Direct CP Violation In B Decays Including $\rho - \omega$ Mixing And Covariant Light-Front Dynamics

Olivier Michel André Leitner
Supervisors:
Prof. Anthony W. Thomas and Prof. Jean-François Mathiot

25th September 2003

Special Research Centre for the Subatomic Structure of Matter (CSSM). School of Chemistry and Physics, University of Adelaide, 5005, Australia,
and
Laboratoire de Physique Corpusculaire (LPC) de Clermont-Ferrand, IN2P3/CNRS Université Blaise Pascal, F-63177 Aubière, France.

à mes parents et mon frère
à Mélissa

Contents

List of Figures

List of Tables

Abstract

Since its discovery in kaon decay in 1964, the origin of CP (Charge-Parity) violation has still not been completely understood. Even though the Standard Model is able to describe this phenomenon, its description involves many theoretical uncertainties. Examples are the parameters of the Cabibbo-Kobayashi-Maskawa (CKM) matrix elements, and the hadronic matrix elements connected to the short and long distance effects. The interest in CP violation has increased with the rise of studies in cosmological physics (baryogenesis) and also with the use of new models so-called "beyond the Standard Model", such as the Higgs model and its derivative, the left-right symmetric models and supersymmetric models.

CP violation can occur via three different modes: it could be an indirect manifestation through the interaction of two initial states, for example $B^0 - \bar{B}^0 \to f$, it could be a direct manifestation due to the initial particle decay, for example, a difference between the decay rates $B^\pm \to \rho^0(\omega)\rho^\pm$, and finally, it could be a combination of the two processes, decay and mixing, as in $B_d^0 \to \psi K_s$. One exciting way to obtain a more accurate understanding of direct CP violation is to study the details of the CP violating asymmetries in the case where $\rho - \omega$ mixing plays a role in the B meson decay. In fact, $\rho - \omega$ mixing provides an opportunity to erase the phase uncertainty mod(π) in the determination of the CKM angles α (in the case of $B \to \rho\pi$) and γ (in the case of $B \to \rho K$) in the unitarity triangle (UT). This phase uncertainty usually arises from the conventional determination of $\sin 2\alpha$ (or $\sin 2\gamma$) in indirect CP violation. Hence, we have an efficient test to check the picture of direct CP violation within the Standard Model.

To achieve this goal, the present thesis is divided in three parts. Firstly, direct CP violation is studied in the following decays: $B^{\pm,0} \to \rho^0(\omega)M^{\pm,0}$ where $M^{\pm,0}$ is either a pion or a kaon. The mixing (through isospin violation) of an ω to ρ^0 which decays into two pions allows us to obtain a difference of the strong phase reaching its maximum at the ω resonance. The calculation of the hadronic matrix elements is carried out using the so-called naive factorization method. This approach utilizes the knowledge of the transition form factors between pseudoscalars and vector particles. In this first part, these form factors will be directly extracted from the literature. By comparing experimental data with theoretical results, it is possible to constrain uncertainties associated with the form factors and parameters ρ and η of the CKM matrix elements. The experimental data (from BELLE, BABAR and CLEO) for branching ratios such as $\mathscr{B}(B \to \rho\pi)$ and $\mathscr{B}(B \to \rho K)$ will be used in this way. Thus, we are able to determine in first approximation (a correct order of magnitude) the CP violating asymmetry parameter, a_{CP},

for the decays $B^{\pm,0} \to \pi^+\pi^- K^{\pm,0}$ and $B^{\pm,0} \to \pi^+\pi^-\pi^{\pm,0}$.

In order to decrease all the uncertainties mentioned previously, it is necessary to evaluate the transition form factors between pseudoscalar and vector particles. To get these form factors, we first need to calculate the wave functions which are involved in these transitions. We take into account several physical constraints to determine the wave functions for the particles π, K, ρ, ω and B; these include the decay constant, electromagnetic form factor, transition form factor and charge radius. We also consider the normalization to fully constrain the wave functions. We apply an explicitly Covariant Light Front Dynamics (CLFD) formalism in our analysis to compute both wave functions and transition form factors. In this formalism, the state vector describing the system under consideration is defined on a light front plane of arbitrary orientation. It is thus decomposed in Fock state components, each one being expressed in terms of a probability amplitude very similar to a non-relativistic wave function. All off-shell amplitudes are thus explicitly dependent on the orientation of the light-front plane, while any physical amplitude should be independent on it.

Then, the last major uncertainty that remains is related to the final state interactions. To compute the hadronic matrix elements without using naive factorization and the Bjorken assumption, we will apply QCD factorization. By assuming some properties lie in energy scales involved in B decays, it allows us to determine as well as possible the non-factorizable terms which arise during the usual hadronic matrix calculation. Finally, only one uncertainty remains uncontrolled, theoretically speaking: these are the CKM matrix parameters ρ and η. By comparing, once again, experimental results for branching ratios $\mathscr{B}(B \to \rho K)$ and $\mathscr{B}(B \to \rho\pi)$ with the theoretical results obtained in this second approach, we can check firstly the transition form factors determined in CLFD. Secondly, we can use these conclusions to predict the CP violating asymmetry parameter, a_{CP}, for decays $B^{\pm,0} \to \pi^+\pi^- K^{\pm,0}$ and $B^{\pm,0} \to \pi^+\pi^-\pi^{\pm,0}$. Finally, based on these results, we determine some limits for the parameters ρ and η of the Cabibbo-Kobayashi-Maskawa matrix.

Résumé

L'origine de la violation CP (Charge-Parité) n'est pas encore complètement comprise depuis sa découverte dans la désintégration du kaon en 1964. Même si le modèle standard décrit de manière assez précise ce phénomène, il prend en compte de nombreuses incertitudes telles que celles sur les paramètres de la matrice Cabibbo-Kobayashi-Maskawa (CKM), celles sur les éléments de la matrice hadronique reliée aux effets à courte et longue distances (problème d'intéraction forte), etc ... L'intérêt de la violation CP s'est accru avec l'essor du domaine cosmologique (étude de la baryogénèse), et avec l'élaboration de nouveaux modèles dits "au-delà du modèle standard", dont on peut citer par exemple le modèle multi-scalaire, le modèle symétrique droite-gauche, les modèles supersymétriques.

La violation CP peut se présenter selon trois modes possibles: soit, c'est une manifestation indirecte dûe au mélange de deux états initiaux qui intéragissent, par exemple $B^0 - \bar{B}^0 \to f$, soit c'est une manifestation directe dûe à la désintégration de la particule initiale, par exemple $B^+ \to \rho^0(\omega)\rho^+$, soit enfin, c'est une combinaison de mélange et de désintégration, par exemple $B_d^0 \to \psi K_s$. Une voie d'étude motivante pour permettre une compréhension plus précise de la violation directe de CP est d'étudier plus en détails les paramètres d'asymétrie dans le cas de la désintégration du méson B tout en tenant compte autant que possible de toutes les incertitudes présentes, et en particulier celles liées à l'intéraction forte.

Pour ce faire, l'étude présentée dans cette thèse est divisée en trois parties. Premièrement, la violation directe de CP est étudiée dans les réactions suivantes: $B^{\pm,0} \to \rho^0(\omega)M^{\pm,0}$ où $M^{\pm,0}$ représente soit un pion soit un kaon. Le mélange $\rho - \omega$ qui se désintègre en deux pions permet d'obtenir à travers la violation d'isospin, un déphasage maximum de la phase forte au voisinage de la résonance ω. Le calcul des éléments hadroniques se fait en utilisant la méthode dite de factorisation naïve où un nombre de couleur effectif, N_c^{eff}, paramétrise les effets hadroniques. Cette méthode implique la connaissance des facteurs de forme de transition entre particules pseudo-scalaires et particules vecteurs. Dans cette première partie, ceux-ci sont directement extraits de la littérature scientifique. En confrontant les données expérimentales et les résultats théoriques, il est alors possible de contraindre les incertitudes théoriques liées aux facteurs de forme, aux éléments ρ et η de la matrice Cabibbo-Kobayashi-Maskawa (CKM) et au nombre de couleur effectif, N_c^{eff}, via principalement les rapports de branchement $\mathscr{B}(B \to \rho\pi)$ et $\mathscr{B}(B \to \rho K)$. Il devient alors possible de déterminer en première approximation le taux d'asymétrie pour les désintégrations $B^{\pm,0} \to \pi^+\pi^- K^{\pm,0}$ et $B^{\pm,0} \to \pi^+\pi^-\pi^{\pm,0}$.

Afin de réduire les présentes incertitudes, il est alors nécessaire d'évaluer

les facteurs de forme de transition entre les particules pseudo-scalaires et vecteurs. Pour obtenir ces facteurs de forme, il est indispensable de calculer les fonctions d'ondes qui sont impliquées dans ces transitions. On prendra en compte les contraintes physiques qui distinguent les particules les unes des autres, i.e., constante de désintégration, facteur de forme électromagnétique, facteur de forme de transition et rayon moyen carré. A ceci s'ajoute la condition de normalisation qui intervient dans toute évaluation de fonction d'onde représentant une particule décrite dans une approche de théorie des champs. Dans notre cas, nous appliquerons un formalisme explicitement covariant et dynamique du front de lumière pour notre analyse. Dans ce formalisme, le vecteur d'état décrivant un système donné est défini sur un plan du front de lumière suivant une orientation arbitraire. Il est alors décomposé en état de Fock où chaque état est exprimé en terme d'amplitude de probabilité. Les amplitudes "off-shell" sont explicitement dépendantes de l'orientation du plan du front de lumière tandis que les amplitudes physiques doivent en être indépandentes.

Ayant déterminé les facteurs de forme de transition entre les particules B, π, K, ρ et ω, la dernière incertitude qui puisse être analysée est celle liée à l'importance des intéractions dans les états finaux. Afin de calculer au mieux les éléments de matrices hadroniques sans utiliser l'hypothèse de Bjorken, nous utiliserons une approche dénommée QCD factorisation. Elle permet, en tenant compte des échelles d'énergie mises en jeu dans les procéssus de désintégration, de calculer la partie généralement non factorisable d'un élément de matrice hadronique, et ainsi d'approximer les intéractions dans les états finaux. Désormais, seule une incertitude subsiste: les éléments ρ et η de la matrice CKM. En comparant les résultats expérimentaux des rapports de branchement et les résultats théoriques obtenus par cette étude, il est alors envisageable à la fois, de vérifier la validité des facteurs de forme déterminés par l'approche CLFD, puis d'extraire des prédictions sur le taux d'asymétrie de la violation directe de CP dans les désintégrations du méson B en trois corps. Finalement, nous exploiterons ces résultats afin d'obtenir des limites sur les éléments ρ et η de la matrice Cabibbo-Kobayashi-Maskawa.

statements

This work contains no material which has been accepted for the award of any other degree or diploma in any university or other tertiary institution and, to the best of my knowledge and belief, contains no material previously published or written by another person, except where due reference has been made in the text.

I give consent to this copy of my thesis, when deposited in the University Library, being made available for loan and photocopying.

date

8/07/03

Acknowledgements

I am going to take the opportunity given by this section to write in french. I hope that noone will be disappointed by that and I am pretty sure that you will guess what it is written in the following sentences.

En écrivant les remerciements, je me rends compte que très bientôt trois ans et demi se seront écoulés depuis mon arrivée en Australie au CSSM le 7 décembre 1999. Ce fut, c'est et cela restera pour moi une formidable expérience qui sans le moindre doute me servira tout au long de ma carrière de physicien. J'ai énormément appris durant toute cette période, que ce soit dans le domaine de la physique des particules, la pratique de l'anglais et la découverte de l'Australie. Tout cela n'eut été possible sans l'accord de deux personnes à qui je dois beaucoup et qui m'ont donné une incroyable opportunité: Jean-François Mathiot et Anthony Thomas. Mes remerciements les plus chaleureux et les plus sincères leur vont en premier. Je ne serais pas ce que je suis aujourd'hui sans la confiance et l'investissement qu'ils ont mis en moi, la liberté qu'ils m'ont donnée dans mon travail de thèse et le temps qu'ils m'ont consacré. Qu'ils sachent que je leur en suis grandement reconnaissant.

Je remercie également Xin-Heng Guo pour tout le travail que nous avons fait ensemble. Il a toujours su être disponible pour toutes les questions que je lui ai posées, pour les discussions que nous avons eues, et a été d'un précieux secours pour contrôler mes étourderies dans les calculs. J'espère que cette collaboration continuera dans le futur. Je voudrais aussi remercier Ian Cloet pour les "morning sessions" où nous discutions de tous les sujets avant de commencer à travailler. Mes remerciements lui vont également entre autre pour les lectures et relectures de ma thèse. Mes remerciements s'adressent aussi aux étudiants du CSSM: James Zanotti, Ross Young, Wassem Kamleh, Will Detmold, Ben Lasscock, Ben Crouch, John Hedditch, Sarah Lawley, Maria Parappilly, Marco Bartolozzi, Frédéric Bonnet et Mark Stanford. Je souhaite également remercier Sharon Johnson et Sara Boffa[1] pour leur disponibilité à mon égard ainsi que Ramona Adorjan pour le temps qu'elle a trouvé pour répondre à toutes mes questions (elles furent nombreuses..) en informatique.

Mes remerciements vont aussi à Anthony Williams ainsi qu'à Alex Kalloniatis, Jianbo Zhang, Ayse Kizilersu, Danielle Morel, Vadim Guzey, Kazuo Tsushima et Andreas Schreiber. Je voudrais mentionner l'exceptionnel convivialité qui règne au CSSM. Je garde en moi le souvenir du petit voyage que nous avons fait courant décembre 2002 pour aller voir l'éclipse totale de

[1]Grazie per aver preso cura dell'appartamento, del gatto, del cane, del pappagallo e delle piante durante il mio soggiorno in Francia.

soleil. Ce voyage à lui seul résume l'amitié présente au laboratoire et l'unité du groupe.

Mes séjours en France au laboratoire LPC de Clermont-Ferrand furent toujours très agréables. Je remercie toute l'équipe de physique théorique du laboratoire ainsi que l'équipe de physique expérimentale LHCb avec laquelle j'ai beaucoup collaboré. Je ne peux oublier de mentionner Hélène Fonvielle pour son accueil et sa gentillesse. Mes remerciements vont aussi à Michèle Chadelas, Janine Pellet et Colette Blisson pour leur efficacité concernant les problèmes administratifs liés à mon statut d'étudiant particulier...

Je remercie également Volodia Karmanov, Jean-Jacques Dugnes, Vincent Morenas, François Bissey, Cécile Rimbault et Ziad Ajaltouni pour leurs participations, leurs commentaires et l'aide qu'ils m'ont apportés durant ma thèse.

Enfin, il ne m'aurait pas été possible de venir en Australie sans le soutien inconditionnel de mes parents, de mon frère et de Mélissa. Pour la présence et l'amour qu'ils m'ont apportés malgré la distance, pour le respect et leur appui dans les choix qui furent les miens, je les en remercie de tout mon coeur. Cette thèse leur est dédiée.

Part I

Matter Antimatter

Chapter 1

Introduction

" Ecrire est difficile, parce qu'on est toujours dépassé par son livre. "

Jean d'Ormesson

A little bit of history...

Why did the matter in our Universe not completely annihilate with antimatter immediately after its creation? The answer to this question has been and remains the quest of many physicists, both experimentalists and theoreticians, in high energy physics since the mid 1950's. The answer lies somewhere within CP violation theory, since it enables us to distinguish in an absolute way matter and anti-matter. For a long time, Charge conjugation C, which transforms a particle into its anti-particle, and Parity P, which reflects the space coordinate $\vec{x}$ into $-\vec{x}$, were considered as exact discrete symmetries in processes such as those involving electromagnetic, strong and weak interactions.

In May 1947 one of the first decays of a neutral particle ($K^0 \to \pi^+\pi^-$) into two charged ones was observed. Almost ten years later (1956), Lee and Yang [1], motivated by the so-called $\theta - \tau$ puzzle, pointed out that parity invariance might be not conserved in weak interactions. Soon after (1957), Wu *et al* [2] and Garwin *et al* [3] verified this theoretical analysis independently and even found that both parity and charge invariance are violated in weak interactions. In 1964 Christenson, Cronin, Fitch and Turlay [4], discovered for the first time CP violation in K^0 meson decays, at Brookhaven National Lab. It was found that two neutral strange mesons could mix by

weak interaction through the decay,

$$K^0 \to (\pi\pi, \pi\pi\pi) \to \bar{K}^0 \ .$$

One way to represent this mixing is to consider two particles, called K_1 and K_2 and defined as a linear combination of K^0 and $\bar{K}^0$:

$$|K_1\rangle = \frac{1}{\sqrt{2}}\Big(|K^0\rangle + |\bar{K}^0\rangle\Big) \ , \tag{1.1}$$

$$|K_2\rangle = \frac{1}{\sqrt{2}}\Big(|K^0\rangle - |\bar{K}^0\rangle\Big) \ . \tag{1.2}$$

K_1 ($K_1 \to K_S$ with short lifetime $\tau_S = 8.92 \times 10^{-11}$ s) decays into two pions and K_2 ($K_2 \to K_L$ with long lifetime $\tau_L = 5.17 \times 10^{-8}$ s) decays into three pions if one assumes CP conservation. What was observed in 1964 was the interference between the particles $K_L \to \pi\pi$ and $K_S \to \pi\pi$. Even though the branching ratio $\mathscr{B}(K_L \to \pi\pi)$ is very small, it was the proof that K_S and K_L should be rewritten as a linear combination of K_1 and K_2 as follows,

$$|K_S\rangle \simeq |K_1\rangle + \epsilon|K_2\rangle \ , \tag{1.3}$$

$$|K_L\rangle \simeq |K_2\rangle + \epsilon|K_1\rangle \ , \tag{1.4}$$

where the epsilon parameter, ϵ, describes the strength of CP violation. $|\epsilon| \simeq 2 \times 10^{-3}$ and $\mathrm{Arg}(\epsilon) \simeq \pi/4$. We had to wait until 1973 to find the theoretical explanation within the Standard Model by M. Kobayashi and T. Maskawa [5] whereas there is still not definitive theoretical explanation beyond the Standard Model. In this work, our analysis will stay within the Standard Model framework.

Plan

CP violation, as it has already been mentioned, is a very exciting field of investigation in particle physics. For almost forty years, physicists have been trying to understand this mechanism. As everyone can imagine, it is not easy to draw an exact picture of CP violation. One way to extract reasonable predictions, since theoretically speaking, one knows the mechanism within the Standard Model, is to use a phenomenological approach which, of course, carries many uncertainties and is very often model dependent.

The aims of this thesis are, first of all, to determine an order of magnitude for the direct CP violation in decays such as $B \to \rho^0(\omega)M^{\pm,0} \to \pi^+\pi^- M^{\pm,0}$ (with M being a kaon or a pion). The $\rho - \omega$ mixing effects in these decays

are also investigated in detail. The second aim is to decrease, within a relativistic and dynamic approach, the uncertainties included in the form factor transitions and wave functions which are involved in our analysis. The third aim is to apply a new kind of factorization of hadronic matrix elements, and hence, to be able to obtain better predictions for the branching ratios as well as the CP violating asymmetry parameter, a_{CP}, in B decays. Comparisons with experimental data (only for branching ratios) provided by the BABAR, BELLE and CLEO collaborations give us an excellent opportunity to finally constrain the Cabibbo-Kobayashi-Maskawa (CKM) matrix element parameters ρ and η.

To study as far as theoretical tools allow us to go, we divide our work into four parts as follows: the first part, so-called "Matter Antimatter", gives the necessary and basic background in particle physics in order to understand the concept of CP violation within the Standard Model. In particular, we recall briefly in Chapter 2, the characteristics of the Standard Model: Gauge theory, Quantum Chromodynamics, Quantum Electrodynamics and Electroweak interaction. It is known that, within the Standard Model framework, the Cabibbo-Kobayashi-Maskawa matrix is the main source of Charge Parity violation. Thus, we introduce it in an extensive way since all of the following work is based on it. Experimentally, it has been observed that CP violation can arise in different ways. To clarify them and to introduce the one which we are going to focus on, we summarize the different observations of CP violation in B meson decays. This first part is very well established and therefore we refer the reader to the plentiful literature for more explanation and detail.

The second part, so-called "Branching Ratio and Direct CP Asymmetry in B Decays", mainly focuses on the analysis of direct CP violation. We begin by explaining the formalism used in our approach: the operator product expansion (OPE), Wilson coefficients and finally the effective Hamiltonian are introduced (Chapter 3). We then describe the calculation of the hadronic matrix elements involved in the decay amplitude, by using the so-called "Naive factorization" method. In Chapter 4, we discuss in detail $\rho-\omega$ mixing, its origin (Vector Meson Dominance model) and its inclusion in our calculations of the branching ratios and CP violating asymmetry parameter a_{CP}. In Chapter 5, we are then able to investigate the branching ratios such as $\mathscr{B}(B \to \rho\pi)$ and $\mathscr{B}(B \to \rho K)$. All the numerical and technical details are described in this chapter. We also list the branching ratios for $\mathscr{B}(B \to \rho\pi)$ and $\mathscr{B}(B \to \rho K)$ measured by CLEO, BABAR and BELLE. Based on our results for the branching ratios and comparisons with the experimental data, we determine in Chapter 6, direct CP violation for the same decays including $\rho - \omega$ mixing effects.

Our calculations contain several uncertainties. One of them is the form factor involved in the factorization method. The third part of this thesis, the so-called "Covariant Light Front Dynamics, Wave Functions and Form Factors", aims to reduce this uncertainty. To increase the accuracy on these transition form factors, we recalculate them in a relativistic and dynamical approach. In Chapter 7, we introduce the main properties and definitions of Covariant Light Front Dynamics (CLFD). In Chapter 8, we determine the wave functions for the following mesons: we evaluate the pseudoscalar particles π, K, B and D and the vector particles ρ and ω. We emphasize that this study takes into account some experimental data (decay constant, charge radius...) in order to parametrize the wave functions. We use the wave functions mentioned previously to compute the transition form factors such as pseudoscalar pseudoscalar transition and pseudoscalar vector transition. This last study is accomplished in Chapter 9.

In order to go further in our investigation, we replace the naive factorization (used as a first approach) by a very recent (1999) and promising theoretical framework. This last part, "QCD Factorization in B Decays", presents the corrections included in our analysis through the "QCD factorization" method. The main idea is to include all of the interactions at the order α_s between quarks and gluons arising in the final states following B decays (in our case). In Chapter 10, we introduce in detail the method applied in our calculations. Expecting to have reduced as far as we can, all the uncertainties involved in the analytical calculation of decay amplitudes, we are able, in Chapter 11, to recalculate the branching ratios $\mathscr{B}(B \to \rho\pi)$ and $\mathscr{B}(B \to \rho K)$. In a similar manner to Chapter 6, we are also able in Chapter 12, to determine more accurate asymmetries in B meson decays. In this final chapter, we also propose some reasonable constraints regarding the Cabibbo-Kobayashi-Maskawa matrix element parameters ρ and η. To end this work, we give some final remarks and draw some conclusions based on this analysis within the Standard Model.

Chapter 2

CP violation, a brief overview

" Les petites choses ont leur importance; c'est toujours par elles qu'on se perd. "

Fiodor Dostoievski

In this chapter, we introduce the formalism and the concept of CP violation [6] within the framework of the Standard Model (SM). We set the scene and describe all the "participants" which are necessary to understand a CP violating asymmetry between matter and antimatter.

2.1 The Standard Model

2.1.1 Basic concepts

The Standard Model of elementary particle physics gives a complete description of the weak, electromagnetic and strong interactions. It is based on the Glashow-Salam-Weinberg Model of the electroweak interaction plus Quantum Chromodynamics. This model is derived from work undertaken in 60's and is built on the principle of local gauge symmetry.

Gauge theory

Within the Standard Model, the fundamental interactions are governed by gauge theory [7]. The free QED or QCD-Lagrangian (for a Dirac particle) described in the framework of gauge theory is not invariant under the phase changes called local gauge transformations. Nevertheless, local gauge invariance can be restored by applying the appropriate covariant derivative $\mathbf{D}_\mu$

acting on the field (fermion field for example). Then, the Lagrangian becomes invariant under any local transformations of a symmetry group. If the symmetry group elements commute, we have an Abelian gauge theory. This is the case for Quantum Electrodynamics (QED) where $U(1)$ defines an Abelian group. This is not the case for Quantum Chromodynamics (QCD) where $SU(3)_{\text{colour}}$, the gauge group of strong interaction, is a non-Abelian group. In the latter group, $SU(3)_{\text{colour}}$, the eight generators correspond to the gluons. The properties of asymptotic freedom and confinement are due to the colour charge carried by the gluons and quarks, which leads to gluons interacting with each other (self-interaction), as well as with quarks.

Quantum ChromoDynamics

QCD [7] is the quantum field theory of strong interaction between quarks and gluons. Since the colour symmetry of the quark model is gauged, the strong interaction is described by an $SU(3)$ colour Yang-Mills theory with each flavour of quarks transforming according to the fundamental triplet representation. By adding the renormalization requirement, the analytical form of the full QCD-Lagrangian density has to be the following:

$$\begin{aligned}\mathcal{L}_{QCD} = & \\ & -\frac{1}{4}(\partial_\mu \mathbf{A}^a_\nu - \partial_\nu \mathbf{A}^a_\mu + g f^{abc}\mathbf{A}^b_\mu \mathbf{A}^c_\nu)(\partial^\mu \mathbf{A}^{a\nu} - \partial^\nu \mathbf{A}^{a\mu} + g f^{ade}\mathbf{A}^{d\mu}\mathbf{A}^{e\nu}) \\ & -\frac{1}{2\xi}(\partial_\mu \mathbf{A}^{a\mu})^2 - \bar{\eta}^a \partial_\mu(\partial^\mu \delta^{ac} - g f^{abc}\mathbf{A}^{b\mu})\eta^c \\ & \qquad + \bar{\psi}\Big[i\gamma_\mu(\partial^\mu - ig\mathbf{A}^{a\mu}\mathbf{T}^a) - m\Big]\psi \ , \quad (2.1)\end{aligned}$$

where the first line refers to the gauge part of the QCD-Lagrangian. $\mathbf{A}^a_\nu, g$ and f^{abc} are the gluon fields, gauge coupling and structure constants of $SU(3)_{\text{colour}}$, respectively. The gluon colour indices take the values, a, b, c equal to $1, \cdots, 8$. The first term of the second line defines the gauge fixing, where ξ could be 1 for Feynman and 't Hooft gauge. The second term of the same line describes the Faddeev-Popov interaction, where η is the ghost field. The following term is the fermion part with the free part given by $\bar{\psi}\big[i\gamma_\mu(\partial^\mu - m)\big]\psi$ and the quark gluon interaction written as $\bar{\psi}\big[\gamma_\mu g A^{a\mu}\mathbf{T}^a\big]\psi$, where ψ refers to the quark field and $\mathbf{T}^a$ to the generators of $SU(3)_{\text{colour}}$.

Quantum ElectroDynamics

QED [7] is the quantum field theory of electrons, positrons and photons. It describes any electromagnetic interactions of these elementary particles. The

fermion field ψ transforms under a local $U(1)$ transformation as:

$$\psi(x) \rightarrow \psi'(x) = \exp(-ie\lambda(x))\,\psi(x)\ . \tag{2.2}$$

To restore the local $U(1)$ gauge invariance of the free Lagrangian for a Dirac particle, we introduce a vector field A_μ (called gauge field) and we replace the ordinary derivative ∂_μ by a covariant derivative $\mathbf{D}_\mu$. Hence, the full QED-Lagrangian density constrained by the $U(1)$ group of transformations reads as,

$$\mathcal{L}_{QED} = -\frac{1}{4}(\partial_\mu \mathbf{A}_\nu - \partial_\nu \mathbf{A}_\mu)^2 - \frac{1}{2\xi}(\partial_\mu \mathbf{A}^\mu)^2 + \bar{\psi}\Big[i\gamma_\mu(\partial^\mu + ie\mathbf{A}^\mu) - m\Big]\psi\ . \tag{2.3}$$

The gauge part of the QED-Lagrangian is given by the first term which is invariant under transformation $A'_\mu \rightarrow A_\mu + \partial_\mu\lambda$. The second term is the gauge fixing condition analogously to the QCD-Lagrangian, but here the photon field is gauged. The last part contains the interaction term, $-\bar{\psi}\gamma_\mu e\mathbf{A}^\mu\psi$ and the free QED-Lagrangian, $\bar{\psi}i\gamma_\mu(\partial^\mu - m)\psi$.

2.1.2 The electroweak interaction

Within the Standard Model (SM), one defines three generations of quarks and leptons [7, 8, 9]. The gauge symmetry which governs these particles is,

$$G_{SM} = SU(3)_c \otimes SU(2)_L \otimes U(1)_Y\ , \tag{2.4}$$

where c, L and Y refer to colour, left and hypercharge respectively. Since one assumes that a scalar field, ϕ, defines a Vacuum Expectation Value like,

$$\langle\phi\rangle = \begin{pmatrix} 0 \\ v/\sqrt{2} \end{pmatrix}\ , \tag{2.5}$$

the gauge group G_{SM} is spontaneously broken down to $SU(2)_L \otimes U(1)_Y$. $SU(2)_L \otimes U(1)_Y$ can also be spontaneously broken to $U(1)_{\mathrm{EM}}$ through the Vacuum Expectation Value of a scalar doublet Higgs field:

$$\langle\phi\rangle = \begin{pmatrix} \phi^+ \\ \phi^0 \end{pmatrix}\ . \tag{2.6}$$

The particles are classified as follows. The left-handed leptons are in $SU(2)_L$ doublets,

$$\begin{pmatrix} \nu_e \\ e^- \end{pmatrix}_L \begin{pmatrix} \nu_\mu \\ \mu^- \end{pmatrix}_L \begin{pmatrix} \nu_\tau \\ \tau^- \end{pmatrix}_L\ , \tag{2.7}$$

and similarly for the quarks,

$$\begin{pmatrix} u \\ d' \end{pmatrix}_L \begin{pmatrix} c \\ s' \end{pmatrix}_L \begin{pmatrix} t \\ b' \end{pmatrix}_L , \tag{2.8}$$

with the corresponding right-handed singlets. Note also that d', s' and b' are related to the mass eigenstates d, s and b by a unitarity transformation. The Standard Model Lagrangian is written down as the most general renormalizable Lagrangian which is consistent with the gauge symmetry. If we focus on the electroweak interaction of quarks and leptons, the massive bosons, $W^{\pm}$, are the mediators describing the electroweak charged current interaction,

$$\frac{g_2}{2\sqrt{2}}(J^+_\mu W^{+\mu} + J^-_\mu W^{-\mu}) , \tag{2.9}$$

where, g_2 is the $SU(2)_L$ coupling constant and the current[1] J^+_μ is given by,

$$J^+_\mu = \sum_f (\bar{q}q')_{V-A} + \sum_f (\bar{\nu}_l l)_{V-A} , \tag{2.10}$$

with q and l denoting respectively quark and lepton. The notation $V - A$ refers to the $\gamma_\mu(1 - \gamma_5)$ structure. We stress that the charged current interactions involve only left-handed quarks and left-handed leptons. For the neutral current interaction, the vectors are Z^0 and the photon A. The corresponding Lagrangian term is,

$$\frac{g_2}{2\cos\theta_W} J^0_\mu Z^\mu + eJ^{em}_\mu A^\mu , \tag{2.11}$$

where the current J^0_μ is defined as,

$$J^0_\mu = \sum_f \bar{f}\gamma_\mu(c^f_V - c^f_A\gamma_5)f . \tag{2.12}$$

In Eq. (2.12), f denotes the quark flavour and c^f_V, c^f_A are written as,

$$c^f_V = T^f_3 - 2Q_f \sin^2\Theta_W \text{ and } c^f_A = T^f_3 , \tag{2.13}$$

where Q_f is the charge, Θ_W is the Weinberg angle and T^f_3 is the third component of the weak isospin. For the current J^{em}_μ, one has,

$$J^{em}_\mu = \sum_f Q_f \bar{f}\gamma_\mu f . \tag{2.14}$$

[1] $J^-_\mu = (J^+_\mu)^\dagger$.

Finally, the weak interaction is related to the Fermi constant, G_F, which plays an important role in the Standard Model,

$$\frac{G_F}{\sqrt{2}} = \frac{g_2^2}{8M_W^2} = \frac{e^2}{8M_W^2 sin^2\Theta_W} , \tag{2.15}$$

where M_W is the boson W mass.

2.2 The Cabibbo-Kobayashi-Maskawa matrix

2.2.1 Sources of CP violation

There are three possibilities which may explain the source of CP violation inside the Standard Model [10, 11, 12]. The first one comes from the strong interaction. If we assume that the vacuum is given by a superposition of degenerate vacua $|n\rangle$ which creates non-trivial quantum fluctuations (instantons), we can include in the Lagrangian the following term:

$$\mathcal{L}_\theta = \theta \cdot \frac{g_s^2}{32\pi^2} G^A_{\mu\nu} G^{\tilde{A}\mu\nu} , \tag{2.16}$$

where θ is the QCD vacuum angle (in fact, the CP violating asymmetry parameter), g_s the QCD gauge coupling and $G^A_{\mu\nu}$ the QCD field strength tensor. The term $\mathcal{L}_\theta$ violates CP symmetry for a non-zero value of $\tilde{\theta} = \theta - \arg(\det \mathrm{M}^\theta)$, where M^θ is the non-diagonal quark mass matrix expressed in the electroweak basis. But, up to now, the so-called *strong CP problem* [13, 14] remains without any available explanation: based on the experimental values on the electric dipole moment of the neutron, $\tilde{\theta}$ has to be less than 10^{-10} which implies a extremely fine value of the QCD vacuum angle θ. The second possible source of CP violation is in the leptonic sector if neutrinos are massive. In this case, the term related to the leptonic sector, in the effective Lagrangian, can give, after symmetry breaking, a Majorana neutrino mass matrix with three CP violating phases. The last way to get CP violation in the quark sector, is the CKM matrix. This possibility is widely detailed in the following.

2.2.2 The CKM matrix

Let us first focus on the Yukawa interaction term in the Lagrangian used in the Standard Model. It reads as,

$$\mathcal{L}_{Yukawa} = -Y^d_{ij} \bar{Q}_{Li} \phi d_{Rj} - Y^u_{ij} \bar{Q}_{Li} \tilde{\phi} u_{Rj} + h.c. , \tag{2.17}$$

where Y_{ij}^q is the Yukawa matrix element, Q_L are the left-handed quark SU(2)-doublets and u_R, d_R are the right-handed SU(2)-singlets. CP asymmetry is violated if and only if,

$$\Im m\{\det[Y^d Y^{d\dagger}, Y^u Y^{u\dagger}]\} \neq 0 \ . \tag{2.18}$$

Now, if we replace ϕ by $(v + H^0)/\sqrt{2}$, the Yukawa Lagrangian becomes massive and gives,

$$\mathcal{L}_{Yukawa} = -(M_d)_{ij}\bar{d}_{Li}d_{Rj} - (M_u)_{ij}\bar{u}_{Li}u_{Rj} + h.c. \ , \tag{2.19}$$

with $M_f = Y^f v/\sqrt{2}$. In the mass basis, one can always find some unitarity matrices V_{fL} and V_{fR} which verify the condition,

$$V_{fL} M_f V_{fR}^\dagger = M_f^{diag} \ , \tag{2.20}$$

where M_f^{diag} is diagonal and real. Then, the mass eigenstates are given by,

$$\begin{aligned} d_{Li} &= (V_{dL})_{ij} d_{Lj} \ , \\ d_{Ri} &= (V_{dR})_{ij} d_{Rj} \ , \\ u_{Li} &= (V_{uL})_{ij} d_{Lj} \ , \\ u_{Ri} &= (V_{dR})_{ij} d_{Rj} \ . \end{aligned}$$

Therefore, after electroweak symmetry breaking, the charged current interaction for quarks is given by,

$$\mathcal{L}_W = -\frac{e}{\sqrt{2}\sin\theta_W}\bar{u}_{Li}\gamma^\mu (V_{uL}V_{dL}^\dagger)_{ij} d_{Lj} W_\mu^+ + h.c. \ , \tag{2.21}$$

where by definition, one puts,

$$V_{CKM} = V_{uL}V_{dL}^\dagger \ . \tag{2.22}$$

This non-diagonal 3×3 matrix is so-called the Cabibbo-Kobayashi-Maskawa and represents the charged current couplings between quark transitions. It describes the only source of flavour changing interaction in the quark sector. The CKM matrix is dependent on nine parameters; three real angles and 6 phases. In order to get a unique matrix, some conventions are adopted: the first is the arrangement of the quark masses from the heaviest to the lightest. We can also illustrate this by taking into account the hierarchy of quark transition through the charged currents (see Fig. 2.1) [15].

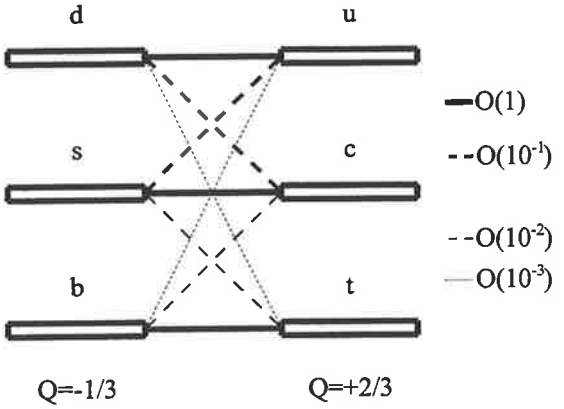

Figure 2.1: Hierarchy of strength of transitions between quarks.

The connection between the electroweak eigenstates (d', s', b') and their mass eigenstates (d, s, b) is given by,

$$\begin{pmatrix} d' \\ s' \\ b' \end{pmatrix} = \begin{pmatrix} V_{ud} & V_{us} & V_{ub} \\ V_{cd} & V_{cs} & V_{cb} \\ V_{td} & V_{ts} & V_{tb} \end{pmatrix} \times \begin{pmatrix} d \\ s \\ b \end{pmatrix} . \tag{2.23}$$

Therefore, the CKM matrix takes the form,

$$V_{CKM} = \begin{pmatrix} V_{ud} & V_{us} & V_{ub} \\ V_{cd} & V_{cs} & V_{cb} \\ V_{td} & V_{ts} & V_{tb} \end{pmatrix} . \tag{2.24}$$

The second convention on the matrix, is to minimize the number of phases in the matrix. When this is realized (in the case of three generations of quarks), the CKM matrix contains only one single physical phase. It is called the Kobayashi-Maskawa phase δ_{KM} and any CP violating physical observable in flavour changing interactions has to be related to this phase. Inside the Standard Model, the phase δ_{KM} is the only source of CP violation in the quark sector.

There are two parametrizations of this matrix. One, called *standard parametrization* reads [16, 17],

$$V_{CKM} = \begin{pmatrix} c_{12}c_{13} & s_{12}c_{13} & s_{13}e^{-i\delta_{KM}} \\ -s_{12}c_{23} - c_{12}s_{23}s_{13}e^{i\delta_{KM}} & c_{12}c_{23} - d_{12}d_{23}s_{13}e^{i\delta_{KM}} & s_{23}c_{13} \\ s_{12}s_{23} - c_{12}c_{23}s_{13}e^{i\delta_{KM}} & -c_{12}s_{23} - s_{12}c_{23}s_{13}e^{i\delta_{KM}} & c_{23}c_{13} \end{pmatrix} , \tag{2.25}$$

where $c_{ij} = \cos\theta_{ij}$ and $s_{ij} = \sin\theta_{ij}$. The three angles θ_{ij}, are real mixing parameters. The c_{ij} and s_{ij} are chosen positive and δ_{KM} can vary in the range $0 < \delta_{KM} < \pi$ since the measurements of CP violation in K decays impose this. In this representation, there are four independent parameters which are,

$$s_{12} = |V_{us}|, \quad s_{13} = |V_{ub}|, \quad s_{23} = |V_{cb}|, \text{ and } \delta_{KM} . \tag{2.26}$$

Another parametrization is widely used in phenomenological applications. This is the *Wolfenstein parametrization* (Wolfenstein 1983) [16, 18, 19]. In this approach, the four independent parameters are λ, A, ρ and η. Then, by expanding each element of the matrix as a power series of the parameter $\lambda = \sin\theta_c = 0.2209$ (θ_c is the GellMan Levy Cabibbo angle), one gets ($O(\lambda^4)$ is neglected),

$$\hat{V}_{CKM} = \begin{pmatrix} 1-\frac{1}{2}\lambda^2 & \lambda & A\lambda^3(\rho - i\eta) \\ -\lambda & 1-\frac{1}{2}\lambda^2 & A\lambda^2 \\ A\lambda^3(1-\rho-i\eta) & -A\lambda^2 & 1 \end{pmatrix} , \tag{2.27}$$

where η plays the role of the CP violating phase. In this parametrization, even though it is an approximation in λ, the CKM matrix satisfies unitarity exactly, which means,

$$\hat{V}^{\dagger}_{CKM} \cdot \hat{V}_{CKM} = \hat{I} = \hat{V}_{CKM} \cdot \hat{V}^{\dagger}_{CKM} . \tag{2.28}$$

The relation between the two parametrizations described above is,

$$\begin{aligned} s_{12} &= \lambda , \\ s_{23} &= A\lambda^2 , \\ s_{13}e^{-i\delta_{KM}} &= A\lambda^3(\rho - i\eta) . \end{aligned}$$

Finally, one can also define a CP violating quantity independent of the parametrization. This quantity is called *Jarlskog* parameter and represents the unique condition for CP violation [10, 20];

$$\mathscr{I}m[V_{ij}V_{kl}V^{\star}_{il}V^{\star}_{kj}] = J_{CP}\sum_{m,n=1}^{3}\epsilon_{ikm}\epsilon_{jln} . \tag{2.29}$$

CP symmetry is violated within the Standard Model if $J_{CP} \neq 0$. From the CKM matrix derived in the Wolfenstein parametrization, one can also obtain 6 normalization relations and 6 orthogonality relations because of the unitarity of the matrix, for example:

$$V_{ud}V^{\star}_{ub} + V_{cd}V^{\star}_{cb} + V_{td}V^{\star}_{tb} = 0 . \tag{2.30}$$

By combining the Wolfenstein parametrization and the unitarity triangle, we can represent the structure of the CKM matrix geometrically in the complex plane $(\bar{\rho}, \bar{\eta})$, as shown in Fig. 2.2. The relations between $(\bar{\rho}, \rho)$ and $(\bar{\eta}, \eta)$ are [21],

$$\bar{\rho} = \left(1 - \frac{\lambda^2}{2}\right)\rho, \quad \bar{\eta} = \left(1 - \frac{\lambda^2}{2}\right)\eta \,. \tag{2.31}$$

The area of all triangles drawn from the orthogonality or normalisation

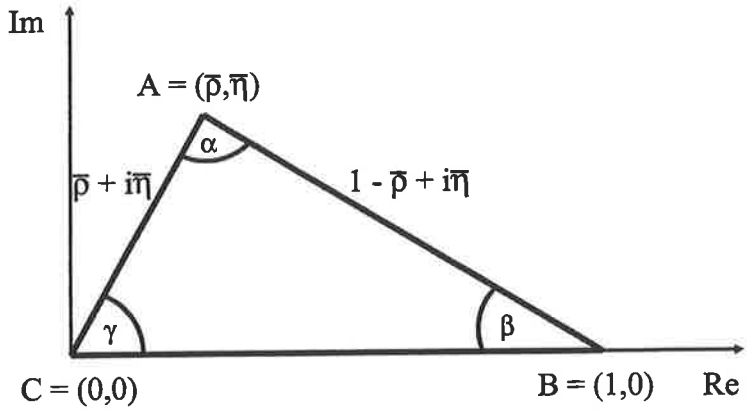

Figure 2.2: The unitarity triangle (UT) of the CKM matrix in the complex plane.

relations is the same and reads [16, 21],

$$2A_\Delta = |J_{CP}| \,, \text{ where } J_{CP} = \lambda^6 A^2 \eta = O(10^{-5}) \,. \tag{2.32}$$

The accuracy between the $(\bar{\rho}, \bar{\eta})$ and (ρ, η) quantities is in the order of 3%. The three angles α, β and γ of the unitarity triangle [22, 23] in can be derived as a function of the CKM matrix elements and one gets,

$$\alpha \equiv \arg\left[-\frac{V_{cd}V_{cb}^\star}{V_{td}V_{tb}^\star}\right], \quad \beta \equiv \arg\left[-\frac{V_{td}V_{tb}^\star}{V_{ud}V_{ub}^\star}\right], \quad \gamma \equiv \arg\left[-\frac{V_{ud}V_{ub}^\star}{V_{cd}V_{cb}^\star}\right] \,, \tag{2.33}$$

which gives analytically the following relations,

$$\begin{aligned}
\sin(2\alpha) &= \frac{2\bar{\eta}(\bar{\eta}^2 + \bar{\rho}^2 - \bar{\rho})}{(\bar{\eta}^2 + \bar{\rho}^2)((1-\bar{\rho}^2)^2 + \bar{\eta}^2)} \,, \\
\sin(2\beta) &= \frac{2\bar{\eta}(1-\bar{\rho})}{(1-\bar{\rho})^2 + \bar{\eta}^2} \,, \\
\sin(2\gamma) &= \frac{2\bar{\eta}\bar{\rho}}{\bar{\rho}^2 + \bar{\eta}^2} \,.
\end{aligned}$$

As regards the lengths CA and BA in the triangle ABC, one has also,

$$R_b \equiv CA \equiv \left|\frac{V_{ud}V_{ub}^\star}{V_{cd}V_{cb}^\star}\right| = \left(1-\frac{\lambda^2}{2}\right)\left|\frac{V_{ub}}{V_{cb}^\star}\right|, \quad R_t \equiv BA \equiv \left|\frac{V_{td}V_{tb}^\star}{V_{cd}V_{cb}^\star}\right| = \frac{1}{\lambda}\left|\frac{V_{td}}{V_{cb}}\right| . \tag{2.34}$$

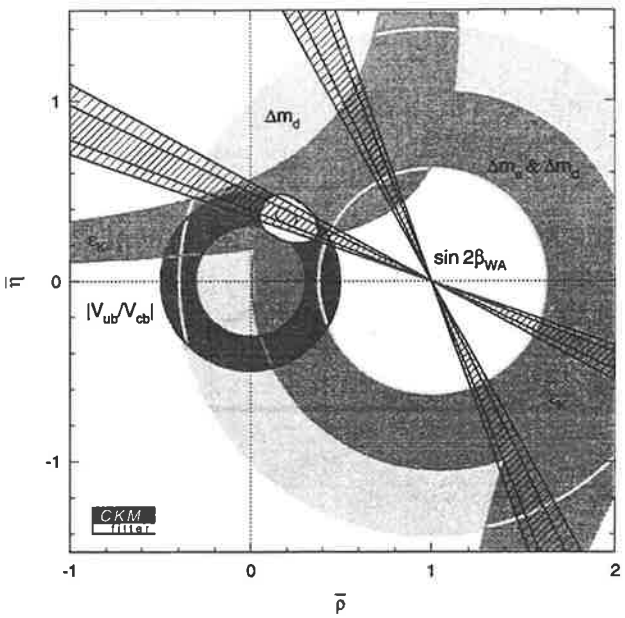

Figure 2.3: Confidence levels, plotted in the plane $(\bar{\rho}, \bar{\eta})$, and obtained from a global fit taking into account many experimental data.

To complete this description, we end by giving the numerical values of the CKM matrix [24]:

$$V_{CKM} = \begin{pmatrix} 0.9741 \text{ to } 0.9756 & 0.219 \text{ to } 0.226 & 0.0025 \text{ to } 0.0048 \\ 0.219 \text{ to } 0.226 & 0.9732 \text{ to } 0.9748 & 0.038 \text{ to } 0.044 \\ 0.004 \text{ to } 0.014 & 0.037 \text{ to } 0.044 & 0.9990 \text{ to } 0.9993 \end{pmatrix} . \tag{2.35}$$

The experimental determination of the matrix elements $U_{qq'}$ are mainly based on β decays, K semi-leptonic decays, B decays, lifetime of B meson, and from unitarity conditions. In Fig 2.3, values of $\bar{\rho}$ and $\bar{\eta}$ are plotted according to the latest experimental constraints [16].

2.3 CP violation in B meson decays

The theory of CP violation predicts large CP violating effects in B meson decays [10, 12, 21, 25], where one can observe three features of CP violation. First, we define the decay amplitude A_{Bf} and $\bar{A}_{Bf}$ by,

$$A_{Bf} = \langle f|H_d|B\rangle \ ,$$
$$\bar{A}_{Bf} = \langle \bar{f}|H_d|\bar{B}\rangle \ ,$$

where H_d is the decay Hamiltonian. We also write down the decay amplitude A_{Bf} as,

$$A_{Bf} = |A_1|e^{i\delta_1 \pm i\phi_1} + |A_2|e^{i\delta_2 \pm i\phi_2} \ , \tag{2.36}$$

where each term is related to a particular Feynman diagram (or set of Feynman diagrams). Two types of phases appear in A_{Bf}. The first phase, ϕ_i, (called *weak phase*) originates from the CKM matrix element through the corresponding electroweak Lagrangian term. The second one, δ_j, (called the *strong phase*) does not violate CP symmetry and arises from the final state interaction processes (absorptive parts in the amplitudes). Let us now describe briefly the different kinds of CP violation.

2.3.1 CP violation in mixing

This requires that two neutral mass eigenstates cannot be chosen to be CP eigenstates [12, 21, 25]. If, one defines the mixing matrix for the two meson system as,

$$\mathcal{M} = M + i\Gamma \ , \tag{2.37}$$

where M and Γ are complex 2×2 matrices, the asymmetry will be proportional to,

$$a_{CP} = \mathcal{I}m\left(\frac{\Gamma_{12}}{M_{12}}\right) \ , \tag{2.38}$$

which means that a relative phase between M_{12} and Γ_{12} is necessary.

2.3.2 CP violation in the interference of decays with and without mixing induced

The feature of CP violation is based on spontaneous oscillations of a particle (see Fig. 2.4) into its antiparticle, which are due to the difference between

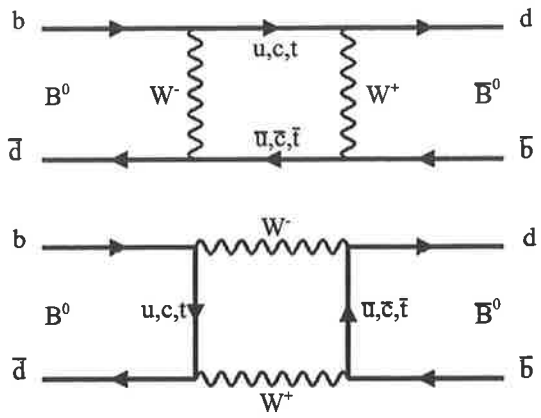

Figure 2.4: Leading box diagrams for $B^0\bar{B}^0$ mixing.

mass eigenstates in the system of $B^0, \bar{B}^0$ [12, 21, 25]. Then, it yields a mixing (in some case) of two states which provides interfering amplitudes and may produce CP violation.
By definition, the time dependent asymmetry is given by,

$$a_{CP}(t, B^0 - \bar{B}^0 \to F) = \frac{\Gamma(B^0(t) \to F) - \Gamma(\bar{B}^0(t) \to \bar{F})}{\Gamma(B^0(t) \to F) + \Gamma(\bar{B}^0(t) \to \bar{F})}\,, \tag{2.39}$$

where $\Gamma(B^0(t) \to F)$ is the decay rate of $B^0(t) \to F$. After decomposition, one gets,

$$a_{CP}(t, B^0 - \bar{B}^0 \to F) = \\ \frac{a_{CP}^{decay}(t, B^0 - \bar{B}^0 \to F)\cos(\Delta M t) + a_{CP}^{mixing}(t, B^0 - \bar{B}^0 \to F)\sin(\Delta M t)}{\cosh(\Delta\Gamma t/2) - a_{CP}^{\Delta\Gamma}(t, B^0 - \bar{B}^0 \to F)\sinh(\Delta\Gamma t/2)}\,, \tag{2.40}$$

where $\Delta M = (0.523 \pm 0.029 \pm 0.031)\ \mathrm{ps}^{-1}$ for the B meson. The expressions for a_{CP}^{decay}, a_{CP}^{mixing} and $a_{CP}^{\Delta\Gamma}$ are the following,

$$a_{CP}^{decay} = \frac{1 - |\xi|^2}{1 + |\xi|^2}\,,$$
$$a_{CP}^{mixing} = \frac{2\mathscr{I}m\xi}{1 + |\xi|^2}\,,$$
$$a_{CP}^{\Delta\Gamma} = \frac{2\mathscr{R}e\xi}{1 + |\xi|^2}\,.$$

The observable ξ has the form:

$$\xi = e^{-i\phi_M} \frac{\bar{A}(\bar{B}^0 \to F)}{A(B^0 \to F)} , \tag{2.41}$$

where ϕ_M represents the weak mixing phase.

2.3.3 Direct CP violation in B decays

This requires that the two CP conjugate processes have different absolute values for their amplitude [12, 13, 21, 25]. This type of CP violation is called *Direct* CP violation. Let us start from the usual definition of asymmetry,

$$a_{CP}(B \to F) = \frac{\Gamma(B \to F) - \Gamma(\bar{B} \to \bar{F})}{\Gamma(B \to F) + \Gamma(\bar{B} \to \bar{F})} , \tag{2.42}$$

which gives,

$$a_{CP}(B \to F) = \frac{|A(B \to F)|^2 - |\bar{A}(\bar{B} \to \bar{F})|^2}{|A(B \to F)|^2 + |\bar{A}(\bar{B} \to \bar{F})|^2} , \tag{2.43}$$

where $A(B \to F)$ is the amplitude for the considered decay. If one uses the definition of the amplitude written in Eq. (2.36), one gets,

$$a_{CP}(B \to F) = \frac{-2|A_1||A_2| \sin(\phi_1 - \phi_2) \sin(\delta_1 - \delta_2)}{|A_1|^2 + 2|A_1||A_2| \cos(\phi_1 - \phi_2) \cos(\delta_1 - \delta_2) + |A_2|^2} . \tag{2.44}$$

Therefore, in order to obtain direct CP violation, the CP asymmetry parameter a_{CP} needs a strong phase *difference* coming from the hadronic matrix *and* a weak phase *difference* coming from the CKM matrix.

Part II

Branching Ratio and Direct CP Asymmetry in B Decays

Chapter 3

Effective Hamiltonian

" La seule écriture valable, c'est celle que l'on invente... C'est cela qui rend les choses réelles. "

Ernest Hemingway

In this chapter, we define the theoretical tools which will be used in order to calculate, in first approximation, the asymmetries and branching ratios in B meson decays [26, 27]. We derive the basic formalism such as the Operator Product Expansion, Wilson coefficients, effective Hamiltonian and *naive* factorization.

3.1 Operator Product Expansion

The Operator Product Expansion (OPE) [28, 29, 30] is used to reproduce the weak interaction of quarks. The decay amplitude, $A(M \to F)$, can be written as,

$$A(M \to F) \propto C_i(\mu)\langle F|O_i(\mu)|M\rangle \ , \tag{3.1}$$

where μ refers to the energy scale and is equal to m_b in our case. In Eq. (3.1), $C_i(\mu)$ are the Wilson coefficients (see Section 3.2) and $O_i(\mu)$ the operators given by the OPE, then, one sees that the OPE separates the calculation of the amplitude, $A(M \to F)$, into two distinct physical regimes. One is called *hard* or short-distance physics, represented by $C_i(\mu)$ and calculated by a perturbative approach. The other is called *soft* or long-distance physics. This part is described by $O_i(\mu)$, and is derived by using a non-perturbative approach such as a $1/N$ expansion [31], QCD sum rules [32, 33], hadronic sum rules...

The operators, O_n, (dependence on μ is removed here for convenience) can be understood as local operators which govern a given decay. They can be written, in a generic form, as,

$$O_n = (\bar{q}_i \Gamma_{n1} q_j)(\bar{q}_k \Gamma_{n2} q_l) \ , \tag{3.2}$$

where Γ_{ni} denotes a combination of gamma matrices. They should respect the Dirac structure, the colour structure and the type of quark relevant for the decay being studied. We can define two kinds of topology which contribute: there is the tree diagram of which the operators are O_1, O_2 [28, 29, 30, 34], and the penguin diagram expressed by the operators O_3 to O_{10} [28, 29, 30, 34]. As regards tree contributions ($W^{\pm}$ exchange), the Feynman diagram is shown Fig. 3.1.

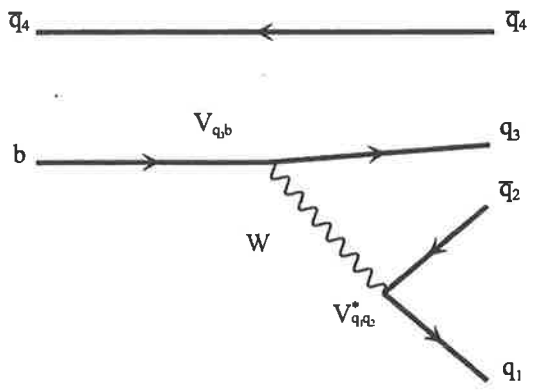

Figure 3.1: Tree diagram.

The current-current operators related to the tree diagram are the following [28, 30],

$$O_1^u = \bar{q}_\alpha \gamma_\mu (1-\gamma_5) u_\beta \bar{u}_\beta \gamma^\mu (1-\gamma_5) b_\alpha \ ,$$
$$O_2^u = \bar{q} \gamma_\mu (1-\gamma_5) u \bar{u} \gamma^\mu (1-\gamma_5) b \ ,$$

or,

$$O_1^s = \bar{q}_\alpha \gamma_\mu (1-\gamma_5) u_\beta \bar{s}_\beta \gamma^\mu (1-\gamma_5) b_\alpha \ ,$$
$$O_2^s = \bar{q} \gamma_\mu (1-\gamma_5) u \bar{s} \gamma^\mu (1-\gamma_5) b \ ,$$

depending on the channel $b \to u$ or $b \to s$, respectively. In the above equations, α and β are the colour indices. The second type of contribution is the penguin one. We can also define two sets of penguin contributions.

The first is called a QCD-penguin (one or two gluons are exchanged) and the second is called an electroweak-penguin (γ and Z^0 exchange). The Feynman diagram for the QCD-penguin is shown in Fig. 3.2 and the corresponding operators are written as follows [28, 30]:

$$O_3 = \bar{q}\gamma_\mu(1-\gamma_5)b\sum_{q'}\bar{q}'\gamma^\mu(1-\gamma_5)q' \ ,$$

$$O_4 = \bar{q}_\alpha\gamma_\mu(1-\gamma_5)b_\beta\sum_{q'}\bar{q}'_\beta\gamma^\mu(1-\gamma_5)q'_\alpha \ ,$$

and for the $(V-A)(V+A)$ transition currents, one has,

$$O_5 = \bar{q}\gamma_\mu(1-\gamma_5)b\sum_{q'}\bar{q}'\gamma^\mu(1+\gamma_5)q' \ ,$$

$$O_6 = \bar{q}_\alpha\gamma_\mu(1-\gamma_5)b_\beta\sum_{q'}\bar{q}'_\beta\gamma^\mu(1+\gamma_5)q'_\alpha \ .$$

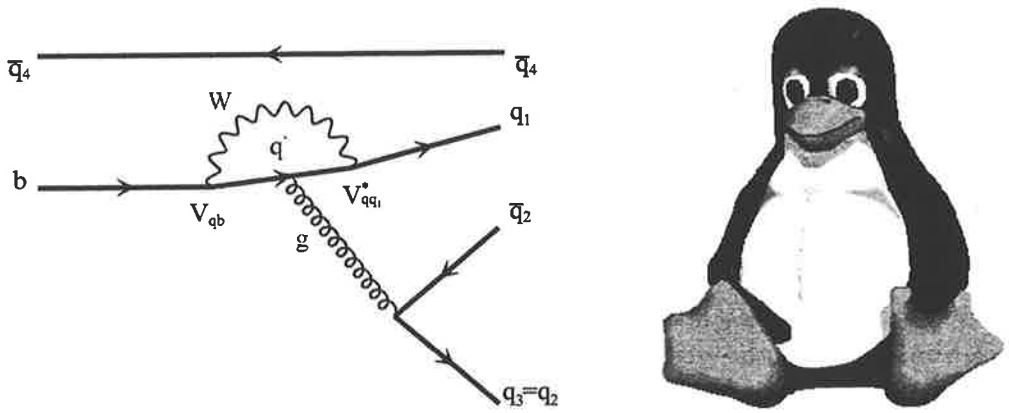

Figure 3.2: QCD-penguin diagram (left hand-side) and real penguin (right hand-side)...

Finally, for the electroweak-penguin, there are two Feynman diagrams represented in Fig. 3.3 (Z, γ exchange from quark line) and Fig. 3.4 (Z, γ exchange from the W line). The structure of O_7 to O_{10} is given by [28, 30],

$$O_7 = \frac{3}{2}\bar{q}\gamma_\mu(1-\gamma_5)b\sum_{q'}e_{q'}\bar{q}'\gamma^\mu(1+\gamma_5)q' \ ,$$

$$O_8 = \frac{3}{2}\bar{q}_\alpha\gamma_\mu(1-\gamma_5)b_\beta\sum_{q'}e_{q'}\bar{q}'_\beta\gamma^\mu(1+\gamma_5)q'_\alpha \ ,$$

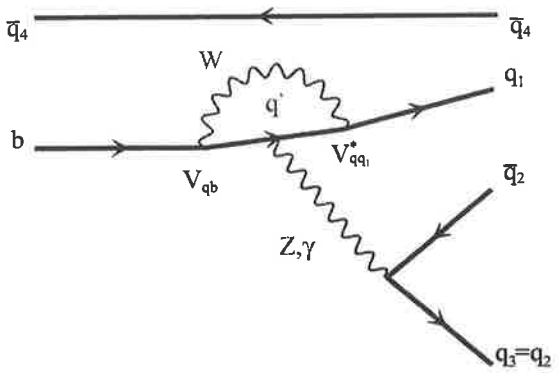

Figure 3.3: Electroweak-penguin diagram.

$$O_9 = \frac{3}{2}\bar{q}\gamma_\mu(1-\gamma_5)b\sum_{q'} e_{q'}\bar{q}'\gamma^\mu(1-\gamma_5)q' \ ,$$

$$O_{10} = \frac{3}{2}\bar{q}_\alpha\gamma_\mu(1-\gamma_5)b_\beta\sum_{q'} e_{q'}\bar{q}'_\beta\gamma^\mu(1-\gamma_5)q'_\alpha \ ,$$

where e_q denotes the quark electric charge and q', the quarks (u, c, s, t) which may contribute in the penguin loop.

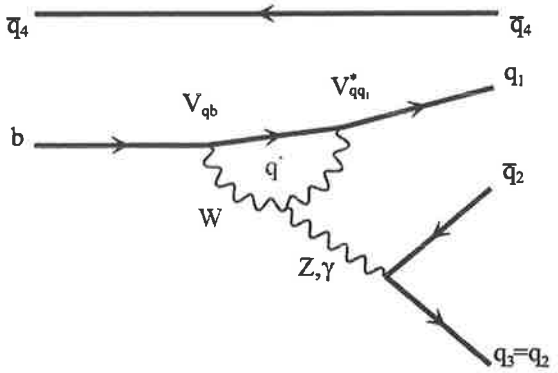

Figure 3.4: Electroweak-penguin diagram (coupling between Z, γ and W).

3.2 Wilson coefficients

As we already mentioned in the previous section (see Section 3.1), the $C_i(\mu)$ are the Wilson coefficients [29]. They represent the physical contributions from scales higher than μ (the OPE describes physics for scales lower than μ), and since QCD has the property of asymptotic freedom, they can be calculated in perturbation theory. The Wilson coefficients include contributions of all heavy particles, such as, the top quark, the W bosons, and the charged Higgs. Usually, the scale μ is chosen to be of the order of $O(m_b)$ for the B decays. Wilson coefficients are calculated to the next-to-leading order (NLO) since this is the first order where one can get some corrections $O(\alpha_s)$ from the leading-log-order (LO). By definition, $C(\mu)$ (we remove for convenience the index i) is given by [28, 29, 30],

$$C(\mu) = U(\mu, M_W)C(M_W) \ , \tag{3.3}$$

where $U(\mu, M_W)$ describes the QCD evolution and reads as,

$$U(\mu, M_W) = \left[1 + \frac{\alpha_s(\mu)}{4\pi}J\right]\left[\frac{\alpha_s(M_W)}{\alpha_s(\mu)}\right]^d\left[1 - \frac{\alpha_s(M_W)}{4\pi}J\right] \ , \tag{3.4}$$

with J the matrix element including the leading order and the next-to-leading order corrections. d is the anomalous dimension. The final expression for $C(\mu)$ in the NLO, with $U^0(\mu, M_W) = \left(\alpha_s(M_W)/\alpha_s(\mu)\right)^d$ is,

$$C(\mu) = \left[1 + \frac{\alpha_s(\mu)}{4\pi}J\right]U^0(\mu, M_W)\left[1 + \frac{\alpha_s(M_W)}{4\pi}(B - J)\right] \ , \tag{3.5}$$

where B is a constant term which depends on the factorization scheme. Since the strong interaction is independent of quark flavour, the $C(\mu)$ are the same for all B decays. At the scale $\mu = m_b = 5$ GeV, $C(\mu)$ take the following values [35, 36, 37, 38] summarized in Table 3.1. To be consistent, the matrix elements of the operators, O_i, should also be renormalized to the one-loop order. This results in the effective Wilson coefficients, C_i', which satisfy the constraint,

$$C_i(m_b)\langle O_i(m_b)\rangle = C_i'\langle O_i\rangle^{tree} \ , \tag{3.6}$$

where $\langle O_i\rangle^{tree}$ are the matrix elements at the tree level. These matrix elements will be evaluated in the factorization approach. From Eq. (3.6), the

$C_i(\mu)$ for $\mu = 5$ GeV			
	C_1	-0.3125	
	C_2	$+1.1502$	
C_3	$+0.0174$	C_5	$+0.0104$
C_4	$+0.0373$	C_6	-0.0459
C_7	-1.050×10^{-5}	C_9	-0.0101
C_8	$+3.839 \times 10^{-4}$	C_{10}	$+1.959 \times 10^{-3}$

Table 3.1: Wilson coefficients to the next-leading order.

relations between C_i' and C_i are [35, 36, 37, 38],

$$\begin{aligned} C_1' &= C_1 \ , & C_2' &= C_2 \ , \\ C_3' &= C_3 - P_s/3 \ , & C_4' &= C_4 + P_s \ , \\ C_5' &= C_5 - P_s/3 \ , & C_6' &= C_6 + P_s \ , \\ C_7' &= C_7 + P_e \ , & C_8' &= C_8 \ , \\ C_9' &= C_9 + P_e \ , & C_{10}' &= C_{10} \ , \end{aligned} \tag{3.7}$$

where

$$\begin{aligned} P_s &= \frac{\alpha_s}{8\pi} C_2 \left(\frac{10}{9} + G(m_c, \mu, q^2) \right) \ , \\ P_e &= \frac{\alpha_{em}}{9\pi} (3C_1 + C_2) \left(\frac{10}{9} + G(m_c, \mu, q^2) \right) \ , \end{aligned}$$

and,

$$G(m_c, \mu, q^2) = 4 \int_0^1 dx \; x(x-1) \ln \frac{m_c^2 - x(1-x)q^2}{\mu^2} \ .$$

Here q^2 is the typical momentum transfer of the gluon or photon in the penguin diagrams and $G(m_c, \mu, q^2)$ has the following explicit expression [39],

$$\begin{aligned} \mathscr{R}e \; G &= \frac{2}{3} \left(\ln \frac{m_c^2}{\mu^2} - \frac{5}{3} - 4\frac{m_c^2}{q^2} + \left(1 + 2\frac{m_c^2}{q^2} \right) \sqrt{1 - 4\frac{m_c^2}{q^2}} \ln \frac{1 + \sqrt{1 - 4\frac{m_c^2}{q^2}}}{1 - \sqrt{1 - 4\frac{m_c^2}{q^2}}} \right) \ , \\ \mathscr{I}m \; G &= -\frac{2}{3} \left(1 + 2\frac{m_c^2}{q^2} \right) \sqrt{1 - 4\frac{m_c^2}{q^2}} \ . \end{aligned} \tag{3.8}$$

Based on simple arguments at the quark level, the value of q^2 is chosen in the range $0.3 < q^2/m_b^2 < 0.5$ [40, 41]. From Eqs. (3.7, 3.8) we can obtain

C_i'	$q^2/m_b^2 = 0.3$	$q^2/m_b^2 = 0.5$
C_1'	-0.3125	-0.3125
C_2'	$+1.1502$	$+1.1502$

Table 3.2: Wilson coefficients for the current-current tree operators.

C_i'	$q^2/m_b^2 = 0.3$	$q^2/m_b^2 = 0.5$
C_3'	$+2.433 \times 10^{-2} + 1.543 \times 10^{-3}i$	$+2.120 \times 10^{-2} + 2.174 \times 10^{-3}i$
C_4'	$-5.808 \times 10^{-2} - 4.628 \times 10^{-3}i$	$-4.869 \times 10^{-2} - 1.552 \times 10^{-2}i$
C_5'	$+1.733 \times 10^{-2} + 1.543 \times 10^{-3}i$	$+1.420 \times 10^{-2} + 5.174 \times 10^{-3}i$
C_6'	$-6.668 \times 10^{-2} - 4.628 \times 10^{-3}i$	$-5.729 \times 10^{-2} - 1.552 \times 10^{-2}i$
C_7'	$-1.435 \times 10^{-4} - 2.963 \times 10^{-5}i$	$-8.340 \times 10^{-5} - 9.938 \times 10^{-5}i$
C_8'	$+3.839 \times 10^{-4}$	$+3.839 \times 10^{-4}$
C_9'	$-1.023 \times 10^{-2} - 2.963 \times 10^{-5}i$	$-1.017 \times 10^{-2} - 9.938 \times 10^{-5}i$
C_{10}'	$+1.959 \times 10^{-3}$	$+1.959 \times 10^{-3}$

Table 3.3: Wilson coefficients related to the electroweak and QCD-penguin operators.

numerical values for C_i'. These values are listed in Tables 3.2 and 3.3, where we have taken $\alpha_s(m_Z) = 0.112$, $\alpha_{em}(m_b) = 1/132.2$, $m_b = 5$ GeV, and $m_c = 1.35$ GeV.

3.3 Effective Hamiltonian

In any phenomenological treatment of the weak decays of hadrons, the starting point is the weak effective Hamiltonian at low energy [28, 29, 30, 34, 42]. It is obtained by integrating out the heavy fields (i.e. the top quark, W and Z bosons) from the Standard Model Lagrangian. It can be written as,

$$\mathcal{H}_{eff} = \frac{G_F}{\sqrt{2}} \sum_i V_{CKM} C_i(\mu) O_i(\mu) \ , \tag{3.9}$$

where G_F is the Fermi constant, V_{CKM} is the CKM matrix element (see Section 2.2.2), $C_i(\mu)$ are the Wilson coefficients (see Section 3.2), $O_i(\mu)$ are the operators entering the Operator Product Expansions (see Section 3.1) and μ represents the renormalization scale. We emphasize that the amplitude corresponding to the effective Hamiltonian for a given decay is independent of the scale μ. In the present case, since we analyse B decays into $\rho\pi$ and into

ρK through $\rho - \omega$ mixing, we take into account tree and penguin diagrams. For the penguin diagrams, we include all operators O_3 to O_{10}. Therefore, the effective Hamiltonian used will be,

$$\mathcal{H}_{eff}^{\Delta B=1} = \frac{G_F}{\sqrt{2}}\left[V_{ub}V_{uq}^*(C_1O_1^q + C_2O_2^q) - V_{tb}V_{tq}^*\sum_{i=3}^{10} C_iO_i\right] + h.c.\,, \qquad (3.10)$$

where $q = d$ or s according to the $b \to u$ or $b \to s$ transitions. Finally, the decay amplitude will be expressed as it follows,

$$A(B \to PV) = \frac{G_F}{\sqrt{2}}\left[V_{ub}V_{uq}^*\Big(C_1\langle PV|O_1^q|B\rangle + C_2\langle PV|O_2^q|B\rangle\Big) - V_{tb}V_{tq}^*\sum_{i=3}^{10} C_i\langle PV|O_i|B\rangle\right] + h.c.\,, \qquad (3.11)$$

where $\langle PV|O_i|B\rangle$ are the hadronic matrix elements. The notation PV means Pseudoscalar Vector. They describe the transition between initial state and final state for scales lower than μ and include, up to now, the main uncertainties in the calculation because of the non-perturbative approach.

3.4 Naive factorization

The computation of the hadronic matrix elements, $\langle PV|O_i|B\rangle$, is not trivial and requires some assumptions. The general method which has to be used is called the "factorization" procedure [43, 44, 45]. This involves the approximation of the matrix element as a product of a transition matrix element between a B meson and one final state meson times a matrix element which describes the creation of the second meson from the vacuum. This can be formulated as,

$$\begin{aligned} \langle PV|O_i|B\rangle &= \langle V|J_{2i}|0\rangle\ \langle P|J_{1i}|B\rangle\,, \\ \text{or}\ \ \langle PV|O_i|B\rangle &= \langle P|J_{4i}|0\rangle\ \langle V|J_{3i}|B\rangle\,, \end{aligned} \qquad (3.12)$$

where the J_{ji} are the transition currents. This approach is called *naive* factorization since it factorizes $\langle PV|O_i|B\rangle$ into a simple product of two quark matrix elements, (see Fig. 3.5). Analytically, Fig. 3.5 can be written down

as,

$$A(B \to PV) \propto \left[\sum_{i=1}^{10} V_{CKM} C_i(\mu) \langle M_1 M_2 | O_i | B \rangle\right]$$
$$\propto \left[\sum_{i=1}^{10} V_{CKM} C_i(\mu) \langle M_1 | J_{2i} | 0 \rangle \langle M_2 | J_{1i} | B \rangle\right] . \quad (3.13)$$

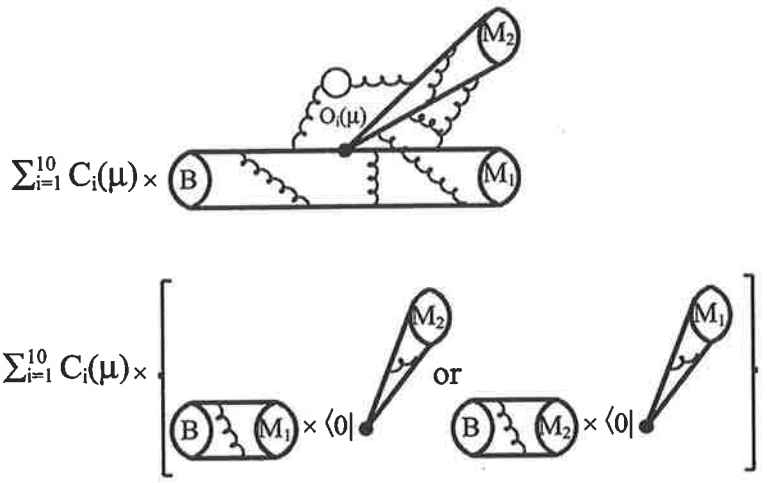

Figure 3.5: Naive factorization, where M_1 and M_2 represent the final meson states.

The justification has been given by Bjorken [46] and is the following: the heavy quark decays are very energetic, so the quark-antiquark pair in a meson in a final state moves very fast away from the localised weak interaction. The hadronization of the quark-antiquark pair occurs far away from the remaining quarks. Then, the meson can be factorized out and the interaction between the quark pair in the meson and the remaining quark is very tiny.

Moreover, by reordering the colour indices (Fierz transformation) with $1/N_c^{eff}$ (N_c^{eff} is the effective number of colours), and also including the colour octet contribution through the variable ξ_i (since it is non-factorizable), the result takes into account the colour-allowed and colour-suppressed contributions which can occur in the decay at the tree level. N_c^{eff} is defined as a parameter which, by assumption, includes all hadronization effects (they cannot be factorized completely) and is written as,

$$\frac{1}{(N_c^{eff})_i} = \frac{1}{3} + \xi_i \text{ , with } i = 1, \cdots, 10 , \quad (3.14)$$

where it is assumed that N_c^{eff} is the same for all operators O_i. Finally, and this is the main uncertainty in the present approach, all of the Final State Interactions (FSI) are not involved. Recall that this work is achieved by applying a phenomenological treatment. In this approach, corrections associated with the limit of validity of the factorization hypothesis are parameterized and may contribute to large uncertainties [47]. However, it should give a good estimate of the magnitude of the B decay amplitude in many cases [48, 49]. We will see in the last part, how it will be possible to incorporate QCD corrections in order to include the FSI (at the first order in α_s) into the factorization approach.

Chapter 4

$\rho - \omega$ mixing

" S'il y avait une seule vérité, on ne pourrait pas faire cent toiles sur le même thème. "

Pablo Picasso

In this chapter, we describe the mechanism of $\rho - \omega$ mixing (coming from the quark mass difference between the u and d quarks [50]) and its implications for B decays (for asymmetries and branching ratios). We explain the origin of the mixing, based on the Vector Meson Dominance model, and how it has been determined (by fitting the pion electromagnetic from factor data).

4.1 Vector Meson Dominance

The idea to incorporate the hadronic contribution of vector mesons in the photon propagator (in other words, the photon propagator is mixed with an intermediate state ρ-propagator) was developed in the early 60's when nuclear form factors were analysed by Nambu [51, 52, 53]. Later, in order to study strong interaction corrections to photon mediated processes at low energy (non-perturbative QCD), the Vector Meson Dominance model [54] (VMD) was proposed. It successfully describes the interactions between photons and hadronic matter by assuming that all photon hadron couplings are governed by vector mesons. Without going into details, we just recall that VMD (VMD1) is build on effective Lagrangian field theory, where the relevant

terms are the following (for the process $\gamma \to \pi^+\pi^-$, see Fig. 4.1) [55]:

$$\mathcal{L} = -\frac{e}{2g_\rho} F_{\mu\nu}\rho^{\mu\nu} - eJ_\mu A^\mu - g_{\rho\pi\pi}\rho^\mu J_\mu \ . \tag{4.1}$$

The first term gives the coupling term (momentum dependent) between the photon and the ρ meson at the $\gamma - \rho$ vertex and ensures that the photon remains massless. The second term represents the direct photon hadronic matter coupling (where J_μ is the hadronic pion current), and the third term shows the coupling between the ρ meson and the pion field. We also stress that global gauge invariance is conserved in the Lagrangian used to develop the VMD1 model [55, 56]. Hence, by applying this approach, it was possi-

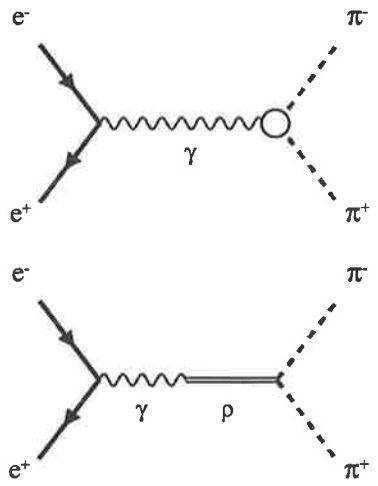

Figure 4.1: $e^+e^- \to \pi^+\pi^-$ described (upper diagram) in the s-channel. The lower diagram represents the Vector Meson Dominance description for the same process (similarly for $e^+e^- \to \mu^+\mu^-$).

ble to reproduce the process, $e^+e^- \to \pi^+\pi^-$, where the amplitude denoted, $\mathcal{M}_\mu^{\gamma\to\pi^+\pi^-}$, includes the vector meson interaction (see Fig. 4.1):

$$\mathcal{M}_\mu^{\gamma\to\pi^+\pi^-} = -e(p_1 - p_2)_\mu F_\pi(q^2) \ , \tag{4.2}$$

where p_1, p_2 are the pion momentum and, $F_\pi(q^2)$, the pion electromagnetic form factor taking into account all intermediate processes. Which can been

defined by [55, 56],

$$F_\pi(q^2) = 1 - g_{\rho\gamma}(q^2)\left[\frac{g_{\rho\pi\pi}}{q^2 - m_\rho^2 + im_\rho\Gamma_\rho(q^2)}\right] - g_{\omega\gamma}(q^2)\left[\frac{1}{q^2 - m_\omega^2 + im_\omega\Gamma_\omega(q^2)}A\exp^{i\phi}\right], \quad (4.3)$$

where $g_{\rho\gamma}$ and $g_{\rho\pi\pi}$ would be equal if we assumed universality (even though experimentally this does not hold exactly). The third term of Eq. (4.3) includes the ω contribution attenuated by a factor real, A, and the Orsay phase, ϕ (both can be extracted from experiment). Other versions of the VMD model (based on various Lagrangians) were established [55, 56]: mainly, VMD2 and HLS (hidden local symmetry [57]). But all of them keep in mind that the interaction between photon and hadronic matter is mediated by a vector meson propagator taking the following form:

$$D_{\mu\nu} = \frac{-g_{\mu\nu}}{q^2 - m_V^2 + im_V\Gamma_V(q^2)}, \quad (4.4)$$

where m_V and Γ_V are the meson mass and momentum dependent width.

4.2 $\rho - \omega$ mixing

4.2.1 $\rho - \omega$ mixing formalism

It is by analysing data from the cross-section for $e^+e^- \to \pi^+\pi^-$ (Fig. 4.2) [58] and references therein that $\rho - \omega$ mixing parameters have been determined. The interference resulting from the narrow resonant ω and the broad resonant ρ produces a significative enhancement in the interaction around $\sqrt{s} \approx 780$ MeV [58].

If we refer to Fig. 4.1 (top diagram), the amplitude, $\mathcal{M}^{\gamma\to\pi\pi}$, which corresponds to the coupling of the photon to the pion pair is given by,

$$\mathcal{M}^{\gamma\to\pi\pi} = \bar{v}(k_2)ie\gamma^\mu u(k_1)iD_{\mu\nu}(q)eF_\pi(q^2)(k_4 - k_3)^\nu, \quad (4.5)$$

where k_1 and k_2 are the momenta of the electron and positron, and k_3 and k_4 are the momenta of the pions. $F_\pi(q^2)$ is the pion electromagnetic form factor and $D_{\mu\nu}(q)$ the photon propagator written as,

$$iD_{\mu\nu}(q) = \frac{-i}{q^2}\left[g_{\mu\nu} + (\xi - 1)\frac{q_\mu q_\nu}{q^2}\right], \quad (4.6)$$

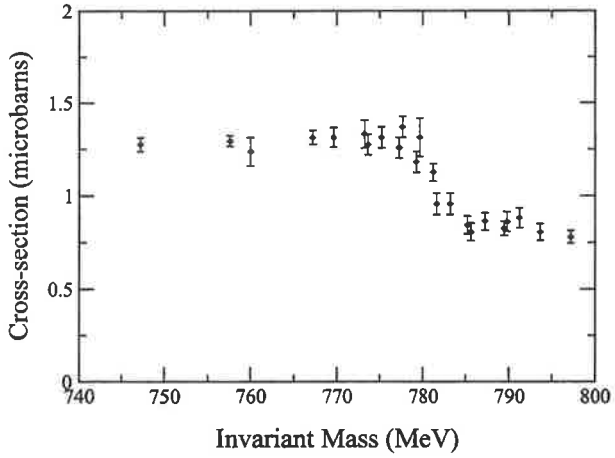

Figure 4.2: Cross-section for $e^+e^- \to \pi^+\pi^-$ in the region where $\rho - \omega$ mixing effects are maximum i.e. where $\sqrt{s} \sim m_\omega$.

where ξ defines the covariant gauge applied. Let us start by assuming that the vector mesons couple to a conserved current, therefore its expression (for one channel) is:

$$D_{\mu\nu} = \frac{1}{q^2 - m^2 - \Pi(q^2)} \left(-g_{\mu\nu} + \frac{(1 - \Pi(q^2))}{q^2} \frac{q_\mu q_\nu}{m^2} \right) , \tag{4.7}$$

where $\Pi(q^2)$ is the one-particle irreducible self-energy. Now, by extending the same formalism to two coupled channels, the full propagator involving $\rho - \omega$ mixing, can be expressed as [59],

$$D_{\mu\nu} = \frac{1}{\alpha} \begin{pmatrix} s_\omega g_{\mu\nu} + a(\rho,\omega) q_\mu q_\nu & \Pi_{\rho\omega}(q^2) T_{\mu\nu} \\ \Pi_{\rho\omega}(q^2) T_{\mu\nu} & s_\rho g_{\mu\nu} + a(\omega,\rho) q_\mu q_\nu \end{pmatrix} , \tag{4.8}$$

where we use the following definitions:

$$\begin{aligned} T_{\mu\nu} &= g_{\mu\nu} - (q_\mu q_\nu / q^2) , \\ s_\omega &= q^2 - \Pi_{\omega\omega}(q^2) - m_\omega^2 = q^2 - m_\omega^2 + i m_\omega \Gamma_\omega(q^2) , \\ s_\rho &= q^2 - \Pi_{\rho\rho}(q^2) - m_\rho^2 = q^2 - m_\rho^2 + i m_\rho \Gamma_\rho(q^2) , \\ a(\rho,\omega) &= \frac{1}{q^2 m_\rho^2} \left(\Pi_{\rho\omega}^2(q^2) - \left[q^2 - \Pi_{\rho\rho}(q^2) \right] s_\omega \right) , \\ \alpha &= \Pi_{\rho\omega}^2(q^2) - s_\rho s_\omega , \end{aligned} \tag{4.9}$$

with, $\Pi_{\rho\omega}^2(q^2)$, the momentum dependent mixing amplitude which vanishes as $q^2 \to 0$. We can now write down the amplitude, $\mathcal{M}_\mu^{\gamma \to \pi\pi}$, where we take

into account the coupling between photon and vector mesons, $f_{\gamma\rho_I}, f_{\gamma\omega_I}$, and also the coupling $g_{\rho_I\pi\pi}$ between ρ_I and the final pion pair ($g_{\omega_I\pi\pi}$ similarly for ω_I). Therefore, one gets,

$$\mathcal{M}_\nu^{\gamma\to\pi\pi} = \left(\mathcal{M}^{\mu;\rho_I\to\pi\pi} \quad \mathcal{M}^{\mu;\omega_I\to\pi\pi}\right) D_{\mu\nu} \begin{pmatrix} \mathcal{M}^{\gamma\to\rho_I} \\ \mathcal{M}^{\gamma\to\omega_I} \end{pmatrix} , \tag{4.10}$$

where, ρ_I and ω_I are the pure isovector ρ and isoscalar ω state. $D_{\mu\nu}$ is given by:

$$D_{\mu\nu} = \begin{pmatrix} 1/s_\rho & \Pi_{\rho\omega}/s_\rho s_\omega \\ \Pi_{\rho\omega}/s_\rho s_\omega & 1/s_\omega \end{pmatrix} g_{\mu\nu} . \tag{4.11}$$

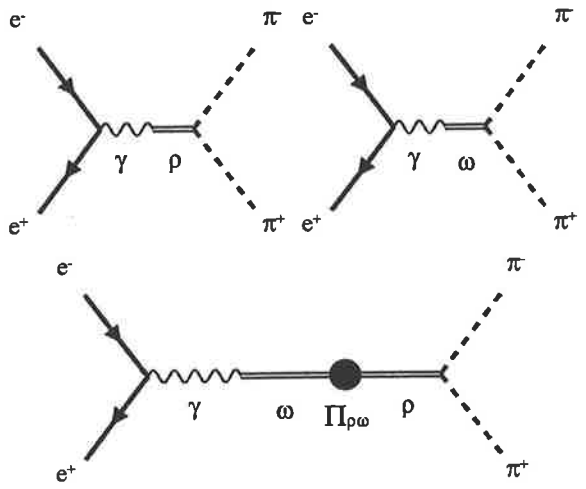

Figure 4.3: $e^+e^- \to \pi^+\pi^-$: leading order diagrams (upper) and leading order in isospin violation diagram (lower).

By expanding Eq. (4.10) one has,

$$\begin{aligned} \mathcal{M}_\mu^{\gamma\to\pi\pi} = \mathcal{M}_\mu^{\rho_I\to\pi\pi}\frac{1}{s_\rho}\mathcal{M}^{\gamma\to\rho_I} + \mathcal{M}_\mu^{\omega_I\to\pi\pi}\frac{\Pi_{\rho\omega}(q^2)}{s_\rho s_\omega}\mathcal{M}^{\gamma\to\rho_I} \\ + \mathcal{M}_\mu^{\rho_I\to\pi\pi}\frac{\Pi_{\rho\omega}(q^2)}{s_\rho s_\omega}\mathcal{M}^{\gamma\to\omega_I} + \mathcal{M}_\mu^{\omega_I\to\pi\pi}\frac{1}{s_\omega}\mathcal{M}^{\gamma\to\omega_I} , \end{aligned} \tag{4.12}$$

where all the above terms are described in Fig. 4.3. However it is more appropriate to analyse the $\rho - \omega$ mixing in the physical basis rather than the isospin pure basis where the G parity can be violated either through the

mixing $\rho_I - \omega_I$ or the direct decay ω_I into the pion pair. We recall that, in the isospin basis, ρ_I and ω_I are exact eigenstates of isospin. MOW (Maltman, O'Connell and Williams) [59, 60] defined a transformation, C, between the physical basis and the isospin basis, which is the following,

$$C = \begin{pmatrix} 1 & -\epsilon_1 \\ \epsilon_2 & 1 \end{pmatrix} , \tag{4.13}$$

and one can therefore write the ρ and ω states explicitly as;

$$\begin{aligned} \rho &= \rho_I - \epsilon_1 \omega_I , \\ \omega &= \epsilon_2 \rho_I + \omega_I , \end{aligned} \tag{4.14}$$

where ϵ_1 and ϵ_2 are two mixing parameters. Since we require that the mixed physical $\rho - \omega$ propagator should not have poles, then ϵ_1 and ϵ_2 read as:

$$\epsilon_1 = \frac{\Pi_{\rho\omega}(m_\omega^2)}{s_\omega - s_\rho}, \quad \epsilon_2 = \frac{\Pi_{\rho\omega}(m_\rho^2)}{s_\omega - s_\rho} . \tag{4.15}$$

It is assumed that, in the vector meson resonance region, the momentum dependence of $\Pi_{\rho\omega}(q^2)$ is negligible, which means that $\Pi_{\rho\omega}(m_\rho^2) = \Pi_{\rho\omega}(m_\omega^2) = \Pi_{\rho\omega}$ [61]. Then, $\Pi_{\rho\omega}$ will be treated as a constant and $\epsilon_1 = \epsilon_2 = \epsilon$ will be given by the expression,

$$\epsilon = \frac{\Pi_{\rho\omega}}{s_\omega - s_\rho} . \tag{4.16}$$

By inserting the transformation matrix, C, (with $CC^{-1} = I$) in Eq. (4.10), we can diagonalize the $D_{\mu\nu}$ matrix propagator:

$$\begin{aligned} \mathcal{M}_\mu^{\gamma\to\pi\pi} = \left(\mathcal{M}_\mu^{\rho_I\to\pi\pi} \quad \mathcal{M}_\mu^{\omega_I\to\pi\pi}\right) CC^{-1} \\ \begin{pmatrix} 1/s_\rho & \Pi_{\rho\omega}/s_\rho s_\omega \\ \Pi_{\rho\omega}/s_\rho s_\omega & 1/s_\omega \end{pmatrix} CC^{-1} \begin{pmatrix} \mathcal{M}^{\gamma\to\rho_I} \\ \mathcal{M}^{\gamma\to\omega_I} \end{pmatrix} , \end{aligned} \tag{4.17}$$

which gives after computation, the amplitude, $\mathcal{M}_\mu^{\gamma\to\pi\pi}$, expressed in the physical basis:

$$\mathcal{M}_\mu^{\gamma\to\pi\pi} = \left(\mathcal{M}_\mu^{\rho\to\pi\pi} \quad \mathcal{M}_\mu^{\omega\to\pi\pi}\right) \begin{pmatrix} 1/s_\rho & 0 \\ 0 & 1/s_\omega \end{pmatrix} \begin{pmatrix} \mathcal{M}^{\gamma\to\rho} \\ \mathcal{M}^{\gamma\to\omega} \end{pmatrix} , \tag{4.18}$$

where one can extract the corresponding amplitudes between both the isospin and physical basis as follows:

$$\begin{aligned} \mathcal{M}_\mu^{\rho\to\pi\pi} &= \mathcal{M}_\mu^{\rho_I\to\pi\pi} + \epsilon \mathcal{M}_\mu^{\omega_I\to\pi\pi} , \\ \mathcal{M}_\mu^{\omega\to\pi\pi} &= -\epsilon \mathcal{M}_\mu^{\rho_I\to\pi\pi} + \mathcal{M}_\mu^{\omega_I\to\pi\pi} , \\ \mathcal{M}^{\gamma\to\rho} &= \mathcal{M}^{\gamma\to\rho_I} + \epsilon \mathcal{M}^{\gamma\to\omega_I} , \\ \mathcal{M}^{\gamma\to\omega} &= -\epsilon \mathcal{M}^{\gamma\to\rho_I} + \mathcal{M}^{\gamma\to\omega_I} . \end{aligned} \tag{4.19}$$

By expanding Eq. (4.18) one finally gets:

$$\mathcal{M}_\mu^{\gamma\to\pi\pi} = \mathcal{M}_\mu^{\rho\to\pi\pi}\frac{1}{s_\rho}\mathcal{M}^{\gamma\to\rho} + \mathcal{M}_\mu^{\omega\to\pi\pi}\frac{1}{s_\omega}\mathcal{M}^{\gamma\to\omega} . \tag{4.20}$$

We stress that $\mathcal{M}^{\omega_I\to\pi\pi}$ cannot be neglected since it provides one of the two sources of G parity violation in the $\rho - \omega$ mixing and has a strong influence on fitting the pion electromagnetic form factor.

4.2.2 Electromagnetic pion form factor

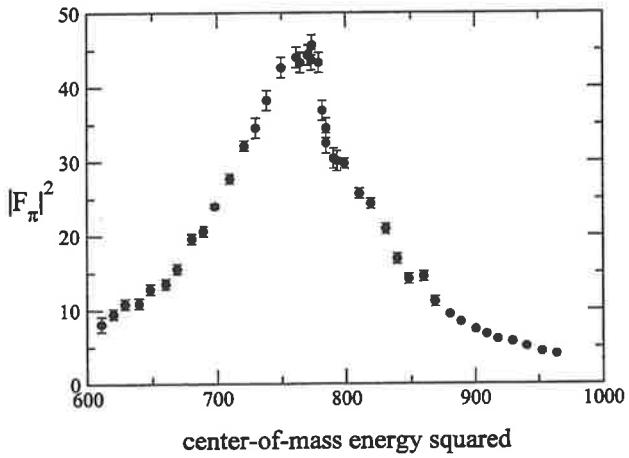

Figure 4.4: Electromagnetic pion form factor data.

Starting from the definition of the pion electromagnetic form factor including $\rho - \omega$ mixing and the $\omega_I \to \pi\pi$ decay, one has,

$$F_\pi(q^2) = \frac{1}{e}\begin{pmatrix} f_{\gamma\rho_I} & f_{\gamma\omega_I}\end{pmatrix}\begin{pmatrix} D^I_{\rho\rho} & D^I_{\rho\rho}\tilde{\Pi}_{\rho\omega}D^I_{\omega\omega} \\ D^I_{\rho\rho}\tilde{\Pi}_{\rho\omega}D^I_{\omega\omega} & D^I_{\omega\omega}\end{pmatrix}\begin{pmatrix} g_{\rho_I\pi\pi} \\ g_{\omega_I\pi\pi}\end{pmatrix} , \tag{4.21}$$

where $D_{VV} = D^I_{VV}$ (see Eq. (4.4)) since we are working to the first order in isospin violation. In order to determine the value for $\tilde{\Pi}_{\rho\omega}$, we chose an appropriate form factor:

$$F_\pi(s) = F_\rho(s)\left[1 + \frac{f_{\omega_I}}{f_{\rho_I\gamma}}\left(\frac{\tilde{\Pi}_{\rho\omega}(s)}{s - m_\omega^2 + im_\omega\Gamma_\omega}\right)\right] , \tag{4.22}$$

where $F_\rho(s)$ is a function incorporating constraints on the form factor and playing the same role as the term $f_{\rho_I\gamma}g_{\rho_I\pi\pi}/s_\rho$.

By fitting the pion form factor data (see Fig. 4.4 [62]), it is therefore possible to extract $\tilde{\Pi}_{\rho\omega}$. Different fits [63, 64] have been realised and the typical average $\rho - \omega$ mixing magnitude is [65]:

$$\tilde{\Pi}_{\rho\omega}(m_\omega^2) = -3500 \pm 300 \text{ MeV}^2 \, . \tag{4.23}$$

The average value also respects the experimental branching ratio for the process $\omega \to \pi\pi$ [66, 67]. Finally, we emphasize that there is no possibility to fix the value of $\rho - \omega$ mixing independent of experimental constraints.

4.3 $\rho - \omega$ mixing in B decays

4.3.1 Inclusion of $\rho - \omega$ mixing in CP violation

Let A be the amplitude for the decay $B \to \rho^0(\omega) M_1 \to \pi^+\pi^- M_1$ (with $M_1 = \{\pi, K\}$), then one has,

$$A = \langle M_1 \pi^- \pi^+ | H^T | B \rangle + \langle M_1 \pi^- \pi^+ | H^P | B \rangle \, , \tag{4.24}$$

with H^T and H^P being the Hamiltonians for the tree and penguin operators. We can define the relative magnitude and phases between these two contributions as follows,

$$\begin{aligned} A &= \langle M_1 \pi^- \pi^+ | H^T | B \rangle \left[1 + r e^{i\delta} e^{i\phi} \right] \, , \\ \bar{A} &= \langle \bar{M}_1 \pi^+ \pi^- | H^T | \bar{B} \rangle \left[1 + r e^{i\delta} e^{-i\phi} \right] \, , \end{aligned} \tag{4.25}$$

where δ and ϕ are strong and weak phases respectively. The phase ϕ arises from the appropriate combination of CKM matrix elements which is $\phi = \arg[(V_{tb} V_{tq}^\star)/(V_{ub} V_{uq}^\star)]$ with $q = \{d, s\}$ for B decays including either π or K. As a result, $\sin\phi$ is equal to $\sin\alpha$ (or $\sin\gamma$) with α (or γ) defined in the standard way [24]. The parameter, r, is the absolute value of the ratio of tree and penguin amplitudes:

$$r \equiv \left| \frac{\langle \rho^0(\omega) M_1 | H^P | B \rangle}{\langle \rho^0(\omega) M_1 | H^T | B \rangle} \right| . \tag{4.26}$$

In order to obtain a large signal for direct CP violation, we need some mechanism to make both $\sin\delta$ and r large. We stress that $\rho - \omega$ mixing has the dual advantages that the strong phase difference is large (passing through 90° at the ω resonance) and is well known [40, 41, 68, 69, 70, 71]. Note as well that working in the naive factorization approach, the only source of strong phase is provided by $\rho - \omega$ mixing. With this mechanism, to first order in

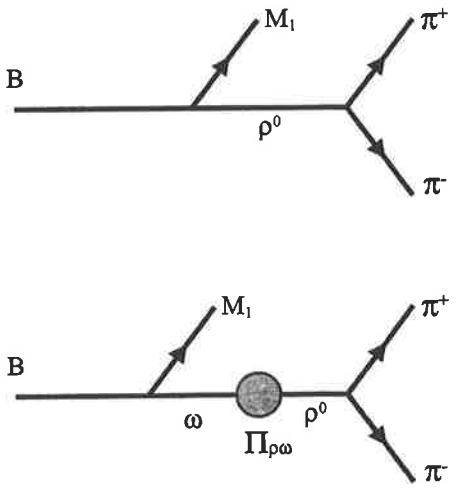

Figure 4.5: B decays without (upper) and with (lower) $\rho - \omega$ mixing.

isospin violation, we have the following results when the invariant mass of $\pi^+\pi^-$ is near the ω resonance mass,

$$\langle M_1\pi^-\pi^+|H^T|B\rangle = \frac{g_\rho}{s_\rho s_\omega}\tilde{\Pi}_{\rho\omega}t_\omega + \frac{g_\rho}{s_\rho}t_\rho \ ,$$
$$\langle M_1\pi^-\pi^+|H^P|B\rangle = \frac{g_\rho}{s_\rho s_\omega}\tilde{\Pi}_{\rho\omega}p_\omega + \frac{g_\rho}{s_\rho}p_\rho \ . \qquad (4.27)$$

Here t_V ($V = \rho$ or ω) is the tree amplitude and p_V the penguin amplitude for producing a vector meson, V, g_ρ is the coupling for $\rho^0 \to \pi^+\pi^-$, $\tilde{\Pi}_{\rho\omega}$ is the effective $\rho - \omega$ mixing amplitude, and s_V is from the inverse propagator of the vector meson V,

$$s_V = s - m_V^2 + im_V\Gamma_V \ , \qquad (4.28)$$

with $\sqrt{s}$ being the invariant mass of the $\pi^+\pi^-$ pair. We stress that the direct coupling $\omega \to \pi^+\pi^-$ is effectively absorbed into $\tilde{\Pi}_{\rho\omega}$ [59, 60, 61, 63, 66], leading to the explicit s dependence of $\tilde{\Pi}_{\rho\omega}$. Making the expansion $\tilde{\Pi}_{\rho\omega}(s) = \tilde{\Pi}_{\rho\omega}(m_\omega^2) + (s - m_\omega^2)\tilde{\Pi}'_{\rho\omega}(m_\omega^2)$, the $\rho - \omega$ mixing parameters were determined in the fit of Gardner and O'Connell [65]: $\mathscr{R}e\ \tilde{\Pi}_{\rho\omega}(m_\omega^2) = -3500 \pm 300\text{MeV}^2$, $\mathscr{I}m\ \tilde{\Pi}_{\rho\omega}(m_\omega^2) = -300 \pm 300\text{MeV}^2$ and $\tilde{\Pi}'_{\rho\omega}(m_\omega^2) = 0.03 \pm 0.04$. In practice, the effect of the derivative term is negligible. From Eqs. (4.25, 4.27) one has,

$$re^{i\delta}e^{i\phi} = \frac{\tilde{\Pi}_{\rho\omega}p_\omega + s_\omega p_\rho}{\tilde{\Pi}_{\rho\omega}t_\omega + s_\omega t_\rho} \ . \qquad (4.29)$$

Defining,

$$\frac{p_\omega}{t_\rho} \equiv r' e^{i(\delta_q+\phi)} \ , \quad \frac{t_\omega}{t_\rho} \equiv \alpha e^{i\delta_\alpha} \ , \quad \frac{p_\rho}{p_\omega} \equiv \beta e^{i\delta_\beta} \ , \tag{4.30}$$

where $\delta_\alpha, \delta_\beta$ and δ_q are strong phases (absorptive part) at short distance. One can rewrite Eq. (4.29) and one finds the following expression,

$$re^{i\delta} = r' e^{i\delta_q} \frac{\tilde{\Pi}_{\rho\omega} + \beta e^{i\delta_\beta} s_\omega}{s_\omega + \tilde{\Pi}_{\rho\omega} \alpha e^{i\delta_\alpha}} \ . \tag{4.31}$$

Letting,

$$\alpha e^{i\delta_\alpha} = f + gi, \quad \beta e^{i\delta_\beta} = b + ci, \quad r' e^{i\delta_q} = d + ei \ , \tag{4.32}$$

and using Eq. (4.31), we obtain the following result when $\sqrt{s} \sim m_\omega$:

$$re^{i\delta} = \frac{C + iD}{(s - m_\omega^2 + f\mathscr{R}e\ \tilde{\Pi}_{\rho\omega} - g\mathscr{I}m\ \tilde{\Pi}_{\rho\omega})^2 + (f\mathscr{I}m\ \tilde{\Pi}_{\rho\omega} + g\mathscr{R}e\ \tilde{\Pi}_{\rho\omega} m_\omega \Gamma_\omega)^2} \ , \tag{4.33}$$

where C and D are defined as:

$$\begin{aligned} C = {} & (s - m_\omega^2 + f\mathscr{R}e\ \tilde{\Pi}_{\rho\omega} - g\mathscr{I}m\ \tilde{\Pi}_{\rho\omega}) \Big\{ d\Big[\mathscr{R}e\ \tilde{\Pi}_{\rho\omega} + b(s - m_\omega^2) - cm_\omega\Gamma_\omega\Big] \\ & - e\Big[\mathscr{I}m\ \tilde{\Pi}_{\rho\omega} + bm_\omega\Gamma_\omega + c(s - m_\omega^2)\Big]\Big\} \\ & + (f\mathscr{I}m\ \tilde{\Pi}_{\rho\omega} + m_\omega\Gamma_\omega + g\mathscr{R}e\ \tilde{\Pi}_{\rho\omega}) \Big\{ e\Big[\mathscr{R}e\ \tilde{\Pi}_{\rho\omega} + b(s - m_\omega^2) - cm_\omega\Gamma_\omega\Big] \\ & + d\Big[\mathscr{I}m\ \tilde{\Pi}_{\rho\omega} + bm_\omega\Gamma_\omega + c(s - m_\omega^2)\Big]\Big\} \ , \end{aligned} \tag{4.34}$$

and,

$$\begin{aligned} D = {} & (s - m_\omega^2 + f\mathscr{R}e\ \tilde{\Pi}_{\rho\omega} - g\mathscr{I}m\ \tilde{\Pi}_{\rho\omega}) \Big\{ e\Big[\mathscr{R}e\ \tilde{\Pi}_{\rho\omega} + d(s - m_\omega^2) - cm_\omega\Gamma_\omega\Big] \\ & + d\Big[\mathscr{I}m\ \tilde{\Pi}_{\rho\omega} + bm_\omega\Gamma_\omega + c(s - m_\omega^2)\Big]\Big\} \\ & - (f\mathscr{I}m\ \tilde{\Pi}_{\rho\omega} + m_\omega\Gamma_\omega + g\mathscr{R}e\ \tilde{\Pi}_{\rho\omega}) \Big\{ d\Big[\mathscr{R}e\ \tilde{\Pi}_{\rho\omega} + b(s - m_\omega^2) - cm_\omega\Gamma_\omega\Big] \\ & - e\Big[\mathscr{I}m\ \tilde{\Pi}_{\rho\omega} + bm_\omega\Gamma_\omega + c(s - m_\omega^2)\Big]\Big\} \ . \end{aligned} \tag{4.35}$$

The quantities $\alpha e^{i\delta_\alpha}$, $\beta e^{i\delta_\beta}$ and $r' e^{i\delta_q}$ will be calculated later. In order to get the CP violating asymmetry, a_{cp}, $\sin\phi$ and $\cos\phi$ are needed, where ϕ is determined by the CKM matrix elements. In the Wolfenstein parametrization [18, 19], one has for the decay $B \to \rho^0(\omega)\pi$,

$$\sin\phi = \frac{\eta}{\sqrt{[\rho(1-\rho)-\eta^2]^2+\eta^2}}\,,$$
$$\cos\phi = \frac{\rho(1-\rho)-\eta^2}{\sqrt{[\rho(1-\rho)-\eta^2]^2+\eta^2}}\,, \tag{4.36}$$

and for the decay $B \to \rho^0(\omega)K$ one has,

$$\sin\phi = \frac{-\eta}{\sqrt{\rho^2+\eta^2}}\,,$$
$$\cos\phi = \frac{-\rho}{\sqrt{\rho^2+\eta^2}}\,. \tag{4.37}$$

The values used for ρ and η will be given in the following chapter.

4.3.2 Inclusion of $\rho - \omega$ mixing in branching ratios

In the Quark Model, the diagram (Fig 4.5 top) describing the $B \to \rho^0 M_1$ decay (with $M_1 = \{\pi, K\}$) is the main contribution. In our case, to be consistent, we should also take into account the ρ–ω mixing contribution (see Fig 4.5 bottom) when we calculate the branching ratio, since we are working to the first order of isospin violation. The application is straightforward and we obtain the branching ratio for $B \to \rho^0 M_1$:

$$\mathscr{B}(B \to \rho^0 M_1) = \frac{G_F^2 |\vec{p}_\rho|^3}{\alpha_K \pi \Gamma_B} \left| \left[V^T_{u,s} A^T_{\rho^0}(a_1, a_2) - V^P_{u,s} A^P_{\rho^0}(a_3, \cdots, a_{10}) \right] \right.$$
$$\left. + \left[V^T_{u,s} A^T_{\omega}(a_1, a_2) - V^P_{u,s} A^P_{\omega}(a_3, \cdots, a_{10}) \right] \frac{\tilde{\Pi}_{\rho\omega}}{(s_\rho - m_\omega^2) + i m_\omega \Gamma_\omega} \right|^2 , \tag{4.38}$$

where the ρ-momentum takes the following form:

$$|\vec{p_\rho}| = \frac{\sqrt{[m_B^2 - (m_\rho + m_{M_1})^2][m_B^2 - (m_\rho - m_{M_1})^2]}}{2m_B}\,. \tag{4.39}$$

In Eq. (4.38) G_F is the Fermi constant, Γ_B, the total width B decay, α_K, an integer related to the given decay $B \to \rho^0 M_1$ (with $M_1 = \{\pi, K\}$) and $V^T_{u,s}$, $V^P_{u,s}$ are the CKM matrix elements involved in the tree and penguin diagram respectively. Finally, $A^T_V(a_i)$ and $A^P_V(a_i)$ are the tree and penguin amplitudes which respect quark interactions in the B decay.

Chapter 5

Branching ratios for B decays into $\rho\pi$ or ρK

" Il y a en chacun de nous des calculs que nous nommons espérance. "

Platon

This chapter is devoted to the application of all the theoretical tools described in the three previous chapters. We start by investigating branching ratios in B decays including in the final state either a π or K particle. We shall calculate branching ratios for the processes $B^{\pm,0} \to \rho^{\pm,0}\pi^{\pm,0}$ and $B^{\pm,0} \to \rho^{\pm,0}K^{\pm,0}$, and shall compare with the experimental results.

5.1 Formalism

With the factorized decay amplitudes, we can compute the decay rates by using the following expression [72],

$$\Gamma(B \to VP) = \frac{|\vec{p_\rho}|^3}{8\pi m_V^2} \left| \frac{A(B \to VP)}{\epsilon_V \cdot p_B} \right|^2 , \tag{5.1}$$

where $\vec{p_\rho}$ is the c.m. momentum of the decay particles (already defined, see Chapter 4), m_V is the mass of the vector V particle, ϵ_V is the polarization vector with the condition $\epsilon_V \cdot P_V = 0$ and $A(B \to VP)$ is the decay amplitude given by,

$$A(B \to VP) = \frac{G_F}{\sqrt{2}} \sum_{i=1}^{10} V_{u,s}^{T,P} a_i \langle VP|O_i|B\rangle . \tag{5.2}$$

In Eq. (5.2), all variables have been introduced in a previous chapter (see Chapter 3). The term denoted $V_{u,s}^{T,P}$ represents the CKM matrix elements involved in the tree and penguin diagrams, for the b into u and b into s transitions, respectively:

$$\left.\begin{array}{ll} V_u^T & = |V_{ub}V_{ud}^\star| \\ V_s^T & = |V_{ub}V_{us}^\star| \end{array}\right\} \text{for} \quad i = 1,2 \quad \text{and} \quad \left.\begin{array}{ll} V_u^P & = |V_{tb}V_{td}^\star| \\ V_s^P & = |V_{tb}V_{ts}^\star| \end{array}\right\} \text{for} \quad i = 3,10 \; .$$

The effective parameters, a_i, which appear in the decay amplitude (see Eq. (5.2)) are the following combinations of effective Wilson coefficients, C_l',

$$a_{2j} = C_{2j}' + \frac{1}{N_c^{eff}} C_{2j-1}', \quad a_{2j-1} = C_{2j-1}' + \frac{1}{N_c^{eff}} C_{2j}', \quad \text{for } j = 1, \cdots, 5 \; . \tag{5.3}$$

As we have already mentioned in Chapter 4, we take into account the $\rho - \omega$ mixing contribution when we calculate the branching ratio, since we are working to the first order of isospin violation. Therefore, for recall, the general expression for the branching ratio is given by:

$$\begin{aligned} \mathscr{B}(B^{\pm,0} \to \rho^{\pm,0} M_1^{\pm,0}) = \frac{G_F^2 |\vec{p}_\rho|^3}{\alpha_k \pi \Gamma_{B^{\pm,0}}} \Bigg| & \left[V_{u,s}^T A_\rho^T(a_1, a_2) - V_{u,s}^P A_\rho^P(a_3, \cdots, a_{10}) \right] \\ + & \left[V_{u,s}^T A_\omega^T(a_1, a_2) - V_{u,s}^P A_\omega^P(a_3, \cdots, a_{10}) \right] \frac{\tilde{\Pi}_{\rho\omega}}{(s_\rho - m_\omega^2) + i m_\omega \Gamma_\omega} \Bigg|^2 \; , \end{aligned} \tag{5.4}$$

where G_F is the Fermi constant, $\Gamma_{B^{\pm,0}}$ is the total width B decay, and α_k is an integer related to the given decay. A_V^T and A_V^P are the tree and penguin amplitudes with V being either ρ or ω. $M_1^{\pm,0}$ is $\{K, \pi\}$. Finally, the term involving $\tilde{\Pi}_{\rho\omega}$ generates the $\rho - \omega$ mixing.

5.2 Calculational details

5.2.1 Factorization

With the Hamiltonian given in Eq. (3.10) (see Chapter 3), we are ready to evaluate the matrix elements for $B^{\pm,0} \to \rho^0(\omega) M_1^{\pm,0}$ where $M_1^{\pm,0}$ is $\pi^{\pm,0}$ or $K^{\pm,0}$. In the factorization approximation [43, 44, 45], either $\rho^0(\omega)$ or $M_1^{\pm,0}$ is generated by one current which has the appropriate quantum numbers in the Hamiltonian. For these decay processes, two kinds of matrix element products are involved after factorization; schematically (i.e. omitting Dirac

matrices and colour labels) $\langle\rho^0(\omega)|(\bar{u}u)|0\rangle\langle M_1^{\pm,0}|(\bar{q}_1 b)|B^{\pm,0}\rangle$ with $q_1 = \{u, s\}$, and $\langle M_1^{\pm,0}|(\bar{q}_3 q_4)|0\rangle\langle\rho^0(\omega)|(\bar{u}b)|B^{\pm,0}\rangle$ with $q_i = \{u, s\}$. We will calculate them in several phenomenological quark models.
The matrix elements for $B \to X$ and $B \to X^\star$ (where X and $X^\star$ denote pseudoscalar and vector mesons, respectively) can be decomposed as follows for the pseudoscalar pseudoscalar transition [73, 74],

$$\langle X|J_\mu|B\rangle = \left(p_B + p_X - \frac{m_B^2 - m_X^2}{k^2}k\right)_\mu F_1(k^2) + \frac{m_B^2 - m_X^2}{k^2}k_\mu F_0(k^2) \,, \tag{5.5}$$

and for the vector transition,

$$\begin{aligned}\langle X^\star|J_\mu|B\rangle = \frac{2}{m_B + m_{X^\star}}\epsilon_{\mu\nu\rho\sigma}\epsilon^{\star\nu}p_B^\rho p_{X^\star}^\sigma V(k^2) + i\Bigg\{\epsilon_\mu^\star(m_B + m_{X^\star})A_1(k^2) \\ - \frac{\epsilon^\star\cdot k}{m_B + m_{X^\star}}(P_B + P_{X^\star})_\mu A_2(k^2) - \frac{\epsilon^\star\cdot k}{k^2}2m_{X^\star}\cdot k_\mu A_3(k^2)\Bigg\} \\ + i\frac{\epsilon^\star\cdot k}{k^2}2m_{X^\star}\cdot k_\mu A_0(k^2) \,,\end{aligned} \tag{5.6}$$

where J_μ is the weak current defined as $J_\mu = \bar{q}\gamma^\mu(1-\gamma_5)b$ with $q = u, d, s$ and $k = p_B - p_{X(X^\star)}$. ϵ_μ is the polarization vector of $X^\star$. F_0, F_1 are the form factors related to the transition $0^- \to 0^-$ and A_0, A_1, A_2, A_3, V the form factors which describe the transition $0^- \to 1^-$. Finally, in order to cancel the poles at $k^2 = 0$ the form factors respect the conditions:

$$F_1(0) = F_0(0), \quad A_3(0) = A_0(0) \,, \tag{5.7}$$

and they also satisfy the following relation:

$$A_3(k^2) = \frac{m_B + m_{X^\star}}{2m_{X^\star}}A_1(k^2) - \frac{m_B - m_{X^\star}}{2m_{X^\star}}A_2(k^2) \,. \tag{5.8}$$

5.2.2 Form factors

The form factors $F_i(k^2)$ and $A_j(k^2)$ depend on the inner structure of the hadrons. We will adopt here three different theoretical approaches. The first was proposed by Bauer, Stech, and Wirbel [73, 74] (BSW model), who used the overlap integrals of wave functions in order to evaluate the meson-meson matrix elements of the corresponding current. The momentum dependence of the form factors is based on a single-pole ansatz. The second one was

developed by Guo and Huang (GH model) [75]. They modified the BSW model by using some wave functions described in the light-cone framework. The BSW (GH) models will be labelled models 1(2) and models 3(4) according to the form factors, $F_1(k^2)$ and $A_0(k^2)$, given in Eq. (5.9) where $n = 1$ and 2, respectively. The last model was given by Ball [76, 77]. In this case, the form factors are calculated from QCD sum rules on the light-cone and leading twist contributions, radiative corrections, and $SU(3)$-breaking effects are included. This model will be labelled model (5). Nevertheless, all these models use phenomenological form factors which are parametrized by making the nearest pole dominance assumption. The explicit k^2 dependence of the form factor is as [72, 73, 74, 75, 76, 77]:

$$F_1(k^2) = \frac{h_1}{\left(1 - \frac{k^2}{m_1^2}\right)^n} , \qquad A_0(k^2) = \frac{h_{A_0}}{\left(1 - \frac{k^2}{m_{A_0}^2}\right)^n} ,$$

or

$$F_1(k^2) = \frac{h_1}{1 - d_1 \frac{k^2}{m_B^2} + b_1 \left(\frac{k^2}{m_B^2}\right)^2} , \qquad A_0(k^2) = \frac{h_{A_0}}{1 - d_0 \frac{k^2}{m_B^2} + b_0 \left(\frac{k^2}{m_B^2}\right)^2} , \tag{5.9}$$

where $n = 1, 2$, m_{A_0}. Note also that m_1 are the pole masses associated with the transition current, h_1 and h_{A_0} are the values of form factors at $k^2 = 0$, and d_i and b_i $(i = 0, 1)$ are parameters in the model of Ball.

5.3 Numerical inputs and experimental results

5.3.1 CKM values

In our numerical calculations we have several parameters: q^2, N_c^{eff}, and the CKM matrix elements in the Wolfenstein parametrization. As mentioned in Chapter 2, the value of q^2 is conventionally chosen to be in the range $0.3 < q^2/{m_b}^2 < 0.5$. The CKM matrix, which should be determined from experimental data, is expressed in terms of the Wolfenstein parameters, A, λ, ρ, and η [18, 19]. Here, we shall use the latest values [78] which were extracted from charmless semileptonic B decays, $(|V_{ub}|)$, charm semileptonic B decays, $(|V_{cb}|)$, s and d mass oscillations, $\Delta m_s, \Delta m_d$, and CP violation in the kaon system (ϵ_K), (ρ, η). Hence, one has,

$$\lambda = 0.2237 , \quad A = 0.8113 , \quad 0.190 < \rho < 0.268 , \quad 0.284 < \eta < 0.366 . \tag{5.10}$$

	α	β	γ
(ρ_{min}, η_{min})	104°47	19°32	56°21
(ρ_{min}, η_{max})	93°13	24°31	62°56
(ρ_{max}, η_{min})	112°14	21°20	46°66
(ρ_{max}, η_{max})	99°66	26°56	53°78

Table 5.1: Values of the CKM unitarity triangle for limiting values of the CKM matrix elements.

These values respect the unitarity triangle as well (see Table 5.1).

5.3.2 Quark masses

The running quark masses are used in order to calculate the matrix elements of penguin operators. The quark mass is taken at the scale $\mu \simeq m_b$ in B decays. Therefore one has [79],

$$\begin{aligned} m_u(\mu = m_b) &= 2.3 \text{ MeV} , & m_d(\mu = m_b) &= 4.6 \text{ MeV} , \\ m_s(\mu = m_b) &= 90 \text{ MeV} , & m_b(\mu = m_b) &= 4.9 \text{ GeV} , \end{aligned} \tag{5.11}$$

which corresponds to $m_s(\mu = 1 \text{ GeV}) = 140$ MeV. For meson masses, we shall use the following values [24]:

$$\begin{aligned} m_{B^\pm} &= 5.279 \text{ GeV} , & m_{B^0} &= 5.279 \text{ GeV} , \\ m_{K^\pm} &= 0.493 \text{ GeV} , & m_{K^0} &= 0.497 \text{ GeV} , \\ m_{\pi^\pm} &= 0.139 \text{ GeV} , & m_{\pi^0} &= 0.135 \text{ GeV} , \\ m_{\rho^0} &= 0.769 \text{ GeV} , & m_\omega &= 0.782 \text{ GeV} . \end{aligned} \tag{5.12}$$

5.3.3 Form factors and decay constants

In Tables 5.2 and 5.3 we list the relevant form factor values at zero momentum transfer [73, 74, 75, 76, 77, 80] for the $B \to K$, $B \to \rho$, and $B \to \pi$ transitions. The different models are defined as follows: models (1) and (3) are the BSW model where the q^2 dependence of the form factors is described by a single ($n = 1$) and a double-pole ($n = 2$) ansatz, respectively. Models (2) and (4) are the GH model with the same momentum dependence as models (1) and (3). We define the decay constants for pseudoscalar (f_P) and vector (f_V) mesons as usual by,

$$\begin{aligned} \langle P(q)|\bar{q}_1\gamma_\mu\gamma_5 q_2|0\rangle &= -if_P q_\mu , \\ \sqrt{2}\langle V(q)|\bar{q}_1\gamma_\mu q_2|0\rangle &= f_V m_V \epsilon_V , \end{aligned} \tag{5.13}$$

	h_{A_0}	h_1	m_{A_0}	m_1	$d_0(d_1)$	$b_0(b_1)$
model 1	0.280	0.290	5.27	5.32		
model 2	0.340	0.625	5.27	5.32		
model 3	0.280	0.290	5.27	5.32		
model 4	0.340	0.625	5.27	5.32		
model 5	0.372	0.305			1.400(0.266)	0.437(-0.752)

Table 5.2: Form factor values for $B \to \rho\pi$ at $k^2 = 0$.

	h_{A_0}	h_1	m_{A_0}	m_1	$d_0(d_1)$	$b_0(b_1)$
model 1	0.280	0.360	5.27	5.41		
model 2	0.340	0.762	5.27	5.41		
model 3	0.280	0.360	5.27	5.41		
model 4	0.340	0.762	5.27	5.41		
model 5	0.372	0.341			1.400(0.410)	0.437(-0.361)

Table 5.3: Form factor values for $B \to \rho K$ at $k^2 = 0$.

with q_μ being the momentum of the pseudoscalar meson, m_V and ϵ_V being the mass and polarization vector of the vector meson, respectively. Numerically, in our calculations, we take [24],

$$f_\pi = 132 \text{ MeV} \ , \ f_K = 160 \text{ MeV} \ , \ f_\rho \simeq f_\omega = 221 \text{ MeV} \ . \tag{5.14}$$

The ρ and ω decay constants are very close and for simplification (without any consequences for results) we choose $f_\rho = f_\omega$.

The numerical values for the CKM matrix elements $V_{u,s}^{T,P}$, the Wilson coefficients, C_i, the $\rho - \omega$ mixing amplitude $\tilde{\Pi}_{\rho\omega}$, the particle masses, $m_{V,P}$, which appear in Eq. (5.4), have been all reported on Chapters 2, 3, 4 and 5, respectively. The Fermi constant is taken equal to be $G_F = 1.166391 \times 10^{-5}\text{GeV}^{-2}$ [24] and for the total B decay width, $\Gamma_B (= 1/\tau_B)$, we use the world average B life-time values (combined results from ALEPH, CDF, DELPHI, L3, OPAL and SLD) [78, 81, 82]:

$$\begin{aligned} \tau_{B^0} &= 1.546 \pm 0.021 \text{ ps} \ , \\ \tau_{B^+} &= 1.647 \pm 0.021 \text{ ps} \ . \end{aligned} \tag{5.15}$$

5.3.4 Experimental results

To compare the theoretical results with experimental data, as well as to determine the constraints on the effective number of colour, N_c^{eff}, the form factors, and the CKM matrix parameters, we shall apply the experimental branching ratios collected at CLEO [83, 84, 85, 86, 87], BELLE [88, 89, 90, 91, 92, 93, 94, 95, 96] and BABAR[1] [98, 99, 100, 101, 102, 103, 104, 105] factories. All the experimental values are summarized in Table 5.4 (for $\rho\pi$) and Table 5.5 (for ρK).

	CLEO	BABAR	BELLE
$\rho^0\pi^\pm$	$10.4^{+3.3}_{-3.4} \pm 2.1^*$	$24 \pm 8 \pm 3^*$ $(\leq 39)^\P$	$8.0^{+2.3+0.7*}_{-2.0-0.7}$ $(\leq 28.8)^\P$
$\rho^\pm\pi^0$	$\leq 43^\P$	–	–
$\rho^\pm\pi^\mp$	$27.6^{+8.4}_{-7.4} \pm 4.2^*$	$28.9 \pm 5.4 \pm 4.3^*$	$20.8^{+6.0+2.8*}_{-6.3-3.1}$
$\rho^0\pi^0$	$1.6^{+2.0}_{-1.4} \pm 0.8^\bullet$ $(\leq 5.5)^\P$	$\leq 10.6^\P$	$\leq 5.3^\P$
$\frac{BR(\rho^\pm\pi^\mp)}{BR(\rho^0\pi^\pm)}$	2.65 ± 1.9	1.20 ± 0.79	2.60 ± 1.31
$\omega\pi^\pm$	$11.3^{+3.3}_{-2.9} \pm 1.4^*$	$6.6^{+2.1}_{-1.8} \pm 0.7^*$	$4.2^{+2.0}_{-1.8} \pm 0.5^*$

Table 5.4: The measured branching ratios by CLEO, BABAR and BELLE factories for B decays into $\rho\pi$ (10^{-6}). Exp. data*, fit$^\bullet$ and upper limit¶.

	CLEO	BABAR	BELLE
$\rho^0 K^\pm$	$8.46^{+4.0}_{-3.4} \pm 1.8^\bullet$ $(\leq 17)^\P$	$10 \pm 6 \pm 2^*$ $(\leq 29)^\P$	$\leq 13.5^\P$
$\rho^\pm K^0$	–	–	$\leq 23.6^\P$
$\rho^\pm K^\mp$	$16.0^{+7.6}_{-6.4} \pm 2.8^\bullet$ $(\leq 32)^\P$	–	$15.8^{+5.1\ +1.7*}_{-4.6\ -3.0}$
$\rho^0 K^0$	–	–	–
$\frac{BR(\rho^\pm K^\mp)}{BR(\rho^0 K^\pm)}$	1.89 ± 1.41	–	–
$\omega K^\pm$	$3.2^{+2.4}_{-1.9} \pm 0.8^\bullet$ $(\leq 7.9)^\P$	$1.4^{+1.3}_{-1.0} \pm 0.3^*$	$9.2^{+2.6}_{-2.3} \pm 1.0^*$

Table 5.5: The measured branching ratios by CLEO, BABAR and BELLE factories for B decays into ρK (10^{-6}). Exp. data*, fit$^\bullet$ and upper limit¶.

[1] We note that BABAR [97] reported preliminary branching ratios for the channels $\mathcal{B}(B^0 \to \rho^\pm\pi^\mp) = (22.6 \pm 1.8 \pm 2.2) \times 10^{-6}$ and $\mathcal{B}(B^0 \to \rho^\pm K^\mp) = (7.3^{+1.3}_{-1.2} \pm 1.3) \times 10^{-6}$ after this thesis was prepared.

5.4 Branching ratios for $B^{\pm,0} \to \rho^{\pm,0}\pi^{\pm,0}$

5.4.1 Formulae

We begin by analysing processes such as $B^{\pm,0} \to \rho^{\pm,0}\pi^{\pm,0}$ and also $B^{\pm} \to \omega\pi^{\pm}$. Two investigated cases include $\rho - \omega$ mixing: $B^- \to \rho^0\pi^-$ and $\bar{B}^0 \to \rho^0\pi^0$. Three other decays (without mixing) are: $B^- \to \rho^-\pi^0$, $\bar{B}^0 \to \rho^-\pi^+$ and $B^- \to \omega\pi^-$. In this section, we give the explicit tree and penguin amplitudes[2] for all these charmless B decays. Therefore, after factorization one gets the following amplitudes[3]:
for the decay $B^- \to \rho^0\pi^-$ ($\alpha_k = 32$ in Eq. (5.4)),

$$\sqrt{2}A_\rho^T(a_1,a_2) = a_1 f_\rho F_1(m_\rho^2) + a_2 f_\pi A_0(m_\pi^2)\,, \tag{5.16}$$

$$\sqrt{2}A_\rho^P(a_3,\cdots,a_{10}) = f_\rho F_1(m_\rho^2)\left\{-a_4 + \frac{3}{2}(a_7+a_9) + \frac{1}{2}a_{10}\right\}$$
$$+ f_\pi A_0(m_\pi^2)\left\{a_4 - 2(a_6+a_8)\left[\frac{m_\pi^2}{(m_u+m_d)(m_b+m_u)}\right] + a_{10}\right\}\,; \tag{5.17}$$

for the decay $B^- \to \omega\pi^-$ ($\alpha_k = 32$ in Eq. (5.4)),

$$\sqrt{2}A_\omega^T(a_1,a_2) = a_1 f_\rho F_1(m_\rho^2) + a_2 f_\pi A_0(m_\pi^2)\,, \tag{5.18}$$

$$\sqrt{2}A_\omega^P(a_3,\cdots,a_{10}) = f_\rho F_1(m_\rho^2)\left\{2(a_3+a_5) + \frac{1}{2}(a_7+a_9) + (a_4 - \frac{1}{2}a_{10})\right\}$$
$$+ f_\pi A_0(m_\pi^2)\left\{-2(a_6+a_8)\left[\frac{m_\pi^2}{(m_u+m_d)(m_b+m_u)}\right] + a_4 + a_{10}\right\}\,; \tag{5.19}$$

for the decay $\bar{B}^0 \to \rho^0\pi^0$ ($\alpha_k = 64$ in Eq. (5.4)),

$$2A_\rho^T(a_1,a_2) = a_1 f_\rho F_1(m_\rho^2) + a_1 f_\pi A_0(m_\pi^2)\,, \tag{5.20}$$

$$2A_\rho^P(a_3,\cdots,a_{10}) = f_\rho F_1(m_\rho^2)\left\{-a_4 + \frac{1}{2}(3a_7 + 3a_9 + a_{10})\right\} +$$
$$f_\pi A_0(m_\pi^2)\left\{-a_4 + (2a_6 - a_8)\left[\frac{m_\pi^2}{2m_d(m_b+m_d)}\right] + \frac{1}{2}(-3a_7 + 3a_9 + a_{10})\right\}\,; \tag{5.21}$$

[2]Read $F_1(m_\rho^2)$ as $F_1^{B\to\pi}(m_\rho^2)$ and $A_0(m_\pi^2)$ as $A_0^{B\to\rho}(m_\pi^2)$.

[3]Note that the integer α_k includes the coefficient written near to the tree or penguin amplitudes on the l.h.s. of Eqs. (5.16)-(5.27).

for the decay $\bar{B}^0 \to \omega\pi^0$ ($\alpha_k = 64$ in Eq. (5.4)),

$$2A_\omega^T(a_1,a_2) = -a_1 f_\rho F_1(m_\rho^2) + a_1 f_\pi A_0(m_\pi^2)\,, \tag{5.22}$$

$$2A_\omega^P(a_3,\cdots,a_{10}) = f_\rho F_1(m_\rho^2)\left\{-2(a_3+a_5) - a_4 - \frac{1}{2}(a_7+a_9-a_{10})\right\}$$
$$+ f_\pi A_0(m_\pi^2)\left\{-a_4 + (2a_6-a_8)\left[\frac{m_\pi^2}{2m_d(m_b+m_d)}\right] + \frac{1}{2}(-3a_7+3a_9+a_{10})\right\}\,; \tag{5.23}$$

for the decay $\bar{B}^0 \to \rho^-\pi^+$ ($\alpha_k = 16$ in Eq. (5.4)),

$$A_\rho^T(a_1,a_2) = a_2 f_\rho F_1(m_\rho^2)\,, \tag{5.24}$$

$$A_\rho^P(a_3,\cdots,a_{10}) = (a_4+a_{10}) f_\rho F_1(m_\rho^2)\,; \tag{5.25}$$

for the decay $B^- \to \rho^-\pi^0$ ($\alpha_k = 32$ in Eq. (5.4)),

$$\sqrt{2}A_\rho^T(a_1,a_2) = a_2 f_\rho F_1(m_\rho^2) + a_1 f_\pi A_0(m_\pi^2)\,, \tag{5.26}$$

$$\sqrt{2}A_\rho^P(a_3,\cdots,a_{10}) = f_\rho F_1(m_\rho^2)(a_4+a_{10}) +$$
$$f_\pi A_0(m_\pi^2)\left\{-a_4 - \frac{1}{2}(3a_7-3a_9-a_{10}) + (2a_6-a_8)\left[\frac{m_\pi^2}{2m_d(m_b+m_d)}\right]\right\}\,. \tag{5.27}$$

We can also calculate the ratio between two branching ratios: $\mathscr{B}(B^0 \to \rho^\pm\pi^\mp)$ and $\mathscr{B}(B^\pm \to \rho^0\pi^\pm)$, in which the uncertainty caused by many systematic errors is removed. We define the ratio, R_π, as:

$$R_\pi = \frac{\mathscr{B}(B^0 \to \rho^\pm\pi^\mp)}{\mathscr{B}(B^\pm \to \rho^0\pi^\pm)}\,, \tag{5.28}$$

and, without taking into account the penguin contribution, one has,

$$R_\pi = \frac{2\Gamma_{B^+}}{\Gamma_{B^0}}\left|\left(\frac{a_1}{a_2} + \frac{f_\pi A_0(m_\pi^2)}{f_\rho F_1(m_\rho^2)}\right)\left(1 + \frac{\tilde{\Pi}_{\rho\omega}}{(s_\rho - m_\omega^2) + i m_\omega \Gamma_\omega}\right)\right|^{-2}\,. \tag{5.29}$$

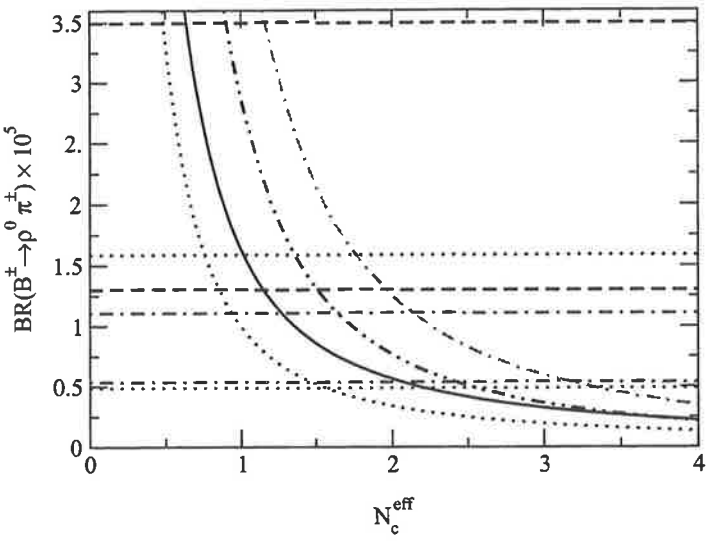

Figure 5.1: Branching ratio for $B^{\pm} \to \rho^0\pi^{\pm}$ for models 1(2), $q^2/m_b^2 = 0.3$ (q^2/m_b^2 is used to calculate the Wilson coefficients) and limiting values of the CKM matrix elements. Solid line (dotted line) for model (1) and max (min) CKM matrix elements. Dot-dashed line (dot-dot-dashed line) for model (2) and max (min) CKM matrix elements. Notation: horizontal dotted lines: CLEO data; dashed lines: BABAR data; dot-dashed lines: BELLE data.

5.4.2 Results and discussions

In order to determine the range of N_c^{eff}, which is allowed by experimental data, we have calculated the branching ratios for $B^{\pm} \to \rho^0\pi^{\pm}$, $B^{\pm} \to \rho^{\pm}\pi^0$, $B^0 \to \rho^{\pm}\pi^{\mp}$, $B^0 \to \rho^0\pi^0$, and $B^{\pm} \to \omega\pi^{\pm}$. All the results are shown in Figs. 5.1, 5.2, 5.3, 5.4, and 5.5 for the corresponding branching ratios listed above. Results are plotted for models (1) and (2), since each of them includes different form factor values, and hence this shows their dependence on form factors. As experimental data, we shall use three sets of data from the CLEO, BABAR and BELLE Collaborations, respectively. Since experimental branching ratios from CLEO are the most accurate, we shall use them to extract the range of N_c^{eff}. The other two, the BABAR and BELLE data, will give us an idea of the magnitude of the experimental uncertainties. It is clear that numerical results are very sensitive to uncertainties coming from the experimental data. Thus, the determination of the allowed range of N_c^{eff} will be done by using all the branching ratio results.

Let us start with the decay processes $B^- \to \rho^0\pi^-$ and $B^- \to \rho^-\pi^0$. In both cases, we have a large range for N_c^{eff} and the CKM matrix elements over which the theoretical results are consistent with experimental data from

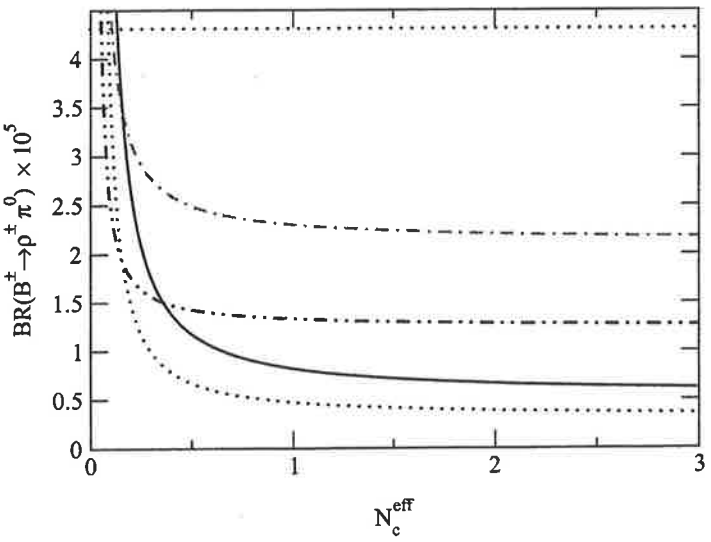

Figure 5.2: Branching ratio for $B^{\pm} \to \rho^{\pm}\pi^0$ for models 1(2), $q^2/m_b^2 = 0.3$ and limiting values of the CKM matrix elements. Solid line (dotted line) for model (1) and max (min) CKM matrix elements. Dot-dashed line (dot-dot-dashed line) for model (2) and max (min) CKM matrix elements. Same notation as in Fig. 5.1 for the horizontal line.

CLEO, BABAR and BELLE. For $B^- \to \rho^-\pi^0$, the lack of data does not allow us to determine the range. However, experiment and theory are consistent in both cases. For $B^- \to \rho^0\pi^-$, the models show considerable variation even though they are all consistent with the experimental data. Numerical results for models (1,3) and (5) are close, as are those for models (2) and (4). We emphasise that the effect of $\rho - \omega$ mixing on the branching ratio $B^{\pm} \to \rho^0\pi^{\pm}$ can be as large as 30%. As regards $\bar{B}^0 \to \rho^-\pi^+$ and $\bar{B}^0 \to \rho^0\pi^0$, the results and conclusions are different from those for $B^{\pm} \to \rho^0\pi^{\pm}$. If we look at the branching ratio for $B^0 \to \rho^{\pm}\pi^{\mp}$, only models (2) and (4) are consistent with the experimental data over a large range of N_c^{eff}, whereas models (1,3) and (5) are not. The strong sensitivity to the results in that case comes from the fact that the decay branching ratios for $B^0 \to \rho^{\pm}\pi^{\mp}$ depend on form factors more sensitively, because in this case only one form factor, $F_1(k^2)$, is involved. In all the other cases, the amplitudes depend on $F_1(k^2)$ and $A_0(k^2)$. Therefore these branching ratios are less sensitive to the magnitude of the form factors. Finally, for the branching ratio $\mathscr{B}(B^{\pm} \to \omega\pi^{\pm})$, plotted in Fig. 5.5, all models give theoretical results in consistency with experimental data. Once again, the difference observed between models (1) and (2) mainly comes from the form factor $F_1(k^2)$ (i.e. from the pion wave function used). Our complete analysis of branching ratios shows that models (1,3) and (5)

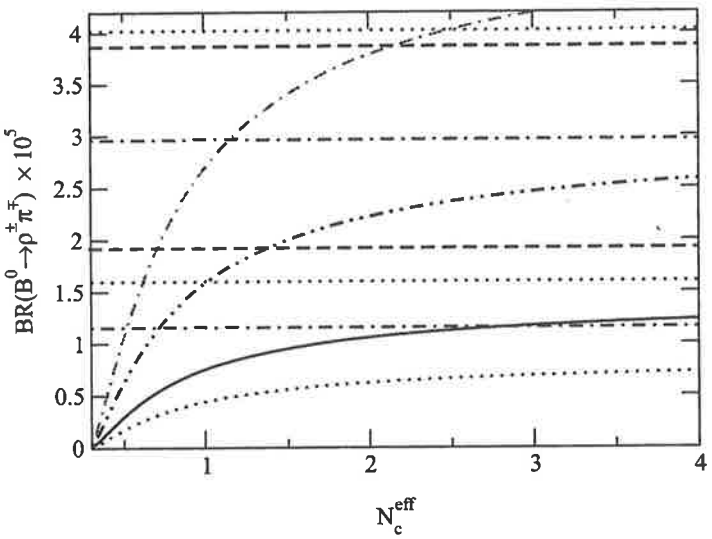

Figure 5.3: Branching ratio for $B^0 \to \rho^{\pm}\pi^{\mp}$ for models 1(2), $q^2/m_b^2 = 0.3$ and limiting values of the CKM matrix elements. Solid line (dotted line) for model (1) and max (min) CKM matrix elements. Dot-dashed line (dot-dot-dashed line) for model (2) and max (min) CKM matrix elements. Same notation as in Fig. 5.1 for the horizontal lines.

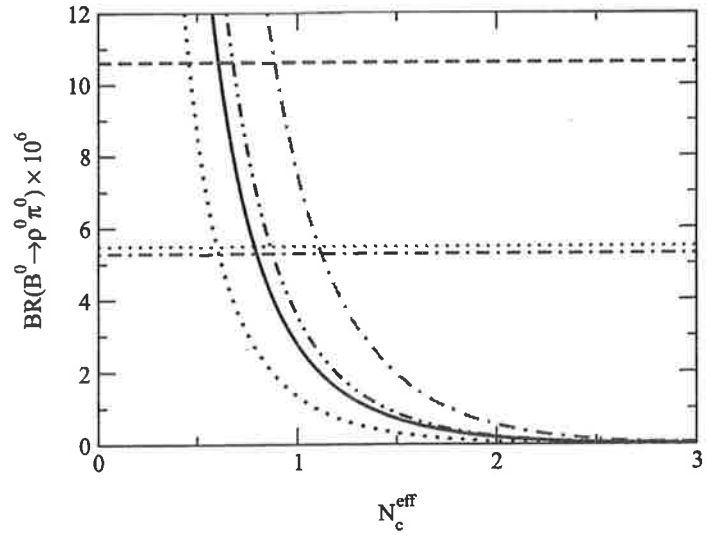

Figure 5.4: Branching ratio for $B^0 \to \rho^0\pi^0$ for models 1(2), $q^2/m_b^2 = 0.3$ and limiting values of the CKM matrix elements. Solid line (dotted line) for model (1) and max (min) CKM matrix elements. Dot-dashed line (dot-dot-dashed line) for model (2) and max (min) CKM matrix elements. Same notation as in Fig. 5.1 for the horizontal lines.

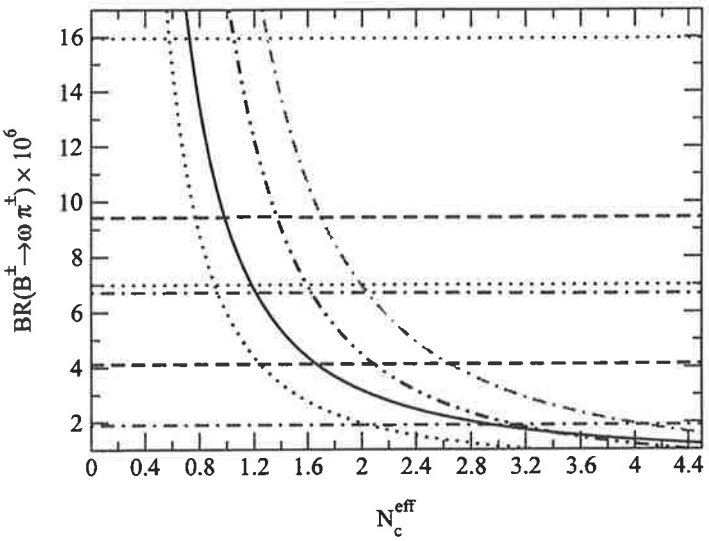

Figure 5.5: Branching ratio for $B^{\pm} \to \omega\pi^{\pm}$ for models 1(2), $q^2/m_b^2 = 0.3$ and limiting values of the CKM matrix elements. Solid line (dotted line) for model (1) and max (min) CKM matrix elements. Dot-dashed line (dot-dot-dashed line) for model (2) and max (min) CKM matrix elements. Same notation as in Fig. 5.1 for the horizontal lines.

cannot give results consistent with all experiments and have to be excluded.

To remove systematic uncertainties coming from experimental results, one can calculate the ratio between two branching ratios for B decays. In the present case (with the data available), the ratio, R_π, is between $\mathscr{B}(B^{\pm} \to \rho^0\pi^{\pm})$ and $\mathscr{B}(B^0 \to \rho^{\pm}\pi^{\mp})$. Results are shown in Fig. 5.6. We observe that the ratios differ markedly between models $(1,3,5)$ and models $(2,4)$. Since models $(1,3)$ and (5) have already been excluded, we will use models (2) and (4) for the determination of the range for N_c^{eff}. If we just

$B \to \rho\pi$	$\{N_c^{eff}\}$
model (2)	1.09;1.63(1.12;1.77)
model (4)	1.10;1.68(1.11;1.80)
maximum range	1.09;1.68(1.11;1.80)
minimum range	1.10;1.63(1.12;1.77)

Table 5.6: Best range of N_c^{eff} determined for $q^2/m_b^2 = 0.3(0.5)$ and for $B \to \rho\pi$ decays.

include tree contributions in the decay amplitudes, R_π becomes independent

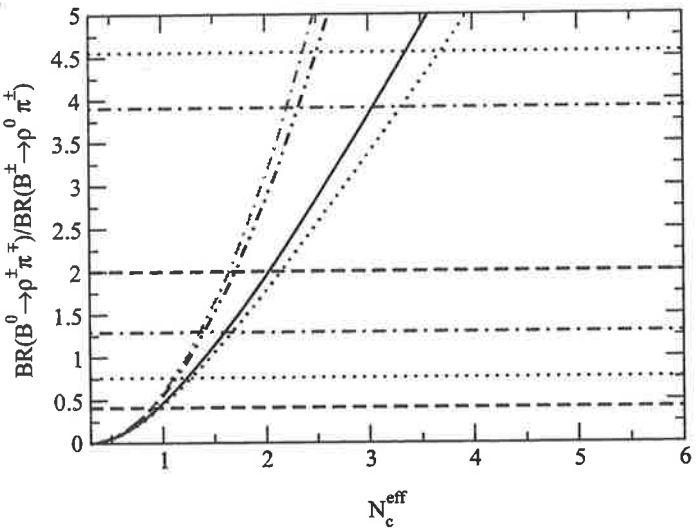

Figure 5.6: The ratio of two $\rho\pi$ branching ratios versus N_c^{eff} for models 1(2) and for limiting values of the CKM matrix elements: solid line (dotted line) for model (1) with max (min) CKM matrix elements. Dot-dashed line (dot-dot-dashed line) for model (2) with max (min) CKM matrix elements. Same notation as in Fig. 5.1 for the horizontal lines.

of the CKM matrix elements. Penguin contributions lead to a relatively weak dependence of R_π on the CKM matrix elements. By comparing numerical results and experimental data, we are now able to extract a range for N_c^{eff} which is consistent with both approaches (experimental and theoretical). To determine the best range of N_c^{eff}, we select the values of N_c^{eff} which are allowed by all constraints for each model. Finally, after excluding models $(1,3)$ and (5) for the obvious reasons mentioned before, we can now fix the upper and the lower limit of the range of N_c^{eff} (Table 5.6). We find that N_c^{eff} should be in the range $1.09(1.11) < N_c^{eff} < 1.68(1.80)$ for $q^2/m_b^2 = 0.3(0.5)$.

5.5 Branching ratios for $B^{\pm,0} \to \rho^{\pm,0} K^{\pm,0}$

5.5.1 Formulae

After the analysis of branching ratios related to $B \to \rho\pi$, we now consider the case $B \to \rho K$. In this section, we start by enumerating the theoretical decay amplitudes. We shall analyse five b into s transitions. Two of them involve $\rho - \omega$ mixing. These are $B^- \to \rho^0 K^-$ and $\bar{B}^0 \to \rho^0 \bar{K}^0$. Two other decays are $\bar{B}^0 \to \rho^- K^+$ and $B^- \to \rho^- \bar{K}^0$ and the last one is $B^- \to \omega K^-$.

We list in the following, the tree and penguin amplitudes which appear in the given transitions[4].
For the decay $B^- \to \rho^0 K^-$ ($\alpha_k = 32$ in Eq. (5.4)),

$$\sqrt{2}A_\rho^T(a_1,a_2) = a_1 f_\rho F_1(m_\rho^2) + a_2 f_K A_0(m_K^2) \ , \tag{5.30}$$

$$\sqrt{2}A_\rho^P(a_3,\cdots,a_{10}) = f_\rho F_1(m_\rho^2)\left\{\frac{3}{2}(a_7+a_9)\right\}$$
$$+ f_K A_0(m_K^2)\left\{a_4+a_{10}-2(a_6+a_8)\left[\frac{m_K^2}{(m_u+m_s)(m_b+m_u)}\right]\right\} \ ; \tag{5.31}$$

for the decay $B^- \to \omega K^-$ ($\alpha_k = 32$ in Eq. (5.4)),

$$\sqrt{2}A_\omega^T(a_1,a_2) = a_1 f_\rho F_1(m_\rho^2) + a_2 f_K A_0(m_K^2) \ , \tag{5.32}$$

$$\sqrt{2}A_\omega^P(a_3,\cdots,a_{10}) = f_\rho F_1(m_\rho^2)\left\{2(a_3+a_5)+\frac{1}{2}(a_7+a_9)\right\}$$
$$+ f_K A_0(m_K^2)\left\{-2(a_8+a_6)\left[\frac{m_K^2}{(m_u+m_s)(m_b+m_u)}\right]+a_4+a_{10}\right\} \ ; \tag{5.33}$$

for the decay $\bar{B}^0 \to \rho^0 \bar{K}^0$ ($\alpha_k = 32$ in Eq. (5.4)),

$$\sqrt{2}A_\rho^T(a_1,a_2) = a_1 f_\rho F_1(m_\rho^2) \ , \tag{5.34}$$

$$\sqrt{2}A_\rho^P(a_3,\cdots,a_{10}) = f_\rho F_1(m_\rho^2)\left\{\frac{3}{2}(a_7+a_9)\right\}$$
$$+ f_K A_0(m_K^2)\left\{-a_4+(2a_6-a_8)\left[\frac{m_K^2}{(m_s+m_d)(m_b+m_d)}\right]+\frac{1}{2}a_{10}\right\} \ ; \tag{5.35}$$

for the decay $\bar{B}^0 \to \omega \bar{K}^0$ ($\alpha_k = 32$ in Eq. (5.4)),

$$\sqrt{2}A_\omega^T(a_1,a_2) = a_1 f_\rho F_1(m_\rho^2) \ , \tag{5.36}$$

$$\sqrt{2}A_\omega^P(a_3,\cdots,a_{10}) = f_\rho F_1(m_\rho^2)\left\{2(a_3+a_5)+\frac{1}{2}(a_7+a_9)\right\}$$
$$+ f_K A_0(m_K^2)\left\{a_4-(2a_6-a_8)\left[\frac{m_K^2}{(m_s+m_d)(m_b+m_d)}\right]-\frac{1}{2}a_{10}\right\} \ ; \tag{5.37}$$

[4]Read $F_1(m_\rho^2)$ as $F_1^{B\to K}(m_\rho^2)$ and $A_0(m_K^2)$ as $A_0^{B\to\rho}(m_K^2)$. See footnote 3 as well.

for the decay $B^- \to \rho^- \bar{K}^0$ ($\alpha_k = 16$ in Eq. (5.4)),

$$A_\rho^T(a_1, a_2) = a_2 f_\rho F_1(m_\rho^2) \ , \tag{5.38}$$

$$A_\rho^P(a_3, \cdots, a_{10}) = f_K A_0(m_K^2)\left\{ a_4 - \frac{1}{2}a_{10} - (2a_6 - a_8)\left[\frac{m_K^2}{(m_s + m_d)(m_b + m_d)}\right]\right\} ; \tag{5.39}$$

for the decay $\bar{B}^0 \to \rho^+ K^-$ ($\alpha_k = 16$ in Eq. (5.4)),

$$A_\rho^T(a_1, a_2) = a_2 f_K A_0(m_K^2) \ , \tag{5.40}$$

$$A_\rho^P(a_3, \cdots, a_{10}) = f_K A_0(m_K^2)\left\{ a_4 + a_{10} - 2(a_6 + a_8)\left[\frac{m_K^2}{(m_s + m_u)(m_b + m_u)}\right]\right\} . \tag{5.41}$$

Moreover, as we did for $B \to \rho\pi$, we can calculate the ratio between two branching ratios, in which the uncertainty caused by systematic errors is removed. We define the ratio R_K as:

$$R_K = \frac{\mathscr{B}(B^0 \to \rho^\pm K^\mp)}{\mathscr{B}(B^\pm \to \rho^0 K^\pm)} \ , \tag{5.42}$$

and, without taking into account the penguin contribution, one has,

$$R_K = \frac{2\Gamma_{B^+}}{\Gamma_{B^0}}\left|\left(1 + \frac{a_1 f_\rho F_1(m_\rho^2)}{a_2 f_K A_0(m_K^2)}\right)\left(1 + \frac{\tilde{\Pi}_{\rho\omega}}{(s_\rho - m_\omega^2) + i m_\omega \Gamma_\omega}\right)\right|^{-2} . \tag{5.43}$$

Finally, we define the ratio R, between the two ratios R_π and R_K defined in Eqs. (5.28) and (5.42), respectively, as,

$$R = \frac{R_\pi}{R_K} . \tag{5.44}$$

Numerically, by using the experimental data from $\rho\pi$ and ρK, one gets a ratio equal to $R = 1.40 \pm 2.04$. By simplification, we can also just include the tree contribution and one obtains therefore:

$$R = \left|\frac{f_\rho}{f_K} \cdot \frac{F_1^{B\to\pi}(m_\rho^2)}{A_0^{B\to\rho}(m_\pi^2)} \cdot \frac{a_1 f_\rho F_1^{B\to K}(m_\rho^2) + a_2 f_\pi A_0^{B\to\rho}(m_K^2)}{a_1 f_\rho F_1^{B\to\pi}(m_\rho^2) + a_2 f_\pi A_0^{B\to\rho}(m_\pi^2)}\right|^2 . \tag{5.45}$$

Further, since $a_2 \ll a_1$, a rough estimation of R can be read as,

$$R = \left|\frac{f_\rho}{f_K} \cdot \frac{F_1^{B\to K}(m_\rho^2)}{A_0^{B\to\rho}(m_\pi^2)}\right|^2 \simeq 3 . \tag{5.46}$$

5.5.2 Results and discussions

In order to determine the range of N_c^{eff} available for calculating the CP violating parameter, a_{CP}, in $B^{\pm,0} \to \rho^0 K^{\pm,0}$, we have calculated the branching ratios for $B^{\pm} \to \rho^0 K^{\pm}$, $B^{\pm} \to \rho^{\pm} K^0$, $B^0 \to \rho^{\pm} K^{\mp}$, $B^0 \to \rho^0 K^0$, and $B^{\pm} \to \omega K^{\pm}$. We show all the results in Figs. 5.7, 5.8, 5.9, 5.10, and 5.11, where branching ratios are plotted as a function of N_c^{eff} for models (1) and (2) (different form factors are used in models (1) and (2)). By taking (just as for $\rho\pi$) experimental data from the CLEO, BABAR and BELLE Collaborations, listed in Table 5.5, and comparing theoretical predictions with experimental results, we expect to extract the allowed range of N_c^{eff} in $B \to \rho K$ and to make the dependence on the form factors explicit between the two classes of models: models $(1,3)$ and (5), and models (2) and (4). We shall mainly use the CLEO data, since the BABAR and BELLE data are (as yet) less numerous and accurate. An exception will be made for the branching ratio $B^{\pm} \to \omega K^{\pm}$, where we shall take the BELLE data for our analysis since they are the most accurate and most recent measurements in that case. Nevertheless, we shall also apply all of them to check the agreement between all the branching ratio data. The CLEO, BABAR and BELLE Collaborations give almost the same experimental branching ratios for all the investigated decays except for the decay $B^- \to \omega K^-$. In the latter case, we observe a strong disagreement between all of them since they provide experimental data in a range from 0.1×10^{-6} to 12.8×10^{-6}. Finally, it is evident that numerical results are very sensitive to uncertainties coming from the experimental data and from the factorization approach applied to calculate hadronic matrix elements in the $B \to K$ transition. Moreover, for $B \to \rho K$, the data are less numerous than for $B \to \rho\pi$, so we cannot expect to get a very accurate range of N_c^{eff}.

For the branching ratio $B^{\pm} \to \rho^0 K^{\pm}$ (Fig. 5.7) we found a large range of values of N_c^{eff} and CKM matrix elements over which the theoretical results are consistent with experimental data from CLEO, BABAR and BELLE. Each of the models $(1,2,3,4)$ and (5), gives an allowed range of N_c^{eff}. Even though strong differences appear between the two classes of models, because of the different form factors used, we are not able to draw strong conclusions about the dependence on the form factors. For the branching ratio $B^{\pm} \to \rho^{\pm} K^0$, (Fig. 5.8), BELLE gives only an upper limit for the branching ratio whereas BABAR and CLEO do not. Our predictions are still consistent with the experimental data for all models, for a large range of N_c^{eff}. In this case, the numerical results for models (1) and (2) are very close to each other and, we need new data to constrain our calculations.

If we consider our results for the branching ratio $B^0 \to \rho^{\pm} K^{\mp}$ (plotted in

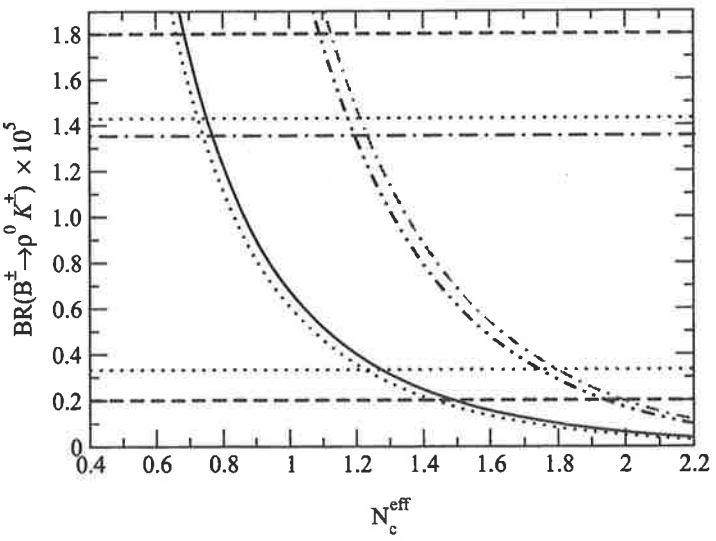

Figure 5.7: Branching ratio for $B^{\pm} \to \rho^0 K^{\pm}$, for models 1(2), $q^2/m_b^2 = 0.3$ and limiting values of the CKM matrix elements. Solid line (dotted line) for model (1) and max (min) CKM matrix elements. Dot-dashed line (dot-dot-dashed line) for model (2) and max (min) CKM matrix elements. Notation: horizontal dotted line: CLEO data; dashed line: BABAR data; dot-dashed line: BELLE data.

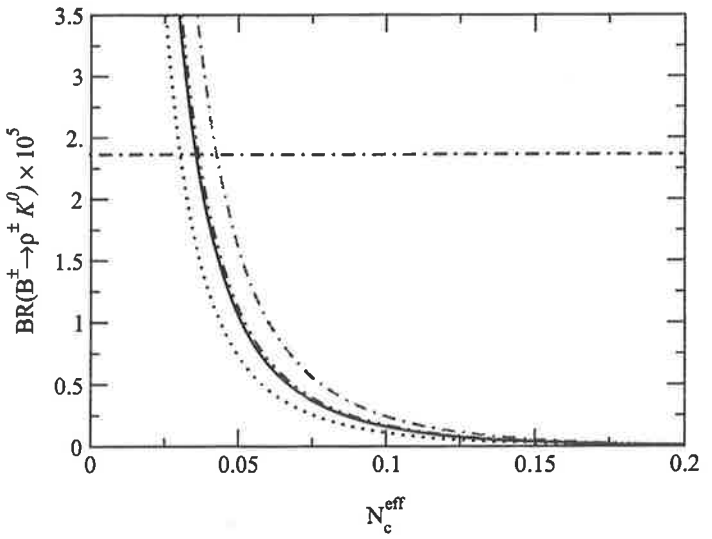

Figure 5.8: Branching ratio for $B^{\pm} \to \rho^{\pm} K^0$, for models 1(2), $q^2/m_b^2 = 0.3$ and limiting values of the CKM matrix elements. Solid line (dotted line) for model (1) and max (min) CKM matrix elements. Dot-dashed line (dot-dot-dashed line) for model (2) and max (min) CKM matrix elements. Same notation as in Fig. 5.7 for the horizontal line.

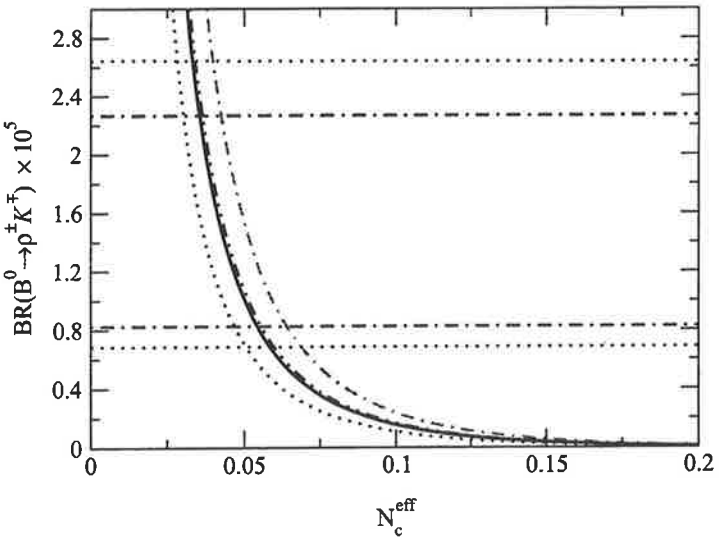

Figure 5.9: Branching ratio for $B^0 \to \rho^{\pm} K^{\mp}$, for models 1(2), $q^2/m_b^2 = 0.3$ and limiting values of the CKM matrix elements. Solid line (dotted line) for model (1) and max (min) CKM matrix elements. Dot-dashed line (dot-dot-dashed line) for model (2) and max (min) CKM matrix elements. Same notation as in Fig. 5.7 for the horizontal lines.

Fig. 5.9), there is agreement between the experimental results from CLEO and BELLE (no data from BABAR) and our theoretical predictions at very low values of N_c^{eff}. All the models $(1, 2, 3, 4)$ and (5), give branching values within the range of branching ratio measurements if N_c^{eff} is less than 0.07. The tiny difference observed between models (1) and (2) comes from the form factor $A_0(k^2)$ (where $A_0(k^2)$ refers to the B to ρ transition taken at $k^2 = m_K^2$) since in that case, the amplitude computed involves only the form factor $A_0(k^2)$. For the branching ratio $B^0 \to \rho^0 K^0$ shown in Fig. 5.10, neither CLEO, BABAR nor BELLE give experimental results. Nevertheless, from models (1) and (2), it appears that this branching ratio is very sensitive to the magnitude of the form factor $F_1(k^2)$ (in our case, $F_1(k^2)$ is uncertain because $h_1 = 0.360$ or 0.762 in models (1) and (2), respectively) since the tree contribution is only proportional to F_1. Moreover, from the range of allowed values of N_c^{eff}, we can estimate the upper limit of this branching ratio to be of the order 4×10^{-6}. Finally, we focus on the branching ratio $B^{\pm} \to \omega K^{\pm}$ which is plotted in Fig. 5.11 for models (1) and (2). We find that both the experimental and theoretical results are in agreement for a large range of values of N_c^{eff}. But, models (1) and (2) do not give similar results because the form factors F_1, applied in these models, are very different. Moreover, the dependence of the branching ratio on the CKM parameters ρ and η indicates

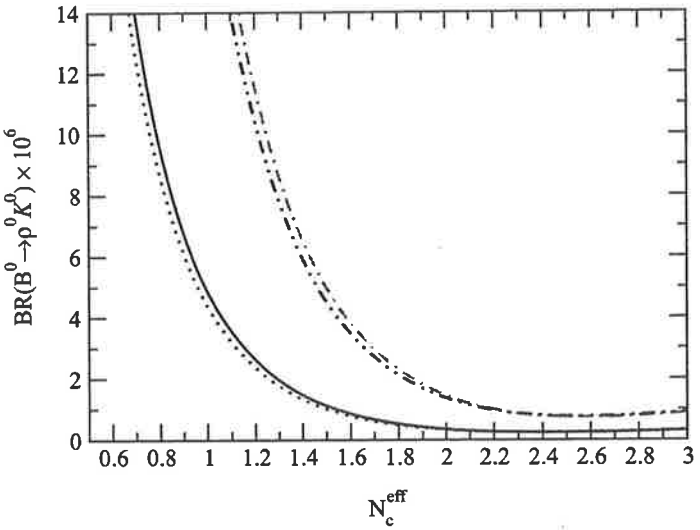

Figure 5.10: Branching ratio for $B^0 \to \rho^0 K^0$, for models 1(2), $q^2/m_b^2 = 0.3$ and limiting values of the CKM matrix elements. Solid line (dotted line) for model (1) and max (min) CKM matrix elements. Dot-dashed line (dot-dot-dashed line) for model (2) and max (min) CKM matrix elements.

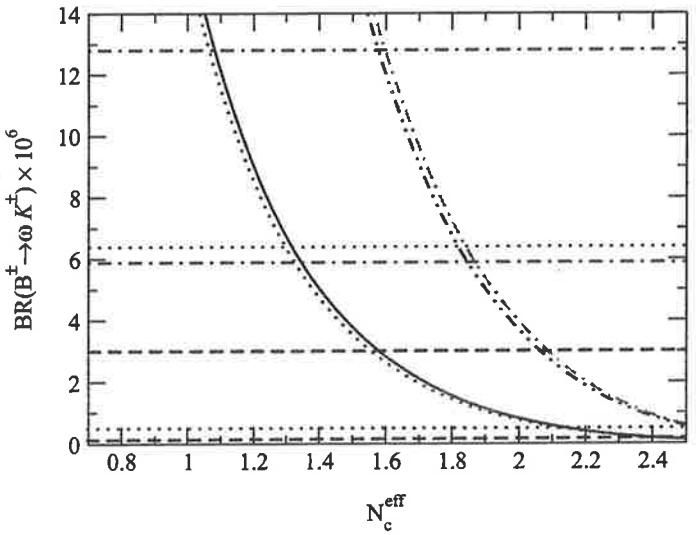

Figure 5.11: Branching ratio for $B^{\pm} \to \omega K^{\pm}$, for models 1(2), $q^2/m_b^2 = 0.3$ and limiting values of the CKM matrix elements. Solid line (dotted line) for model (1) and max (min) CKM matrix elements. Dot-dashed line (dot-dot-dashed line) for model (2) and max (min) CKM matrix elements. Same notation as in Fig. 5.7 for the horizontal lines.

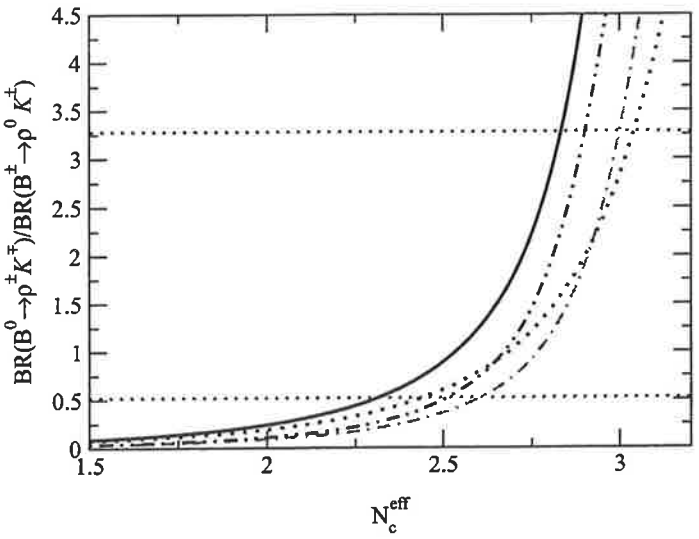

Figure 5.12: The ratio of two ρK branching ratios versus N_c^{eff} for models 1(2) and for limiting values of the CKM matrix elements. Solid line (dotted line) for model (1) with max (min) CKM matrix elements. Dot-dashed line (dot-dot-dashed line) for model (2) with max (min) CKM matrix elements. Same notation as in Fig. 5.7 for the horizontal lines.

that it would be possible to strongly constrain ρ and η with a very accurate experimental measurement for the decay $B^- \to \omega K^-$.

To remove systematic errors in branching ratios given by the B factories, we look at the ratio, R_K, between the two branching ratios $\mathscr{B}(B^0 \to \rho^\pm K^\mp)$ and $\mathscr{B}(B^\pm \to \rho^0 K^\mp)$. The ratio is plotted in Fig. 5.12 as a function of N_c^{eff}, for models (1) and (2) and for limiting values of the CKM matrix elements. These results indicate that the ratio is very sensitive to both N_c^{eff} and to the magnitude of the form factors. The sensitivity increases with the value of N_c^{eff} and gives a large difference between models $(1,3)$ and (5) and models (2) and (4). We found that for a definite range of N_c^{eff}, all models investigated give a ratio consistent with the experimental data from CLEO. It should be noted that R_K is not very sensitive to the CKM matrix elements. Indeed, if we only take into account the tree contributions, R_K is independent of the CKM parameters ρ and η. The difference which appears comes from the penguin contribution and has to be taken into account in any approach since they are not negligible. To extract a common behaviour for both $B \to \rho\pi$ and $B \to \rho K$ decays, we calculate the ratio, R, between R_π and R_K, defined in Eqs. (5.28) and (5.42), respectively. In Fig 5.13, the ratio is given as a function of N_c^{eff} for models (1) and (2). The results show that model (1) is agreement with the experimental data (CLEO) for

$B \to \rho K$	$\{N_c^{eff}\}$
model (1)	0.66;2.68(0.61;2.68)
model (2)	1.17;2.84(1.09;2.82)
maximum range	0.66;2.84(0.61;2.82)
minimum range	1.17;2.68(1.09;2.68)

Table 5.7: Best range of N_c^{eff} determined for $q^2/m_b^2 = 0.3(0.5)$ and for $B \to \rho K$ decays.

a range of N_c^{eff} varying between 2.5 to 4.2, whereas it agrees from 2.8 and 3.45 for model (2). In addition to the CKM matrix elements and form factor effects (already discussed in detail previously), both models (1) and (2) have a critical point (minimum value of the ratio R) near $N_c^{eff} = N_c = 3$.

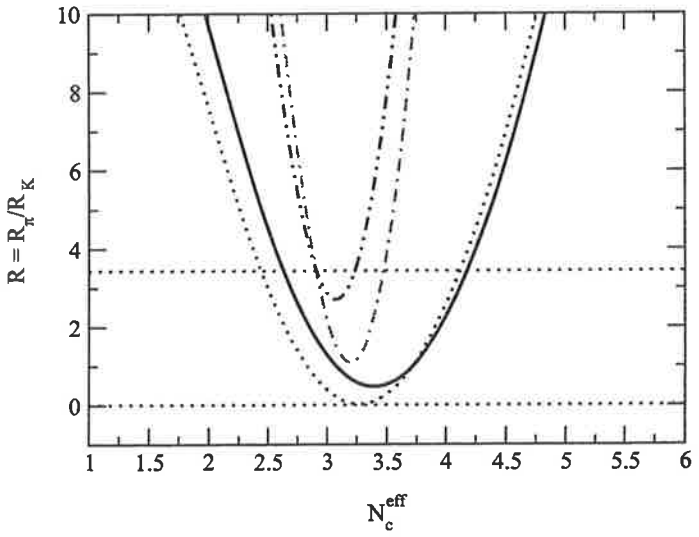

Figure 5.13: Ratio, R, between R_π and R_K for models 1(2), $q^2/m_b^2 = 0.3$ and limiting values of the CKM matrix elements. Solid line (dotted line) for model (1) and max (min) CKM matrix elements. Dot-dashed line (dot-dot-dashed line) for model (2) and max (min) CKM matrix elements. Same notation as in Fig. 5.7 for the horizontal lines.

We have summarized for each model, each branching ratio and each set of limiting values of CKM matrix elements, the allowed range of N_c^{eff} within which the experimental data and numerical results are consistent. To determine the best range of N_c^{eff}, we have to find some intersection of values

of N_c^{eff} for each model and each set of CKM matrix elements, for which the theoretical and experimental results are consistent. Since the experimental results are not numerous and not as accurate as one would like, it is more reasonable to fix the upper and lower limits of N_c^{eff} which allow us the maximum of agreement between the theoretical and experimental approaches. By using the limiting values of the CKM matrix elements we show in Table 5.7, the range of allowed values of N_c^{eff} with $\rho - \omega$ mixing. Even though in the previous study for $B \to \rho\pi$, we have restricted ourselves to models (2) and (4) rather than models $(1,3)$ and (5), here, we cannot exclude one of the models $(1,2,3,4)$ and (5) because of the lack of accurate experimental data. We find that N_c^{eff} should be in the following range: $0.66(0.61) < N_c^{eff} < 2.84(2.82)$, where the values outside and inside brackets correspond to the choice $q^2/m_b^2 = 0.3(0.5)$.

5.6 Summary

We have calculated the branching ratios $B^\pm \to \rho^0\pi^\pm$, $B^\pm \to \rho^\pm\pi^0$, $B^0 \to \rho^\pm\pi^\mp$, $B^0 \to \rho^0\pi^0$ and $B^\pm \to \omega\pi^\pm$ and compared the results with experimental data coming from the CLEO, BABAR and BELLE Collaborations. We have shown that for models (2) and (4) there is a range for N_c^{eff}, $1.09(1.11) < N_c^{eff} < 1.68(1.80)$, in which theoretical results are consistent with experimental data. Models $(1,3)$ and (5) are excluded since the form factor $F_1(k^2)$ in these models cannot produce results consistent with experiment. For a deeper investigation into this problem, some resonant and non-resonant contributions [106, 107, 108, 109, 110, 111] which may carry bigger effects than expected in the calculation of branching ratios in $\rho\pi$ may have to be considered seriously.

As regards theoretical results for the branching ratios $B^\pm \to \rho^0 K^\pm$, $B^\pm \to \rho^\pm K^0$, $B^0 \to \rho^\pm K^\mp$, $B^0 \to \rho^0 K^0$ and $B^\pm \to \omega K^\pm$, we made comparison by using experimental data from the same factories as for $\rho\pi$. We found that it is possible to have agreement between the theoretical results and experimental branching ratio data for $B^\pm \to \rho^0 K^\pm$, $B^\pm \to \rho^\pm K^0$, $B^\pm \to \omega K^\pm$, $B^0 \to \rho^\pm K^\mp$, and R. For $B^0 \to \rho^0 K^0$, the lack of results does not allow us to draw conclusions. Only an estimate for the upper limit (4×10^{-6}) has been determined.

In comparison with the situation for $B \to \rho\pi$, it is not possible in the case of $B \to \rho K$, to exclude one of the models because of the lack of experimental data. Nevertheless, we have determined a range of value of N_c^{eff}, $0.66(0.61) < N_c^{eff} < 2.84(2.82)$, inside of which the experimental data and theoretical calculations are consistent for all the models. We have to keep in

mind that, because of the difficulty in dealing with non-factorizable effects associated with final state interactions (FSI), which are more complex for decays involving an s quark, we have weakly constrained the range of value of N_c^{eff}.

global maximum range	0.66;2.84(0.61;2.82)
global minimum range	1.17;1.63(1.12;1.77)

Table 5.8: Global range of N_c^{eff} from both B decays.

Finally, if we take into account the allowed range of N_c^{eff} determined from decays such as $B \to \rho\pi$ and $B \to \rho K$ we find a maximum global allowed range of N_c^{eff} which should be in the range $0.66(0.61) < N_c^{eff} < 2.84(2.82)$ (see Table 5.8). This gives us a mean average value for N_c^{eff} around 1.75.

Chapter 6

Direct CP violation via $\rho - \omega$ mixing

" Avec l'avion, nous avons appris la ligne droite. "

Antoine de Saint-Exupéry

After the computation of branching ratios in $B \to \rho M_1$, where M_1 is either K or π, and the comparison with experimental data from three main factories (BABAR, BELLE, and CLEO), we are now able to constrain the investigation of CP violating asymmetry through the effective number of colours, N_c^{eff}. This chapter first starts by analysing the CP violating asymmetry, a_{CP}, in the process $B^{\pm,0} \to \pi^+\pi^-\pi^{\pm,0}$. Then, we also shall study the process $B^{\pm,0} \to \pi^+\pi^- K^{\pm,0}$ in a similar way in order to give some predictions concerning direct CP violation in B decays.

6.1 Calculational details

The calculation of the CP violating asymmetry, including $\rho - \omega$ mixing, has already been discussed in detail in Chapter 4. We just remind that the asymmetry, a_{CP}, can be written as,

$$a_{CP} \equiv \frac{|A|^2 - |\bar{A}|^2}{|A|^2 + |\bar{A}|^2} = \frac{-2r \sin\delta \sin\phi}{1 + 2r \cos\delta \cos\phi + r^2} \,, \tag{6.1}$$

where all quantities are explained in Chapter 4. As we see in Eq. (6.1), the asymmetry, a_{CP}, can be expressed in terms of r (the ratio between the tree and penguin amplitudes), and the strong and weak phases, δ and ϕ, respectively. Therefore, to determine these quantities, we shall use (see Chapter 4

for more details) the following expression which involves the $\rho - \omega$ mixing amplitude, $\tilde{\Pi}_{\rho\omega}$:

$$re^{i\delta}e^{i\phi} = \frac{\tilde{\Pi}_{\rho\omega}p_\omega + s_\omega p_\rho}{\tilde{\Pi}_{\rho\omega}t_\omega + s_\omega t_\rho} \ . \tag{6.2}$$

As regards the calculational details, we apply the factorization approximation to evaluate the matrix elements which arise in the penguin and tree amplitudes. For the form factors $F_1(k^2)$ and $A_0(k^2)$, we adopt, the same models as we did for the calculation of branching ratios. More details can be found in Chapter 5. Finally, all the numerical inputs (CKM values, quark masses and decay constants) are also listed in Chapter 5.

6.2 $B^{\pm,0} \to \pi^+\pi^-\pi^{\pm,0}$

6.2.1 Formulae

In this section, we apply the formalism derived in Chapter 4 and write down all the analytical expressions necessary to calculate the CP violating asymmetry parameter, a_{CP}. We first focus on the case where $M_1 = \{\pi^-\}$.

Case of $B^- \to \pi^+\pi^-\pi^-$

Using the decomposition given in Eqs. (5.5, 5.6), one has for the tree operator contribution,

$$t_\rho = m_B|\vec{p}_\rho|\left[(C_1' + \frac{1}{N_c}C_2')f_\rho F_1(m_\rho^2) + (C_2' + \frac{1}{N_c}C_1')f_\pi A_0(m_\pi^2)\right] \ . \tag{6.3}$$

where $\vec{p}_\rho$ is the three momentum of the ρ. In the same way, we find $t_\omega = t_\rho$, so that gives us,

$$\alpha e^{i\delta_\alpha} = t_\omega/t_\rho = 1 \ . \tag{6.4}$$

After calculating the ρ and ω penguin operator contributions, one has first,

$$\begin{aligned}\beta e^{i\delta_\beta} = \frac{p_\rho}{p_\omega} = \frac{m_B|\vec{p}_\rho|}{p_\omega}\Bigg\{ & (C_4' + \frac{1}{N_c}C_3')[-f_\rho F_1(m_\rho^2) + f_\pi A_0(m_\pi^2)] \\ & + \frac{3}{2}[(C_7' + \frac{1}{N_c}C_8') + (C_9' + \frac{1}{N_c}C_{10}')]f_\rho F_1(m_\rho^2) \\ & - [(C_6' + \frac{1}{N_c}C_5') + (C_8' + \frac{1}{N_c}C_7')]\left[\frac{2m_\pi^2 f_\pi A_0(m_\pi^2)}{(m_u + m_d)(m_b + m_u)}\right] \\ & + (C_{10}' + \frac{1}{N_c}C_9')[\frac{1}{2}f_\rho F_1(m_\rho^2) + f_\pi A_0(m_\pi^2)]\Bigg\} \ , \end{aligned} \tag{6.5}$$

and the ratio between the ω penguin and ρ tree (from which we can extract the weak CKM matrix phase ϕ) is,

$$r'e^{i\delta_q} = -\frac{p_\omega}{(C_1' + \frac{1}{N_c}C_2')f_\rho F_1(m_\rho^2) + (C_2' + \frac{1}{N_c}C_1')f_\pi A_0(m_\pi^2)} \left|\frac{V_{tb}V_{td}^\star}{V_{ub}V_{ud}^\star}\right| . \quad (6.6)$$

The expression for the matrix element of the ω penguin operator is,

$$\begin{aligned} p_\omega = m_B|\vec{p}_\rho|\Bigg\{ & 2\left[(C_3' + \frac{1}{N_c}C_4') + (C_5' + \frac{1}{N_c}C_6')\right] f_\rho F_1(m_\rho^2) \\ & + \frac{1}{2}\left[(C_7' + \frac{1}{N_c}C_8') + (C_9' + \frac{1}{N_c}C_{10}')\right] f_\rho F_1(m_\rho^2) \\ & - 2\left[(C_8' + \frac{1}{N_c}C_7') + (C_6' + \frac{1}{N_c}C_5')\right]\left[\frac{m_\pi^2 f_\pi A_0(m_\pi^2)}{(m_u + m_d)(m_b + m_u)}\right] \\ & + (C_4' + \frac{1}{N_c}C_3')\left[f_\pi A_0(m_\pi^2) + f_\rho F_1(m_\rho^2)\right] \\ & + (C_{10}' + \frac{1}{N_c}C_9')\left[f_\pi A_0(m_\pi^2) - \frac{1}{2}f_\rho F_1(m_\rho^2)\right]\Bigg\} , \end{aligned} \quad (6.7)$$

while the ratio of CKM matrix elements ratio is:

$$\left|\frac{V_{tb}V_{td}^\star}{V_{ub}V_{ud}^\star}\right| = \frac{\sqrt{(1-\rho)^2 + \eta^2}}{(1 - \lambda^2/2)\sqrt{\rho^2 + \eta^2}} = \left(1 - \frac{\lambda^2}{2}\right)^{-1}\left|\frac{\sin\gamma}{\sin\beta}\right| , \quad (6.8)$$

where the angles γ and β are defined in the unitarity triangle (see Chapter 2). To simplify the formulas we used N_c for N_c^{eff} in Eqs. (5.3)-(5.11))

Case of $\bar{B}^0 \to \pi^+\pi^-\pi^0$

In a similar way, we write down the expressions[1] necessary to calculate the asymmetry when $M_1 = \{\pi^0\}$. The ρ tree operator contribution for this given decay is,

$$t_\rho = m_B|\vec{p}_\rho|\left[(C_1' + \frac{1}{N_c}C_2')\right]\left(f_\rho F_1(m_\rho^2) + f_\pi A_0(m_\pi^2)\right) , \quad (6.9)$$

where all the variables are as previously defined. We find in this case that $t_\omega \neq t_\rho$, and we have:

$$\alpha e^{i\delta_\alpha} = \frac{-f_\rho F_1(m_\rho^2) + f_\pi A_0(m_\pi^2)}{f_\rho F_1(m_\rho^2) + f_\pi A_0(m_\pi^2)} . \quad (6.10)$$

[1]Read $F_1(m_\rho^2)$ as $F_1^{B\to\pi}(m_\rho^2)$ and $A_0(m_\pi^2)$ as $A_0^{B\to\rho}(m_\pi^2)$.

After calculating the penguin operator contributions, one gets,

$$\begin{aligned}\beta e^{i\delta_\beta} = \frac{m_B|\vec{p}_\rho|}{p_\omega}\Bigg\{ & -(C'_4+\frac{1}{N_c}C'_3)[f_\rho F_1(m_\rho^2)+f_\pi A_0(m_\pi^2)] \\ & -\frac{3}{2}[(C'_7+\frac{1}{N_c}C'_8)-(C'_9+\frac{1}{N_c}C'_{10})]f_\pi A_0(m_\pi^2) \\ & +\frac{3}{2}[(C'_7+\frac{1}{N_c}C'_8)+(C'_9+\frac{1}{N_c}C'_{10})]f_\rho F_1(m_\rho^2) \\ & +[(C'_6+\frac{1}{N_c}C'_5)-\frac{1}{2}(C'_8+\frac{1}{N_c}C'_7)]\left[\frac{2m_\pi^2 f_\pi A_0(m_\pi^2)}{(m_d+m_d)(m_b+m_d)}\right] \\ & +\frac{1}{2}(C'_{10}+\frac{1}{N_c}C'_9)[f_\rho F_1(m_\rho^2)+f_\pi A_0(m_\pi^2)]\Bigg\}, \end{aligned} \tag{6.11}$$

$$r'e^{i\delta_q} = -\frac{p_\omega}{(C'_1+\frac{1}{N_c}C'_2)\left(f_\rho F_1(m_\rho^2)+f_\pi A_0(m_\pi^2)\right)}\left|\frac{V_{tb}V_{td}^*}{V_{ub}V_{ud}^*}\right| . \tag{6.12}$$

Once again the ratio of CKM matrix elements is given in Eq. (6.8) and the ω penguin operator has the following expression,

$$\begin{aligned} p_\omega = m_B|\vec{p}_\rho|\Bigg\{ & -2\left[(C'_3+\frac{1}{N_c}C'_4)+(C'_5+\frac{1}{N_c}C'_6)\right]f_\rho F_1(m_\rho^2) \\ & -\frac{1}{2}\left[(C'_7+\frac{1}{N_c}C'_8)+(C'_9+\frac{1}{N_c}C'_{10})\right]f_\rho F_1(m_\rho^2) \\ & -\left[\frac{1}{2}(C'_8+\frac{1}{N_c}C'_7)-(C'_6+\frac{1}{N_c}C'_5)\right]\left[\frac{2m_\pi^2 f_\pi A_0(m_\pi^2)}{(m_d+m_d)(m_b+m_d)}\right] \\ & -(C'_4+\frac{1}{N_c}C'_3)\left[f_\pi A_0(m_\pi^2)+f_\rho F_1(m_\rho^2)\right] \\ & +\frac{1}{2}(C'_{10}+\frac{1}{N_c}C'_9)\left[f_\pi A_0(m_\pi^2)+f_\rho F_1(m_\rho^2)\right]\Bigg\} . \end{aligned} \tag{6.13}$$

6.2.2 Results and discussions

In our analysis, we are going to show the dependence on the CKM matrix elements and form factors of the direct CP violating asymmetry in B decays. We aim to include the latest values of the Wolfenstein CKM parameters, ρ and η. In the following numerical calculations, we apply all the formalism detailed previously and we investigate more precisely two channels of B decay asymmetries. These are $\bar{B}^0 \to \pi^+\pi^-\pi^0$ and $B^- \to \pi^+\pi^-\pi^-$. We find

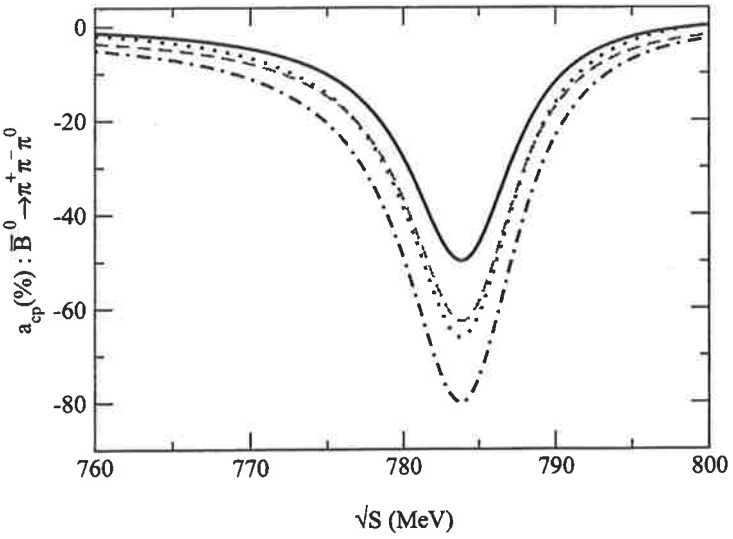

Figure 6.1: CP violating asymmetry, a_{CP}, for $\bar{B}^0 \to \pi^+\pi^-\pi^0$, for $q^2/m_b^2 = 0.3$, $N_c^{eff} = 1.09(1.68)$ and limiting values of the CKM matrix elements for model (1): solid line (dotted line) for $N_c^{eff} = 1.09$ and max(min) CKM matrix elements. Dashed line (dot-dashed line) for $N_c^{eff} = 1.68$ and max(min) CKM matrix elements.

that for a fixed N_c^{eff}, there is a maximum value, a_{max}, for the CP violating parameter, a_{CP}, when the invariant mass of the $\pi^+\pi^-$ is in the vicinity of the ω resonance. In Figs. 6.1 and 6.2, we show the CP violating asymmetries for $\bar{B}^0 \to \pi^+\pi^-\pi^0$, $q^2/m_b^2 = 0.3$ with $N_c^{eff} = 1.09(1.68)$, and $q^2/m_b^2 = 0.5$ with $N_c^{eff} = 1.11(1.80)$, and for limiting values of CKM matrix elements, respectively. These results are shown for model (1), as an example. In Figs. 6.3 and 6.4, CP violating asymmetries are also given in the case $B^- \to \pi^+\pi^-\pi^-$. Both studies are done with the same approach. We investigate five models, with five different form factors in order to show the model dependence of a_{CP}.

As regards the maximum CP violating asymmetry for $\bar{B}^0 \to \pi^+\pi^-\pi^0$, a_{max}, varies from $-51\%(-38\%)$ to $-84\%(-69\%)$ in the allowed range of ρ, η for $q^2/m_b^2 = 0.3(0.5)$. From the numerical results listed in Table 6.1, for $N_{cmin}^{eff} = 1.09(1.11)$ and $N_{cmax}^{eff} = 1.68(1.80)$, we can see that the five models fall into two classes: models $(1,3)$ and (5) and models (2) and (4). For models $(1,3)$ and (5), and for $N_{cmin}^{eff} = 1.09(1.11)$, the maximum asymmetry, a_{max}, is around $-54\%(-40\%)$ for the set (ρ_{max}, η_{max}) and around $-69\%(-53.6\%)$ for the set (ρ_{min}, η_{min}), leading to the ratio between them around 1.28(1.34). In each of these models and for $N_{cmax}^{eff} = 1.68(1.80)$, the maximum value of the asymmetry, a_{max}, reaches $-62.6\%(-48.6\%)$ for the set (ρ_{max}, η_{max}) to

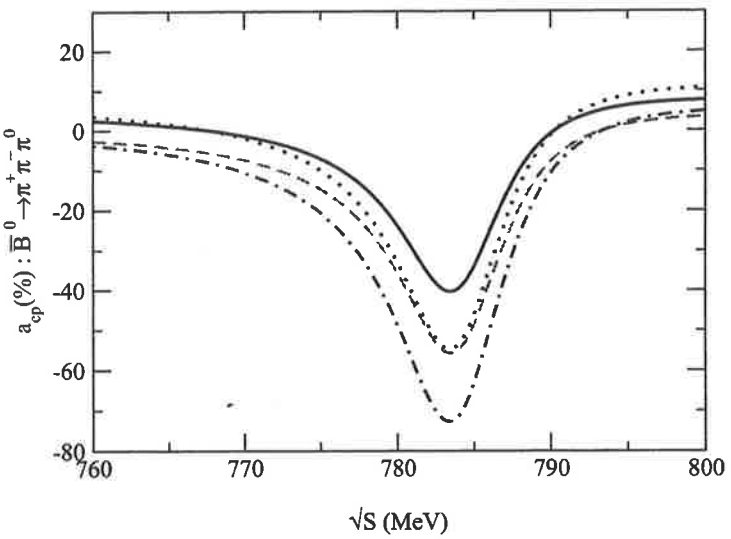

Figure 6.2: CP violating asymmetry, a_{CP}, for $\bar{B}^0 \to \pi^+\pi^-\pi^0$, for $q^2/m_b^2 = 0.5$, $N_c^{eff} = 1.11(1.80)$ and limiting values of the CKM matrix elements for model (1): solid line (dotted line) for $N_c^{eff} = 1.11$ and max(min) CKM matrix elements. Dashed line (dot-dashed line) for $N_c^{eff} = 1.80$ and max(min) CKM matrix elements.

around $-77.3\%(-64.6\%)$ for the set (ρ_{min}, η_{min}). In that case, the ratio is equal to 1.23(1.32). If we consider models (2) and (4), the maximum asymmetry, a_{max}, where $N_{cmin}^{eff} = 1.09(1.11)$, is around $-63.5\%(-48\%)$ for the set (ρ_{max}, η_{max}) and around $-78.5\%(-62\%)$ for the set (ρ_{min}, η_{min}). This yields a ratio of order 1.24(1.29). When $N_{cmax}^{eff} = 1.68(1.80)$, one has a maximum of asymmetry around $-71\%(-56.5\%)$ for the set (ρ_{max}, η_{max}) and around $-84\%(-69\%)$ for the set (ρ_{min}, η_{min}), leading to a ratio around 1.18(1.22).

Now let us consider $B^- \to \pi^+\pi^-\pi^-$. All the numerical values can be found in Table 6.2. Once again, the models fall into two classes as in $\bar{B}^0 \to \pi^+\pi^-\pi^0$. For models (1,3) and (5), and for $N_{cmin}^{eff} = 1.09(1.11)$, one finds the maximum value of the CP violating asymmetry, a_{max}, around $-32.3\%(-25.3\%)$ for the set (ρ_{max}, η_{max}) and around $-43.6\%(-34.3\%)$ for the set (ρ_{min}, η_{min}). For $N_{cmax}^{eff} = 1.68(1.80)$, we find that the value of a_{max} is around $-29.6\%(-20.3\%)$ and $-40.3\%(-27.6\%)$ for the given maximum and minimum sets of (ρ, η). The corresponding ratios between asymmetries are around 1.34(1.35) and 1.36(1.36). For the second class of model (models (2) and (4)), the maximum CP violating asymmetry, a_{max}, for $N_{cmin}^{eff} = 1.09(1.11)$, is around $-38\%(-30\%)$ and around $-50.5\%(-40.5\%)$ for the maximum and minimum set of (ρ, η), respectively. Finally, for $N_{cmax}^{eff} = 1.68(1.80)$, one gets $-38.5\%(-27.5\%)$ and $-52.5\%(-38\%)$. The ratio is

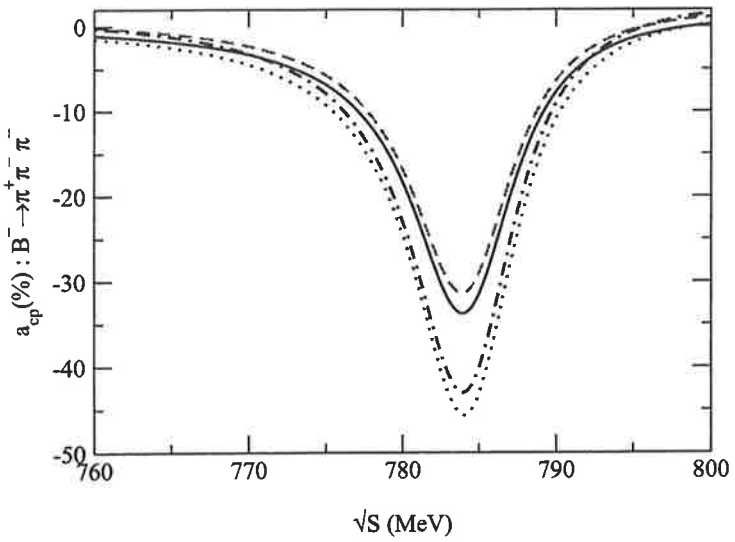

Figure 6.3: CP violating asymmetry, a_{CP}, for $B^- \to \pi^+\pi^-\pi^-$, for $q^2/m_b^2 = 0.3$, $N_c^{eff} = 1.09(1.68)$ and limiting values of the CKM matrix elements for model (1): solid line (dotted line) for $N_c^{eff} = 1.09$ and max(min) CKM matrix elements. Dashed line (dot-dashed line) for $N_c^{eff} = 1.68$ and max(min) CKM matrix elements.

equal to 1.32(1.35) when $N_{cmin}^{eff} = 1.09(1.11)$ and is around 1.36(1.38) when $N_{cmax}^{eff} = 1.68(1.80)$.

From all these results, many comments can be enumerated. Although the maximum asymmetry, a_{max}, still varies over some range in both cases ($B^- \to \pi^+\pi^-\pi^-$ and $\bar{B}^0 \to \pi^+\pi^-\pi^0$), we want to stress that by using more accurate CKM element values than before, a more precise CP violating asymmetry is obtained. The reason is primarily the matrix elements V_{td} and V_{ub} which are involved in the $b \to d$ transition through the ratio of p_ω to t_ρ. In our preliminary CP violation study where we used the values $A = 0.815, \lambda = 0.2205, 0.09 < \rho < 0.254$ and $0.323 < \eta < 0.442$, for the process $B^- \to \pi^+\pi^-\pi^-$, we found that the ratio between maximum and minimum asymmetry related to the minimum and maximum set of (ρ, η), was around 1.6. By comparison, in the present work, this ratio is reduced to 1.3. The difference is related to the improvement in the measurement of the CKM matrix elements, and shows the strong effect of the CKM parameters, ρ and η, on limiting asymmetry values.

With regard to the CKM matrix elements, it appears that if we take their upper limit, we obtain a smaller asymmetry, a_{CP}, and vice-versa. As we found before, there is still a strong dependence of the CP violating asymmetry on the form factors. The difference between the two classes of models,

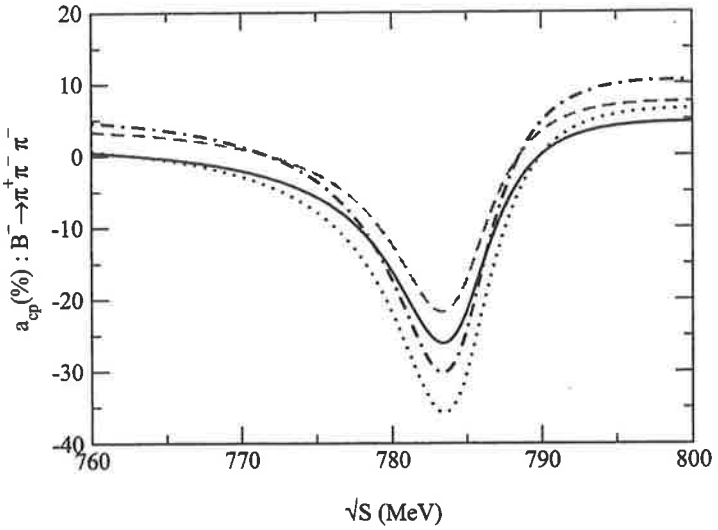

Figure 6.4: CP violating asymmetry, a_{CP}, for $B^- \to \pi^+\pi^-\pi^-$, for $q^2/m_b^2 = 0.5$, $N_c^{eff} = 1.11(1.80)$ and limiting values of the CKM matrix elements for model (1): solid line (dotted line) for $N_c^{eff} = 1.11$ and max(min) CKM matrix elements. Dashed line (dot-dashed line) for $N_c^{eff} = 1.80$ and max(min) CKM matrix elements.

$(1,3,5)$ and $(2,4)$, comes mainly from the magnitudes of the form factors. In fact, the form factor $F_1(k^2)$, which describes the transition $B \to \pi$, is mainly responsible for this dependence. In both classes, we find a stronger dependence of the CP violating asymmetry on the CKM matrix elements than that on the form factors or the effective parameter N_c^{eff}. The difference observed in our results between $q^2/m_b^2 = 0.3$ and $q^2/m_b^2 = 0.5$ arises from the renormalization scheme of the Wilson coefficients in the weak effective Hamiltonian. Finally, since N_c^{eff} (treated as a free parameter) is related to hadronization effects through the factorization approach, it is not possible to determine its value accurately since non-factorizable effects are not well known. That is why the asymmetry also varies in some range of N_c^{eff}. It is obvious that a more accurate value for N_c^{eff} (which requires a more accurate approach with non-factorizable effects being taken into account), and hadronic decay form factors (which requires better a understanding of the pion structure and the $B \to \pi$ transition) are needed in order to determine the CKM matrix elements.

In spite of all the uncertainties mentioned above, we stress that the $\rho - \omega$ mixing mechanism in the $B \to \rho\pi$ decay can be used to remove ambiguity concerning the sign of $\sin\delta$. As the internal top quark dominates the $b \to d$ transition, the weak phase in the asymmetry is proportional to $\sin\alpha$ (=

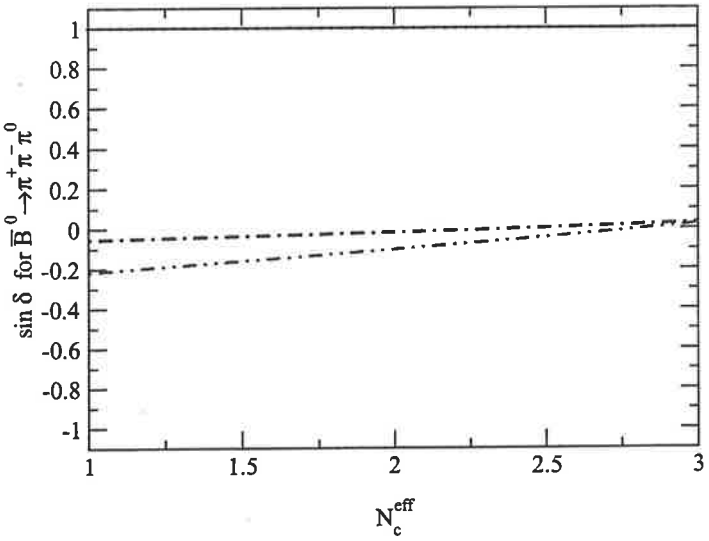

Figure 6.5: $\sin\delta$ as a function of N_c^{eff}, for $\bar{B}^0 \to \pi^+\pi^-\pi^0$, for $q^2/m_b^2 = 0.3(0.5)$ and for model (1). The solid (dotted) line at $\sin\delta = +1$ corresponds the case $\tilde{\Pi}_{\rho\omega} = (-3500; -300)$, where $\rho - \omega$ mixing is included. The dot-dashed (dot-dot-dashed) line corresponds to $\tilde{\Pi}_{\rho\omega} = (0; 0)$, where $\rho-\omega$ mixing is not included.

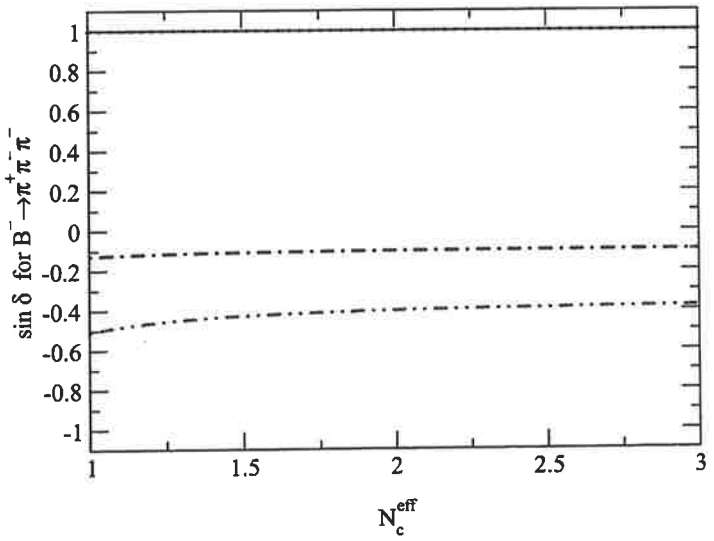

Figure 6.6: $\sin\delta$ as a function of N_c^{eff}, for $B^- \to \pi^+\pi^-\pi^-$, for $q^2/m_b^2 = 0.3(0.5)$ and for model (1). The solid (dotted) line at $\sin\delta = +1$ corresponds the case $\tilde{\Pi}_{\rho\omega} = (-3500; -300)$, where $\rho - \omega$ mixing is included. The dot-dashed (dot-dot-dashed) line corresponds to $\tilde{\Pi}_{\rho\omega} = (0; 0)$, where $\rho-\omega$ mixing is not included.

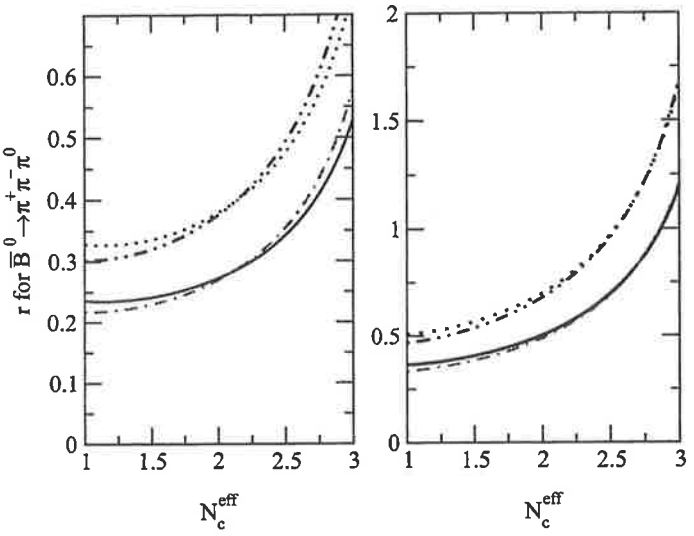

Figure 6.7: The ratio of penguin to tree amplitudes, r, as a function of N_c^{eff}, for $\bar{B}^0 \to \pi^+\pi^-\pi^0$, for $q^2/m_b^2 = 0.3(0.5)$, for limiting values of the CKM matrix elements (ρ, η) max(min), for $\tilde{\Pi}_{\rho\omega} = (-3500; -300)(0, 0)$, (i.e. with(without) $\rho - \omega$ mixing) and for model (1). Figure 6.7a (left): for $\tilde{\Pi}_{\rho\omega} = (0; 0)$, solid line (dotted line) for $q^2/m_b^2 = 0.3$ and (ρ, η) max(min). Dot-dashed line (dot-dot-dashed line) for $q^2/m_b^2 = 0.5$ and (ρ, η) max(min). Figure 6.7b (right): same caption but for $\tilde{\Pi}_{\rho\omega} = (-3500; -300)$.

$\sin\phi$), where $\alpha = \arg\left[-\frac{V_{td}V_{tb}^*}{V_{ud}V_{ub}^*}\right]$. Hence knowing the sign of $\sin\delta$ enables us to determine that of $\sin\alpha$ from a measurement of the asymmetry, a_{CP}. In Figs. 6.5 and 6.6 we show $\sin\delta$ as a function of N_c^{eff} for $\bar{B}^0 \to \pi^+\pi^-\pi^0$ and $B^- \to \pi^+\pi^-\pi^-$, respectively, when we have maximum CP violation. In our determined range of N_c^{eff}, $(1.09(1.68) < N_c^{eff} < 1.11(1.80))$, one finds that its sign is always positive for all the models studied and for all the form factors. Therefore, by measuring the CP violating asymmetry in $B^{\pm,0} \to \pi^+\pi^-\pi^{\pm,0}$ decays, we can remove the mod(π) uncertainty which appears in the determination for α from the usual indirect measurements which yield $\sin 2\alpha$.

In Figs. 6.7 and 6.8, the ratio of the penguin and tree amplitudes, as a function of N_c^{eff}, is plotted for limiting values of the CKM matrix elements, ρ, η, for the processes $B^{\pm,0} \to \pi^+\pi^-\pi^{\pm,0}$. Even though one gets a large value of $\sin\delta$ around $N_c^{eff} = 1$, for $\bar{B}^0 \to \pi^+\pi^-\pi^0$, without $\rho - \omega$ mixing, one still has a small value for r around this value of N_c^{eff}. Similarly, we observe the same phenomena for $B^- \to \pi^+\pi^-\pi^-$ when $N_c^{eff} = 0.5$. In both cases, the CP violating asymmetry, a_{CP}, remains very small without $\rho - \omega$ mixing.

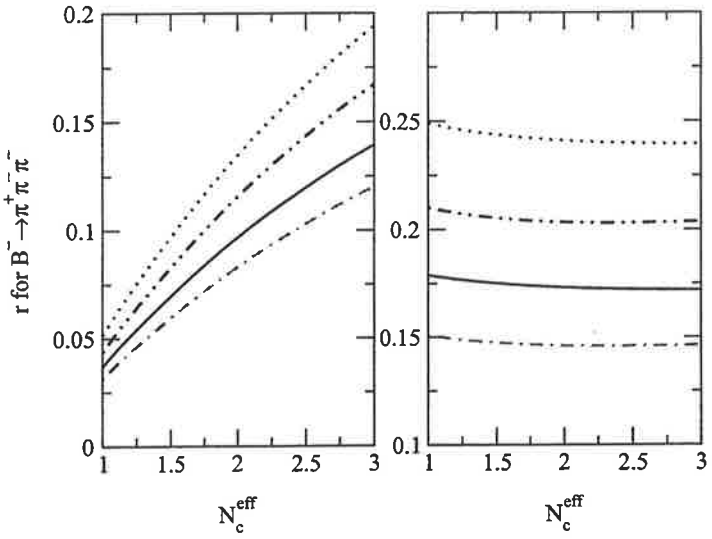

Figure 6.8: The ratio of penguin to tree amplitudes, r, as a function of N_c^{eff} for $B^- \to \pi^+\pi^-\pi^-$. Same caption for Figure 6.8a (left) and Figure 6.8b (right) as in Fig. 6.7.

	$N_{cmin}^{eff} = 1.09(1.11)$	$N_{cmax}^{eff} = 1.68(1.80)$
model (1)		
ρ_{max}, η_{max}	-55(-41)	-65(-51)
ρ_{min}, η_{min}	-72(-55)	-80(-65)
model (2)		
ρ_{max}, η_{max}	-63(-48)	-71(-56)
ρ_{min}, η_{min}	-78(-62)	-84(-69)
model (3)		
ρ_{max}, η_{max}	-56(-41)	-65(-51)
ρ_{min}, η_{min}	-72(-55)	-80(-69)
model (4)		
ρ_{max}, η_{max}	-64(48)	-71(-57)
ρ_{min}, η_{min}	-79(62)	-84(-69)
model (5)		
ρ_{max}, η_{max}	-51(-38)	-58(-44)
ρ_{min}, η_{min}	-63(-51)	-72(-60)

Table 6.1: Maximum CP violating asymmetry $a_{max}(\%)$ for $\bar{B}^0 \to \pi^+\pi^-\pi^0$, for all models, limiting (upper and lower) values of the CKM matrix elements, and $q^2/m_b^2 = 0.3(0.5)$.

	$N_{c_{min}}^{eff} = 1.09(1.11)$	$N_{c_{max}}^{eff} = 1.68(1.80)$
model (1)		
ρ_{max}, η_{max}	-33(-26)	-32(-22)
ρ_{min}, η_{min}	-45(-36)	-43(-30)
model (2)		
ρ_{max}, η_{max}	-38(-30)	-38(-27)
ρ_{min}, η_{min}	-50(-40)	-52(-38)
model (3)		
ρ_{max}, η_{max}	-34(-27)	-32(-22)
ρ_{min}, η_{min}	-45(-36)	-44(-30)
model (4)		
ρ_{max}, η_{max}	-38(-30)	-39(-28)
ρ_{min}, η_{min}	-51(-41)	-53(-38)
model (5)		
ρ_{max}, η_{max}	-30(-23)	-25(-17)
ρ_{min}, η_{min}	-41(-31)	-34(-23)

Table 6.2: Maximum CP violating asymmetry $a_{max}(\%)$ for $B^- \to \pi^+\pi^-\pi^-$, for all models, limiting values of the CKM matrix elements (upper and lower limit), and for $q^2/m_b^2 = 0.3(0.5)$.

Thus $\rho - \omega$ mixing plays an essential role in both enhancing the direct CP violation and rendering the analysis of the result free of ambiguity.

6.3 $B^{\pm,0} \to \pi^+\pi^- K^{\pm,0}$

6.3.1 Formulae

After the study of direct CP violation in the $b \to d$ transition, we now investigate the CP violating asymmetry, a_{CP}, in the $b \to s$ quark transition. We begin by calculating all the tree and penguin operator contributions[2] in the charged decay $B^\pm \to \pi^+\pi^- K^\pm$.

[2]Read $F_1(m_\rho^2)$ as $F_1^{B\to K}(m_\rho^2)$ and $A_0(m_K^2)$ as $A_0^{B\to\rho}(m_K^2)$.

Case of $B^- \to \pi^+\pi^-K^-$

As usual, we start by computing the ρ tree operator contribution which takes the following form,

$$t_\rho = m_B|\vec{p}_\rho|\left[(C_1' + \frac{1}{N_c}C_2')f_\rho F_1(m_\rho^2) + (C_2' + \frac{1}{N_c}C_1')f_K A_0(m_K^2)\right] , \quad (6.14)$$

where f_ρ and f_K are the decay constants of the ρ and K respectively. In the same way, we find $t_\omega = t_\rho$, therefore one has,

$$\alpha e^{i\delta_\alpha} = 1 . \quad (6.15)$$

After calculating the penguin operator contributions for ρ and ω, one gets,

$$\begin{aligned}\beta e^{i\delta_\beta} = \frac{m_B|\vec{p}_\rho|}{p_\omega}\Bigg\{&(C_4' + \frac{1}{N_c}C_3')f_K A_0(m_K^2) \\ &+ \frac{3}{2}\Big((C_7' + \frac{1}{N_c}C_8') + (C_9' + \frac{1}{N_c}C_{10}')\Big)f_\rho F_1(m_\rho^2) + (C_{10}' + \frac{1}{N_c}C_9')f_K A_0(m_K^2) \\ &- 2\Big((C_6' + \frac{1}{N_c}C_5') + (C_8' + \frac{1}{N_c}C_7')\Big)\left[\frac{m_K^2 f_K A_0(m_K^2)}{(m_u + m_s)(m_b + m_u)}\right]\Bigg\} , \quad (6.16)\end{aligned}$$

and the ratio between penguin and tree operator contributions, which involves CKM matrix elements, is given by,

$$r' e^{i\delta_q} = -\frac{p_\omega}{(C_1' + \frac{1}{N_c}C_2')f_\rho F_1(m_\rho^2) + (C_2' + \frac{1}{N_c}C_1')f_K A_0(m_K^2)}\left|\frac{V_{tb}V_{ts}^*}{V_{ub}V_{us}^*}\right| . \quad (6.17)$$

In Eqs. (6.16, 6.17), the ω penguin contribution, p_ω is:

$$\begin{aligned}p_\omega = m_B|\vec{p}_\rho|\Bigg\{&2\Big((C_3' + \frac{1}{N_c}C_4') + (C_5' + \frac{1}{N_c}C_6')\Big)f_\rho F_1(m_\rho^2) \\ &+ \frac{1}{2}\Big((C_7' + \frac{1}{N_c}C_8') + (C_9' + \frac{1}{N_c}C_{10}')\Big)f_\rho F_1(m_\rho^2) \\ &+ \Big((C_4' + \frac{1}{N_c}C_3') + (C_{10}' + \frac{1}{N_c}C_9')\Big)f_K A_0(m_K^2) \\ &- 2\Big((C_8' + \frac{1}{N_c}C_7') + (C_6' + \frac{1}{N_c}C_5')\Big)\left[\frac{m_K^2}{(m_u + m_s)(m_b + m_u)}\right]f_K A_0(m_K^2)\Bigg\} ,\end{aligned} \quad (6.18)$$

and the ratio of CKM amplitude which arises in the $b \to s$ transition is,

$$\left|\frac{V_{tb}V_{ts}^{\star}}{V_{ub}V_{us}^{\star}}\right| = \frac{1}{\lambda^2}\frac{1}{\sqrt{\rho^2+\eta^2}} = \frac{1}{\lambda^2}\frac{1}{|\sin\beta|} \ . \tag{6.19}$$

To simplify the formulas we used N_c for N_c^{eff} in Eqs. (5.14)-(5.24))

Case of $\bar{B}^0 \to \pi^+\pi^-\bar{K}^0$

Finally, in the case of neutral decay ($\bar{B}^0 \to \pi^+\pi^-\bar{K}^0$), by applying the same formalism one gets:

$$t_\rho = m_B|\vec{p}_\rho|(C_1' + \frac{1}{N_c}C_2')f_\rho F_1(m_\rho^2) \ , \tag{6.20}$$

The computation of ω tree contribution gives $t_\omega = t_\rho$, therefore one has again,

$$\alpha e^{i\delta_\alpha} = 1 \ . \tag{6.21}$$

The ratio between p_ω and p_ρ is expressed as,

$$\begin{aligned}\beta e^{i\delta_\beta} = \frac{m_B|\vec{p}_\rho|}{p_\omega}\Bigg\{\frac{3}{2}\Bigg((C_7'+\frac{1}{N_c}C_8')+(C_9'+\frac{1}{N_c}C_{10}')\Bigg)f_\rho F_1(m_\rho^2)+ \\ \Bigg(-(C_4'+\frac{1}{N_c}C_3')+\frac{1}{2}(C_{10}'+\frac{1}{N_c}C_9')+\Bigg(2(C_6'+\frac{1}{N_c}C_5')-(C_8'+\frac{1}{N_c}C_7')\Bigg) \\ \Bigg[\frac{m_K^2}{(m_b+m_d)(m_d+m_s)}\Bigg]\Bigg)f_K A_0(m_K^2)]\Bigg\} \ ,\end{aligned} \tag{6.22}$$

and,

$$r'e^{i\delta_q} = -\frac{p_\omega}{(C_1'+\frac{1}{N_c}C_2')f_\rho F_1(m_\rho^2)}\left|\frac{V_{tb}V_{ts}^{\star}}{V_{ub}V_{us}^{\star}}\right| \ , \tag{6.23}$$

where p_ω gives, after calculation the following expression:

$$\begin{aligned}p_\omega = m_B|\vec{p}_\rho|\Bigg\{2\Bigg((C_3'+\frac{1}{N_c}C_4')+(C_5'+\frac{1}{N_c}C_6')\Bigg)f_\rho F_1(m_\rho^2) \\ +\frac{1}{2}\Bigg((C_7'+\frac{1}{N_c}C_8')+(C_9'+\frac{1}{N_c}c_{10}')\Bigg)f_\rho F_1(m_\rho^2) \\ +\Bigg((C_8'+\frac{1}{N_c}C_7')-2(C_6'+\frac{1}{N_c}C_5')\Bigg)\Bigg[\frac{m_K^2 f_K A_0(m_K^2)}{(m_b+m_d)(m_d+m_s)}\Bigg] \\ +\Bigg((C_4'+\frac{1}{N_c}C_3')-\frac{1}{2}(C_{10}'+\frac{1}{N_c}C_9')\Bigg)f_K A_0(m_K^2)\Bigg\} \ .\end{aligned} \tag{6.24}$$

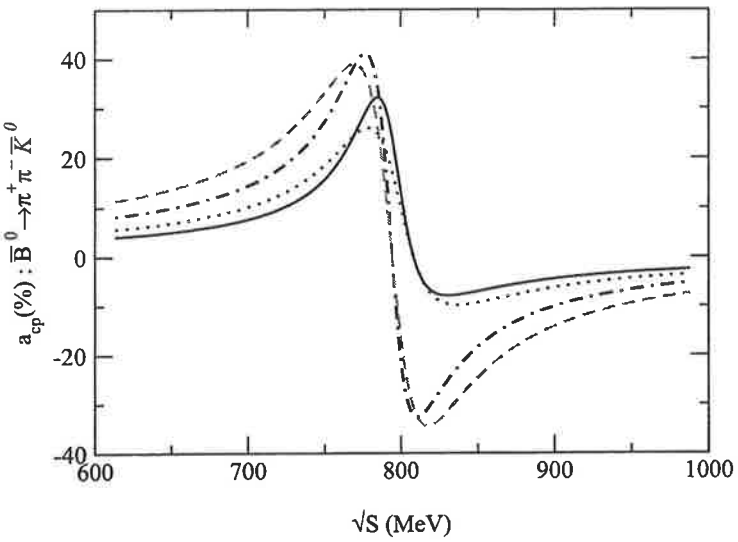

Figure 6.9: CP violating asymmetry, a_{CP}, for $\bar{B}^0 \to \pi^+\pi^-\bar{K}^0$, for $q^2/m_b^2 = 0.3(0.5)$, for $N_c^{eff} = 0.66, 0.61$ and for limiting values, max (min), of the CKM matrix elements for model (1): solid line (dotted line) for $N_c^{eff} = 0.66$. Dashed line (dot-dashed line) for $N_c^{eff} = 0.61$.

The CKM weak phase expression involved in this decay is identical to the one given in Eq. (6.19).

6.3.2 Results and discussions

We have investigated the CP violating asymmetry, a_{CP}, for the two B decays: $\bar{B}^0 \to \rho^0\bar{K}^0 \to \pi^+\pi^-\bar{K}^0$ and $B^- \to \rho^0 K^- \to \pi^+\pi^- K^-$. The results are shown in Figs. 6.9, 6.10 and 6.11 for $\bar{B}^0 \to \pi^+\pi^-\bar{K}^0$, ($a_{CP} = [\Gamma(\bar{B}^0 \to \pi^+\pi^-\bar{K}^0) - \Gamma(B^0 \to \pi^-\pi^+ K^0)]/[\Gamma(\bar{B}^0 \to \pi^+\pi^-\bar{K}^0) + \Gamma(B^0 \to \pi^-\pi^+ K^0)]$), with $q^2/m_b^2 = 0.3(0.5)$ and for N_c^{eff} equal to $0.61, 0.66, 2.65, 2.69, 2.82$ and 2.84. Similarly, in Figs. 6.12, 6.13 and 6.14, the CP violating asymmetry, a_{CP}, ($= [\Gamma(B^- \to \pi^+\pi^- K^-) - \Gamma(B^+ \to \pi^-\pi^+ K^+)]/[\Gamma(B^- \to \pi^+\pi^- K^-) + \Gamma(B^+ \to \pi^-\pi^+ K^+)]$), is plotted for $B^- \to \pi^+\pi^- K^-$, where $q^2/m_b^2 = 0.3(0.5)$ and for the same values of N_c^{eff} previously applied for $\bar{B}^0 \to \pi^+\pi^-\bar{K}^0$. In our numerical calculations, we found that the CP violating parameter, a_{CP}, reaches a maximum value, a_{max}, when the invariant mass of the $\pi^+\pi^-$ is in the vicinity of the ω resonance, for a fixed value of N_c^{eff}. We have studied the model dependence of a with five models where different form factors have been applied. Numerical results for $\bar{B}^0 \to \pi^+\pi^-\bar{K}^0$ and $B^- \to \pi^+\pi^- K^-$ are listed in Tables 6.3 and 6.4, respectively. It appears that the form factor dependence of a_{CP} for all models, and in both decays, is weaker than the

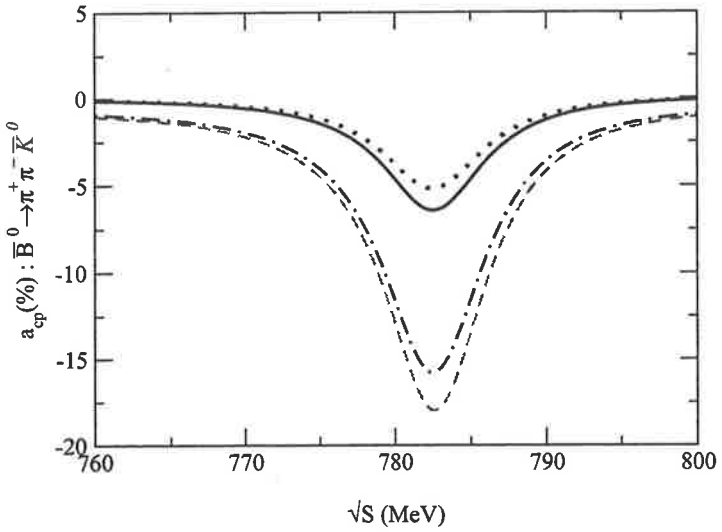

Figure 6.10: CP violating asymmetry, a_{CP}, for $\bar{B}^0 \to \pi^+\pi^-\bar{K}^0$, for $q^2/m_b^2 = 0.3$, for $N_c^{eff} = 2.69, 2.84$ and for limiting values, max (min), of the CKM matrix elements for model (1): solid line (dotted line) for $N_c^{eff} = 2.69$. Dashed line (dot-dashed line) for $N_c^{eff} = 2.84$.

N_c^{eff} dependence.

For $\bar{B}^0 \to \pi^+\pi^-\bar{K}^0$, we have determined the range of the maximum asymmetry parameter, a_{max}, when N_c^{eff} varies between 0.66(0.61) and 2.84(2.82), in the case of $q^2/m_b^2 = 0.3(0.5)$. The evaluation of a_{max} gives allowed values from 37%(55%) to $-20\%(-24\%)$ for the range of N_c^{eff} and CKM matrix elements indicated before. The sign of a_{max} stays positive until N_c^{eff} reaches 2.5. If we look at the numerical results for the asymmetries (Table 6.3), for $N_{cmin}^{eff} = 0.66(0.61)$ and $q^2/m_b^2 = 0.3(0.5)$, we find good agreement between all the models, with a maximum asymmetry, a_{max}, around 33%(45.6%) for the set (ρ_{max}, η_{max}), and around 26%(33.2%) for the set (ρ_{min}, η_{min}). The ratio between asymmetries associated with the upper and lower limits of (ρ, η) is around 1.26(1.37). If we consider the maximum asymmetry parameter, a_{max}, for $N_{cmax}^{eff} = 2.84(2.82)$, we observe a distinction between the models. Indeed, two classes of model appear: models (2) and (4) and models (1, 3) and (5). For models (2) and (4), one has an asymmetry, a_{max}, around $-6\%(-7\%)$ and around $-9\%(-10\%)$ for the upper and lower set of (ρ, η), respectively. The ratio between them is around 1.50(1.42). For models (1, 3) and (5), the maximum asymmetry is of order $-14.3\%(-16.3\%)$ for (ρ_{max}, η_{max}) and around $-19.3\%(-23.0\%)$ for (ρ_{min}, η_{min}). In this case, the ratio between asymmetries is around 1.34(1.41).

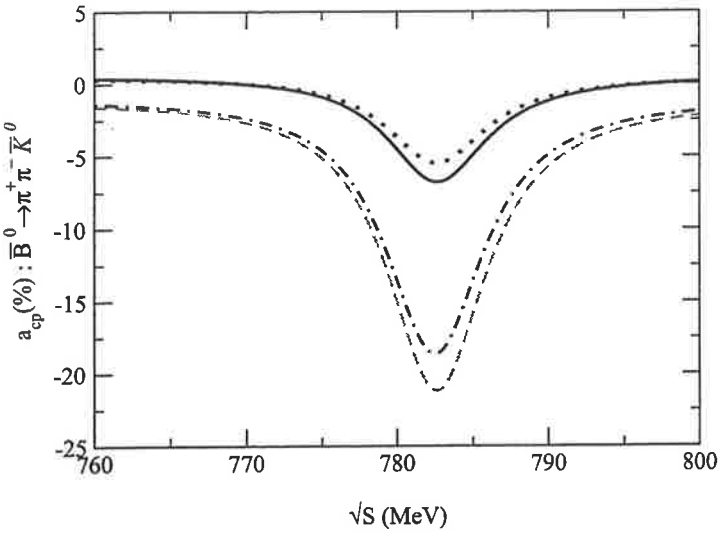

Figure 6.11: CP violating asymmetry, a_{CP}, for $\bar{B}^0 \to \pi^+\pi^-\bar{K}^0$, for $q^2/m_b^2 = 0.5$, for $N_c^{eff} = 2.65, 2.82$ and for limiting values, max (min), of the CKM matrix elements for model (1): solid line (dotted line) for $N_c^{eff} = 2.65$. Dashed line (dot-dashed line) for $N_c^{eff} = 2.82$.

	$N_{c_{min}}^{eff} = 0.66(0.61)$	$N_{c_{max}}^{eff} = 2.84(2.82)$
model (1)		
ρ_{max}, η_{max}	32(46)	-14(-16)
ρ_{min}, η_{min}	25(33)	-19(-22)
model (2)		
ρ_{max}, η_{max}	32(41)	-6(-7)
ρ_{min}, η_{min}	27(30)	-9(-10)
model (3)		
ρ_{max}, η_{max}	32(45)	-14(-16)
ρ_{min}, η_{min}	25(33)	-20(-23)
model (4)		
ρ_{max}, η_{max}	32(41)	-6(-7)
ρ_{min}, η_{min}	27(30)	-9(-10)
model (5)		
ρ_{max}, η_{max}	37(55)	-15(-17)
ρ_{min}, η_{min}	26(40)	-19(-24)

Table 6.3: Maximum CP violating asymmetry $a_{max}(\%)$ for $\bar{B}^0 \to \pi^+\pi^-\bar{K}^0$, for all models, limiting values (upper and lower) of the CKM matrix elements, and for $q^2/m_b^2 = 0.3(0.5)$.

	$N_{cmin}^{eff} = 0.66(0.61)$	$N_{cmax}^{eff} = 2.84(2.82)$
model (1)		
ρ_{max}, η_{max}	47(45)	-15(-17)
ρ_{min}, η_{min}	34(35)	-21(-23)
model (2)		
ρ_{max}, η_{max}	45(41)	-11(-13)
ρ_{min}, η_{min}	33(32)	-17(-18)
model (3)		
ρ_{max}, η_{max}	47(44)	-15(-17)
ρ_{min}, η_{min}	34(35)	-20(-23)
model (4)		
ρ_{max}, η_{max}	45(42)	-12(-13)
ρ_{min}, η_{min}	33(32)	-17(-18)
model (5)		
ρ_{max}, η_{max}	49(46)	-17(-19)
ρ_{min}, η_{min}	36(35)	-22(-25)

Table 6.4: Maximum CP violating asymmetry $a_{max}(\%)$ for $B^- \to \pi^+\pi^-K^-$, for all models, limiting values of the CKM matrix elements (upper and lower limit), and for $q^2/m_b^2 = 0.3(0.5)$.

The first reason why the maximum asymmetry, a_{max}, can vary so much comes from the element V_{ub}. The other CKM matrix elements V_{tb}, V_{ts} and V_{us}, all proportional to A and λ, are very well measured experimentally and thus do not interfere in our results. Only V_{ub}, which contains the ρ and η parameters, provides large uncertainties, and thus, large variations for the maximum asymmetry. The second reason is the non-factorizable effects in the transition $b \to s$. It is well known that decays including a K meson (and therefore an s quark) carry more uncertainties than those involving only a π meson (u,d quarks). If we look at the asymmetries at N_{cmin}^{eff}, all models give almost the same values, whereas at N_{cmax}^{eff}, we obtain different asymmetry values (with moreover a change of sign for the CP violating asymmetry). The CP asymmetry parameter is more sensitive to form factors at high values of N_c^{eff} than at low values of N_c^{eff}. It appears therefore that all of the models investigated can be divided in two classes, referring to the two classes of form factors.

For $B^- \to \pi^+\pi^-K^-$, we have similarly investigated the CP violating asymmetry. The values of maximum asymmetry parameter, a_{max}, for a range of N_c^{eff} from 0.66(0.61) to 2.84(2.82), where $q^2/m_b^2 = 0.3(0.5)$ and for the five models analysed, are given in Table 6.4. We found that for this decay, the CP

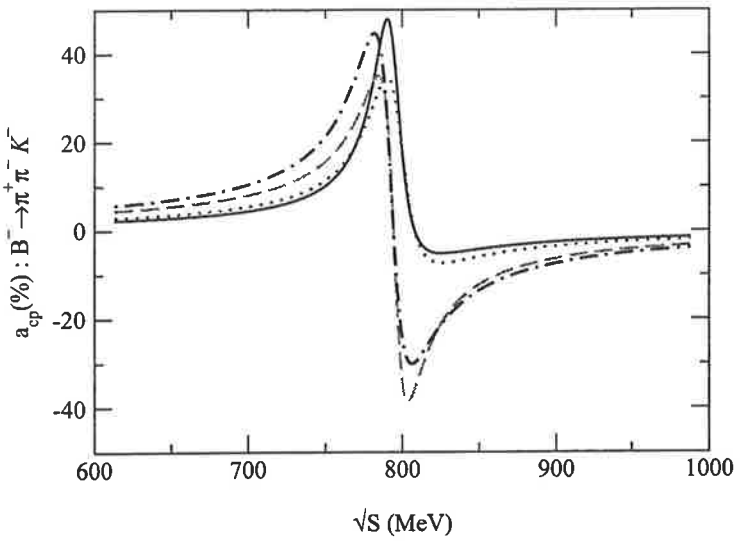

Figure 6.12: CP violating asymmetry, a_{CP}, for $B^- \to \pi^+\pi^- K^-$, for $q^2/m_b^2 = 0.3$, for $N_c^{eff} = 0.66, 0.61$ and for limiting values, max (min), of the CKM matrix elements for model (1): solid line (dotted line) for $N_c^{eff} = 0.66$. Dashed line (dot-dashed line) for $N_c^{eff} = 0.61$.

violating parameter, a_{CP}, takes values around 49%(46%) to $-22\%(-25\%)$ for the limiting CKM matrix values of ρ and η defined before. Once again, the sign of the asymmetry parameter, a_{CP}, is positive if the value of N_c^{eff} stays below 2.7. If we focus on N_{cmin}^{eff} equal to 0.66(0.61), models $(1, 2, 3, 4)$ and (5) give almost the same value which is around 46.6%(43.6%) for the maximum values of the CKM matrix elements. For the set (ρ_{min}, η_{min}), the maximum asymmetry, a_{max}, is around 34.0%(33.8%). The ratio between asymmetry values taken at upper and lower limiting ρ and η values is around 1.37(1.28). Let us have a look at the CP asymmetry values at N_{cmax}^{eff}. As we observed for the decay $\bar{B}^0 \to \pi^+\pi^-\bar{K}^0$, all models are separated into two distinct classes related to their form factors. For models $(1, 3)$ and (5), the value of maximum asymmetry, a_{max}, is around $-15.6\%(-17.6\%)$ and around $-21\%(-23.6\%)$ for the maximum and minimum values of set (ρ, η), respectively. The calculated ratio is around 1.34(1.34), between these two asymmetries. As regards models (2) and (4), for the same set of (ρ, η), one gets $-11.5\%(-13\%)$ and $-17\%(-18\%)$. In this case, one has 1.47(1.38) for the ratio. The reasons for the differences between the maximum asymmetry parameter, a_{max}, are the same as in the decay $\bar{B}^0 \to \pi^+\pi^-\bar{K}^0$.

By analysing the B decays, such as $\bar{B}^0 \to \pi^+\pi^-\bar{K}^0$ and $B^- \to \pi^+\pi^- K^-$, we found that the CP violating asymmetry, a_{CP}, depends on the CKM ma-

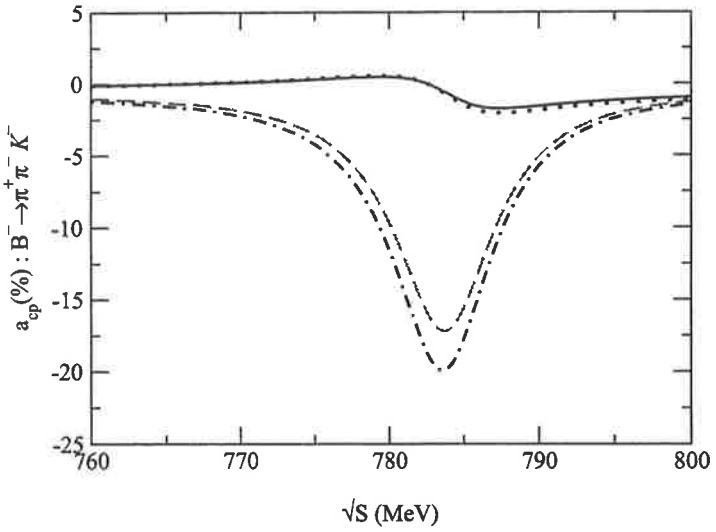

Figure 6.13: CP violating asymmetry, a_{CP}, for $B^- \to \pi^+\pi^- K^-$, for $q^2/m_b^2 = 0.3$, for $N_c^{eff} = 2.69, 2.84$ and for limiting values, max (min), of the CKM matrix elements for model (1): solid line (dotted line) for $N_c^{eff} = 2.69$. Dashed line (dot-dashed line) for $N_c^{eff} = 2.84$.

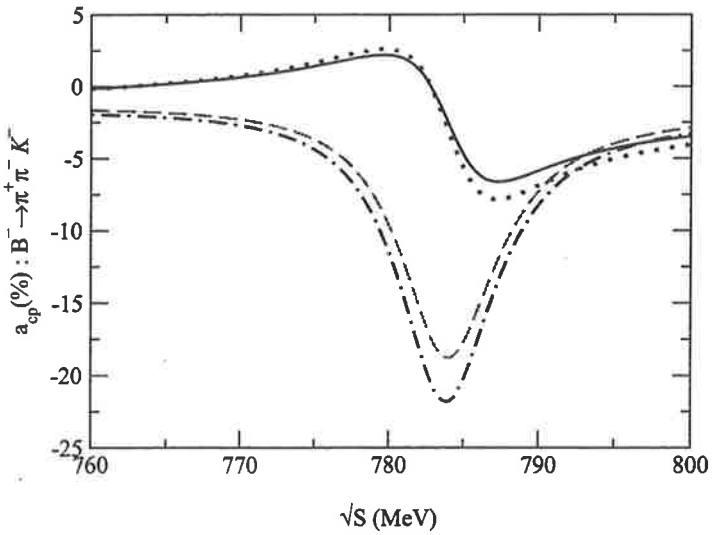

Figure 6.14: CP violating asymmetry, a_{CP}, for $B^- \to \pi^+\pi^- K^-$, for $q^2/m_b^2 = 0.5$, for $N_c^{eff} = 2.65, 2.82$ and for limiting values, max (min), of the CKM matrix elements for model (1): solid line (dotted line) for $N_c^{eff} = 2.65$. Dashed line (dot-dashed line) for $N_c^{eff} = 2.82$.

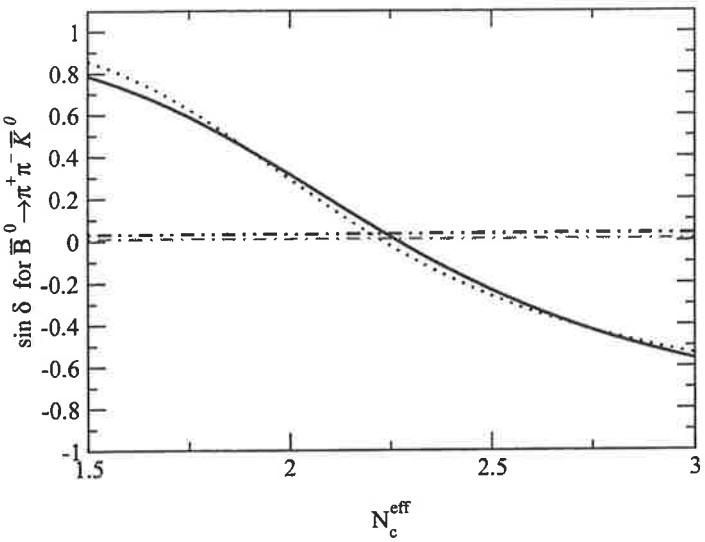

Figure 6.15: $\sin\delta$, as a function of N_c^{eff}, for $\bar{B}^0 \to \pi^+\pi^-\bar{K}^0$, for $q^2/m_b^2 = 0.3(0.5)$ and for model (1). The solid (dotted) line corresponds the case $\tilde{\Pi}_{\rho\omega} = (-3500; -300)$, where $\rho - \omega$ mixing is included. The dot-dashed (dot-dot-dashed) line corresponds to $\tilde{\Pi}_{\rho\omega} = (0; 0)$, where $\rho - \omega$ mixing is not included.

trix elements, form factors and the effective parameter N_c^{eff} (in order of increasing dependence). As regards the CKM matrix elements, the dependence through the element, V_{ub}, contributes to the asymmetry in the ratio between the ω penguin and the ρ tree contributions. It also appears that for the upper limit of set (ρ, η), we get the higher value asymmetry, a_{CP}, and vice-versa. With regard to the form factors, the dependence at low values of N_c^{eff} is very weak although there was a considerable difference between the phenomenological form factors (models (2) and (4) and models (1,3) and (5)) applied in our calculations. At high values of N_c^{eff}, the dependence becomes strong and then, the asymmetry appears very sensitive to form factors. For the effective parameter, N_c^{eff}, (related to hadronic non-factorizable effects), our results show explicitly the dependence of the asymmetry parameter on it. Because of the energy carried by the quark s, intermediate states and final state interactions are not well taken into account and may explain this strong sensitivity.

Finally, results obtained at $q^2/m_b^2 = 0.3(0.5)$, also show renormalization effects of the Wilson coefficients involved in the weak effective hadronic Hamiltonian. For the ratio between asymmetries, results give an average value of order 1.36(1.40) for $\bar{B}^0 \to \pi^+\pi^-\bar{K}^0$ and 1.39(1.33) for $B^- \to \pi^+\pi^-K^-$. This ratio is mainly governed by the term $1/\sin\beta$, where the

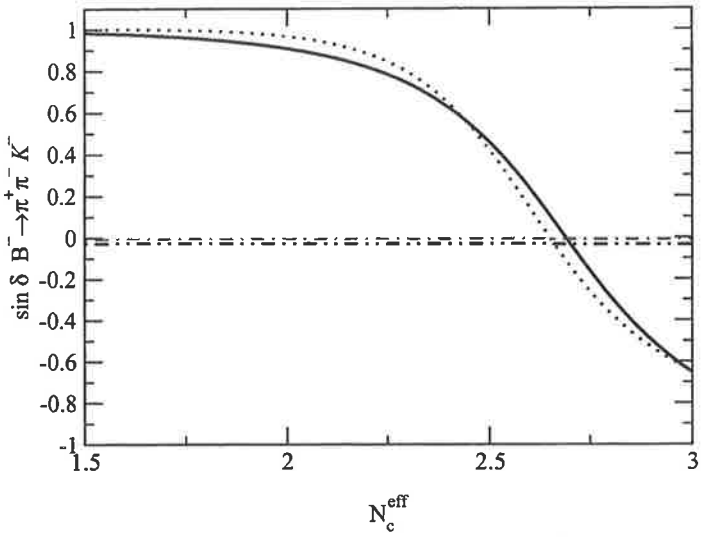

Figure 6.16: $\sin\delta$, as a function of N_c^{eff} for $B^- \to \pi^+\pi^-K^-$, for $q^2/m_b^2 = 0.3(0.5)$ and for model (1). The solid (dotted) line corresponds the case $\tilde{\Pi}_{\rho\omega} = (-3500; -300)$, where $\rho-\omega$ mixing is included. The dot-dashed (dot-dot-dashed) line corresponds to $\tilde{\Pi}_{\rho\omega} = (0; 0)$, where $\rho-\omega$ mixing is not included.

values of the angles α, β and γ are listed in Table 5.1. As a first conclusion based on these numerical results, it is obvious that the dependence of the asymmetry on the effective parameter N_c^{eff} is dramatic and therefore it is absolutely necessary to more efficiently constrain its value, in order to use asymmetry, a_{CP}, to determine the CKM parameters ρ and η.

We know that the effects of $\rho-\omega$ mixing only exist around the ω resonance. Nevertheless, at small values of N_c^{eff}, i.e. $\simeq 0.6$, (see Figs. 6.9 and 6.12), the curves show large asymmetry values far away from $\rho-\omega$ mixing, which is a priori unexpected. In fact, if we assume that non-factorizable effects are not as important as factorizable contributions, then N_c^{eff} should be much bigger. From previous analysis on some other B decays such as $B \to D\pi, B \to \omega\pi, B \to \omega K$, it was found that N_c^{eff} should be around 2 [112]. Therefore, although small values of N_c^{eff} are allowed by the experimental data, we expect that the value of N_c^{eff} cannot be so small with more accurate data. Thus, with a very small value of N_c^{eff}, non-factorizable effects have been overestimated. This means that soft gluon exchanges between $\rho^0(\omega)$ and K may effect $\rho-\omega$ mixing and hence lead to the large CP asymmetries in a region far away from ω resonance. However, at $\sqrt{s}$ energy very far from ω resonance, the CP asymmetries go to zero as expected.

In spite of the uncertainties discussed previously, the main effect of $\rho-\omega$

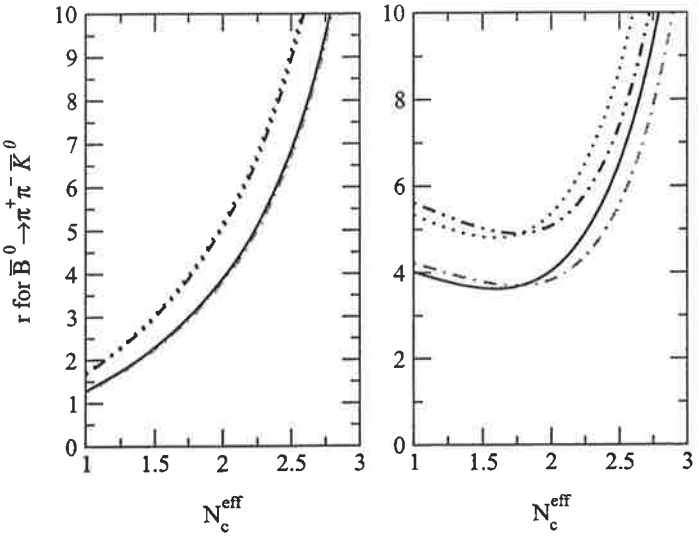

Figure 6.17: The ratio of penguin to tree amplitudes, r, as a function of N_c^{eff}, for $\bar{B}^0 \to \pi^+\pi^-\bar{K}^0$, for $q^2/m_b^2 = 0.3(0.5)$, for limiting values of the CKM matrix elements (ρ, η) max(min), for $\tilde{\Pi}_{\rho\omega} = (-3500; -300)(0, 0)$, (i.e. with(without) $\rho - \omega$ mixing) and for model (1). Figure 6.17a (left): for $\tilde{\Pi}_{\rho\omega} = (0; 0)$, solid line (dotted line) for $q^2/m_b^2 = 0.3$ and (ρ, η) max(min). Dot-dashed line (dot-dot-dashed line) for $q^2/m_b^2 = 0.5$ and (ρ, η) max(min). Figure 6.17b (right): same caption but for $\tilde{\Pi}_{\rho\omega} = (-3500; -300)$.

mixing in $B \to \rho K$ is the removal of the ambiguity concerning the strong phase, $\sin\delta$. In the $b \to s$ transition, the weak phase in the rate asymmetry is proportional to $\sin\gamma$ where $\gamma = arg[-(V_{ts}V_{tb}^*/(V_{us}V_{ub}^*)]$. Knowing the sign of $\sin\delta$, we are then able to determine the sign of $\sin\gamma$ from a measurement of the asymmetry, a_{CP}. In Figs. 6.15 and 6.16, the value of $\sin\delta$ is plotted as a function of N_c^{eff} for $\bar{B}^0 \to \pi^+\pi^-\bar{K}^0$ and $B^- \to \pi^+\pi^- K^-$, respectively. It appears, in both cases, when $\rho - \omega$ mixing mechanism is included, that the sign of $\sin\delta$ is positive, for all models studied, until $N_c^{eff} \simeq 2.5$ for both $B^- \to \pi^+\pi^- K^-$ and $\bar{B}^0 \to \pi^+\pi^-\bar{K}^0$, when $q^2/m_b^2 = 0.3(0.5)$. For values of N_c^{eff} bigger than this limit, $\sin\delta$ becomes negative. At the same time, the sign of the asymmetry also changes.

In Figs. 6.17b and 6.18b, the ratio of penguin to tree amplitudes is shown for $B^{\pm,0} \to \pi^+\pi^- K^{\pm,0}$, in the case of $\tilde{\Pi}_{\rho\omega} = (-3500, -300)$. The critical point around $N_c^{eff} = 2.7$, refers to the change of sign of $\sin\delta$. Clearly, we can use a measurement of the asymmetry, a_{CP}, to eliminate the uncertainty $\mathrm{mod}(\pi)$ which is usually involved in the determination of γ (through $\sin 2\gamma$). If we do not take into account $\rho - \omega$ mixing, the CP violating asymmetry, a_{CP},

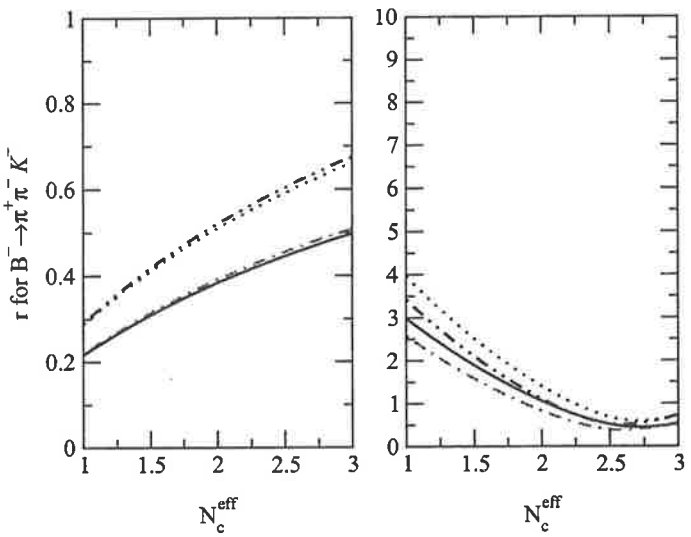

Figure 6.18: The ratio of penguin to tree amplitudes, r, for $B^- \to \pi^+\pi^-K^-$. Same caption for Figure 6.18a (left) and Figure 6.18b (right) as in Fig. 6.17.

remains very small (just a few percent) in both decays. In Figs. 6.15 and 6.16 (for the evolution of $\sin\delta$) and in Figs. 6.17a and 6.18a (for the evolution of penguin to tree amplitudes), for $B^{\pm,0} \to \pi^+\pi^-K^{\pm,0}$, we plot $\sin\delta$ and r when $\tilde{\Pi}_{\rho\omega} = (0,0)$ –i.e. without $\rho-\omega$ mixing. There is a critical point at $N_c^{eff} = 1$ (for $\bar{B}^0 \to \pi^+\pi^-\bar{K}^0$) and $N_c^{eff} = 0.24$ (for $B^- \to \pi^+\pi^-K^-$) for which the value of $\sin\delta$ is at its maximum and corresponds (for the same value of N_c^{eff}), to the lowest value of r. Anywhere else, the value of $\sin\delta$ is closed to zero. The last results show the double effect of the $\rho-\omega$ mixing: the CP violating asymmetry increases and the sign of the strong phase δ is determined.

6.4 Summary

The aim of the present work was to apply recent values of the CKM matrix elements, e.g. A, λ, η and ρ, to study direct CP violation for B decays such as $B^{\pm,0} \to \rho^0(\omega)\pi^{\pm,0} \to \pi^+\pi^-\pi^{\pm,0}$ and $B^{\pm,0} \to \rho^0(\omega)K^{\pm,0} \to \pi^+\pi^-K^{\pm,0}$ where the $\rho-\omega$ mixing mechanism must be included. When the invariant mass of the $\pi^+\pi^-$ pair is in the vicinity of the ω resonance, it is found that the CP violating asymmetry, a_{CP}, has a maximum a_{max}. To calculate the CP violating asymmetry, a_{CP}, we started from the weak Hamiltonian in which the OPE separates hard and soft physical regimes. We worked in the factorization approximation where the hadronic matrix elements are treated in some phenomenological quark models. The effective parameter, N_c^{eff}, was

used in order to take into account, as well as possible, the non-factorizable effects involved in $B \to \rho\pi$ and $B \to \rho K$decays. Although one must have some doubts about factorization, it has been pointed out that it may be quite reliable in energetic weak decays [48, 49, 113].

We started by analysing the direct CP violating asymmetry in the two B decays: $B^- \to \pi^-\pi^+\pi^-$ and $\bar{B}^0 \to \pi^-\pi^+\pi^0$. We found that the CP violation parameter, a_{CP}, is very sensitive to the parameters ρ and η in the CKM matrix, and also to the magnitude of the form factors appearing in the five phenomenological models we investigated. For $\bar{B}^0 \to \pi^-\pi^+\pi^0$, we have calculated the maximum asymmetry, a_{max}, as a function of the effective parameter, N_c^{eff}, with the limiting values of the CKM matrix elements. We found that the CP violating asymmetry, a_{max}, can vary from -37% to -84%. For $B^- \to \pi^-\pi^+\pi^-$, we also determined the range for the maximum asymmetry, a_{max}, namely -17% to -53%. As we already determined in a first preliminary study, the ratio between the asymmetries for limiting values of the CKM matrix elements is mainly governed by η. We found a ratio equal to 1.64 where the CKM values used were the following: $A = 0.815, \lambda = 0.2205$, $0.09 < \rho < 0.254$, and $0.323 < \eta < 0.442$. In the final work, one finds for the same decay, a ratio equal to 1.30. The more accurate value for η has reduced uncertainties on both the CP violating asymmetry and the ratio, $\Gamma(B^+ \to \pi^-\pi^+\pi^+)/\Gamma(B^0 \to \pi^-\pi^+\pi^0)$.

We have also studied CP violation in B decay process such as $B^{\pm,0} \to \rho^0 K^{\pm,0} \to \pi^+\pi^- K^{\pm,0}$. We have explicitly shown that the direct CP violating asymmetry is very sensitive to the CKM matrix elements, the magnitude of the form factors $A_0(k^2)$ and $F_1(k^2)$, and also to the effective parameter N_c^{eff} (in order of increasing dependence). We have determined a range for the maximum asymmetry, a_{max}, as a function of the parameter N_c^{eff}, the limits of CKM matrix elements and the choice of $q^2/m_b^2 = 0.3(0.5)$. For the decay $\bar{B}^0 \to \pi^+\pi^-\bar{K}^0$ and from all models investigated, we found that the largest CP violating asymmetry varies from $+37\%(+55\%)$ to $-20\%(-24\%)$. As regards $B^- \to \pi^+\pi^- K^-$, one gets $+49\%(+46\%)$ to $-22\%(-25\%)$. For $B^{\pm,0} \to \pi^+\pi^- K^{\pm,0}$, the sign of a_{max} stays positive as long as the value of N_c^{eff} is less than 2.7. In both decays ($B \to \rho K$), the ratio between asymmetry values which are taken at upper and lower limiting ρ and η values is mainly governed by the term $1/\sin\beta$. It appears also that the direct CP violating asymmetry is very sensitive to the form factors at high values of N_c^{eff}.

We underline that without the inclusion of $\rho - \omega$ mixing, we would not have a large CP violating asymmetry, a_{CP}, since a_{CP} is proportional to both $\sin\delta$ and r (for $B \to \rho\pi$ and $B \to \rho K$). Without $\rho - \omega$ mixing, we found a critical point for which $\sin\delta$ reaches the value $+1$, but at the same time, r becomes very tiny. Therefore, the asymmetry, a_{CP} is also very

tiny. We emphasise that the advantage of $\rho - \omega$ mixing is the large strong phase difference which varies extremely rapidly near the ω resonance. In our calculations, we found that for $B^{\pm,0} \to \pi^+\pi^- K^{\pm,0}$, the sign of $\sin\delta$ is positive until N_c^{eff} reaches roughly 2.5 when $q^2/m_b^2 = 0.3(0.5)$. For $B^{\pm,0} \to \rho^0\pi^{\pm,0} \to \pi^+\pi^-\pi^{\pm,0}$, the sign of $\sin\delta$ stays positive.

By measuring a_{CP} for values of N_c^{eff}, within the limits given above, we can remove the phase uncertainty mod(π) in the determination of the CKM angle α in $B^{\pm,0} \to\to \pi^+\pi^-\pi^{\pm,0}$. In a similar way, it has been also possible to remove the phase uncertainty mod(π) in the determination of the CKM angle γ by analysing direct CP violation in $B \to \pi^+\pi^- K$. Thus by combining both previous results, we can finally remove the phase uncertainty mod(π) which appears in the analysis of the CKM angle β through the study of $b \to c$ transition and hence, to constrain the unitarity triangle condition.

The investigation of branching ratios such as $B^{\pm,0} \to \rho^{\pm,0}\pi^{\pm,0}$ and $B^{\pm,0} \to \rho^{\pm,0}K^{\pm,0}$, allowed us to make comparisons between our theoretical results and experimental data from the CLEO, BABAR and BELLE Collaborations (see Chapter 5). We have applied five phenomenological models in order to show their dependence on form factors, CKM matrix elements and the effective parameter N_c^{eff} in our approach. In output, we determine for both decays ($B \to \rho\pi$ and $B \to \rho K$), the range for N_c^{eff} which constrains the direct CP violation asymmetry parameter, a_{CP}. With more accurate CKM matrix elements values, i.e. ρ and η, we are able to give more precise CP violating asymmetries, and the main uncertainties remaining are from the factorization approach and the hadronic decay form factors. The QCD factorization will provide a more efficient way to deal with non-factorizable effects. With regard to form factors, we have shown that some models for the $B \to \pi$ transition are not consistent with the experimental branching ratios, whereas for $B \to K$, we cannot draw firm conclusions.

Therefore, in the following and in order to go further in our investigation, we shall determine in a covariant light cone framework, wave functions for π, K, B and D. Then, we shall calculate form factors based on these functions determined from physical observables. Finally, in the last part, we shall apply QCD factorization, where the new form factors will be involved, to obtain (better and more accurate) predictions on direct CP violation in B decays.

Part III

Covariant Light-Front Dynamics, Wave Functions and Form Factors

Chapter 7

Covariant Light-Front Dynamics - Main properties

" La théorie, c'est quand on sait tout et que rien ne fonctionne. La pratique, c'est quand tout fonctionne et que personne ne sait pourquoi. "

Albert Einstein

In this third section of the thesis, we are going to apply the Covariant Light-Front Dynamics (CLFD) formalism to determine wave functions for pseudoscalar particles B, D, K, π and for vector particles ρ, ω (see Chapter 8). Then, we will calculate transition form factors (see Chapter 9) for $P \to P$ and $P \to V$ where P (pseudoscalar) and V (vector) are the particles mentioned previously. In this first chapter, we recall the theoretical background of Covariant Light-Front Dynamics. We will start by giving some basic properties of Light-Front Dynamics (LFD), then we will summarize briefly the dynamical approach used in the covariant formulation of light-front dynamics.

7.1 Light-Front Dynamics

The first requirement to build a dynamical theory is that it should be invariant under the ten generators of the Poincaré group. These generators include space time translations (four generators), space rotations (three generators) and Lorentz boost (three generators). The time translation operator is the Hamiltonian. Three forms of dynamics have been derived and defined a long time ago, in one of Dirac's famous papers [114]. There are the instant form, the point form and the front form (see Fig. 7.1 [115]). Among the ten

generators of the Poincaré group, the ones which do not leave the light-front plane $\omega \cdot x = \text{cte}$ invariant are called dynamical, i.e. they should depend on the interaction. The other ones are called kinematical.

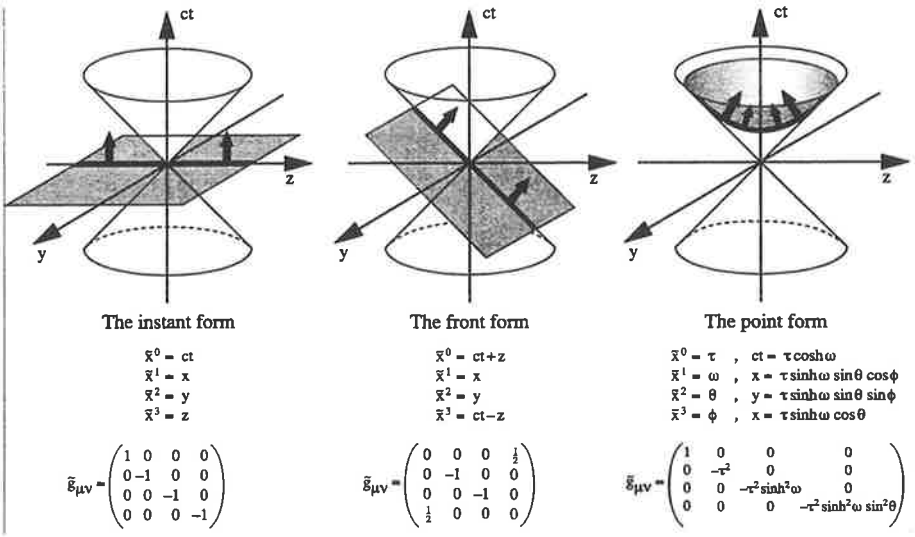

Figure 7.1: Dirac's three forms of dynamics.

The instant form describes in a four dimensional space, the evolution of one system from one three dimensional plane, $t = \text{const}$, to another one. The point form describes the evolution of one system on any four dimensional space like surface $t^2 - \vec{r}^{\,2} = \text{const}$. A physical process can also be described in the observer's system (t', x', y', z') which is moving with velocity v along the z-axis in the laboratory system (t, x, y, z). Then, the evolution is investigated from one plane $t' = \text{const}$ in the moving system (or $t + zv/c^2 = \text{const}$ if we refer to the laboratory system) to another plane. If $v \to c$, the wave function is therefore determined on the plane $t + zv/c = \text{const}$ which corresponds to the equation for the light-front plane $z = -ct$ moving along $-z$ axis. In this so-called front form, the coordinates are defined as (z_+, x, y, z_-) where $z_+ = t + z$ and $z_- = t - z$. While the front form is interesting since the boost operator along the z axis gets kinematical, the plane $z_+ = \text{cte}$ is not invariant under all spatial rotations. The angular momentum operators are therefore dynamical. In order to treat in a transparent way the dependence of these operators on the dynamics, an explicitly covariant light front dynamics has been derived by V.A. Karmanov [116, 117, 118, 119, 120, 121, 122, 123].

7.2 Covariant Light-Front Dynamics

7.2.1 Main properties

In the past few years, a Covariant formulation of Light-Front Dynamics (CLFD) has been proposed [122, 123, 124] and applied to relativistic particle and nuclear physics. This formulation is particularly useful for describing hadrons, and all observables related to them, within the constituent quark model. In CLFD [122, 123, 124], the state vector which describes the physical bound state is defined on the light-front plane given by the equation $\omega \cdot x = 0$, where ω is an unspecified light-like four vector ($\omega^2 = 0$). It defines the position of the light-front plane. This approach is a generalization of the standard Light-Front Dynamics (LFD) [125]. This latter can easily be recovered with a special choice of the light-front orientation, $\omega = (1, 0, 0, -1)$.

The description of relativistic systems in the covariant formalism of LFD provides several advantages as compared to the standard formulation. The main properties are the following [122, 123, 124]:

- The formalism does not involve vacuum fluctuation contributions because of Lorentz time dilatation. The state vector describing the physical bound state contains a definite number of particle, described by Fock state components.

- The Fock components of the state vector satisfy a three dimensional equation, and the relativistic wave function has the same meaning, namely a probability amplitude, as the non-relativistic one. This is very convenient in the framework of the constituent quark model.

- Relativistic wave functions and off-shell amplitudes have a dependence on the orientation of the light-front plane which is fully parametrized in term of the four vector ω. Approximate on-shell physical amplitudes also depend on ω, whereas, the exact on-shell physical amplitudes do not depend on the orientation of the light-front plane.

In contrast to LFD, where the covariance is lost, CLFD proposes a formulation in which the evolution for a given system is expressed in terms of covariant expressions. Therefore, any four vector describing a phenomena can be transformed from one system of reference to another one by using a unique standard matrix which depends only on kinematical parameters and on ω.

7.2.2 Kinematical and dynamical transformations

The kinematical transformations are associated with transformations of the coordinate systems, while dynamical transformations correspond to transformations of the hypersurface on which the state vector is defined.

Consider first the case of kinematical transformations. The transformation of the system of reference under both translation ($x \to x' = x + a$) and infinitesimal rotation ($x_\mu \to x'_\mu = g x_\mu = x_\mu + \epsilon_{\nu\mu} x^\nu$) transform the state vector, $\phi_\omega(\sigma)$, where $\sigma = \omega \cdot x$ is the light-front time, as:

$$\phi_\omega(\sigma) \to \phi'_{\omega'}(\sigma') = \left[U_{P^0}(a) + U_{J^0}(g) \right] \phi_\omega(\sigma) \ , \tag{7.1}$$

with $U_{P^0}(a) = \exp(iP^0 \cdot a)$ and $U_{J^0}(g) = 1 + 1/2 J^0_{\mu\nu} \epsilon^{\mu\nu}$. P^0 and J^0 are respectively the free part of the operators associated to the four momentum P_μ and four angular momentum $J_{\mu\nu}$ defined by,

$$\begin{aligned} \hat{P}_\mu &= \int T_{\mu\nu} \omega^\nu \delta(\omega \cdot x - \sigma) \mathrm{d}^4 x = \hat{P}^0_\mu + \hat{P}^{\mathrm{int}}_\mu \ , \\ \hat{J}_{\mu\nu} &= \int M^\rho_{\mu\nu} \omega_\rho \delta(\omega \cdot x - \sigma) \mathrm{d}^4 x = \hat{J}^0_{\mu\nu} + \hat{J}^{\mathrm{int}}_{\mu\nu} \ , \end{aligned} \tag{7.2}$$

where the int superscripts indicate the interacting part of the operators. In Eq. (7.2), $M^\rho_{\mu\nu}$ and $T_{\mu\nu}$ are the angular and energy momentum tensors. The free operator parts fully control all the kinematic transformations and do not contain any interaction term. They describe the transformation of the state vector under transformation of the reference system. The operators $\hat{P}^{\mathrm{int}}$ and $\hat{J}^{\mathrm{int}}$ contain the interaction Hamiltonian $H^{\mathrm{int}}(x)$:

$$\begin{aligned} \hat{P}^{\mathrm{int}}_\mu &= \omega_\mu \int H^{\mathrm{int}}(x) \delta(\omega \cdot x - \sigma) \mathrm{d}^4 x \ , \\ \hat{J}^{\mathrm{int}}_{\mu\nu} &= \int H^{\mathrm{int}}(x) (x_\mu \omega_\nu - x_\nu \omega_\mu) \delta(\omega \cdot x - \sigma) \mathrm{d}^4 x \ . \end{aligned} \tag{7.3}$$

The dynamical transformation of the state vector is completely defined by the part of the operators containing the interaction Hamiltonian $H^{\mathrm{int}}(x)$ according to the Tomonaga-Schwinger equation [126]:

$$i \delta\phi / \delta\sigma(x) = H^{\mathrm{int}}(x) \phi \ . \tag{7.4}$$

These operators describe the transformation of the state vector under translations and rotations of the light-front plane. In the case of a rotation of the light-front plane, it is easy to find [122, 123, 124] for instance:

$$\phi_\omega(\sigma) \to \phi_{\omega+\delta\omega}(\sigma) = \phi_\omega + \delta\phi_\omega, \text{ with } \delta\phi_\omega = \frac{1}{2} \varepsilon_{\mu\nu} \left(\omega^\mu \frac{\partial}{\partial \omega_\nu} - \omega^\nu \frac{\partial}{\partial \omega_\mu} \right) \phi_\omega(\sigma) \ . \tag{7.5}$$

It is then possible to express the interacting part of the angular momentum operator, acting on the state vector, according to,

$$\hat{J}^{\rm int}_{\mu\nu}\phi_\omega(\sigma) = \hat{L}_{\mu\nu}(\omega)\phi_\omega(\sigma) \ , \tag{7.6}$$

where,

$$\hat{L}_{\mu\nu}(\omega) = i\left(\omega_\mu \frac{\partial}{\partial\omega^\nu} - \omega_\nu \frac{\partial}{\partial\omega^\mu}\right) . \tag{7.7}$$

With this "angular condition", it is possible to determine (without any ambiguity) the state vector for a definite angular momentum as well as the dependence of ϕ_ω on the orientation of the light front. Moreover, it allows this determination in terms of kinematical transformation properties of the wave function, letting the dynamical transformation of the system appear through the dependence of the wave function on the orientation ω of the light-front plane (see Refs. [122, 123, 124] for more details).

7.2.3 *S*-matrix

In CLFD, the S-matrix is calculated from the light-front graph techniques. For technical details regarding CLFD graphs rules, we refer to the extensive review in Refs. [122, 123, 124]. The S-matrix which gives the time evolution of the wave function from one light-front plane to another in the direction of the light-front time is written as:

$$S = T_\omega \exp\left[-i \int H^{\rm int}_\omega(x) d^4x\right] , \tag{7.8}$$

where the T-product orders the operators with respect to the light-front time $\sigma = \omega\cdot x$, and $H^{\rm int}_\omega$ is the interaction part of the Hamiltonian. The S-matrix can thus be decomposed as follows:

$$S = 1 + \sum_n \int (-i)^n H^{\rm int}_\omega(x_1)\theta(\omega\cdot(x_1-x_2))H^{\rm int}_\omega(x_2)\theta(\omega\cdot(x_2-x_3))\cdots \\ \theta(\omega\cdot(x_{n-1}-x_n))H^{\rm int}_\omega(x_n)\mathrm{d}^4x_1\cdots\mathrm{d}^4x_n \ . \tag{7.9}$$

Since the S-matrix is expanded in terms of (light-front) time ordered contributions, all particles are on their mass-shell, while any intermediate state is off energy shell. Thus, all amplitudes and equations of motion can be expressed in terms of three-dimensional quantities (like the momenta for instance). This enables us to have a clear physical relationship between light

front relativistic and non-relativistic amplitudes, as we shall illustrate in the following sections. The final expression for the S-matrix takes the following form:

$$S = 1 + \int_{-\infty}^{+\infty} \frac{\exp(i\tau\sigma)}{2\pi i(\tau - i\epsilon)} R(\omega\tau)\mathrm{d}\tau \ , \tag{7.10}$$

with $R(\omega\tau)$ given by:

$$R(\omega\tau) = \sum_n (-i)^n \int \tilde{H}_\omega(\omega\tau - \omega\tau_1)\frac{\mathrm{d}\tau_1}{2\pi i(\tau_1 - i\epsilon)}$$
$$\tilde{H}_\omega(\omega\tau_1 - \omega\tau_2)\frac{\mathrm{d}\tau_2}{2\pi i(\tau_2 - i\epsilon)} \cdots \tilde{H}_\omega(\omega\tau - \omega\tau_{n-1})\frac{\mathrm{d}\tau_{n-1}}{2\pi i(\tau_{n-1} - i\epsilon)} \ . \tag{7.11}$$

Here $\tilde{H}_\omega$ is the Fourier transformation of the interaction part of the Hamiltonian. The full S-matrix and therefore any physical amplitudes do not depend on ω but the off-shell energy amplitudes do.

7.3 Wave function

The particle is described by a wave function expressed in terms of Fock components of the state vector [127, 128, 129] which respects the properties required under any transformation and therefore respects the angular momentum condition –see Eq. (7.6). Recall that the state vector is to be an irreducible representation of the Poincaré group and is to be fully defined by a mass, M, a four momentum, p, a total angular momentum, J, and a z-axis projection of angular momentum, λ. The state vector describing a meson of momentum p, defined on a light-front plane characterized by ω (with $\omega\cdot x = 0$ for simplicity), is given by:

$$|p,\lambda\rangle_\omega = \phi^{J\lambda}(p) = (2\pi)^{3/2}\int \Phi^{J\lambda}_{j_1\sigma_1 j_2\sigma_2}(k_1,k_2,p,\omega\tau)a^\dagger_{\sigma_1}(\mathbf{k}_1)a^\dagger_{\sigma_2}(\mathbf{k}_2)|0\rangle$$
$$\times\,\delta^{(4)}(k_1+k_2-p-\omega\tau)\exp(i\tau\sigma)2(\omega\cdot p)\mathrm{d}\tau\frac{\mathrm{d}^3k_1}{(2\pi)^{3/2}\sqrt{2\varepsilon_{k_1}}}\frac{\mathrm{d}^3k_2}{(2\pi)^{3/2}\sqrt{2\varepsilon_{k_2}}}$$
$$+\,(2\pi)^{3/2}\int \Phi^{J\lambda}_{j_1\sigma_1 j_2\sigma_2 j_3\sigma_3}(k_1,k_2,k_3,p,\omega\tau)a^\dagger_{\sigma_1}(\mathbf{k}_1)a^\dagger_{\sigma_2}(\mathbf{k}_3)a^\dagger_{\sigma_3}(\mathbf{k}_2)|0\rangle$$
$$\times\,\delta^{(4)}(k_1+k_2+k_3-p-\omega\tau)\exp(i\tau\sigma)2(\omega\cdot p)$$
$$\mathrm{d}\tau\frac{\mathrm{d}^3k_1}{(2\pi)^{3/2}\sqrt{2\varepsilon_{k_1}}}\frac{\mathrm{d}^3k_2}{(2\pi)^{3/2}\sqrt{2\varepsilon_{k_2}}}\frac{\mathrm{d}^3k_3}{(2\pi)^{3/2}\sqrt{2\varepsilon_{k_3}}}\cdots \ , \tag{7.12}$$

where $\varepsilon_{k_i} = \sqrt{\mathbf{k}_i^2 + m_i^2}$ and $\mathbf{k}_i$ is the momentum of the quark i. λ is the projection of the total angular momentum of the system on the z axis in the rest frame and $\sigma_1, \sigma_2, \sigma_3$ are the spin projections of the particles 1 to 3 in the corresponding rest systems. If we retain the two body component only [127, 128, 129], from the delta function ensuring momentum conservation, one gets:

$$\mathcal{P} = p + \omega\tau = k_1 + k_2 \ . \tag{7.13}$$

To keep track of this conservation law, we shall represent on any diagram

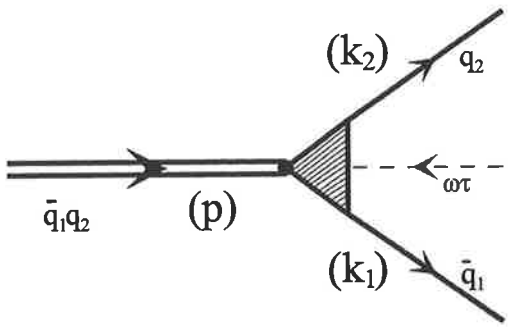

Figure 7.2: Diagrammatic representation of the two body wave function on the light-front.

(see Fig. 7.2) the four-vector $\omega\tau$ by a dashed line (the so-called spurion line, see [122, 123, 124] for more details). We emphasize that the bound state wave function is always an off-energy shell object ($\tau \neq 0$ due to binding energy) and depends on the light-front orientation. There is no fictitious particle in the physical state vector, although a momentum is assigned to the spurion. The parameter τ is entirely determined by the on-mass shell condition for the individual constituents.

7.3.1 Various parametrizations

The two-body wave function $\Phi(k_1, k_2, p, \omega\tau)$ written in Eq. (7.12) can be parametrized in terms of various sets of variables. In order to make a close connection to the non-relativistic case, it would be more convenient to introduce another pair of variables [122, 123, 124] defined by:

$$\mathbf{k} = L^{-1}(\mathcal{P})\mathbf{k}_1 = \mathbf{k}_1 - \frac{\mathcal{P}}{\sqrt{\mathcal{P}^2}}\left[k_{10} - \frac{\mathbf{k}_1 \cdot \mathcal{P}}{\sqrt{\mathcal{P}^2} + \mathcal{P}_0}\right] \ , \tag{7.14}$$

$$\mathbf{n} = \frac{L^{-1}(\mathcal{P})\omega}{|L^{-1}(\mathcal{P})\omega|} = \sqrt{\mathcal{P}^2}\frac{L^{-1}(\mathcal{P})\omega}{\omega \cdot p} \ , \tag{7.15}$$

where $\mathcal{P} = k_1 + k_2$, and $L^{-1}(\mathcal{P})$ is the Lorentz boost. The relativistic, relative momentum, $\mathbf{k}$, corresponds, in the frame where $\mathbf{k_1} + \mathbf{k_2} = \mathbf{0}$, to the usual relative momentum between the two particles. Note that this choice of variable does not assume that we restrict ourselves to this particular frame. The unit vector $\mathbf{n}$ corresponds, in this frame, to the spatial direction of ω.

The second set of variables which we shall use in the following are the usual light-front coordinates $(x, \mathbf{R}_\perp)$, which are defined by analogy to the equal time function in the infinite momentum frame as:

$$\begin{aligned} x &= \frac{\omega \cdot k_1}{\omega \cdot p} , \\ R_1 &= k_1 - xp , \end{aligned}$$

and where R_1 is decomposed in its spatial components parallel and perpendicular to the direction of the light-front, $R_1 = (R_0, \mathbf{R}_\perp, \mathbf{R}_{||})$. We have by definition $R_1 \cdot \omega = 0$, and thus $R_1^2 = -\mathbf{R}_\perp^2$. We can easily express these variables in terms of the previous ones. All details can be found in Refs. [122, 123, 124]. The relations between $(x, \mathbf{R}_\perp)$ and $(\mathbf{k}^2, \mathbf{n}\cdot\mathbf{k})$ are the following,

$$\begin{aligned} \mathbf{R}_\perp^2 &= \mathbf{k}^2 - (\mathbf{n}\cdot\mathbf{k})^2 , \\ x &= \frac{1}{2}\left[1 - \frac{(\mathbf{n}\cdot\mathbf{k})}{\epsilon_k}\right] , \end{aligned} \tag{7.16}$$

with $\epsilon_k = \sqrt{k^2 + m^2}$ in the case of equal masses. The inverse relations read:

$$\begin{aligned} \mathbf{k}^2 &= \frac{\mathbf{R}_\perp^2 + m^2}{4x(1-x)} - m^2 , \\ \mathbf{n}\cdot\mathbf{k} &= \left[\frac{\mathbf{R}_\perp^2 + m^2}{x(1-x)}\right]^{1/2} \left(\frac{1}{2} - x\right) , \end{aligned} \tag{7.17}$$

where $\mathbf{k}^2$ and $\mathbf{n}\cdot\mathbf{k}$ are the rotation and Lorentz invariants. The wave function can therefore be expressed at any time as:

$$\Phi(\mathbf{R}_\perp, x) \equiv \tilde{\Phi}(\mathbf{k}^2, \mathbf{n}\cdot\mathbf{k}) . \tag{7.18}$$

7.3.2 Equation of motion

The two-body component Φ is the solution of a three dimensional equation, Eq. (7.19). It is shown schematically by the diagram of Fig. 7.3. For simplicity, let us just first consider the case of a scalar system composed of two scalar

particles. The wave function is scalar, and can be parametrized in terms of $\Phi(x, \mathbf{R}_\perp)$. The homogeneous equation which Φ should satisfy is given by:

$$\left(\frac{\mathbf{R}_\perp^2 + m^2}{x(1-x)} - M^2\right)\Phi(x, \mathbf{R}_\perp) = \frac{1}{(2\pi)^3}\int \Phi(x', \mathbf{R}'_\perp)\mathcal{K}(x', \mathbf{R}'_\perp; x, \mathbf{R}_\perp, M^2)\frac{\mathrm{d}^2\mathbf{R}'_\perp \mathrm{d}x'}{2x'(1-x')}\ , \quad (7.19)$$

where m is the constituent quark mass (for two identical particles) and M is the bound state mass. In this form, this equation is similar to the Weinberg equation. The kernel $\mathcal{K}$ of the equation, defined graphically by the shaded area in Fig. 7.3, depends on the dynamics of the system. In our case, we shall use a kernel with one gluon exchange. This exchange is shown in Fig. 8.1 and will be discussed later in Chapter 8. The relativistic wave function is

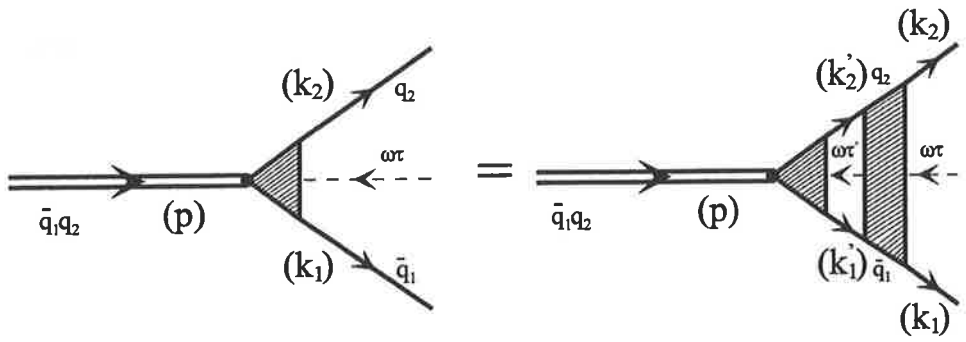

Figure 7.3: Two body relativistic wave function equation.

an equal-time wave function on the light-front which turns out to be the non-relativistic wave function when $c \to \infty$.

7.3.3 Normalization

As regards the normalization, the state vector which describes a physical particle is normalized according to:

$$\langle p', \lambda' | p, \lambda \rangle = 2p_0\delta^{(3)}(\mathbf{p} - \mathbf{p}')N^{\lambda'\lambda}\ , \quad (7.20)$$

where $N^{\lambda'\lambda} = \sum_n N_n^{\lambda'\lambda}$ with $N_n^{\lambda'\lambda}$ being the contribution from the n-body Fock components. Its expression in terms of x and $\mathbf{R}_\perp$ is given by [122, 123,

124],

$$N_n^{\lambda'\lambda} = (2\pi)^3 \int \sum_{\sigma_1 \cdots \sigma_n} \Phi^{J\lambda'*}_{j_1 \sigma_1 \cdots j_n \sigma_n} \Phi^{J\lambda}_{j_1 \sigma_1 \cdots j_n \sigma_n} \delta^{(2)}\Big(\sum_{i=1}^{n} \mathbf{R}_{\perp i}\Big) \delta\Big(\sum_{i=1}^{n} x_i - 1\Big) 2 \prod_{i=1}^{n} \frac{\mathrm{d}^2\mathbf{R}_{\perp i}\mathrm{d}x_i}{(2\pi)^3 2x_i} , \quad (7.21)$$

where J, λ, j_i, and σ_i are defined as in Eq. (7.12) and where Φ is the wave function expressed in the Fock state decomposition (see Eq. (7.12)). In the case where the total angular momentum is equal to zero ($J = 0$), the normalization condition for the corresponding pseudoscalar or scalar particles becomes:

$$\sum_n N_n = 1 , \quad (7.22)$$

where we take into account all the n-body Fock components. If the total angular momentum is equal to one ($J = 1$), the normalization condition for the corresponding pseudovector or vector particles takes the following form:

$$N_n^{\lambda'\lambda} = e_\mu^{*(\lambda')}(p) I_n^{\mu\nu} e_\nu^{(\lambda)}(p) , \quad (7.23)$$

where $e_\nu^{(\lambda)}(p)$ is the polarization vector for the system and $I_n^{\mu\nu}$ is a tensor written as,

$$I_n^{\mu\nu} = -A_n g^{\mu\nu} + B_n p^\mu p^\nu + C_n(p^\mu \omega^\nu + p^\nu \omega^\mu) + D_n(p^\mu \omega^\nu - p^\nu \omega^\mu) + E_n\left(\frac{\omega^\mu \omega^\nu}{(\omega \cdot p)^2} + \frac{g_{\mu\nu}}{3M^2}\right) . \quad (7.24)$$

In Eq. (7.24) A_n, B_n, C_n, D_n and E_n are constants with $\sum_n C_n = \sum_n D_n = \sum_n E_n = 1$ and M is the mass of the system.

Although each contribution to the normalization may depend on ω (this is the case for $J = 1$ but not for $J = 0$), the total result will be independent of ω if all the n-body Fock components are included.

Chapter 8

Meson wave functions

" Il n'est pas certain que tout soit certain. "

Blaise Pascal

Many theoretical frameworks are used to understand the internal structure of hadrons - for example we can mention QCD sum rules [130, 131, 132], perturbative QCD [133, 134, 135], lattice QCD [136, 137], chiral perturbation theory [138, 139], constituent quark model [140], heavy quark effective theory [141], heavy quark symmetry and light-front quark models [122, 142, 143]. In our work we chose to follow the formalism of Covariant Light-Front Dynamics, detailed in the previous chapter. We will start by applying this formalism to determine in a phenomenological way the wave functions of pseudoscalar particles such as B, D, K, π and the vector particles ρ, ω.

8.1 Pseudoscalar wave function

8.1.1 Structure of the bound state

The explicit covariance of our approach allows us to write down explicitly the general structure of the two-body bound state. For a pseudoscalar particle composed of an antiquark and a quark of mass m_1 and m_2 respectively, it has the form:

$$\Psi_{PS} = \frac{1}{\sqrt{2}}\bar{u}(k_2)\left[A_1\frac{1}{m_r} + A_2\frac{\not{\omega}}{\omega\cdot p}\right]\gamma_5 v(k_1)\ , \tag{8.1}$$

where $v(k_1)$ and $\bar{u}(k_2)$ are the usual Dirac spinors, and A_1 and A_2 are the two scalar components of the wave function. Note that the colour factor is not

included in the wave function written in Eq. (8.1). The mass m_r is defined by $m_r = \frac{2m_1m_2}{m_1+m_2}$ and is chosen here just for convenience. The representation of this wave function in terms of the variables $\mathbf{k}$ and $\mathbf{n}$ is given by:

$$\Psi_{PS} = \frac{1}{\sqrt{2}} w_2^t \left(g_1 + \frac{i\sigma\cdot[\mathbf{n}\times\mathbf{k}]}{k} g_2 \right) w_1 \ , \tag{8.2}$$

where w_i is the Pauli spinor. One can easily express A_1 and A_2 in terms of g_1 and g_2. One finds for A_1:

$$\begin{aligned} A_1 = +\frac{m_r}{\sqrt{\varepsilon_{k,1}+m_1}\sqrt{\varepsilon_{k,2}+m_2}} \left(1+\frac{\mathbf{k}^2}{(\varepsilon_{k,1}+m_1)(\varepsilon_{k,2}+m_2)}\right)^{-1} \left\{ g_1 + \frac{g_2}{k} \right. \\ \times \left[1 - \frac{\mathbf{k}^2}{(\varepsilon_{k,1}+m_1)(\varepsilon_{k,2}+m_2)} - \mathbf{n}\cdot\mathbf{k}\left(\frac{1}{\varepsilon_{k,1}+m_1} - \frac{1}{\varepsilon_{k,2}+m_2}\right)\right] \\ \left. \times \left(\frac{1}{\varepsilon_{k,1}+m_1} + \frac{1}{\varepsilon_{k,2}+m_2}\right)^{-1} \right\} , \end{aligned} \tag{8.3}$$

and for A_2:

$$A_2 = -\frac{\sqrt{\varepsilon_{k,1}+m_1}\sqrt{\varepsilon_{k,2}+m_2}}{k} \left(1+\frac{m_1+m_2}{\varepsilon_{k,1}+\varepsilon_{k,2}}\right)^{-1} g_2 \ , \tag{8.4}$$

where one defines $\varepsilon_{k,i} = \sqrt{\mathbf{k}^2+m_i^2}$.

The components g_1 and g_2 will be parametrized by gaussian wave functions written as $g_i = 4\pi^2\alpha_i\beta_i \exp(-\beta_i\mathbf{k}^2)$ where α_i and β_i are two parameters to be determined from experimental data. In terms of the variables $(x, \mathbf{R}_\perp)$, we have for the relative momentum between two quarks of different masses:

$$\mathbf{k}^2 = \frac{(\mathbf{R}_\perp^2 + (m_1(x-1)-xm_2)^2)(\mathbf{R}_\perp^2 + (m_1(x-1)+xm_2)^2)}{4x(1-x)(\mathbf{R}_\perp^2 + (1-x)m_1^2 + xm_2^2)} \ . \tag{8.5}$$

8.1.2 Radiative corrections to the wave function

In our phenomenological study of wave functions, we shall start from a gaussian parametrization of the components g_1 and g_2, as given above. However, it is necessary to correct these wave functions in some way in order to incorporate the high momentum tail given by the one-gluon exchange mechanism (see Fig. 8.1). We shall achieve this using perturbation theory, starting from the zeroth order wave function parametrized as gaussian, and calculate the corrected wave function using the equation of motion analogous to Eq. (7.19).

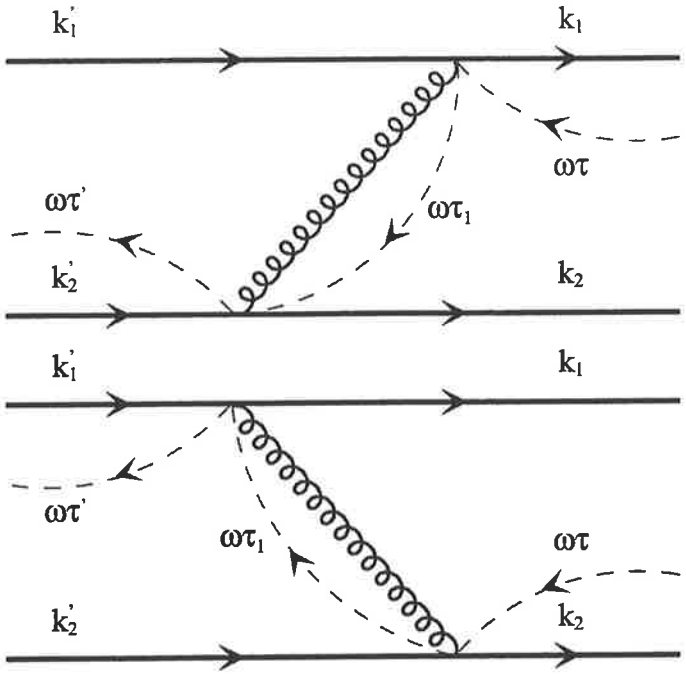

Figure 8.1: One-gluon exchange kernel.

This equation is, for spin 1/2 particles:

$$(s-M^2)\,\bar{u}(k_2)\vartheta v(k_1) = \frac{1}{(2\pi)^3}\int \bar{u}(k_2)\left[\gamma_\mu(\not{k}_2'+m_2)\vartheta'(m_1-\not{k}_1')\gamma_\nu\right]K^{\mu\nu}v(k_1)\frac{\mathrm{d}^3\mathbf{k_1}'}{2\varepsilon_{k_1'}(1-x')}\,, \quad (8.6)$$

with:

$$s=\frac{\mathbf{R}_\perp^2+m_1^2}{x}+\frac{\mathbf{R}_\perp^2+m_2^2}{(1-x)}\,, \quad (8.7)$$

$$\vartheta=\frac{1}{\sqrt{2}}\left[\frac{A_1}{m_r}+A_2\frac{\not{\omega}}{\omega\cdot p}\right]\gamma_5\,,\ \text{and}\ \vartheta'=\frac{1}{\sqrt{2}}\left[\frac{A_1'}{m_r}+A_2'\frac{\not{\omega}}{\omega\cdot p}\right]\gamma_5\,. \quad (8.8)$$

The kernel[1] $K^{\mu\nu}$ can be written as $K^{\mu\nu}=-g^{\mu\nu}\mathcal{K}$, with:

$$\mathcal{K}=g^2\int\theta(\omega\cdot(k_1-k_1'))\delta((k_1-k_1'+\omega\tau_1-\omega\tau)^2-\mu^2)\frac{d\tau_1}{\tau_1-i\epsilon} + g^2\int\theta(\omega\cdot(k_1'-k_1))\delta((k_1'-k_1+\omega\tau_1-\omega\tau')^2-\mu^2)\frac{d\tau_1}{\tau_1-i\epsilon}\,, \quad (8.9)$$

[1]Note that a colour factor $-\frac{4}{3}$ has to be added.

which gives,

$$\mathcal{K} = \frac{g^2\theta(\omega\cdot(k_1-k_1'))}{\mu^2-(k_1-k_1')^2+2\tau\omega\cdot(k_1-k_1')-i\epsilon} + \frac{g^2\theta(\omega\cdot(k_1'-k_1))}{\mu^2-(k_1'-k_1)^2+2\tau'\omega\cdot(k_1'-k_1)-i\epsilon}\ , \quad (8.10)$$

where τ and τ' are defined by,

$$\tau = \frac{s-M^2}{2\,\omega\cdot p}\ , \quad \text{and} \quad \tau' = \frac{s'-M^2}{2\,\omega\cdot p}\ . \quad (8.11)$$

The two items in Eq. (8.9) cannot be both non-zero simultaneously. After developing all scalar products, one gets the following final expression for $\mathcal{K}$, in the variables $(x, \mathbf{R}_\perp)$:

$$\begin{aligned}\mathcal{K}(x,x',\mathbf{R}_\perp,\mathbf{R}'_\perp;M) = \\ \left\{\left(-(x-1)\big(x'^2+x'+x(x'-1)\big)m_1^2 - 2\mathbf{R}'_\perp\cdot\mathbf{R}_\perp(x-1)x'\right.\right. \\ \left.\left. - M^2x'(x-1)(x-x') + \mathcal{K}'(x,x',\mathbf{R}_\perp,\mathbf{R}'_\perp)\right)\frac{1}{x'(x-1)}\right\}^{-1}\Theta(x'-x) + \\ \left\{\left(-(x'-1)\big(x^2+x+x'(x-1)\big)m_1^2 - 2\mathbf{R}'_\perp\cdot\mathbf{R}_\perp(x'-1)x\right.\right. \\ \left.\left. - M^2x(x'-1)(x'-x) + \mathcal{K}'(x,x',\mathbf{R}_\perp,\mathbf{R}'_\perp)\right)\frac{1}{x(x'-1)}\right\}^{-1}\Theta(x-x')\ ,\end{aligned} \quad (8.12)$$

where,

$$\mathcal{K}'(x,x',\mathbf{R}_\perp,\mathbf{R}'_\perp) = \mathbf{R}_\perp^2x'(x'-1) + \mathbf{R}_\perp'^2x(x-1) + m_2^2xx'(x+x'-2)\ . \quad (8.13)$$

In order to extract the two components A_1 and A_2, one should proceed as follows. We first multiply both sides of Eq. (8.6) by $u(k_2)$ on the left and $\bar{v}(k_1)$ on the right, then sum over polarization states. We then multiply both sides successively by γ_5 and $\not{\omega}\gamma_5$, and then take the trace. We end up with the following system of equations:

$$\begin{aligned}&\mathrm{Tr}\Big[\gamma_5(\not{k}_2+m_2)\vartheta(\not{k}_1-m_1)\Big] = \\ &\frac{1}{(s-M^2)(2\pi)^3}\int \mathrm{Tr}\Big[\gamma_5(\not{k}_2+m_2)A_{\mu\nu}(\not{k}_1-m_1)\Big]K^{\mu\nu}\frac{\mathrm{d}^2\mathbf{R}'_\perp\mathrm{d}x'}{2x'(1-x')}\ ,\end{aligned} \quad (8.14)$$

$$\mathrm{Tr}\Big[\psi\gamma_5(\not k_2+m_2)\vartheta(\not k_1-m_1)\Big]=$$
$$\frac{1}{(s-M^2)(2\pi)^3}\int \mathrm{Tr}\Big[\psi\gamma_5(\not k_2+m_2)A_{\mu\nu}(\not k_1-m_1)\Big]K^{\mu\nu}\frac{\mathrm{d}^2\mathbf{R}'_\perp\mathrm{d}x'}{2x'(1-x')}\ , \quad (8.15)$$

with:

$$A_{\mu\nu}=\gamma_\mu(\not k'_2+m_2)\vartheta'(m_1-\not k'_1)\gamma_\nu\ . \quad (8.16)$$

In perturbation theory, we take $A'_{1,2}=A^{0\prime}_{1,2}$ in the r.h.s. of Eq. (8.14) and Eq. (8.15), where $A^{0\prime}_{1,2}$ are given by Eq. (8.3) and Eq. (8.4) with gaussian wave functions for $g_{1,2}$. The correction to the wave function is then given by solving the system of equations Eq. (8.14) and Eq. (8.15). We finally get:

$$A^1_{1,2}=A^{0\prime}_{1,2}+A'_{1,2}\ , \quad (8.17)$$

where,

$$A'_{1,2}=\int_0^1\int_0^\infty\Big[\chi_{1,2}(x,x',\mathbf{R}_\perp,\mathbf{R}'_\perp)A^{0\prime}_1+\Omega_{1,2}(x,x',\mathbf{R}_\perp,\mathbf{R}'_\perp)A^{0\prime}_2\Big]$$
$$\times\mathcal{K}(x,x',\mathbf{R}_\perp,\mathbf{R}'_\perp;M)\frac{1}{s-M^2}\frac{\mathrm{d}^2\mathbf{R}'_\perp\mathrm{d}x'}{(2\pi)^3 2x'(1-x')}\ , \quad (8.18)$$

where the expressions for $\chi_{1,2}$ and $\Omega_{1,2}$ are reported in Appendix A.

8.1.3 Physical constraints

Normalization

According to the spirit of the constituent quark model, the state vector is decomposed in Fock components, and only the two-body component is retained. Since the state vector is normalized as:

$$\langle p',\lambda'|p,\lambda\rangle=2p_0\delta^{(3)}(\mathbf{p}-\mathbf{p}')\delta^{\lambda'\lambda}\ , \quad (8.19)$$

it gives for a state of zero total angular momentum, the following normalization condition [124]:

$$N_2\equiv 1=\int_D\sum_{\lambda_1\lambda_2}\Psi_{\lambda_1\lambda_2}\Psi^\star_{\lambda_1\lambda_2}D\ , \quad (8.20)$$

where D is an invariant phase space element defined by:

$$D=\frac{1}{(2\pi)^3}\frac{\mathrm{d}^3\mathbf{k}_1}{(1-x)2\varepsilon_{k_1}}=\frac{1}{(2\pi)^3}\frac{\mathrm{d}^3\mathbf{k}}{\varepsilon_k}=\frac{1}{(2\pi)^3}\frac{\mathrm{d}^2\mathbf{R}_\perp\mathrm{d}x}{2x(1-x)}\ . \quad (8.21)$$

With the pseudoscalar wave function written in Eq. (8.1), the normalization condition is therefore [124]:

$$1 = \int_D \left[\left\{ \frac{\mathbf{R}_\perp^2 + (m_2 x + m_1(1-x))^2}{m_r^2 x(1-x)} \right\} A_1^2 + 4A_1 A_2 \left\{ \frac{m_1(1-x) + m_2 x}{m_r} \right\} + 4x(1-x)A_2^2 \right] D \ . \quad (8.22)$$

Decay constant

The pseudoscalar decay amplitude is given by the diagram in Fig. 8.2. According to the usual definition, the decay amplitude is $\Gamma_\mu = \langle 0|J_\mu|PS\rangle$ where J_μ is the $\gamma_\mu\gamma_5$ current. Since our formulation is explicitly covariant, we can decompose Γ_μ in terms of all momenta available in our system, i.e. the incoming meson momentum p_μ and ω_μ. We have therefore:

$$\Gamma_\mu = f_{PS}\ p_\mu + B\ \omega_\mu \ , \quad (8.23)$$

where f_{PS} is the physical decay constant. In an exact calculation of Γ_μ, B should be zero. Since $\omega^2 = 0$, the decay constant can be obtained according to:

$$f_{PS} = \frac{\Gamma\cdot\omega}{\omega\cdot p} \ . \quad (8.24)$$

Using the diagrammatic rules of CLFD, we can calculate Γ_μ from the dia-

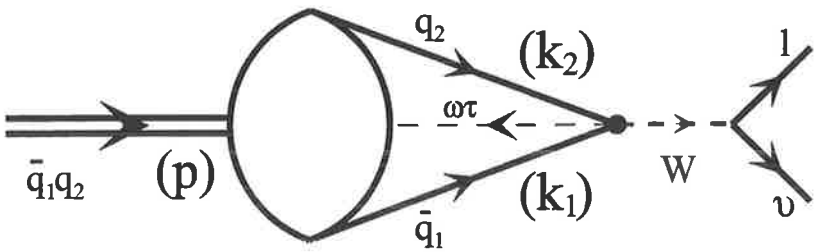

Figure 8.2: Decay diagram.

gram shown in Fig. 8.2. One gets:

$$\Gamma_\mu = \sqrt{3}\int_D \mathrm{Tr}\left[\frac{1}{\sqrt{2}}\left(\frac{A_1}{m_r} + A_2\frac{\not\omega}{\omega\cdot p}\right)\gamma_5(m_1 - \not k_1)\gamma_\mu(1-\gamma_5)(\not k_2 + m_2)\right] D \ . \quad (8.25)$$

Having calculated the trace, the decay constant is then given by:

$$f_{PS} = 2\sqrt{6}\int_D \left[\left\{\frac{(m_1(1-x)+m_2x)}{m_r}\right\}A_1 + 2x(1-x)A_2\right] D\ . \qquad (8.26)$$

Electromagnetic form factor

The electromagnetic form factor is one of the most useful tools with which we can probe the internal structure of a bound state. Moreover, from the electromagnetic form factor at low Q^2, it is possible to determine the charge radius for a given particle. This physical observable is therefore very powerful in order to constrain the phenomenological structure of the wave function. The leading order (impulse approximation) for the electromagnetic form factor is shown in Fig. 8.3.

In CLFD, the general physical electromagnetic amplitude of a spinless system can be decomposed as [124, 144]:

$$J_\rho = \langle PS|\bar{q}\gamma_\rho q|PS\rangle = (p+p')_\rho\ F_{PS}(Q^2) + \frac{\omega_\rho}{\omega\cdot p}B(Q^2)\ , \qquad (8.27)$$

where $F_{PS}(Q^2)$ is the physical form factor. In any exact calculation, $B(Q^2)$ should be zero. We choose for convenience $\omega\cdot q = 0$. This implies automatically that the form factors $F_{PS}(Q^2)$ and $B(Q^2)$ depend on $Q^2 = -q^2$ only, since from homogeneity arguments they can depend only on $\omega\cdot p/\omega\cdot p' \equiv 1$. The physical electromagnetic form factor $F_{PS}(Q^2)$ can be obtained by contracting both sides in Eq. (8.27) with ω_ρ. One then has:

$$F_{PS}(Q^2) = \frac{J\cdot\omega}{2\,\omega\cdot p}\ . \qquad (8.28)$$

By using the diagrammatic rules of CLFD, we can write down the electromagnetic amplitude corresponding to Fig. 8.3 where the photon interacts with a quark. Assuming that quarks are pointlike, one obtains:

$$F_{PS}^{\gamma q}(Q^2) = e_q\int_D \mathrm{Tr}\left[-\bar{\vartheta}'(\not{k}_2'+m_2)\frac{\not{\omega}}{2(1-x)\omega\cdot p}(\not{k}_2+m_2)\vartheta(m_1-\not{k}_1)\right] D\ , \qquad (8.29)$$

with, e_q, the quark electric charge and where $\bar{\vartheta}$ is defined by:

$$\bar{\vartheta} = \gamma^0\vartheta^\dagger\gamma^0\ , \qquad (8.30)$$

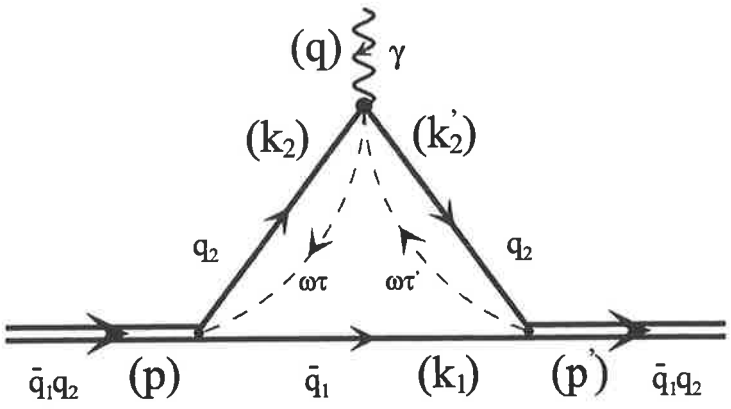

Figure 8.3: Electromagnetic form factor, $F_{PS}^{\gamma q}(Q^2)$, of a two body bound state where the photon interacts with the quark. A similar diagram can be drawn in the case of $F_{PS}^{\gamma\bar{q}}(Q^2)$ where the photon interacts with the antiquark.

with ϑ and ϑ' given in Eq. (8.8). After simplification one obtains,

$$F_{PS}^{\gamma q}(Q^2) = e_q \int_D \left[\frac{(m_1(1-x)+m_2 x)^2 + \mathbf{R}_\perp^2 - x\mathbf{R}_\perp\cdot\Delta}{x(1-x)m_r^2} A_1 A_1' \right.$$
$$\left. + 2(A_1 A_2' + A_1' A_2)\frac{(m_1(1-x)+m_2 x)}{m_r} + 4x(1-x)A_2 A_2' \right] D \ . \quad (8.31)$$

The wave functions A_1' and A_2' depend on $(x', \mathbf{R}_\perp')$, with $x = x'$ in the impulse approximation. If we define the four momentum transfer q by $q = (q_0, \Delta, \mathbf{q}_{||})$, with $\Delta\cdot\omega = 0$ and $\mathbf{q}_{||}$ parallel to ω, we have $Q^2 = -q^2 \equiv \Delta^2$, and thus $\mathbf{R}_\perp' = \mathbf{R}_\perp - x\Delta$. In the case where the photon interacts with an antiquark, one gets:

$$F_{PS}^{\gamma\bar{q}}(Q^2) = e_{\bar{q}} \int_D \mathrm{Tr}\left[-\vartheta(m_2 - \not{k}_2)\frac{\not{\omega}}{2(1-x)\omega\cdot p}(m_2 - \not{k}_2')\bar{\vartheta}'(m_1 + \not{k}_1) \right] D \ . \quad (8.32)$$

Finally, for the electromagnetic form factor, $F_{PS}(Q^2)$, one obtains:

$$F_{PS}(Q^2) = F_{PS}^{\gamma q}(Q^2) + F_{PS}^{\gamma\bar{q}}(Q^2) \ . \quad (8.33)$$

From the form factor, we can extract two major pieces of information: the first is the charge radius of the bound state defined by:

$$\langle r_{PS}^2 \rangle = -6\frac{\mathrm{d}}{\mathrm{d}Q^2} F_{PS}(Q^2)\Big|_{Q^2=0} \ , \quad (8.34)$$

and the second is the behaviour of the electromagnetic form factor at high Q^2 (i.e. its asymptotic form).

Asymptotic behaviour of the electromagnetic form factor

It is now well accepted that the asymptotic behaviour of the pion form factor, $F_{PS}(Q^2) \sim 1/Q^2$, is fully determined by the one gluon exchange mechanism. This mechanism can either be considered explicitly in the hard scattering amplitude, or incorporated in the relativistic wave function of the meson. Here we adopt the second strategy. At asymptotically large Q^2, the form factor is dominated by the contribution from the relativistic A_2 component in Eq. (8.1). The high momentum tail of the wave function is thus generated by the one-gluon exchange kernel, as detailed in Section 8.1.2. We will assume that the asymptotic behaviour of the kaon form factor is similar to that of the pion.

Transition form factor

The quantum numbers of the π transition amplitude, $\pi \to \gamma^*\gamma$, are similar to the deuteron electrodisintegration amplitude near threshold, as detailed in Ref. [124]. The exact physical amplitude has the form:

$$F_{\mu\rho} = \frac{-i}{2} e_{\rho\mu\nu\lambda} q^\nu P^\lambda F^{\pi\gamma} \ , \tag{8.35}$$

where $P = p + p'$ and $q = p' - p$. In any approximate calculation, the amplitude $F_{\mu\rho}$ has to depend on ω. It should therefore be decomposed in terms of all possible tensor structures compatible with the quantum numbers of the transition, as we did above for the decay constant and the electromagnetic form factor. One thus has [124]:

$$\begin{aligned} F_{\mu\rho} = {} & \frac{-i}{2} e_{\rho\mu\nu\gamma} q^\nu P^\gamma F^{\pi\gamma} + e_{\rho\mu\nu\gamma} q^\nu \omega^\gamma B_1 + e_{\rho\mu\nu\gamma} p^\nu \omega^\gamma B_2 \\ & + (V_\mu q_\rho + V_\rho q_\mu) B_3 + (V_\rho \omega_\rho + V_\rho \omega_\mu) B_4 + \frac{1}{2m^2 \omega \cdot p} (V_\mu p_\rho + V_\rho p_\mu) B_5 \ , \end{aligned} \tag{8.36}$$

where $V_\mu = e_{\mu\alpha\beta\gamma} \omega^\alpha q^\beta p^\gamma$. From Eq. (8.36) we can extract the physical form factor $F^{\pi\gamma}$ by the following contraction:

$$F^{\pi\gamma} = \frac{-i}{2Q^2(\omega \cdot p)} e^{\mu\rho\nu\lambda} q_\nu \omega_\lambda F_{\mu\rho} \ . \tag{8.37}$$

For the transition form factor to leading order, the two relevant diagrams are indicated on Fig. 8.4 ($F^a_{\mu\rho}$) and Fig. 8.5 ($F^b_{\mu\rho}$), respectively. By applying

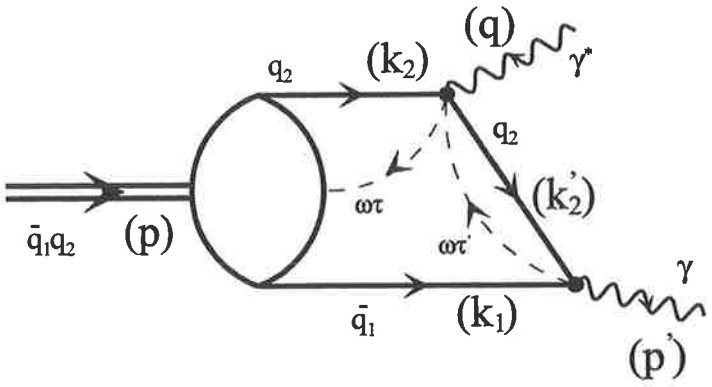

Figure 8.4: The leading contribution ($F^a_{\mu\rho}$) to the transition form factor, $\pi \to \gamma^*\gamma$ (first diagram).

the diagrammatic rules of CLFD, we can derive the corresponding amplitude and one finds:

$$F^a_{\mu\rho} = \frac{\sqrt{3}}{2}(e_u^2 - e_d^2)$$
$$\int_D \mathrm{Tr}\Big[\vartheta(m - \not{k}_1)\gamma_\mu(\not{k}'_2 - \omega\tau' + m)\gamma_\rho(\not{k}_2 + m)\Big]\frac{D}{m^2 - (p+q-k_1)^2}\,, \quad (8.38)$$

where e_q is the quark electric charge. The second diagram which is necessary to compute the transition form factor can be calculated similarly, and one gets for $F^b_{\mu\rho}$,

$$F^b_{\mu\rho} = \frac{\sqrt{3}}{2}(e_u^2 - e_d^2)$$
$$\int_D \mathrm{Tr}\Big[\vartheta(m - \not{k}_1)\gamma_\rho(m - \not{k}'_1 + \omega\tau')\gamma_\mu(\not{k}_2 + m)\Big]\frac{D}{m^2 - (p+q-k_2)^2}\,. \quad (8.39)$$

Other diagrams which should be taken into account at leading order either correspond to vacuum diagrams or are equal to zero for $\omega\cdot q = 0$. The total amplitude for the transition form factor therefore reads:

$$F_{\pi\gamma}(Q^2) = \sqrt{3}(e_u^2 - e_d^2)$$
$$\times \int_D \frac{2D}{4\varepsilon_k^2(1-x) - 2\mathbf{R}_\perp\cdot\Delta + xQ^2}$$
$$\left[A_1 + 2A_2x(1-x) + A_2\frac{\mathbf{R}_\perp\cdot\Delta}{Q^2}(1-x)\right]\,. \quad (8.40)$$

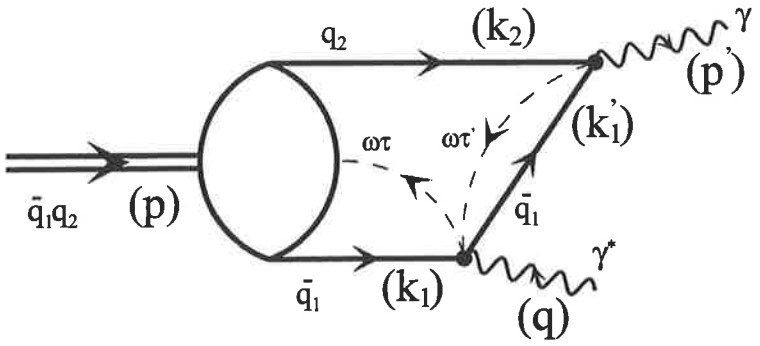

Figure 8.5: The leading contribution ($F^b_{\mu\rho}$) to the transition form factor, $\pi \to \gamma^*\gamma$ (second diagram).

Axial anomaly The constraint from the axial anomaly is defined at $Q^2 = 0$ GeV^2. It gives the transition form factor when both photons are on their mass-shell. One should have [145, 146, 147]:

$$F_{\pi\gamma}(Q^2 = 0) = \frac{1}{4\pi^2 f_\pi} \,. \tag{8.41}$$

Asymptotic behaviour At high Q^2, the transition form factor behaves like $1/Q^2$. In this limit, we can simplify Eq. (8.40) and one obtains:

$$Q^2 F_{\pi\gamma}(Q^2)\Big|_{Q^2\to\infty} = 2\sqrt{3}(e_u^2 - e_d^2)\int_D \frac{1}{x}\Big[A_1 + 2A_2 x(1-x)\Big] D \,. \tag{8.42}$$

In the approximation $x = 1/2$, the transition form factor can be expressed as a function of the decay constant obtaining,

$$Q^2 F_{\pi\gamma}(Q^2)\Big|_{Q^2\to\infty} = \sqrt{2}(e_u^2 - e_d^2) f_\pi \,. \tag{8.43}$$

8.1.4 Numerical results

Data

The wave function is expressed in terms of the scalar functions A_1 and A_2, which means that we have to determine 5 parameters in our analysis. There are two parameters per scalar function, A_i, and the strong coupling constant as well. In order to have an accurate phenomenological investigation, we will deal with only 3 parameters which are α and β from the scalar function A_1 and the strong coupling constant from the one-gluon exchange. Therefore,

the analysis will start by using a scalar function A_1 and by applying the kernel to it we will generate the scalar function A_2 without any additional fit parameter. We will separate our analysis into two parts. The first concerns heavy particles, such as B and D, and the second focuses on light particles, such as π and K.

Regarding the particles B and D, it has been explained in Ref. [148] that the relativistic component A_2 goes to zero in the heavy quark limit. We can thus safety restrict our choice by taking only the scalar function A_1 as initial ansatz wave function. Since we work in a constituent quark model, we use the following quark masses and decay constants for the numerical applications:

$$m_1 = m_b = 4.930 \text{ GeV}, \text{ and } m_2 = m_u = 0.35 \text{ GeV} ,$$
$$m_1 = m_c = 1.620 \text{ GeV}, \text{ and } m_2 = m_u = 0.35 \text{ GeV} ,$$
$$f_D = (0.225 \pm 0.028) \text{ GeV [149] , and } f_B = (0.200 \pm 0.030) \text{ GeV [150, 151]} .$$

Unfortunately, there is no experimental data for decay constants of heavy mesons. Therefore, we will use values for the decay constants f_D and f_B extracted mainly from lattice QCD and QCD sum rules, even though it can be observed that their values may vary according to the framework applied. Note also that we modify slightly the value of m_1 in order to have $m_1 + m_2 \geq M$. For the meson masses we take,

$$M_B = 5.279 \text{ GeV} , \quad M_D = 1.968 \text{ GeV} .$$

The strong coupling constant is evaluated at the next to leading order according to the heavy quark mass for the B and D mesons. Working in the constituent quark model framework, we will assume that the normalization of the wave function is equal to one.

The second part of our analysis concerns the light particles π and K. For light quark systems like π or K, one would have to consider both components A_1 and A_2 as initial ansatz. For the reason previously explained, (number of parameters and simplicity) we will consider only as input the scalar wave function A_1 and we will obtain the relativistic component A_2 through radiative corrections. The initial scalar wave function for π and K will thus be determined using only three parameters: α, β and the strong coupling constant, α_s. For the numerical applications, we take for the quark masses:

$$m_1 = m_u = 0.350 \text{ GeV}, \qquad m_2 = m_u = 0.350 \text{ GeV} ,$$
$$m_1 = m_s = 0.510 \text{ GeV}, \qquad m_2 = m_u = 0.350 \text{ GeV} ,$$

and concerning the meson masses, one uses:

$$M_\pi = 0.135 \text{ GeV} , \quad M_K = 0.497 \text{ GeV} .$$

The coupling constant, α_s, is determined according to the asymptotic behaviour of the electromagnetic form factor. Its value for the pion and kaon will be discussed in the next section. Both particles K and π are more easily constrained than B and D, because of the numerous available experimental data. In our analysis, we will take into account the decay constant and the observables extracted from the electromagnetic form factor. For the decay constant, we take the following values:

$$f_\pi = 0.129 \pm 0.01 \text{ GeV} ,$$
$$f_K = 0.159 \pm 0.01 \text{ GeV} .$$

As has already been mentioned in the previous section, one important physical property and one specific physical behaviour can be obtained from the electromagnetic form factor. These are the charge radius and the asymptotic electromagnetic form factor. We use for the charge radius the following experimental values:

$$\langle r_\pi^2 \rangle_{\text{exp}} = (0.439 \pm 0.03) \text{ fm}^2 \text{ [152]} ,$$
$$\langle r_K^2 \rangle_{\text{exp}} = (0.340 \pm 0.05) \text{ fm}^2 \text{ [153]} .$$

Recently, experimental data has been re-analysed for the pion asymptotic electromagnetic form factor at high Q^2. Usually, the value 0.3 GeV^2 [154] has been used for $Q^2 F_\pi(Q^2)$ when Q^2 becomes large. Since the re-analysis of experimental data sets from DESY [155] and those extracted from the longitudinal cross section at Jefferson Lab [156], we will use the following asymptotic limit:

$$\lim_{Q^2 \to \infty} Q^2 F_\pi(Q^2) = (0.45 \pm 0.10) \text{ GeV}^2 .$$

Unfortunately, for the kaon electromagnetic form factor, we do not have any accurate experimental data sets. By assuming that the kaon is similar to the pion by $SU(3)$ symmetry, we will consider the same asymptotic behaviour as for the pion, however with a larger uncertainty. Thus one has:

$$\lim_{Q^2 \to \infty} Q^2 F_K(Q^2) = (0.45 \pm 0.15) \text{ GeV}^2 .$$

Finally, we will assume that the normalization is equal to one in the spirit of the constituent quark model.

Discussion

By solving the system of physical constraints detailed previously, we have extracted the wave functions for the pseudoscalar mesons B, D, π and K.

In order to compare the theoretical predictions $\{y\}$ with the experimental measurements $\{x \pm \sigma_x\}$, we defined the following χ^2 by:

$$\chi^2 = \sum \left(\frac{x-y}{\sigma_x} \right)^2 . \tag{8.44}$$

We also define the light cone distribution amplitude[2], $\Phi(x)$ as a function of the momentum fraction carried by one quark as,

$$\Phi(x) = \int_0^\infty \frac{\mathrm{d}^2\mathbf{R}_\perp}{(2\pi)^3 2x(1-x)} \phi(x, \mathbf{R}_\perp) . \tag{8.45}$$

We consider the normalization and decay constant as our input parameters for the evaluation of the B and D mesons and we choose for the value of the strong coupling constant (calculated to next leading order) that given at the scale $\mu = m_b$ and $\mu = m_c$ for the B and D mesons respectively. The average transverse momentum $\sqrt{\langle \mathbf{R}_\perp^2 \rangle}$ is the only output in the case of heavy mesons. For the pion and kaon wave functions, we consider in addition to the two previous input parameters, the asymptotic electromagnetic form factor. Then as output parameters, one obtains the charge radius, the transverse momentum $\sqrt{\langle \mathbf{R}_\perp^2 \rangle}$ and the asymptotic transition form factor (the latter case is only valid for the pion).

B	D	π	K
$\alpha_1 = 0.2804$	$\alpha_1 = 0.2426$	$\alpha_1 = 0.056$	$\alpha_1 = 0.099$
$\beta_1 = 1.4680$	$\beta_1 = 2.100$	$\beta_1 = 31.12$	$\beta_1 = 19.01$
$\alpha_s = 0.2190$	$\alpha_s = 0.3200$	$\alpha_s = 0.92$	$\alpha_s = 0.68$

Table 8.1: Parameters $\alpha_1, \beta_1(\mathrm{GeV}^{-2})$ and α_s for the B, D, K and π wave functions.

The input parameters have been fitted and the results for the constants α_1, β_1 and α_s are listed in Table 8.1 for all of the mesons mentioned previously. For the heavy quark systems, such as the pseudoscalars B and D, the values of α_1 and β_1 are strongly related to the value of the decay constant $f_{B(D)}$. In Fig. 8.6, the distribution amplitudes for B and D are shown. It can be seen that the distributions $\Phi(x)$ for B and D are peaked at high values of x and vanish at low values of x. This behaviour originates from the heavy c and b quark masses. Their distributions reach the maximum when x is around $x_B^{max} = 0.93$ and $x_D^{max} = 0.86$, respectively. This roughly corresponds to

[2]Note that $\Phi(x)$ refers to the scalar function A_1.

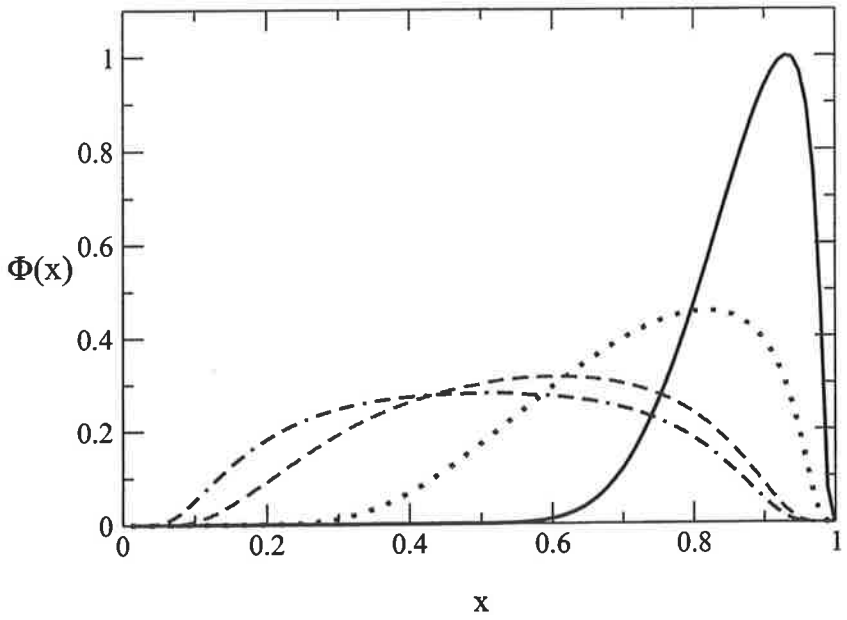

Figure 8.6: Pseudoscalar distribution amplitude. Full line, dotted line, dashed line and dot-dashed line represent the distribution amplitude for B, D, K and π respectively.

the ratios m_b/M_B and m_c/M_D. Finally, the average transverse momentum, $\sqrt{\langle \mathbf{R}_\perp^2 \rangle}$, is equal to 0.530 GeV for the B meson and takes the value 0.413 GeV for the D meson. These results are listed in Table 8.2.

Now let us focus on light particles. We are mainly interested in the pion and the kaon pseudoscalar mesons. Regarding the pion wave function, many studies have been performed in the past and it is still under investigation. We can refer to the Gaussian model [141, 157], the BSW approach [75] and the B.F. (Braun and Filyanov) wave function [158, 159]. We can also cite the very well known asymptotic form [160, 161, 162] and the C.Z.-like wave function [161, 163, 164] (Chernyak and Zhitnitsky). Note as well that wave function distribution amplitudes can be expanded in terms of Gegenbauer polynomials, where their coefficients are calculated using Light Cone Sum Rules (LCSR).

In order to determine the pion wave function, recall that we use as input parameters the decay constant, the electromagnetic form factor at high Q^2 and the normalization. As output parameters we obtain the electromagnetic form factor at low Q^2 (that gives us the charge radius), the transition form factor, the axial anomaly and the transverse momentum $\sqrt{\langle \mathbf{R}_\perp^2 \rangle}$. The coefficients α_1, β_1 and α_s which are necessary to obtain our wave function are listed in Table 8.1. The distribution amplitude is shown in Fig. 8.6 as well as

	B	D	π	K
input				
Normalization	1.00	1.00	1.00	1.00
Decay constant (GeV)	0.200	0.225	0.129	0.159
Asymptotic $Q^2F_{PS}(Q^2)$			0.35	0.37
output				
Asymptotic $Q^2F_\gamma(Q^2)$			0.166	
Charge radius (fm^2)			0.410	0.386
$\sqrt{\langle \mathbf{R}_\perp^2 \rangle}$ (GeV)	0.530	0.413	0.290	0.320
χ^2	0.0	0.0	1.0	0.28

Table 8.2: Physical constraints for pseudoscalar particles.

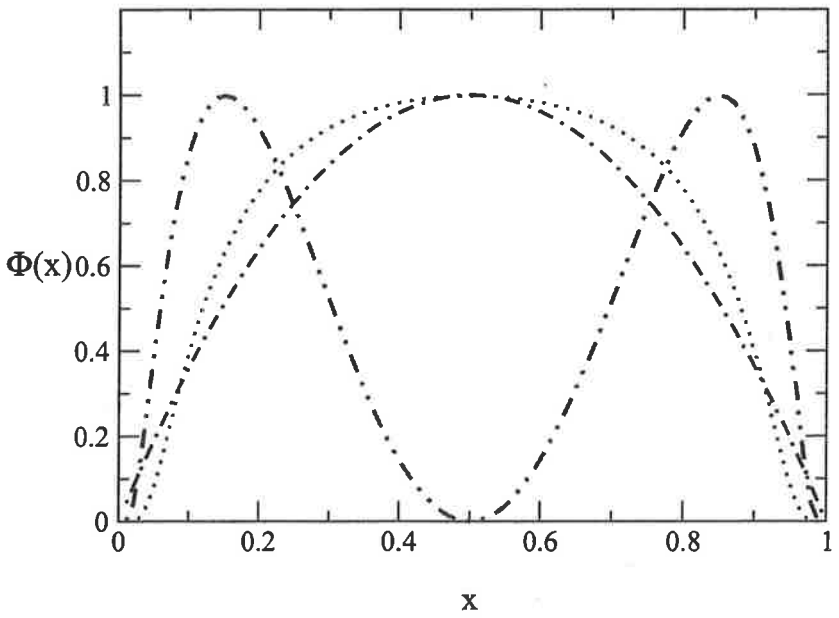

Figure 8.7: Different pion wave functions, asymptotic (dot-dashed line), C.Z. (dot-dotted dashed line), our work (dotted line).

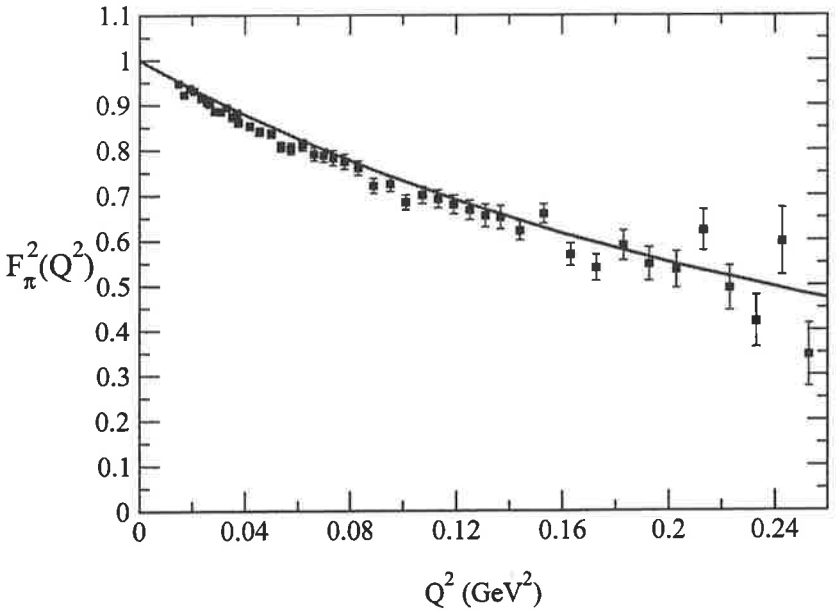

Figure 8.8: Pion electromagnetic form factor. Experimental data are taken from Ref. [165] (solid square).

in Fig. 8.7 where comparisons[3] can be made with the C.Z. and asymptotic pion wave functions. In Fig. 8.7 the C.Z. and asymptotic pion wave functions are:

$$\Phi(x)^{asym} = 6x(1-x) \ ,$$
$$\Phi(x)^{CZ} = A(1-2x)^2 \exp\left[-\frac{\mathbf{R}_\perp^2 + m^2}{8\gamma^2 x(1-x)}\right] \ ,$$

where A and γ are parameters that define the wave function. In Figs. 8.8, 8.9 and 8.10 are shown respectively, the pion electromagnetic form factor squared at low Q^2, the pion electromagnetic form factor at high Q^2 and finally the transition form factor. For the electromagnetic form factor one obtains very good agreement with experimental data at low Q^2. The pion charge radius given by the slope of the electromagnetic form factor curve at $Q^2 = 0$ GeV is equal to $\langle r_\pi^2 \rangle = 0.410$ fm^2. This is inside the experimental uncertainty range. At high Q^2 (see Fig. 8.9), the electromagnetic form has been fitted and therefore it is consistent with the data sets [156]. We underline that we take into account the one gluon exchange process which contributes strongly to the quark momentum distribution at high Q^2. We refer the reader to

[3]The distributions have been plotted in order to get a maximum equal to one.

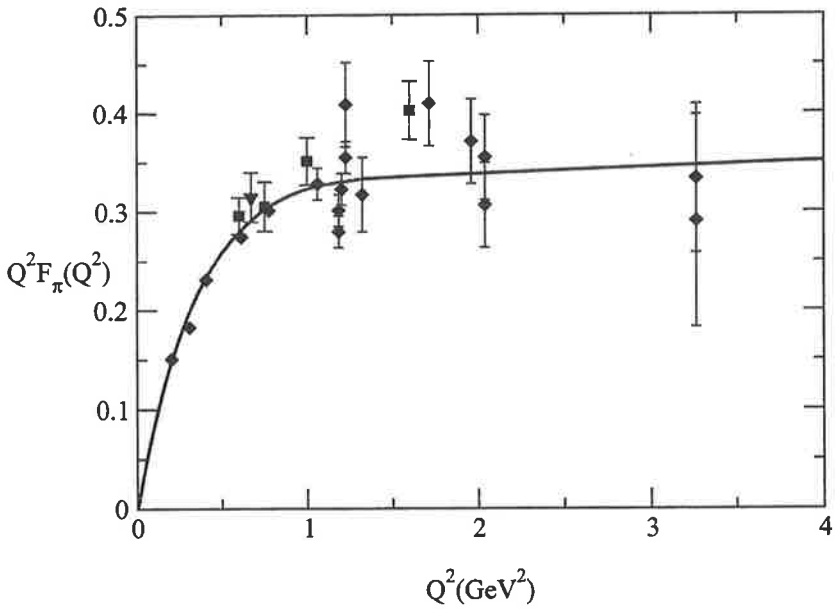

Figure 8.9: Asymptotic pion electromagnetic form factor. Experimental data sets are: full diamonds [172], full triangle down [155] and full square [156].

literature regarding the pion electromagnetic form factor [166, 167, 168, 169, 170] for comparisons. The transition form factor shown in Fig. 8.10, gives good agreement with the experimental data [171] at high Q^2 and it also agrees with the theoretical limit. The only experimental constraint which is not well reproduced is the axial anomaly. A summary of the results is given in Table 8.2. Finally, we have also computed the transverse momentum for which one obtains the following value: $\sqrt{\langle \mathbf{R}_\perp^2 \rangle} = 0.290$ GeV.

In a similar way to that for the pion, we investigate the structure of the kaon wave function. We apply exactly the same approach as outlined previously, with the same input and output parameters except that we do not use the transition form factor and the axial anomaly. In Figs. 8.11 and 8.12 are shown respectively the electromagnetic form factor squared at low Q^2 and the electromagnetic form factor at high Q^2. The coefficients α_1, β_1 and α_s obtained by fitting the physical observables mentioned previously are listed in Table 8.1. In Table 8.2 are given the values of our input and output parameters.

For the electromagnetic form factor, we mainly focus on low Q^2 since we do not have enough accurate experimental data. However, we can check our results at high Q^2 because of assumptions (kaon is similar to the pion by $SU(3)$ symmetry) that give us an asymptotic value of $Q^2 F_K(Q^2)$ around 0.37 GeV^2. We observe that our theoretical results and the experimental

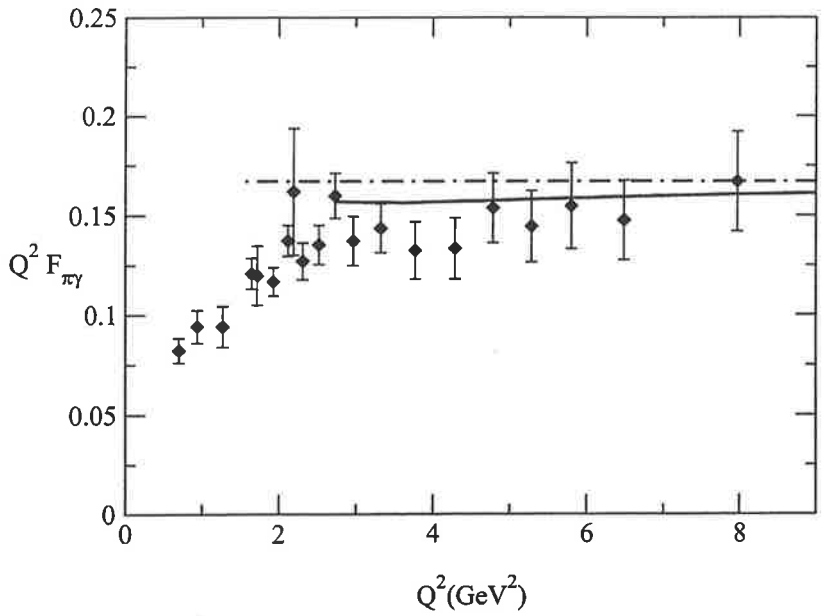

Figure 8.10: Asymptotic pion transition form factor compared to the data [171]. The dot-dashed line is the analytical asymptotic transition form factor from CLFD and the full line is the asymptotic behaviour of the pion transition form factor.

data sets are consistent at low Q^2 as well as in very good agreement with other theoretical approaches, such as soft QCD [173, 174]. By calculating the electromagnetic form factor slope at $Q^2 = 0$ GeV one is able to obtain the kaon charge radius. In our work one has $\langle r_K^2 \rangle = 0.386$ fm^2. As for the pion, the charge radius is inside experimental uncertainty. Regarding the electromagnetic form factor at high Q^2, we have good agreement with the expectation of obtaining a similar behaviour to the pion electromagnetic form factor. This comes from the inclusion of the one gluon exchange that allows the electromagnetic form factor to become flat and stable at high Q^2.

Finally the distribution amplitude of the kaon wave function is shown in Fig. 8.6. We emphasize that the asymmetry in the distribution arises from the s quark mass as expected. From the distribution amplitude, we can also calculate the kaon transverse momentum which is around $\sqrt{\langle \mathbf{R}_\perp^2 \rangle} = 0.320$ GeV. The study of the kaon ends the analysis regarding the pseudoscalar mesons. In the next section we investigate the vector particles such as the ρ and ω.

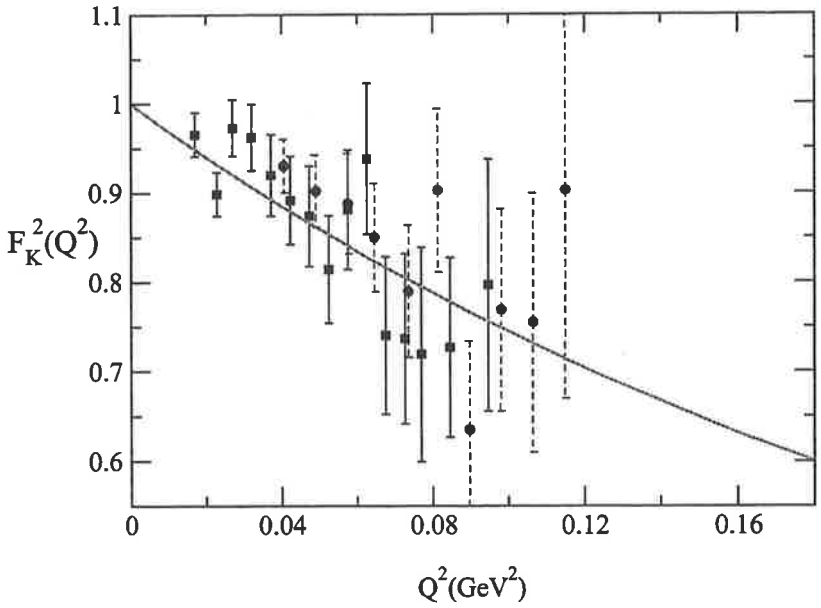

Figure 8.11: Kaon electromagnetic form factor compared to data [153] (solid squares) and to data [175](solid circles).

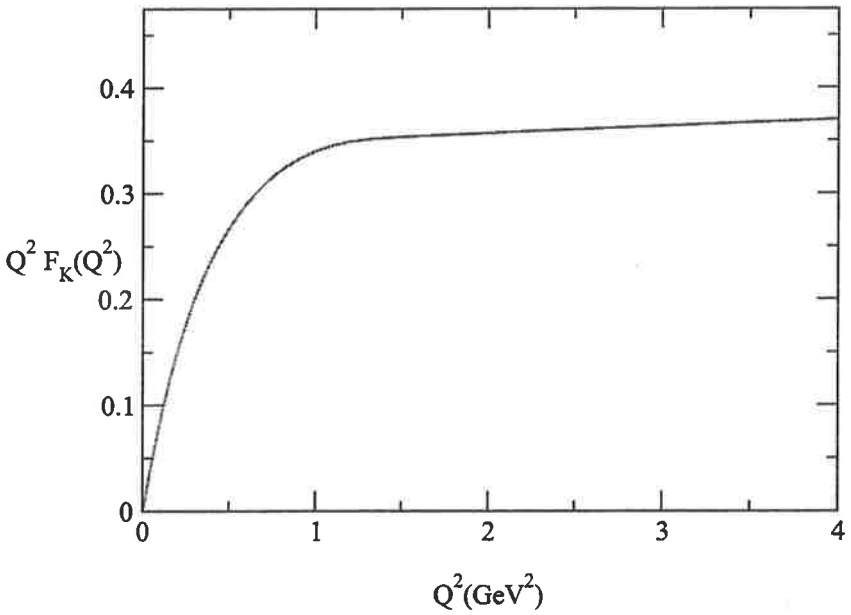

Figure 8.12: Asymptotic kaon electromagnetic form factor.

8.2 Vector mesons

8.2.1 Formalism

We shall now concentrate on the structure of vector mesons $J^P = 1^-$. Following the same approach as for the pseudoscalar mesons, the wave function is decomposed in terms of all possible independent spin structures. One obtains [124]:

$$\Phi^{\lambda}_{\sigma_2\sigma_1}(k_1, k_2, p, \omega\tau) = \sqrt{m}\; e^{\lambda}_{\mu}(p)\; \bar{u}^{\sigma_2}(k_2)\; \phi_{\mu}\; v^{\sigma_1}(k_1)\;, \tag{8.46}$$

with:

$$\phi_{\mu} = \varphi_1 \frac{(k_1 - k_2)_{\mu}}{2m^2} + \varphi_2 \frac{1}{m}\gamma_{\mu} + \varphi_3 \frac{\omega_{\mu}}{\omega\cdot p} + \varphi_4 \frac{(k_1 - k_2)_{\mu}\not{\omega}}{2\omega\cdot p} - \varphi_5 \frac{i}{m^2 \omega\cdot p}\gamma_5 \epsilon_{\mu\nu\rho\gamma} k_{1\nu} k_{2\rho} \omega_{\gamma} + \varphi_6 \frac{m\omega_{\mu}\not{\omega}}{(\omega\cdot p)^2}\;, \tag{8.47}$$

where $e^{\lambda}_{\mu}(p)$ is the polarization vector of the vector meson, and m is the mass of the quark and antiquark. We consider here only the case of equal masses for the quark and antiquark. The wave function[4] is determined by six invariant functions φ_{1-6}, which depend on two invariant scalar variables. This decomposition is similar to the deuteron wave function used in previous studies [176, 177]. In terms of the variables $\mathbf{k}$ and $\mathbf{n}$, the wave function takes the form [124]:

$$\Psi^{\lambda}_{\sigma_2\sigma_1}(\mathbf{k}, \mathbf{n}) = \sqrt{m} w^{\dagger}_{\sigma_2} \psi^{\lambda}(\mathbf{k}, \mathbf{n}) w_{\sigma_1}\;, \tag{8.48}$$

with:

$$\psi(\mathbf{k}, \mathbf{n}) = f_1 \frac{1}{\sqrt{2}}\sigma + f_2 \frac{1}{2}\left(\frac{3\mathbf{k}(\mathbf{k}\cdot\sigma)}{\mathbf{k}^2} - \sigma\right) + f_3 \frac{1}{2}\left(3\mathbf{n}(\mathbf{n}\cdot\sigma) - \sigma\right) + f_4 \frac{1}{2k}\left(3\mathbf{k}(\mathbf{n}\cdot\sigma) + 3\mathbf{n}(\mathbf{k}\cdot\sigma) - 2(\mathbf{k}\cdot\mathbf{n})\sigma\right) + f_5 \sqrt{\frac{3}{2}}\frac{i}{k}\left[\mathbf{k}\times\mathbf{n}\right] + f_6 \frac{\sqrt{3}}{2k}\left[\left[\mathbf{k}\times\mathbf{n}\right]\times\sigma\right]\;, \tag{8.49}$$

where w_{σ} is the two-component Pauli spinor normalised to $w^{\dagger}_{\sigma} w_{\sigma} = 1$, and σ are the usual Pauli matrices. The relation between $\psi^{\lambda}(\mathbf{k}, \mathbf{n})$ and $\psi(\mathbf{k}, \mathbf{n})$, is the same as the relation between the spherical function $Y^{\lambda}_1(\mathbf{n})$ and $\mathbf{n}$.

The coefficients of the spin structures in Eq. (8.47) and Eq. (8.49) are scalar functions of two independent invariants, which we can choose to be $\mathbf{k}^2$

[4]Note that the wave function written in Eq. (8.47) does not include the colour factor.

and $\mathbf{k}\cdot\mathbf{n}$, since these variables are only rotated by a Lorentz boost [124]. In the non-relativistic limit, only two components remain, f_1 and f_2, and they only depend on $\mathbf{k}^2$. This can be easily seen if we keep track of the c factors, and then let c go to infinity to obtain the non-relativistic limit. We shall neglect in the first approximation the tensor component, f_2, so one is left with the non-relativistic wave function $f_1 \equiv \phi^{NR}(\mathbf{k}^2)$. The relation between $\varphi_1(\mathbf{k}^2)$, $\varphi_2(\mathbf{k}^2)$ and $\phi^{NR}(\mathbf{k}^2)$ is given by [178]:

$$\varphi_1(\mathbf{k}^2) = \frac{m^2}{4\varepsilon_k(\varepsilon_k+m)}\sqrt{2}\phi^{NR}(\mathbf{k}^2)\ , \tag{8.50}$$

$$\varphi_2(\mathbf{k}^2) = \frac{m}{4\varepsilon_k}\sqrt{2}\phi^{NR}(\mathbf{k}^2)\ . \tag{8.51}$$

Finally, the wave function $\phi^{NR}(\mathbf{k}^2)$ should be normalized according to [178] and one obtains,

$$N_2 \equiv 1 = m\int_D |\phi^{NR}(\mathbf{k}^2)|^2 D\ . \tag{8.52}$$

8.2.2 Decay constant

The vector decay diagram is similar to the one for the pseudo-scalar particles. It is shown in Fig. 8.13. The decay amplitude $\mathcal{M}^{\mu\rho}$ to produce a photon with

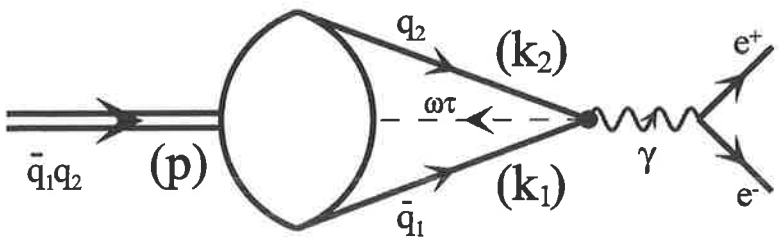

Figure 8.13: Leptonic decay diagram.

polarisation ϵ^μ from a vector state of polarisation ϵ^ρ can be decomposed in terms of all possible tensor structures. Therefore we can write $\mathcal{M}^{\mu\rho}$ [178] as:

$$\mathcal{M}^{\mu\rho} = Fa_1^{\mu\rho} + \frac{B_1}{2\omega\cdot p}a_2^{\mu\rho} + \frac{B_2}{2\omega\cdot p}a_3^{\mu\rho} + \frac{B_3M^2}{(\omega\cdot p)^2}a_4^{\mu\rho} + Da_5^{\mu\rho}\ , \tag{8.53}$$

where the tensors $a_i^{\mu\rho}$ are defined as followed:

$$\begin{aligned} a_1^{\mu\rho} &= g^{\mu\rho} - \frac{p^\mu p^\rho}{M^2} , \\ a_2^{\mu\rho} &= p^\mu \omega_\rho + p^\rho \omega_\mu , \\ a_3^{\mu\rho} &= p^\mu \omega_\rho - p^\rho \omega_\mu , \\ a_4^{\mu\rho} &= \omega^\mu \omega^\rho , \\ a_5^{\mu\rho} &= \frac{p^\mu p^\rho}{M^2} . \end{aligned}$$

By algebraic manipulations [178], we can isolate the physical amplitude F as a function of $\mathcal{M}^{\mu\rho}$, and one obtains:

$$F = \frac{1}{2}(I_1 - 2I_2 + I_4 + I_5) , \quad \text{where} \quad I_i = \mathcal{M}_{\mu\rho} a_i^{\mu\rho} . \tag{8.54}$$

The decay amplitude can be calculated by using CLFD diagrammatical rules and we obtain:

$$\mathcal{M}_{\mu\rho} = \sqrt{3m} \int_D \mathrm{Tr}\Big[\phi_\rho (m - \not{k}_1)\gamma_\mu (1 - \gamma_5)(\not{k}_2 + m)\Big] D . \tag{8.55}$$

One can thus extract the physical amplitude, F, which can be written as:

$$F = \int_D \Big[m \tilde{F} \phi^{NR}(\mathbf{k}^2)\Big] D , \tag{8.56}$$

where one has:

$$\tilde{F} = \frac{-2\sqrt{6m}}{3} \left[1 - 2\left(\frac{m}{\varepsilon_k} + \frac{\varepsilon_k}{m}\right)\right] . \tag{8.57}$$

For two identical quarks, the relative momentum, $\mathbf{k}$, is defined by:

$$\mathbf{k}^2 = \frac{\mathbf{R}_\perp^2 + m^2}{4x(1-x)} - m^2 , \tag{8.58}$$

and the non-relativistic wave function $\phi^{NR}(\mathbf{k}^2)$ is parametrized as a gaussian:

$$\phi^{NR}(\mathbf{k}^2) = \psi(x)\, \Sigma(x, \mathbf{R}_\perp) , \tag{8.59}$$

with $\psi(x)$ given by:

$$\psi(x) = \alpha \exp\left[-\beta\left(\frac{m^2}{4x(1-x)} - m^2\right)\right] . \tag{8.60}$$

Here, α and β are two parameters determined from experimental data sets. The function $\Sigma(x, \mathbf{R}_\perp)$ has the form,

$$\Sigma(x, \mathbf{R}_\perp) = 4\pi^2\beta \exp\left[-\beta \frac{\mathbf{R}_\perp^2}{4x(1-x)}\right] , \tag{8.61}$$

with the following normalization:

$$\int_0^\infty \frac{\mathrm{d}^2\mathbf{R}_\perp}{2x(1-x)} \frac{1}{(2\pi)^3} \Sigma(x, \mathbf{R}_\perp) = 1 . \tag{8.62}$$

After averaging over the polarization states of the vector, one obtains for the decay width:

$$\Gamma(V \to e^+e^-) = \frac{4\pi}{3M^3}\alpha_e^2 E_q^2 |F|^2 , \tag{8.63}$$

where E_q is a factor arising from the electric charges of the constituent quarks, M is the mass of the vector meson and α_e is the electromagnetic fine structure constant. In the non-relativistic limit, one obtains the following decay width $\Gamma^{NR}(V \to e^+e^-)$,

$$\Gamma^{NR}(V \to e^+e^-) = 32\pi \frac{m}{M^3}\alpha_e^2 E_q^2 |\phi^{NR}(\mathbf{r}=0)|^2 , \tag{8.64}$$

where $\phi^{NR}(\mathbf{r})$ is written at the origin as,

$$\phi^{NR}(\mathbf{r}=0) = \frac{\alpha\sqrt{\pi}}{2\sqrt{\beta}} . \tag{8.65}$$

8.2.3 Numerical results

Data

Because of the lack of experimental data for the vector mesons on which we are now focused, we will start our derivation by using a non-relativistic wave function. The vector wave function, $\phi^{NR}(\mathbf{k}^2)$, is determined by two parameters, α and β, which are calculated from the two following constraints: the normalization condition and the leptonic decay. In our numerical applications, we use the constituent quark masses for u and d quarks as previously defined. Regarding the vector masses, one takes:

$$M_\rho = 0.770 \text{ GeV} , \quad M_\omega = 0.782 \text{ GeV} .$$

ρ	ω
$\alpha = 0.213$	$\alpha = 0.204$
$\beta = 5.840$	$\beta = 6.589$

Table 8.3: Parameters $\alpha, \beta(\mathrm{GeV}^{-2})$ for the ρ, ω wave functions.

The leptonic decay is the only physical constraint which is used in our analysis. We apply the following experimental data for our simulations:

$$\Gamma_{ee}(\rho) = (6.77 \pm 0.32)\ \mathrm{KeV}\ ,$$
$$\Gamma_{ee}(\omega) = (0.60 \pm 0.020)\ \mathrm{KeV}\ .$$

The charge factor E_q which arises in the decay width formulation has the following form:

$$E_q^2(\rho) = \frac{1}{2}(e_u - e_d)^2,\ \ E_q^2(\omega) = \frac{1}{2}(e_u + e_d)^2\ , \tag{8.66}$$

where e_u and e_d are the quark electric charges. We also assume that the normalization is chosen to equal one for all the vector mesons analysed. As output, we will get the mean relative momentum square $\langle \mathbf{k}^2 \rangle$, and the averaged transverse momentum square $\langle \mathbf{R}_\perp^2 \rangle$.

Discussions

In solving the system of physical constraints (normalization and leptonic decay width) detailed in Section 8.2.1, we have determined the wave functions corresponding to the vectors ρ and ω. The parameters α and β included in our ansatz wave function have been listed in Table 8.3.

The distribution amplitudes for these vectors are plotted in Fig. 8.13. We investigated the mesons ρ and ω where no radiative corrections have been taken into account. As output results, we obtain the mean relative momentum square $\langle \mathbf{k}^2 \rangle$ and the averaged transverse momentum squared $\langle \mathbf{R}_\perp^2 \rangle$ for all of the vectors studied. Their values are also enumerated in Table 8.4.

One defines in the non-relativistic limit the mean relative momentum square of the bound state by,

$$\langle \mathbf{k}^2 \rangle = \int_0^\infty \frac{\mathrm{d}^3 k}{(2\pi)^3} \mathbf{k}^2 |\phi^{NR}(\mathbf{k}^2)|^2\ . \tag{8.67}$$

Regarding the determination of the ρ and ω wave functions, the leptonic decay width used as a constraint does not include radiative corrections

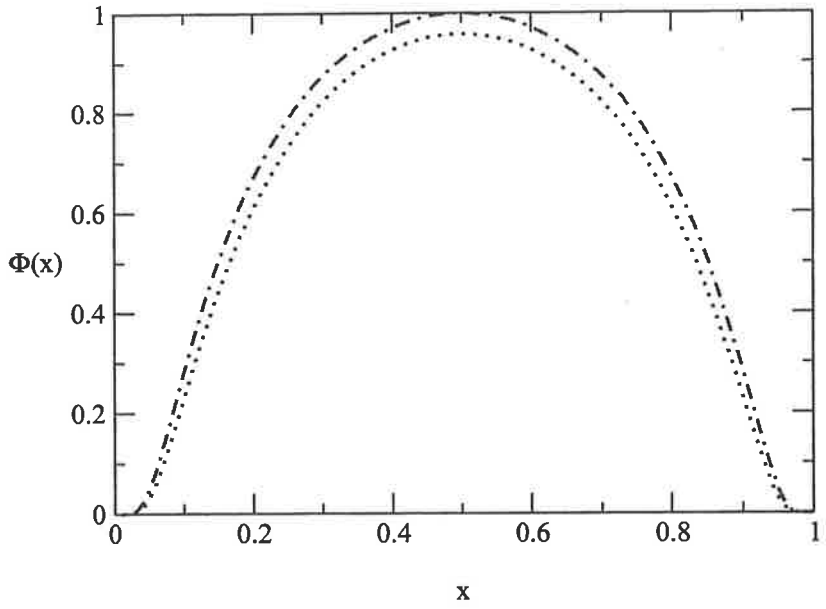

Figure 8.14: Vector meson distribution amplitude: the dotted line and dot-dashed line represent the results for the distribution amplitude of ω and ρ, respectively.

through the one-gluon-exchange. Their distribution amplitudes are plotted in Fig. 8.13 and it appears that they are very close to each other as expected. We are working within the constituent quark picture where the normalization is equal to one for both vectors. The decay constant that is very similar for ρ and ω ($f_\rho = 221$ MeV and $f_\omega = 218$ MeV) is used as the second constraint through the leptonic decay width. These two reasons mainly explain why their distribution amplitudes are very similar.

The low values obtained for the mean relative momentum squared (an output), $\langle \mathbf{k}^2 \rangle$, (see Table 8.4) are in total agreement with the expectation of large radii for the particles ω and ρ. One calculated the mean relative momentum and one obtains $\langle \mathbf{k}^2 \rangle / m_u^2 = 1.420$ for ρ and $\langle \mathbf{k}^2 \rangle / m_u^2 = 1.224$ for ω. According to the parameters determined with the constraints detailed previously, we have determined the averaged transverse momenta for ρ, ω. Their values, which are listed in Table 8.4, respect the hierarchy created by the constituent quark model, since the transverse momentum for ρ and ω (0.459 GeV and 0.434 GeV, respectively) are bigger than those for π and K but smaller than those for B and D. This consistency over the quark scale in the investigated vector and pseudo-scalar mesons is conserved.

Finally, we analyse the distribution amplitude $\Phi_2(\mathbf{R}_\perp)$ as a function of the

	ρ	ω
input		
Normalization	1.00	1.00
Decay width (KeV)	6.77	0.60
output		
$\sqrt{\langle \mathbf{R}_\perp^2 \rangle}$ (GeV)	0.459	0.434
$\langle \mathbf{k}^2 \rangle$ (GeV)^2	0.174	0.150
χ^2	0.0	0.0

Table 8.4: Physical constraints for vector particles.

transverse momentum $\mathbf{R}_\perp$. This can be evaluated by the following expression,

$$\Phi_2(\mathbf{R}_\perp) = \int_0^1 \frac{1}{(2\pi)^3 2x(1-x)} \psi(x)\, \Sigma(x, \mathbf{R}_\perp)\, \mathrm{d}x \ , \tag{8.68}$$

where $\Sigma(x, \mathbf{R}_\perp)$ and $\psi(x)$ have been defined in Eq. (8.60) and Eq. (8.61), respectively. The distribution $\Phi_2(\mathbf{R}_\perp)$ is plotted for the vectors ω and ρ in Fig. 8.15. For ω and ρ, the distribution in terms of the transverse momentum $\mathbf{R}_\perp^2$ is almost identical and indicates once again the similar constitution of these two particles. We note that the average transverse momentum for these particles is around 0.35 at $\mathbf{R}_\perp^2 = 0$ GeV and goes down to 0 near $\mathbf{R}_\perp^2 = 1$ GeV. It emphasises the properties carried by a system of light quarks. Note also that taking the slope of the distribution amplitude $\Phi_2(\mathbf{R}_\perp)$ at the half width, gives the constituent quark mass for the given particles. Hence, one obtains a quark mass around 0.45 GeV for ρ and ω. That finalizes the analysis of light vector mesons.

8.3 Summary

Here we focused on four pseudoscalar particles. Heavy quark and light quark systems have been analysed through the mesons B, D, π, and K. Regarding vector particles, we have studied the ρ and ω mesons. In using all the available physical constraints, we have determined the unknown parameters involved in our ansatz wave functions. According to the experimental data, we have described meson particles by fitting our parameters and by including one-gluon exchange (except for the ρ and ω). The physical constraints (depending on the considered particle) that have been taken into account are

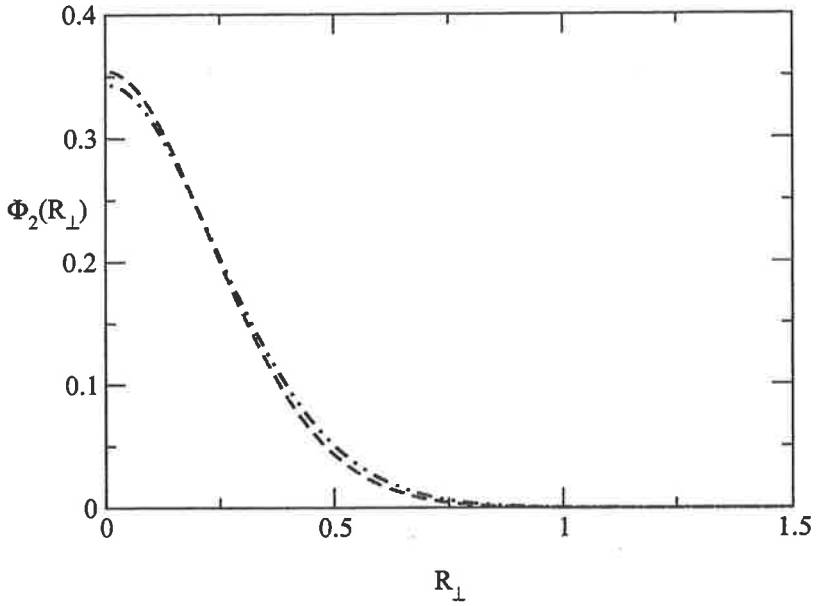

Figure 8.15: Vector distribution amplitude as a function of $\mathbf{R}_\perp$. Dashed line and dot-dashed line represent the results for ω and ρ respectively.

the electromagnetic form factor (asymptotic behaviour and charge radius), transition form factor, decay constant and leptonic decay. The normalization condition has also been utilized. As output results, we have calculated the mean relative momentum square $\langle \mathbf{k}^2 \rangle$, and the averaged transverse momentum square $\langle \mathbf{R}_\perp^2 \rangle$. Now, since one has fully parameterized the wave functions for B, D, π, and K as well as for ρ and ω, we are able to calculate the weak transition form factors between them in the next chapter.

Chapter 9

Transition form factors

" Choisis toujours le chemin qui semble le meilleur même s'il paraît plus difficile: l'habitude le rendra bientôt agréable. "

Pythagore

Having determined the wave functions for the particles B, D, π, K, ρ and ω, we can now investigate the transition form factors between two pseudoscalar mesons and between pseudoscalar and vector mesons. We mainly concentrate our study on B decays, however we also include D decays for completeness. We begin our analysis with the semi leptonic decays of pseudoscalar into pseudoscalar mesons described in the usual formalism (i.e. quark model) and in the CLFD framework. Similar investigations will be made for semi leptonic decays of pseudo scalar into vector mesons.

9.1 Weak decay form factors for $P \to P$ transitions

9.1.1 Usual formalism

Many studies have been done regarding the pseudoscalar pseudoscalar transition. Some of them have been performed in the quark model using heavy quark theory [179, 180, 181, 182, 183], the light front formalism [141, 184] and applying the Isgur-Wise function [185, 186]. Note also that in lattice QCD [187, 188, 189, 190, 191, 192, 193], perturbative QCD [160, 194] and QCD sum rules [76, 195, 196, 197] calculations were derived to analyse this type of transition.

The b and d decays are mainly controlled by the following weak current $J^{\mu}_{b(d)}$ (even though just $\bar{q}\gamma^{\mu}q_{b(d)}$ is relevant),

$$J^{\mu}_{b(d)} = \bar{q}\gamma^{\mu}(1-\gamma_5)q_{b(d)} \ , \tag{9.1}$$

where q is a light or a heavy quark. As usual, one can define the physical amplitude for the semi-leptonic decay $X \to Yl\nu_l$ by the expression:

$$\mathcal{M} = \frac{G_f V_{q_1 q_2}}{\sqrt{2}} \langle P_2|J^{\mu}|P_1\rangle J^{lep}_{\mu} \ , \tag{9.2}$$

where J^{lep}_{μ} is the leptonic current and G_f is the Fermi constant which takes the value $1.166391 \times 10^{-5}\mathrm{GeV}^{-2}$. In Eq. (9.2), $\langle P_2|J^{\mu}|P_1\rangle$ is the hadronic matrix element including the weak current as defined previously. The hadronic matrix element can be given by the following decomposition:

$$\langle P_2|J^{\mu}|P_1\rangle = (P_1+P_2)^{\mu} f_+(q^2) + (P_1-P_2)^{\mu} f_-(q^2) \ , \tag{9.3}$$

where $f_+(q^2)$ and $f_-(q^2)$ are the transition form factors. P_1 and P_2 are respectively the four-momentum related to the initial and final particle states, involved in the hadronic current. By introducing another set of form factors $F_0(q^2)$ and $F_1(q^2)$, the amplitude can be expressed by,

$$\langle P_2|J^{\mu}|P_1\rangle = F_1(q^2)\left[P_1+P_2-\frac{M_1^2-M_2^2}{q^2}q\right]^{\mu} + F_0(q^2)\left[\frac{M_1^2-M_2^2}{q^2}q^{\mu}\right] \ . \tag{9.4}$$

In Eq. (9.4) M_1 and M_2 are the particle masses and q is defined as $q = P_1 - P_2$. It is straightforward to derive the relationship between the two sets of form factors. One obtains,

$$F_1(q^2) = f_+(q^2) \ , \tag{9.5}$$

$$F_0(q^2) = f_+(q^2) + \frac{q^2}{M_1^2-M_2^2} f_-(q^2) \ . \tag{9.6}$$

In the helicity basis, the form factors $F_1(q^2)$ and $F_0(q^2)$ represent the transition amplitudes corresponding to the exchange of a vector and a scalar boson in the t-channel. Note that at $q^2 = 0$, one obtains $F_1(q^2=0) = F_0(q^2=0) = f_+(q^2=0)$. This means that the exchange of either a vector or a scalar boson are similar at $q^2 = 0$ in the t-channel. It is also possible to compare our results with the usual assumption of pole dominance which is currently

applied when the whole q^2 range is not accessible. In this case, the form factors $f_\pm(q^2)$ are described by,

$$f_\pm(q^2) = \frac{f_\pm(0)}{\left(1 - q^2/M^2_{pole}\right)^n} , \tag{9.7}$$

where M_{pole} denotes the meson mass and n refers to a single pole or double pole dominance. This latter expression has been derived according to experimental data.

9.1.2 CLFD formalism

In the Covariant Light-Front Dynamics formalism, the exact transition amplitude does not depend on the light front orientation. However, in any approximate computation the dependence is explicit. But we can parametrise this dependence since our formalism is covariant. Hence, the approximate amplitude expressed in CLFD is given by the following hadronic matrix [148],

$$\langle P_2|J^\mu|P_1\rangle^{CLFD} = (P_1 + P_2)^\mu f_+(q^2) + (P_1 - P_2)^\mu f_-(q^2) + B(q^2)\omega^\mu , \tag{9.8}$$

where $B(q^2)$ is a non-physical form factor which has to be zero in any exact calculation. The last term represents the explicit dependence of the amplitude on the light front orientation ω. In order to extract the physical form factor $f_\pm(q^2)$, without any dependence on ω, from the amplitude $\langle P_2|J^\mu|P_1\rangle^{CLFD}$, we will proceed as follow. Firstly, we calculate the following scalar products $\mathcal{X}, \mathcal{Y}$ and $\mathcal{Z}$ which are defined by,

$$\mathcal{X} = (P_1 + P_2)_\mu \cdot \langle P_2|J^\mu|P_1\rangle^{CLFD} =$$
$$f_+(q^2)\left[2(M_1^2 + M_2^2) - q^2\right] + f_-(q^2)(M_1^2 - M_2^2) + B(q^2)P_1\cdot\omega\,(1+y) , \tag{9.9}$$

$$\mathcal{Y} = (P_1 - P_2)_\mu \cdot \langle P_2|J^\mu|P_1\rangle^{CLFD} =$$
$$f_-(q^2)q^2 + f_+(q^2)(M_1^2 - M_2^2) + B(q^2)P_1\cdot\omega\,(1-y) , \tag{9.10}$$

and finally,

$$\mathcal{Z} = \frac{\omega_\mu \cdot \langle P_2|J^\mu|P_1\rangle^{CLFD}}{\omega\cdot P_1} = f_-(q^2)(1-y) + f_+(q^2)(1+y) . \tag{9.11}$$

In Eqs. (9.9, 9.10, 9.11) the term y defines the ratio between the two momenta P_1 and P_2 times the light-like four vector ω as,

$$y = \frac{\omega\cdot P_2}{\omega\cdot P_1} = \frac{M_2^2 + P_1\cdot P_2}{M_1^2 + P_1\cdot P_2} , \quad \text{with} \quad P_1\cdot P_2 = \frac{1}{2}(M_1^2 + M_2^2 - q^2) . \tag{9.12}$$

For $q^2 > 0$, it is convenient to restrict ourselves to the plane defined by $\vec{\omega}\cdot\vec{q} = \vec{0}$. This condition is allowed in the system of reference where $\vec{P}_1 + \vec{P}_2 = \vec{0}$ with $P_{10} - P_{20} \neq 0$. From the scalar products $\mathcal{X}, \mathcal{Y}$ and $\mathcal{Z}$ we can isolate the form factors $f_\pm(q^2)$ from $B(q^2)$. Then, one gets the expressions for the form factors $f_\pm(q^2)$:

$$f_\pm(q^2) = \Omega(y, q^2)\Psi_\pm(y, q^2, \mathcal{X}, \mathcal{Y}, \mathcal{Z}) \ , \tag{9.13}$$

where $\Omega(y, q^2)$ is identical for both form factors $f_\pm(q^2)$:

$$\Omega(y, q^2) = \frac{1}{4\big[((y-1)M_1^2 + q^2)y - M_2^2(y-1)\big]} \ , \tag{9.14}$$

and where the functions $\Psi_\pm(y, q^2, \mathcal{X}, \mathcal{Y}, \mathcal{Z})$ have the following form:

$$\begin{aligned}
&\Psi_-(y, q^2, \mathcal{X}, \mathcal{Y}, \mathcal{Z}) = \\
&\quad \mathcal{Y}(y+1)^2 + \mathcal{X}(y^2-1) + \Big[(1-3y)M_1^2 - M_2^2(y-3) + q^2(y-1)\Big]\mathcal{Z} \ , \\
&\Psi_+(y, q^2, \mathcal{X}, \mathcal{Y}, \mathcal{Z}) = \\
&\mathcal{Y}(y^2-1) + \mathcal{X}(y-1)^2 + \Big[(y-1)M_1^2 - M_2^2(y-1) + q^2(y+1)\Big]\mathcal{Z} \ .
\end{aligned} \tag{9.15}$$

The second step is to express the amplitude $\langle P_2|J^\mu|P_1\rangle^{CLFD}$ without using the form factors $f_\pm(q^2)$. In CLFD the leading contribution to the transition amplitude $\langle P_2|J^\mu|P_1\rangle^{CLFD}$ is given by the diagram shown in Fig. 9.1.

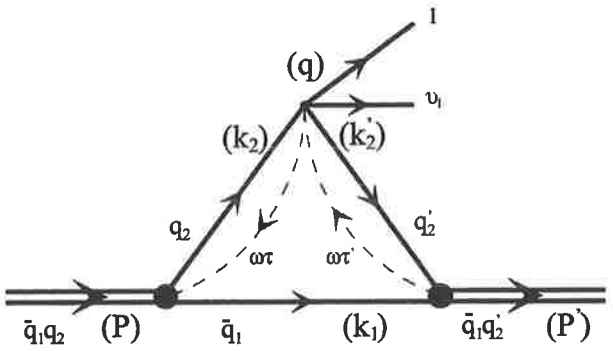

Figure 9.1: Transition between two pseudoscalar particles (leading contribution).

By using the CLFD rules (see Ref. [124]), one can derive the matrix

elements from the diagram (Fig. 9.1) and one has,

$$\langle P_2|J^\mu|P_1\rangle_g^{CLFD} = \int \mathrm{Tr}\left[-\bar{\vartheta}_2(m_2' + \not{k}_2')\gamma^\mu(1-\gamma_5)(m_2+\not{k}_2)\vartheta_1(m_1-\not{k}_1)\right]\frac{1}{1-x'}D \ , \quad (9.16)$$

where ϑ_j is defined by:

$$\vartheta_j = \frac{1}{\sqrt{2}}\left[\frac{A_{1,j}}{m_{r_j}} + A_{2,j}\frac{\not{\omega}}{\omega\cdot p_j}\right]\gamma_5 \ \text{ and } \ \bar{\vartheta}_j = \gamma_0\vartheta_j^t\gamma_0 \ . \quad (9.17)$$

$A_{i,j}$ are the scalar wave functions defined previously in Chapter 8. The indices $i = 1,2$ denote the scalar component of wave functions whereas the indices $j = 1,2$ refer to the initial and final meson, respectively.

Note that x and x' are the fraction of the momentum carried by a quark q_1 (spectator quark) as given by:

$$x = \frac{\omega\cdot k_1}{\omega\cdot p_1} \ , \quad \text{and} \quad x' = \frac{\omega\cdot k_1}{\omega\cdot p_2} \ . \quad (9.18)$$

Finally, recall D is the invariant phase space element given by:

$$D = \frac{1}{(2\pi)^3}\frac{\mathrm{d}^3\mathbf{k}_1}{(1-x)2\varepsilon_{k_1}} = \frac{1}{(2\pi)^3}\frac{\mathrm{d}^3\mathbf{k}}{\varepsilon_k} = \frac{1}{(2\pi)^3}\frac{\mathrm{d}^2\mathbf{R}_\perp \mathrm{d}x}{2x(1-x)} \ . \quad (9.19)$$

Now, one can replace the hadronic matrix element $\langle P_2|J^\mu|P_1\rangle^{CLFD}$, which appears in the scalar products $\mathcal{X}, Y, Z$ defined in Eqs. (9.9, 9.10, 9.11), by the hadronic matrix elements $\langle P_2|J^\mu|P_1\rangle_g^{CLFD}$ calculated by applying the CLFD diagrammatic rules and given in Eq. (9.16). Hence, by using Eq. (9.13) we are able to compute the form factors $f_\pm(q^2)$ as a function of q^2 and this over the whole available momentum range $0 < q^2 < q^2_{max}$.

9.1.3 Semi-leptonic decay

The form factor $f_-(q^2)$ yields a contribution to the semi-leptonic decay which is proportional to the lepton mass and therefore can be safety neglected in first approximation in the calculation of the decay rate. Using this assumption, the usual semi-leptonic decay rate is proportional to just the form factor $F_1(q^2) = f_+(q^2)$ and takes the form,

$$\Gamma = \Gamma_0 \int_{\eta_{min}}^{\eta_{max}} \mathrm{d}\eta \ (\eta^2-1)^{3/2} f_+^2(\eta) \ , \quad (9.20)$$

where η is defined as $\eta = P_1 \cdot P_2 / M_1 M_2$. $\eta_{min} = 1$ (zero recoil) and $\eta_{max} = (M_1^2 + M_2^2)/2M_1M_2$ - these correspond to $q^2 = q^2_{max} = (M_1 - M_2)^2$ and $q^2 = q^2_{min} = 0$, respectively. By writing the form factor $h_+(\eta)$ as a function of $f_+(\eta)$, $h_+(\eta)$ is normalized to one at the point of zero recoil ($\eta = 1$) and its slope near 1 is the so-called Isgur-Wise function ρ^2:

$$h_+(\eta) = 1 - \rho^2(\eta - 1) + O[(\eta - 1)^2] \; . \tag{9.21}$$

The other parameters in Eq. (9.20) are:

$$\Gamma_0 = |V_{\bar{q}_1 q_2}|^2 \frac{G_F^2 M_1^5}{12\pi^3} \xi^4 \;\text{ with }\; \xi = \frac{M_2}{M_1} \; , \tag{9.22}$$

where $V_{\bar{q}_1 q_2}$ is the relevant CKM matrix element. An extraction of the CKM matrix element could be made by comparing experimental data with theoretical predictions for the semi-leptonic decay.

	This work	BSW model	Lattice	QCDSR
$B \to D$				
$F_0(0)$	0.72	0.69	–	–
$B \to \pi$				
$F_0(0)$	0.35	0.33	0.28	0.30
$B \to K$				
$F_0(0)$	0.40	0.37	0.30	0.29
$D \to \pi$				
$F_0(0)$	0.67	0.69	0.65	0.50
$D \to K$				
$F_0(0)$	0.72	0.76	0.73	0.60

Table 9.1: Form factors for the pseudoscalar pseudoscalar transition. BSW model [73, 74, 80], Lattice QCD [187, 188, 189, 190, 191, 192] and QCDSR [76, 195, 196, 197].

9.1.4 Numerical results for $P \to Pl\nu_l$

We calculated the transition form factors in the case of the pseudoscalar pseudoscalar transitions, such as $B \to D$, $B \to \pi$, $B \to K$, $D \to \pi$ and $D \to K$. We are working in a constituent quark model where the CLFD formalism is applied. The wave functions used to describe the particles B, D, K, and π

have been determined using the same approach as that for the form factors (we refer the reader to the previous chapter for all the details regarding their determination) and have been constrained by several physical observables such as decay constant and electromagnetic form factor. We recall that all of the wave functions include the effect of one gluon exchange, which provides indirectly radiative corrections to the transition form factor.

Each of the weak hadronic transitions mentioned previously are induced by a charge current quark transition. The $B \to D$ transition is induced by $b \to c$, the $B \to \pi$ by $b \to d$, the $B \to K$ by $b \to s$, the $D \to \pi$ by $c \to d$, and the $D \to K$ by the $c \to s$ charged quark transition. In Table 9.1 we list the form factors at $q^2 = 0$, computed in our work, and comparisons with other approaches (Lattice QCD, QCDSR and BSW) are shown as well. Because of Eq. (9.5) we expect to obtain similar results for $F_0(q^2)$ and $F_1(q^2)$ at $q^2 = 0$. We observe that our results are qualitatively in agreement with the three other frameworks, lattice QCD, QCDSR and BSW. However, it appears that our results are closer to those obtained by BSW than those given by QCDSR and lattice QCD. This can be understood by the fact that both BSW and our work are derived in a constituent quark model approach. This is not the case for the QCDSR and lattice QCD formalisms. In the next section, we investigate the weak transition form factors in the case of $B \to V l \nu_l$ and $D \to V l \nu_l$.

9.2 Weak decay form factors for $P \to V$ transitions

Numerous studies of the weak decay form factors in $P \to V$ transitions can be found in the literature. As for the $P \to P$ transition, different frameworks have been applied. We refer the reader to theoretical approaches such as using HQET [198, 199, 182, 183], light front and Isgur-Wise function [185, 186], lattice QCD [187, 188, 189, 190, 191, 192, 193], perturbative QCD [160, 194], QCD sum rules [76, 195, 196, 197] and "exotic" analysis [200, 201, 202, 203]. All of them investigate the hadronic matrix elements that drives the weak decay transition between two hadronic states.

9.2.1 Vector current

Since the Lorentz invariance is maintained, one can define the hadronic form factors as a covariant decomposition of hadronic matrix elements of vector and axial currents. For a transition between a pseudoscalar and vector meson, one has usually four form factors - three for the axial current and one for the

vector current. We first focus on the vector current V_μ, where $V_\mu = \bar{q}_2\gamma_\mu q_1$. In that case the transition can be written as:

$$\langle P_2, \epsilon|V_\mu|P_1\rangle = \frac{2i}{M_1+M_2} e_{\mu\nu\alpha\beta}\epsilon^{*\nu}(P_2)P_1^\alpha P_2^\beta V(q^2) \ . \tag{9.23}$$

The form factor $V(q^2)$ can be understood as the 1^- intermediate state in the transition $0^- \to 1^-$. It is sometimes more convenient to define the form factor $V(q^2)$ by,

$$\langle P_2, \epsilon|V_\mu|P_1\rangle = ig(q^2)e_{\mu\nu\alpha\beta}\ \epsilon^{*\nu}(P_2)(P_1+P_2)^\alpha q^\beta \ , \tag{9.24}$$

where $g(q^2)$ is related to the previous form factor $V(q^2)$ by the following expression,

$$g(q^2) = \frac{-1}{M_1+M_2} V(q^2) \ . \tag{9.25}$$

In Eqs. (9.23, 9.24, 9.25), M_j and P_j are respectively the mass and momentum of the initial and final states. $\epsilon^{*\nu}(P_2)$ defines the vector polarization with the condition $\epsilon^\nu(P_2)\cdot P_{2\nu} = 0$ and $q = P_1 - P_2$.

We can also express the pseudoscalar-vector transition form factor in the explicitly covariant light-front formalism. By analogy the amplitude of the pseudo-scalar-vector transition is similar to the $\rho - \pi$ transition. The transition $\langle 1^-|J_\mu|0^-\rangle$ has the same structure since the decomposition is determined by the kinematic components only. In our case, the spins and parities of the particles are the same for $\langle 1^-|J_\mu|0^-\rangle$ and $\langle 0^-|J_\mu|1^-\rangle$. Therefore, in the impulse approximation the corresponding amplitude of the pseudo-scalar vector transition for the vector part is given by [124],

$$\langle P_2, \epsilon|V_\mu|P_1\rangle^{CLFD} = \frac{2}{M_2^2} e_{\mu\rho\nu\gamma}\epsilon^{*\rho}(P_2)q^\nu P_2^\gamma A(q^2) \ , \tag{9.26}$$

with $A(q^2)$ a dimensionless scalar function. One has to decompose the hadronic matrix element $\langle P_2, \epsilon|V_\mu|P_1\rangle^{CLFD}$ on the general invariant amplitudes in order to show explicitly the dependence of the transition amplitude on ω. Then, one obtains,

$$\langle P_2, \epsilon|V_\mu|P_1\rangle^{CLFD} = \epsilon^{*\rho}(P_2)\tilde{F}_{\rho\mu} \ , \tag{9.27}$$

where $\tilde{F}_{\rho\mu}$ contains all of the possible terms that are a function of ω [124]:

$$\begin{aligned}\tilde{F}_{\rho\mu} = {} & \frac{2}{M_2^2} e_{\mu\rho\nu\gamma}q^\nu P_2^\gamma A(q^2) + e_{\mu\rho\nu\gamma}q^\nu\omega^\gamma B_1 + e_{\mu\rho\nu\gamma}P_2^\nu\omega^\gamma B_2 \\ & + (V_\rho q_\mu + V_\mu q_\rho)B_3 + (V_\rho\omega_\mu + V_\mu\omega_\rho)B_4 + \frac{2}{M_2^2\omega\cdot P_2}(V_\rho P_{2\mu} + V_\mu P_{2\rho})B_5 \ ,\end{aligned} \tag{9.28}$$

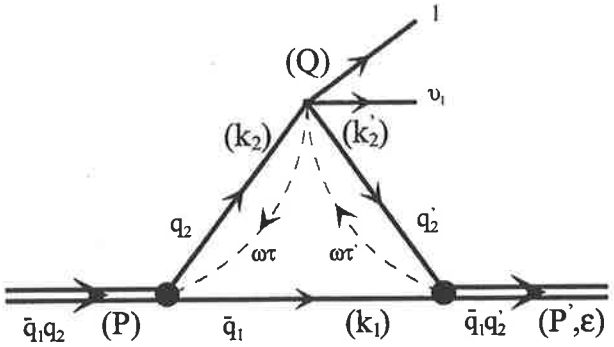

Figure 9.2: Transition between pseudoscalar and vector particles (leading contribution).

with $V_\rho = e_{\rho\alpha\beta\gamma}\omega^\alpha q^\beta P_2^\gamma$. The terms, B_i $(i = 1,5)$, are scalar functions (carrying no physical meaning) that are equal to zero in any exact calculation but which, in any approximate calculation, parametrize the dependence of the transition amplitude on ω. By separating the ω-independent parts from the non-physical ω-dependent ones in Eq. (9.28), one can extract the physical form factor $A(q^2)$ and one finds:

$$A(q^2) = -\frac{M_2^2 e^{\mu\rho\nu\gamma}((y-1)P_{2\nu} + yq_\nu)\omega_\gamma}{4(\omega\cdot P_1)(((y-1)M_1^2 + q^2)y - M_2^2(y-1))}\tilde{F}_{\mu\rho} \ . \tag{9.29}$$

Now one has to express $\tilde{F}_{\mu\rho}$ by applying the diagrammatic CLFD rules in order to determine $\langle P_2, \epsilon|J_\mu|P_1\rangle^{CLFD}$ (see Eq. (9.27)) without including the form factor $A(q^2)$. Then one has,

$$\begin{aligned}\langle P_2, \epsilon|J_\mu|P_1\rangle_g^{CLFD} &= \epsilon^{\rho\star}(P_2)\tilde{F}_{\rho\mu} = \\ &\int_D \left\{ \frac{1}{\sqrt{2}}\epsilon^{\rho\star}(P_2)\mathrm{Tr}\left[-\bar{\phi}_\rho(m_2' + \not{k}_2')\gamma_\mu(m_2 + \not{k}_2) \right.\right. \\ &\left.\left. \times \left(\frac{A_{1,1}}{m_r} + A_{2,1}\frac{\not{\omega}}{\omega\cdot P_1}\right)\gamma_5(m_1 - \not{k}_1)\right]\frac{1}{1-x'}\right\} D \ , \end{aligned} \tag{9.30}$$

where, ϕ_ρ, the vector wave function is given by,

$$\Phi_{\sigma_2\sigma_1\rho}{}^\lambda(k_1, k_2, P_2, \omega\tau) = \sqrt{m}\ \epsilon_\rho^\lambda(P_2)\ \bar{u}^{\sigma_2}(k_2)\ \phi_\rho\ v^{\sigma_1}(k_1) \ . \tag{9.31}$$

We refer the reader to Chapter 8 as well as Ref. [124] for all of the definitions regarding the vector wave function. Replacing $\tilde{F}_{\rho\mu}$ in Eq. (9.29) by its

expression given in Eq. (9.30) one obtains the physical form factor $A(q^2)$. The relationship between the form factor derived in CLFD, $A(q^2)$, and in the usual formalism, $g(q^2)$, is the following:

$$g(q^2) = \frac{-iA(q^2)}{M_2^2} \,. \tag{9.32}$$

In a similar way and for completeness one can determine the relationship between the form factors $A(q^2)$ and $V(q^2)$. One has,

$$V(q^2) = \frac{i(M_1 + M_2)A(q^2)}{M_2^2} \,. \tag{9.33}$$

It is then possible to calculate the form factor $A(q^2)$, $V(q^2)$ and $g(q^2)$ over the full range of values for q^2.

9.2.2 Axial current

After the extraction of the vector form factor, $V(q^2)$, we investigate the three form factors noted, $A_0(q^2), A_1(q^2), A_3(q^2)$, that describe the axial transition between pseudoscalar and vector particles. Their usual expression is the following:

$$\begin{aligned}\langle P_2, \epsilon | A_\rho | P_1 \rangle = \Bigg\{ & (M_1 + M_2)\epsilon_\rho^\star A_1(q^2) \\ & - \frac{\epsilon^\star(P_2)\cdot q}{M_1 + M_2}(P_1 + P_2)_\rho A_2(q^2) - 2M_2 \frac{\epsilon^\star(P_2)\cdot q}{q^2} q_\rho \Big(A_3(q^2) - A_0(q^2) \Big) \Bigg\} \,,\end{aligned} \tag{9.34}$$

where the momentum transfer q is defined as $q = P_1 - P_2$, the axial current A_ρ is $\bar{q}_2 \gamma_\rho \gamma_5 q_1$ and the zero q^2-momentum condition $A_0(0) = A_3(0)$ is required. Moreover, the form factor $A_3(q^2)$ can be written in terms of $A_1(q^2)$ and $A_2(q^2)$ by,

$$A_3(q^2) = \frac{M_1 + M_2}{2M_2} A_1(q^2) - \frac{M_1 - M_2}{2M_2} A_2(q^2) \,. \tag{9.35}$$

The physical meaning of the form factors $A_i(q^2)$ is the following: $A_1(q^2)$ and $A_2(q^2)$ are related to the 1^+ intermediate states, whereas $A_0(q^2)$ refers to the 0^+ state. We can also define another set of form factors in terms of $a_\pm(q^2)$

and $f(q^2)$. They take the following expression:

$$\langle P_2, \epsilon | A_\rho | P_1 \rangle = -f(q^2)\epsilon^\star_\rho(P_2) - \epsilon^\star(P_2)\cdot(P_1 - P_2)\left[a_+(q^2)(P_1 + P_2)_\rho + a_-(q^2)(P_1 - P_2)_\rho\right] , \quad (9.36)$$

where the form factors $a_\pm(q^2)$ and $f(q^2)$ can be linked to $A_0(q^2), A_1(q^2)$, $A_2(q^2)$ and $A_3(q^2)$ by the relations:

$$f(q^2) = -(M_1 + M_2)A_1(q^2) , \quad (9.37)$$

$$a_+(q^2) = \frac{1}{M_1 + M_2}A_2(q^2) , \quad (9.38)$$

$$a_-(q^2) = \frac{2M_2}{q^2}\left[A_3(q^2) - A_0(q^2)\right] . \quad (9.39)$$

The general transition amplitude regarding the axial current can be written by analogy to that one for the $\pi - A_1$ transition. The transition $\langle 1^-|J_\rho|0^-\rangle$ for the axial current, corresponds to the same change of parity as the transition $\langle 1^+|J_\rho|0^-\rangle$ for the vector current. Therefore, the transition amplitude expressed in the covariant light-front formalism becomes as [124]:

$$\langle P_2, \epsilon | J_\rho | P_1 \rangle^{CLFD} = \epsilon^\star_\mu(P_2)\Big\{ F_1(q^2)\left[(P_2\cdot q)g^\mu_\rho - P_{2\rho}q^\mu\right] + F_2(q^2)\left[q_\rho q^\mu - q^2 g^\mu_\rho\right] + F_3(q^2)P_1^\mu q_\rho \Big\} . \quad (9.40)$$

Here, $\epsilon_\mu(P_2)$ is the vector polarization of the outgoing particle with the condition $\epsilon_\mu(P_2)P_2^\mu = 0$. The amplitude describing the pseudoscalar vector axial transition (written in light-front dynamics) is determined by three form factors $F_1(q^2), F_2(q^2)$ and $F_3(q^2)$. We emphasise again that in any approximate calculation, this amplitude should incorporate the ω-dependent contributions. This is explicitly given by [124],

$$\langle P_2, \epsilon | J_\rho | P_1 \rangle^{CLFD} = \epsilon^\star_\mu(P_2)\tilde{G}^\mu_\rho , \quad (9.41)$$

where,

$$\tilde{G}_{\rho\mu} = F_1(q^2)\left[(P_2\cdot q)g_{\rho\mu} - P_{2\rho}q_\mu\right] + F_2(q^2)\left[q_\rho q_\mu - q^2 g_{\rho\mu}\right] + F_3(q^2)P_{1\mu}q_\rho + A' P_{2\mu}\left[P_{1\rho} - q_\rho(q\cdot P_1)/q^2\right] + C' P_{2\mu}q_\rho + B_1 q^2\omega_\mu P_{1\rho}/\omega\cdot P_2 + B_2 P_{1\mu}\omega_\rho + B'_2 P_{2\mu}\omega_\rho + B_3\omega_\mu q_\rho + B_4\omega_\mu\omega_\rho , \quad (9.42)$$

where $F_1(q^2), F_2(q^2)$ and $F_3(q^2)$ are the three physical form factors. On the other hand, $A', C', B_1, B_2, B_2', B_3$ and B_4 are the non-physical terms used to express the ω dependence. By solving Eq. (9.41) we can extract the form factors $F_1(q^2), F_2(q^2)$ and $F_3(q^2)$, and can write them as a function of $\tilde{G}_{\rho\mu}$:

$$F_{1,2,3}(q^2) = \frac{2q^2\tilde{G}_{\rho\mu}}{F^{(d)}_{1,2,3}} \times \left\{ \frac{1}{\omega\cdot P_1}\Big[F^{(1)}_{1,2,3}\, P_{1\rho}\omega_\mu + F^{(2)}_{1,2,3}\, q_\rho\omega_\mu + F^{(3)}_{1,2,3}\, P_{1\mu}\omega_\rho + F^{(4)}_{1,2,3}\, q_\mu\omega_\rho \Big] + \frac{1}{(\omega\cdot P_1)^2} F^{(5)}_{1,2,3}\, \omega_\mu\omega_\rho + F^{(6)}_{1,2,3}\, g^{\mu\rho} + F^{(7)}_{1,2,3}\, P_{1\rho}q_\mu + F^{(8)}_{1,2,3}\, q_\rho q_\mu + F^{(9)}_{1,2,3}\, P_{1\mu}q_\rho + F^{(10)}_{1,2,3}\, P_{1\rho}P_{1\mu} \right\}, \quad (9.43)$$

where the analytic expressions for the kinematical terms $F^{(i)}_{1,2,3}$ and the function $F^{(d)}_{1,2,3}$ can be found in Appendix B. By analogy to the method applied to calculate the term $\tilde{F}_{\mu\rho}$ in the amplitude related to the vector current V_μ, we can also derive $\tilde{G}^{\mu\nu}$ by using the diagrammatic CLFD rules:

$$\langle P_2, \epsilon | J_\rho | P_1 \rangle_g^{CLFD} = \epsilon^\star_\mu(P_2)\tilde{G}^\mu_\rho = \int_D \left\{ \frac{1}{\sqrt{2}}\epsilon^\star_\mu(P_2)\mathrm{Tr}\Big[-\bar{\phi}^\mu(m_2' + \not{k}_2')(-\gamma_\rho\gamma_5)(m_2 + \not{k}_2) \times \left(\frac{A_{1,1}}{m_r} + A_{2,1}\frac{\not{\omega}}{\omega\cdot P_1} \right)\gamma_5(m_1 - \not{k}_1)\Big] \frac{1}{1-x'} \right\} D\,. \quad (9.44)$$

Finally, one replaces in Eq. (9.43) the expression for $\tilde{G}_{\mu\nu}$ given by Eq. (9.44) and one obtains the form factors $F_1(q^2), F_2(q^2)$ and $F_3(q^2)$, derived in the light-front formalism. The correspondence between the form factors $a_\pm(q^2)$ and $f(q^2)$, and $F_{i=1,3}(q^2)$ are:

$$a_-(q^2) = -\Big[F_2(q^2) + F_3(q^2) + \frac{1}{2}F_1(q^2) \Big]\,, \quad (9.45)$$

$$a_+(q^2) = \frac{1}{2}F_1(q^2)\,, \quad (9.46)$$

$$f(q^2) = \frac{1}{2}F_1(q^2)\Big[M_2^2 - M_1^2 + q^2 \Big] + q^2 F_2(q^2)\,. \quad (9.47)$$

Note that the relationship between the form factors $F_{i=1,3}(q^2)$, and the usual $A_i(q^2)$ is:

$$A_0(q^2) = \frac{1}{4M_2}\Big[2q^2F_3(q^2) + F_1(q^2)(M_1^2 - M_2^2)\Big] ,$$
$$A_1(q^2) = \frac{1}{2(M_1+M_2)}\Big[2F_1(q^2)(M_1^2 - M_2^2) - (F_1(q^2) + 2F_2(q^2))q^2\Big] ,$$
$$A_2(q^2) = \frac{1}{2}F_1(q^2)(M_1 + M_2) . \tag{9.48}$$

By following this formalism, we can calculate all of the form factors $A_{i=0,3}(q^2)$ over the full range of q^2-momentum according, in terms of the form factors $F_{i=1,3}(q^2)$ derived in CLFD.

9.2.3 Semi-leptonic decay

For completeness, we detail the semi-leptonic decay rate for the pseudo-scalar vector transition. The usual definition can be written as:

$$\Gamma = \Gamma_0 \int_1^{\eta_{max}} d\eta(\eta^2 - 1)^{1/2}\left[(1 + \xi^2 - 2\xi\eta)\Big\{H_-^2(\eta) + H_+^2(\eta)\Big\} + H_0^2(\eta)\right] , \tag{9.49}$$

where all of the terms proportional to the lepton masses have been neglected. In Eq. (9.49) the upper limit for $\eta_{max} = (M_1^2 + M_2^2)/2M_1M_2$ where M_1 and M_2 always define the ingoing and outgoing particle masses. The expressions for the "bare" semi-leptonic decay rate, Γ_0, is the following:

$$\Gamma_0 = |V_{\bar{q}_1q_2}|^2\frac{G_F^2M_1^5}{48\pi^3}\xi^2 , \tag{9.50}$$

with $\xi = M_2/M_1$ and $V_{\bar{q}_1q_2}$ denoting a CKM matrix element involved in the semi-leptonic decay. The helicity amplitudes, $H_0(\eta)$, $H_\pm(\eta)$, which appear in the semi-leptonic decay rate take the form:

$$H_0(\eta) = \left[(\eta - \xi)(1 + \xi)A_1(\eta) - 2(\eta^2 - 1)\xi\frac{A_2(\eta)}{1+\xi}\right] , \tag{9.51}$$

and,

$$H_\pm(\eta) = (1 + \xi)A_1(\eta) \mp 2(\eta^2 - 1)^{1/2}\xi\frac{V(\eta)}{1+\xi} . \tag{9.52}$$

$A_i(\eta)$ and $V(\eta)$ are the previously defined form factors, expressed as functions of η. By comparing theoretical with experimental results regarding the semi-leptonic decays, we are able to determine in a reasonable way the CKM matrix elements, $V_{\bar{q}_1q_2}$, arising for a given decay.

9.2.4 Numerical results for $P \to V l \nu_l$

By applying the formalism detailed previously we can calculate the weak transition form factor in the case of a pseudoscalar vector transition. We were focused on those like $B \to \rho$, $B \to \omega$ as well as $D \to \rho$ and $D \to \omega$. The first two transitions correspond to a decay induced by the charge current $b \to d$ quark transition whereas the last two transitions correspond to a $c \to d$ quark transition. We list in Table 9.2 our results obtained for the vector current, i.e. the form factor $V(q^2)$, as well as those obtained for the axial current - i.e. the four form factors $A_i(q^2)$ (with $i = 0, 1, 2, 3$). For comparison we also list the results given by lattice QCD and the QCDSR formalism.

	$V(0)$	$A_0(0)$	$A_1(0)$	$A_2(0)$	$A_3(0)$
$B \to \rho$					
This work	0.34	0.32	0.30	0.29	0.32
BSW model	0.32	0.28	0.28	0.28	0.28
Lattice	0.37	0.30	0.27	0.26	0.30
QCDSR	0.34	0.38	0.26	0.22	0.38
$B \to \omega$					
This work	0.34	0.32	0.30	0.29	0.32
BSW model	0.32	0.28	0.28	0.28	0.28
Lattice	–	–	–	–	–
QCDSR	–	–	–	–	–
$D \to \rho$					
This work	1.19	0.66	0.75	0.87	0.66
BSW model	1.23	0.68	0.78	0.92	0.68
Lattice	1.1	0.59	0.65	0.55	0.59
QCDSR	1.0	0.57	0.5	0.4	0.57
$D \to \omega$					
This work	1.19	0.66	0.75	0.87	0.66
BSW model	1.23	0.68	0.78	0.92	0.68
Lattice	–	–	–	–	–
QCDSR	–	–	–	–	–

Table 9.2: Form factors for the pseudoscalar vector transition within the BSW model [73, 74, 80], Lattice QCD [187, 188, 189, 190, 191, 192, 204, 205] and QCDSR [76, 195, 196, 197, 206].

It appears, as in the previous case ($P \to P$), that our results are in

agreement with those from QCDSR, lattice QCD and the BSW model. The small discrepancy which can be observed between all of the results may come from the different formalisms applied but it is still smaller in the case of $P \to V$ than $P \to P$.

9.3 Summary

Based on the covariant light front dynamics formalism, we derived the weak transition form factors in the case of pseudoscalar pseudoscalar transitions as well as pseudo scalar vector transitions. The wave functions (see Chapter 8) describing the particles B, D, π, K, ρ and ω have been taken into account in our approach. This yields a dependence of the form factors on these wave functions. It has to be noticed that our results for the form factors have been shown at $q^2 = 0$ only. In theory we derived all of the equations which are necessary to obtain the behaviour of the form factors according to the momentum q^2. However, in practice we are not able to compute the form factors over the full range of q^2 because of problems related to numerical simulations. This work is still in progress.

We also compared our results with QCD sum rules and lattice QCD. We emphasize that both approaches have a limited range of applicability. QCD sum rules gives correct results only at low q^2, whereas lattice QCD gives correct results only in the high q^2 region. However, comparisons between all of the transition form factors in both cases give good agreement.

Knowing the values for the form factors $F_{0,1}^{B\to\pi}$, $F_{0,1}^{B\to K}$ and $A_0^{B\to\rho}$ at $q^2 = 0$, we can now focus on the final state interactions that arise in B decays and make an estimate of them in the calculation of the hadronic matrix elements.

Part IV

QCD Factorization in B Decays

Chapter 10

QCD factorization

" Avoir un système borne son horizon; n'en avoir pas est impossible. Le mieux est d'en posséder plusieurs. "

Raymond Queneau

In this final part, we are explicitly taking into account all the final state interactions at the order α_s and we are evaluating them in B decays. QCD factorization will be applied to reach this goal instead of naive factorization. Form factors and wave functions determined in CLFD will also be used in our analysis. In this chapter we introduce, in an extensive way, the formalism of QCD factorization (derived by M. Beneke, G. Buchalla, M. Neubert and C.T. Sachrajda [207], so-called BBNS approach) necessary to calculate the hadronic matrix elements arising in B decay amplitudes.

10.1 QCD factorization in $B \to PV$ decays

Factorization in charmless B decays involves three fundamental scales: the weak interaction scale M_W, the b quark mass scale m_b, and the strong interaction scale Λ_{QCD}. It is well known that the non-leptonic decay amplitude for $B \to PV$ is proportional to:

$$A(B \to PV) \propto \sum_i C_i(\mu) \langle PV|O_i(\mu)|B\rangle \ , \tag{10.1}$$

where we have omitted the CKM factor and Fermi constant for simplicity. The matrix elements $\langle PV|O_i(\mu)|B\rangle$ that depend on both m_b and Λ_{QCD}, contain perturbative and non-perturbative effects which are not accurately estimated in the naive factorization. The coefficients $C_i(\mu)$, include strong

interaction effects from the scales M_W down to m_b, and have been under control for a long time. The aim is therefore to obtain a good estimate of the matrix elements without using naive factorization, where the matrix element of a four fermion operator is directly replaced by the product of the matrix elements of two currents, one semi-leptonic and another purely leptonic. In QCD factorization [208], assuming a heavy quark expansion such as $m_b \gg \Lambda_{QCD}$ and soft collinear factorization where the particle energies are bigger than the scale Λ_{QCD}, the matrix elements $\langle PV|O_i(\mu)|B\rangle$ can be written as [209]:

$$\langle PV|O_i(\mu)|B\rangle = \langle P|j_1|B\rangle\langle V|j_2|0\rangle\left[1+\sum_n r_n\alpha_s^n + \mathcal{O}(\Lambda_{QCD}/m_b)\right] , \quad (10.2)$$

where r_n refers to the radiative corrections in α_s and j_i are the quark currents. It is straightforward to see that if we neglect the corrections at the order α_s, we recover the conventional naive factorization. We can rewrite the matrix elements $\langle PV|O_i(\mu)|B\rangle$, at the leading order in Λ_{QCD}/m_b, in the QCDF approach by using a partonic language and one has [209, 210, 211, 212, 213, 214]:

$$\begin{aligned}\langle PV|O_i(\mu)|B\rangle = F_j^{B\to P}(0)\int_0^1 dx T_{ij}^I(x)\phi_V(x) + A_k^{B\to V}(0)\int_0^1 dy T_{ik}^I(y)\phi_p(y) \\ + \int_0^1 d\xi\int_0^1 dx\int_0^1 dy T_i^{II}(\xi,x,y)\phi_B(\xi)\phi_V(x)\phi_P(y) , \quad (10.3)\end{aligned}$$

where ϕ_M with $M = V, P, B$ are the leading twist light cone distribution amplitudes (LCDA) of the valence quark Fock states. The light cone momentum fractions of the constituent quarks of the vector, pseudoscalar and B mesons are given respectively by x, y, and ξ. The form factors for $B \to P$ and $B \to V$ semi-leptonic decays evaluated at $k^2 = 0$ are denoted by $F_j^{B\to P}(0)$ and $A_k^{B\to V}(0)$. Eq. (10.3) can be understood via Fig. 10.1 where a graphical representation of the factorization formula is given. The hadronic decay

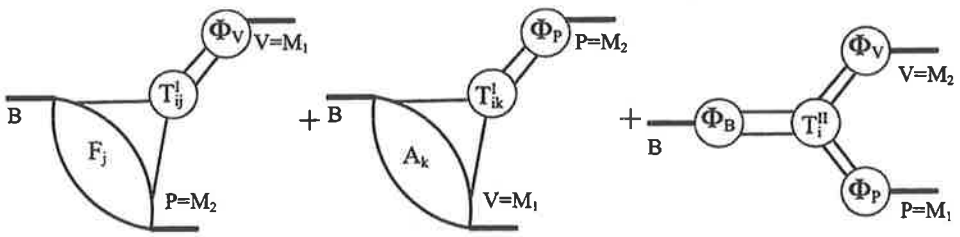

Figure 10.1: Graphical representation of the factorization formula.

amplitude involves both soft and hard contributions. At leading order, all the non-perturbative effects are assumed to be contained in the semileptonic form factors (Fig. 10.2) and the light cone distributions amplitudes. Then, non-factorizable interactions are dominated by hard gluon exchanges (in the case where the $O(\Lambda_{QCD}/m_b)$ terms are neglected) and can be calculated perturbatively, in order to correct the naive factorization approximation. These hard scattering kernels [209, 210, 211, 212, 213, 214, 215], T_{ik}^I and T_i^{II}, are calculable order by order in perturbation theory. The naive factorization terms are recovered by the leading terms of T_{ik}^I coming from the tree level, whereas vertex corrections (see diagrams (a-d) in Fig. 10.3) and penguin corrections (see diagrams (g-h) in Fig. 10.4) are included at the order of α_s in T_{ik}^I. The hard interactions (at order $O(\alpha_s)$) between the spectator quark and the emitted meson (see diagrams (e-f) in Fig. 10.4), at large gluon momentum, are taken into account by T_i^{II}.

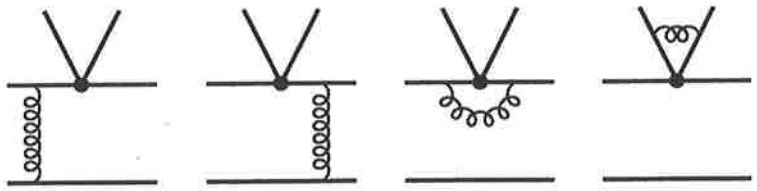

Figure 10.2: Soft corrections at the order α_s.

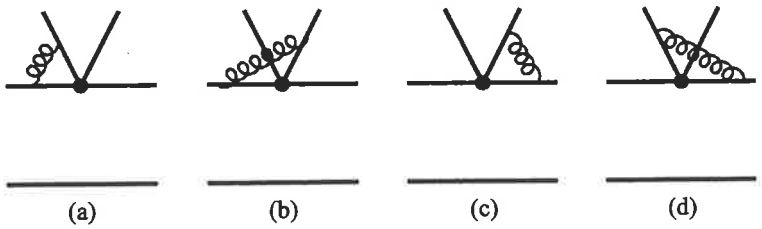

Figure 10.3: Order α_s corrections to the hard scattering kernels: vertex corrections.

10.2 Effective Hamiltonian

Phenomenological studies in charmless hadronic B decays are based on an effective Hamiltonian. We refer to Chapter 2 for details, definitions and explanations and just recall that the Hamiltonian results from a sum of local operators $O_i(\mu)$, times Wilson coefficients $C_i(\mu)$, times the quark mixing

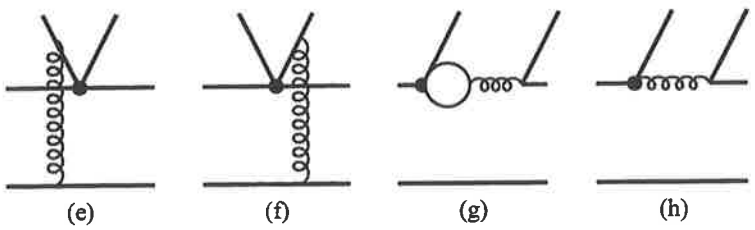

Figure 10.4: Order α_s corrections to the hard scattering kernels: penguin corrections and hard spectator scattering.

matrix element V_{qp}. In this part, we will use a Hamiltonian which includes electromagnetic, $Q_{7\gamma}$, and chromomagnetic, Q_{8g}, operators as well as annihilation contributions, b_i. This gives us,

$$\mathcal{H}_{\rm eff} = \frac{G_F}{\sqrt{2}}\Bigg\{ V_{ub}V_{uq}^*(C_1\,O_1^q + C_2\,O_2^q) \\ -V_{tb}V_{tq}^*\Bigg[\sum_{i=3,\ldots,10} C_i\,O_i + C_{7\gamma}\,O_{7\gamma} + C_{8g}\,O_{8g}\Bigg] + \sum_{i=1,\ldots,4} V_{qb}V_{qs}^* f_B f_{M_1} f_{M_2} b_i \Bigg\} + h.c.\,. \tag{10.4}$$

The definitions of the operators O_i are recalled for completeness:

$$\begin{aligned}
O_1^p &= (\bar{p}_\alpha b_\beta)_{V-A}(\bar{q}_\beta p_\alpha)_{V-A}\,, & O_2^p &= (\bar{p}_\alpha b_\alpha)_{V-A}(\bar{q}_\beta p_\beta)_{V-A}\,,\\
O_3 &= (\bar{q}_\alpha b_\alpha)_{V-A}\textstyle\sum_{q'}(\bar{q}'_\beta q_\beta)_{V-A}\,, & O_4 &= (\bar{q}_\alpha b_\beta)_{V-A}\textstyle\sum_{q'}(\bar{q}'_\beta q_\alpha)_{V-A}\,,\\
O_5 &= (\bar{q}_\alpha b_\alpha)_{V-A}\textstyle\sum_{q'}(\bar{q}'_\beta q_\beta)_{V+A}\,, & O_6 &= (\bar{q}_\alpha b_\beta)_{V-A}\textstyle\sum_{q'}(\bar{q}'_\beta q_\alpha)_{V+A}\,,\\
O_7 &= (\bar{q}_\alpha b_\alpha)_{V-A}\textstyle\sum_{q'}\frac{3}{2}e'_q(\bar{q}'_\beta q_\beta)_{V+A}\,, & O_8 &= (\bar{q}_\alpha b_\beta)_{V-A}\textstyle\sum_{q'}\frac{3}{2}e'_q(\bar{q}'_\beta q_\alpha)_{V+A}\,,\\
O_9 &= (\bar{q}_\alpha b_\alpha)_{V-A}\textstyle\sum_{q'}\frac{3}{2}e'_q(\bar{q}'_\beta q_\beta)_{V-A}\,, & O_{10} &= (\bar{q}_\alpha b_\beta)_{V-A}\textstyle\sum_{q'}\frac{3}{2}e'_q(\bar{q}'_\beta q_\alpha)_{V-A}\,,
\end{aligned} \tag{10.5}$$

where $(\bar{q}_1 q_2)_{V\pm A} = \bar{q}_1\gamma_\mu(1\pm\gamma_5)q_2$, α,β are colour indices, e'_q are the electric charges of the quarks in units of $|e|$, and a summation over all the active quarks, at the scale $\mu = O(m_b)$, $q' = u,d,s,c,b$, is implied. In Eq. (10.5) p and q denote the quark u or s according to the given transition $b\to u$ or $b\to s$. Expressions for the operators $O_{7\gamma}$ and O_{8g} are,

$$\begin{aligned}
O_{7\gamma} &= \frac{-e}{8\pi^2}\,m_b\,\bar{s}\sigma_{\mu\nu}(1+\gamma_5)F^{\mu\nu}b\,,\\
O_{8g} &= \frac{-g_s}{8\pi^2}\,m_b\,\bar{s}\sigma_{\mu\nu}(1+\gamma_5)G^{\mu\nu}b\,.
\end{aligned} \tag{10.6}$$

In Eq. (10.6) the definition of the dipole operators $O_{7\gamma}$ and O_{8g} corresponds to the sign convention applied for the gauge-covariant derivative $iD^\mu = i\partial^\mu + g_s A_a^\mu t_a$. Listed in Table 10.1 are the Wilson coefficients, C_i, calculated at the scale $\mu = m_b$, in the Naive Dimensional Regularization (NDR) scheme [207, 216]. The following sections will present in detail the necessary formalism used to factorize the hadronic matrix elements.

NLO	C_1	C_2	C_3	C_4	C_5	C_6
$\mu = m_b$	-0.190	1.081	0.014	-0.036	0.009	-0.0042
NLO	C_7/α	C_8/α	C_9/α	C_{10}/α		
$\mu = m_b$	-0.011	0.060	-1.254	0.223		
LO					$C_{7\gamma}^{eff}$	C_{8g}^{eff}
					-0.318	-0.151

Table 10.1: Wilson coefficients C_i in the NDR scheme. Input parameters are $\Lambda_{\overline{\rm MS}}^{(5)} = 0.225\,{\rm GeV}$, $m_t(m_t) = 167\,{\rm GeV}$, $m_b(m_b) = 4.2\,{\rm GeV}$, $M_W = 80.4\,{\rm GeV}$, $\alpha = 1/129$, and $\sin^2\theta_W = 0.23$.

10.2.1 The QCD coefficients a_i

The coefficients a_i [207, 216] have been calculated at next-to-leading order. They contain all the non-factorizable effects at the first order in α_s. In order to clearly separate every contribution, the coefficients a_i are written in two parts:

$$a_i = a_{i,I} + a_{i,II} \ , \tag{10.7}$$

where the first term includes the naive factorization, the vertex and penguin corrections, while the second term contains the hard spectator interactions. According to the final states, the terms a_i have to be expressed for two different cases: case A corresponds to the situation where the recoiling meson M_1 is a vector and the emitted meson M_2 is a pseudoscalar, and vice-versa for case B. For case A, the coefficients a_i take the form [207, 216],

$$a_{1,I} = C_1 + \frac{C_2}{N_c}\left[1 + \frac{C_F\alpha_s}{4\pi}V_M\right] \ , \quad a_{1,II} = \frac{\pi C_F\alpha_s}{N_c^2}C_2 H(BM_1, M_2) \ ,$$
$$a_{2,I} = C_2 + \frac{C_1}{N_c}\left[1 + \frac{C_F\alpha_s}{4\pi}V_M\right] \ , \quad a_{2,II} = \frac{\pi C_F\alpha_s}{N_c^2}C_1 H(BM_1, M_2) \ ,$$

$$
\begin{aligned}
a_{3,I} &= C_3 + \frac{C_4}{N_c}\Big[1 + \frac{C_F\alpha_s}{4\pi}V_M\Big] , & a_{3,II} &= \frac{\pi C_F\alpha_s}{N_c^2}C_4 H(BM_1, M_2) , \\
a^p_{4,I} &= C_4 + \frac{C_3}{N_c}\Big[1 + \frac{C_F\alpha_s}{4\pi}V_M\Big] + a^p_{4,I,b} , & a_{4,II} &= \frac{\pi C_F\alpha_s}{N_c^2}C_3 H(BM_1, M_2) , \\
a_{5,I} &= C_5 + \frac{C_6}{N_c}\Big[1 - \frac{C_F\alpha_s}{4\pi}V'_M\Big] , & -a_{5,II} &= \frac{\pi C_F\alpha_s}{N_c^2}C_6 H'(BM_1, M_2) , \\
a^p_{6,I} &= C_6 + \frac{C_5}{N_c}\Big[1 - 6\frac{C_F\alpha_s}{4\pi}\Big] + a^p_{6,I,b} , & a_{6,II} &= 0 , \\
a_{7,I} &= C_7 + \frac{C_8}{N_c}\Big[1 - \frac{C_F\alpha_s}{4\pi}V'_M\Big] , & -a_{7,II} &= \frac{\pi C_F\alpha_s}{N_c^2}C_8 H'(BM_1, M_2) , \\
a^p_{8,I} &= C_8 + \frac{C_7}{N_c}\Big[1 - 6\frac{C_F\alpha_s}{4\pi}\Big] + a^p_{8,I,b} , & a_{8,II} &= 0 , \\
a_{9,I} &= C_9 + \frac{C_{10}}{N_c}\Big[1 + \frac{C_F\alpha_s}{4\pi}V_M\Big] , & a_{9,II} &= \frac{\pi C_F\alpha_s}{N_c^2}C_{10} H(BM_1, M_2) , \\
a^p_{10,I} &= C_{10} + \frac{C_9}{N_c}\Big[1 + \frac{C_F\alpha_s}{4\pi}V_M\Big] + a^p_{10,I,b} , & a_{10,II} &= \frac{\pi C_F\alpha_s}{N_c^2}C_9 H(BM_1, M_2) ,
\end{aligned}
\tag{10.8}
$$

where the terms $a^p_{4,I,b}, a^p_{6,I,b}, a^p_{8,I,b}$ and $a^p_{10,I,b}$ are,

$$
\begin{aligned}
a^p_{4,I,b} &= \frac{C_F\alpha_s}{4\pi}\frac{P^p_{M,2}}{N_c} , & a^p_{6,I,b} &= \frac{C_F\alpha_s}{4\pi}\frac{P^p_{M,3}}{N_c} , \\
a^p_{8,I,b} &= \frac{\alpha}{9\pi}\frac{P^{p,ew}_{M,3}}{N_c} , & a^p_{10,I,b} &= \frac{\alpha}{9\pi}\frac{P^{p,ew}_{M,2}}{N_c} ,
\end{aligned}
\tag{10.9}
$$

where the subscripts 2 and 3 refer to the corresponding twist-2 and twist-3 LCDAs of the mesons. In Eqs. (10.8) and (10.9) V_M, V'_M represent the vertex corrections, H, H' describe hard gluon exchanges between the spectator quark in the B meson and the emitted meson (pseudoscalar or vector). $P^p_{M,2}, P^p_{M,3}, P^{p,ew}_{M,3}, P^{p,ew}_{M,2}$ are the QCD penguin contributions and electroweak penguin contributions, respectively. These quantities contain all of the non-perturbative dynamics and are a result of the convolution of hard scattering kernels g, with meson distribution amplitudes, Φ. The other parameters are $C_i \equiv C_i(\mu)$ (in NDR), $\alpha_s \equiv \alpha_s(\mu)$ (next to leading order), $C_F = (N_c^2-1)/2N_c$ with $N_c = 3$. The vertex corrections V_M and V'_M involved in $a_{i,I}$ are given by [207, 216],

$$
\begin{aligned}
V_M &= 12\,\ln\frac{m_b}{\mu} - 18 + \int_0^1 dx\, g(x)\,\Phi_M(x) , \\
V'_M &= 12\,\ln\frac{m_b}{\mu} - 6 + \int_0^1 dx\, g(1-x)\,\Phi_M(x) ,
\end{aligned}
\tag{10.10}
$$

with the kernel $g(x)$ having the following form,

$$g(x) = 3\left(\frac{1-2x}{1-x}\ln x - i\pi\right) + \left[2\,\mathrm{Li}_2(x) - \ln^2 x + \frac{2\ln x}{1-x} - (3+2i\pi)\ln x - (x \leftrightarrow 1-x)\right] . \quad (10.11)$$

We assume that one can neglect the higher order terms in the expansion involving Gegenbauer polynomials for the leading-twist light cone amplitudes, $\Phi_M(x)$, given by,

$$\Phi_M(x) = 6x(1-x)\left[1 + \sum_{n=1}^{\infty} \alpha_n^M(\mu) C_n^{3/2}(2x-1)\right] , \quad (10.12)$$

where $\alpha_n^M(\mu)$ are the Gegenbauer moments that depend on the scale μ. $C_n^{3/2}(u)$ are coefficients defined such as $C_1^{3/2}(u) = 3u$ for $n = 1$ and $C_2^{3/2}(u) = (3/2)(5u^2 - 1)$ for $n = 2$. Since the corrections to the asymptotic form are very small, we use $\Phi_M(x) = 6x(1-x)$ and we obtain the result,

$$\int_0^1 dx\, g(x)\,\Phi_M(x) = \int_0^1 dx\, g(1-x)\,\Phi_M(x) = -\frac{1}{2} - 3i\pi . \quad (10.13)$$

Regarding the QCD penguin contributions, $P_{M,i}^p$, one has [207, 216],

$$\begin{aligned}
P_{M,2}^p &= C_1\left[\frac{4}{3}\ln\frac{m_b}{\mu} + \frac{2}{3} - G_M(s_p)\right] \\
&\quad + (C_3 - \frac{1}{2}C_9)\left[\frac{8}{3}\ln\frac{m_b}{\mu} + \frac{4}{3} - G_M(0) - G_M(1)\right] \\
&+ \sum_{q=q'}(C_4 + C_6 + \frac{3}{2}e_q C_8 + \frac{3}{2}e_q C_{10})\left[\frac{4}{3}\ln\frac{m_b}{\mu} - G_M(s_q)\right] - 2C_{8g}^{eff}\int_0^1 dx \frac{\phi_M(x)}{1-x} , \\
P_{M,3}^p &= C_1\left[\frac{4}{3}\ln\frac{m_b}{\mu} + \frac{2}{3} - \hat{G}_M(s_p)\right] \\
&\quad + (C_3 - \frac{1}{2}C_9)\left[\frac{8}{3}\ln\frac{m_b}{\mu} + \frac{4}{3} - \hat{G}_M(0) - \hat{G}_M(1)\right] \\
&+ \sum_{q=q'}(C_4 + C_6 + \frac{3}{2}e_q C_8 + \frac{3}{2}e_q C_{10})\left[\frac{4}{3}\ln\frac{m_b}{\mu} - \hat{G}_M(s_q)\right] - 2C_{8g}^{eff} , \quad (10.14)
\end{aligned}$$

while for the electroweak penguin contributions, $P_{M,i}^{p,EW}$, one finds:

$$P_{M,2}^{p,EW} = (C_1 + N_c C_2)\left[\frac{4}{3}\ln\frac{m_b}{\mu} + \frac{2}{3} - G_M(s_p)\right] - (C_3 + N_c C_4)\left[\frac{4}{3}\ln\frac{m_b}{\mu} + \frac{2}{3} - \frac{1}{2}G_M(0) - \frac{1}{2}G_M(1)\right] + \sum_{q=q'}(N_c C_3 + C_4 + N_c C_5 + C_6)\frac{3}{2}e_q\left[\frac{4}{3}\ln\frac{m_b}{\mu} - G_M(s_q)\right] - N_c C_{7\gamma}^{eff}\int_0^1 dx\frac{\phi_M(x)}{1-x}\,, \tag{10.15}$$

and,

$$P_{M,3}^{p,EW} = (C_1 + N_c C_2)\left[\frac{4}{3}\ln\frac{m_b}{\mu} + \frac{2}{3} - \hat{G}_M(s_p)\right] - (C_3 + N_c C_4)\left[\frac{4}{3}\ln\frac{m_b}{\mu} + \frac{2}{3} - \frac{1}{2}\hat{G}_M(0) - \frac{1}{2}\hat{G}_M(1)\right] + \sum_{q=q'}(N_c C_3 + C_4 + N_c C_5 + C_6)\frac{3}{2}e_q\left[\frac{4}{3}\ln\frac{m_b}{\mu} - \hat{G}_M(s_q)\right] - N_c C_{7\gamma}^{eff}\,, \tag{10.16}$$

where the subscripts 2 and 3 refer to the corresponding twist-2 and twist-3 LCDAs of the mesons. $s_q = m_q^2/m_b^2$ is the mass ratio and can be equal to $s_u = s_d = 0, s_c = m_c^2/m_b^2$ or $s_b = 1$. All active quarks at the scale $\mu = \mathcal{O}(m_b)$ are represented by $q' = u, d, s, c, b$. The functions $G_M(s)$ and $\hat{G}_M(s)$ have the following expressions:

$$G_M(s) = \int_0^1 dx\, G(s - i\epsilon, 1-x)\,\Phi_M(x)\,,$$
$$\hat{G}_M(s) = \int_0^1 dx\, G(s - i\epsilon, 1-x)\,\Phi_M^p(x)\,, \tag{10.17}$$

where $G(s,x)$ takes the form,

$$G(s,x) = -4\int_0^1 du\, u(1-u)\ln[s - u(1-u)x] = \frac{2(12s + 5x - 3x\ln s)}{9x} - \frac{4\sqrt{4s-x}\,(2s+x)}{3x^{3/2}}\arctan\sqrt{\frac{x}{4s-x}}\,. \tag{10.18}$$

Explicitly, in Eqs. (10.14-10.16), the terms $G_M(s_c), G_M(0)$ and $G_M(1)$ are given analytically by,

$$G_M(s_c) = \frac{5}{3} - \frac{2}{3}\ln s_c + \frac{32}{3}s_c + 16s_c^2 - \frac{2}{3}\sqrt{1-4s_c}(1+2s_c+24s_c^2)$$
$$\times \left(2\arctan\sqrt{1-4s_c} - i\pi\right) + 12s_c^2\left(1-\frac{4}{3}s_c\right)\left(2\arctan\sqrt{1-4s_c} - i\pi\right)^2 ,$$
$$G_M(0) = \frac{5}{3} + \frac{2\pi}{3}i ,$$
$$G_M(1) = \frac{85}{3} - 3\sqrt{3}\pi + \frac{4\pi^2}{9} , \qquad (10.19)$$

and the terms $\hat{G}_M(s_c), \hat{G}_M(1)$ and $\hat{G}_M(0)$ are given by,

$$\hat{G}_M(s_c) = \frac{16}{9}(1-3s_c) - \frac{2}{3}\left[\ln s_c + (1-4s_c)^{3/2}\left(2\arctan\sqrt{1-4s_c} - i\pi\right)\right] ,$$
$$\hat{G}_M(0) = \frac{16}{9} + \frac{2\pi}{3}i ,$$
$$\hat{G}_M(1) = \frac{2\pi}{\sqrt{3}} - \frac{32}{9} . \qquad (10.20)$$

The vertex and penguin corrections to the hard-scattering kernels are evaluated at the scale $\mu \sim m_b$. The imaginary parts arising in both penguin functions $g(x)$ and $G(s,x)$, give us two sources of strong rescattering phases. Finally the hard scattering contributions, including chirally-enhanced contributions in the coefficients $a_{i,II}$, are written as [207, 216],

$$H(BV,P) = \frac{f_B f_V}{m_B^2 A_0^{B\to V}(0)} \int_0^1 d\xi \int_0^1 dx \int_0^1 dy \frac{\phi_B(\xi)}{\xi}\frac{\phi_P(x)}{1-x}\frac{\phi_V(y)}{1-y} ,$$
$$H'(BV,P) = \frac{f_B f_V}{m_B^2 A_0^{B\to V}(0)} \int_0^1 d\xi \int_0^1 dx \int_0^1 dy \frac{\phi_B(\xi)}{\xi}\frac{\phi_P(x)}{x}\frac{\phi_V(y)}{1-y} , \qquad (10.21)$$

with the usual definitions for $f_B, f_V, A_0^{B\to V}(0)$ and m_B. For case B where a vector is emitted, the expressions for a_i are similar to those in case A except for the parameters of $H(BV,P)$ and $H'(BV,P)$ which take the form:

$$H(BP,V) = \frac{f_B f_P}{m_B^2 F_1^{B\to P}(0)} \int_0^1 d\xi \int_0^1 dx \int_0^1 dy \frac{\phi_B(\xi)}{\xi}\frac{\phi_V(x)}{1-x}$$
$$\times \left[\frac{\phi_P(y)}{1-y} + \frac{2\mu_P}{m_b}\frac{1-x}{x}\frac{\phi_P^p(y)}{1-y}\right] ,$$

$$H'(BP,V) = -\frac{f_B f_P}{m_B^2 F_1^{B\to P}(0)} \int_0^1 d\xi \int_0^1 dx \int_0^1 dy \frac{\phi_B(\xi)}{\xi} \frac{\phi_V(x)}{x} \times \left[\frac{\phi_P(y)}{1-y} + \frac{2\mu_P}{m_b} \frac{x}{1-x} \frac{\phi_P^p(y)}{1-y} \right], \quad (10.22)$$

where the chirally enhanced factor is parameterized by the factor $\mu_P = m_P^2/(m_1 + m_2)$, with m_1 and m_2 being the current quark masses of the meson. The divergence coming from the twist-3 contribution is treated phenomenologically by,

$$X_H = \int_0^1 dy \frac{\phi_P^p(y)}{1-y} = \int_0^1 dy \frac{1}{1-y} = (1 + \varrho_H\, e^{i\phi_H}) \ln \frac{m_B}{\Lambda_h}\,. \quad (10.23)$$

In the above equation, the phase ϕ_H and the coefficient ϱ_H are chosen in an arbitrary way. Because the gluon is off-shell the strong coupling constant $\alpha_s(\mu)$, the Wilson coefficients $C_i(\mu)$ and then the hard-scattering contributions $H(BV,P)$ or $H(BP,V)$ (with prime or not), involved in the terms $a_{i,II}$, are evaluated at the scale $\mu_h = \sqrt{\Lambda_h \mu}$, with $\Lambda_h = 0.5$ GeV rather than the scale $\mu = m_b$.

10.2.2 The weak annihilation coefficients b_i

It has been shown in Refs [217, 218] that weak annihilation contributions should not be neglected in B meson decays, even though they are power suppressed in the heavy-quark limit ($\Lambda_{QCD}/m_b \to 0$). Moreover, their contributions could carry large strong phases with QCD corrections and hence, large CP violation might be obtained in B meson decays. Annihilation contributions, at leading order in α_s, are given by the diagrams drawn in Fig. 10.5. They do not appear in QCD factorization formulae and they cannot be cal-

Figure 10.5: Order α_s corrections to the weak annihilation.

culated within QCD-based factorization approach [209, 210, 211, 212, 213, 214, 215]. Nevertheless, their contributions denoted by $A(M_1, M_2)^a$, are approximated in terms of convolutions of hard scattering kernels with light

cone expansions for the final state mesons. Since they differ according to the final states, $A(M_1, M_2)^a$ is divided into two different cases: (recall) case A is where M_1 is a vector meson and M_2 is a pseudoscalar meson. Case B corresponds to the opposite situation. If we define x as the longitudinal momentum fraction of a quark contained in M_2 and $\bar{y} = 1 - y$, the momentum fraction of an antiquark contained in M_1, then the diagrams related to the annihilation contributions (without including the B decay constant) can be expressed (for case A) in terms of [207, 216]:

$$
\begin{aligned}
A^f_{1,2}(V,P)^a &= 0 \,, \\
A^f_3(V,P)^a &= \pi\alpha_s \int_0^1 dx \int_0^1 dy\, \Phi_V(x)\Phi^p_P(y) \frac{2\mu_P}{m_b} \frac{2(1+\bar{x})}{\bar{x}^2 y} \,, \\
A^i_1(V,P)^a &= \pi\alpha_s \int_0^1 dx \int_0^1 dy\, \Phi_V(x)\Phi_P(y) \left[\frac{1}{y(1-x\bar{y})} + \frac{1}{\bar{x}^2 y} \right] \,, \\
A^i_2(V,P)^a &= -\pi\alpha_s \int_0^1 dx \int_0^1 dy\, \Phi_V(x)\Phi_P(y) \left[\frac{1}{\bar{x}(1-x\bar{y})} + \frac{1}{\bar{x}y^2} \right] \,, \\
A^i_3(V,P)^a &= \pi\alpha_s \int_0^1 dx \int_0^1 dy\, \Phi_V(x)\Phi^p_P(y) \frac{2\mu_P}{m_b} \frac{2\bar{y}}{\bar{x}y(1-x\bar{y})} \,.
\end{aligned}
\tag{10.24}
$$

If we consider case B, one has:

$$
\begin{aligned}
A^f_{1,2}(P,V)^a &= 0 \,, \\
A^f_3(P,V)^a &= -\pi\alpha_s \int_0^1 dx \int_0^1 dy\, \Phi^p_P(x)\Phi_V(y) \frac{2\mu_P}{m_b} \frac{2(1+y)}{\bar{x}y^2} \,, \\
A^i_1(P,V)^a &= \pi\alpha_s \int_0^1 dx \int_0^1 dy\, \Phi_P(x)\Phi_V(y) \left[\frac{1}{y(1-x\bar{y})} + \frac{1}{\bar{x}^2 y} \right] , \\
A^i_2(P,V)^a &= -\pi\alpha_s \int_0^1 dx \int_0^1 dy\, \Phi_P(x)\Phi_V(y) \left[\frac{1}{\bar{x}(1-x\bar{y})} + \frac{1}{\bar{x}y^2} \right] \,, \\
A^i_3(P,V)^a &= \pi\alpha_s \int_0^1 dx \int_0^1 dy\, \Phi^p_P(x)\Phi_V(y) \frac{2\mu_P}{m_b} \frac{2x}{\bar{x}y(1-x\bar{y})} \,,
\end{aligned}
\tag{10.25}
$$

where $\Phi_V(x)$ is the leading twist light cone distribution amplitude of the vector meson ρ or ω and $\Phi_P(x)$ and $\Phi^p_P(x)$ refer to the twist-2 and twist-3 LCDA's (asymptotic forms) for the pseudoscalar π or K. In Eqs. (10.24) and (10.25), the superscripts i and f on $A^f(M_1, M_2)^a$ correspond respectively to the gluon emitted from an initial state or a final state quark. Finally, the subscript $k = (1, 3)$ on $A^i_k(M_1, M_2)^a$ describes the three Dirac structures involved in the annihilation contributions: $(V-A)\otimes(V-A), (V-A)\otimes(V+A)$

and $(-2)(S-P)\otimes(S+P)$. Considering the case where LCDA's of light mesons are symmetric under $x \to \bar{x}$, and assuming $SU(3)$ flavour symmetry conservation, one can simplify Eqs. (10.24) and (10.25) and one obtains the following approximation for the weak annihilation amplitudes,

$$\begin{aligned}
A_1^i(V,P)^a &= -A_2^i(V,P)^a \simeq 18\pi\alpha_s\Big(X_A - 4 + \frac{\pi^2}{3}\Big) \,, \\
A_1^i(P,V)^a &= -A_2^i(P,V)^a \simeq 18\pi\alpha_s\Big(X_A - 4 + \frac{\pi^2}{3}\Big) \,, \\
A_3^i(V,P)^a &= +A_3^i(P,V)^a \simeq \pi\alpha_s r_\chi\Big[2\pi^2 - 6\Big(X_A^2 + 2X_A\Big)\Big] \,, \\
A_3^f(V,P)^a &= -A_3^f(P,V)^a \simeq 6\pi\alpha_s r_\chi\Big(2X_A^2 - X_A\Big) \,,
\end{aligned} \tag{10.26}$$

with the factor r_χ is defined by $r_\chi^{M_1}(\mu) = 2M_1^2/m_b(\mu)(m_{q_1}(\mu) + m_{q_2}(\mu))$. Following Ref. [209], the divergent endpoint integral $\int_0^1 dx/x$ is parameterized by X_A and will be treated as a phenomenological parameter with the same value for all the annihilation terms $A(M_1,M_2)^a$. That is, in a similar way to X_H, the parameterization is the following:

$$X_A = (1 + \varrho_A\, e^{i\phi_A})\ln\frac{m_B}{\Lambda_h} \,, \tag{10.27}$$

with ϕ_A an arbitrary phase. Taking into account the flavour structure of the various operators involved in the weak annihilation topologies, the annihilation amplitude can be written as,

$$A^a(B \to PV) \propto f_B f_P f_V \sum_{p=u,c}\sum_{i=1,4} V_{pb}V_{ps}^* b_i \,. \tag{10.28}$$

In the above equation, f_B, f_P and f_V refer to B, pseudoscalar and vector meson decay constants, respectively. The coefficients b_i in Eq. (10.28) expressed in terms of linear combinations of $A(M_1,M_2)^a$, have the following form [207, 216]:

$$\begin{aligned}
b_1(M_1,M_2) &= \frac{C_F}{N_c^2}C_1 A_1^i(M_1,M_2)^a \,, \\
b_2(M_1,M_2) &= \frac{C_F}{N_c^2}C_2 A_1^i(M_1,M_2)^a \,, \\
b_3(M_1,M_2) &= \frac{C_F}{N_c^2}\Bigg\{C_3 A_1^i(M_1,M_2)^a + C_5 A_3^i(M_1,M_2)^a \\
&\qquad + \Big[C_5 + N_c C_6\Big]A_3^f(M_1,M_2)^a\Bigg\} \,,
\end{aligned}$$

$$b_4(M_1,M_2) = \frac{C_F}{N_c^2}\Big\{C_4 A_1^i(M_1,M_2)^a + C_6 A_2^i(M_1,M_2)^a\Big\}\,,$$

$$b_3^{ew}(M_1,M_2) = \frac{C_F}{N_c^2}\Bigg\{C_9 A_1^i(M_1,M_2)^a + C_7 A_3^i(M_1,M_2)^a + \Big[C_7 + N_c C_8\Big] A_3^f(M_1,M_2)^a\Bigg\}\,,$$

$$b_4^{ew}(M_1,M_2) = \frac{C_F}{N_c^2}\Big\{C_{10} A_1^i(M_1,M_2)^a + C_8 A_2^i(M_1,M_2)^a\Big\}\,, \qquad (10.29)$$

where $b_1(M_1,M_2)$ and $b_2(M_1,M_2)$ are the current-current annihilation parameters arising from the hadronic matrix elements of the effective operators $O_{1,2}$. $b_3(M_1,M_4)$ and $b_4(M_1,M_2)$ are the QCD penguin annihilation parameters (the most relevant effects) and $b_3^{EW}(M_1,M_4)$ and $b_4^{EW}(M_1,M_2)$ are the electroweak penguin annihilation parameters coming respectively from the effective operators O_{3-6} and O_{7-10}. The quantities b_i depend on the final state mesons through the terms $A(M_1,M_2)^a$ defined previously. It is crucial to note that the terms $A(M_1,M_2)^a$ are independent of the form of the B meson amplitude because the momentum fraction of the quark spectator in the B meson, ξ, has been neglected in front of $x, \bar{x}, y$ and $\bar{y}$, assuming hard scattering. This approximation may need to be improved in future, however it is expected to give the correct order of magnitude of the weak annihilation effects.

10.3 Input parameters

10.3.1 Form factors, decay constants, CKM matrix elements and quark masses

As defined previously, $F_{0,1}(k^2), V(k^2)$ and $A_{0,1,2,3}(k^2)$ are the form factors describing transitions between pseudoscalar and vector particles, where k^2 defines the momentum transfer involved in the corresponding transition. We refer the reader to Chapter 5 for the usual definitions and properties of the form factors. In our numerical computations, we will use those calculated in CLFD (see Chapter 9). Recall, for the case of $B \to \rho\pi$, their values are:

$$F_{0,1}^{B\to\pi} = 0.35\,, \qquad A_0^{B\to\rho} = 0.34\,, \qquad (10.30)$$

and for $B \to \rho K$, their values are:

$$F_{0,1}^{B\to K} = 0.40\,, \qquad A_0^{B\to\rho} = 0.34\,. \qquad (10.31)$$

The decay constants, f_B, f_π, f_ρ, f_K and the CKM matrix element parameters A, λ, ρ, η, have the same values as those applied in Chapter 5 of Part I. The quark masses that appear in the calculations, contribute to the QCD penguin $P^p_{M,i}$ and electroweak penguin corrections $P^{p,EW}_{M,i}$, as well as the hard scattering kernels $G_M(s_q)$ and $\hat{G}_M(s_q)$ via the term $s_q = m_q^2/m_b^2$. For the numerical applications we take the following quark masses:

$$m_u = 0 = m_d = m_s = 0 \ , \quad m_c = 1.45 \text{ GeV} \ , \text{ and } m_b = 4.6 \text{ GeV} \ . \quad (10.32)$$

The evaluation of the hadronic matrix elements of the $(S+P)\otimes(S-P)$ operators, via the equation of motion and the twist-3 LCDA's of the mesons, yields a chirally enhanced factor proportional to the quark masses (which are renormalization scale dependent). The quark mass values have already been listed in Chapter 5.

10.3.2 Light cone distribution amplitude (LCDA) of the mesons

QCD factorization involves the light cone distribution amplitude (LCDA) of the mesons [207, 216] where the leading twist (twist-2) and subleading twist (twist-3) [219] distribution amplitudes are taken into account. For a light pseudoscalar meson the LCDA is defined as,

$$\langle P(k)|\bar{q}(z_2)q(z_1)|0\rangle = \frac{if_P}{4}\int_0^1 dx\ e^{i(xk\cdot z_2+\bar{x}k\cdot z_1)}\left\{\not{k}\gamma_5\Phi_P(x) - \mu_P\gamma_5\left[\Phi_P^p(x) - \sigma_{\mu\nu}k^\mu z^\nu\frac{\Phi_P^\sigma(x)}{6}\right]\right\} , \quad (10.33)$$

where f_P is a decay constant, μ_P is the chiral enhancement factor and $z = z_2 - z_1$. $\Phi_P(x), \Phi_P^p(x)$ and $\Phi_P^\sigma(x)$ are the leading twist and subleading twist LCDA's of the mesons, respectively. All distributions are normalized to one. Neglecting three-particle distributions such as quark-antiquark-gluon, it follows from the equations of motion that the asymptotic forms of the LCDA's must be used. They take the forms:

$$\Phi_P(x) = 6x(1-x), \quad \Phi_P^p(x) = 1, \quad \Phi_P^\sigma(x) = 6x(1-x) \ . \quad (10.34)$$

For the LCDAs of the vector mesons, the usual definitions applied here are,

$$\langle 0|\bar{q}(0)\sigma_{\mu\nu}q(z)|V(k,\lambda)\rangle = i(\epsilon_\mu^\lambda k_\nu - \epsilon_\nu^\lambda k_\mu)f_V^\perp\int_0^1 dx\ e^{-ixk\cdot z}\Phi_V^\perp(x) \ , \quad (10.35)$$

$$\langle 0|\bar{q}(0)\gamma_\mu q(z)|V(k,\lambda)\rangle = k_\mu\frac{\epsilon^\lambda\cdot z}{k\cdot z}f_V m_V\int_0^1 dx\ e^{-ixk\cdot z}\Phi_V^\parallel(x) \ , \quad (10.36)$$

where ϵ is the polarization vector. $\Phi_V^{\perp}(x)$ and $\Phi_V^{\parallel}(x)$ are the transverse and longitudinal quark distributions of the polarized mesons. Assuming that the contributions from $\Phi_V^{\perp}(x)$ are power suppressed, $\Phi_V(x)$ takes the following form,

$$\Phi_V(x) = \Phi_V^{\parallel}(x) = 6x(1-x) \; . \tag{10.37}$$

For the wave function of the B meson, we will use the distribution amplitude determined in CLFD (see Chapter 8). To conclude this chapter, the end-point divergences parameterized by the terms X_A and X_H, and included in hard spectator scattering kernels and weak annihilation contributions, will be treated by taking the following values: the phases ϕ_A and ϕ_H are equal to 0^o and the constants ϱ_A and ϱ_H are equal to one. Despite the fact that several studies [220, 221] have fitted ϕ_A and ϕ_H from different experimental data, we shall use conventional values for them since the uncertainties carried by $\phi_{A,H}$ are large. Recall that theoretically speaking $\phi_{A,H}$ could vary in the range $\{-180, +180\}$.

Chapter 11

Branching ratios for B decays into $\rho\pi$ or ρK in QCDF

" Il n'y a pas moyen de contenter ceux qui veulent savoir le pourquoi des pourquoi. "

Leibniz

Now that we have introduced QCD factorization, we can apply this formalism to the calculation of the branching ratios for the decays $B \to \rho\pi$ and $B \to \rho K$. Hence, we can again (see Chapter 5) compare our results with experimental data providing by BABAR, BELLE and CLEO.

11.1 Generalities

Investigating the branching ratios for B decays is not an easy task since we have to deal with the high to low energy scale involved in the hadronic matrix elements that arise in the B decay amplitude. Many studies have been performed in the past regarding this subject. We could refer (for the QCD factorization framework) to that for B decays into two vectors [222], into two pseudo-scalars [223], into pseudoscalar and vector [224], into two pions and into pion kaon [225]... Branching ratios have been analysed in an extensive way by using the naive factorization formalism [226, 227, 228] as well as in perturbative QCD factorization [229, 230, 231]. Before beginning the analysis of branching ratios for B decaying into $\rho\pi$ or into ρK, we shall make a few comments regarding our approach.

- As in Chapter 10, the input parameters such as the parameters of the CKM matrix, A, λ, ρ and η, the decay constants $f_\pi, f_K, f_\rho, f_\omega$, the quark masses m_u, m_d, m_b, m_s, and the B life-time values τ_{B^0}, τ_{B^+} (as listed in Chapter 5) will be used in our numerical applications.

- Regarding the form factors involved in our calculations, we shall use those listed in Chapter 9 and determined in the CLFD approach. We fix the value for the form factor $A_0(k^2)$ which describes the transition $B \to \rho$, and we keep free the other form factor $F_1(k^2)$ - that describes the transition $B \to \pi$ or $B \to K$ - since its value is not determined with the same accuracy and still needs improvement.

- Because of the complexity of the QCD factorization method and the different uncertainties carried by many parameters included in the formulation (for example, the phenomenological parametrization of the divergent point integral, X_A or X_H, in the annihilation and hard scattering contributions, respectively), we shall fix all of the parameters such as $\varrho_{A,H}, \phi_{A,H}$, except the form factor $F_1(k^2)$ and the CKM matrix parameters ρ and η.

  According to previous studies where numerous fits have been applied to experimental data and where various constraints have been obtained, we expect to have reduced the effects of uncertainties in our results and hence, we will just focus on the uncertainties included in $F_1(k^2)$, ρ and η. Recall that the values of A and λ are very well determined and do not need more accuracy. Note as well that we replace N_c by N_c^{eff} in the QCDF formulation since the colour octet contributions cannot be neglected[1] and are not exactly factorizable. Therefore their contributions are taken into account through the variable ξ_i into N_c^{eff} (see Chapter 3). We shall use, according to results obtained in naive factorization, the average value for N_c^{eff} that is equal to 1.5 in the case of $B \to \rho\pi$ and around 1.75 in the case of $B \to \rho K$. Thus we shall express all of our results as a function of the form factor $F_1(k^2)$ and as a function of the CKM parameters ρ and η.

- As when naive factorization was applied, we shall include the $\rho - \omega$ mixing contribution every time that it can contribute - i.e. in all of the B decay channels such as $B \to \rho^0 M$, with M being K or π.

- It has been shown that annihilation contributions could play an important role in B decays. Even though they are power suppressed in QCD

[1]Note that we used $N_c = 3$ for the calculation of α_s and C_F.

factorization, they may give large strong phases due to QCD corrections and then, they cannot be neglected. Although we did not include them in the naive factorization, we will take them into account in our second approach.

- It has also been pointed out that charming-penguin contribution effects could have been underestimated and may affect the evaluation of hadronic matrix elements. It is assumed that charm-anticharm intermediate states can be created by the weak interaction and may turn into non-charmed final states by strong rescattering. Nevertheless, we will not include these contributions because they are not yet under good control, and carry large uncertainties and unknown parameters.

- Finally, in order to compare our results with experimental data and to determine the constraints on the form factors $F_1^{B\to\pi}$, $F_1^{B\to K}$ and the CKM matrix parameters ρ and η, we shall use the experimental branching ratios of $B \to \rho\pi$, $B \to \rho K$, $B \to \rho\pi$ and $B \to \omega K$ from BABAR, BELLE and CLEO. We refer the reader to Chapter 5 for their listed values. At the time, we will have an opportunity to check the agreement (or not) between naive factorization and QCD factorization according to the experimental results.

11.2 Branching ratios for $B \to \rho\pi$

11.2.1 Weak annihilation contributions

We analyse processes such as $B^{\pm,0} \to \rho^{\pm,0}\pi^{\pm,0}$ and also $B^{\pm} \to \omega\pi^{\pm}$. Two of them include $\rho - \omega$ mixing: $B^- \to \rho^0\pi^-$ and $\bar{B}^0 \to \rho^0\pi^0$. The three other decays without $\rho - \omega$ mixing effects are $B^- \to \rho^-\pi^0$, $\bar{B}^0 \to \rho^-\pi^+$ and $B^- \to \omega\pi^-$. Recall that the branching ratio of $B \to PV$ decays can be written in the B meson rest frame as,

$$\mathscr{B}(B\to PV) = \frac{\tau_B}{8\pi}\frac{|p_\rho|}{m_B^2}\left|\mathcal{A}(B\to PV) + \mathcal{A}^a(B\to PV)\right|^2 , \qquad (11.1)$$

where $|p_\rho|$ is a kinematical factor referring to the c.m. momentum of the decay particles. $\mathcal{A}(B\to PV)$ is the amplitude coming from the tree and penguin diagrams and $\mathcal{A}^a(B\to PV)$ is the annihilation amplitude. We emphasise that annihilation contributions depend strongly on the value of the phase ϕ_A that could be subject to discussions. In this section, we give the explicit annihilation amplitudes for all these charmless B decays. Their contributions are added to the tree and penguin amplitudes. We refer the reader to Chapter

5 for the explicit tree and penguin amplitudes. Note that there is a factor $m_B|p_\rho|$ that needs to be added to obtain the correct branching ratios accordingly to Eq. (11.1). Moreover, an inversion between a_1 and a_2 has to be made to follow the usual definition of the tree diagram contributions. Below, we list the annihilation amplitudes:
for the decay $\bar{B}^0 \to \rho^-\pi^+$,

$$\mathcal{A}^a(\overline{B}^0 \to \rho^-\pi^+) = \frac{G_F}{\sqrt{2}} f_B f_\pi f_\rho \Big\{ V_{ub}V_{ud}^* b_1(\pi^+,\rho^-) + (V_{ub}V_{ud}^* + V_{cb}V_{cd}^*)\Big[b_3(\rho^-,\pi^+) + b_4(\pi^+,\rho^-) + b_4(\rho^-,\pi^+) - \frac{1}{2}b_3^{ew}(\rho^-,\pi^+) + b_4^{ew}(\pi^+,\rho^-) - \frac{1}{2}b_4^{ew}(\rho^-,\pi^+)\Big]\Big\}\ ; \quad (11.2)$$

for the decay $\bar{B}^0 \to \rho^0\pi^0$,

$$\mathcal{A}^a(\overline{B}^0 \to \rho^0\pi^0) = \frac{G_F}{2\sqrt{2}} f_B f_\pi f_\rho \Big\{ V_{ub}V_{ud}^* \Big[b_1(\rho^0,\pi^0) + b_1(\pi^0,\rho^0)\Big] + (V_{ub}V_{ud}^* + V_{cb}V_{cd}^*)\Big[b_3(\rho^0,\pi^0) + b_3(\pi^0,\rho^0) + 2b_4(\pi^0,\rho^0) + 2b_4(\rho^0,\pi^0) - \frac{1}{2}b_3^{ew}(\rho^0,\pi^0) - \frac{1}{2}b_3^{ew}(\pi^0,\rho^0) + \frac{1}{2}b_4^{ew}(\pi^0,\rho^0) + \frac{1}{2}b_4^{ew}(\rho^0,\pi^0)\Big]\Big\}\ ; \quad (11.3)$$

for the decay $\bar{B}^0 \to \omega\pi^0$,

$$\mathcal{A}^a(\overline{B}^0 \to \omega\pi^0) = \frac{G_F}{2\sqrt{2}} f_B f_\pi f_\omega \Big\{ V_{ub}V_{ud}^* \Big[b_1(\omega,\pi^0) + b_1(\pi^0,\omega)\Big] + (V_{ub}V_{ud}^* + V_{cb}V_{cd}^*)\Big[- b_3(\pi^0,\omega) - b_3(\omega,\pi^0) + \frac{1}{2}b_3^{ew}(\pi^0,\omega) + \frac{1}{2}b_3^{ew}(\omega,\pi^0) + \frac{3}{2}b_4^{ew}(\pi^0,\omega) + \frac{3}{2}b_4^{ew}(\omega,\pi^0)\Big]\Big\}\ ; \quad (11.4)$$

for the decay $B^- \to \rho^0\pi^-$,

$$\mathcal{A}^a(B^- \to \rho^0\pi^-) = \frac{G_F}{2} f_B f_\pi f_\rho \Big\{ V_{ub}V_{ud}^* \Big[b_2(\pi^-,\rho^0) - b_2(\rho^0,\pi^-)\Big] + (V_{ub}V_{ud}^* + V_{cb}V_{cd}^*)\Big[b_3(\pi^-,\rho^0) - b_3(\rho^0,\pi^-) + b_3^{ew}(\pi^-,\rho^0) - b_3^{ew}(\rho^0,\pi^-)\Big]\Big\}\ ; \quad (11.5)$$

for the decay $B^- \to \omega\pi^-$,

$$\mathcal{A}^a(B^- \to \omega\pi^-) = \frac{G_F}{2} f_B f_\pi f_\omega \Big\{ V_{ub}V_{ud}^* \Big[b_2(\pi^-,\omega) + b_2(\omega,\pi^-) \Big] + (V_{ub}V_{ud}^* + V_{cb}V_{cd}^*) \Big[b_3(\pi^-,\omega) + b_3(\omega,\pi^-) + b_3^{ew}(\pi^-,\omega) + b_3^{ew}(\omega,\pi^-) \Big] \Big\} ; \tag{11.6}$$

for the decay $B^- \to \rho^-\pi^0$,

$$\mathcal{A}^a(B^- \to \rho^-\pi^0) = \frac{G_F}{2} f_B f_\pi f_\rho \Big\{ V_{ub}V_{ud}^* \Big[b_2(\rho^-,\pi^0) - b_2(\pi^0,\rho^-) \Big] + (V_{ub}V_{ud}^* + V_{cb}V_{cd}^*) \Big[b_3(\rho^-,\pi^0) - b_3(\pi^0,\rho^-) + b_3^{ew}(\rho^-,\pi^0) - b_3^{ew}(\pi^0,\rho^-) \Big] \Big\} . \tag{11.7}$$

All the coefficients b_i have been defined in the previous chapter. The expressions for the CKM matrix elements V_{ub}, V_{ud}^*, V_{cb} and V_{cd}^* can be found in Chapter 2. As in Chapter 5, we shall also calculate the ratio between $\mathscr{B}(B^0 \to \rho^\pm\pi^\mp)$ and $\mathscr{B}(B^\pm \to \rho^0\pi^\pm)$, since in that case, the uncertainties caused by many systematic errors are removed. Recall, we define the ratio R_π as,

$$R_\pi = \frac{\mathscr{B}(B^0 \to \rho^\pm\pi^\mp)}{\mathscr{B}(B^\pm \to \rho^0\pi^\pm)} . \tag{11.8}$$

11.2.2 Results and discussions

Assuming that all of the parameters involved in QCD factorization have been constrained by independent studies where the input parameters related to factorization were fitted, we concentrate our efforts on the form factor $F_1^{B\to\pi}$ and the CKM matrix parameters ρ and η. In order to reach this aim, we have calculated the branching ratios for B decays such as $B^\pm \to \rho^0\pi^\pm$, $B^\pm \to \rho^\pm\pi^0$, $B^0 \to \rho^\pm\pi^\mp$, $B^0 \to \rho^0\pi^0$ and $B^\pm \to \omega\pi^\pm$, where the annihilation and $\rho-\omega$ mixing contributions were taken into account. All the results are shown in Figs. 11.1, 11.2, 11.3, 11.4, 11.5 and 11.6, and the branching ratios are plotted as a function of the form factor $F_1^{B\to\pi}$ and as a function of the values of ρ and η as well. By taking into account experimental data from CLEO, BABAR and BELLE collaborations, and comparing theoretical predictions with experimental results, we expect to obtain a constraint on the form factor

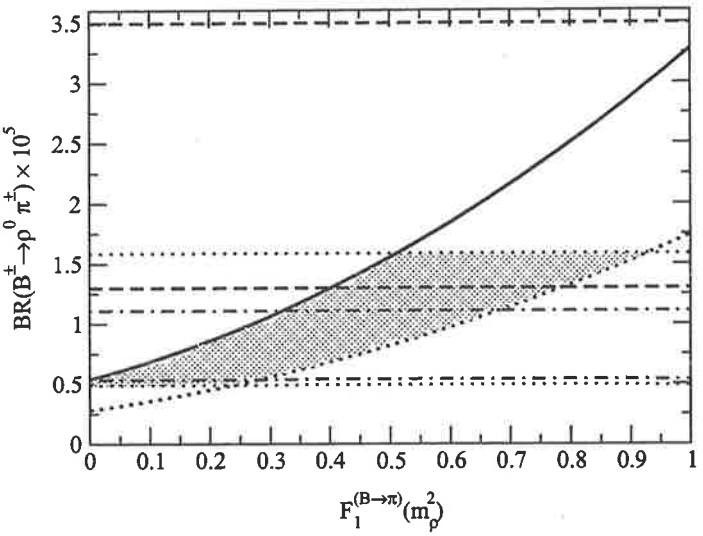

Figure 11.1: Branching ratio for $B^{\pm} \to \rho^0\pi^{\pm}$, for limiting values of the CKM matrix elements. Solid line (dotted line) for max (min) CKM matrix elements. Notation: horizontal dotted lines: CLEO data; dashed lines: BABAR data; dot-dashed lines: BELLE data.

$F_1^{B\to\pi}$ as well as some limits for the CKM matrix element parameters ρ and η. Because of their accuracy, we shall mainly use the CLEO and BELLE data for our analysis rather than those from BABAR. Our results should depend more on uncertainties coming from the experimental data than those from the factorization approach (as opposed to naive factorization) applied to calculate hadronic matrix element $\langle\rho\pi|J_\mu|B\rangle$.

For the branching ratio $B^{\pm} \to \rho^0\pi^{\pm}$ (Fig. 11.1), we found total consistency between the theoretical results and experimental data from CLEO and BELLE. However, these results allow us to determine a limit (between 0.3 and 0.50 with an average value around 0.42) for the value of the form factor $F_1^{B\to\pi}$ whereas they do not allow us to constrain for the CKM matrix parameters ρ and η. The weak dependence of the branching ratio on the form factor, $F_1^{B\to\pi}$, is related to the tree and penguin amplitudes which are mainly governed by the form factor $A_0^{B\to\rho}$ rather than $F_1^{B\to\pi}$. Therefore, this branching ratio cannot be used as an efficient test to constrain the form factor $F_1^{B\to\pi}$. Note also that the comparison with BABAR data shows an agreement between theory and experiment at a little over one σ but for a value of $F_1^{B\to\pi}$ bigger than 0.4.

For the branching ratio $B^{\pm} \to \rho^{\pm}\pi^0$ (Fig. 11.2), CLEO gives only an upper limit for the branching ratio, whereas BABAR and BELLE do not. According to this upper limit, the value of the form factor $F_1^{B\to\pi}$ is to be lower

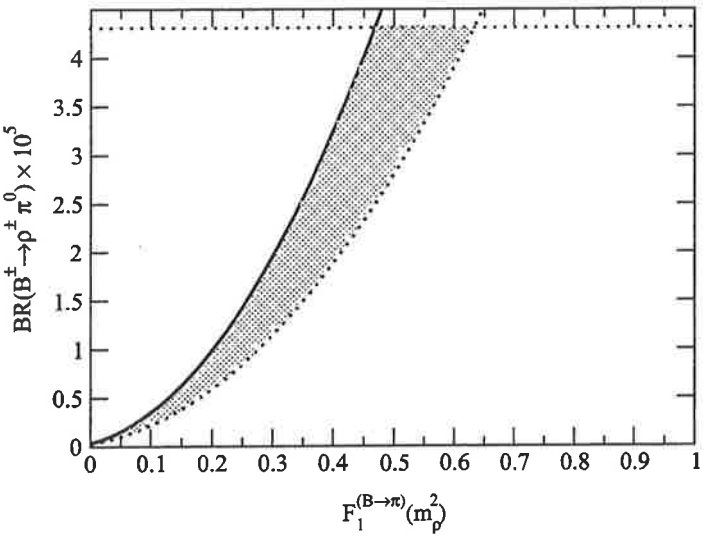

Figure 11.2: Branching ratio for $B^{\pm} \to \rho^{\pm}\pi^0$, for limiting values of the CKM matrix elements. Solid line (dotted line) for max (min) CKM matrix elements. Same notation as in Fig. 11.1 for the horizontal line.

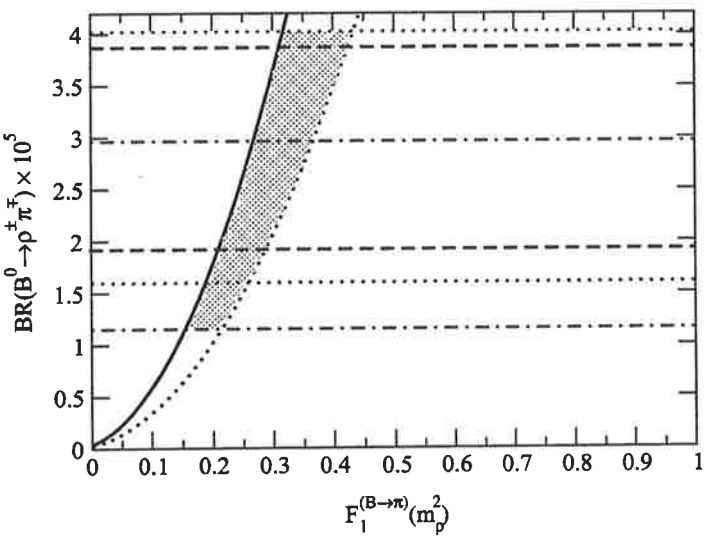

Figure 11.3: Branching ratio for $B^0 \to \rho^{\pm}\pi^{\mp}$, for limiting values of the CKM matrix elements. Solid line (dotted line) for max (min) CKM matrix elements. Same notation as in Fig. 11.1 for the horizontal lines.

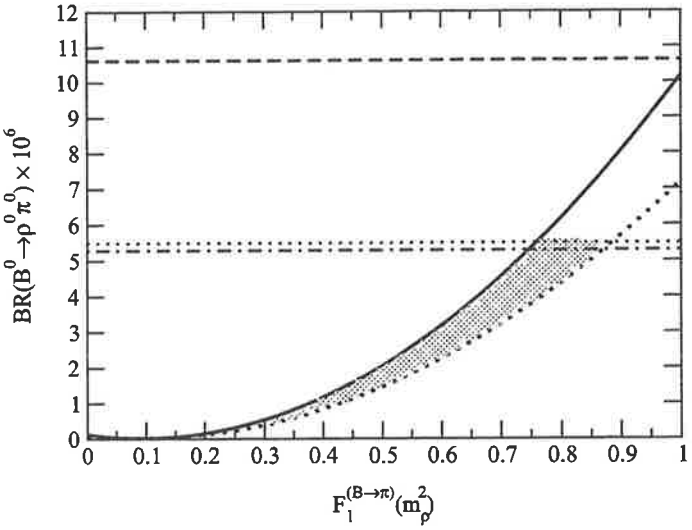

Figure 11.4: Branching ratio for $B^0 \to \rho^0\pi^0$, for limiting values of the CKM matrix elements. Solid line (dotted line) for max (min) CKM matrix elements. Same notation as in Fig. 11.1 for the horizontal lines.

than 0.62. We emphasize that this branching ratio is strongly dependent on the form factor $F_1^{B\to\pi}$ and could be an efficient test to constrain the value of $F_1^{B\to\pi}$. For the branching ratio $B^0 \to \rho^\pm\pi^\mp$ (shown in Fig. 11.3), BELLE, BABAR and CLEO give coherent experimental data. The decay amplitude related to this branching ratio is proportional to the form factor $F_1^{B\to\pi}$ and thus allows us to constrain the form factor. Requiring agreement between experimental values and theoretical results yields a mean average value for $F_1^{B\to\pi}$ equal to 0.28. Note that for these first three branching ratios their dependence on the CKM matrix elements ρ and η is strong. Hence we expect to be able to determine limits for their values when more B decay channels are taken into account.

For the branching ratio $B^0 \to \rho^0\pi^0$ (Fig. 11.4), BABAR, BELLE and CLEO only give an upper limit for the branching ratio. Moreover, the branching ratio does not appear to be very sensitive to the CKM matrix elements ρ and η. We therefore need new data to go further in this case. Finally, we focus on the branching ratio $B^\pm \to \omega\pi^\pm$, plotted in Fig. 11.5. There is no agreement with the CLEO data for values of the form factor $F_1^{B\to\pi}$ lower than 0.2 whereas there is a good agreement with BABAR and BELLE for a large range of values of $F_1^{B\to\pi}$. BABAR gives an average value of $F_1^{B\to\pi}$ around 0.35. Note that the sensitivity of the branching ratio to the CKM matrix elements is bigger than that to the form factor $F_1^{B\to\pi}$ and this does not allow us to draw any conclusions regarding the value of $F_1^{B\to\pi}$.

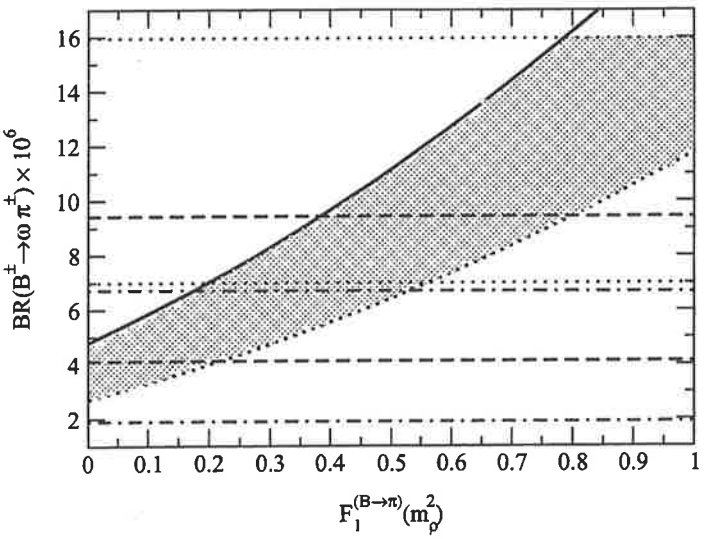

Figure 11.5: Branching ratio for $B^{\pm} \to \omega\pi^{\pm}$, for limiting values of the CKM matrix elements. Solid line (dotted line) for max (min) CKM matrix elements. Same notation as in Fig. 11.1 for the horizontal lines.

To remove systematic errors in branching ratio data given by the B factories, we can look at the ratio R_π, between the two following branching ratios: $\mathscr{B}(B^0 \to \rho^{\pm}\pi^{\mp})$ and $\mathscr{B}(B^{\pm} \to \rho^0\pi^{\pm})$. In Fig. 11.6 we show the ratio R_π as a function of the form factor $F_1^{B\to\pi}$. All the B factory data are in good agreement with theoretical predictions. The results indicate that the ratio is weakly sensitive to the CKM matrix elements ρ and η whereas it is strongly sensitive to the value of $F_1^{B\to\pi}$. Comparison with BELLE data allows us to obtain a value for $F_1^{B\to\pi}$ of between 0.15 and 0.37, with BABAR it is between 0.05 and 0.20 and with CLEO it is 0.08 - 0.42. According to the first conclusion for the value of $F_1^{B\to\pi}$, it seems to us that the value of the form factor $F_1^{B\to\pi}$ which describes the transition $B \to \pi$ taken at $k^2 = m_\rho^2$ might be around 0.3-0.4. Based on this result taking into account only the branching ratio $B \to \rho\pi$, it is also possible to give some predictions concerning the branching ratios for the decays $B^0 \to \rho^{\pm}\pi^0$ and $B^0 \to \rho^0\pi^0$. Their predicted values are the following: $\mathscr{B}(B^0 \to \rho^{\pm}\pi^0) \approx 17.5 \times 10^{-6}$ and $\mathscr{B}(B^0 \to \rho^0\pi^0) < 1 \times 10^{-6}$.

It has to be pointed out that the annihilation contributions in B decays play a major role since they contribute significantly to the magnitude of the amplitude. As an example, in Fig. 11.7 we show the annihilation contributions for the branching ratio $B^- \to \rho^0\pi^-$. The annihilation diagram contribution to the total decay amplitude strongly enhances (in a positive or negative way) the branching ratio $B^- \to \rho^0\pi^-$ according to the value chosen

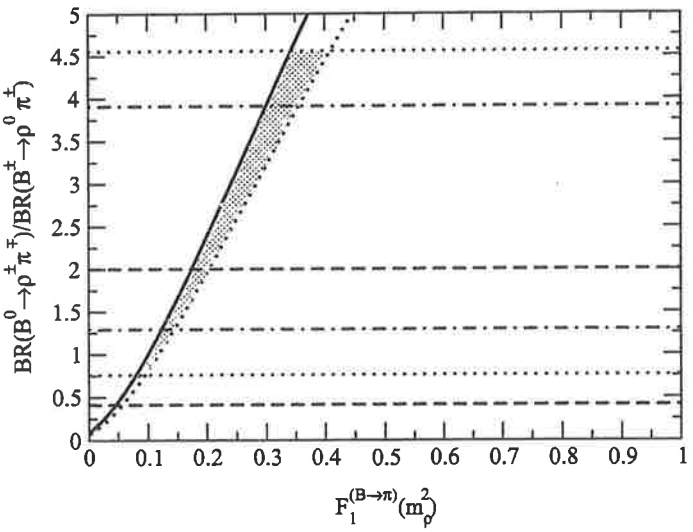

Figure 11.6: The ratio of two $\rho\pi$ branching ratios for limiting values of the CKM matrix elements: solid line (dotted line) for max (min) CKM matrix elements. Same notation as in Fig. 11.1 for the horizontal lines.

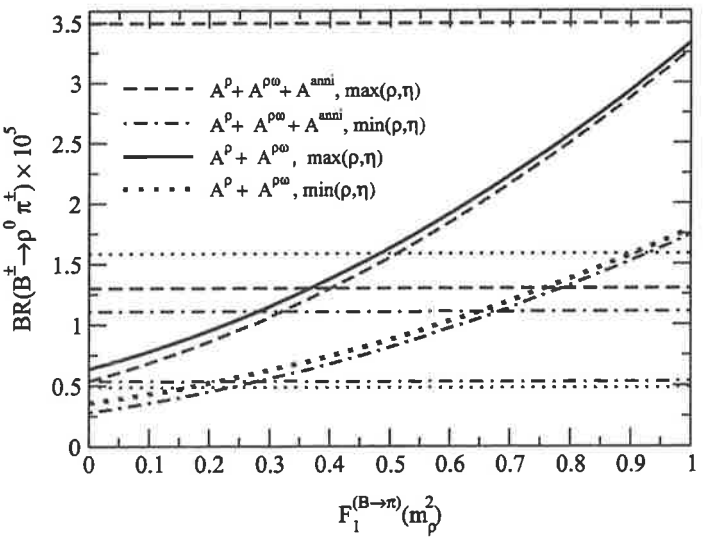

Figure 11.7: Annihilation contributions to the branching ratio for $B^{\pm} \to \rho^0 K^{\pm}$, for limiting values of the CKM matrix elements. Same notation as in Fig. 11.1 for the horizontal lines. $A^{\rho-\omega}$ and A^{a} are the ρ^0 amplitude including $\rho - \omega$ mixing effects and annihilation contributions, respectively.

for the phase ϕ_A. This contribution could be bigger than that of $\rho-\omega$ mixing but carries more uncertainties because of the endpoint divergence (see Chapter 10). We emphasise that these two contributions ($\rho - \omega$ mixing effects and annihilation contributions) are not just simple corrections to the total amplitude but they fully contribute to obtain a correct description of the B decay amplitude.

We emphasize as well that the value of the form factor $F_1^{B\to\pi}$ determined in covariant light front dynamics fully satisfies this analysis since $F_1^{B\to\pi}$ is equal to 0.35 in CLDF. Finally, the results obtained by applying QCD factorization are qualitatively in agreement with naive factorization used in the first part of this thesis. However, the QCD factorization approach is more powerful since we are able to calculate the branching ratios as a function of the uncertainty related to one physical parameter, the form factor $F_1^{B\to\pi}$, rather than one phenomenological parameter, the effective number of colours N_c^{eff}. According to this analysis of branching ratios for the $B \to \rho\pi$ decays, the value obtained for the form factor $F_1^{B\to\pi}$ would support the BSW model rather than the GH model. In the next section, we are going to analyse the branching ratios $B \to \rho K$ and then draw some conclusions regarding the form factor $F_1^{B\to K}$.

11.3 Branching ratios for $B \to \rho K$

11.3.1 Weak annihilation contributions

Now, let us consider the case where M is a kaon (i.e. $B \to \rho K$). As in the previous section, where five $b \to u$ transitions were analysed, here we investigate five $b \to s$ transitions. These are the following B decays: $B^- \to \rho^0 K^-$, $\bar{B}^0 \to \rho^0 \bar{K}^0$, $\bar{B}^0 \to \rho^- K^+$, $B^- \to \rho^- \bar{K}^0$ and finally $B^- \to \omega K^-$. As usual, the reader will find in Chapter 5 all of the expressions for the tree and penguin amplitudes related to the analysed decays. Recall the inversion of a_1 with a_2 and the factor $m_B|p_\rho|$ for the branching ratio formula in Eq. (11.1). In the following, we enumerate the annihilation amplitudes which will be included in the usual branching ratio amplitude for the five decays mentioned previously:
for the decay $\bar{B}^0 \to \rho^+ K^-$,

$$\mathcal{A}^a(\overline{B}^0 \to \rho^+ K^-) = \frac{G_F}{\sqrt{2}} f_B f_K f_\rho \Big\{ (V_{ub}V_{us}^* + V_{cb}V_{cs}^*) \Big[b_3(K^-, \rho^+) - \frac{1}{2} b_3^{ew}(K^-, \rho^+) \Big] \Big\} \; ; \quad (11.9)$$

for the decay $\bar{B}^0 \to \rho^0 \bar{K}^0$,

$$\mathcal{A}^a(\overline{B}^0 \to \rho^0 \overline{K}^0) = -\frac{G_F}{2} f_B f_K f_\rho \Big\{ (V_{ub}V_{us}^* + V_{cb}V_{cs}^*) \Big[b_3(\overline{K}^0, \rho^0) - \frac{1}{2} b_3^{ew}(\overline{K}^0, \rho^0) \Big] \Big\} \; ; \quad (11.10)$$

for the decay $\bar{B}^0 \to \omega \bar{K}^0$,

$$\mathcal{A}^a(\overline{B}^0 \to \omega \overline{K}^0) = \frac{G_F}{2} f_B f_K f_\omega \Big\{ (V_{ub}V_{us}^* + V_{cb}V_{cs}^*) \Big[b_3(\overline{K}^0, \omega) - \frac{1}{2} b_3^{ew}(\overline{K}^0, \omega) \Big] \Big\} \; ; \quad (11.11)$$

for the decay $B^- \to \omega K^-$,

$$\mathcal{A}^a(B^- \to \omega K^-) = \frac{G_F}{2} f_B f_K f_\omega \Big\{ V_{ub}V_{us}^* b_2(K^-, \omega) + (V_{ub}V_{us}^* + V_{cb}V_{cs}^*) \Big[b_3(K^-, \omega) + b_3^{ew}(K^-, \omega) \Big] \Big\} \; ; \quad (11.12)$$

for the decay $B^- \to \rho^0 K^-$,

$$\mathcal{A}^a(B^- \to \rho^0 K^-) = \frac{G_F}{2} f_B f_K f_\rho \Big\{ V_{ub}V_{us}^* b_2(K^-, \rho^0) + (V_{ub}V_{us}^* + V_{cb}V_{cs}^*) \Big[b_3(K^-, \rho^0) + b_3^{ew}(K^-, \rho^0) \Big] \Big\} \; ; \quad (11.13)$$

for the decay $B^- \to \rho^- \bar{K}^0$,

$$\mathcal{A}^a(B^- \to \rho^- \overline{K}^0) = \frac{G_F}{\sqrt{2}} f_B f_K f_\rho \Big\{ V_{ub}V_{us}^* b_2(\overline{K}^0, \rho^-) + (V_{ub}V_{us}^* + V_{cb}V_{cs}^*) \Big[b_3(\overline{K}^0, \rho^-) + b_3^{ew}(\overline{K}^0, \rho^-) \Big] \Big\} \; . \quad (11.14)$$

All of the terms involved in the above expressions can be found in Chapter 9. We shall evaluate the ratio, R_K, between the two branching ratios $\mathscr{B}(B^0 \to \rho^\pm K^\mp)$ and $\mathscr{B}(B^\pm \to \rho^0 K^\pm)$ as follows:

$$R_K = \frac{\mathscr{B}(B^0 \to \rho^\pm K^\mp)}{\mathscr{B}(B^\pm \to \rho^0 K^\pm)} \; . \quad (11.15)$$

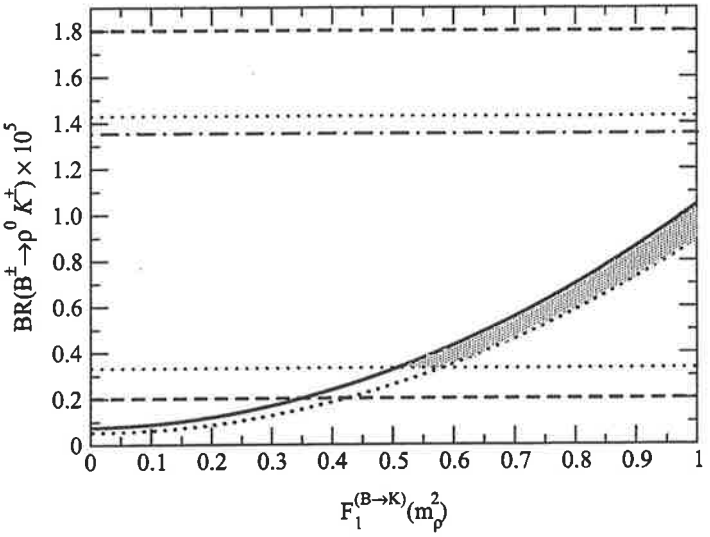

Figure 11.8: Branching ratio for $B^{\pm} \to \rho^0 K^{\pm}$, for limiting values of the CKM matrix elements. Solid line (dotted line) for max (min) CKM matrix elements. Notation: horizontal dotted line: CLEO data; dashed line: BABAR data; dot-dashed line: BELLE data.

To end this analysis, we shall also calculate the ratio, R, defined as the ratio between R_π and R_K, by

$$R = \frac{R_\pi}{R_K} \,. \tag{11.16}$$

11.3.2 Results and discussions

This section aims to discuss the numerical results of branching ratios for B decays such as $B \to \rho K$. The branching ratios for $B^- \to \rho^0 K^-$, $\bar{B}^0 \to \rho^0 \bar{K}^0$, $\bar{B}^0 \to \rho^- K^+$, $B^- \to \rho^- \bar{K}^0$ and $B^- \to \omega K^-$ have been calculated in the QCD factorization framework rather than in the naive factorization approach, as in Chapter 5. Results are plotted in Figs. 11.8, 11.9, 11.10, 11.11, 11.12 and 11.13. Annihilation contributions and $\rho - \omega$ mixing effects have been included in the B decay amplitudes.

We shall compare our theoretical predictions with experimental data provided mainly by CLEO since the BABAR and BELLE data are less numerous and need some improvement. Nevertheless, for the branching ratio $B^- \to \omega K^-$ we shall take the BELLE data, which are the most recent and accurate measurements in that case. It is also necessary to notice that all of these branching ratio data are less numerous and carry more uncertainties than those of $B \to \rho\pi$. All of the branching ratios are plotted as a function

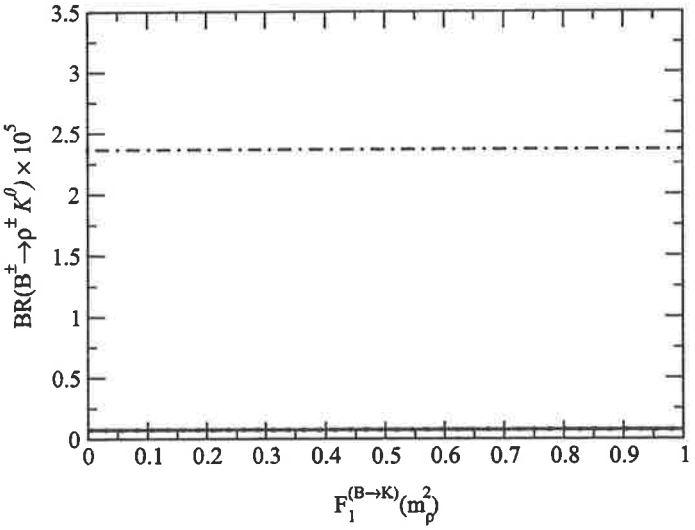

Figure 11.9: Branching ratio for $B^{\pm} \to \rho^{\pm} K^0$, for limiting values of the CKM matrix elements. Solid line (dotted line) for max (min) CKM matrix elements. Same notation as in Fig. 11.8 for the horizontal line.

of the transition form factor $F_1^{B\to K}$, where $F_1^{B\to K}$ describes the transition $B \to K$ at $k^2 = m_\rho^2$. In order to constrain the value of this transition form factor, we shall use some experimental data and hence we expect to obtain some limits regarding its value. As usual, we also show the dependence of the branching ratios on the CKM matrix parameters ρ and η.

For the branching ratio $B^- \to \rho^0 K^-$ (see Fig. 11.8), theoretical results and experimental data from CLEO and BABAR are in good agreement. BELLE only gives an upper limit for this branching ratio which is still consistent with our results. Note, that the dependence of the branching ratio on the form factor, $F_1^{B\to K}$, is stronger than that on the CKM matrix parameters ρ, and η. Nevertheless, no firm conclusion can be drawn from this branching ratio except for a lower limit for the form factor $F_1^{B\to K}$ that is around 0.33 (assuming the largest range of experimental data). For the branching ratio $B^- \to \rho^- \bar{K}^0$ plotted in Fig. 11.9, we observe a total lack of dependence of the branching ratio on the form factor $F_1^{B\to K}$ that explains the flat curves. This lack of dependence on $F_1^{B\to K}$ can be seen as well from the tree and penguin expressions. Only BELLE gives an upper experimental limit and that is consistent with our results. Moreover, the variation of CKM matrix elements ρ and η has a very weak influence on the branching ratio predictions. This channel cannot be used to constrain both the form factor $F_1^{B\to K}$ and the parameters ρ and η. Similarly, the branching ratio for the $\bar{B}^0 \to \rho^- K^+$ decay (see Fig. 11.10) is independent of the form factor $F_1^{B\to K}$

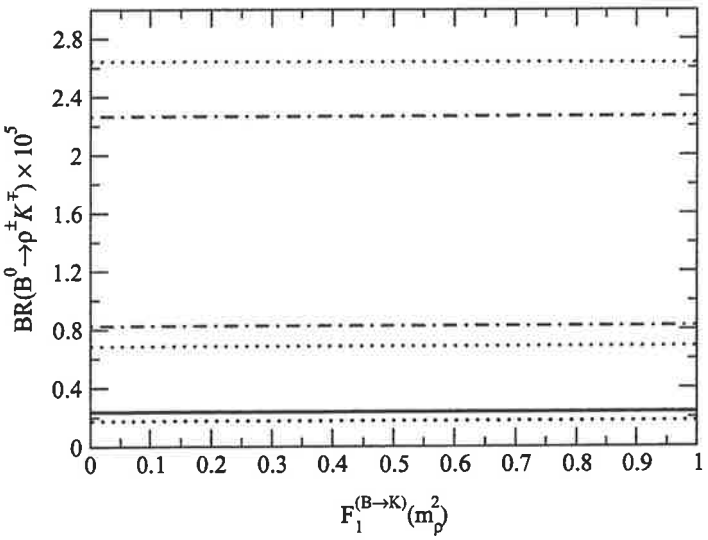

Figure 11.10: Branching ratio for $B^0 \to \rho^{\pm} K^{\mp}$, for limiting values of the CKM matrix elements. Solid line (dotted line) for max (min) CKM matrix elements. Same notation as in Fig. 11.8 for the horizontal lines.

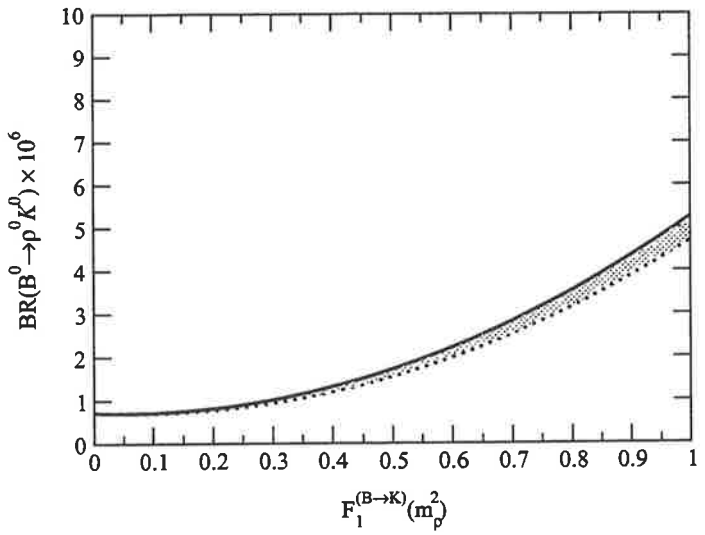

Figure 11.11: Branching ratio for $B^0 \to \rho^0 K^0$, for limiting values of the CKM matrix elements. Solid line (dotted line) for max (min) CKM matrix elements.

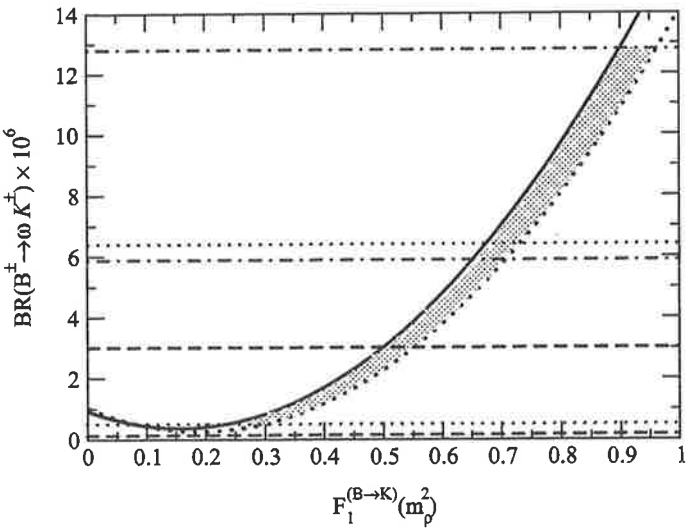

Figure 11.12: Branching ratio for $B^{\pm} \to \omega K^{\pm}$, for limiting values of the CKM matrix elements. Solid line (dotted line) for max (min) CKM matrix elements. Same notation as in Fig. 11.8 for the horizontal lines.

and no constraint regarding this form factor can be extracted. We observed that the branching ratio is more dependent on the parameters ρ and η than in the previous case but it is still not sufficient to derive information about the sensitivity of the branching ratio sensitivity to these parameters. We also mention that our theoretical results are not in agreement with experimental data from CLEO and BELLE. More investigations are needed in that case.

Next we consider the branching ratio $\bar{B}^0 \to \rho^0 \bar{K}^0$ shown in Fig. 11.11. Since there is no experimental data from BELLE, CLEO or BABAR, no conclusions about the form factor $F_1^{B\to K}$ can be drawn. Due to the strong sensitivity of the branching ratio on $F_1^{B\to K}$ and to the weak dependence on the CKM parameters ρ and η, it would be useful to have new data to constrain the transition $B \to K$. In Fig. 11.12 the branching ratio $B^- \to \omega K^-$ is plotted. It turns out that our result is in agreement with BABAR and CLEO data for values of $F_1^{B\to K}$ lower than 0.75 whereas lies outside the one σ range for BELLE. The curves have a strong dependence on the form factor $F_1^{B\to K}$. Assuming that the experimental data from BABAR and CLEO are more accurate than those from BELLE, it yields an upper limit for the form factor around 0.55 (BABAR) and 0.75 (CLEO).

By calculating the ratio R_K between $\mathscr{B}(B^0 \to \rho^{\pm} K^{\mp})$ and $\mathscr{B}(B^{\pm} \to \rho^0 K^{\pm})$, systematic errors can be removed. This ratio is shown in Fig. 11.13 as a function of $F_1^{B\to K}$ and for limiting values of the CKM parameters ρ and η. It appears that an agreement between experimental data provided by

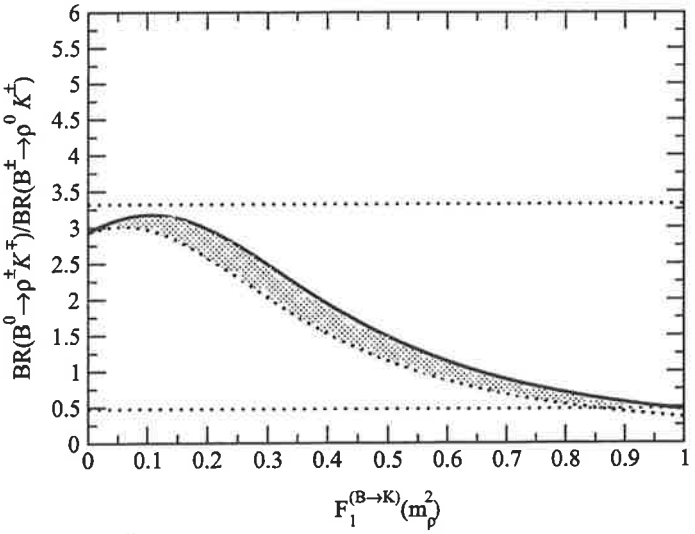

Figure 11.13: The ratio of two ρK branching ratios for limiting values of the CKM matrix elements. Solid line (dotted line) for max (min) CKM matrix elements. Same notation as in Fig. 11.8 for the horizontal lines.

CLEO and our results is almost found whatever the value of the form factor $F_1^{B\to K}$ is. Assuming that $F_1^{B\to K}$ is similar to $F_1^{B\to\pi}$ we can also compute the ratio R between the two previous ratios R_π and R_K and the result is shown in Fig. 11.14. Like the ratio R_K, the ratio R indicates that the upper limit for the value of the form factor $F_1^{B\to K}$ has to be around 0.45. Note that this limit can be applied on $F_1^{B\to\pi}$ as well due to the assumption made previously.

From this analysis, some conclusions can be drawn. First, it seems that the GH model, where $F_1^{B\to K} = 0.762$ at $k^2 = m_\rho^2$, does not lead to agreement with the experimental results in the QCD factorization framework. It appears as well that the BSW model might give a better approximation of this form factor transition than the GH model. Nevertheless, in the $B \to \rho K$ channel, we cannot effectively constrain our free parameter $F_1^{B\to K}$ because of the lack of experimental data. However, we are able to give a prediction regarding the branching ratio $\bar{B}^0 \to \rho^0 \bar{K}^0$ where data is currently not available. According to our analysis, $\mathscr{B}(\bar{B}^0 \to \rho^0 \bar{K}^0)$ might be lower than 3×10^{-6}. This prediction is consistent with our results obtained by using naive factorization in Chapter 5. As for the branching ratios for the $B \to \rho\pi$ channel, we observe a qualitative agreement between the naive factorization and QCD factorization even though the second method can give more theoretical predictions.

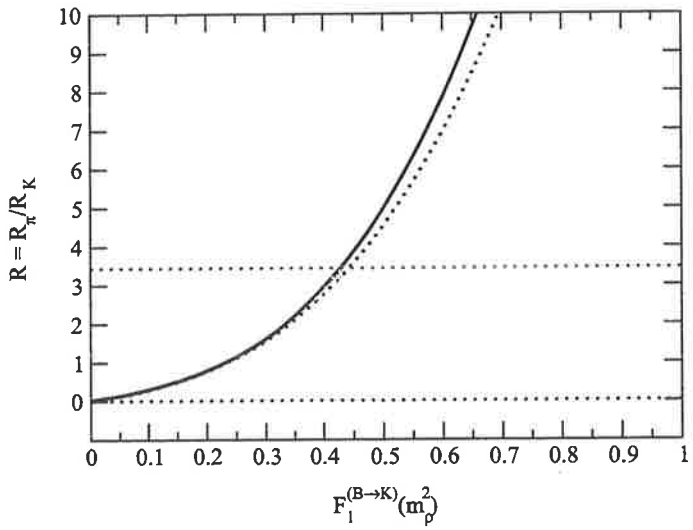

Figure 11.14: Ratio, R, between R_π and R_K limiting values of the CKM matrix elements. Solid line (dotted line) for max (min) CKM matrix elements. Same notation as in Fig. 11.8 for the horizontal lines.

11.4 Summary

We have mainly calculated the branching ratios in two different channels, $B \to \rho\pi$ and $B \to \rho K$. These calculations have been performed by applying the so-called QCD factorization approach, which takes into account explicitly the radiative corrections, at order α_s, coming from the hard scattering contributions. Our results are shown as a function of the form factor $F_1^{B\to\pi}$, in the case of $B \to \rho\pi$, and as a function of the form factor $F_1^{B\to K}$, in the case $B \to \rho K$, since these transition form factors could carry large uncertainties according to different models (BSW and GH models). We have also included uncertainties from the CKM matrix parameters, ρ and η, in our theoretical predictions. In order to constrain in an efficient way the form factors $F_1^{B\to\pi}$, $F_1^{B\to K}$ and the parameters ρ and η, we have compared our results with experimental data coming from CLEO, BABAR and BELLE. Since these experiments do not always give the same experimental branching ratios, we have tried to focus on those which are the most recent and accurate depending on the branching ratio analysed.

Regarding theoretical results for the branching ratios $B^\pm \to \rho^0\pi^\pm, B^\pm \to \rho^\pm\pi^0, B^0 \to \rho^\pm\pi^\mp, B^0 \to \rho^0\pi^0$ and $B^\pm \to \omega\pi^\pm$, we found that the BSW model provides a good agreement with experimental results whereas the GH model does not. It has been possible to obtain a best fit for the form factor describing the transition $B \to \pi$ at $k^2 = m_\rho^2$ that is $F_1^{B\to\pi} = 0.35$. Moreover,

predictions for the branching ratios $B^{\pm} \to \rho^{\pm}\pi^0$ and $B^0 \to \rho^0\pi^0$ have been made as well. These are $\mathscr{B}(B^{\pm} \to \rho^{\pm}\pi^0) \approx 17.5 \times 10^{-6}$ and $\mathscr{B}(B^0 \to \rho^0\pi^0) < 1 \times 10^{-6}$.

For the branching ratios $B^- \to \rho^0 K^-$, $\bar{B}^0 \to \rho^0 \bar{K}^0$, $\bar{B}^0 \to \rho^- K^+$, $B^- \to \rho^- \bar{K}^0$ and $B^- \to \omega K^-$, it has not been possible to determine precisely the value of the form factor $F_1^{B\to K}$ that describes the transition $B \to K$. At least, we found that the value for the form factor might be less than 0.65. This once again supports the BSW model in comparison with the GH model. A prediction for the branching ratio $\bar{B}^0 \to \rho^0 \bar{K}^0$ has also been made: $\mathscr{B}(\bar{B}^0 \to \rho^0 \bar{K}^0) < 3 \times 10^{-6}$.

We would like to emphasize that QCD factorization gives more accurate results than naive factorization as expected. However in a qualitative way naive factorization is still able to give the correct order of magnitude for the branching ratios analysed in our case. This does not mean that it is true for all types of B decays. Secondly, the form factors $F_1^{B\to\pi}$ and $F_1^{B\to K}$ for the transitions $B \to \pi$ and $B \to K$, calculated in the covariant light front dynamics framework, are in total agreement with the experimental data. Recall that we found the following values for the form factors when the CLFD approach was applied: $F_{1,(CLFD)}^{B\to\pi}(m_\rho^2) = 0.35$ and $F_{1,(CLFD)}^{B\to K}(m_\rho^2) = 0.40$. We refer the reader to Chapter 9 for more details. Unfortunately, it is not possible to constrain efficiently the parameters ρ and η with an analysis based only on the channels $B \to \rho\pi$ and $B \to \rho K$, because of the lack of experimental data. We need more accurate data if we want to improve the values of the CKM matrix parameters ρ and η. We need also to include more B decay channels such as $B \to K^*\pi, B \to K^*\eta, B \to K\phi$ to be able to obtain constraints on the parameters ρ and η. The conclusions drawn from this analysis are going to help us to determine the CP violating asymmetry parameter, a_{CP}, more precisely than when naive factorization was used. The next and final chapter introduces our asymmetry predictions for the direct CP violation in B decays into the channels $\rho\pi$ and ρK.

Chapter 12

Direct CP violation in B decays in QCDF

" On ne peut se passer d'une méthode pour se mettre en quête de la vérité des choses. "

René Descartes

We end our analysis by investigating the direct CP violating asymmetry, a_{CP}, in B decays, limiting our study to the decay $B \to \pi^+\pi^- M$, where as usual, M is a kaon or a pion. Isospin violation is taken into account through $\rho - \omega$ mixing and QCD factorization is applied in this work instead of naive factorization.

12.1 Asymmetry in B decays including annihilation contributions and $\rho - \omega$ mixing effects

It has been shown in the first part of this thesis that the $\rho - \omega$ mixing effects strongly enhance the direct CP violating asymmetry parameter a_{CP}. When the invariant mass of the $\pi^+\pi^-$ pair is in the vicinity of the ω resonance, it is found that the CP violating asymmetry, a_{CP}, reaches its maximum, a_{max}. We refer the reader to Chapter 4 for more details about $\rho - \omega$ mixing and to Chapter 6 for its use in the determination of the CP violating asymmetry parameter, a_{CP}, within the naive factorization approach. We emphasise that in this framework (i.e. naive factorization) the asymmetry, a_{CP}, is very small (near to 0) without the $\rho - \omega$ mixing effects. Remember that large direct

asymmetry requires at least a large strong phase difference and only $\rho - \omega$ mixing can provide it within naive factorization.

It has also been pointed out that annihilation amplitudes could contribute significantly to the total decay amplitude. However, their determination still needs to be improved and cannot be derived directly from the usual QCDF framework. Despite this they were included in our analysis of the branching ratios, where their contributions have been controlled by using a default value for the phase, ϕ_a. We shall not include them in the following work since their effects could provide large uncertainties in the direct CP asymmetry. The reader may refer to Chapters 9 and 10 for discussions regarding the annihilation contributions.

Nevertheless, for completeness we detail below how these annihilation contributions can be included in the usual calculations of asymmetry including $\rho - \omega$ mixing. As seen in Chapter 9, Section 9.2.2, the coefficients $b_i(M_1, M_2)$ – that describe the annihilation contributions – are expressed in terms of functions, $A_j^i(V,P)^a$, with the Wilson coefficients, C_k, related to the tree and electroweak (or QCD) penguin diagrams. Recall that the functions $A_j^i(V,P)^a$ arise from the convolution of hard scattering kernels with leading twist light cone distributions.

All of the details regarding the calculation of the CP violating asymmetry parameter, a_{CP}, can be found in Chapters 4 and 6. However we will emphasise one technical detail about the inclusion of the annihilation amplitudes in the total amplitude. It is known that CP violating asymmetry needs a strong phase difference, δ, coming from the hadronic matrix *and* a weak phase difference, ϕ, coming from the CKM matrix to obtain direct CP violation. In Chapter 4 the equations that define the ratios between the tree, t_ρ, t_ω, and penguin p_ρ, p_ω, amplitudes were derived. They take the following form:

$$\frac{p_\omega}{t_\rho} \equiv r' e^{i(\delta_q+\phi)} \ , \quad \frac{t_\omega}{t_\rho} \equiv \alpha e^{i\delta_\alpha} \ , \quad \frac{p_\rho}{p_\omega} \equiv \beta e^{i\delta_\beta} \ . \tag{12.1}$$

Following the previous discussion in Sect. 10.2.2, we can separate tree (b_1, b_2) from penguin $(b_3, b_3^{ew}, b_4, b_4^{ew})$ contributions in the annihilation amplitude. Therefore, we rewrite Eq. (12.1) as,

$$\frac{p_\omega + p_\omega^a}{t_\rho + t_\rho^a} \equiv r' e^{i(\delta_q+\phi)} \ , \quad \frac{t_\omega + t_\omega^a}{t_\rho + t_\rho^a} \equiv \alpha e^{i\delta_\alpha} \ , \quad \frac{p_\rho + p_\rho^a}{p_\omega + p_\omega^a} \equiv \beta e^{i\delta_\beta} \ , \tag{12.2}$$

where $t_\rho^a, t_\omega^a, p_\rho^a$ and p_ω^a are the tree and penguin annihilation contributions, respectively for the $\langle \rho M \rangle$ and $\langle \omega M \rangle$ amplitudes. The expressions for $t_\rho^a, t_\omega^a, p_\rho^a$ and p_ω^a for every decay channel on which we are going to focus can be very

easily determined. We refer the reader to Appendix C for their expressions. As mentioned in the title of this chapter, the tree and penguin amplitudes involved in the decay channel $B \to \pi^+\pi^- M$ are calculated in the QCD factorization framework. Their expressions are proportional to the coefficients a_k ($\propto C_k$) and are listed in Chapter 6. The reader will replace the coefficients, a_k^{NF}, determined in naive factorization by those obtained in QCDF, a_k^{QCDF}, in Chapter 9. It is a straightforward substitution since the global expression for the tree and penguin amplitudes does not change; simply, a_k^{NF} becomes a_k^{QCDF}.

12.2 CP violation in $B^{\pm,0} \to \pi^+\pi^-\pi^{\pm,0}$

In this section, we analyse the direct CP violating asymmetry parameter, a_{CP}, in the decay channels $B^- \to \rho^0(\omega)\pi^- \to \pi^+\pi^-\pi^-$ as well as $\bar{B}^0 \to \rho^0(\omega)\pi^0 \to \pi^+\pi^-\pi^0$.

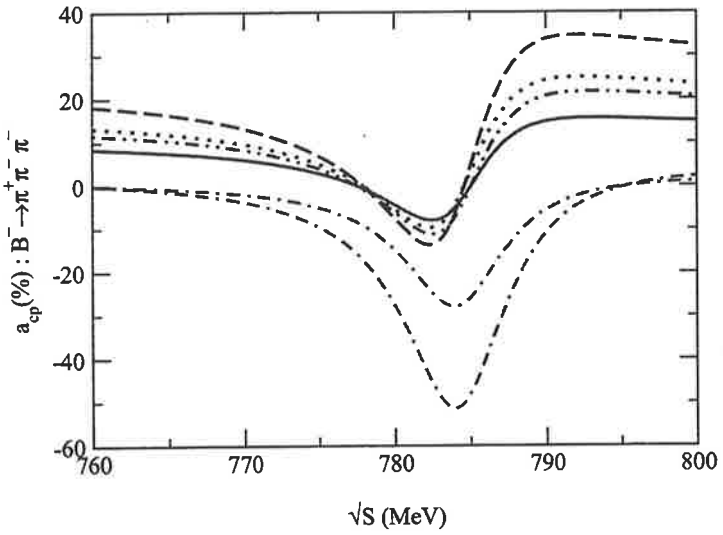

Figure 12.1: CP violating asymmetry, a_{CP}, for $B^- \to \pi^+\pi^-\pi^-$ for limiting values of the CKM matrix elements and for different values of the form factor $F_1^{B\to\pi}(m_\rho^2)$. Solid line (dotted line) for max CKM matrix elements and $F_1^{B\to\pi}(m_\rho^2) = 0.3$ (0.5). Dot-dot-dashed line (dashed line) for min CKM matrix elements and $F_1^{B\to\pi}(m_\rho^2) = 0.3$ (0.5). For comparison, we plot the asymmetry a_{CP} determined in naive factorization. (Dot-dashed and dot dash-dashed lines for minimum and maximum asymmetry values.)

In Figs. 12.1 and 12.2 we show the CP violating asymmetries for $B^- \to \rho^0(\omega)\pi^- \to \pi^+\pi^-\pi^-$ and $\bar{B}^0 \to \rho^0(\omega)\pi^0 \to \pi^+\pi^-\pi^0$ respectively, as a func-

tion of the energy $\sqrt{S}$, the form factor $F_1^{B\to\pi}(m_\rho^2)$ and the CKM matrix element parameters ρ and η.

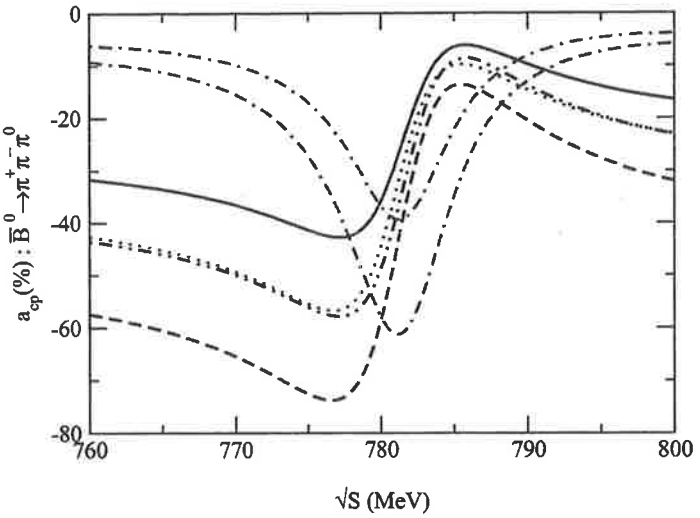

Figure 12.2: CP violating asymmetry, a_{CP}, for $\bar{B}^0 \to \pi^+\pi^-\pi^0$ for limiting values of the CKM matrix elements and for different values of the form factor $F_1^{B\to\pi}(m_\rho^2)$. Solid line (dotted line) for max CKM matrix elements and $F_1^{B\to\pi}(m_\rho^2) = 0.3$ (0.5). Dot-dot-dashed line (dashed line) for min CKM matrix elements and $F_1^{B\to\pi}(m_\rho^2) = 0.3$ (0.5). For comparison, we plot the asymmetry a_{CP} determined in naive factorization. (Dot-dashed and dot dash-dashed lines for minimum and maximum asymmetry values.)

Focusing first on Fig. 12.1, where the asymmetry for $B^- \to \rho^0(\omega)\pi^- \to \pi^+\pi^-\pi^-$ is plotted, we observe that the CP violating asymmetry parameter, a_{CP}, can be large and can even reach $20\% - 30\%$ outside the region where the invariant mass of the $\pi^+\pi^-$ pair is in the vicinity of the ω resonance. This is the first consequence of QCD factorization, since within this framework the strong phase can be generated not only by the $\rho - \omega$ mechanism but also by the Wilson coefficients. We recall that the Wilson coefficients include all of the final state interactions at order α_s. This shows as well that the non factorizable contribution effects are important and can modify the strong interaction phase. Because of the strong phase[1] that is either at the order of α_s or power suppressed by Λ_{QCD}/m_b, the CP violating asymmetry, a_{CP}, may be small but a large asymmetry cannot be excluded. Note that at the ω resonance, the asymmetry parameter a_{CP} is around -10%. In comparison,

[1]In comparison with QCDF, pQCD predicts large strong phases and direct CP asymmetries.

we show on the same figure the asymmetry parameter, a_{CP}, obtained by applying naive factorization. The results are quite different between these approaches because of the strong phase mentioned previously.

The second observation is that the form factor $F_1^{B\to\pi}(m_\rho^2)$ contributes very strongly to the asymmetry. If the form factor $F_1^{B\to\pi}(m_\rho^2)$ is equal to 0.3 then the asymmetry reaches 8% far away from the ω resonance whereas when $F_1^{B\to\pi}(m_\rho^2)$ is equal to 0.5 the asymmetry reaches 18%. This comes directly from the hard scattering contribution (included in the Wilson coefficients) that is dependent on the form factor $F_1^{B\to\pi}(m_\rho^2)$. Finally, it appears that the asymmetry is dependent on the CKM matrix parameters ρ and η, as expected. Note that this dependence is qualitatively as large as that for the form factor $F_1^{B\to\pi}(m_\rho^2)$.

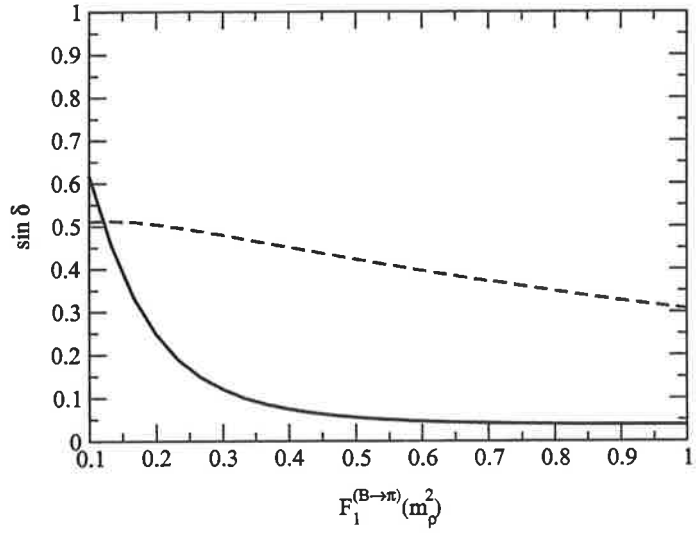

Figure 12.3: $\sin\delta$ as a function of the form factor $F_1^{B\to\pi}(m_\rho^2)$, for $B^- \to \pi^+\pi^-\pi^-$ (full line) and $\bar{B}^0 \to \pi^+\pi^-\pi^0$ (dashed line) for the case $\tilde{\Pi}_{\rho\omega} = (-3500; -300)$, where $\rho-\omega$ mixing is included.

In Fig. 12.2, the asymmetry, a_{CP}, is shown for $\bar{B}^0 \to \rho^0(\omega)\pi^0 \to \pi^+\pi^-\pi^0$. As for the previous case, we observe a strong sensitivity of the asymmetry to the form factor $F_1^{B\to\pi}(m_\rho^2)$ as well as the CKM matrix element parameters ρ and η. The CP violating asymmetry is predicted to be large, around -40% without the $\rho-\omega$ mixing effects. Again we show the comparison with naive factorisation, where there is agreement near the ω resonance. However, we emphasise that the results are quite different from those obtained by using the naive factorization framework where the strong phase only arises from $\rho-\omega$ mixing and hence allows for a large asymmetry only near ω and nowhere

else. With the knowledge of the asymmetry it will be possible to constrain the form factor $F_1^{B\to\pi}(m_\rho^2)$.

As mentioned, one of the main reasons for the interest in $\rho-\omega$ mixing is to provide an opportunity to remove the phase uncertainty mod(π) in the determination of the CKM angle α in the case of the $b\to u$ transition. Knowing the sign of the CP violating asymmetry at the ω resonance gives us the angle α without any ambiguity. This provides an efficient test for the Standard Model. In Fig. 12.3, we present the evolution of $\sin\delta$ as a function of the form factor $F_1^{B\to\pi}(m_\rho^2)$, for $B^-\to\pi^+\pi^-\pi^-$ and for $\bar{B}^0\to\pi^+\pi^-\pi^0$.

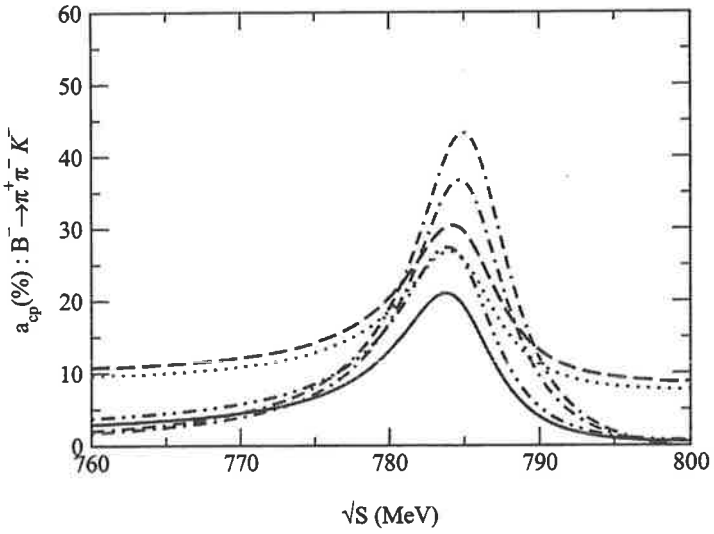

Figure 12.4: CP violating asymmetry, a_{CP}, for $B^-\to\pi^+\pi^-K^-$ for limiting values of the CKM matrix elements and for different values of the form factor $F_1^{B\to K}(m_\rho^2)$. Solid line (dotted line) for max CKM matrix elements and $F_1^{B\to K}(m_\rho^2)=0.3$ (0.5). Dot-dot-dashed line (dashed line) for min CKM matrix elements and $F_1^{B\to K}(m_\rho^2)=0.3$ (0.5). For comparison, we plot the asymmetry a_{CP} determined in naive factorization. (Dot-dashed and dot dash-dashed lines for minimum and maximum asymmetry values.)

12.3 CP violation in $B^{\pm,0}\to\pi^+\pi^-K^{\pm,0}$

After the analysis of the CP asymmetry in $B^{\pm,0}\to\rho^0(\omega)\pi^{\pm,0}\to\pi^+\pi^-\pi^{\pm,0}$, we finally conclude our work by focusing on the asymmetry in $B^{\pm,0}\to\pi^+\pi^-K^{\pm,0}$. Plotted in Figs. 12.4 and 12.5 is the direct CP violating asymmetry, a_{CP}, for $B^-\to\rho^0(\omega)K^-\to\pi^+\pi^-K^-$ and for $\bar{B}^0\to\rho^0(\omega)\bar{K}^0\to\pi^+\pi^-\bar{K}^0$

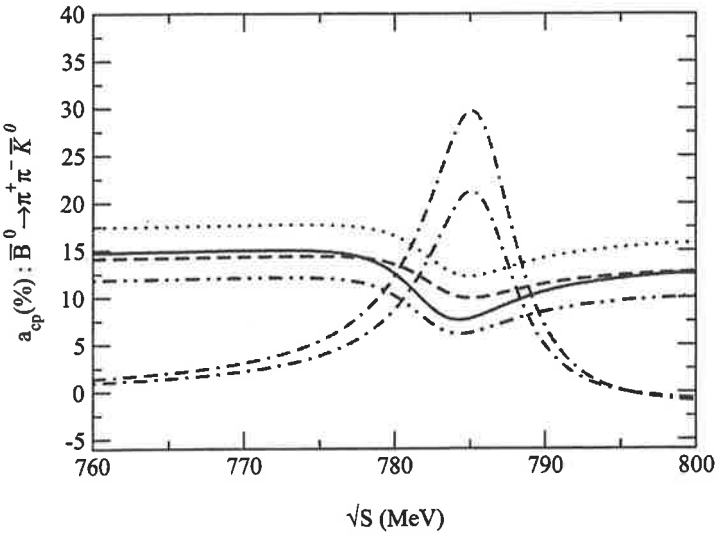

Figure 12.5: CP violating asymmetry, a_{CP}, for $\bar{B}^0 \to \pi^+\pi^-\bar{K}^0$ for limiting values of the CKM matrix elements and for different values of the form factor $F_1^{B\to K}(m_\rho^2)$. Solid line (dotted line) for max CKM matrix elements and $F_1^{B\to K}(m_\rho^2) = 0.3$ (0.5). Dot-dot-dashed line (dashed line) for min CKM matrix elements and $F_1^{B\to K}(m_\rho^2) = 0.3$ (0.5). For comparison, we plotted the asymmetry a_{CP} determined in naive factorization. (Dot-dashed and dot dash-dashed lines for minimum and maximum asymmetry values.)

respectively, for limiting values of CKM matrix parameters ρ and η and for different values of the form factor $F_1^{B\to K}(m_\rho^2)$.

In Fig. 12.4, we show the CP asymmetry for $B^- \to \rho^0(\omega)K^- \to \pi^+\pi^-K^-$. Similar conclusions can be drawn to that of previous case, regarding the sensitivity of the asymmetry parameter, a_{CP}, on the form factor $F_1^{B\to K}(m_\rho^2)$ and the CKM matrix element parameters ρ and η. There is no agreement for the value of asymmetry between naive factorization and QCD factorization at the ω resonance except that the CP violating asymmetry reaches its maximum in the vicinity of ω in both cases. However, when the asymmetry goes to zero far from the ω resonance in naive factorization, it is around 10% in QCDF.

The CP asymmetry for $\bar{B}^0 \to \rho^0(\omega)\bar{K}^0 \to \pi^+\pi^-\bar{K}^0$ is plotted in Fig. 12.5. The $\rho - \omega$ mixing effects still enhance the asymmetry near the ω resonance. However, we notice that outside this "window" the asymmetry remains large in QCDF, whereas it goes to zero in naive factorization. As usual, the asymmetry depends strongly on the form factor $F_1^{B\to K}(m_\rho^2)$ and the CKM matrix parameters ρ and η. Similarly to the case of $B^\pm \to \pi^+\pi^-\pi^\pm$, a measurement

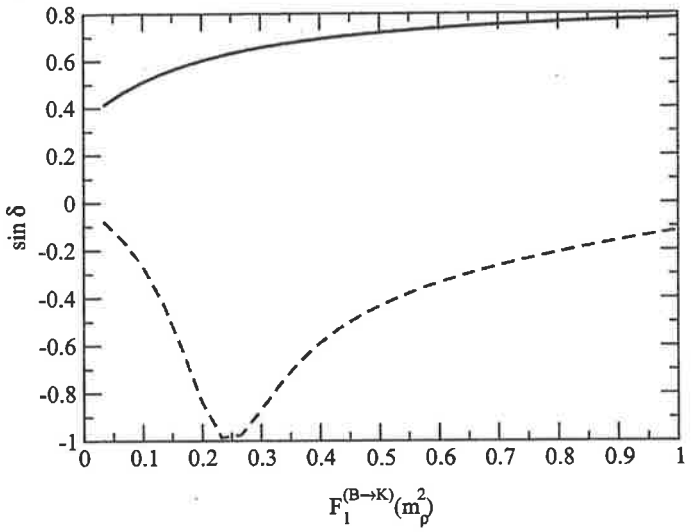

Figure 12.6: $\sin\delta$ as a function of the form factor $F_1^{B\to K}(m_\rho^2)$, for $B^- \to \pi^+\pi^-K^-$ (full line) and $\bar{B}^0 \to \pi^+\pi^-\bar{K}^0$ (dashed line) for the case $\tilde{\Pi}_{\rho\omega} = (-3500; -300)$, where $\rho - \omega$ mixing is included.

of the asymmetry would yield a constraint on the form factor $F_1^{B\to K}(m_\rho^2)$ and thus on the wave function describing the Kaon.

As we did for B decaying into $\pi\pi\pi$ we can remove the ambiguity for the determination of the angle γ that arises from the conventional determination of $\sin 2\gamma$ in indirect CP violation. In Fig. 12.6 $\sin\delta$ as a function of the form factor $F_1^{B\to K}(m_\rho^2)$, for $B^- \to \pi^+\pi^-K^-$ and $\bar{B}^0 \to \pi^+\pi^-\bar{K}^0$ is shown. We notice that the sign of $\sin\delta$ does not change over the range of $F_1^{B\to K}(m_\rho^2)$. This is very useful since we are then able to check the picture of direct CP violation within the Standard Model by measuring the asymmetry in case of B decaying into $\pi\pi K$.

As already mentioned, we obtain a large asymmetry in some decays in QCDF because of the large strong phase arising in the Wilson coefficients. The function $G(s,x)$, given in Eq. (10.18), depends on the ratio $s = m_q^2/m_b^2$ and on the fraction of momentum x. However, it has no dependence on the invariant mass, q^2, of the virtual gluon in the penguin diagram -unlike the case of naive factorization (see Eq. (3.8) in Chapter 3). As a result, when $s = 0$, i.e. for u and d quarks, $G_M(0)$ given in Eq. (10.19) (after integration of $G(s,x)$ over x) acquires a large imaginary part. The QCD penguin contribution written in Eq. (10.14), $P_{M,i}^p$, depends on $G_M(0)$. Therefore the effect of the large imaginary part appears in the QCD penguin contributions, in particular in the term involving C_1 in Eq. (10.14).

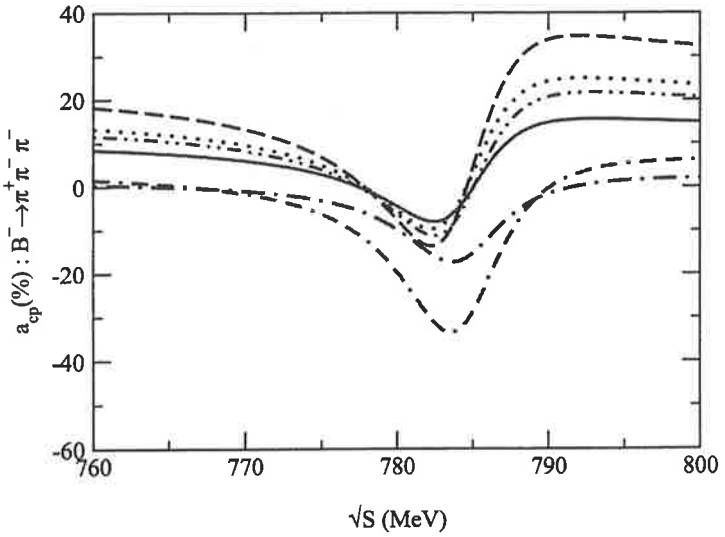

Figure 12.7: CP violating asymmetry, a_{CP}, for $B^- \to \pi^+\pi^-\pi^-$. Comparison (dot-dash-dashed lines for various values of $F_1^{B\to\pi}(m_\rho^2) = 0.3\ (0.5)$) is made in the case where $\mathcal{I}m(G_M(0)) = 0$ but only for the term involving C_1 in Eq. (10.14). See Fig. 12.1 for the other definitions.

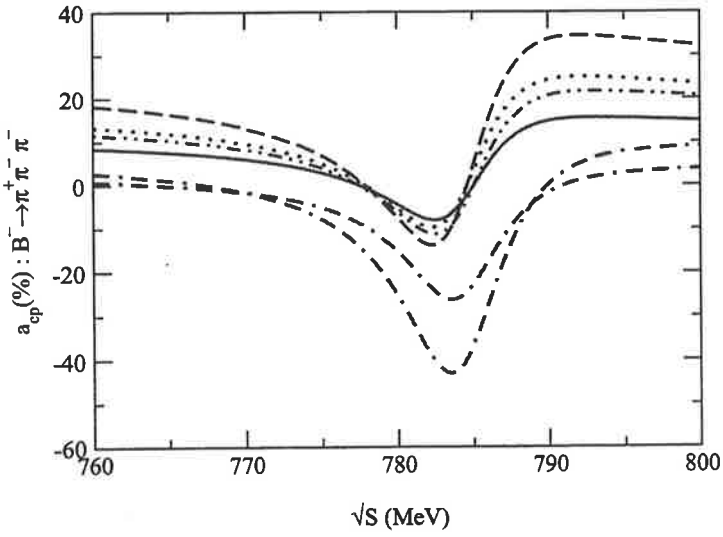

Figure 12.8: CP violating asymmetry, a_{CP}, for $B^- \to \pi^+\pi^-\pi^-$. Comparison (dot-dash-dashed lines for various values of $F_1^{B\to\pi}(m_\rho^2) = 0.3\ (0.5)$) is made in the case where a_4 from QCDF is replaced by that given in naive factorization. See Fig. 12.1 for the other definitions.

If the imaginary part of $G_M(0)$ is removed, we obtain results similar to those found in naive factorization. As an example, Fig. 12.7 shows the CP violating asymmetry, a_{CP}, for the decay $B^- \to \pi^+\pi^-\pi^-$ where the imaginary part of $G_M(0)$ is taken to be zero but only for the term involving C_1 in Eq. (10.14). As a result, no large CP violating asymmetry is obtained far from the ω resonance. For the same decay, Fig. 12.8 shows the case where we replace the value of a_4 determined in QCD factorization by that given in naive factorization [37, 36, 35]. In other words, the dependence on q^2 is included in the function $G(m_c, \mu, q^2)$ [39]. Once again, no large CP violating asymmetry is found far from the ω resonance. In these two illustrations, we obtain a convergence of the CP violating asymmetry, a_{CP}, close to zero outside the ω window.

From these investigations, it is clear that the omission of any q^2 dependence in $G(s, x)$ (Eq. (10.18)) is the reason for the difference between the QCDF and the naive factorization approach. In fact, the effect of this difference is negligible for the branching ratios considered in Chapter 11, and is only significant for CP violating asymmetry, a_{CP}, because that is proportional to $\sin\delta$. Apart from this, the corrections associated with hard scattering introduced in QCDF are satisfactorily convergent, producing relatively small corrections to naive factorization. For the future, it is crucial to work towards a consensus on the most appropriate approach to the calculation of the quark loop contribution shown in Fig. 10.4 (g).

We determined within the QCD factorization framework the CP violating asymmetry parameter a_{CP} in B decays into three particles. The computation of both asymmetry and branching ratios reveal once again that, unfortunately, uncertainties play a major role in hadronic physics. However, thanks to the experimental branching ratios provided by many facilities in the world, it could be possible to strongly constrain our predictions. The following section presents how and which conclusions can be drawn regarding our parameters.

12.4 Constraints

All these studies about direct CP violation and branching ratios in B decays have been performed by involving some free parameters such as form factors $F_1^{B\to\pi}(m_\rho^2), F_1^{B\to K}(m_\rho^2)$. By comparing experimental data with theoretical predictions for branching ratios we determined some constraints concerning these free parameters. We were mainly focused on the effective number of colours, N_c^{eff}, the form factors $F_1^{B\to\pi}(m_\rho^2)$ and $F_1^{B\to K}(m_\rho^2)$ as well as the CKM matrix element parameters ρ and η. In the following section, we draw

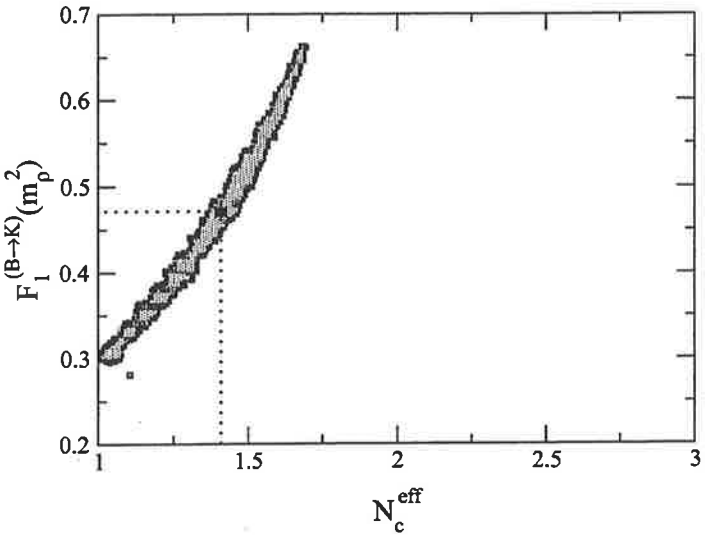

Figure 12.9: Fit of branching ratios for the decays $B \to \rho K$, $B \to \omega K$, including the uncertainties from the CKM matrix parameters ρ and η and the experimental data provided by BELLE and CLEO.

some conclusions about these constraints.

12.4.1 Constraints on form factors

Form factors play a major role in the factorization method (naive or QCDF) since they represent the transition between two hadronic states where the energy transition scale can vary from heavy quark to light quark masses (if we consider $b \to u$ or $b \to s$). Their computation is non trivial and may carry large uncertainties, according to which model you are using. We refer the reader to Chapters 5 and 8 for a list of available form factors determined within different frameworks such as QCD sum rules, heavy quark limit, lattice QCD or light cone QCD... The reason why we kept the form factors $F_1^{B\to\pi}(m_\rho^2)$ and $F_1^{B\to K}(m_\rho^2)$ free came from the necessity to constrain indirectly but efficiently the wave functions describing the pion and kaon mesons. These two light particles are subject to intensive research because of their complex physical properties.

It has to be noticed that to constrain a form factor requires constraints on the effective number of colours, N_c^{eff}. Therefore it is not possible to draw conclusions about one without the other. In Figs. 12.9 and 12.10 we show the results for the form factors $F_1^{B\to K}(m_\rho^2)$ and $F_1^{B\to\pi}(m_\rho^2)$, respectively. We have fitted all the branching ratios for B decaying into $\rho\pi$, into ρK, into ωK or into $\omega\pi$ with the experimental data provided by the CLEO and BELLE

facilities. We have excluded the data from BABAR since they are currently not numerous and accurate enough. We have included uncertainties for the CKM matrix parameters ρ and η and we have applied the QCD factorization method where all of the final state interaction corrections arising at order α_s are incorporated. Finally we emphasize that the following results are model independent.

In Fig. 12.9 we show the constraints for the form factor $F_1^{B\to K}(m_\rho^2)$ as well as the effective number of colours N_c^{eff}. Based on their experimental data, we observe that the common region for BELLE and CLEO is very small. The form factor $F_1^{B\to K}(m_\rho^2)$ is allowed to vary between 0.3 and 0.65. At the same time, the effective number of colours can vary between 1 and 1.75. Their mean average values are $F_1^{B\to K}(m_\rho^2) = 0.47$ and $N_c^{eff} = 1.40$. As we have already mentioned in the previous chapter, these results seem consistent with the BSW model rather than the GH model. However, it is not possible to draw any strong conclusions regarding $F_1^{B\to K}(m_\rho^2)$ since the experimental data for the branching ratios in B decays such as $B \to \rho K$ or $B \to \omega K$ are unfortunately not accurate.

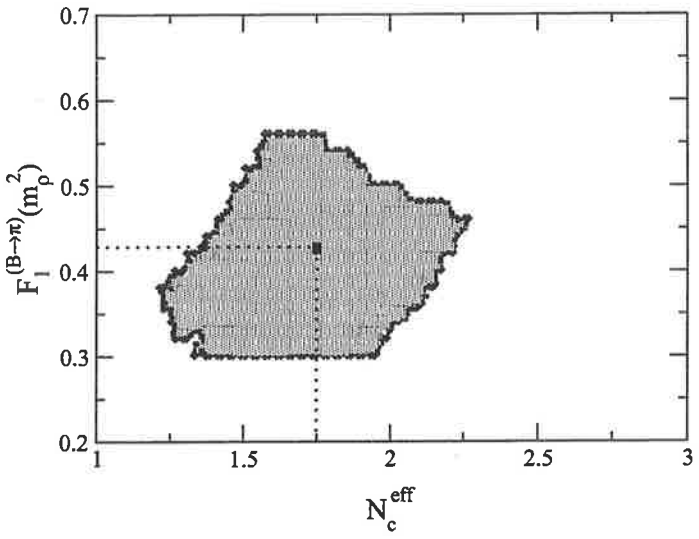

Figure 12.10: Fit of branching ratios for the decays $B \to \rho\pi$, $B \to \omega\pi$, including the uncertainties from the CKM matrix parameters ρ and η and the experimental data provided by BELLE and CLEO.

In Fig. 12.10, the constraints for the form factor, $F_1^{B\to\pi}(m_\rho^2)$, and the effective number of colours, N_c^{eff}, are plotted by using the same fit method as that for $B \to \rho K$. In contrast to the previous case, we found a large common region between BELLE and CLEO for the B decay into $\rho\pi$. From

our analysis, $F_1^{B\to\pi}(m_\rho^2)$ varies between 0.3 and 0.57 and N_c^{eff} can take values from 1.25 to 2.25. Their mean average values are $F_1^{B\to\pi}(m_\rho^2) = 0.43$ and $N_c^{eff} = 1.75$. These results which have a higher confidence level than those for decays $B \to \rho K$ give a strong constraint on the form factor $F_1^{B\to\pi}(m_\rho^2)$ and hence on the pion wave function. Once again, if we consider the average values, it appears that the BSW model is in better agreement with our results than the GH model.

The results obtained for the form factors $F_1^{B\to\pi}(m_\rho^2)$ and $F_1^{B\to K}(m_\rho^2)$ reduce one of the main uncertainties in the factorization process that may enhances results in asymmetry. Those obtained for the effective number of colours, N_c^{eff}, confirm previous analysis where naive factorization was applied for the same decays. Together, they increase the precision on theoretical predictions and allow us to focus on the most significant parameters that govern the direct CP violating asymmetry within the Standard Model. Next, we discuss the CKM matrix parameters ρ and η.

12.4.2 Constraints on the CKM matrix parameters ρ and η

It is well known that the CKM matrix parameters ρ and η are the main "key" to CP violation within the Standard Model. Recall that the weak phase is mainly governed by the parameter η that provides the imaginary part which is absolutely necessary to obtain an asymmetry between matter and antimatter. Based on our analysis, we are not able from branching ratios for $B \to \rho\pi$ and $B \to \rho K$ to efficiently constrain the CKM matrix parameters ρ and η. In fact, the common region allowed by CLEO and BELLE for branching ratios in both cases $B \to \rho\pi$ and $B \to \rho K$ does not constrain the parameters ρ and η. As input parameters for ρ and η, we used the values $0.190 < \rho < 0.268$ and $0.284 < \eta < 0.366$. The common region obtained in our analysis fully satisfies these limits.

However, we can try to get some constraints by only taking into account the mean values for the form factors $F_1^{B\to\pi}(m_\rho^2)$, $F_1^{B\to K}(m_\rho^2)$ as well as the effective number of colours N_c^{eff}. The results are listed in Table 12.1. According to our work, we find the following limits: $0.214 < \rho < 0.251$ and $0.300 < \eta < 0.351$. This reduces by around 47% and 62%, respectively, the allowed ranges for the parameters ρ and η. These results seem promising but they only include the branching ratios from the BELLE and CLEO facilities for the channels $B \to \rho\pi$, $B \to \rho K$ and are available for the mean values for our constraints. It is clear that the ranges obtained in our work for the CKM parameters ρ and η satisfy all of the experimental data, since we have

BELLE and CLEO	
	ρ
$B \to \rho\pi$	$\rho_{min} = 0.205$, $\rho_{max} = 0.251$
$B \to \rho K$	$\rho_{min} = 0.214$, $\rho_{max} = 0.268$
common region	$\rho_{min} = 0.214$, $\rho_{max} = 0.251$
	η
$B \to \rho\pi$	$\eta_{min} = 0.300$, $\eta_{max} = 0.351$
$B \to \rho K$	$\eta_{min} = 0.284$, $\eta_{max} = 0.366$
common region	$\eta_{min} = 0.300$, $\eta_{max} = 0.351$

Table 12.1: Limits for the CKM matrix element parameters ρ and η.

used as inputs, the initial values ($0.190 < \rho < 0.268$ and $0.284 < \eta < 0.366$) for the CKM parameters derived by fitting branching ratios and asymmetry data for numerous decay channels.

It has to be noticed that our results regarding the constraints for the form factors, $F_1^{B\to\pi}$ and $F_1^{B\to K}$, as well as those for the CKM matrix parameters, ρ and η, are calculated in using the mean value of the input parameters. For example, the variation of the quark mass values on the results are negligible. If now we consider a variation of the parameter ρ_H and the corresponding phase ϕ_H, (used in the calculation of the hard-scattering contributions, $H(BV,P)$ and $H(BP,V)$, see Chapter 10) the effect on the results is small enough to be ignored. We can draw the same conclusion for the parameter ρ_A (used in the calculation of the annihilation contributions, $A(P,V)$ and $A(V,P)$, see Chapter 10) as for the parameter ρ_H. Finally, the phase, ϕ_A, corresponding to the parameter, ρ_A, is the only main parameter which can affect our results. A variation up to 30% of this parameter may change significantly our results. We have to mention as well that our fits have been performed by using several experimental branching ratios which can be subject to some variations in the future. Therefore, our results are strongly dependent on these experimental data.

Through our analysis of branching ratios in B decays, we have constrained the form factors, $F_1^{B\to\pi}(m_\rho^2)$, $F_1^{B\to K}(m_\rho^2)$, the effective number of colours, N_c^{eff}, and the CKM matrix parameters ρ and η. By determining the sign of $\sin\alpha$ for the transition $b \to u$, the sign of $\sin\gamma$ for the transition $b \to s$

and by an independent method $\sin\beta$, we can see if there really is a unitarity triangle like is the prediction of the Standard Model. Now we have to wait for more experimental data regarding branching ratios and asymmetries in B decays in order to provide more accurate results. We expect that our work will be helpful in the quest to gain further knowledge of direct CP violation in B decays.

Chapter 13

Conclusion

" Les théories servent à irriter les philistins, à séduire les esthètes et à faire rire les autres. "

Amélie Nothomb

Direct CP violation in B decays

We have investigated direct CP violation in B decays, such as $B \to \pi\pi\pi$ and $B \to \pi\pi K$. Because of the energy scale involved in these transitions, the calculation of the hadronic matrix elements that arise in the B decay amplitude is non trivial and requires several physical assumptions. The effective Hamiltonian is the starting point of any phenomenological treatment of the weak decays of hadrons. It can be mainly written as a product of CKM matrix elements describing the change of flavour, with Wilson coefficients describing the short distance physics and operators describing the long distance physics. The main difficulty is then to express the hadronic matrix elements which represent the transition between the meson B and the final state.

As a first approach, we used the so-called "naive factorization" method where the hadronic matrix is governed by the product of a decay constant times a transition form factor between the meson B and one of the two final mesons. Through the Wilson coefficients, this method includes a few of the final state interactions but not all of them at the order α_s. The colour octet contribution is reproduced by an effective number of colours. By applying this framework we have calculated the branching ratios for $B \to \rho\pi$ and $B \to \rho K$ and we have extracted some constraints for the effective number of

colours treated as a free parameter. Comparing our theoretical results with experimental branching ratios provided by BELLE, BABAR and CLEO, we have been able to determine a limited range for this free parameter. With this value we then computed the direct CP violating asymmetry parameter a_{CP} for decays[1] such as $B \to \pi\pi\pi$ and $B \to \pi\pi K$.

We included $\rho-\omega$ mixing in order to analyse its effect on this asymmetry. The mixing through isospin violation of an ω to ρ, which then decays into two pions allows us to obtain a difference of the strong phase reaching its maximum at the ω resonance. $\rho - \omega$ mixing provides an opportunity to remove the phase uncertainty mod(π) in the determination of two CKM angles, α in the case of $B \to \rho\pi$ and γ in the case of $B \to \rho K$. This phase uncertainty usually arises from the conventional determination of $\sin 2\alpha$ or $\sin 2\gamma$ in indirect CP violation.

In order to decrease uncertainties involved in our calculations, we evaluated the transition form factors used in our work. To obtain these form factors, we first investigated the wave functions related to the particles playing a role in the decay. By working in an explicit covariant light front formalism, we determined the wave functions related for the particles π, ρ, ω, K, B where the decay constant, electromagnetic form factor, charge radius and normalization were applied to constrain our parameters. Based on these functions, we calculated the transition form factors between pseudoscalars and between pseudoscalar and vector mesons.

To end our analysis we replaced naive factorization by QCD factorization where all of the final state interactions at the order α_s are included. Assuming some properties (i.e. heavy quark expansion) lie at the energy scale of B decays, this allows us to determine a good approximation to the non factorizable terms which arise during the usual hadronic matrix calculation. Note that if we neglect corrections at the order α_s we recover naive factorization. We then investigated the branching ratios for $B \to \rho\pi, B \to \rho K, B \to \omega\pi$ and $B \to \omega K$ by applying this method. Comparisons were made with experimental results from BABAR, BELLE and CLEO. As in the first part, we then computed the direct CP asymmetry violating parameter a_{CP} in the decays $B \to \pi\pi\pi$ and $B \to \pi\pi K$.

Having reduced all of the uncertainties entering the calculation, we have constrained the form factors $F_1^{B\to\pi}$ and $F_1^{B\to K}$. At the same time, we evaluated the effective number of colours N_c^{eff}. Using the fit obtained for the branching ratios $\rho\pi$ and ρK, and assuming that the values for the parameters A and λ are accurate enough, we extracted some limits regarding the CKM

[1]Direct CP violating asymmetry, a_{CP}, in $B \to \pi\pi K$ decays has been investigated where the χ_{c0} resonance [232] is included. A large asymmetry is predicted.

matrix parameters ρ and η. Finally, knowing the sign of the asymmetry in B decays into $\pi\pi\pi$ or into $\pi\pi K$, we provide an efficient test to constrain the value of the angles α and γ in the unitarity triangle. This gives the opportunity to check the picture of direct CP violation within the Standard Model.

Main results

- **Factorization**
  As we said previously we used two approaches in order to factorize the hadronic matrix involved in the amplitude, the so-called "naive factorization" and "QCD factorization" methods. We have calculated the branching ratios for $B \to \rho\pi$, $B \to \rho K$, $B \to \omega\pi$ and $B \to \omega K$, and compared the results with experimental data coming from the CLEO, BABAR and BELLE Collaborations.

  By applying the naive factorization method we have shown that the range for N_c^{eff} in which theoretical branching ratio results are consistent with experimental data is $1.09(1.11) < N_c^{eff} < 1.68(1.80)$ for $B \to \rho\pi$ and is $0.66(0.61) < N_c^{eff} < 2.84(2.82)$ for $B \to \rho K$. Finally, if we take into account the allowed range of N_c^{eff} determined from decays such as $B \to \rho\pi$ and $B \to \rho K$ we find a mean average value for N_c^{eff} around 1.75 ± 1.1.

  By applying the QCD factorization method, we have shown that the range allowed for the form factor, $F_1^{B\to\pi}$, in the case of $B \to \rho\pi$, is $0.30 < F_1^{B\to\pi} < 0.57$ and is $0.30 < F_1^{B\to K} < 0.65$ in the case of $B \to \rho K$ for the form factor, $F_1^{B\to K}$. It has been possible to fit the form factor describing the transition $B \to \pi$ at $k^2 = m_\rho^2$ that is $F_1^{B\to\pi} = 0.35$. Similarly we obtained for the transition $B \to K$, $F_1^{B\to K} = 0.47$ at $k^2 = m_\rho^2$. We recall that we found the following values for the form factors when the CLFD approach was applied: $F_{1,(CLFD)}^{B\to\pi}(m_\rho^2) = 0.35$ and $F_{1,(CLFD)}^{B\to K}(m_\rho^2) = 0.40$.

  Moreover, predictions for the branching ratios $B^\pm \to \rho^\pm\pi^0$ and $B^0 \to \rho^0\pi^0$ have been made as well. These are $\mathscr{B}(B^\pm \to \rho^\pm\pi^0) \approx 17.5 \times 10^{-6}$ and $\mathscr{B}(B^0 \to \rho^0\pi^0) < 1 \times 10^{-6}$. Regarding the branching ratio $\bar{B}^0 \to \rho^0\bar{K}^0$, one has $\mathscr{B}(\bar{B}^0 \to \rho^0\bar{K}^0) < 3 \times 10^{-6}$.

  We would like to emphasize that QCD factorization gives more accurate results than naive factorization as expected. However in a qualitative way naive factorization is still able to give the correct order of magnitude for the branching ratios analysed in our case.

- **$\rho - \omega$ mixing**
  In order to obtain a large signal for direct CP violation, we already stressed that $\rho - \omega$ mixing has the dual advantages that the strong phase difference is large and varies extremely rapidly near the ω resonance. When the invariant mass of the $\pi^+\pi^-$ pair is in the vicinity of the ω resonance, it is found that the CP violating asymmetry, a_{CP}, has a maximum a_{max} whereas it goes to zero outside the ω resonance in the naive factorization method and may remain large in the QCD factorization method. The direct CP violating asymmetry, a_{CP}, has been analysed in the B decays $B^{\pm,0} \to \rho^0(\omega)\pi^{\pm,0} \to \pi^+\pi^-\pi^{\pm,0}$ as well as $B^{\pm,0} \to \rho^0(\omega)K^{\pm,0} \to \pi^+\pi^-K^{\pm,0}$ where the $\rho-\omega$ mixing mechanism must be included.

  We found that the CP violation parameter, a_{CP}, is very sensitive to the parameters ρ and η in the CKM matrix, and also to the magnitude of the form factors. We found that the CP violating asymmetry, a_{max}, can vary from -37% to -84% for $\bar{B}^0 \to \pi^-\pi^+\pi^0$ and -17% to -53% for $B^- \to \pi^-\pi^+\pi^-$. In the case of $\bar{B}^0 \to \pi^+\pi^-\bar{K}^0$ we found a_{max} varying from $+37\%(+55\%)$ to $-20\%(-24\%)$ and from $+49\%(+46\%)$ to $-22\%(-25\%)$ for $B^- \to \pi^+\pi^-K^-$.

  By measuring the CP violating asymmetry, a_{CP}, where the effects of $\rho - \omega$ mixing are taken into account, we can remove the phase uncertainty mod(π) in the determination of the CKM angle α in $B^{\pm,0} \to \pi^+\pi^-\pi^{\pm,0}$. In a similar way, it has been also possible to remove the phase uncertainty mod(π) in the determination of the CKM angle γ by analysing direct CP violation in $B \to \pi^+\pi^-K$. Therefore the interferences generated by the $\rho - \omega$ mixing allow us to eliminate the phase ambiguity on the unitarity angles α and γ.

  Finally, even though it is not possible to constrain efficiently the parameters ρ and η with an analysis based only on the channels $B \to \rho\pi$ and $B \to \rho K$, we have determined a range of values for ρ that is $0.214 < \rho < 0.251$ and that is $0.300 < \eta < 0.351$ for η. We recall that the results listed previously about the form factors, $F_1^{B\to\pi}$ and $F_1^{B\to K}$, as well as those for the CKM matrix parameters, ρ and η, are stable against reasonable variation of the input parameters used in our analysis.

  It is clear that the inclusion of $\rho-\omega$ mixing into the calculation of direct CP violating asymmetry, a_{CP}, provides the opportunity to go further into the knowledge of CP violation since we can indirectly check the unitarity triangle (UT) by measuring experimentally the direct asym-

metry. We expect that the CLEO, BABAR and BELLE Collaborations will be able to provide soon useful data regarding our analysis.

In the future...

- This work could be extended to more B decays. It would be very interesting to constrain our parameters by investigating other channels than $\rho\pi$ and ρK for branching ratios and asymmetries. By including more channels such as $B \to K^*\pi, B \to K^*\eta, B \to K\phi$, we will use more experimental data and hence be able to obtain better constraints on our parameters.

- We largely focused our analysis on the case of B decaying into pseudoscalar plus vector mesons where the $\rho-\omega$ mixing effects were included. We have also analysed (but not included in this thesis) the results for B decays into two vectors, such as ρ and K^*. This analysis is very promising and we refer the reader to the publications [233, 234] for more details[2]. This work was performed in collaboration with the LHCb experimental group of Clermont-Ferrand.

- In the QCD factorization (QCDF) framework, hard scattering and annihilation contributions need further investigation. Clarifying these points would be very helpful in avoiding any over or under estimation of our theoretical predictions. For example, it is important to solve the problem related to the end point integral divergence which is parameterized without any strong physical motivation. Moreover, the annihilation contributions are not derived within the QCDF method. To obtain a consistent framework, it would be better to find a way to include them in QCDF.

- It has been shown in the previous chapter that the reason for the large CP violating asymmetry outside the ω window in QCDF is the large strong phase included in the QCD penguin contribution through the term $G_M(0)$. It is clear that the omission of any q^2 dependence in $G(s,x)$ (Eq. (10.18)) is the reason for the difference between the QCDF and the naive factorization approach. For the future, it is crucial to work towards a consensus on the most appropriate approach to the calculation of the quark loop contribution shown in Fig. 10.4 (g). Clari-

[2]Recently, BELLE [235, 236] and BABAR [237] published new branching ratio results for B decays into two vectors which are in total agreement with our work.

fication of this point would be helpful to obtain more accurate results for the CP violating asymmetry, a_{CP}, in B decays.

- The work performed in CLFD (Covariant Light Front Dynamics) is very promising since it shows that this formalism can be applied to most kinds of phenomenological studies. Even though this framework still needs to be improved, it provides excellent results for the wave functions and transition form factors investigated in this thesis. It would very be interesting to extend this analysis to more particles, including baryons. As such, we are not restricted just to particle physics, but can investigate phenomenological applications in nuclear physics as well.

Beyond the Standard Model...

To explain the predominance of matter over antimatter in our universe requires CP violation. It is well established that CP symmetry is not an exact symmetry in nature, because for example it is observed that the baryon number of the universe does not vanish. B decays seem to be one of the most ideal tools with which to investigate CP violation, since all of the three families of quarks can be involved through the Cabibbo-Kobayashi-Maskawa matrix.

Within the Standard Model, the CKM parameters A, λ, ρ and η constitute all of the fundamental quantities which can be described by the so-called Unitarity Triangle [22]. The better we know this triangle and its shape, the better we will be able to infer the intervention of any new physics which future theoretical predictions and experimental data may reveal. Even though a correct understanding of CP violation is expected within the Standard Model, we do not have to exclude any other possibilities [238] to explain CP violation in B decays. Some other sources beyond the Standard Model might be found such as those based on left and right symmetric model [239] and Higgs model [240]. We can also mention supersymmetry [241, 242, 243, 244], bariogenesis [245] and the neutrino sector [246] as an opportunity to explore CP violation.

In any case, the understanding of CP violation remains a great challenge and, without any doubt, needs a strong interaction between experiment and theory if we want to develop a deeper understanding of our universe.

Appendix A

The kernel, one-gluon exchange in CLFD

" On ne fait jamais attention à ce qui a été fait; on ne voit que ce qui reste à faire. "

Marie Curie

In this appendix, we present the complete expressions for the functions χ_i and Ω_i used to determine the radiative corrections in the calculation of wave functions including a one-gluon exchange. We refer the reader to Chapter 8 for all of the definitions.

A.1 Functions $\Omega_{1,2}$

For $\Omega_{1,2}(x,x',\mathbf{R}_\perp,\mathbf{R}'_\perp)$ one has the following expressions:

$$\begin{aligned}
&\Omega_1(x,x',\mathbf{R}_\perp,\mathbf{R}'_\perp) = \\
&\frac{1}{\mathbf{R}_\perp^2}\Bigg\{2m_r\Bigg[m_1^3(-1+x)(-1+x')x' + m_1^2 m_2 x(-1+x')x' - m_1(-1+x') \\
&\times\Big(2\mathbf{R}_\perp^2(-1+x') + m_2^2(-1+x)x'\Big) + m_2x'\Big(-2\mathbf{R}_\perp^2x' + m_2^2(x-xx')\Big) \\
&\qquad + 2\Big(m_1(-1+x)(-1+x') + m_2xx'\Big)\mathbf{R}'_\perp\cdot\mathbf{R}_\perp\Bigg]\Bigg\}\,, \qquad \text{(A.1)}
\end{aligned}$$

$$\Omega_2(x,x',\mathbf{R}_\perp,\mathbf{R}'_\perp)=\frac{-1}{\mathbf{R}^2_\perp(-1+x)x}\Big\{-2m_1m_2\mathbf{R}^2_\perp(-1+x)x+$$
$$m_1^4(-1+x)^2(-1+x')x'+m_2^4x^2(-1+x')x'+2\mathbf{R}^2_\perp\Big(\mathbf{R}'^2_\perp(-1+x)x+$$
$$\mathbf{R}^2_\perp(-1+x')x'\Big)+m_2^2\mathbf{R}^2_\perp\Big[-(-1+x)x+x'+2(-3+x)xx'$$
$$+(-1+4x)x'^2\Big]+m_1^2\Big[-m_2^2(1+2(-1+x)x)(-1+x')x'+$$
$$\mathbf{R}^2_\perp\Big(x^2(1-2x')+3(-1+x')x'+x(-1+6x'-4x'^2)\Big)\Big]+2\Big[m_1m_2(-1+x)x+$$
$$m_1^2(-1+x)^2(-1+x')-m_2^2x^2x'+\mathbf{R}^2_\perp\Big(-1+x+x'-2xx'\Big)\Big]\mathbf{R}'_\perp\cdot\mathbf{R}_\perp\Big\}\,. \tag{A.2}$$

A.2 Functions $\chi_{1,2}$

For $\chi_{1,2}(x,x',\mathbf{R}_\perp,\mathbf{R}'_\perp)$ one has the following expressions:

$$\chi_1(x,x',\mathbf{R}_\perp,\mathbf{R}'_\perp)=\frac{1}{\mathbf{R}^2_\perp(-1+x')x'}\Big\{2\mathbf{R}'^2_\perp\mathbf{R}^2_\perp+m_1^4(-1+x)(-1+x')^2x'$$
$$+m_2^2x'^2\Big(m_2^2x(-1+x')+2\mathbf{R}^2_\perp x'\Big)+m_1^3m_2x'\Big(x-(1+x)x'+x'^2\Big)$$
$$-m_1m_2(-1+x')x'\Big(2\mathbf{R}^2_\perp+m_2^2(-x+x')\Big)-m_1^2(-1+x')$$
$$\times\Big[2\mathbf{R}^2_\perp(-1+x')^2+m_2^2x'\Big(1-x'+x(-1+2x')\Big)\Big]$$
$$+2(m_1-m_2)(m_1(-1+x)+m_2x)(-1+x')x'\mathbf{R}'_\perp\cdot\mathbf{R}_\perp\Big\}\,, \tag{A.3}$$

$$\chi_2(x,x',\mathbf{R}_\perp,\mathbf{R}'_\perp)=\frac{-1}{2m_r\mathbf{R}^2_\perp(-1+x)x(-1+x')x'}\Big\{m_1^5(-1+x)^2$$
$$(-1+x')^2x'-m_1^4m_2(-1+x)^2(-1+x')x'^2+m_1^2m_2(-1+x')$$
$$\Big[m_2^2\Big(1+2(-1+x)x\Big)x'^2+\mathbf{R}^2_\perp\Big(-2(-1+x)x+2(-1+x)xx'+$$
$$(-3+4x)x'^2\Big)\Big]+m_1x'\Big[2\mathbf{R}^2_\perp\Big(\mathbf{R}'^2_\perp(-1+x)x+\mathbf{R}^2_\perp(-1+x')^2\Big)$$

$$+ m_2^4 x^2(-1+x')^2 + m_2^2 \mathbf{R}_\perp^2 \Big(-1+4x+2(1+(-5+x)x)x' + (-1+4x)x'^2\Big)\Big] - m_1^3(-1+x')x'\Big[m_2^2(1+2(-1+x)x)(-1+x') + \mathbf{R}_\perp^2\Big(3-3x'+2x(-3+x+2x')\Big)\Big] - m_2(-1+x')\Big[2\mathbf{R}_\perp'^2\mathbf{R}_\perp^2(-1+x)x + x'\Big(2\mathbf{R}_\perp^4 x' + m_2^4 x^2 x' + m_2^2\mathbf{R}_\perp^2(-x'+2x(-1+x+2x'))\Big)\Big] + 2(m_1-m_2) \times \Big[\mathbf{R}_\perp^2 + m_1^2(-1+x)^2 - x(2\mathbf{R}_\perp^2 + m_2^2 x)\Big](-1+x')x'\mathbf{R}_\perp'\cdot\mathbf{R}_\perp\Bigg\}. \quad \text{(A.4)}$$

Appendix B

Transition form factor in CLFD

" Le monde et la science ont leurs données propres, qui se touchent et ne se pénètrent pas. L'une nous montre à quel but nous devons viser, l'autre, le but étant donné, nous donne les moyens de l'atteindre. "

Henri Poincaré

In this appendix, we present the complete expressions regarding the calculation of the transition form factor in the case of pseudoscalar vector transition. All of the terms used in this section have been defined in Chapters 7, 8 and 9. We refer the reader to these chapters for their definitions. The functions $F_i^{(j)}$ are the kinematic terms involved in the transition form factor.

B.1 Functions $F_1^{(j)}, F_2^{(j)}$

The functions $F_1^{(j)}$ take the following form:

$$F_1^{(1)} = \left[\frac{(1-y)}{yq^2}\right] X^{(1)} ,$$

$$F_1^{(2)} = \left[\frac{(1-y)}{yq^2}\right] X^{(2)} ,$$

$$F_1^{(3)} = \left[\frac{(y-1)^2(M_2^2 - M_1^2) - q^2(y^2-1)}{q^2(q^2y^2 - M_2^2(y-1)^2)}\right] X^{(3)} ,$$

$$
\begin{aligned}
F_1^{(4)} &= \left[\frac{M_1^2(y-1)^2 - q^2}{q^2(M_2^2 - M_1^2 y^2)}\right] X^{(4)} \,, \\
F_1^{(5)} &= X^{(5)} \\
&\left[\frac{-(y-1)^2 M_2^4 + q^2(2(y-1)y-1)M_2^2 - q^4 y^2 + M_1^2(M_2^2(y-1)^2 + q^2 y^2)}{q^2\big(((y-2)y+2)M_2^4 - 2(M_1^2 + q^2(y-1))yM_2^2 + (M_1^2 - q^2)^2 y^2\big)}\right] \,, \\
F_1^{(6)} &= \left[\frac{(1-y)}{yq^2}\right] X^{(6)} \,, \\
F_1^{(7)} &= \left[\frac{(1-y)}{yq^2}\right] X^{(7)} \,, \\
F_1^{(8)} &= \left[\frac{(1-y)}{yq^2}\right] X^{(8)} \,, \\
F_1^{(9)} &= \left[\frac{(1-y)}{yq^2}\right] X^{(9)} \,, \\
F_1^{(10)} &= \left[\frac{(1-y)}{yq^2}\right] X^{(10)} \,,
\end{aligned}
\tag{B.1}
$$

where the terms $X^{(j)}$ read as:

$$
\begin{aligned}
X^{(1)} &= 2q^2 y\big(q^2 y^2 - M_2^2(y-1)^2\big) \,, \\
X^{(2)} &= 2q^2 y\big(M_2^2 - M_1^2 y^2\big) \,, \\
X^{(3)} &= X^{(1)} \,, \\
X^{(4)} &= X^{(2)} \,, \\
X^{(5)} &= q^2\Big(\big((y-2)y+2\big)M_2^4 - 2\big(M_1^2 + q^2(y-1)\big)yM_2^2 + (M_1^2 - q^2)^2 y^2\Big) \,, \\
X^{(6)} &= -2q^2 y^2\big(((y-1)M_1^2 + q^2)y - M_2^2(y-1)\big) \,, \\
X^{(7)} &= 4q^2(y-1)y^2 \,, \\
X^{(8)} &= 4q^2 y^2 \,, \\
X^{(9)} &= X^{(7)} \,, \\
X^{(10)} &= (y-1)X^{(7)} \,.
\end{aligned}
\tag{B.2}
$$

The functions $F_2^{(j)}$ can be expressed in terms of $F_3^{(j)}$ and $X^{(j)}$ as follows,

$$
F_2^{(j)} + F_3^{(j)} = X^{(j)} \,.
$$

B.2 Functions $F_3^{(j)}$

The functions $F_3^{(j)}$ are defined as,

$$
\begin{aligned}
F_3^{(1)} &= -(y-1)((y-1)(M_1^2-M_2^2)+q^2(y+1))F_3' \,, \\
F_3^{(2)} &= -(q^2-M_1^2(y-1)^2)F_3' \,, \\
F_3^{(3)} &= (y-1)\big((y-1)^2M_2^4+q^2(1-2(y-1)y)M_2^2 \\
&\quad +q^4y^2-M_1^2(M_2^2(y-1)^2+q^2y^2)\big) \,, \\
F_3^{(4)} &= -(1-y)\big(y^2M_1^4+(M_2^4((y-4)y+1)-q^2y^2)M_1^2+M_2^2(M_2^2-q^2)\big) \,, \\
F_3^{(5)} &= -(1/2)((M_1+M_2)^2-q^2)((M_1-M_2)^2-q^2)(y-1)F_3' \,, \\
F_3^{(6)} &= (y-1)\big(((y-1)M_1^2+q^2)y-M_2^2(y-1)\big)F_3' \,, \\
F_3^{(7)} &= -2(y-1)(M_2^2(y-1)^2-q^2y^2) \,, \\
F_3^{(8)} &= F_3^{(7)}/(y-1) \,, \\
F_3^{(9)} &= F_3^{(7)} \,, \\
F_3^{(10)} &= (y-1)F_3^{(7)} \,,
\end{aligned}
\tag{B.3}
$$

where $F_3' = ((y-2)M_2^2+(M_1^2-q^2)y)$ and the expression for $F_{1,2,3}^{(d)}$ is written as:

$$
F_{1,2,3}^{(d)} = 4q^4\Big[M_2^2(y-1)-\big((y-1)M_1^2+q^2\big)y\Big]^2 \,. \tag{B.4}
$$

B.3 Transition form factor diagrams

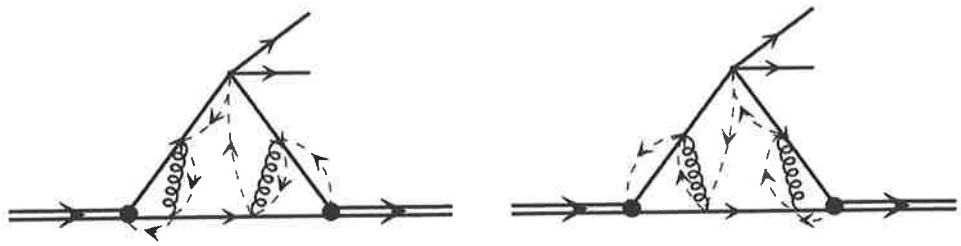

Figure B.1: Diagrams included in the case of the weak decay pseudoscalar pseudoscalar transitions (a).

The one gluon exchange process included in the calculation of wave function (see Chapter 8) allows us to take into account the following diagrams

in the investigation of the weak decay transition (see Chapter 9). Note that all of the diagrams which can include a one gluon exchange process are not calculated in our work but only those shown in Figs. B.1, B.2 and B.3. We refer the reader to Chapters 7, 8 and 9 for all of the definitions.

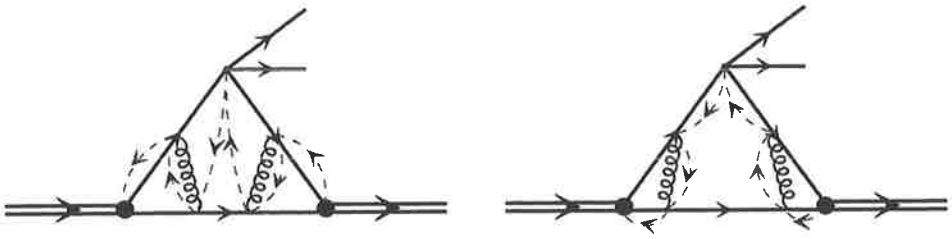

Figure B.2: Diagrams included in the case of the weak decay pseudoscalar pseudoscalar transitions (b).

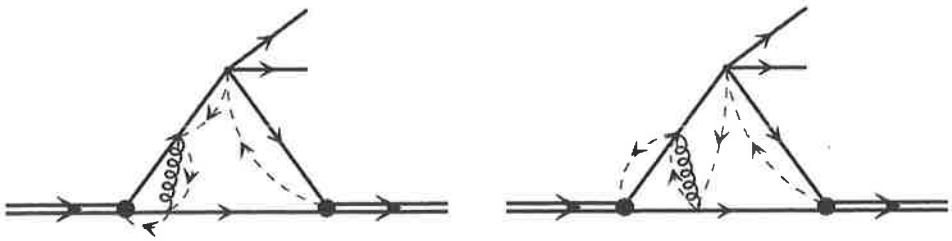

Figure B.3: Diagrams included in the calculation of the weak decay pseudoscalar vector transitions.

Appendix C

Annihilation amplitudes in $B \to \pi^+\pi^- M$

" Il y a un véritable agacement à essayer de trouver le mot précis pour les pensées que l'on a. "

Charlie Chaplin

In this appendix, we present the complete expressions for the annihilation amplitudes in $B \to \pi^+\pi^- M$ where M is π or K. We refer the reader to Chapters 10 and 11 for all of the definitions.

C.1 Transition $b \to u$

$\overline{B}^0 \to \pi^0\rho^0$

$$\begin{aligned} t^a_\rho &= b_1(\rho^0,\pi^0) + b_1(\pi^0,\rho^0)\ , \\ p^a_\rho &= b_3(\rho^0,\pi^0) + b_3(\pi^0,\rho^0) + 2b_4(\pi^0,\rho^0) + 2b_4(\rho^0,\pi^0) \\ &\quad + \frac{1}{2}\Big(- b^{ew}_3(\rho^0,\pi^0) - b^{ew}_3(\pi^0,\rho^0) + b^{ew}_4(\pi^0,\rho^0) + b^{ew}_4(\rho^0,\pi^0)\Big)\ . \end{aligned} \tag{C.1}$$

$\overline{B}^0 \to \pi^0\omega$

$$\begin{aligned} t^a_\omega &= b_1(\omega,\pi^0) + b_1(\pi^0,\omega)\ , \\ p^a_\omega &= -b_3(\pi^0,\omega) - b_3(\omega,\pi^0) \\ &\quad + \frac{1}{2}\Big(b^{ew}_3(\pi^0,\omega) + b^{ew}_3(\omega,\pi^0)\Big) + \frac{3}{2}\Big(b^{ew}_4(\pi^0,\omega) + b^{ew}_4(\omega,\pi^0)\Big)\ . \end{aligned} \tag{C.2}$$

$B^- \to \pi^- \rho^0$

$$\begin{aligned} t^a_\rho &= b_2(\pi^-, \rho^0) - b_2(\rho^0, \pi^-) \,, \\ p^a_\rho &= b_3(\pi^-, \rho^0) - b_3(\rho^0, \pi^-) + b_3^{ew}(\pi^-, \rho^0) - b_3^{ew}(\rho^0, \pi^-) \,. \end{aligned} \tag{C.3}$$

$B^- \to \pi^- \omega$

$$\begin{aligned} t^a_\omega &= b_2(\pi^-, \omega) + b_2(\omega, \pi^-) \,, \\ p^a_\omega &= b_3(\pi^-, \omega) + b_3(\omega, \pi^-) + b_3^{ew}(\pi^-, \omega) + b_3^{ew}(\omega, \pi^-) \,. \end{aligned} \tag{C.4}$$

C.2 Transition $b \to s$

$\overline{B}^0 \to \overline{K}^0 \rho^0$

$$\begin{aligned} t^a_\rho &= 0 \,, \\ p^a_\rho &= b_3(\overline{K}^0, \rho^0) - \frac{1}{2} b_3^{ew}(\overline{K}^0, \rho^0) \,. \end{aligned} \tag{C.5}$$

$\overline{B}^0 \to \overline{K}^0 \omega$

$$\begin{aligned} t^a_\omega &= 0 \,, \\ p^a_\omega &= b_3(\overline{K}^0, \omega) - \frac{1}{2} b_3^{ew}(\overline{K}^0, \omega) \,. \end{aligned} \tag{C.6}$$

$B^- \to K^- \rho^0$

$$\begin{aligned} t^a_\rho &= b_2(K^-, \rho^0) \,, \\ p^a_\rho &= b_3(K^-, \rho^0) + b_3^{ew}(K^-, \rho^0) \,. \end{aligned} \tag{C.7}$$

$B^- \to K^- \omega$

$$\begin{aligned} t^a_\omega &= b_2(K^-, \omega) \,, \\ p^a_\omega &= b_3(K^-, \omega) + b_3^{ew}(K^-, \omega) \,. \end{aligned} \tag{C.8}$$

Bibliography

[1] T. D. Lee and C.-N. Yang, Phys. Rev. **104**, 254 (1956).

[2] C. S. Wu, E. Ambler, R. W. Hayward, D. D. Hoppes, and R. P. Hudson, Phys. Rev. **105**, 1413 (1957).

[3] R. L. Garwin, L. M. Lederman, and M. Weinrich, Phys. Rev. **105**, 1415 (1957).

[4] J. H. Christenson, J. W. Cronin, V. L. Fitch, and R. Turlay, Phys. Rev. Lett. **13**, 138 (1964).

[5] M. Kobayashi and T. Maskawa, Prog. Theor. Phys. **49**, 652 (1973).

[6] A. Le Yaouanc, L. Oliver, O. Pene, and J. C. Raynal, Contribution to Capri Mtg. on Particle Physics, Capri, Italy, May 1991.

[7] M. E. Peskin and S. D. V., Perseus Books Publishing L.L.C. (1995).

[8] Y. Nir, (1999), hep-ph/9911321.

[9] C. Quigg, (2002), hep-ph/0204104.

[10] H. Quinn, (2001), hep-ph/0111177.

[11] M. Neubert, Int. J. Mod. Phys. **A17**, 2936 (2002), hep-ph/0110301.

[12] J. L. Rosner, (2000), hep-ph/0005258.

[13] M. Beneke, (2002), hep-ph/0201137.

[14] Z. Ligeti and Y. Nir, Nucl. Phys. Proc. Suppl. **111**, 82 (2002), hep-ph/0202117.

[15] J. L. Rosner, Nucl. Phys. Proc. Suppl. **59**, 1 (1997), hep-ph/9612327.

[16] A. Hocker, H. Lacker, S. Laplace, and F. Le Diberder, Eur. Phys. J. **C21**, 225 (2001), hep-ph/0104062.

[17] L.-L. Chau and W.-Y. Keung, Phys. Rev. Lett. **53**, 1802 (1984).

[18] L. Wolfenstein, Phys. Rev. Lett. **51**, 1945 (1983).

[19] L. Wolfenstein, Phys. Rev. Lett. **13**, 562 (1964).

[20] C. Jarlskog, Phys. Rev. Lett. **55**, 1039 (1985).

[21] A. J. Buras, (2001), hep-ph/0109197.

[22] M. Battaglia *et al.*, (2003), hep-ph/0304132.

[23] C. T. Sachrajda, Int. J. Mod. Phys. **A17**, 3140 (2002), hep-ph/0110304.

[24] Particle Data Group, K. Hagiwara *et al.*, Phys. Rev. **D66**, 010001 (2002).

[25] R. Fleischer, (2000), hep-ph/0011323.

[26] C. T. Sachrajda, (1998), hep-ph/9801343.

[27] C. T. Sachrajda, (1997), hep-ph/9711386.

[28] A. J. Buras, Lect. Notes Phys. **558**, 65 (2000), hep-ph/9901409.

[29] A. J. Buras, (1998), hep-ph/9806471.

[30] G. Buchalla, A. J. Buras, and M. E. Lautenbacher, Rev. Mod. Phys. **68**, 1125 (1996), hep-ph/9512380.

[31] V. A. Novikov, M. A. Shifman, A. I. Vainshtein, and V. I. Zakharov, Nucl. Phys. **B249**, 445 (1985).

[32] M. A. Shifman, A. I. Vainshtein, and V. I. Zakharov, Nucl. Phys. **B147**, 385 (1979).

[33] M. A. Shifman, A. I. Vainshtein, and V. I. Zakharov, Nucl. Phys. **B147**, 448 (1979).

[34] B. Stech, (1997), hep-ph/9706384.

[35] N. G. Deshpande and X.-G. He, Phys. Rev. Lett. **74**, 26 (1995), hep-ph/9408404.

[36] R. Fleischer, Z. Phys. **C62**, 81 (1994).

[37] R. Fleischer, Z. Phys. **C58**, 483 (1993).

[38] R. Fleischer, Int. J. Mod. Phys. **A12**, 2459 (1997), hep-ph/9612446.

[39] G. Kramer, W. F. Palmer, and H. Simma, Nucl. Phys. **B428**, 77 (1994), hep-ph/9402227.

[40] R. Enomoto and M. Tanabashi, Phys. Lett. **B386**, 413 (1996), hep-ph/9606217.

[41] S. Gardner, H. B. O'Connell, and A. W. Thomas, Phys. Rev. Lett. **80**, 1834 (1998), hep-ph/9705453.

[42] A. J. Buras, Nucl. Instrum. Meth. **A368**, 1 (1995), hep-ph/9509329.

[43] D. Fakirov and B. Stech, Nucl. Phys. **B133**, 315 (1978).

[44] N. Cabibbo and L. Maiani, Phys. Lett. **B73**, 418 (1978).

[45] M. J. Dugan and B. Grinstein, Phys. Lett. **B255**, 583 (1991).

[46] J. D. Bjorken, Nucl. Phys. Proc. Suppl. **11**, 325 (1989).

[47] H. R. Quinn, (1999), hep-ph/9912325.

[48] H.-Y. Cheng, Phys. Lett. **B335**, 428 (1994), hep-ph/9406262.

[49] H.-Y. Cheng, Phys. Lett. **B395**, 345 (1997), hep-ph/9610283.

[50] H. Fritzsch and A. S. Muller, Nucl. Phys. Proc. Suppl. **96**, 273 (2001), hep-ph/0011278.

[51] Y. Nambu and E. Shrauner, Phys. Rev. **128**, 862 (1962).

[52] Y. Nambu, Nuovo Cim. 9 (1958) 610-623. In *Eguchi, T. (ed.) et al.: Broken symmetry* 77-90.

[53] Y. Nambu, Phys. Rev. Lett. **4**, 380 (1960).

[54] J. J. Sakurai, University of Chicago Press (1969).

[55] H. B. O'Connell, B. C. Pearce, A. W. Thomas, and A. G. Williams, Prog. Part. Nucl. Phys. **39**, 201 (1997), hep-ph/9501251.

[56] A. G. Williams, (1997), hep-ph/9712405.

[57] M. Benayoun, P. David, L. DelBuono, P. Leruste, and H. B. O'Connell, will be published in Eur. Phys. J. (2003), nucl-th/0301037.

[58] H. B. O'Connell, Austral.J.Phys. **50**, 255 (1997), hep-ph/9604375.

[59] H. B. O'Connell, B. C. Pearce, A. W. Thomas, and A. G. Williams, Phys. Lett. **B336**, 1 (1994), hep-ph/9405273.

[60] K. Maltman, H. B. O'Connell, and A. G. Williams, Phys. Lett. **B376**, 19 (1996), hep-ph/9601309.

[61] H. B. O'Connell, A. W. Thomas, and A. G. Williams, Nucl. Phys. **A623**, 559 (1997), hep-ph/9703248.

[62] CMD-2, R. R. Akhmetshin *et al.*, Phys. Lett. **B527**, 161 (2002), hep-ex/0112031.

[63] A. G. Williams, H. B. O'Connell, and A. W. Thomas, Nucl. Phys. **A629**, 464c (1998), hep-ph/9707253.

[64] H. B. O'Connell, B. C. Pearce, A. W. Thomas, and A. G. Williams, Phys. Lett. **B354**, 14 (1995), hep-ph/9503332.

[65] S. Gardner and H. B. O'Connell, Phys. Rev. **D57**, 2716 (1998), hep-ph/9707385.

[66] S. Gardner and H. B. O'Connell, Phys. Rev. **D59**, 076002 (1999), hep-ph/9809224.

[67] M. Benayoun *et al.*, Eur. Phys. J. **C2**, 269 (1998), hep-ph/9707509.

[68] X. H. Guo and A. W. Thomas, Phys. Rev. **D58**, 096013 (1998), hep-ph/9805332.

[69] X. H. Guo and A. W. Thomas, Phys. Rev. **D61**, 116009 (2000), hep-ph/9907370.

[70] S. Gardner, (1998), hep-ph/9809479.

[71] S. Gardner, H. B. O'Connell, and A. W. Thomas, (1997), hep-ph/9707414.

[72] Y.-H. Chen, H.-Y. Cheng, B. Tseng, and K.-C. Yang, Phys. Rev. **D60**, 094014 (1999), hep-ph/9903453.

[73] M. Bauer, B. Stech, and M. Wirbel, Z. Phys. **C34**, 103 (1987).

[74] M. Wirbel, B. Stech, and M. Bauer, Z. Phys. **C29**, 637 (1985).

[75] X.-H. Guo and T. Huang, Phys. Rev. **D43**, 2931 (1991).

[76] P. Ball, JHEP **09**, 005 (1998), hep-ph/9802394.

[77] P. Ball and V. M. Braun, Phys. Rev. **D58**, 094016 (1998), hep-ph/9805422.

[78] ALEPH, D. Abbaneo *et al.*, (2001), hep-ex/0112028.

[79] H.-Y. Cheng and A. Soni, Phys. Rev. **D64**, 114013 (2001), hep-ph/0105246.

[80] D. Melikhov and B. Stech, Phys. Rev. **D62**, 014006 (2000), hep-ph/0001113.

[81] BABAR, C.-h. Cheng, Int. J. Mod. Phys. **A16S1A**, 413 (2001), hep-ex/0011007.

[82] BABAR, B. Aubert *et al.*, (2003), hep-ex/0303043.

[83] CLEO, Y. Gao and F. Wurthwein, (1999), hep-ex/9904008.

[84] CLEO, C. P. Jessop *et al.*, Phys. Rev. Lett. **85**, 2881 (2000), hep-ex/0006008.

[85] CLEO, H. Schwarthoff, (2002), hep-ex/0205015.

[86] CLEO, R. A. Briere, AIP Conf. Proc. **618**, 159 (2002), hep-ex/0202029.

[87] X. Zhao, (2001), hep-ex/0101013.

[88] Belle, K. Abe *et al.*, (2001), hep-ex/0107051.

[89] the Belle, A. Bozek, (2001), hep-ex/0104041.

[90] R. S. Lu *et al.*, Phys. Rev. Lett. **89**, 191801 (2002), hep-ex/0207019.

[91] Belle, B. C. K. Casey *et al.*, Phys. Rev. **D66**, 092002 (2002), hep-ex/0207090.

[92] Belle, K. Abe *et al.*, Phys. Rev. **D65**, 092005 (2002), hep-ex/0201007.

[93] BELLE, A. Garmash, (2002), hep-ex/0207003.

[94] Belle, A. Gordon *et al.*, Phys. Lett. **B542**, 183 (2002), hep-ex/0207007.

[95] BELLE, T. Iijima, (2001), hep-ex/0105005.

[96] BELLE, K. Kinoshita, Nucl. Instrum. Meth. **A462**, 77 (2001), hep-ex/0101033.

[97] G. H. De Monchenault, (2003), hep-ex/0305055.

[98] BABAR, B. Aubert *et al.*, Phys. Rev. Lett. **87**, 221802 (2001), hep-ex/0108017.

[99] BABAR, B. Aubert *et al.*, (2002), hep-ex/0206004.

[100] BABAR, J. Olsen, Int. J. Mod. Phys. **A16S1A**, 468 (2001), hep-ex/0011031.

[101] BABAR, B. Aubert *et al.*, (2000), hep-ex/0008058.

[102] BABAR, T. Schietinger, (2001), hep-ex/0105019.

[103] BABAR, G. Sciolla, Nucl. Phys. Proc. Suppl. **99B**, 135 (2001), hep-ex/0101004.

[104] BABAR, G. Cavoto, (2001), hep-ex/0105018.

[105] BABAR, B. Aubert *et al.*, Phys. Rev. Lett. **87**, 151802 (2001), hep-ex/0105061.

[106] A. Deandrea and A. D. Polosa, Phys. Rev. Lett. **86**, 216 (2001), hep-ph/0008084.

[107] U.-G. Meissner, (2002), hep-ph/0206125.

[108] A. Deandrea, R. Gatto, M. Ladisa, G. Nardulli, and P. Santorelli, Phys. Rev. **D62**, 036001 (2000), hep-ph/0002038.

[109] S. Gardner and U.-G. Meissner, Phys. Rev. **D65**, 094004 (2002), hep-ph/0112281.

[110] A. Deandrea, (2000), hep-ph/0005014.

[111] J. Tandean and S. Gardner, Phys. Rev. **D66**, 034019 (2002), hep-ph/0204147.

[112] H.-Y. Cheng and B. Tseng, (1997), hep-ph/9708211.

[113] H.-Y. Cheng and B. Tseng, Phys. Rev. **D58**, 094005 (1998), hep-ph/9803457.

[114] P. A. M. Dirac, Rev. Mod. Phys. **21**, 392 (1949).

[115] H. C. Pauli, Nucl. Phys. Proc. Suppl. **90**, 259 (2000), hep-ph/0103106.

[116] V. A. Karmanov, Prepared for 4th International Workshop on Light Cone Quantization and Non-Perturbative Dynamics, Polana Zgorzelisko, Poland, 15-25 Aug 1994.

[117] V. A. Karmanov, Zh. Eksp. Teor. Fiz. **71**, 399 (1976).

[118] V. A. Karmanov, Sov. Phys. JETP **48**, 598 (1978).

[119] V. A. Karmanov, Nucl. Phys. **B166**, 378 (1980).

[120] V. A. Karmanov, Nucl. Phys. **A362**, 331 (1981).

[121] V. A. Karmanov, JETP Lett. **35**, 276 (1982).

[122] V. A. Karmanov, (1999), nucl-th/9907037.

[123] V. A. Karmanov and J. Carbonell, (2002), nucl-th/0207075.

[124] J. Carbonell, B. Desplanques, V. A. Karmanov, and J. F. Mathiot, Phys. Rept. **300**, 215 (1998), nucl-th/9804029.

[125] S. J. Brodsky, H.-C. Pauli, and S. S. Pinsky, Phys. Rept. **301**, 299 (1998), hep-ph/9705477.

[126] J. Schwinger, (1958), Quantum Electrodynamics, Selected Papers, Dover, New York.

[127] J. Carbonell, M. Mangin-Brinet, and V. A. Karmanov, (2002), nucl-th/0202042.

[128] M. Mangin-Brinet, J. Carbonell, and V. A. Karmanov, Phys. Rev. **D64**, 125005 (2001), hep-th/0107235.

[129] M. Mangin-Brinet, J. Carbonell, and V. A. Karmanov, Phys. Rev. **D64**, 027701 (2001), hep-th/0102068.

[130] A. P. Bakulev and S. V. Mikhailov, Phys. Lett. **B436**, 351 (1998), hep-ph/9803298.

[131] A. P. Bakulev, S. V. Mikhailov, and N. G. Stefanis, Phys. Lett. **B508**, 279 (2001), hep-ph/0103119.

[132] V. M. Belyaev and M. B. Johnson, Phys. Rev. **D56**, 1481 (1997), hep-ph/9702207.

[133] I. V. Musatov and A. V. Radyushkin, Phys. Rev. **D56**, 2713 (1997), hep-ph/9702443.

[134] H.-n. Li and G. Sterman, Nucl. Phys. **B381**, 129 (1992).

[135] R. Jakob and P. Kroll, Phys. Lett. **B315**, 463 (1993), hep-ph/9306259.

[136] M. Burkardt and S. K. Seal, Phys. Rev. **D65**, 034501 (2002), hep-ph/0102245.

[137] S. K. Seal and M. Burkardt, (2002), hep-ph/0204015.

[138] J. A. Oller, E. Oset, and J. E. Palomar, Phys. Rev. **D63**, 114009 (2001), hep-ph/0011096.

[139] E. Ruiz Arriola and W. Broniowski, Phys. Rev. **D66**, 094016 (2002), hep-ph/0207266.

[140] V. Anisovich, D. Melikhov, and V. Nikonov, Phys. Rev. **D52**, 5295 (1995), hep-ph/9503473.

[141] H.-Y. Cheng, C.-Y. Cheung, C.-W. Hwang, and W.-M. Zhang, Phys. Rev. **D57**, 5598 (1998), hep-ph/9709412.

[142] C.-W. Hwang, Eur. Phys. J. **C19**, 105 (2001), hep-ph/0005163.

[143] J. Speth and V. R. Zoller, Phys. Lett. **B351**, 533 (1995), hep-ph/9502382.

[144] V. A. Karmanov and J. F. Mathiot, Nucl. Phys. **A602**, 388 (1996).

[145] S. L. Adler, Phys. Rev. **177**, 2426 (1969).

[146] J. S. Bell and R. Jackiw, Nuovo Cim. **A60**, 47 (1969).

[147] L. Trentadue and M. Verbeni, Nucl. Phys. **B583**, 307 (2000), hep-ph/0006113.

[148] F. Bissey and J. F. Mathiot, Eur. Phys. J. **C16**, 131 (2000).

[149] CP-PACS, A. Ali Khan *et al.*, Phys. Rev. **D64**, 034505 (2001), hep-lat/0010009.

[150] M. Jamin and B. O. Lange, Phys. Rev. **D65**, 056005 (2002), hep-ph/0108135.

[151] C. Gay, Ann. Rev. Nucl. Part. Sci. **50**, 577 (2000), hep-ex/0103016.

[152] N. F. Nasrallah, Phys. Rev. **D63**, 054028 (2001), hep-ph/0005017.

[153] S. R. Amendolia *et al.*, Phys. Lett. **B178**, 435 (1986).

[154] A. F. Krutov and V. E. Troitsky, (2000), nucl-th/0010076.

[155] P. Brauel *et al.*, Zeit. Phys. **C3**, 101 (1979).

[156] The Jefferson Lab F(pi), J. Volmer *et al.*, Phys. Rev. Lett. **86**, 1713 (2001), nucl-ex/0010009.

[157] T. Heinzl, Nucl. Phys. Proc. Suppl. **90**, 83 (2000), hep-ph/0008314.

[158] V. M. Braun and I. E. Halperin, Z. Phys. **C44**, 157 (1989).

[159] V. M. Braun and I. E. Halperin, Z. Phys. **C48**, 239 (1990).

[160] G. Sterman and P. Stoler, Ann. Rev. Nucl. Part. Sci. **47**, 193 (1997), hep-ph/9708370.

[161] F.-G. Cao, T. Huang, and B.-Q. Ma, Phys. Rev. **D53**, 6582 (1996), hep-ph/9603330.

[162] P. Kroll and M. Raulfs, Phys. Lett. **B387**, 848 (1996), hep-ph/9605264.

[163] V. L. Chernyak and A. R. Zhitnitsky, Nucl. Phys. **B201**, 492 (1982).

[164] R. Jakob, P. Kroll, and M. Raulfs, J. Phys. **G22**, 45 (1996), hep-ph/9410304.

[165] NA7, S. R. Amendolia *et al.*, Nucl. Phys. **B277**, 168 (1986).

[166] C. A. Dominguez, (2001), hep-ph/0102190.

[167] H.-C. Pauli, Nucl. Phys. **A705**, 73 (2002), hep-ph/0107302.

[168] C.-W. Hwang, Eur. Phys. J. **C23**, 585 (2002), hep-ph/0112237.

[169] P. Kroll, (1997), hep-ph/9701319.

[170] A. Schmedding and O. I. Yakovlev, Phys. Rev. **D62**, 116002 (2000), hep-ph/9905392.

[171] CLEO, J. Gronberg *et al.*, Phys. Rev. **D57**, 33 (1998), hep-ex/9707031.

[172] C. J. Bebek *et al.*, Phys. Rev. **D17**, 1693 (1978).

[173] P. Maris and P. C. Tandy, Phys. Rev. **C62**, 055204 (2000), nucl-th/0005015.

[174] P. C. Tandy, (2001), nucl-th/0106031.

[175] E. B. Dally *et al.*, Phys. Rev. Lett. **45**, 232 (1980).

[176] V. A. Karmanov, Fiz. Elem. Chast. Atom. Yadra **19**, 525 (1988).

[177] J. Carbonell and V. A. Karmanov, Nucl. Phys. **A581**, 625 (1995).

[178] S. Louise, J. J. Dugne, and J. F. Mathiot, Phys. Lett. **B472**, 357 (2000).

[179] C.-Y. Cheung, C.-W. Hwang, and W.-M. Zhang, Z. Phys. **C75**, 657 (1997), hep-ph/9602309.

[180] N. B. Demchuk, I. L. Grach, I. M. Narodetski, and S. Simula, Phys. Atom. Nucl. **59**, 2152 (1996), hep-ph/9601369.

[181] I. L. Grach, I. M. Narodetsky, and S. Simula, Phys. Lett. **B385**, 317 (1996), hep-ph/9605349.

[182] A. Le Yaouanc, L. Oliver, O. Pene, and J. C. Raynal, Phys. Lett. **B365**, 319 (1996), hep-ph/9507342.

[183] A. Le Yaouanc, L. Oliver, O. Pene, and J. C. Raynal, (1995), hep-ph/9504267.

[184] N. B. Demchuk, P. Y. Kulikov, I. M. Narodetsky, and P. J. O'Donnell, Phys. Atom. Nucl. **60**, 1292 (1997), hep-ph/9701388.

[185] H.-Y. Cheng, C.-Y. Cheung, and C.-W. Hwang, Phys. Rev. **D55**, 1559 (1997), hep-ph/9607332.

[186] F. Cardarelli and S. Simula, Phys. Lett. **B421**, 295 (1998), hep-ph/9711207.

[187] D. Becirevic, S. Prelovsek, and J. Zupan, (2003), hep-lat/0305001.

[188] UKCQD, C. M. Maynard, Nucl. Phys. Proc. Suppl. **73**, 396 (1999), hep-lat/9809064.

[189] UKQCD, C. M. Maynard, Nucl. Phys. Proc. Suppl. **94**, 367 (2001), hep-lat/0010016.

[190] UKQCD, J. Gill, Nucl. Phys. Proc. Suppl. **106**, 391 (2002), hep-lat/0109035.

[191] UKQCD, L. Del Debbio, J. M. Flynn, L. Lellouch, and J. Nieves, Phys. Lett. **B416**, 392 (1998), hep-lat/9708008.

[192] UKQCD, K. C. Bowler, G. Douglas, R. D. Kenway, G. N. Lacagnina, and C. M. Maynard, Nucl. Phys. **B637**, 293 (2002), hep-lat/0202029.

[193] C. T. Sachrajda, Nucl. Instrum. Meth. **A462**, 23 (2001), hep-lat/0101003.

[194] T. Kurimoto, H.-n. Li, and A. I. Sanda, Phys. Rev. **D65**, 014007 (2002), hep-ph/0105003.

[195] T. M. Aliev, H. Koru, A. Ozpineci, and M. Savci, Phys. Lett. **B400**, 194 (1997), hep-ph/9702209.

[196] S. Weinzierl and O. I. Yakovlev, J. Phys. **G26**, 737 (2000), hep-ph/9911530.

[197] A. Khodjamirian, R. Ruckl, and C. W. Winhart, Phys. Rev. **D58**, 054013 (1998), hep-ph/9802412.

[198] N. B. Demchuk, JHEP **08**, 008 (1998), hep-ph/9807333.

[199] J. M. Soares, (1998), hep-ph/9810402.

[200] I. L. Grach, I. M. Narodetsky, S. Simula, and K. A. Ter-Martirosian, Nucl. Phys. **B502**, 227 (1997), hep-ph/9603239.

[201] B. L. G. Bakker, H.-M. Choi, and C.-R. Ji, (2003), hep-ph/0303002.

[202] M. A. Ivanov and Y. M. Valit, (1996), hep-ph/9606404.

[203] D. S. Hwang and D.-W. Kim, (1998), hep-ph/9806362.

[204] J. M. Flynn and C. T. Sachrajda, Adv. Ser. Direct. High Energy Phys. **15**, 402 (1998), hep-lat/9710057.

[205] A. Abada *et al.*, Nucl. Phys. Proc. Suppl. **83**, 268 (2000), hep-lat/9910021.

[206] P. Colangelo, F. De Fazio, P. Santorelli, and E. Scrimieri, Phys. Rev. **D53**, 3672 (1996), hep-ph/9510403.

[207] M. Beneke, G. Buchalla, M. Neubert, and C. T. Sachrajda, Nucl. Phys. **B606**, 245 (2001), hep-ph/0104110.

[208] C. T. Sachrajda, Acta Phys. Polon. **B32**, 1821 (2001).

[209] M. Beneke, G. Buchalla, M. Neubert, and C. T. Sachrajda, Phys. Rev. Lett. **83**, 1914 (1999), hep-ph/9905312.

[210] M. Neubert, AIP Conf. Proc. **602**, 168 (2001), hep-ph/0110093.

[211] M. Neubert, Nucl. Phys. Proc. Suppl. **99B**, 113 (2001), hep-ph/0011064.

[212] M. Beneke, J. Phys. **G27**, 1069 (2001), hep-ph/0009328.

[213] M. Beneke, (2002), hep-ph/0207228.

[214] M. Beneke, (1999), hep-ph/9910505.

[215] M. Beneke, G. Buchalla, M. Neubert, and C. T. Sachrajda, (2000), hep-ph/0007256.

[216] M. Beneke, G. Buchalla, M. Neubert, and C. T. Sachrajda, Nucl. Phys. **B591**, 313 (2000), hep-ph/0006124.

[217] Y. Y. Keum, H.-N. Li, and A. I. Sanda, Phys. Rev. **D63**, 054008 (2001), hep-ph/0004173.

[218] Y.-Y. Keum and H.-n. Li, Phys. Rev. **D63**, 074006 (2001), hep-ph/0006001.

[219] D.-s. Du, D. Yang, and G. Zhu, Phys. Lett. **B509**, 263 (2001), hep-ph/0102077.

[220] D.-s. Du, J.-f. Sun, D.-s. Yang, and G.-h. Zhu, Phys. Rev. **D67**, 014023 (2003), hep-ph/0209233.

[221] R. Aleksan, P. F. Giraud, V. Morenas, O. Pene, and A. S. Safir, (2003), hep-ph/0301165.

[222] H.-Y. Cheng and K.-C. Yang, Phys. Lett. **B511**, 40 (2001), hep-ph/0104090.

[223] D.-s. Du, H.-u. Gong, J.-f. Sun, D.-s. Yang, and G.-h. Zhu, Phys. Rev. **D65**, 074001 (2002), hep-ph/0108141.

[224] D.-s. Du, H.-j. Gong, J.-f. Sun, D.-s. Yang, and G.-h. Zhu, Phys. Rev. **D65**, 094025 (2002), hep-ph/0201253.

[225] D.-s. Du, D.-s. Yang, and G.-h. Zhu, Phys. Lett. **B488**, 46 (2000), hep-ph/0005006.

[226] A. Ali, G. Kramer, and C.-D. Lu, Phys. Rev. **D59**, 014005 (1999), hep-ph/9805403.

[227] A. Ali, G. Kramer, and C.-D. Lu, Phys. Rev. **D58**, 094009 (1998), hep-ph/9804363.

[228] H.-Y. Cheng and K.-C. Yang, Phys. Rev. **D62**, 054029 (2000), hep-ph/9910291.

[229] A. J. Buras and L. Silvestrini, Nucl. Phys. **B548**, 293 (1999), hep-ph/9806278.

[230] C.-D. Lu, K. Ukai, and M.-Z. Yang, Phys. Rev. **D63**, 074009 (2001), hep-ph/0004213.

[231] C.-D. Lu and M.-Z. Yang, Eur. Phys. J. **C23**, 275 (2002), hep-ph/0011238.

[232] S. Fajfer, R. J. Oakes, and T. N. Pham, Phys. Lett. **B539**, 67 (2002), hep-ph/0203072.

[233] Z. J. Ajaltouni, O. Leitner, and C. Rimbault, (2003), hep-ph/0302037.

[234] Z. J. Ajaltouni, O. Leitner, P. Perret, C. Rimbault, and A. W. Thomas, will be published in Eur. Phys. J. (2003), hep-ph/0302156.

[235] BELLE, J. Zhang *et al.*, (2003), hep-ex/0306007.

[236] BELLE, K. Abe *et al.*, (2003), hep-ex/0307077.

[237] BABAR, B. Aubert, (2003), hep-ex/0307026.

[238] S. Khalil and V. Sanz, (2003), hep-ph/0306171.

[239] M. Gronau and D. London, Phys. Rev. **D55**, 2845 (1997), hep-ph/9608430.

[240] G.-H. Wu, K. Kiers, and A. Soni, (1999), hep-ph/9903343.

[241] D. I. Kazakov and A. V. Gladyshev.

[242] P. Fayet, Nucl. Phys. Proc. Suppl. **101**, 81 (2001), hep-ph/0107228.

[243] G. C. Branco, F. Kruger, J. C. Romao, and A. M. Teixeira, JHEP **07**, 027 (2001), hep-ph/0012318.

[244] D. I. Kazakov, (2000), hep-ph/0012288.

[245] M. B. Gavela, P. Hernandez, J. Orloff, and O. Pene, Prepared for International Seminar: Quarks - 94, Vladimir, Russia, 11-18 May 1994.

[246] R. Battiston and B. Bertucci, Prepared for 2nd International Workshop on Matter, Anti- Matter and Dark Matter, Trento, Italy, 29-30 Oct 2001.

Papers

Publications in progress

- **Enhanced Direct CP Violation in QCD Factorization in $B^{\pm,0} \to \pi^+\pi^- {M_1}^{\pm,0}$**

  By O. Leitner, X.H. Guo and A.W. Thomas.

- **Phenomenological Meson Wave Functions In Covariant Light-Front Dynamics**

  By O. Leitner, J.-F. Mathiot and A.W. Thomas.

- **Transition Form Factors For B And D Decays In Covariant Light-Front Dynamics**

  By O. Leitner, J.-F. Mathiot and A.W. Thomas.

List of publications

- **Direct CP Violation in $B \to \pi^+\pi^-\pi$: Determination of α Without Discrete Ambiguity**

  By O. Leitner, X.H. Guo and A.W. Thomas. *Euro. Phys. J.* **Cxx**: xxxxxx, 2003, [hep-ph/0211003].

- **Direct CP Violation in $B \to \pi^+\pi^- V$ With $\rho - \omega$ Mixing Effects: Phenomenological Approach**

  By Z. Ajaltouni, O. Leitner, P. Perret, C. Rimbault and A.W. Thomas. *Euro. Phys. J.* **C29** 215, 2003, [hep-ph/0302156].

- **$B^{0(\pm)}$ Decays Into Two Vector Mesons**

  By Z.J. Ajaltouni, O. Leitner and C. Rimbault. CERN publication, LHCb-PHYS-2001-041, [hep-ph/0302037].

- **Enhanced Direct CP Violation In $B^\pm \to \rho^0\pi^\pm$.**

  By X.H. Guo, O. Leitner and A.W. Thomas. *Phys. Rev.* **D63**: 056012, 2001, [hep-ph/0009042].

- **Enhanced Direct CP Violation in $B^{\pm,0} \to \pi^+\pi^- K^{\pm,0}$**

  By O. Leitner, X.H. Guo and A.W. Thomas. *Phys. Rev.* **D66**: 096008, 2002, [hep-ph/0208198].

List of proceedings and talks

- **Covariant Light-Front Dynamics and its application to the meson wave functions.**

  By O. Leitner, J.-F. Mathiot and A.W. Thomas. Will be published in Proceedings of the Workshop on Physics at the Japan Hadron Facility (JHF), Adelaide, Australia, 14-21 March 2002, World Scientific, 222-231, (2002).

- **Covariant Light-Front Dynamics and its application to the meson wave functions and form factors.**

  By O. Leitner, J.-F. Mathiot and A.W. Thomas. Published in Proceedings of the 15th AIP Biennial Congress 2002, Sydney, Australia, 8-11 July, 2002.

- **QCD Factorization in B Decays into $\rho\pi$**

  By O. Leitner, X.H. Guo and A.W. Thomas. Will be published by the American Institute of Physics (AIP) in Proceedings of the Workshop on Fourth Tropical Workshop on Particle Physics, Cosmology: Neutrinos, Flavour Physics and Precision Cosmology, Palm Cove, Queensland, Australia, June 9-13, 2003. [hep-ph/0307201]

- **Simulation Methods of Processes $B \to \pi^+\pi^- V$ with $\rho^0 - \omega$ Mixing**

  By Z. Ajaltouni, O. Leitner, P. Perret, C. Rimbault, and A.W. Thomas. Talk presented at the CERN Workshop on Event Generators, CERN, Geneva, July 22-26, 2003.

PHYSICAL REVIEW D 66, 096008 (2002)

Enhanced direct CP violation in $B^{\pm,0}\to\pi^+\pi^-K^{\pm,0}$

O. Leitner*
Department of Physics and Mathematical Physics and Special Research Center for the Subatomic Structure of Matter, University of Adelaide, Adelaide 5005, Australia
and Laboratoire de Physique Corpusculaire, Université Blaise Pascal, CNRS/IN2P3, 24 avenue des Landais, 63177 Aubière Cedex, France

X.-H. Guo† and A. W. Thomas‡
Department of Physics and Mathematical Physics and Special Research Center for the Subatomic Structure of Matter, University of Adelaide, Adelaide 5005, Australia
(Received 22 August 2002; published 25 November 2002)

We investigate in a phenomenological way direct CP violation in the hadronic decays $B^{\pm,0}\to\pi^+\pi^-K^{\pm,0}$ where the effect of ρ-ω mixing is included. If N_c^{eff} (the effective parameter associated with factorization) is constrained using the most recent experimental branching ratios (to ρ^0K^0, $\rho^\pm K^\mp$, $\rho^\pm K^0$, $\rho^0K^\pm$ and $\omega K^\pm$) from the BABAR, BELLE and CLEO Collaborations, we get a maximum CP violating asymmetry a_{max} in the range -25% to $+49\%$ for $B^-\to\pi^+\pi^-K^-$ and -24% to $+55\%$ for $\bar{B}^0\to\pi^+\pi^-\bar{K}^0$. We also find that CP violation is strongly dependent on the Cabibbo-Kobayashi-Maskawa matrix elements. Finally, we show that the sign of $\sin\delta$ is always positive in the allowed range of N_c^{eff} and hence, a measurement of direct CP violation in $B^{\pm,0}\to\pi^+\pi^-K^{\pm,0}$ would remove the mod(π) ambiguity in arg$[-V_{ts}V_{tb}^*/V_{us}V_{ub}^*]$.

DOI: 10.1103/PhysRevD.66.096008 PACS number(s): 11.30.Er, 12.39.−x, 13.25.Hw

I. INTRODUCTION

The study of CP violation in B decays is one of the most important aims for the B factories. The relative large CP violating effects expected in B meson decays should provide efficient tests of the standard model through the Cabibbo-Kobayashi-Maskawa (CKM) matrix. It is usually assumed that a nonzero imaginary phase angle η is responsible for the CP violating phenomena. This is why, in the past few years, numerous theoretical studies and experiments have been conducted in the B meson system [1,2] in order to reduce uncertainties in calculations (e.g. CKM matrix elements, hadronic matrix elements and nonfactorizable effects) and increase our understanding of CP violation within the standard model framework.

Direct CP violating asymmetries in B decays occur through the interference of at least two amplitudes with different weak phase ϕ *and* strong phase δ. In order to extract the weak phase (which is determined by the CKM matrix elements) through the measurement of a CP violating asymmetry, one must know the strong phase δ and this is usually not well determined. In addition, in order to have a large signal, we have to appeal to some phenomenological mechanism to obtain a large δ. The charge symmetry violating mixing between ρ^0 and ω can be extremely important in this regard. In particular, it can lead to a large CP violation in B decays, such as $B^{\pm,0}\to\rho^0(\omega)K^{\pm,0}\to\pi^+\pi^-K^{\pm,0}$, because the strong phase passes through 90° at the ω resonance [3–5].

We have collected the latest data for b to s transitions concentrating on the CLEO, BABAR and BELLE branching ratio results in our approach. The aim of the present work is multiple. The main one is to constrain the CP violating calculation in $B^{\pm,0}\to\rho^0(\omega)K^{\pm,0}\to\pi^+\pi^-K^{\pm,0}$, including ρ-ω mixing and using the most recent experimental data for $B\to\rho K$ decays. The second one is to extract consistent constraints for B decays into $\rho(PS)$ where PS can be either π or K. In order to extract the strong phase δ, we shall use the factorization approach, in which the hadronic matrix elements of operators are saturated by vacuum intermediate states. Moreover, we approximate non-factorizable effects by introducing an effective number of colors, N_c^{eff}.

In this paper we investigate five phenomenological models with different weak form factors and determine the CP violating asymmetry, a, for $B^{\pm,0}\to\rho^0(\omega)K^{\pm,0}\to\pi^+\pi^-K^{\pm,0}$ in these models. We select models which are consistent with all the data and determine the allowed range for N_c^{eff} $[0.66(0.61)<N_c^{eff}<2.84(2.82)]$. Then, we study the sign of $\sin\delta$ in this range of N_c^{eff} for all these models. We also discuss the model dependence of our results in detail.

The remainder of this paper is organized as it follows. In Sec. II, we present the form of the effective Hamiltonian which is based on the operator product expansion, together with the values of the corresponding Wilson coefficients. In Sec. III, we give the phenomenological formalism for the CP violating asymmetry in decay processes including ρ-ω mixing, where all aspects of the calculation of direct CP violation, the CKM matrix, ρ-ω mixing, factorization and form factors are discussed in detail. In Sec. IV we list all the numerical inputs which are needed for calculating the asymmetry, a, in $B^{\pm,0}\to\rho^0(\omega)K^{\pm,0}\to\pi^+\pi^-K^{\pm,0}$. Section V is devoted to results and discussions for these decays. In Sec. VI we calculate branching ratios for decays such as $B^{\pm,0}$

*Email address: oleitner@physics.adelaide.edu.au
†Email address: xhguo@physics.adelaide.edu.au
‡Email address: athomas@physics.adelaide.edu.au

$\to\rho^{\pm,0}K^{\pm,0}$ and $B^{\pm}\to\omega K^{\pm}$ as well, and present numerical results over the range of N_c^{eff} which is allowed by experimental data from the CLEO, BABAR, and BELLE Collaborations. In Sec. VII, we summarize our results and determine the allowed range of N_c^{eff} which is consistent with data for both $\rho\pi$ and ρK decays. Uncertainties in our approach and conclusions are also discussed in this section.

II. THE EFFECTIVE HAMILTONIAN

A. Operator product expansion

Operator product expansion (OPE) [6] is a useful tool introduced to analyze the weak interaction of quarks. Defining the decay amplitude $A(M\to F)$ as

$$A(M\to F)\propto C_i(\mu)\langle F|O_i(\mu)|M\rangle, \tag{1}$$

where $C_i(\mu)$ are the Wilson coefficients (see Sec. II B) and $O_i(\mu)$ the operators given by the OPE, one sees that OPE separates the calculation of the amplitude, $A(M\to F)$, into two distinct physical regimes. One is related to *hard* or short-distance physics, represented by $C_i(\mu)$ and calculated by a perturbative approach. The other is the *soft* or long-distance regime. This part must be treated by non-perturbative approaches such as the $1/N$ expansion [7], QCD sum rules [8] or hadronic sum rules.

The operators, O_i, are local operators which can be written in the general form

$$O_n=(\bar{q}_i\Gamma_{n1}q_j)(\bar{q}_k\Gamma_{n2}q_l), \tag{2}$$

where Γ_{n1} and Γ_{n2} denote a combination of gamma matrices and q the quark flavor. They should respect the Dirac structure, the color structure and the types of quarks relevant for the decay being studied. They can be divided into two classes according to topology: tree operators (O_1,O_2), and penguin operators (O_3 to O_{10}). For tree contributions ($W^{\pm}$ is exchanged), the Feynman diagram is shown Fig. 1. The current-current operators related to the tree diagram are the following:

$$\begin{aligned} O_1^s&=\bar{q}_\alpha\gamma_\mu(1-\gamma_5)u_\beta\bar{s}_\beta\gamma^\mu(1-\gamma_5)b_\alpha,\\ O_2^s&=\bar{q}\gamma_\mu(1-\gamma_5)u\bar{s}\gamma^\mu(1-\gamma_5)b, \end{aligned} \tag{3}$$

where α and β are the color indices. The penguin terms can be divided into two sets. The first is from the QCD penguin diagrams (gluons are exchanged) and the second is from the electroweak penguin diagrams (γ and Z^0 exchanged). The Feynman diagram for the QCD penguin diagram is shown in Fig. 2 and the corresponding operators are written as follows:

$$\begin{aligned} O_3&=\bar{q}\gamma_\mu(1-\gamma_5)b\sum_{q'}\bar{q}'\gamma^\mu(1-\gamma_5)q',\\ O_4&=\bar{q}_\alpha\gamma_\mu(1-\gamma_5)b_\beta\sum_{q'}\bar{q}'_\beta\gamma^\mu(1-\gamma_5)q'_\alpha, \end{aligned} \tag{4}$$

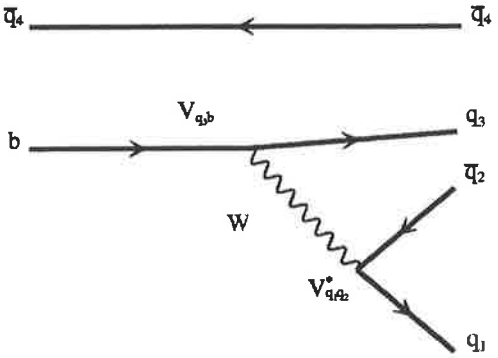

FIG. 1. Tree diagram for B decays.

$$\begin{aligned} O_5&=\bar{q}\gamma_\mu(1-\gamma_5)b\sum_{q'}\bar{q}'\gamma^\mu(1+\gamma_5)q',\\ O_6&=\bar{q}_\alpha\gamma_\mu(1-\gamma_5)b_\beta\sum_{q'}\bar{q}'_\beta\gamma^\mu(1+\gamma_5)q'_\alpha, \end{aligned} \tag{5}$$

where $q'=u,d,s,c$. Finally, the electroweak penguin operators arise from the two Feynman diagrams represented in Fig. 3 (Z,γ exchanged from a quark line) and Fig. 4 (Z,γ exchanged from the W line). They have the following expressions:

$$\begin{aligned} O_7&=\frac{3}{2}\bar{q}\gamma_\mu(1-\gamma_5)b\sum_{q'}e_{q'}\bar{q}'\gamma^\mu(1+\gamma_5)q',\\ O_8&=\frac{3}{2}\bar{q}_\alpha\gamma_\mu(1-\gamma_5)b_\beta\sum_{q'}e_{q'}\bar{q}'_\beta\gamma^\mu(1+\gamma_5)q'_\alpha,\\ O_9&=\frac{3}{2}\bar{q}\gamma_\mu(1-\gamma_5)b\sum_{q'}e_{q'}\bar{q}'\gamma^\mu(1-\gamma_5)q',\\ O_{10}&=\frac{3}{2}\bar{q}_\alpha\gamma_\mu(1-\gamma_5)b_\beta\sum_{q'}e_{q'}\bar{q}'_\beta\gamma^\mu(1-\gamma_5)q'_\alpha, \end{aligned} \tag{6}$$

where $e_{q'}$ denotes the electric charge of q'.

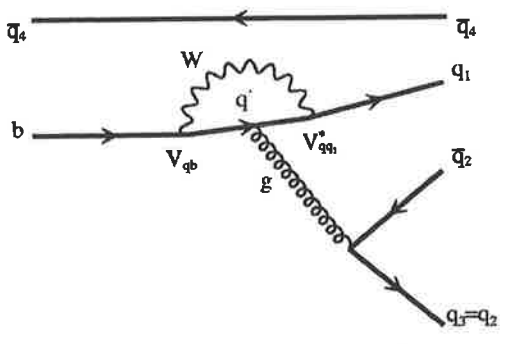

FIG. 2. QCD penguin diagram, for B decays.

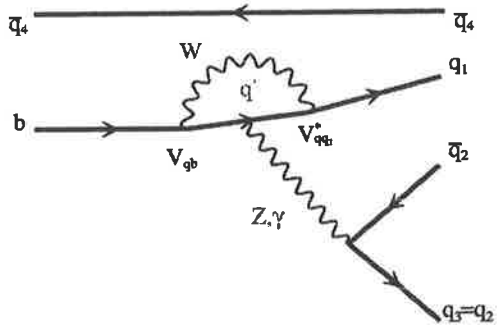

FIG. 3. Electroweak-penguin diagram for B decays.

B. Wilson coefficients

As we mentioned in the preceding section, the Wilson coefficients [9], $C_i(\mu)$, represent the physical contributions from scales higher than μ (the OPE describes physics for scales lower than μ). Since QCD has the property of asymptotic freedom, they can be calculated in perturbation theory. The Wilson coefficients include contributions of all heavy particles, such as the top quark, the W bosons, and the charged Higgs boson. Usually, the scale μ is chosen to be of order $O(m_b)$ for B decays. Wilson coefficients have been calculated to the next-to-leading order (NLO). The evolution of $C(\mu)$ [the matrix that includes $C_i(\mu)$] is given by

$$C(\mu)=U(\mu,M_W)C(M_W), \tag{7}$$

where $U(\mu,M_W)$ is the QCD evolution matrix:

$$U(\mu,M_W)=\left[1+\frac{\alpha_s(\mu)}{4\pi}J\right]U^0(\mu,M_W)\left[1-\frac{\alpha_s(M_W)}{4\pi}J\right], \tag{8}$$

with J the matrix summarizing the next-to-leading order corrections and $U^0(\mu,M_W)$ the evolution matrix in the leading-logarithm approximation. Since the strong interaction is independent of quark flavor, the $C(\mu)$ are the same for all B decays. At the scale $\mu=m_b=5$ GeV, $C(\mu)$ take the values summarized in Table I [10,11].

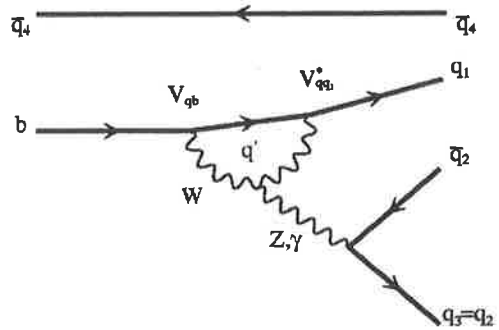

FIG. 4. Electroweak-penguin diagram (coupling between Z, γ, and W) for B decays.

TABLE I. Wilson coefficients to the next-leading order (see the reference in text).

$C_i(\mu)$ for $\mu=5$ GeV			
	C_1	-0.3125	
	C_2	$+1.1502$	
C_3	$+0.0174$	C_5	$+0.0104$
C_4	$+0.0373$	C_6	-0.0459
C_7	-1.050×10^{-5}	C_9	-0.0101
C_8	$+3.839\times10^{-4}$	C_{10}	$+1.959\times10^{-3}$

To be consistent, the matrix elements of the operators, O_i, should also be renormalized to the one-loop order. This results in the effective Wilson coefficients, C_i', which satisfy the constraint

$$C_i(m_b)\langle O_i(m_b)\rangle=C_i'\langle O_i\rangle^{tree}, \tag{9}$$

where $\langle O_i\rangle^{tree}$ are the matrix elements at the tree level. These matrix elements will be evaluated in the factorization approach. From Eq. (9), the relations between C_i' and C_i are [10,11]

$$\begin{aligned} &C_1'=C_1, \quad C_2'=C_2,\\ &C_3'=C_3-P_s/3, \quad C_4'=C_4+P_s,\\ &C_5'=C_5-P_s/3, \quad C_6'=C_6+P_s,\\ &C_7'=C_7+P_e, \quad C_8'=C_8,\\ &C_9'=C_9+P_e, \quad C_{10}'=C_{10}, \end{aligned} \tag{10}$$

where

$$\begin{aligned} P_s&=(\alpha_s/8\pi)C_2[10/9+G(m_c,\mu,q^2)],\\ P_e&=(\alpha_{em}/9\pi)(3C_1+C_2)[10/9+G(m_c,\mu,q^2)], \end{aligned} \tag{11}$$

and

$$G(m_c,\mu,q^2)=4\int_0^1 dx x(x-1)\ln\frac{m_c^2-x(1-x)q^2}{\mu^2}. \tag{12}$$

Here q^2 is the typical momentum transfer of the gluon or photon in the penguin diagrams and $G(m_c,\mu,q^2)$ has the following explicit expression [12]:

TABLE II. Effective Wilson coefficients related to the tree operators, electroweak and QCD penguin operators (see the reference in text).

C_i'	$q^2/m_b^2=0.3$	$q^2/m_b^2=0.5$
C_1'	-0.3125	-0.3125
C_2'	$+1.1502$	$+1.1502$
C_3'	$+2.433\times10^{-2}+1.543\times10^{-3}i$	$+2.120\times10^{-2}+2.174\times10^{-3}i$
C_4'	$-5.808\times10^{-2}-4.628\times10^{-3}i$	$-4.869\times10^{-2}-1.552\times10^{-2}i$
C_5'	$+1.733\times10^{-2}+1.543\times10^{-3}i$	$+1.420\times10^{-2}+5.174\times10^{-3}i$
C_6'	$-6.668\times10^{-2}-4.628\times10^{-3}i$	$-5.729\times10^{-2}-1.552\times10^{-2}i$
C_7'	$-1.435\times10^{-4}-2.963\times10^{-5}i$	$-8.340\times10^{-5}-9.938\times10^{-5}i$
C_8'	$+3.839\times10^{-4}$	$+3.839\times10^{-4}$
C_9'	$-1.023\times10^{-2}-2.963\times10^{-5}i$	$-1.017\times10^{-2}-9.938\times10^{-5}i$
C_{10}'	$+1.959\times10^{-3}$	$+1.959\times10^{-3}$

$$\mathrm{Re}G=\frac{2}{3}\left(\ln\frac{m_c^2}{\mu^2}-\frac{5}{3}-4\frac{m_c^2}{q^2}+\left(1+2\frac{m_c^2}{q^2}\right)\times\sqrt{1-4\frac{m_c^2}{q^2}}\ln\frac{1+\sqrt{1-4\frac{m_c^2}{q^2}}}{1-\sqrt{1-4\frac{m_c^2}{q^2}}}\right), \tag{13}$$

$$\mathrm{Im}G=-\frac{2}{3}\left(1+2\frac{m_c^2}{q^2}\right)\sqrt{1-4\frac{m_c^2}{q^2}}.$$

Based on simple arguments at the quark level, the value of q^2 is chosen in the range $0.3<q^2/m_b^2<0.5$ [3,4]. From Eqs. (10)–(13) we can obtain numerical values for C_i'. These values are listed in Table II, where we have taken $\alpha_s(m_Z)=0.112$, $\alpha_{em}(m_b)=1/132.2$, $m_b=5$ GeV, and $m_c=1.35$ GeV.

C. Effective Hamiltonian

In any phenomenological treatment of the weak decays of hadrons, the starting point is the weak effective Hamiltonian at low energy [13]. It is obtained by integrating out the heavy fields (e.g. the top quark, W and Z bosons) from the standard model Lagrangian. It can be written as,

$$\mathcal{H}_{eff}=\frac{G_F}{\sqrt{2}}\sum_i V_{CKM}C_i(\mu)O_i(\mu), \tag{14}$$

where G_F is the Fermi constant, V_{CKM} is the CKM matrix element (see Sec. III A), $C_i(\mu)$ are the Wilson coefficients (see Sec. II B), $O_i(\mu)$ are the operators from the operator product expansion (see Sec. II A), and μ represents the renormalization scale. We emphasize that the amplitude corresponding to the effective Hamiltonian for a given decay is independent of the scale μ. In the present case, since we analyze direct CP violation in B decays, we take into account both tree and penguin diagrams. For the penguin diagrams, we include all operators O_3 to O_{10}. Therefore, the effective Hamiltonian used will be

$$\mathcal{H}_{eff}^{\Delta B=1}=\frac{G_F}{\sqrt{2}}\left[V_{ub}V_{us}^*(C_1O_1^s+C_2O_2^s)-V_{tb}V_{ts}^*\sum_{i=3}^{10}C_iO_i\right]+\mathrm{H.c.}, \tag{15}$$

and consequently, the decay amplitude can be expressed as follows:

$$A(B\to PV)=\frac{G_F}{\sqrt{2}}\left[V_{ub}V_{us}^*(C_1\langle PV|O_1^s|B\rangle+C_2\langle PV|O_2^s|B\rangle)-V_{tb}V_{ts}^*\sum_{i=3}^{10}C_i\langle PV|O_i|B\rangle\right]+\mathrm{H.c.}, \tag{16}$$

where $\langle PV|O_i|B\rangle$ are the hadronic matrix elements. They describe the transition between the initial state and the final state for scales lower than μ and include, up to now, the main uncertainties in the calculation since they involve nonperturbative effects.

III. *CP* VIOLATION IN $B^{\pm,0}\to\rho^0(\omega)K^{\pm,0}\to\pi^+\pi^-K^{\pm,0}$

Direct CP violation in a decay process requires that the two CP conjugate decay processes have different absolute

values for their amplitudes [14]. Let us start from the usual definition of asymmetry,

$$a(B\to F)=\frac{\Gamma(B\to F)-\Gamma(\bar{B}\to\bar{F})}{\Gamma(B\to F)+\Gamma(\bar{B}\to\bar{F})}, \tag{17}$$

which gives

$$a(B\to F)=\frac{|A(B\to F)|^2-|\bar{A}(\bar{B}\to\bar{F})|^2}{|A(B\to F)|^2+|\bar{A}(\bar{B}\to\bar{F})|^2}, \tag{18}$$

where $A(B\to F)$ is the amplitude for the considered decay, which in general can be written as $A(B\to F)=|A_1|e^{i\delta_1+i\phi_1}+|A_2|e^{i\delta_2+i\phi_2}$. Hence one gets

$$a(B\to F)=\frac{-2|A_1||A_2|\sin(\phi_1-\phi_2)\sin(\delta_1-\delta_2)}{|A_1|^2+2|A_1||A_2|\cos(\phi_1-\phi_2)\cos(\delta_1-\delta_2)+|A_2|^2}. \tag{19}$$

Therefore, in order to obtain direct CP violation, the CP asymmetry parameter a needs a strong phase *difference*, $\delta_1-\delta_2$, coming from the hadronic matrix *and* a weak phase *difference*, $\phi_1-\phi_2$, coming from the CKM matrix.

A. CKM matrix

In phenomenological applications, the widely used CKM matrix parametrization is the *Wolfenstein parametrization* [15]. In this approach, the four independent parameters are λ, A, ρ and η. Then, by expanding each element of the matrix as a power series of the parameter $\lambda=\sin\theta_c=0.2209$ (θ_c is the Gell-Mann–Levy–Cabibbo angle), one gets [$O(\lambda^4)$ is neglected]

$$\hat{V}_{CKM}=\begin{pmatrix} 1-\frac{1}{2}\lambda^2 & \lambda & A\lambda^3(\rho-i\eta) \\ -\lambda & 1-\frac{1}{2}\lambda^2 & A\lambda^2 \\ A\lambda^3(1-\rho-i\eta) & -A\lambda^2 & 1 \end{pmatrix}, \tag{20}$$

where η plays the role of the CP-violating phase. In this parametrization, even though it is an approximation in λ, the CKM matrix satisfies unitarity exactly, which means,

$$\hat{V}^\dagger_{CKM}\cdot\hat{V}_{CKM}=\hat{I}=\hat{V}_{CKM}\cdot\hat{V}^\dagger_{CKM}. \tag{21}$$

B. ρ-ω mixing

In the vector meson dominance model [16], the photon propagator is dressed by coupling to vector mesons. From this, the ρ-ω mixing mechanism [17] was developed. Let A be the amplitude for the decay $B\to\rho^0(\omega)K\to\pi^+\pi^-K$, then one has

$$A=\langle K\pi^-\pi^+|H^T|B\rangle+\langle K\pi^-\pi^+|H^P|B\rangle, \tag{22}$$

with H^T and H^P being the Hamiltonians for the tree and penguin operators. We can define the relative magnitude and phases between these two contributions as follows:

$$\begin{aligned} A&=\langle K\pi^-\pi^+|H^T|B\rangle[1+re^{i\delta}e^{i\phi}], \\ \bar{A}&=\langle\bar{K}\pi^+\pi^-|H^T|\bar{B}\rangle[1+re^{i\delta}e^{-i\phi}], \end{aligned} \tag{23}$$

where δ and ϕ are strong and weak phases, respectively. The phase ϕ arises from the appropriate combination of CKM matrix elements, and $\phi=\arg[(V_{tb}V^*_{ts})/(V_{ub}V^*_{us})]$. As a result, $\sin\phi$ is equal to $\sin\gamma$ with γ defined in the standard way [18]. The parameter, r, is the absolute value of the ratio of tree and penguin amplitudes:

$$r\equiv\left|\frac{\langle\rho^0(\omega)K|H^P|B\rangle}{\langle\rho^0(\omega)K|H^T|B\rangle}\right|. \tag{24}$$

In order to obtain a large signal for direct CP violation, we need some mechanism to make both $\sin\delta$ and r large. We stress that ρ-ω mixing has the dual advantages that the strong phase difference is large (passing through 90° at the ω resonance) and well known [4,5]. With this mechanism, to first order in isospin violation, we have the following results when the invariant mass of $\pi^+\pi^-$ is near the ω resonance mass:

$$\begin{aligned} \langle K\pi^-\pi^+|H^T|B\rangle&=\frac{g_\rho}{s_\rho s_\omega}\tilde{\Pi}_{\rho\omega}t_\omega+\frac{g_\rho}{s_\rho}t_\rho, \\ \langle K\pi^-\pi^+|H^P|B\rangle&=\frac{g_\rho}{s_\rho s_\omega}\tilde{\Pi}_{\rho\omega}p_\omega+\frac{g_\rho}{s_\rho}p_\rho. \end{aligned} \tag{25}$$

Here t_V ($V=\rho$ or ω) is the tree amplitude and p_V the penguin amplitude for producing a vector meson, V, g_ρ is the coupling for $\rho^0\to\pi^+\pi^-$, $\tilde{\Pi}_{\rho\omega}$ is the effective ρ-ω mixing amplitude, and s_V is from the inverse propagator of the vector meson V,

$$s_V=s-m_V^2+im_V\Gamma_V, \tag{26}$$

with $\sqrt{s}$ being the invariant mass of the $\pi^+\pi^-$ pair. We stress that the direct coupling $\omega\to\pi^+\pi^-$ is effectively absorbed into $\tilde{\Pi}_{\rho\omega}$ [19], leading to the explicit s dependence of $\tilde{\Pi}_{\rho\omega}$. Making the expansion $\tilde{\Pi}_{\rho\omega}(s)=\tilde{\Pi}_{\rho\omega}(m_\omega^2)+(s-m_\omega^2)\tilde{\Pi}'_{\rho\omega}(m_\omega^2)$, the ρ-ω mixing parameters were determined in the fit of Gardner and O'Connell [20]: $\Re e\tilde{\Pi}_{\rho\omega}(m_\omega^2)=-3500\pm300$ MeV^2, $\Im m\tilde{\Pi}_{\rho\omega}(m_\omega^2)=-300\pm300$ MeV^2, and $\tilde{\Pi}'_{\rho\omega}(m_\omega^2)=0.03\pm0.04$. In practice, the effect of the derivative term is negligible. From Eqs. (22), (25) one has

$$re^{i\delta}e^{i\phi}=\frac{\tilde{\Pi}_{\rho\omega}p_\omega+s_\omega p_\rho}{\tilde{\Pi}_{\rho\omega}t_\omega+s_\omega t_\rho}. \tag{27}$$

Defining

$$\frac{p_\omega}{t_\rho}\equiv r' e^{i(\delta_q+\phi)}, \quad \frac{t_\omega}{t_\rho}\equiv \alpha e^{i\delta_\alpha}, \quad \frac{p_\rho}{p_\omega}\equiv \beta e^{i\delta_\beta}, \tag{28}$$

where $\delta_\alpha, \delta_\beta$ and δ_q are strong phases (absorptive part). Substituting Eq. (28) into Eq. (27), one finds

$$re^{i\delta}=r' e^{i\delta_q}\frac{\tilde{\Pi}_{\rho\omega}+\beta e^{i\delta_\beta} s_\omega}{s_\omega+\tilde{\Pi}_{\rho\omega}\alpha e^{i\delta_\alpha}}, \tag{29}$$

where

$$\alpha e^{i\delta_\alpha}=f, \quad \beta e^{i\delta_\beta}=b+ci, \quad r' e^{i\delta_q}=d+ei, \tag{30}$$

and using Eq. (29), we obtain the following result when $\sqrt{s}\sim m_\omega$:

$$re^{i\delta}=\frac{C+iD}{(s-m_\omega^2+f\Re e\tilde{\Pi}_{\rho\omega})^2+(f\Im m\tilde{\Pi}_{\rho\omega}+m_\omega\Gamma_\omega)^2}. \tag{31}$$

Here C and D are defined as

$$\begin{aligned}C=&(s-m_\omega^2+f\Re e\tilde{\Pi}_{\rho\omega})\{d[\Re e\tilde{\Pi}_{\rho\omega}+b(s-m_\omega^2)-cm_\omega\Gamma_\omega]\\&-e[\Im m\tilde{\Pi}_{\rho\omega}+bm_\omega\Gamma_\omega+c(s-m_\omega^2)]\}\\&+(f\Im m\tilde{\Pi}_{\rho\omega}+m_\omega\Gamma_\omega)\{e[\Re e\tilde{\Pi}_{\rho\omega}+b(s-m_\omega^2)-cm_\omega\Gamma_\omega]\\&+d[\Im m\tilde{\Pi}_{\rho\omega}+bm_\omega\Gamma_\omega+c(s-m_\omega^2)]\},\end{aligned} \tag{32}$$

and

$$\begin{aligned}D=&(s-m_\omega^2+f\Re e\tilde{\Pi}_{\rho\omega})\{e[\Re e\tilde{\Pi}_{\rho\omega}+d(s-m_\omega^2)-cm_\omega\Gamma_\omega]\\&+d[\Im m\tilde{\Pi}_{\rho\omega}+bm_\omega\Gamma_\omega+c(s-m_\omega^2)]\}\\&-(f\Im m\tilde{\Pi}_{\rho\omega}+m_\omega\Gamma_\omega)\{d[\Re e\tilde{\Pi}_{\rho\omega}+b(s-m_\omega^2)-cm_\omega\Gamma_\omega]\\&-e[\Im m\tilde{\Pi}_{\rho\omega}+bm_\omega\Gamma_\omega+c(s-m_\omega^2)]\}.\end{aligned} \tag{33}$$

$\alpha e^{i\delta_\alpha}$, $\beta e^{i\delta_\beta}$, and $r' e^{i\delta_q}$ will be calculated later. In order to get the CP violating asymmetry, a, $\sin\phi$ and $\cos\phi$ are needed, where ϕ is determined by the CKM matrix elements. In the Wolfenstein parametrization [15], the weak phase comes from $[V_{tb}V_{ts}^*/V_{ub}V_{us}^*]$ and one has for the decay $B\to\rho^0(\omega)K$,

$$\sin\phi=\frac{-\eta}{\sqrt{\rho^2+\eta^2}}, \quad \cos\phi=\frac{-\rho}{\sqrt{\rho^2+\eta^2}}. \tag{34}$$

The values used for ρ and η will be discussed in Sec. IV A.

C. Factorization

With the Hamiltonian given in Eq. (15) (see Sec. II C), we are ready to evaluate the matrix elements for $B^{\pm,0}\to\rho^0(\omega)K^{\pm,0}$. In the factorization approximation [21], either $\rho^0(\omega)$ or $K^{\pm,0}$ is generated by one current which has the appropriate quantum numbers in the Hamiltonian. For these decay processes, two kinds of matrix element products are involved after factorization (i.e. omitting Dirac matrices and color labels): $\langle\rho^0(\omega)|(\bar{u}u)|0\rangle\langle K^{\pm,0}|(\bar{s}b)|B^{\pm,0}\rangle$ and $\langle K^{\pm,0}|(\bar{q}_1q_2)|0\rangle\langle\rho^0(\omega)|(\bar{u}b)|B^{\pm,0}\rangle$, where q_1 and q_2 could be u, s or d. We will calculate them in several phenomenological quark models.

The matrix elements for $B\to X$ and $B\to X^*$ (where X and X^* denote pseudoscalar and vector mesons, respectively) can be decomposed as follows [22]:

$$\begin{aligned}\langle X|J_\mu|B\rangle=&\left(p_B+p_X-\frac{m_B^2-m_X^2}{k^2}k\right)_\mu F_1(k^2)\\&+\frac{m_B^2-m_X^2}{k^2}k_\mu F_0(k^2),\end{aligned} \tag{35}$$

and

$$\begin{aligned}\langle X^*|J_\mu|B\rangle=&\frac{2}{m_B+m_{X^*}}\epsilon_{\mu\nu\rho\sigma}\epsilon^{*\nu}p_B^\rho p_{X^*}^\sigma V(k^2)\\&+i\left\{\epsilon_\mu^*(m_B+m_{X^*})A_1(k^2)-\frac{\epsilon^*\cdot k}{m_B+m_{X^*}}\right.\\&\left.\times(P_B+P_{X^*})_\mu A_2(k^2)-\frac{\epsilon^*\cdot k}{k^2}2m_{X^*}\cdot k_\mu A_3(k^2)\right\}\\&+i\frac{\epsilon^*\cdot k}{k^2}2m_{X^*}\cdot k_\mu A_0(k^2),\end{aligned} \tag{36}$$

where J_μ is the weak current, defined as $J_\mu=\bar{q}\gamma^\mu(1-\gamma_5)b$ with $q=u,d,s$ and $k=p_B-p_{X(X^*)}$. ϵ_μ is the polarization vector of X^*. F_0 and F_1 are the form factors related to the transition $0^-\to0^-$, while A_0, A_1, A_2, A_3 and V are the form factors that describe the transition $0^-\to1^-$. Finally, in order to cancel the poles at $q^2=0$, the form factors respect the conditions

$$F_1(0)=F_0(0), \quad A_3(0)=A_0(0), \tag{37}$$

and they also satisfy the following relations:

$$A_3(k^2)=\frac{m_B+m_{X^*}}{2m_{X^*}}A_1(k^2)-\frac{m_B-m_{X^*}}{2m_{X^*}}A_2(k^2). \tag{38}$$

An argument for factorization has been given by Bjorken [23]: the heavy quark decays are very energetic, so the quark-antiquark pair in a meson in a final state moves very fast away from the localized weak interaction. The hadronization of the quark-antiquark pair occurs far away from the

remaining quarks. Then, the meson can be factorized out and the interaction between the quark pair in the meson and the remaining quark should be tiny.

In the evaluation of matrix elements, the effective number of colors, N_c^{eff}, enters through a Fierz transformation. In general, for operator O_i, one can write

$$\frac{1}{(N_c^{eff})_i}=\frac{1}{3}+\xi_i \quad \text{with} \quad i=1,\ldots,10, \tag{39}$$

where ξ_i describes non-factorizable effects. We assume ξ_i is universal for all the operators O_i. We also ignore the final state interactions (FSI). After factorization, and using the decomposition in Eqs. (35),(36), one obtains, for the process $\bar{B}^0\to\rho^0(\omega)\bar{K}^0$,

$$t_\rho=m_B|\vec{p}_\rho|\left(C_1'+\frac{1}{N_c}C_2'\right)f_\rho F_1(m_\rho^2), \tag{40}$$

where f_ρ is the ρ decay constant [and to simplify the formulas we use N_c for N_c^{eff} in Eqs. (40)–(50)]. In the same way, we find $t_\omega=t_\rho$, so that

$$\alpha e^{i\delta_\alpha}=1. \tag{41}$$

After calculating the penguin operator contributions, one has

$$r'e^{i\delta_q}=-\frac{p_\omega}{\left(C_1'+\frac{1}{N_c}C_2'\right)f_\rho F_1(m_\rho^2)}\left|\frac{V_{tb}V_{ts}^*}{V_{ub}V_{us}^*}\right|, \tag{42}$$

and

$$\beta e^{i\delta_\beta}=\frac{m_B|\vec{p}_\rho|}{p_\omega}\left(\frac{3}{2}\left[\left(C_7'+\frac{1}{N_c}C_8'\right)+\left(C_9'+\frac{1}{N_c}C_{10}'\right)\right]f_\rho F_1(m_\rho^2)+\left\{\left(C_4'+\frac{1}{N_c}C_3'\right)-\frac{1}{2}\left(C_{10}'+\frac{1}{N_c}C_9'\right)\right.$$
$$\left.+\left[-2\left(C_6'+\frac{1}{N_c}C_5'\right)+\left(C_8'+\frac{1}{N_c}C_7'\right)\right]\left[\frac{m_K^2}{(m_b+m_d)(m_d+m_s)}\right]\right\}f_K A_0(m_K^2)\Bigg), \tag{43}$$

where f_K is the K decay constant. In Eqs. (42), (43), p_ω has the following form:

$$p_\omega=m_B|\vec{p}_\rho|\left\{2\left[\left(C_3'+\frac{1}{N_c}C_4'\right)+\left(C_5'+\frac{1}{N_c}C_6'\right)\right]f_\rho F_1(m_\rho^2)+\frac{1}{2}\left[\left(C_7'+\frac{1}{N_c}C_8'\right)+\left(C_9'+\frac{1}{N_c}c_{10}'\right)\right]f_\rho F_1(m_\rho^2)\right.$$
$$\left.+\left[\left(C_8'+\frac{1}{N_c}C_7'\right)-2\left(C_6'+\frac{1}{N_c}C_5'\right)\right]\left[\frac{m_K^2 f_K A_0(m_K^2)}{(m_b+m_d)(m_d+m_s)}\right]+\left[\left(C_4'+\frac{1}{N_c}C_3'\right)-\frac{1}{2}\left(C_{10}'+\frac{1}{N_c}C_9'\right)\right]f_K A_0(m_K^2)\right\}, \tag{44}$$

and the CKM amplitude entering the $b\to s$ transition is

$$\left|\frac{V_{tb}V_{ts}^*}{V_{ub}V_{us}^*}\right|=\frac{1}{\lambda^2}\frac{1}{\sqrt{\rho^2+\eta^2}}=\frac{1}{\lambda^2}\frac{1}{|\sin\beta|}, \tag{45}$$

with β defined as the unitarity triangle as usual. Similarly, by applying the same formalism, one gets for the decay $B^-\to\rho^0(\omega)K^-$,

$$t_\rho=m_B|\vec{p}_\rho|\left[\left(C_1'+\frac{1}{N_c}C_2'\right)f_\rho F_1(m_\rho^2)+\left(C_2'+\frac{1}{N_c}C_1'\right)f_K A_0(m_K^2)\right]. \tag{46}$$

In the same way, we find $t_\omega=t_\rho$, therefore one has, again,

$$\alpha e^{i\delta_\alpha}=1. \tag{47}$$

The ratio between penguin and tree operator contributions, which involves CKM matrix elements, is given by

$$r' e^{i\delta_q} = -\frac{p_\omega}{\left(C_1' + \frac{1}{N_c}C_2'\right) f_\rho F_1(m_\rho^2) + \left(C_2' + \frac{1}{N_c}C_1'\right) f_K A_0(m_K^2)} \left|\frac{V_{tb}V_{ts}^*}{V_{ub}V_{us}^*}\right|, \tag{48}$$

and finally,

$$\beta e^{i\delta_\beta} = \frac{m_B|\vec{p}_\rho|}{p_\omega}\left\{\left(C_4' + \frac{1}{N_c}C_3'\right) f_K A_0(m_K^2) + \frac{3}{2}\left[\left(C_7' + \frac{1}{N_c}C_8'\right) + \left(C_9' + \frac{1}{N_c}C_{10}'\right)\right] f_\rho F_1(m_\rho^2) + \left(C_{10}' + \frac{1}{N_c}C_9'\right) f_K A_0(m_K^2) - 2\left[\left(C_6' + \frac{1}{N_c}C_5'\right) + \left(C_8' + \frac{1}{N_c}C_7'\right)\right]\left[\frac{m_K^2 f_K A_0(m_K^2)}{(m_u + m_s)(m_b + m_u)}\right]\right\}, \tag{49}$$

where the ω penguin operator contribution, p_ω, is

$$p_\omega = m_B|\vec{p}_\rho|\left\{2\left[\left(C_3' + \frac{1}{N_c}C_4'\right) + \left(C_5' + \frac{1}{N_c}C_6'\right)\right] f_\rho F_1(m_\rho^2) + \frac{1}{2}\left[\left(C_7' + \frac{1}{N_c}C_8'\right) + \left(C_9' + \frac{1}{N_c}C_{10}'\right)\right] f_\rho F_1(m_\rho^2) + \left[\left(C_4' + \frac{1}{N_c}C_3'\right) + \left(C_{10}' + \frac{1}{N_c}C_9'\right)\right] f_K A_0(m_K^2) - 2\left[\left(C_8' + \frac{1}{N_c}C_7'\right) + \left(C_6' + \frac{1}{N_c}C_5'\right)\right]\left[\frac{m_K^2}{(m_u + m_s)(m_b + m_u)}\right] f_K A_0(m_K^2)\right\}. \tag{50}$$

D. Form factors

The form factors $F_i(k^2)$ and $A_j(k^2)$ depend on the inner structure of the hadrons. We will adopt here three different theoretical approaches. The first was proposed by Bauer, Stech, and Wirbel (BSW) [22], who used the overlap integrals of wave functions in order to evaluate the meson-meson matrix elements of the corresponding current. The momentum dependence of the form factors is based on a single-pole ansatz. The second one was developed by Guo and Huang (GH) [24]. They modified the BSW model by using some wave functions described in the light-cone framework. The last model was given by Ball [25] and Ball and Braun [26]. In this case, the form factors are calculated from QCD sum rules on the light-cone and leading twist contributions, radiative corrections, and $SU(3)$-breaking effects are included. Nevertheless, all these models use phenomenological form factors which are parametrized by making the nearest pole dominance assumption. The explicit k^2 dependence of the form factor is as [22,24–27]:

$$F_1(k^2) = \frac{h_1}{\left(1 - \frac{k^2}{m_1^2}\right)^n},$$

$$A_0(k^2) = \frac{h_{A_0}}{\left(1 - \frac{k^2}{m_{A_0}^2}\right)^n},$$

or

$$F_1(k^2) = \frac{h_1}{1 - d_1\frac{k^2}{m_B^2} + b_1\left(\frac{k^2}{m_B^2}\right)^2},$$

$$A_0(k^2) = \frac{h_{A_0}}{1 - d_0\frac{k^2}{m_B^2} + b_0\left(\frac{k^2}{m_B^2}\right)^2}, \tag{51}$$

where $n = 1,2$, m_{A_0} and m_1 are the pole masses associated with the transition current, h_1 and h_{A_0} are the values of form factors at $q^2 = 0$, and d_i and b_i $(i = 0,1)$ are parameters in the model of Ball.

IV. NUMERICAL INPUTS

A. CKM values

In our numerical calculations we have several parameters: q^2, N_c, and the CKM matrix elements in the Wolfenstein parametrization. As mentioned in Sec. II B, the value of q^2 is conventionally chosen to be in the range $0.3 < q^2/m_b^2 < 0.5$. The CKM matrix, which should be determined from experi-

TABLE III. Values of the CKM unitarity triangle for limiting values of the CKM matrix elements.

	α	β	γ
(ρ_{min}, η_{min})	104°47	19°32	56°21
(ρ_{min}, η_{max})	93°13	24°31	62°56
(ρ_{max}, η_{min})	112°14	21°20	46°66
(ρ_{max}, η_{max})	99°66	26°56	53°78

TABLE IV. Form factor values for $B\to\rho$ and $B\to K$ at $q^2=0$ (see the reference in text).

	h_{A_0}	h_1	m_{A_0}	m_1	$d_0(d_1)$	$b_0(b_1)$
model (1)	0.280	0.360	5.27	5.41		
model (2)	0.340	0.762	5.27	5.41		
model (3)	0.280	0.360	5.27	5.41		
model (4)	0.340	0.762	5.27	5.41		
model (5)	0.372	0.341			1.400(0.410)	0.437(−0.361)

mental data, is expressed in terms of the Wolfenstein parameters, A, λ, ρ, and η [15]. Here, we shall use the latest values [28] which were extracted from charmless semileptonic B decays, ($|V_{ub}|$), charm semileptonic B decays, ($|V_{cb}|$), s and d mass oscillations, Δm_s, Δm_d, and CP violation in the kaon system (ϵ_K),(ρ,η). Hence, one has

$$\lambda=0.2237,\ A=0.8113,\ 0.190<\rho<0.268,\qquad 0.284<\eta<0.366. \tag{52}$$

These values respect the unitarity triangle as well (see also Table III).

B. Quark masses

The running quark masses are used in order to calculate the matrix elements of penguin operators. The quark mass is taken at the scale $\mu\simeq m_b$ in B decays. Therefore one has [29]

$$m_u(\mu=m_b)=2.3\ \text{MeV},\quad m_d(\mu=m_b)=4.6\ \text{MeV},\qquad m_s(\mu=m_b)=90\ \text{MeV},\quad m_b(\mu=m_b)=4.9\ \text{GeV}, \tag{53}$$

which corresponds to $m_s(\mu=1\ \text{GeV})=140$ MeV. For meson masses, we shall use the following values [18]:

$$m_{B^\pm}=5.279\ \text{GeV},\quad m_{B^0}=5.279\ \text{GeV},\qquad m_{K^\pm}=0.493\ \text{GeV},\quad m_{K^0}=0.497\ \text{GeV},\qquad m_{\pi^\pm}=0.139\ \text{GeV},\quad m_{\pi^0}=0.135\ \text{GeV},\qquad m_{\rho^0}=0.769\ \text{GeV},\quad m_\omega=0.782\ \text{GeV}. \tag{54}$$

C. Form factors and decay constants

In Table IV we list the relevant form factor values at zero momentum transfer [22,24–26,30] for the $B\to K$ and $B\to\rho$ transitions. The different models are defined as follows: models (1) and (3) are the BSW model where the q^2 dependence of the form factors is described by a single- and a double-pole ansatz, respectively. Models (2) and (4) are the GH model with the same momentum dependence as models (1) and (3). Finally, model (5) refers to the Ball model. We define the decay constants for pseudo-scalar (f_P) and vector (f_V) mesons as usual by,

$$\langle P(q)|\bar q_1\gamma_\mu\gamma_5 q_2|0\rangle=if_P q_\mu,\qquad \sqrt{2}\langle V(q)|\bar q_1\gamma_\mu q_2|0\rangle=f_V m_V\epsilon_V, \tag{55}$$

with q_μ being the momentum of the pseudo-scalar meson, m_V and ϵ_V being the mass and polarization vector of the vector meson, respectively. Numerically, in our calculations, we take [18],

$$f_K=160\ \text{MeV},\quad f_\rho\simeq f_\omega=221\ \text{MeV}. \tag{56}$$

The ρ and ω decay constants are very close and for simplification (without any consequences for results) we choose $f_\rho=f_\omega$.

V. RESULTS AND DISCUSSION

We have investigated the CP violating asymmetry, a, for the two B decays: $\bar B^0\to\rho^0\bar K^0\to\pi^+\pi^-\bar K^0$ and $B^-\to\rho^0K^-\to\pi^+\pi^-K^-$. The results are shown in Figs. 5 and 6 for $\bar B^0\to\pi^+\pi^-\bar K^0$, ($a=[\Gamma(\bar B^0\to\pi^+\pi^-\bar K^0)-\Gamma(B^0\to\pi^-\pi^+K^0)]/[\Gamma(\bar B^0\to\pi^+\pi^-\bar K^0)+\Gamma(B^0\to\pi^-\pi^+K^0)]$), where $k^2/m_b^2=0.3(0.5)$ and for N_c^{eff} equal to 0.61, 0.66, 2.65, 2.69, 2.82 and 2.84. Similarly, in Figs. 7 and 8, the CP violating asymmetry, a, ($=[\Gamma(B^-\to\pi^+\pi^-K^-)-\Gamma(B^+\to\pi^-\pi^+K^+)]/[\Gamma(B^-\to\pi^+\pi^-K^-)+\Gamma(B^+\to\pi^-\pi^+K^+)]$), is plotted for $B^-\to\pi^+\pi^-K^-$, where $k^2/m_b^2=0.3(0.5)$ and for the same values of N_c^{eff} previously applied for $\bar B^0\to\pi^+\pi^-\bar K^0$. In our numerical calculations,

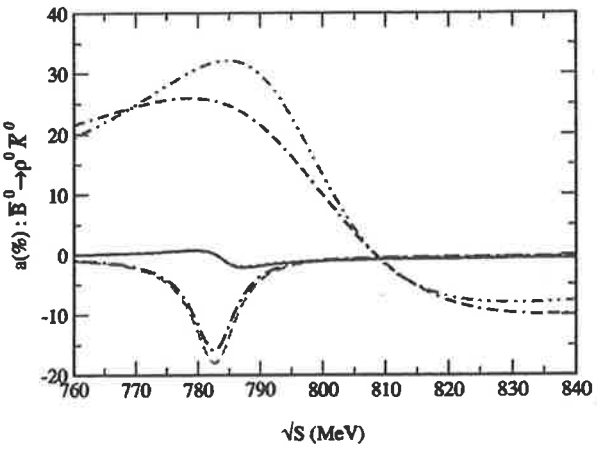

FIG. 5. CP violating asymmetry, a, for $\bar B^0\to\pi^+\pi^-\bar K^0$, for $k^2/m_b^2=0.3$, for $N_c^{eff}=0.66,2.69,2.84$ and for limiting values, max (min), of the CKM matrix elements for model (1): dot-dot-dashed line (dot-dash-dashed line) for $N_c^{eff}=0.66$. Solid line (dotted line) for $N_c^{eff}=2.69$. Dashed line (dot-dashed line) for $N_c^{eff}=2.84$.

TABLE IV. Form factor values for $B\to\rho$ and $B\to K$ at $q^2=0$ (see the reference in text).

	h_{A_0}	h_1	m_{A_0}	m_1	$d_0(d_1)$	$b_0(b_1)$
model (1)	0.280	0.360	5.27	5.41		
model (2)	0.340	0.762	5.27	5.41		
model (3)	0.280	0.360	5.27	5.41		
model (4)	0.340	0.762	5.27	5.41		
model (5)	0.372	0.341			1.400(0.410)	0.437(−0.361)

mental data, is expressed in terms of the Wolfenstein parameters, A, λ, ρ, and η [15]. Here, we shall use the latest values [28] which were extracted from charmless semileptonic B decays, ($|V_{ub}|$), charm semileptonic B decays, ($|V_{cb}|$), s and d mass oscillations, Δm_s, Δm_d, and CP violation in the kaon system (ϵ_K),(ρ,η). Hence, one has

$$\lambda=0.2237,\quad A=0.8113,\quad 0.190<\rho<0.268,\qquad 0.284<\eta<0.366. \tag{52}$$

These values respect the unitarity triangle as well (see also Table III).

B. Quark masses

The running quark masses are used in order to calculate the matrix elements of penguin operators. The quark mass is taken at the scale $\mu\simeq m_b$ in B decays. Therefore one has [29]

$$m_u(\mu=m_b)=2.3\ \text{MeV},\quad m_d(\mu=m_b)=4.6\ \text{MeV},\qquad m_s(\mu=m_b)=90\ \text{MeV},\quad m_b(\mu=m_b)=4.9\ \text{GeV}, \tag{53}$$

which corresponds to $m_s(\mu=1\ \text{GeV})=140$ MeV. For meson masses, we shall use the following values [18]:

$$m_{B^\pm}=5.279\ \text{GeV},\quad m_{B^0}=5.279\ \text{GeV},\qquad m_{K^\pm}=0.493\ \text{GeV},\quad m_{K^0}=0.497\ \text{GeV},\qquad m_{\pi^\pm}=0.139\ \text{GeV},\quad m_{\pi^0}=0.135\ \text{GeV},\qquad m_{\rho^0}=0.769\ \text{GeV},\quad m_\omega=0.782\ \text{GeV}. \tag{54}$$

C. Form factors and decay constants

In Table IV we list the relevant form factor values at zero momentum transfer [22,24–26,30] for the $B\to K$ and $B\to\rho$ transitions. The different models are defined as follows: models (1) and (3) are the BSW model where the q^2 dependence of the form factors is described by a single- and a double-pole ansatz, respectively. Models (2) and (4) are the GH model with the same momentum dependence as models (1) and (3). Finally, model (5) refers to the Ball model. We define the decay constants for pseudo-scalar (f_P) and vector (f_V) mesons as usual by,

$$\langle P(q)|\bar q_1\gamma_\mu\gamma_5 q_2|0\rangle=if_P q_\mu,\qquad \sqrt{2}\langle V(q)|\bar q_1\gamma_\mu q_2|0\rangle=f_V m_V\epsilon_V, \tag{55}$$

with q_μ being the momentum of the pseudo-scalar meson, m_V and ϵ_V being the mass and polarization vector of the vector meson, respectively. Numerically, in our calculations, we take [18],

$$f_K=160\ \text{MeV},\quad f_\rho\simeq f_\omega=221\ \text{MeV}. \tag{56}$$

The ρ and ω decay constants are very close and for simplification (without any consequences for results) we choose $f_\rho=f_\omega$.

V. RESULTS AND DISCUSSION

We have investigated the CP violating asymmetry, a, for the two B decays: $\bar B^0\to\rho^0\bar K^0\to\pi^+\pi^-\bar K^0$ and $B^-\to\rho^0K^-\to\pi^+\pi^-K^-$. The results are shown in Figs. 5 and 6 for $\bar B^0\to\pi^+\pi^-\bar K^0$, ($a=[\Gamma(\bar B^0\to\pi^+\pi^-\bar K^0)-\Gamma(B^0\to\pi^-\pi^+K^0)]/[\Gamma(\bar B^0\to\pi^+\pi^-\bar K^0)+\Gamma(B^0\to\pi^-\pi^+K^0)]$), where $k^2/m_b^2=0.3(0.5)$ and for N_c^{eff} equal to 0.61, 0.66, 2.65, 2.69, 2.82 and 2.84. Similarly, in Figs. 7 and 8, the CP violating asymmetry, a, ($=[\Gamma(B^-\to\pi^+\pi^-K^-)-\Gamma(B^+\to\pi^-\pi^+K^+)]/[\Gamma(B^-\to\pi^+\pi^-K^-)+\Gamma(B^+\to\pi^-\pi^+K^+)]$), is plotted for $B^-\to\pi^+\pi^-K^-$, where $k^2/m_b^2=0.3(0.5)$ and for the same values of N_c^{eff} previously applied for $\bar B^0\to\pi^+\pi^-\bar K^0$. In our numerical calculations,

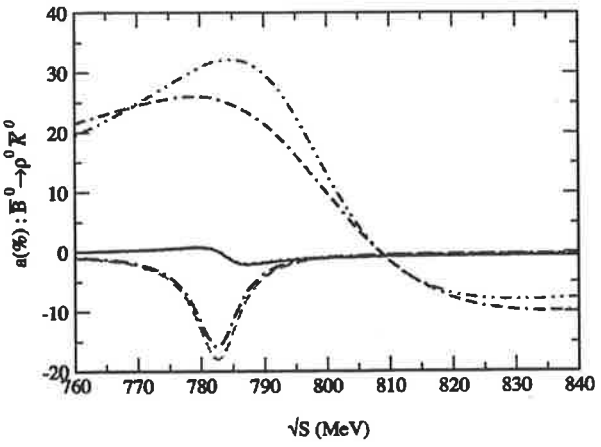

FIG. 5. CP violating asymmetry, a, for $\bar B^0\to\pi^+\pi^-\bar K^0$, for $k^2/m_b^2=0.3$, for $N_c^{eff}=0.66,2.69,2.84$ and for limiting values, max (min), of the CKM matrix elements for model (1): dot-dot-dashed line (dot-dash-dashed line) for $N_c^{eff}=0.66$. Solid line (dotted line) for $N_c^{eff}=2.69$. Dashed line (dot-dashed line) for $N_c^{eff}=2.84$.

TABLE VI. Maximum CP violating asymmetry $a_{max}(\%)$ for $B^-\to\pi^+\pi^-K^-$ for all models, limiting values of the CKM matrix elements (upper and lower limit), and for $k^2/m_b^2=0.3(0.5)$.

	$N_{cmin}^{eff}=0.66(0.61)$	$N_{cmax}^{eff}=2.84(2.82)$
model (1)		
ρ_{max},η_{max}	47(45)	$-15(-17)$
ρ_{min},η_{min}	34(35)	$-21(-23)$
model (2)		
ρ_{max},η_{max}	45(41)	$-11(-13)$
ρ_{min},η_{min}	33(32)	$-17(-18)$
model (3)		
ρ_{max},η_{max}	47(44)	$-15(-17)$
ρ_{min},η_{min}	34(35)	$-20(-23)$
model (4)		
ρ_{max},η_{max}	45(42)	$-12(-13)$
ρ_{min},η_{min}	33(32)	$-17(-18)$
model (5)		
ρ_{max},η_{max}	49(46)	$-17(-19)$
ρ_{min},η_{min}	36(35)	$-22(-25)$

(ρ,η) is around 1.26(1.37). If we consider the maximum asymmetry parameter, a_{max}, for $N_{cmax}^{eff}=2.84(2.82)$, we observe a distinction between the models. Indeed, two classes of models appear: models (2) and (4) and models (1), (3) and (5). For models (2) and (4), one has an asymmetry, a_{max}, around $-6\%(-7\%)$ and around $-9\%(-10\%)$ for the upper and lower set of (ρ,η), respectively. The ratio between them is around 1.50(1.42). For models (1), (3) and (5), the maximum asymmetry is of order -14.3% (-16.3%) for (ρ_{max},η_{max}) and around -19.3% (-23.0%) for (ρ_{min},η_{min}). In this case, the ratio between asymmetries is around 1.34(1.41).

The first reason why the maximum asymmetry, a_{max}, can vary so much comes from the element V_{ub}. The other CKM matrix elements V_{tb}, V_{ts} and V_{us}, all proportional to A and λ, are very well measured experimentally and thus do not interfere in our results. Only V_{ub}, which contains the ρ and η parameters, provides large uncertainties, and thus, large variations for the maximum asymmetry. The second reason is the non-factorizable effects in the transition $b\to s$. It is well known that decays including a K meson (and therefore an s quark) carry more uncertainties than those involving only a π meson (u, d quarks). If we look at the asymmetries at N_{cmin}^{eff}, all models give almost the same values, whereas at N_{cmax}^{eff}, we obtain different asymmetry values (with, moreover, a change of sign for the CP violating asymmetry). The CP asymmetry parameter is more sensitive to form factors at high values of N_c^{eff} than at low values of N_c^{eff}. It appears therefore that all of the models investigated can be divided in two classes, referring to the two classes of form factors.

For $B^-\to\pi^+\pi^-K^-$, we have similarly investigated the CP violating asymmetry. The values of maximum asymmetry parameter, a_{max}, for a range of N_c^{eff} from 0.66(0.61) to 2.84(2.82), where $k^2/m_b^2=0.3(0.5)$ and for the five models analyzed, are given in Table VI. We found that for this decay, the CP violating parameter, a, takes values around 49%(46%) to $-22\%(-25\%)$ for the limiting CKM matrix values of ρ and η defined before. Once again, the sign of the asymmetry parameter, a, is positive if the value of N_c stays below 2.7. If we focus on N_{cmin}^{eff} equal to 0.66(0.61), models (1), (2), (3), (4) and (5) give almost the same value which is around 46.6%(43.6%) for the maximum values of the CKM matrix elements. For the set (ρ_{min},η_{min}), the maximum asymmetry, a, is around 34.0%(33.8%). The ratio between asymmetry values taken at upper and lower limiting ρ and η values is around 1.37(1.28). Let us have a look at the CP asymmetry values at N_{cmax}^{eff}. As we observed for the decay $\bar{B}^0\to\pi^+\pi^-\bar{K}^0$, all models are separated into two distinct classes related to their form factors. For models (1), (3) and (5), the value of maximum asymmetry, a_{max}, is around $-15.6\%(-17.6\%)$ and around $-21\%(-23.6\%)$ for the maximum and minimum values of set (ρ,η), respectively. The calculated ratio is around 1.34(1.34), between these two asymmetries. As regards models (2) and (4), for the same set of (ρ,η), one gets $-11.5\%(-13\%)$ and -17% (-18%). In this case, one has 1.47(1.38) for the ratio. The reasons for the differences between the maximum asymmetry parameter, a_{max}, are the same as in the decay $\bar{B}^0\to\pi^+\pi^-\bar{K}^0$.

By analyzing the B decays, such as $\bar{B}^0\to\pi^+\pi^-\bar{K}^0$ and $B^-\to\pi^+\pi^-K^-$, we found that the CP violating asymmetry, a, depends on the CKM matrix elements, form factors and the effective parameter N_c^{eff} (in order of increasing dependence). As regards the CKM matrix elements, the dependence through the element, V_{ub}, contributes to the asymmetry in the ratio between the ω penguin contributions and the ρ tree contributions. It also appears that for the upper limit of set (ρ,η), we get the higher value asymmetry, a, and vice versa. With regard to the form factors, the dependence at low values of N_c^{eff} is very weak although the huge difference between the phenomenological form factors [models (2) and (4) and models (1), (3) and (5)] applied in our calculations. At high values of N_c^{eff} the dependence becomes strong and then, the asymmetry appears very sensitive to form factors. For the effective parameter, N_c^{eff} (related to hadronic non-factorizable effects), our results show explicitly the dependence of the asymmetry parameter on it. Because of the energy carried by the quark s, intermediate states and final state interactions are not well taken into account and may explain this strong sensitivity. Finally, results obtained at $k^2/m_b^2=0.3(0.5)$ also show renormalization effects of the Wilson coefficients involved in the weak effective hadronic Hamiltonian. For the ratio between asymmetries, results give an average value of order 1.36(1.40) for $\bar{B}^0\to\pi^+\pi^-\bar{K}^0$ and 1.39(1.33) for $B^-\to\pi^+\pi^-K^-$. This ratio is mainly governed by the term $1/\sin\beta$, where the values of the angles α, β and γ are listed in Table III.

As a first conclusion on these numerical results, it is obvious that the dependence of the asymmetry on the effective

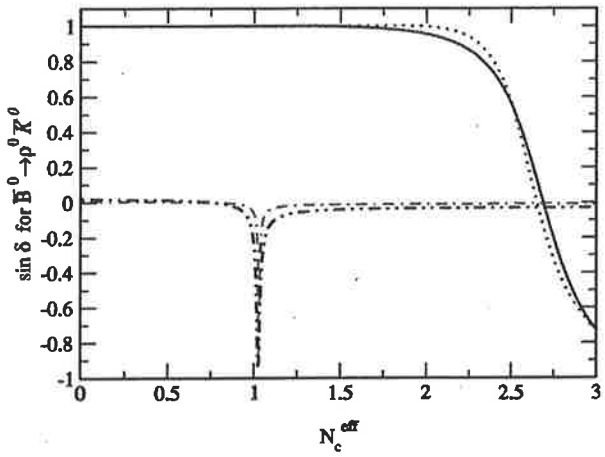

FIG. 9. $\sin\delta$, as a function of N_c^{eff}, for $\bar{B}^0 \to \pi^+\pi^-\bar{K}^0$, for $k^2/m_B^2 = 0.3(0.5)$ and for model (1). The solid (dotted) line at $\sin\delta = +1$ corresponds to the case $\tilde{\Pi}_{\rho\omega} = (-3500; -300)$, where ρ-ω mixing is included. The dot-dashed (dot-dot-dashed) line corresponds to $\tilde{\Pi}_{\rho\omega} = (0;0)$, where ρ-ω mixing is not included.

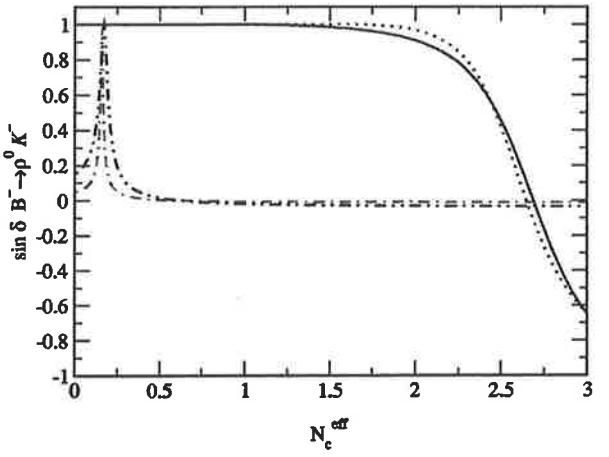

FIG. 10. $\sin\delta$, as a function of N_c^{eff}, for $B^- \to \pi^+\pi^-K^-$, for $k^2/m_B^2 = 0.3(0.5)$ and for model (1). The solid (dotted) line at $\sin\delta = +1$ corresponds to the case $\tilde{\Pi}_{\rho\omega} = (-3500; -300)$, where ρ-ω mixing is included. The dot-dashed (dot-dot-dashed) line corresponds to $\tilde{\Pi}_{\rho\omega} = (0;0)$ where ρ-ω mixing is not included.

parameter N_c^{eff} is dramatic and therefore it is absolutely necessary to more efficiently constrain its value, in order to use asymmetry, a, to determine the CKM parameters ρ and η. We know that the effects of ρ-ω mixing only exist around ω resonance. Nevertheless, in Figs. 5, 6, 7, and 8, at small values of N_c^{eff}, e.g. $\simeq 0.6$, the curves show large asymmetry values far away from ω resonance, which is *a priori* unexpected. In fact, if we assume that nonfactorizable effects are not as important as factorizable contributions, then N_c^{eff} should be much bigger [see Eq. (39)]. From previous analysis on some other B decays such as $B \to D\pi$, $B \to \omega\pi$, and $B \to \omega K$, it was found that N_c^{eff} should be around 2 [31]. Therefore, although small values of N_c^{eff} are allowed by the experimental data we are considering in this paper, we expect that the value of N_c^{eff} cannot be so small with more accurate data. We have checked that when N_c^{eff} is larger than 1 the large CP asymmetries are confined in the ω resonance region. With a very small value of N_c^{eff}, nonfactorizable effects have been overestimated. This means that soft gluon exchanges between $\rho^0(\omega)$ and K may affect ρ-ω mixing and hence lead to the large CP asymmetries in a region far away from ω resonance. However, when $\sqrt{s}$ is very far from ω resonance, the CP asymmetries go to zero as expected.

In spite of the uncertainties discussed previously, the main effect of ρ-ω mixing in $B \to \pi^+\pi^-K$ is the removal of the ambiguity concerning the strong phase, $\sin\delta$. In the $b \to s$ transition, the weak phase in the rate asymmetry is proportional to $\sin\gamma$ where $\gamma = \arg[-(V_{ts}V_{tb}^*)/(V_{us}V_{ub}^*)]$. Knowing the sign of $\sin\delta$, we are then able to determine the sign of $\sin\gamma$ from a measurement of the asymmetry, a. In Figs. 9 and 10, the value of $\sin\delta$ is plotted as a function of N_c^{eff} for $\bar{B}^0 \to \pi^+\pi^-\bar{K}^0$ and $B^- \to \pi^+\pi^-K^-$, respectively. It appears, in both cases, when ρ-ω mixing mechanism is included, that the sign of $\sin\delta$ is positive, for all models studied, until N_c^{eff} reaches 2.69(2.65) for both $B^- \to \pi^+\pi^-K^-$ and $\bar{B}^0 \to \pi^+\pi^-\bar{K}^0$, when $k^2/m_b^2 = 0.3(0.5)$. For values of N_c^{eff} bigger than this limit, $\sin\delta$ becomes negative. At the same time, the sign of the asymmetry also changes. In Figs. 11(b) and 12(b), the ratio of penguin to tree amplitudes is shown for $B^{\pm,0} \to \pi^+\pi^-K^{\pm,0}$, in the case of $\tilde{\Pi}_{\rho\omega} = (-3500, -300)$. The critical point around $N_c^{eff} = 2.7$ refers to the change of sign of $\sin\delta$. Clearly, we can use a measurement of the asymmetry, a, to eliminate the uncertainty mod(π) which is usually involved in the determination of γ

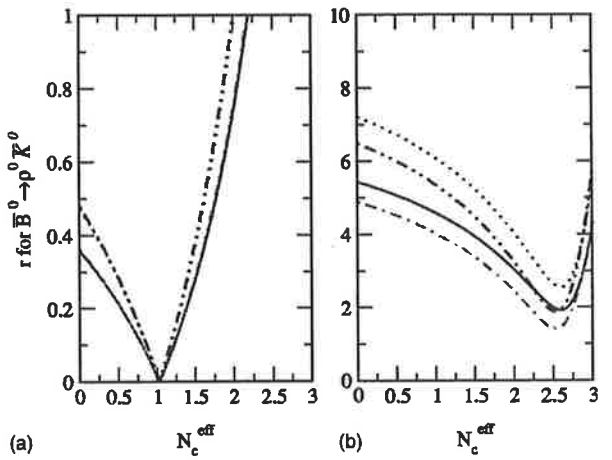

FIG. 11. The ratio of penguin to tree amplitudes, r, as a function of N_c^{eff}, for $\bar{B}^0 \to \pi^+\pi^-\bar{K}^0$, for $k^2/m_B^2 = 0.3(0.5)$, for limiting values of the CKM matrix elements (ρ,η)max (min), for $\tilde{\Pi}_{\rho\omega} = (-3500; -300)(0,0)$ [i.e. with (without) ρ-ω mixing] and for model (1). (a) For $\tilde{\Pi}_{\rho\omega} = (0;0)$, solid line (dotted line) for $k^2/m_B^2 = 0.3$ and (ρ,η)max (min). Dot-dashed line (dot-dot-dashed line) for $k^2/m_B^2 = 0.5$ and (ρ,η)max (min). (b) The same caption as (a) but for $\tilde{\Pi}_{\rho\omega} = (-3500; -300)$.

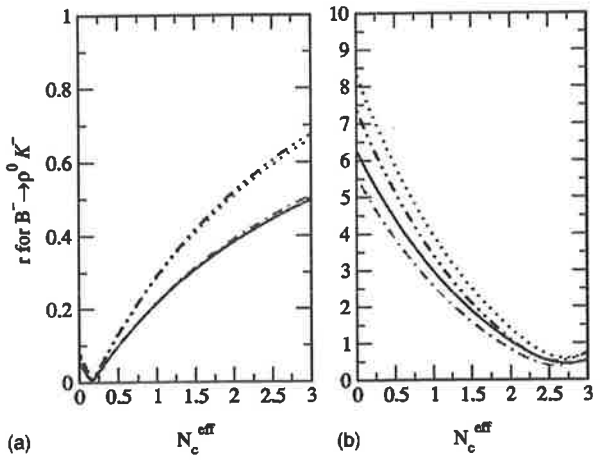

FIG. 12. The ratio of penguin to tree amplitudes, r, for $B^-\to\pi^+\pi^-K^-$. We have the same caption for (a) and (b) as in Fig. 11.

(through $\sin 2\gamma$). If we do not take into account ρ-ω mixing, the CP violating asymmetry, a, remains very small (just a few percent) in both decays. In Figs. 9 and 10 (for the evolution of $\sin\delta$) and in Figs. 11(a) and 12(a) (for the evolution of penguin to tree amplitudes), for $B^{\pm,0}\to\pi^+\pi^-K^{\pm,0}$, we plot $\sin\delta$ and r when $\tilde{\Pi}_{\rho\omega}=(0,0)$—i.e. without ρ-ω mixing. There is a critical point at $N_c^{eff}=1$ (for $\bar{B}^0\to\pi^+\pi^-\bar{K}^0$) and $N_c^{eff}=0.24$ (for $B^-\to\pi^+\pi^-K^-$) for which the value of $\sin\delta$ is at its maximum and corresponds (for the same value of N_c^{eff}), to the lowest value of r. The last results show the double effect of the ρ-ω mixing: the CP violating asymmetry increases and the sign of the strong phase δ is determined.

VI. BRANCHING RATIOS FOR $B^{\pm,0}\to\rho^0K^{\pm,0}$

A. Formalism

With the factorized decay amplitudes, we can compute the decay rates by using the following expression [27]:

$$\Gamma(B\to VP)=\frac{|\vec{p}_\rho|^3}{8\pi m_V^2}\left|\frac{A(B\to VP)}{\epsilon_V\cdot p_B}\right|^2, \tag{57}$$

where $\vec{p}_\rho$ is the c.m. momentum of the decay particles defined as

$$|\vec{p}_\rho|=\frac{\sqrt{[m_B^2-(m_1+m_2)^2][m_B^2-(m_1-m_2)^2]}}{2m_B}. \tag{58}$$

m_1 (m_2) is the mass of the vector (pseudo-scalar) $V(P)$ particle, ϵ_V is the polarization vector and $A(B\to VP)$ is the decay amplitude given by

$$A(B\to VP)=\frac{G_F}{\sqrt{2}}\sum_{i=1,10}V_s^{T,P}a_i\langle VP|O_i|B\rangle, \tag{59}$$

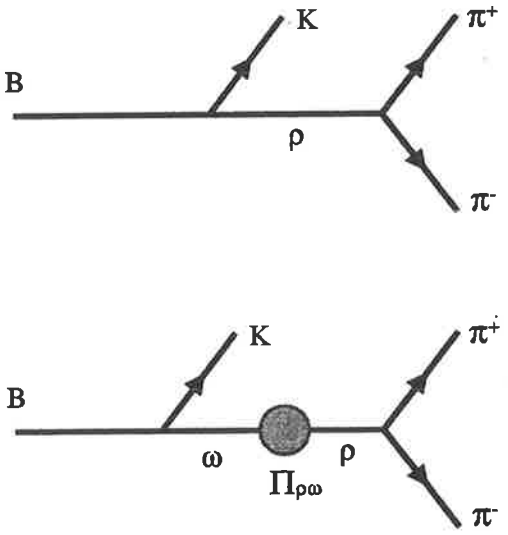

FIG. 13. B decays without (upper) and with (lower) ρ-ω mixing.

where the effective parameters, a_i, which are involved in the decay amplitude, are the following combinations of effective Wilson coefficients:

$$a_{2j}=C'_{2j}+\frac{1}{N_c^{eff}}C'_{2j-1},$$
$$a_{2j-1}=C'_{2j-1}+\frac{1}{N_c^{eff}}C'_{2j}\quad\text{for } j=1,\ldots,5. \tag{60}$$

All other variables in Eq. (59) have been introduced earlier. In the Quark Model, the diagram (Fig. 13 top) gives the main contribution to the $B\to\rho^0K$ decay. In our case, to be consistent, we should also take into account the ρ-ω mixing contribution (Fig. 13 bottom) when we calculate the branching ratio, since we are working to the first order of isospin violation. The application is straightforward and we obtain the branching ratio for $B\to\rho^0K$:

$$\mathrm{BR}(B\to\rho^0K)=\frac{G_F^2|\vec{p}_\rho|^3}{\alpha_k\pi\Gamma_B}\Big|[V_s^TA_{\rho^0}^T(a_1,a_2)-V_s^PA_{\rho^0}^P(a_3,\ldots,a_{10})]+[V_s^TA_\omega^T(a_1,a_2)-V_s^PA_\omega^P(a_3,\ldots,a_{10})]\frac{\tilde{\Pi}_{\rho\omega}}{(s_\rho-m_\omega^2)+im_\omega\Gamma_\omega}\Big|^2. \tag{61}$$

In Eq. (61) G_F is the Fermi constant, Γ_B is the total width B decay, and α_k is an integer related to the given decay. A_V^T and A_V^P are the tree and penguin amplitudes which respect quark interactions in the B decay. $V_s^{T,P}$ [in Eq. (59)] or V_s^T, V_s^P [in Eq. (61)] represent the CKM matrix elements involved in the tree and penguin diagrams, respectively:

$$V_s^T=|V_{ub}V_{us}^*| \text{ for } i=1,2,$$
$$V_s^P=|V_{tb}V_{ts}^*| \text{ for } i=3,\ldots,10. \quad (62)$$

B. Calculational details

In this section we enumerate the theoretical decay amplitudes. We shall analyze five b into s transitions. Two of them involve ρ-ω mixing. These are $B^-\to\rho^0K^-$ and $\bar{B}^0\to\rho^0\bar{K}^0$. Two other decays are $\bar{B}^0\to\rho^-K^+$ and $B^-\to\rho^-\bar{K}^0$ and the last one is $B^-\to\omega K^-$. We list in the following the tree and penguin amplitudes which appear in the given transitions.

For the decay $B^-\to\rho^0K^-$ [$\alpha_k=32$ in Eq. (61)],

$$\sqrt{2}A_\rho^T(a_1,a_2)=a_1f_\rho F_1(m_\rho^2)+a_2f_KA_0(m_K^2), \quad (63)$$

$$\sqrt{2}A_\rho^P(a_3,\ldots,a_{10})=f_\rho F_1(m_\rho^2)\left\{\frac{3}{2}(a_7+a_9)\right\}+f_KA_0(m_K^2)\times\left\{a_4+a_{10}-2(a_6+a_8)\times\left[\frac{m_K^2}{(m_u+m_s)(m_b+m_u)}\right]\right\}; \quad (64)$$

for the decay $B^-\to\omega K^-$ [$\alpha_k=32$ in Eq. (61)],

$$\sqrt{2}A_\omega^T(a_1,a_2)=a_1f_\rho F_1(m_\rho^2)+a_2f_KA_0(m_K^2), \quad (65)$$

$$\sqrt{2}A_\omega^P(a_3,\ldots,a_{10})=f_\rho F_1(m_\rho^2)\left\{2(a_3+a_5)+\frac{1}{2}(a_7+a_9)\right\}+f_KA_0(m_K^2)\left\{-2(a_8+a_6)\times\left[\frac{m_K^2}{(m_u+m_s)(m_b+m_u)}\right]+a_4+a_{10}\right\}; \quad (66)$$

for the decay $\bar{B}^0\to\rho^0\bar{K}^0$ [$\alpha_k=32$ in Eq. (61)],

$$\sqrt{2}A_\rho^T(a_1,a_2)=a_1f_\rho F_1(m_\rho^2), \quad (67)$$

$$\sqrt{2}A_\rho^P(a_3,\ldots,a_{10})=f_\rho F_1(m_\rho^2)\left\{\frac{3}{2}(a_7+a_9)\right\}+f_KA_0(m_K^2)\times\left\{a_4-(2a_6-a_8)\times\left[\frac{m_K^2}{(m_s+m_d)(m_b+m_d)}\right]-\frac{1}{2}a_{10}\right\}; \quad (68)$$

for the decay $\bar{B}^0\to\omega\bar{K}^0$ [$\alpha_k=32$ in Eq. (61)],

$$\sqrt{2}A_\omega^T(a_1,a_2)=a_1f_\rho F_1(m_\rho^2), \quad (69)$$

$$\sqrt{2}A_\omega^P(a_3,\ldots,a_{10})=f_\rho F_1(m_\rho^2)\left\{2(a_3+a_5)+\frac{1}{2}(a_7+a_9)\right\}+f_KA_0(m_K^2)\left\{a_4-(2a_6-a_8)\times\left[\frac{m_K^2}{(m_s+m_d)(m_b+m_d)}\right]-\frac{1}{2}a_{10}\right\}; \quad (70)$$

for the decay $B^-\to\rho^-\bar{K}^0$ [$\alpha_k=16$ in Eq. (61)],

$$A_\rho^T(a_1,a_2)=a_2f_\rho F_1(m_\rho^2), \quad (71)$$

$$A_\rho^P(a_3,\ldots,a_{10})=f_KA_0(m_K^2)\left\{a_4-\frac{1}{2}a_{10}-(2a_6-a_8)\times\left[\frac{m_K^2}{(m_s+m_d)(m_b+m_d)}\right]\right\}; \quad (72)$$

for the decay $\bar{B}^0\to\rho^+K^-$ [$\alpha_k=16$ in Eq. (61)],

$$A_\rho^T(a_1,a_2)=a_2f_KA_0(m_K^2), \quad (73)$$

$$A_\rho^P(a_3,\ldots,a_{10})=f_KA_0(m_K^2)\left\{a_4+a_{10}-2(a_6+a_8)\times\left[\frac{m_K^2}{(m_s+m_u)(m_b+m_u)}\right]\right\}. \quad (74)$$

Moreover, we can calculate the ratio between two branching ratios, in which the uncertainty caused by many systematic errors is removed. We define the ratio R as

$$R=\frac{\mathrm{BR}(B^0\to\rho^\pm K^\mp)}{\mathrm{BR}(B^\pm\to\rho^0K^\pm)}, \quad (75)$$

and, without taking into account the penguin contribution, one has

$$R=\frac{2\Gamma_{B^+}}{\Gamma_{B^0}}\left|\left(1+\frac{a_1f_\rho F_1(m_\rho^2)}{a_2f_KA_0(m_K^2)}\right)\times\left(1+\frac{\tilde{\Pi}_{\rho\omega}}{(s_\rho-m_\omega^2)+im_\omega\Gamma_\omega}\right)\right|^{-2}. \quad (76)$$

C. Numerical results

The numerical values for the CKM matrix elements $V_s^{T,P}$, the ρ-ω mixing amplitude $\tilde{\Pi}_{\rho\omega}$, and the particle masses $m_{V,P}$, which appear in Eq. (61), have been all reported in Sec. IV. The Fermi constant is taken to be $G_F=1.166391\times10^{-5}$ GeV^{-2} [18], and for the total width B decay, $\Gamma_B(=1/\tau_B)$, we use the world average B lifetime values [combined results from ALEPH, Collider Detector at Fermilab (CDF), DELPHI, L3, OPAL and SLAC Large Detector (SLD)] [28]:

TABLE VII. The measured branching ratios by CLEO, BABAR and BELLE factories for B decays into ρK (10^{-6}) (see the reference in text).

	CLEO	BABAR	BELLE
$\rho^0K^\pm$	$8.46^{+4.0}_{-3.4}\pm1.8^a$ (≤17)^b	$10\pm6\pm2^c$ (≤29)^b	$\leq13.5^b$
$\rho^\pm K^0$	–	–	$\leq23.6^b$
$\rho^\pm K^\mp$	$16.0^{+7.6}_{-6.4}\pm2.8^a$ (≤32)^b	–	$15.8^{+5.1+1.7c}_{-4.6-3.0}$
ρ^0K^0	–	–	–
$\frac{BR(\rho^\pm K^\mp)}{BR(\rho^0K^\pm)}$	1.89 ± 1.41	–	–
$\omega K^\pm$	$3.2^{+2.4}_{-1.9}\pm0.8^a$ (≤7.9)^b	$1.4^{+1.3}_{-1.0}\pm0.3^c$	$9.2^{+2.6}_{-2.3}\pm1.0^c$

[a]Fit.
[b]Upper limit.
[c]Experimental data.

$$\tau_{B^0}=1.546\pm0.021\ \text{ps},\qquad \tau_{B^+}=1.647\pm0.021\ \text{ps}. \tag{77}$$

To compare the theoretical results with experimental data, as well as to determine the constraints on the effective number of color, N_c^{eff}, the form factors, and the CKM matrix parameters, we shall apply the experimental branching ratios collected at CLEO [32], BELLE [33–35] and BABAR [36,37] factories. All the experimental values are summarized in Table VII.

In order to determine the range of N_c^{eff} available for calculating the CP violating parameter, a, in $B^{\pm,0}\to\rho^0K^{\pm,0}$, we have calculated the branching ratios for $B^\pm\to\rho^0K^\pm$, $B^\pm\to\rho^\pm K^0$, $B^0\to\rho^\pm K^\mp$, $B^0\to\rho^0K^0$, and $B^\pm\to\omega K^\pm$. We show all the results in Figs. 14, 15, 16, 17, and 18, where branching ratios are plotted as a function of N_c^{eff} for models (1) and (2) [different form factors are used in models (1) and (2)]. By taking experimental data from CLEO, BABAR and BELLE Collaborations, listed in Table VII, and comparing theoretical predictions with experimental results, we expect to extract the allowed range of N_c^{eff} in $B\to\rho K$ and to make the dependence on the form factors explicit between the two classes of models: models (1), (3) and (5), and models (2) and (4). We shall mainly use the CLEO data, since the BABAR and BELLE data are (as yet) less numerous and accurate. An exception will be made for the branching ratio $B^\pm\to\omega K^\pm$, where we shall take the BELLE data for our analysis since they are the most accurate and most recent measurements in that case. Nevertheless, we shall also apply all of them to check the agreement between all the branching ratio data. The CLEO, BABAR and BELLE Collaborations give almost the same experimental branching ratios for all the investigated decays except for the decay $B^-\to\omega K^-$. In this later case, we observe a strong disagreement between all of them since they provide experimental data in a range from 0.1×10^{-6} to 12.8×10^{-6}. Finally, it is evident that numerical results are very sensitive to uncertainties coming from the experimental data and from the factorization approach ap-

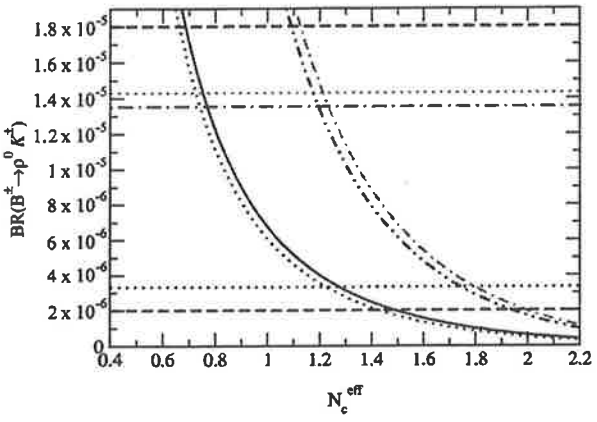

FIG. 14. Branching ratio for $B^\pm\to\rho^0K^\pm$ for models (1) [(2)], $k^2/m_B^2=0.3$ and limiting values of the CKM matrix elements. The solid line (dotted line) is for model (1) and max (min) CKM matrix elements. Dot-dashed line (dot-dot-dashed line) is for model (2) and max (min) CKM matrix elements. The notation is as follows: horizontal dotted line: CLEO data; dashed line: BABAR data; dot-dashed line: BELLE data.

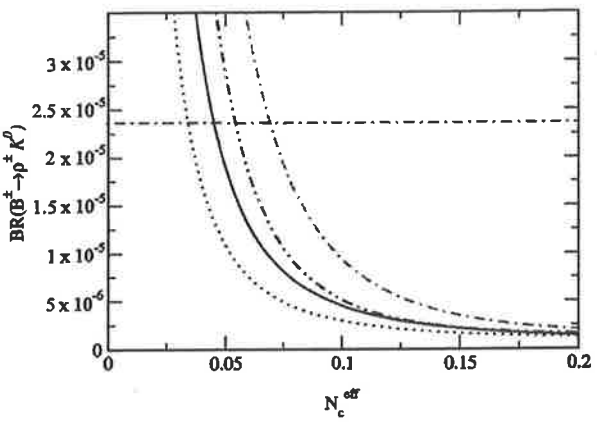

FIG. 15. Branching ratio for $B^\pm\to\rho^\pm K^0$, for models (1) [(2)], $k^2/m_B^2=0.3$ and limiting values of the CKM matrix elements. Solid line (dotted line) is for model (1) and max (min) CKM matrix elements. Dot-dashed line (dot-dot-dashed line) is for model (2) and max (min) CKM matrix elements. Same notation as in Fig. 14, but only experimental upper limits are available.

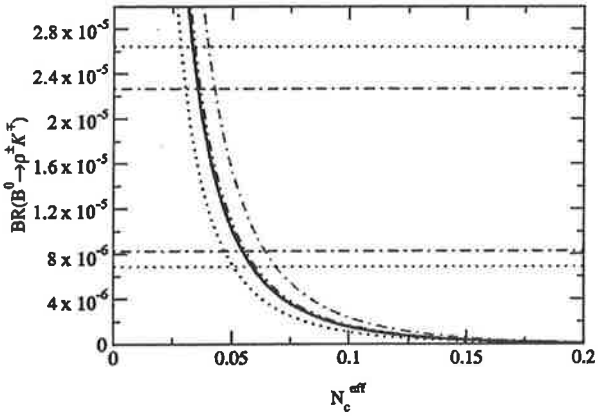

FIG. 16. Branching ratio for $B^0 \to \rho^{\pm} K^{\mp}$, for models (1) [(2)], $k^2/m_B^2 = 0.3$ and limiting values of the CKM matrix elements. Solid line (dotted line) is for model (1) and max (min) CKM matrix elements. Dot-dashed line (dot-dot-dashed line) is for model (2) and max (min) CKM matrix elements. Same notation as in Fig. 14.

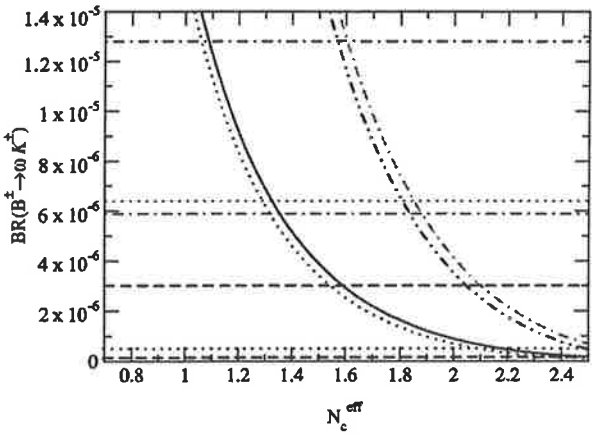

FIG. 18. Branching ratio for $B^{\pm} \to \omega K^{\pm}$, for models (1) [(2)], $k^2/m_B^2 = 0.3$ and limiting values of the CKM matrix elements. Solid line (dotted line) is for model (1) and max (min) CKM matrix elements. Dot-dashed line (dot-dot-dashed line) is for model (2) and max (min) CKM matrix elements. Same notation as in Fig. 14.

plied to calculate hadronic matrix elements in the $B \to K$ transition. Moreover, for $B \to \rho K$, the data are less numerous than for $B \to \rho \pi$, so we cannot expect to get a very accurate range of N_c^{eff}.

For the branching ratio $B^{\pm} \to \rho^0 K^{\pm}$ (Fig. 14) we found a large range of values of N_c^{eff} and CKM matrix elements over which the theoretical results are consistent with experimental data from CLEO, BABAR and BELLE. Each of the models, (1), (2), (3), (4) and (5), gives an allowed range of N_c^{eff}. Even though strong differences appear between the two classes of models, because of the different used form factors, we are not able to draw strong conclusions about the dependence on the form factors. For the branching ratio $B^{\pm} \to \rho^{\pm} K^0$ (Fig. 15), BELLE gives only an upper branching ratio limit whereas BABAR and CLEO do not. Our predictions are still consistent with the experimental data for all models, for a large range of N_c^{eff}. In this case, the numerical results for models (1) and (2) are very close to each other and we need new data to constrain our calculations.

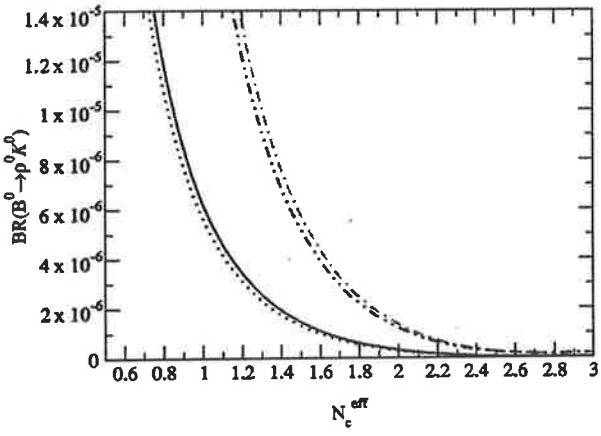

FIG. 17. Branching ratio for $B^0 \to \rho^0 K^0$, for models (1) [(2)], $k^2/m_B^2 = 0.3$ and limiting values of the CKM matrix elements. Solid line (dotted line) is for model (1) and max (min) CKM matrix elements. Dot-dashed line (dot-dot-dashed line) is for model (2) and max (min) CKM matrix elements.

If we consider our results for the branching ratio $B^0 \to \rho^{\pm} K^{\mp}$ (plotted in Fig. 16), there is agreement between the experimental results from CLEO and BELLE (no data from BABAR) and our theoretical predictions at very low values of N_c^{eff} and the CKM matrix elements. All the models (1), (2), (3), (4) and (5) give branching values within the range of branching ratio measurements if N_c^{eff} is less than 0.07. The tiny difference observed between models (1) and (2) comes from the form factor $A_0(k^2)$ [where $A_0(k^2)$ refers to the B to ρ transition taken at $k^2 = m_K^2$] since in that case the amplitude computed involves only the form factor $A_0(k^2)$. For the branching ratio $B^0 \to \rho^0 K^0$ shown in Fig. 17, neither CLEO, BABAR nor BELLE give experimental results. Nevertheless, from models (1) and (2), it appears that this branching ratio is very sensitive to the magnitude of the form factor $F_1(k^2)$ [in our case, $F_1(k^2)$ is uncertain because $h_1 = 0.360$ or 0.762 in models (1) and (2), respectively] since the tree contribution is only proportional to F_1. Moreover, from the range of allowed values of N_c^{eff}, we can estimate the upper limit of this branching ratio to be of the order 20×10^{-6}. Finally, we focus on the branching ratio $B^{\pm} \to \omega K^{\pm}$ which is plotted in Fig. 18 for models (1) and (2). We find that both the experimental and theoretical results are in agreement for a large range of values of N_c^{eff}. But, the models (1) and (2) do not give similar results because the form factor F_1, applied in these models, is very different in both cases. Moreover, the dependence of the branching ratio on the CKM parameters ρ and η indicates that it would be possible to strongly constrain ρ and η with a very accurate experimental measurement for the decay $B^- \to \omega K^-$.

To remove systematic errors in branching ratios given by the B factories, we look at the ratio, R, between the two

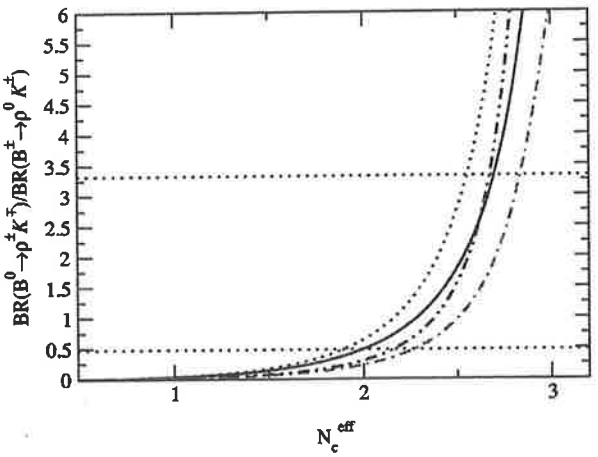

FIG. 19. The ratio of two ρK branching ratios versus N_c^{eff} for models (1) [(2)] and for limiting values of the CKM matrix elements: solid line (dotted line) is for model (1) with max (min) CKM matrix elements. Dot-dashed line (dot-dot-dashed line) is for model (2) with max (min) CKM matrix elements. Same notation as in Fig. 14.

following branching ratios: $\mathrm{BR}(B^0\to\rho^\pm K^\mp)$ and $\mathrm{BR}(B^\pm\to\rho^0K^\mp)$. The ratio is plotted in Fig. 19 as a function of N_c^{eff} for models (1) and (2) and for limiting values of the CKM matrix elements. These results indicate that the ratio is very sensitive to both N_c^{eff} and to the magnitude of the form factors. The sensitivity increases with the value of N_c^{eff} and gives a large difference between models (1), (3) and (5) and models (2) and (4). We found that for a definite range of N_c^{eff}, all models investigated give a ratio consistent with the experimental data from CLEO. It should be noted that R is not very sensitive to the CKM matrix elements. Indeed, if we only take into account the tree contributions, R is independent of the CKM parameters ρ and η. The difference which appears comes from the penguin contribution and has to be taken into account in any approach since they are not negligible.

We have summarized for each model, each branching ratio and each set of limiting values of CKM matrix elements, the allowed range of N_c^{eff} within which the experimental data and numerical results are consistent. To determine the best range of N_c^{eff}, we have to find some intersection of values of N_c^{eff} for each model and each set of CKM matrix elements, for which the theoretical and experimental results are consistent. Since the experimental results are not numerous and not as accurate as one would like, it is more reasonable to fix the upper and lower limits of N_c^{eff} which allow us the maximum of agreement between the theoretical and experimental approaches. By using the limiting values of the CKM matrix elements, we show in Table VIII, the range of allowed values of N_c^{eff} with ρ-ω mixing. Even though in our previous study for $B\to\rho\pi$, we have restricted ourselves to models (2) and (4) rather than models (1), (3) and (5), here we cannot exclude one of the models (1), (2), (3), (4) and (5) due to the lack of accurate experimental data. We find that N_c^{eff} should

TABLE VIII. Best range of N_c^{eff} determined for $k^2/m_b^2=0.3(0.5)$ and for $B\to\rho K$ decays (upper). Also range of N_c^{eff} determined previously for $B\to\rho\pi$ decays [39] (updated). Finally global range of N_c^{eff} from both B decays (lower).

$B\to\rho K$	$\{N_c^{eff}\}$
model (1)	0.66;2.68(0.61;2.68)
model (2)	1.17;2.84(1.09;2.82)
maximum range	0.66;2.84(0.61;2.82)
minimum range	1.17;2.68(1.09;2.68)
$B\to\rho\pi$	$\{N_c^{eff}\}$
model (2)	1.09;1.63(1.12;1.77)
model (4)	1.10;1.68(1.11;1.80)
maximum range	1.09;1.68(1.11;1.80)
minimum range	1.10;1.63(1.12;1.77)
Global range	$\{N_c^{eff}\}$
global maximum range	0.66;2.84(0.61;2.82)
global minimum range	1.17;1.63(1.12;1.77)

be in the following range: $0.66(0.61)<N_c^{eff}<2.84(2.82)$, where the values outside and inside brackets correspond to the choice $k^2/m_b^2=0.3(0.5)$. Finally, if we take into account the allowed range of N_c^{eff} determined for decays such as $B\to\rho\pi$ and $B\to\rho K$ we find a minimum global allowed range of N_c^{eff} which should be in the range $1.17(1.12)<N_c^{eff}<1.63(1.77)$.

VII. SUMMARY AND DISCUSSION

We have studied direct CP violation in decay process such as $B^{\pm,0}\to\rho^0K^{\pm,0}\to\pi^+\pi^-K^{\pm,0}$ with the inclusion of ρ-ω mixing. When the invariant mass of the $\pi^+\pi^-$ pair is in the vicinity of the ω resonance, it is found that the CP violating asymmetry, a, has a maximum a_{max}. We have also investigated the branching ratios $B^0\to\rho^0K^0$, $B^0\to\rho^\pm K^\mp$, $B^\pm\to\rho^\pm K^0$, $B^\pm\to\rho^0K^\pm$, and $B^\pm\to\omega K^\pm$. From our theoretical results, we make comparisons with experimental data from the CLEO, BABAR and BELLE Collaborations. We have applied five phenomenological models in order to show their dependence on form factors, CKM matrix elements and the effective parameter N_c^{eff} in our approach.

To calculate the CP violating asymmetry, a, and the branching ratios, we started from the weak Hamiltonian in which the OPE separates hard and soft physical regimes. We worked in the factorization approximation where the hadronic matrix elements are treated in some phenomenological quark models. The effective parameter, N_c^{eff}, was used in order to take into account, as well as possible, the non-factorizable effects involved in $B\to\rho K$ decays. Although one must have some doubts about factorization, it has been pointed out that it may be quite reliable in energetic weak decays [38].

With the present work, we have explicitly shown that the direct CP violating asymmetry is very sensitive to the CKM

matrix elements, the magnitude of the form factors $A_0(k^2)$ and $F_1(k^2)$, and also to the effective parameter N_c^{eff} (in order of increasing dependence). We have determined a range for the maximum asymmetry, a_{max}, as a function of the parameter N_c^{eff}, the limits of CKM matrix elements and the choice of $k^2/m_b^2=0.3(0.5)$. For the decay $\bar{B}^0\to\pi^+\pi^-\bar{K}^0$ and from all models investigated, we found that the largest CP violating asymmetry varies from $+37\%(+55\%)$ to $-20\%(-24\%)$. As regards $B^-\to\pi^+\pi^-K^-$, one gets $+49\%(+46\%)$ to $-22\%(-25\%)$. For $B^{\pm,0}\to\pi^+\pi^-K^{\pm,0}$, the sign of a_{max} stays positive as long as the value of N_c is less than 2.7. In both decays, the ratio between asymmetry values which are taken at upper and lower limiting ρ and η values is mainly governed by the term $1/\sin\beta$. It appears also that the direct CP violating asymmetry is very sensitive to the form factors at high values of N_c^{eff}. We underline that without the inclusion of ρ-ω mixing, we would not have a large CP violating asymmetry, a, since a is proportional to both $\sin\delta$ and r. We found a critical point for which $\sin\delta$ reaches the value $+1$, but at the same time, r becomes very tiny. We emphazise that the advantage of ρ-ω mixing is the large strong phase difference which varies extremely rapidly near the ω resonance. In our calculations, we found that for $B^{\pm,0}\to\pi^+\pi^-K^{\pm,0}$, the sign of $\sin\delta$ is positive until N_c^{eff} reaches 2.69(2.65) when $k^2/m_b^2=0.3(0.5)$. Then, by measuring a for values of N_c^{eff} lower than the limits given above, we can remove the phase uncertainty $\mathrm{mod}(\pi)$ in the determination of the CKM angle γ.

As regards theoretical results for the branching ratios $B^\pm\to\rho^0K^\pm$, $B^\pm\to\rho^\pm K^0$, $B^0\to\rho^\pm K^\mp$, $B^0\to\rho^0K^0$ and $B^\pm\to\omega K^\pm$, we made comparison with data from the CLEO (mainly), BABAR and BELLE (for $B^\pm\to\omega K^\pm$) Collaborations. We found that it is possible to have agreement between the theoretical results and experimental branching ratio data for $B^\pm\to\rho^0K^\pm$, $B^\pm\to\rho^\pm K^0$, $B^\pm\to\omega K^\pm$, $B^0\to\rho^\pm K^\mp$, and R. For $B^0\to\rho^0K^0$, the lack of results does not allow us to draw conclusions. Only an estimation for the upper limit (20×10^{-6}) has been determined. Nevertheless, we have determined a range of value of N_c^{eff}, $0.66(0.61)<N_c^{eff}<2.84(2.82)$, inside of which the experimental data and theoretical calculations are consistent. We have to keep in mind that, because of the difficulty in dealing with nonfactorizable effects associated with final state interactions (FSI), which are more complex for decays involving an s quark, we have weakly constrained the range of value of N_c^{eff}.

From the CP violating asymmetry and the branching ratios, we expect to determine the CKM matrix elements. In order to reach our aim, all uncertainties in our calculations have to be decreased: the transition form factors for $B\to\rho$ and $B\to K$ have to be well determined and non-factorizable effects have to be treated in the future by using generalized QCD factorization. Moreover, we strongly need more numerous and accurate experimental data in $B\to\rho K$ decays if we want to understand direct CP violation in B decays better.

ACKNOWLEDGMENTS

This work was supported in part by the Australian Research Council and the University of Adelaide.

[1] A.B. Carter and A.I. Sanda, Phys. Rev. Lett. **45**, 952 (1980); Phys. Rev. D **23**, 1567 (1981); I.I. Bigi and A.I. Sanda, Nucl. Phys. **B193**, 85 (1981).

[2] *Proceedings of the Workshop on CP Violation*, Adelaide, Australia, 1998, edited by X.-H. Guo, M. Sevior, and A. W. Thomas (World Scientific, Singapore, 2000).

[3] R. Enomoto and M. Tanabashi, Phys. Lett. B **386**, 413 (1996).

[4] S. Gardner, H.B. O'Connell, and A.W. Thomas, Phys. Rev. Lett. **80**, 1834 (1998).

[5] X.-H. Guo and A.W. Thomas, Phys. Rev. D **58**, 096013 (1998); **61**, 116009 (2000).

[6] A.J. Buras, in *Quantum Field Theory*, Lecture Notes in Physics Vol. 558, edited by P. Breitenlohner and D. Maison (Springer, Heidelberg, 2000), p. 65; also in "Recent Developments in Quantum Field Theory," edited by P. Breitenlohner, D. Maison, and J. Wess (Springer-Verlag, Berlin, in press), hep-ph/9901409.

[7] V.A. Novikov, M.A. Shifman, A.I. Vainshtein, and V.I. Zakharov, Nucl. Phys. **B249**, 445 (1985); Yad. Fiz. **41**, 1063 (1985).

[8] M.A. Shifman, A.I. Vainshtein, and V.I. Zakharov, Nucl. Phys. **B147**, 385 (1979); **B147**, 448 (1979).

[9] A.J. Buras, in *Probing the Standard Model of Particle Interactions* (Elsevier Science, New York, 1998).

[10] N.G. Deshpande and X.-G. He, Phys. Rev. Lett. **74**, 26 (1995).

[11] R. Fleischer, Int. J. Mod. Phys. A **12**, 2459 (1997); Z. Phys. C **62**, 81 (1994); **58**, 483 (1993).

[12] G. Kramer, W. Palmer, and H. Simma, Nucl. Phys. **B428**, 77 (1994).

[13] G. Buchalla, A.J. Buras, and M.E. Lautenbacher, Rev. Mod. Phys. **68**, 1125 (1996).

[14] M. Beneke, plenary talk at the International Europhysics Conference on High Energy Physics (HEP 2001), Budapest, Hungary, 2001, hep-ph/0201137.

[15] L. Wolfenstein, Phys. Rev. Lett. **51**, 1945 (1983); **13**, 562 (1964).

[16] J.J. Sakurai, *Currents and Mesons* (University of Chicago Press, Chicago, 1969).

[17] H.B. O'Connell, B.C. Pearce, A.W. Thomas, and A.G. Williams, Prog. Part. Nucl. Phys. **39**, 201 (1997); H.B. O'Connell, A.G. Williams, M. Bracco, and G. Krein, Phys. Lett. B **370**, 12 (1996); H.B. O'Connell, Aust. J. Phys. **50**, 255 (1997).

[18] Particle Data Group, D.E. Groom *et al.*, Eur. Phys. J. C **15**, 1 (2000).

[19] H.B. O'Connell, A.W. Thomas, and A.G. Williams, Nucl. Phys. **A623**, 559 (1997); K. Maltman, H.B. O'Connell, and A.G. Williams, Phys. Lett. B **376**, 19 (1996).

[20] S. Gardner and H.B. O'Connell, Phys. Rev. D **57**, 2716 (1998).

[21] J. Schwinger, Phys. Rev. **12**, 630 (1964); D. Farikov and B. Stech, Nucl. Phys. **B133**, 315 (1978); N. Cabibbo and L. Maiani, Phys. Lett. **73B**, 418 (1978); M.J. Dugan and B. Grinstein, Phys. Lett. B **255**, 583 (1991).
[22] M. Bauer, B. Stech, and M. Wirbel, Z. Phys. C **34**, 103 (1987); M. Wirbel, B. Stech, and M. Bauer, *ibid.* **29**, 637 (1985).
[23] J.D. Bjorken, Nucl. Phys. B (Proc. Suppl.) **11**, 325 (1989).
[24] X.-H. Guo and T. Huang, Phys. Rev. D **43**, 2931 (1991).
[25] P. Ball, J. High Energy Phys. **09**, 005 (1998).
[26] P. Ball and V.M. Braun, Phys. Rev. D **58**, 094016 (1998).
[27] Y.-H. Chen, H.-Y. Cheng, B. Tseng, and K.-C. Yang, Phys. Rev. D **60**, 094014 (1999).
[28] ALEPH Collaboration, CDF Collaboration, DELPHI Collaboration, L3 Collaboration, OPAL Collaboration, and SLD Collaboration, D. Abbaneo *et al.*, hep-ex/0112028.
[29] H.-Y. Cheng and A. Soni, Phys. Rev. D **64**, 114013 (2001).
[30] D. Melikhov and B. Stech, Phys. Rev. D **62**, 014006 (2000).
[31] H.-Y. Cheng and B. Tseng, hep-ph/9708211.
[32] CLEO Collaboration, C.P. Jessop *et al.*, Phys. Rev. Lett. **85**, 2881 (2000).
[33] BELLE Collaboration, A. Bozek, in Proceedings of the 4th International Conference on B Physics and CP Violation, Ise-Shima, Japan, 2001, hep-ex/0104041.
[34] BELLE Collaboration, K. Abe *et al.*, in Proceedings of the XX International Symposium on Lepton and Photon Interactions at High Energies, Roma, Italy, 2001, BELLE-CONF-0115.
[35] BELLE Collaboration, A. Garmash *et al.*, Phys. Rev. D **65**, 092005 (2002); BELLE Collaboration, R.S. Lu *et al.*, Phys. Rev. Lett. **89**, 191801 (2002).
[36] BABAR Collaboration, T. Schietinger, Proceedings of the Lake Louise Winter Institute on Fundamental Interactions, Alberta, Canada, 2001, hep-ex/0105019.
[37] BABAR Collaboration, B. Aubert *et al.*, hep-ex/0008058; BABAR Collaboration, B. Aubert *et al.*, Phys. Rev. Lett. **87**, 221802 (2001).
[38] H.-Y. Cheng, Phys. Lett. B **335**, 428 (1994); **395**, 345 (1997); H.-Y. Cheng and B. Tseng, Phys. Rev. D **58**, 094005 (1998).
[39] X.-H. Guo, O. Leitner, and A.W. Thomas, Phys. Rev. D **63**, 056012 (2001).

PHYSICAL REVIEW D, VOLUME 63, 056012

Enhanced direct CP violation in $B^{\pm}\to\rho^0\pi^{\pm}$

X.-H. Guo*
Department of Physics and Mathematical Physics, Adelaide University, Adelaide 5005, Australia and Special Research Center for the Subatomic Structure of Matter, Adelaide University, Adelaide 5005, Australia

O. Leitner†
Department of Physics and Mathematical Physics, Adelaide University, Adelaide 5005, Australia, Special Research Center for the Subatomic Structure of Matter, Adelaide University, Adelaide 5005, Australia, and Laboratoire de Physique Corpusculaire, Université Blaise Pascal, CRS/IN2P3, 24 Avenue des Landais, 63177 Aubière Cedex, France

A. W. Thomas‡
Department of Physics and Mathematical Physics, Adelaide University, Adelaide 5005, Australia and Special Research Center for the Subatomic Structure of Matter, Adelaide University, Adelaide 5005, Australia

(Received 6 September 2000; published 9 February 2001)

We study direct CP violation in the hadronic decay $B^{\pm}\to\rho^0\pi^{\pm}$, including the effect of $\rho-\omega$ mixing. We find that the CP violating asymmetry is strongly dependent on the CKM matrix elements, especially the Wolfenstein parameter η. For fixed N_c (the effective parameter associated with factorization), the CP violating asymmetry a has a maximum of order 30%–50% when the invariant mass of the $\pi^+\pi^-$ pair is in the vicinity of the ω resonance. The sensitivity of the asymmetry a to N_c is small. Moreover, if N_c is constrained using the latest experimental branching ratios from the CLEO Collaboration, we find that the sign of $\sin\delta$ is always positive. Thus, a measurement of direct CP violation in $B^{\pm}\to\rho^0\pi^{\pm}$ would remove the mod(π) ambiguity in $\arg[-[V_{td}V_{tb}^*/V_{ud}V_{ub}^*]$.

DOI: 10.1103/PhysRevD.63.056012 PACS number(s): 11.30.Er, 12.39.−x, 13.25.Hw

I. INTRODUCTION

Even though CP violation has been known of since 1964, we still do not know the source of CP violation clearly. In the standard model, a non-zero phase angle in the Cabibbo-Kobayashi-Maskawa (CKM) matrix is responsible for CP violating phenomena. In the past few years, numerous theoretical studies have been conducted on CP violation in the B meson system [1,2]. However, we need a lot of data to check these approaches because there are many theoretical uncertainties—e.g. CKM matrix elements, hadronic matrix elements and nonfactorizable effects. The future aim would be to reduce all these uncertainties.

Direct CP violating asymmetries in B decays occur through the interference of at least two amplitudes with different weak phase ϕ and strong phase δ. In order to extract the weak phase (which is determined by the CKM matrix elements), one must know the strong phase δ, and this is usually not well determined. In addition, in order to have a large signal, we have to appeal to some phenomenological mechanism to obtain a large δ. The charge symmetry violating mixing between ρ^0 and ω can be extremely important in this regard. In particular, it can lead to a large CP violation in B decays such as $B^{\pm}\to\rho^0(\omega)\pi^{\pm}\to\pi^+\pi^-\pi^{\pm}$, because the strong phase passes through 90° at the ω resonance [3–5]. Recently, CLEO reported new data [6] on $B\to\rho\pi$. It is the aim of the present work to analyze direct CP violation in $B^{\pm}\to\rho^0(\omega)\pi^{\pm}\to\pi^+\pi^-\pi^{\pm}$, including $\rho-\omega$ mixing, using the latest data from the CLEO Collaboration to constrain the calculation. In order to extract the strong phase δ, we use the factorization approach, in which the hadronic matrix elements of operators are saturated by vacuum intermediate states.

In this paper, we investigate five phenomenological models with different weak form factors and determine the CP violating asymmetry for $B^{\pm}\to\rho^0(\omega)\pi^{\pm}\to\pi^+\pi^-\pi^{\pm}$ in these models. We select models which are consistent with the CLEO data and determine the allowed range of N_c ($0.98(0.94)<N_c<2.01(1.95)$). Then, we study the sign of $\sin\delta$ in the range of N_c allowed by experimental data in all these models. We discuss the model dependence of our results in detail.

The remainder of this paper is organized as follows. In Sec. II, we present the form of the effective Hamiltonian and the values of Wilson coefficients. In Sec. III, we give the formalism for the CP violating asymmetry in $B^+\to\rho^0(\omega)\pi^+\to\pi^+\pi^-\pi^+$, for all the models which will be checked. We also show numerical results in this section (asymmetry, a, and the value of $\sin\delta$). In Sec. IV, we calculate branching ratios for $B^+\to\rho^0\pi^+$ and $B^0\to\rho^+\pi^-$ and present numerical results over the range of N_c allowed by the CLEO data. In the last section, we summarize our results and suggest further work.

II. THE EFFECTIVE HAMILTONIAN

In order to calculate the direct CP violating aymmetry in hadronic decays, one can use the following effective weak

*Email address: xhguo@physics.adelaide.edu.au
†Email address: oleitner@physics.adelaide.edu.au
‡Email address: athomas@physics.adelaide.edu.au

Hamiltonian, based on the operator product expansion [7]:

$$\mathcal{H}_{\Delta B=1}=\frac{G_F}{\sqrt{2}}\left[\sum_{q=d,s} V_{ub}V_{uq}^{*}(c_1O_1^u+c_2O_2^u) - V_{tb}V_{tq}^{*}\sum_{i=3}^{10} c_iO_i\right]+\text{H.c.}, \quad (1)$$

where $c_i(i=1,\ldots,10)$ are the Wilson coefficients. They are calculable in renormalization group improved perturbation theory and are scale dependent. In the present case, we use their values at the renormalization scale $\mu\approx m_b$. The operators O_i have the following form:

$$O_1^u=\bar{q}_\alpha\gamma_\mu(1-\gamma_5)u_\beta\bar{u}_\beta\gamma^\mu(1-\gamma_5)b_\alpha,$$

$$O_2^u=\bar{q}\gamma_\mu(1-\gamma_5)u\bar{u}\gamma^\mu(1-\gamma_5)b,$$

$$O_3=\bar{q}\gamma_\mu(1-\gamma_5)b\sum_{q'}\bar{q}'\gamma^\mu(1-\gamma_5)q',$$

$$O_4=\bar{q}_\alpha\gamma_\mu(1-\gamma_5)b_\beta\sum_{q'}\bar{q}'_\beta\gamma^\mu(1-\gamma_5)q'_\alpha,$$

$$O_5=\bar{q}\gamma_\mu(1-\gamma_5)b\sum_{q'}\bar{q}'\gamma^\mu(1+\gamma_5)q',$$

$$O_6=\bar{q}_\alpha\gamma_\mu(1-\gamma_5)b_\beta\sum_{q'}\bar{q}'_\beta\gamma^\mu(1+\gamma_5)q'_\alpha,$$

$$O_7=\frac{3}{2}\bar{q}\gamma_\mu(1-\gamma_5)b\sum_{q'}e_{q'}\bar{q}'\gamma^\mu(1+\gamma_5)q',$$

$$O_8=\frac{3}{2}\bar{q}_\alpha\gamma_\mu(1-\gamma_5)b_\beta\sum_{q'}e_{q'}\bar{q}'_\beta\gamma^\mu(1+\gamma_5)q'_\alpha,$$

$$O_9=\frac{3}{2}\bar{q}\gamma_\mu(1-\gamma_5)b\sum_{q'}e_{q'}\bar{q}'\gamma^\mu(1-\gamma_5)q',$$

$$O_{10}=\frac{3}{2}\bar{q}_\alpha\gamma_\mu(1-\gamma_5)b_\beta\sum_{q'}e_{q'}\bar{q}'_\beta\gamma^\mu(1-\gamma_5)q'_\alpha, \quad (2)$$

where α and β are color indices, and $q'=u$, d or s are quarks. In Eq. (2), O_1^u and O_2^u are the tree level operators, O_3–O_6 are QCD penguin operators, and O_7–O_{10} arise from electroweak penguin diagrams.

The Wilson coefficients, c_i, are known to the next-to-leading logarithmic order. At the scale $\mu=m_b=5$ GeV, they take the following values [8,9]:

$$c_1=-0.3125, \quad c_2=1.1502, \quad (3)$$

$$c_3=0.0174, \quad c_4=-0.0373,$$

$$c_5=0.0104, \quad c_6=-0.0459,$$

$$c_7=-1.050\times10^{-5}, \quad c_8=3.839\times10^{-4},$$

$$c_9=-0.0101, \quad c_{10}=1.959\times10^{-3}.$$

To be consistent, the matrix elements of the operators O_i should also be renormalized to the one-loop order. This results in the effective Wilson coefficients, c_i', which satisfy the constraint

$$c_i(m_b)\langle O_i(m_b)\rangle=c_i'\langle O_i\rangle^{tree}, \quad (4)$$

where $\langle O_i\rangle^{tree}$ is the matrix element at the tree level, which will be evaluated in the factorization approach. From Eq. (4), the relations between c_i' and c_i are [8,9]

$$c_1'=c_1, \quad c_2'=c_2,$$

$$c_3'=c_3-P_s/3, \quad c_4'=c_4+P_s,$$

$$c_5'=c_5-P_s/3, \quad c_6'=c_6+P_s,$$

$$c_7'=c_7+P_e, \quad c_8'=c_8,$$

$$c_9'=c_9+P_e, \quad c_{10}'=c_{10}, \quad (5)$$

where

$$P_s=(\alpha_s/8\pi)c_2(10/9+G(m_c,\mu,q^2)),$$

$$P_e=(\alpha_{em}/9\pi)(3c_1+c_2)(10/9+G(m_c,\mu,q^2)),$$

with

$$G(m_c,\mu,q^2)=4\int_0^1 dx\,x(x-1)\ln\frac{m_c^2-x(1-x)q^2}{\mu^2}.$$

Here q^2 is the typical momentum transfer of the gluon or photon in the penguin diagrams. $G(m_c,\mu,q^2)$ has the following explicit expression [10]:

$$\Re G=\frac{2}{3}\left(\ln\frac{m_c^2}{\mu^2}-\frac{5}{3}-4\frac{m_c^2}{q^2}+\left(1+2\frac{m_c^2}{q^2}\right)\times\sqrt{1-4\frac{m_c^2}{q^2}}\ln\frac{1+\sqrt{1-4\frac{m_c^2}{q^2}}}{1-\sqrt{1-4\frac{m_c^2}{q^2}}}\right),$$

$$\Im G=-\frac{2}{3}\left(1+2\frac{m_c^2}{q^2}\right)\sqrt{1-4\frac{m_c^2}{q^2}}. \quad (6)$$

Based on simple arguments at the quark level, the value of q^2 is chosen in the range $0.3<q^2/m_b^2<0.5$ [3,4]. From Eqs. (5),(6) we can obtain numerical values for c_i'.

When $q^2/m_b^2=0.3$,

$$c_1'=-0.3125,\quad c_2'=1.1502,$$
$$c_3'=2.433\times10^{-2}+1.543\times10^{-3}i,$$
$$c_4'=-5.808\times10^{-2}-4.628\times10^{-3}i,$$
$$c_5'=1.733\times10^{-2}+1.543\times10^{-3}i,$$
$$c_6'=-6.668\times10^{-2}-4.628\times10^{-3}i,$$
$$c_7'=-1.435\times10^{-4}-2.963\times10^{-5}i,$$
$$c_8'=3.839\times10^{-4},$$
$$c_9'=-1.023\times10^{-2}-2.963\times10^{-5}i,$$
$$c_{10}'=1.959\times10^{-3}, \tag{7}$$

and when $q^2/m_b^2=0.5$, one has

$$c_1'=-0.3125,\quad c_2'=1.1502,$$
$$c_3'=2.120\times10^{-2}+2.174\times10^{-3}i,$$
$$c_4'=-4.869\times10^{-2}-1.552\times10^{-2}i,$$
$$c_5'=1.420\times10^{-2}+5.174\times10^{-3}i,$$
$$c_6'=-5.729\times10^{-2}-1.552\times10^{-2}i,$$
$$c_7'=-8.340\times10^{-5}-9.938\times10^{-5}i,$$
$$c_8'=3.839\times10^{-4},$$
$$c_9'=-1.017\times10^{-2}-9.938\times10^{-5}i,$$
$$c_{10}'=1.959\times10^{-3}, \tag{8}$$

where we have taken $\alpha_s(m_Z)=0.112$, $\alpha_{em}(m_b)=1/132.2$, $m_b=5$ GeV, and $m_c=1.35$ GeV.

III. CP VIOLATION IN $B^+\to\rho^0(\omega)\pi^+\to\pi^+\pi^-\pi^+$

A. Formalism

The formalism for CP violation in hadronic B meson decays is the following: Let A be the amplitude for the decay $B^+\to\pi^+\pi^-\pi^+$, and then one has

$$A=\langle\pi^+\pi^-\pi^+|H^T|B^+\rangle+\langle\pi^+\pi^-\pi^+|H^P|B^+\rangle, \tag{9}$$

with H^T and H^P being the Hamiltonians for the tree and penguin operators, respectively. We can define the relative magnitude and phases between these two contributions as follows:

$$A=\langle\pi^+\pi^-\pi^+|H^T|B^+\rangle[1+re^{i\delta}e^{i\phi}], \tag{10}$$

$$\bar{A}=\langle\pi^+\pi^-\pi^-|H^T|B^-\rangle[1+re^{i\delta}e^{-i\phi}], \tag{11}$$

where δ and ϕ are strong and weak phases, respectively. The phase ϕ arises from the appropriate combination of CKM matrix elements, which is $\phi=\arg[(V_{tb}V_{td}^*)/(V_{ub}V_{ud}^*)]$. As a result, $\sin\phi$ is equal to $\sin\alpha$ with α defined in the standard way [11]. The parameter r is the absolute value of the ratio of tree and penguin amplitudes:

$$r\equiv\left|\frac{\langle\rho^0(\omega)\pi^+|H^P|B^+\rangle}{\langle\rho^0(\omega)\pi^+|H^T|B^+\rangle}\right|. \tag{12}$$

The CP violating asymmetry, a, can be written as

$$a\equiv\frac{|A|^2-|\bar{A}|^2}{|A|^2+|\bar{A}|^2}=\frac{-2r\sin\delta\sin\phi}{1+2r\cos\delta\cos\phi+r^2}. \tag{13}$$

It can be seen explicitly from Eq. (13) that both weak and strong phase differences are needed to produce CP violation. In order to obtain a large signal for direct CP violation, we need some mechanism to make both $\sin\delta$ and r large. We stress that $\rho-\omega$ mixing has the dual advantages that the strong phase difference is large (passing through 90° at the ω resonance) and well known [4,5]. With this mechanism, to first order in isospin violation, we have the following results when the invariant mass of $\pi^+\pi^-$ is near the ω resonance mass:

$$\langle\pi^-\pi^+\pi^+|H^T|B^+\rangle=\frac{g_\rho}{s_\rho s_\omega}\tilde{\Pi}_{\rho\omega}t_\omega+\frac{g_\rho}{s_\rho}t_\rho, \tag{14}$$

$$\langle\pi^-\pi^+\pi^+|H^P|B^+\rangle=\frac{g_\rho}{s_\rho s_\omega}\tilde{\Pi}_{\rho\omega}p_\omega+\frac{g_\rho}{s_\rho}p_\rho. \tag{15}$$

Here, $t_V(V=\rho$ or $\omega)$ is the tree amplitude and p_V is the penguin amplitude for producing a vector meson, V, g_ρ is the coupling for $\rho^0\to\pi^+\pi^-$, $\tilde{\Pi}_{\rho\omega}$ is the effective $\rho-\omega$ mixing amplitude, and s_V is from the inverse propagator of the vector meson V,

$$s_V=s-m_V^2+im_V\Gamma_V, \tag{16}$$

with $\sqrt{s}$ being the invariant mass of the $\pi^+\pi^-$ pair.

We stress that the direct coupling $\omega\to\pi^+\pi^-$ is effectively absorbed into $\tilde{\Pi}_{\rho\omega}$ [12], leading to the explicit s dependence of $\tilde{\Pi}_{\rho\omega}$. Making the expansion $\tilde{\Pi}_{\rho\omega}(s)=\tilde{\Pi}_{\rho\omega}(m_\omega^2)+(s-m_\omega^2)\tilde{\Pi}'_{\rho\omega}(m_\omega^2)$, the $\rho-\omega$ mixing parameters were determined in the fit of Gardner and O'Connell [13]: $\Re\tilde{\Pi}_{\rho\omega}(m_\omega^2)=-3500\pm300$ MeV^2, $\Im\tilde{\Pi}_{\rho\omega}(m_\omega^2)=-300\pm300$ MeV^2 and $\tilde{\Pi}'_{\rho\omega}(m_\omega^2)=0.03\pm0.04$. In practice, the effect of the derivative term is negligible. From Eqs. (10),(14),(15) one has

$$re^{i\delta}e^{i\phi}=\frac{\tilde{\Pi}_{\rho\omega}p_\omega+s_\omega p_\rho}{\tilde{\Pi}_{\rho\omega}t_\omega+s_\omega t_\rho}. \tag{17}$$

Defining

$$\frac{p_\omega}{t_\rho}\equiv r' e^{i(\delta_q+\phi)}, \quad \frac{t_\omega}{t_\rho}\equiv \alpha e^{i\delta_\alpha}, \quad \frac{p_\rho}{p_\omega}\equiv \beta e^{i\delta_\beta}, \tag{18}$$

where $\delta_\alpha, \delta_\beta$ and δ_q are strong phases, one finds the following expression from Eq. (18):

$$re^{i\delta}=r' e^{i\delta_q}\frac{\tilde{\Pi}_{\rho\omega}+\beta e^{i\delta_\beta} s_\omega}{s_\omega+\tilde{\Pi}_{\rho\omega}\alpha e^{i\delta_\alpha}}. \tag{19}$$

It will be shown that in the factorization approach, we have $\alpha e^{i\delta_\alpha}=1$ in our case. Letting

$$\beta e^{i\delta_\beta}=b+ci, \quad r' e^{i\delta_q}=d+ei, \tag{20}$$

and using Eq. (19), we obtain the following result when $\sqrt{s}\sim m_\omega$:

$$re^{i\delta}=\frac{C+Di}{(s-m_\omega^2+\Re\tilde{\Pi}_{\rho\omega})^2+(\Im\tilde{\Pi}_{\rho\omega}+m_\omega\Gamma_\omega)^2}, \tag{21}$$

where

$$\begin{aligned}C=&(s-m_\omega^2+\Re\tilde{\Pi}_{\rho\omega})\{d[\Re\tilde{\Pi}_{\rho\omega}+b(s-m_\omega^2)-cm_\omega\Gamma_\omega]\\&-e[\Im\tilde{\Pi}_{\rho\omega}+bm_\omega\Gamma_\omega+c(s-m_\omega^2)]\}\\&+(\Im\tilde{\Pi}_{\rho\omega}+m_\omega\Gamma_\omega)\{e[\Re\tilde{\Pi}_{\rho\omega}+b(s-m_\omega^2)-cm_\omega\Gamma_\omega]\\&+d[\Im\tilde{\Pi}_{\rho\omega}+bm_\omega\Gamma_\omega+c(s-m_\omega^2)]\},\\D=&(s-m_\omega^2+\Re\tilde{\Pi}_{\rho\omega})\{e[\Re\tilde{\Pi}_{\rho\omega}+d(s-m_\omega^2)-cm_\omega\Gamma_\omega]\\&+d[\Im\tilde{\Pi}_{\rho\omega}+bm_\omega\Gamma_\omega+c(s-m_\omega^2)]\}-(\Im\tilde{\Pi}_{\rho\omega}+m_\omega\Gamma_\omega)\\&\times\{d[\Re\tilde{\Pi}_{\rho\omega}+b(s-m_\omega^2)-cm_\omega\Gamma_\omega]-e[\Im\tilde{\Pi}_{\rho\omega}+bm_\omega\Gamma_\omega\\&+c(s-m_\omega^2)]\}.\end{aligned} \tag{22}$$

$\beta e^{i\delta_\beta}$ and $r' e^{i\delta_q}$ will be calculated later. Then, from Eq. (22), we can obtain $r\sin\delta$ and $r\cos\delta$. In order to get the CP violating asymmetry, a, in Eq. (13), $\sin\phi$ and $\cos\phi$ are needed, where ϕ is determined by the CKM matrix elements. In the Wolfenstein parametrization [14], one has

$$\sin\phi=\frac{\eta}{\sqrt{[\rho(1-\rho)-\eta^2]^2+\eta^2}}, \tag{23}$$

$$\cos\phi=\frac{\rho(1-\rho)-\eta^2}{\sqrt{[\rho(1-\rho)-\eta^2]^2+\eta^2}}. \tag{24}$$

B. Calculational details

With the Hamiltonian given in Eq. (1), we are ready to evaluate the matrix elements for $B^+\to\rho^0(\omega)\pi^+$. In the factorization approximation, either the $\rho^0(\omega)$ or the π^+ is generated by one current which has the appropriate quantum numbers in the Hamiltonian. For this decay process, two kinds of matrix element products are involved after factorization. Schematically (i.e. omitting Dirac matrices and color labels) $\langle\rho^0(\omega)|(\bar{u}u)|0\rangle\langle\pi^+|(\bar{d}b)|B^+\rangle$ and $\langle\pi^+|(\bar{d}u)|0\rangle\langle\rho^0(\omega)|(\bar{u}b)|B^+\rangle$. We will calculate them in some phenomenological quark models.

The matrix elements for $B\to X$ and $B\to X^*$ (where X and X^* denote pseudoscalar and vector mesons, respectively) can be decomposed as [15]

$$\begin{aligned}\langle X|J_\mu|B\rangle=&\left(p_B+p_X-\frac{m_B^2-m_X^2}{k^2}k\right)_\mu F_1(k^2)\\&+\frac{m_B^2-m_X^2}{k^2}k_\mu F_0(k^2),\end{aligned} \tag{25}$$

$$\begin{aligned}\langle X^*|J_\mu|B\rangle=&\frac{2}{m_B+m_{X^*}}\epsilon_{\mu\nu\rho\sigma}\epsilon^{*\nu}p_B^\rho p_{X^*}^\sigma V(k^2)\\&+i\left\{\epsilon_\mu^*(m_B+m_{X^*})A_1(k^2)-\frac{\epsilon^*\cdot k}{m_B+m_{X^*}}\right.\\&\times(P_B+P_{X^*})_\mu A_2(k^2)\\&\left.-\frac{\epsilon^*\cdot k}{k^2}2m_{X^*}\cdot k_\mu A_3(k^2)\right\}\\&+i\frac{\epsilon^*\cdot k}{k^2}2m_{X^*}\cdot k_\mu A_0(k^2),\end{aligned} \tag{26}$$

where J_μ is the weak current ($J_\mu=\bar{q}\gamma^\mu(1-\gamma_5)b$ with $q=u,d$), $k=p_B-p_{X(X^*)}$ and ϵ_μ is the polarization vector of X^*. The form factors included in our calculations satisfy $F_1(0)=F_0(0)$, $A_3(0)=A_0(0)$ and $A_3(k^2)=[(m_B+m_{X^*})/2m_{X^*}]A_1(k^2)-[(m_B-m_{X^*})/2m_{X^*}]A_2(k^2)$. Using the decomposition in Eqs. (25), (26), one has

$$\begin{aligned}t_\rho=m_B|\vec{p}_\rho|\left[\left(c_1'+\frac{1}{N_c}c_2'\right)f_\rho F_1(m_\rho^2)\right.\\\left.+\left(c_2'+\frac{1}{N_c}c_1'\right)f_\pi A_0(m_\pi^2)\right],\end{aligned} \tag{27}$$

where f_ρ and f_π are the decay constants of ρ and π, respectively, and $\vec{p}_\rho$ is the three momentum of the ρ. In the same way, we find $t_\omega=t_\rho$, so that

$$\alpha e^{i\delta_\alpha}=1. \tag{28}$$

After calculating the penguin operator contributions, one has

$$\beta e^{i\delta_\beta}=\frac{m_B|\vec{p}_\rho|}{p_\omega}\left\{\left(c_4'+\frac{1}{N_c}c_3'\right)[-f_\rho F_1(m_\rho^2)+f_\pi A_0(m_\pi^2)]+\frac{3}{2}\left[\left(c_7'+\frac{1}{N_c}c_8'\right)+\left(c_9'+\frac{1}{N_c}c_{10}'\right)\right]f_\rho F_1(m_\rho^2)\right.$$
$$\left.-\left[\left(c_6'+\frac{1}{N_c}c_5'\right)+\left(c_8'+\frac{1}{N_c}c_7'\right)\right]\left[\frac{2m_\pi^2 f_\pi A_0(m_\pi^2)}{(m_u+m_d)(m_b+m_u)}\right]+\left(c_{10}'+\frac{1}{N_c}c_9'\right)\left[\frac{1}{2}f_\rho F_1(m_\rho^2)+f_\pi A_0(m_\pi^2)\right]\right\},$$

$$r'e^{i\delta_q}=-\frac{p_\omega}{\left(c_1'+\frac{1}{N_c}c_2'\right)f_\rho F_1(m_\rho^2)+\left(c_2'+\frac{1}{N_c}c_1'\right)f_\pi A_0(m_\pi^2)}\left|\frac{V_{tb}V_{td}^*}{V_{ub}V_{ud}^*}\right|, \tag{29}$$

where

$$p_\omega=m_B|\vec{p}_\rho|\left\{2\left[\left(c_3'+\frac{1}{N_c}c_4'\right)+\left(c_5'+\frac{1}{N_c}c_6'\right)\right]f_\rho F_1(m_\rho^2)+\frac{1}{2}\left[\left(c_7'+\frac{1}{N_c}c_8'\right)+\left(c_9'+\frac{1}{N_c}c_{10}'\right)\right]f_\rho F_1(m_\rho^2)\right.$$
$$-2\left[\left(c_8'+\frac{1}{N_c}c_7'\right)+\left(c_6'+\frac{1}{N_c}c_5'\right)\right]\left[\frac{m_\pi^2 f_\pi A_0(m_\pi^2)}{(m_u+m_d)(m_b+m_u)}\right]+\left(c_4'+\frac{1}{N_c}c_3'\right)[f_\pi A_0(m_\pi^2)+f_\rho F_1(m_\rho^2)]$$
$$\left.+\left(c_{10}'+\frac{1}{N_c}c_9'\right)\left[f_\pi A_0(m_\pi^2)-\frac{1}{2}f_\rho F_1(m_\rho^2)\right]\right\},$$

and

$$\left|\frac{V_{tb}V_{td}^*}{V_{ub}V_{ud}^*}\right|=\frac{\sqrt{(1-\rho)^2+\eta^2}}{(1-\lambda^2/2)\sqrt{\rho^2+\eta^2}}=\left(1-\frac{\lambda^2}{2}\right)^{-1}\left|\frac{\sin\gamma}{\sin\beta}\right|. \tag{30}$$

C. Numerical results

In our numerical calculations we have several parameters: q^2, N_c and the CKM matrix elements in the Wolfenstein parametrization. As mentioned in Sec. II, the value of q^2 is conventionally chosen to be in the range $0.3<q^2/m_b^2<0.5$. The CKM matrix, which should be determined from experimental data, has the following form in term of the Wolfenstein parameters, A,λ,ρ,η [14]:

$$V=\begin{pmatrix} 1-\frac{1}{2}\lambda^2 & \lambda & A\lambda^3(\rho-i\eta) \\ -\lambda & 1-\frac{1}{2}\lambda^2 & A\lambda^2 \\ A\lambda^3(1-\rho-i\eta) & -A\lambda^2 & 1 \end{pmatrix}, \tag{31}$$

where $O(\lambda^4)$ corrections are neglected. We use $\lambda=0.2205$, $A=0.815$ and the range for ρ and η as the following [16,17]:

$$0.09<\rho<0.254, \quad 0.323<\eta<0.442. \tag{32}$$

The form factors $F_1(m_\rho^2)$ and $A_0(m_\pi^2)$ depend on the inner structure of the hadrons. Under the nearest pole dominance assumption, the k^2 dependence of the form factors is:

for model 1(2) [15,18]:

$$F_1(k^2)=\frac{h_1}{1-\frac{k^2}{m_1^2}}, \quad A_0(k^2)=\frac{h_{A_0}}{1-\frac{k^2}{m_{A_0}^2}}, \tag{33}$$

where $h_1=0.330(0.625)$, $h_{A_0}=0.28(0.34)$, $m_1=5.32$ GeV, $m_{A_0}=5.27$ GeV,

for model 3(4) [15,18,19]:

$$F_1(k^2)=\frac{h_1}{\left(1-\frac{k^2}{m_1^2}\right)^2}, \quad A_0(k^2)=\frac{h_{A_0}}{\left(1-\frac{k^2}{m_{A_0}^2}\right)^2}, \tag{34}$$

where $h_1=0.330(0.625)$, $h_{A_0}=0.28(0.34)$, $m_1=5.32$ GeV, $m_{A_0}=5.27$ GeV, for model 5 [20,21]:

$$F_1(k^2)=\frac{h_1}{1-a_1\frac{k^2}{m_B^2}+b_1\left(\frac{k^2}{m_B^2}\right)^2},$$

$$A_0(k^2)=\frac{h_{A_0}}{1-a_0\frac{k^2}{m_B^2}+b_0\left(\frac{k^2}{m_B^2}\right)^2}, \tag{35}$$

where $h_1=0.305$, $h_{A_0}=0.372$, $a_1=0.266$, $b_1=-0.752$, $a_0=1.4$, $b_0=0.437$.

The decay constants used in our calculations are: $f_\rho=f_\omega=221$ MeV and $f_\pi=130.7$ MeV.

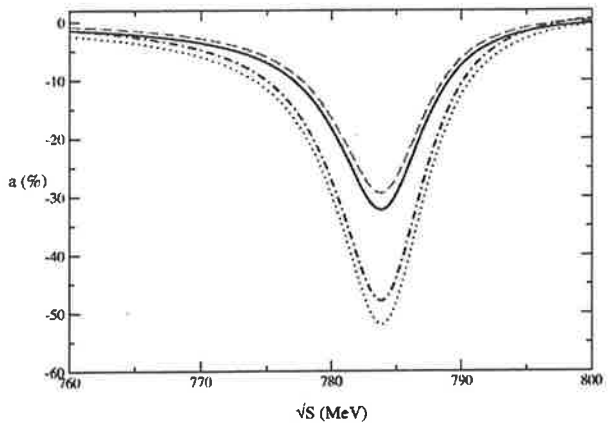

FIG. 1. Asymmetry, a, for $k^2/m_b^2=0.3$, $N_c=0.98(2.01)$ and limiting values of the CKM matrix elements for model 1. Solid line (dot line) stands for $N_c=0.98$ and max (min) CKM matrix elements. Dashed line (dot dashed line) stands for $N_c=2.01$ and max (min) CKM matrix elements.

In the numerical calculations, it is found that for a fixed N_c, there is a maximum value, a_{max}, for the CP violating parameter, a, when the invariant mass of the $\pi^+\pi^-$ is in the vicinity of the ω resonance. The results are shown in Figs. 1 and 2, for $k^2/m_b^2=0.3(0.5)$ and N_c in the range $0.98(0.94)<N_c<2.01(1.95)$—for reasons which will be explained later (Sec. IV). We investigate five models with different form factors to study the model dependence of a. It appears that this dependence is strong (Table I).

The maximum asymmetry parameter, a_{max}, varies from $-24\%(-19\%)$ to $-59\%(-48\%)$ for N_c in both the chosen range $k^2/m_b^2=0.3(0.5)$ and the range of CKM matrix elements indicated earlier. If we look at the numerical results for the asymmetries (Table I) for $N_{cmax}=2.01(1.95)$ and $k^2/m_b^2=0.3(0.5)$, we obtain for models 1, 3, and 5 an asymmetry, a_{max}, around $-27.3\%(-21.6\%)$ for the set (ρ_{max},η_{max}), and around $-44.3\%(-35.0\%)$ for the set (ρ_{min},η_{min}). We find a ratio equal to 1.62(1.62) between the asymmetries associated with the upper and lower limits of (ρ,η). The reason why the maximum asymmetry, a_{max}, can have large variation, comes from the $b\to d$ transition, where V_{td} and V_{ub} appear. These are functions of (ρ,η) and contribute to the asymmetry [Eq. (31)] through the ratio between the ω penguin diagram and the ρ tree diagram.

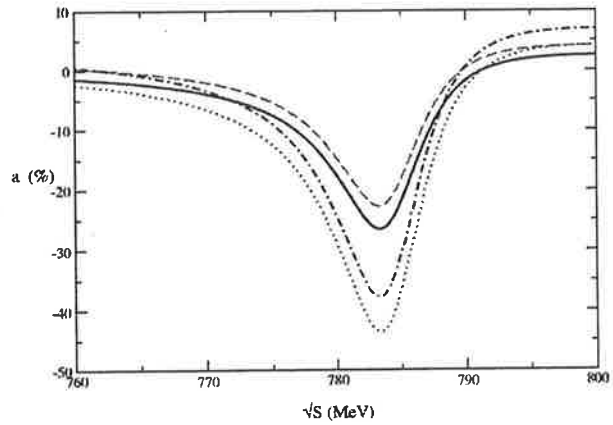

FIG. 2. Asymmetry, a, for $k^2/m_b^2=0.5$, $N_c=0.94(1.95)$ and limiting values of the CKM matrix elements for model 1. Solid line (dot line) stands for $N_c=0.94$ and max (min) CKM matrix elements. Dashed line (dot dashed line) stands for $N_c=1.95$ and max (min) CKM matrix elements.

TABLE I. Maximum CP violating asymmetry a_{max} (%) for $B^+\to\pi^+\pi^-\pi^+$, for all models, limiting values of the CKM matrix elements (upper and lower limit), and for $k^2/m_b^2=0.3(0.5)$.

	$N_{cmin}=0.98(0.94)$	$N_{cmax}=2.01(1.95)$
model 1		
ρ_{max},η_{max}	$-33(-27)$	$-29(-23)$
ρ_{min},η_{min}	$-52(-43)$	$-47(-37)$
model 2		
ρ_{max},η_{max}	$-36(-29)$	$-37(-28)$
ρ_{min},η_{min}	$-57(-48)$	$-59(-46)$
model 3		
ρ_{max},η_{max}	$-32(-26)$	$-29(-23)$
ρ_{min},η_{min}	$-51(-43)$	$-47(-37)$
model 4		
ρ_{max},η_{max}	$-36(-29)$	$-37(-28)$
ρ_{min},η_{min}	$-57(-48)$	$-59(-46)$
model 5		
ρ_{max},η_{max}	$-29(-24)$	$-24(-19)$
ρ_{min},η_{min}	$-48(-40)$	$-39(-31)$

For models 2 and 4, one has a maximum asymmetry, a_{max}, around $-37\%(-28\%)$ for the set (ρ_{max},η_{max}) and around $-59\%(-46\%)$ for the set (ρ_{min},η_{min}). We find a ratio between the asymmetries equal to 1.59(1.64) in this case. The difference between these two sets of models comes from the magnitudes of the form factors, where $F_1(k^2)$ is larger for models 2 and 4 than for models 1, 3, and 5. Now, if we look at the numerical results for the asymmetry for $N_{cmin}=0.98(0.94)$, we find, for models 1, 3, and 5, $k^2/m_b^2=0.3(0.5)$, and the set (ρ_{max},η_{max}), an asymmetry, a_{max}, around $-31.3\%(-25.6\%)$, and for the set (ρ_{min},η_{min}) we find an asymmetry, a_{max}, around $-50.3\%(-42.0\%)$. In this case, one has a ratio equal to 1.61(1.64). Finally, for models 2 and 4, we get $-36\%(-29\%)$ for the set (ρ_{max},η_{max}) and $-57\%(-48\%)$ for the set (ρ_{min},η_{min}) with a ratio equal to 1.58(1.65).

These results show explicitly the dependence of the CP violating asymmetry on form factors, CKM matrix elements and the effective parameter N_c. For the CKM matrix elements, it appears that if we take their upper limit, we obtain a smaller asymmetry, a, and vice versa. The difference between $k^2/m_b^2=0.3(0.5)$ in our results comes from the renormalization of the matrix elements of the operators in the weak Hamiltonian. Finally, the dependence on N_c comes from the fact that N_c is related to hadronization effects, and consequently, we cannot exactly determine N_c in our calculations. Therefore, we treat N_c as a free effective parameter.

TABLE II. Values of the CKM unitarity triangle for limiting values of the CKM matrix elements.

	$(\rho,\eta)_{min}$	$(\rho,\eta)_{max}$
α	86°02	89°23
β	19°50	30°64
γ	74°43	60°11

As regards the ratio between the asymmetries, we have found a ratio equal to 1.61(1.63). This is mainly determined by the ratio $\sin\gamma/\sin\beta$, and more precisely by η. In Table II, we show the values for the angles α,β,γ. From all these numerical results, we can conclude that we need to determine the value of N_c and the hadronic decay form factors more precisely, if we want to use the asymmetry, a, to constrain the CKM matrix elements.

In spite of the uncertainties just discussed, it is vital to realize that the effect of $\rho-\omega$ mixing in the $B\to\rho\pi$ decay is to remove any ambiguity concerning the strong phase, $\sin\delta$. As the internal top quark dominates the $b\to d$ transition, the weak phase in the rate asymmetry is proportional to $\sin\alpha$ $(=\sin\phi)$, where $\alpha=\arg[-(V_{td}V_{tb}^*/V_{ud}V_{ub}^*)]$, and knowing the sign of $\sin\delta$ enables us to determine that of $\sin\alpha$ from a measurement of the asymmetry, a. We show in Fig. 3 that the sign of $\sin\delta$ is always positive in our range, $0.98(0.94)<N_c<2.01(1.95)$, for all the models studied. Indeed, at the $\pi^+\pi^-$ invariant mass, where the asymmetry parameter, a, reaches a maximum, the value of $\sin\delta$ is equal to one—provided $\rho-\omega$ mixing is included—over the entire range of N_c and for all the form factors studied. So, we can remove, with the help of asymmetry, a, the uncertainty $\mathrm{mod}(\pi)$, which appears in α from the usual indirect measurements [5] which yield $\sin 2\alpha$. By contrast, in the case where we do not take $\rho-\omega$ mixing into account, we find a small value for $\sin\delta$. In Figs. 3 and 4 we plot the role of $\rho-\omega$ mixing in our

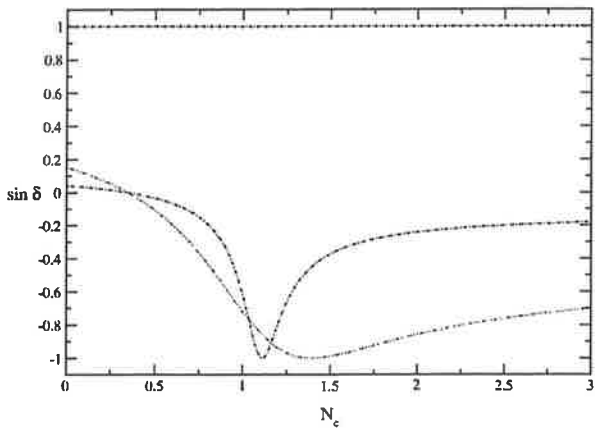

FIG. 3. Determination of the strong phase difference, $\sin\delta$, for $k^2/m_B^2=0.3(0.5)$ and for model 1. Solid line (dot line) at $\sin\delta=+1$ stands for $\tilde{\Pi}_{\rho\omega}=(-3500;-300)$ (i.e. with $\rho-\omega$ mixing). Dot dashed line (dot dot dashed line) stands for $\tilde{\Pi}_{\rho\omega}=(0;0)$, (i.e. with no $\rho-\omega$ mixing).

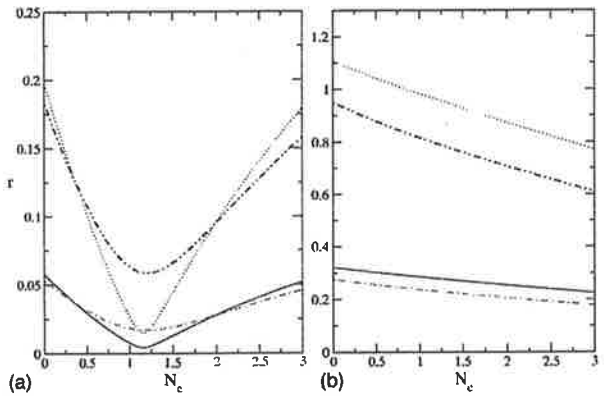

FIG. 4. Evolution of the ratio of penguin to tree amplitudes, r, for $k^2/m_B^2=0.3(0.5)$, limiting values of the CKM matrix elements (ρ,η) max(min), $\tilde{\Pi}_{\rho\omega}=(-3500;-300)(0,0)$, [i.e. with(without) $\rho-\omega$ mixing] and for model 1. Figure 4(a) (left): for $\tilde{\Pi}_{\rho\omega}=(0;0)$, solid line (dot line) stands for $k^2/m_B^2=0.3$ and (ρ,η) max (min). Dot dashed line (dot dot dashed line) stands for $k^2/m_B^2=0.5$ and (ρ,η) max (min). Figure 4(b) (right): same caption but for $\tilde{\Pi}_{\rho\omega}=(-3500;-300)$.

calculations. We stress that, even though one has a large value of $\sin\delta$ around $N_c=1$ with no $\rho-\omega$ mixing, one still has a very small value for r (Fig. 4). Hence, the CP violating asymmetry, a, remains very small in that case.

IV. BRANCHING RATIOS FOR $B^+\to\rho^0\pi^+$ AND $B^0\to\rho^+\pi^-$

A. Formalism

With the factorized decay amplitudes, we can compute the decay rates by using the following expression [19]:

$$\Gamma(B\to VP)=\frac{|\vec{p}_\rho|^3}{8\pi m_V^2}\left|\frac{A(B\to VP)}{\epsilon\cdot p_B}\right|^2, \tag{36}$$

where

$$|\vec{p}_\rho|=\frac{\sqrt{[m_B^2-(m_1+m_2)^2][m_B^2-(m_1-m_2)^2]}}{2m_B} \tag{37}$$

is the c.m. momentum of the decay particles, $m_1(m_2)$ is the mass of the vector (pseudoscalar) $V(P)$, and $A(B\to VP)$ is the decay amplitude

$$A(B\to VP)=\frac{G_F}{\sqrt{2}}\sum_{i=1,10}V_u^{T,P}a_i\langle VP|O_i|B\rangle. \tag{38}$$

Here $V_u^{T,P}$ is CKM factor

$$V_u^T=|V_{ub}V_{ud}^*| \quad \text{for } i=1,2$$

$$\text{and } V_u^P=|V_{tb}V_{td}^*| \text{ for } i=3,\ldots,10$$

where the effective parameters are the following combinations:

$$a_{2j}=c'_{2j}+\frac{1}{N_c}c'_{2j-1},$$

$$a_{2j-1}=c'_{2j-1}+\frac{1}{N_c}c'_{2j},\quad \text{for } j=1,\ldots,5$$

and $\langle VP|O_i|B\rangle$ is a matrix element which is evaluated in the factorization approach. In the quark model, the diagram coming from the $B^+\to\rho^0\pi^+$ decay is the only contribution. In our case, to be consistent, we should also take into account the $\rho-\omega$ mixing contribution when we calculate the branching ratio since we are working to the first order of isospin violation. Explicitly, we obtain, for $B^+\to\rho^0\pi^+$,

$$\begin{aligned}BR(B^+\to\rho^0\pi^+)&=\frac{G_F^2|\vec{p}_\rho|^3}{32\pi\Gamma_{B^+}}\Big|[V_u^TA^T_{\rho^0}(a_1,a_2)-V_u^PA^P_{\rho^0}(a_3,\cdots,a_{10})]\\&\quad+[V_u^TA^T_{\omega}(a_1,a_2)-V_u^PA^P_{\omega}(a_3,\cdots,a_{10})]\\&\quad\times\frac{\tilde{\Pi}_{\rho\omega}}{(s_\rho-m_\omega^2)+im_\omega\Gamma_\omega}\Big|^2,\end{aligned}\tag{39}$$

where the tree and penguin amplitudes are

$$\sqrt{2}A^T_{\rho^0}(a_1,a_2)=a_1f_\rho F_1(m_\rho^2)+a_2f_\pi A_0(m_\pi^2),$$

$$\begin{aligned}\sqrt{2}A^P_{\rho^0}(a_3,\cdots,a_{10})&=a_4[-f_\rho F_1(m_\rho^2)+f_\pi A_0(m_\pi^2)]\\&\quad+a_{10}\left[\frac{1}{2}f_\rho F_1(m_\rho^2)+f_\pi A_0(m_\pi^2)\right]\\&\quad+\frac{3}{2}(a_7+a_9)f_\rho F_1(m_\rho^2)-2(a_6+a_8)\\&\quad\times\left[\frac{m_\pi^2f_\pi A_0(m_\pi^2)}{(m_u+m_d)(m_b+m_u)}\right],\end{aligned}$$

$$\sqrt{2}A^T_{\omega}(a_1,a_2)=a_1f_\rho F_1(m_\rho^2)+a_2f_\pi A_0(m_\pi^2),$$

$$\begin{aligned}\sqrt{2}A^P_{\omega}(a_3,\cdots,a_{10})&=\left[2(a_3+a_5)+\frac{1}{2}(a_7+a_9)\right]f_\rho F_1(m_\rho^2)\\&\quad-2(a_8+a_6)\left[\frac{m_\pi^2f_\pi A_0(m_\pi^2)}{(m_u+m_d)(m_b+m_u)}\right]\\&\quad+a_4[f_\pi A_0(m_\pi^2)+f_\rho F_1(m_\rho^2)]\\&\quad+a_{10}\left[f_\pi A_0(m_\pi^2)-\frac{1}{2}f_\rho F_1(m_\rho^2)\right],\end{aligned}$$

where $\langle\rho^0|\bar{u}u|0\rangle=1/\sqrt{2}f_\rho m_\rho\epsilon_\rho$ and $\langle\pi^+|\bar{u}d|0\rangle=if_\pi p_\mu$.

For $B^0\to\rho^+\pi^-$ we obtain

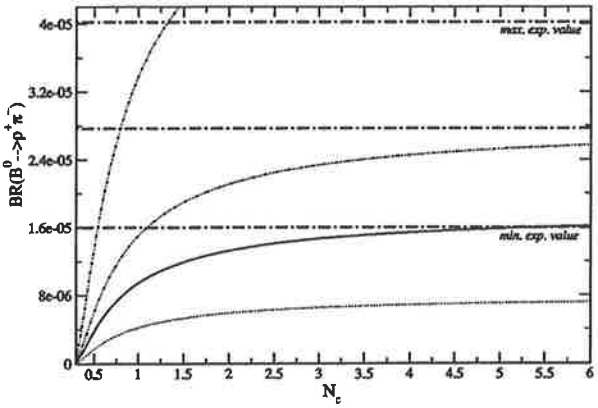

FIG. 5. Branching ratio for $B^0\to\rho^+\pi^-$ for models 1(2), $k^2/m_B^2=0.3$ and limiting values of the CKM matrix elements. Solid line (dot line) stands for model 1 and max (min) CKM matrix elements. Dot dashed line (dot dot dashed line) stands for model 2 and max (min) CKM matrix elements.

$$\begin{aligned}BR(B^0\to\rho^+\pi^-)=\frac{G_F^2|\vec{p}_\rho|^3}{16\pi\Gamma_{B^0}}&|V_u^TA^T_{\rho^+}(a_2)\\&-V_u^PA^P_{\rho^+}(a_3,\cdots,a_{10})|^2,\end{aligned}\tag{40}$$

where

$$A^T_{\rho^+}(a_2)=a_2f_\rho F_1(m_\rho^2),$$

$$A^P_{\rho^+}(a_3,\cdots,a_{10})=(a_4+a_{10})f_\rho F_1(m_\rho^2).$$

Moreover, we can calculate the ratio between these two branching ratios, in which the uncertainty caused by many systematic errors is removed. We define the ratio R as

$$R=\frac{BR(B^0\to\rho^+\pi^-)}{BR(B^+\to\rho^0\pi^+)},\tag{41}$$

and, without taking into account the penguin contribution, one has

$$\begin{aligned}R=\frac{2\Gamma_{B^+}}{\Gamma_{B^0}}&\left|\left(\frac{a_1}{a_2}+\frac{f_\pi A_0(m_\pi^2)}{f_\rho F_1(m_\rho^2)}\right)\right.\\&\left.\times\left(1+\frac{\tilde{\Pi}_{\rho\omega}}{(s_\rho-m_\omega^2)+im_\omega\Gamma_\omega}\right)\right|^{-2}.\end{aligned}\tag{42}$$

B. Numerical results

The latest experimental data from the CLEO Collaboration [6] are

$$BR(B^+\to\rho^0\pi^+)=(10.4^{+3.3}_{-3.4}\pm2.1)\times10^{-6},$$

$$BR(B^0\to\rho^+\pi^-)=(27.6^{+8.4}_{-7.4}\pm4.2)\times10^{-6},$$

$$R=2.65\pm1.9.$$

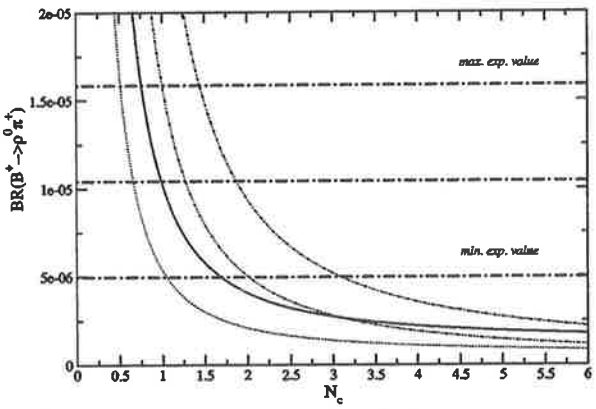

FIG. 6. Branching ratio for $B^+\to\rho^0\pi^+$ for models 1(2), $k^2/m_B^2=0.3$ and limiting values of the CKM matrix elements. Solid line (dot line) stands for model 1 and max (min) CKM matrix elements. Dot dashed line (dot dot dashed line) stands for model 2 and max (min) CKM matrix elements.

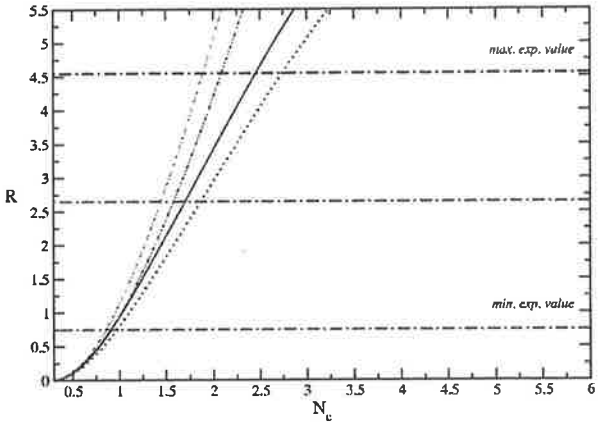

FIG. 7. Calculation of the ratio of the two $\rho\pi$ branching ratios versus N_c for models 1(2) and for limiting values of the CKM matrix elements. Solid line (dot line) stands for model 1 with max (min) CKM matrix elements. Dot dashed line (dot dot dashed line) stands for model 2 with max (min) CKM matrix elements.

TABLE III. Summary of the range of values of N_c, which is determined from the experimental data for various models and input parameters (numbers outside (inside) brackets are for $k^2/m_b^2=0.3(0.5)$). The notation: (number;number) means that there is an upper and lower limit for N_c. (number; $\star\star$) means that there is no upper limit for N_c in the range N_c [0;10]. (– ; –) means that there is no range of N_c which is consistent with experimental data.

	B^+	B^0	R
model 1			
ρ_{max} , η_{max}	0.76;1.69(0.73;1.62)	5.50; $\star\star$ (– ; –)	0.92;2.57(0.90;2.52)
ρ_{min} , η_{min}	0.52;1.04(0.49;0.98)	– ; – (– ; –)	0.97;2.88(0.94;2.76)
ρ_{max} , η_{min}	0.61;1.25(0.59;1.20)	– ; – (– ; –)	0.92;2.58(0.91;2.54)
ρ_{min} , η_{max}	0.69;1.46(0.66;1.39)	– ; – (– ; –)	0.95;2.75(0.90;2.66)
model 2			
ρ_{max} , η_{max}	1.44;3.06(1.40;2.95)	0.54;1.33(0.54;1.38)	0.86;1.89(0.84;1.86)
ρ_{min} , η_{min}	1.00;2.01(0.96;1.90)	1.10; $\star\star$ (1.15; $\star\star$)	0.92;2.09(0.89;2.01)
ρ_{max} , η_{min}	1.15;2.32(1.12;2.22)	0.70; $\star\star$ (0.72; $\star\star$)	0.87;1.89(0.85;1.86)
ρ_{min} , η_{max}	1.32;2.78(1.25;2.60)	0.63;2.77(0.62;3.12)	0.90;2.00(0.84;1.94)
model 3			
ρ_{max} , η_{max}	0.74;1.65(0.72;1.60)	– ; – (– ; –)	0.92;2.65(0.92;2.60)
ρ_{min} , η_{min}	0.51;1.02(0.49;0.98)	– ; – (– ; –)	0.97;2.95(0.94;2.85)
ρ_{max} , η_{min}	0.60;1.22(0.57;1.19)	– ; – (– ; –)	0.93;2.66(0.92;2.61)
ρ_{min} , η_{max}	0.67;1.43(0.65;1.37)	– ; – (– ; –)	0.92;2.79(0.92;2.71)
model 4			
ρ_{max} , η_{max}	1.41;3.04(1.36;2.92)	0.56;1.44(0.57;1.52)	0.86;1.91(0.85;1.87)
ρ_{min} , η_{min}	0.98;1.96(0.94;1.87)	1.16; $\star\star$ (1.23; $\star\star$)	0.90;2.10(0.89;2.03)
ρ_{max} , η_{min}	1.14;2.29(1.10;2.21)	0.72; $\star\star$ (0.74; $\star\star$)	0.86;1.92(0.85;1.88)
ρ_{min} , η_{max}	1.30;2.74(1.24;2.59)	0.64;3.49(0.66;4.03)	0.89;2.01(0.86;1.95)
model 5			
ρ_{max} , η_{max}	0.75;2.18(0.73;2.10)	– ; – (– ; –)	1.03; $\star\star$ (1.02; $\star\star$)
ρ_{min} , η_{min}	0.50;1.08(0.47;1.03)	– ; – (– ; –)	1.09; $\star\star$ (1.06; $\star\star$)
ρ_{max} , η_{min}	0.58;1.38(0.55;1.34)	– ; – (– ; –)	1.03; $\star\star$ (1.02; $\star\star$)
ρ_{min} , η_{max}	0.66;1.71(0.64;1.62)	– ; – (– ; –)	1.04; $\star\star$ (1.04; $\star\star$)

TABLE IV. Determination of the intersection of the values of N_c which are consistent with various subsets of the data for all models and all sets of CKM matrix elements [numbers outside (inside) brackets are for $k^2/m_b^2=0.3(0.5)$]. The notation: – (–) means that no common range of N_c can be extracted from the data.

	$\{N_c\}_{B^+}\cap\{N_c\}_{B^0}$	$\{N_c\}_{B^+}\cap\{N_c\}_R$	$\{N_c\}_{B^0}\cap\{N_c\}_R$
model 1			
ρ_{max},η_{max}	– (–)	0.92;1.69(0.90;1.62)	– (–)
ρ_{min},η_{min}	– (–)	0.97;1.04(0.94;0.98)	– (–)
ρ_{max},η_{min}	– (–)	0.92;1.25(0.91;1.20)	– (–)
ρ_{min},η_{max}	– (–)	0.95;1.46(0.90;1.39)	– (–)
model 2			
ρ_{max},η_{max}	– (–)	1.44;1.89(1.40;1.86)	0.86;1.33(0.84;1.38)
ρ_{min},η_{min}	1.10;2.01(1.15;1.90)	1.00;2.01(0.96;1.90)	1.10;2.09(1.15;2.01)
ρ_{max},η_{min}	1.15;2.32(1.12;2.22)	1.15;1.89(1.12;1.86)	0.87;1.89(0.85;1.86)
ρ_{min},η_{max}	1.32;2.78(1.25;2.60)	1.32;2.00(1.25;1.94)	0.90;2.00(0.84;1.94)
model 3			
ρ_{max},η_{max}	– (–)	0.92;1.65(0.92;1.60)	– (–)
ρ_{min},η_{min}	– (–)	0.97;1.02(0.94;0.98)	– (–)
ρ_{max},η_{min}	– (–)	0.93;1.22(0.92;1.19)	– (–)
ρ_{min},η_{max}	– (–)	0.92;1.43(0.92;1.37)	– (–)
model 4			
ρ_{max},η_{max}	1.41;1.44(1.36;1.52)	1.41;1.91(1.36;1.87)	0.86;1.44(0.85;1.52)
ρ_{min},η_{min}	1.16;1.96(1.23;1.87)	0.98;1.96(0.94;1.87)	1.16;2.10(1.23;2.03)
ρ_{max},η_{min}	1.14;2.29(1.10;2.21)	1.14;1.92(1.10;1.88)	0.86;1.92(0.85;1.88)
ρ_{min},η_{max}	1.30;2.74(1.24;2.59)	1.30;2.01(1.24;1.95)	0.89;2.01(0.86;1.95)
model 5			
ρ_{max},η_{max}	– (–)	1.03;2.18(1.02;2.10)	– (–)
ρ_{min},η_{min}	– (–)	– (–)	– (–)
ρ_{max},η_{min}	– (–)	1.03;1.38(1.02;1.34)	– (–)
ρ_{min},η_{max}	– (–)	1.04;1.71(1.04;1.62)	– (–)

We have calculated the branching ratios for $B^0\to\rho^+\pi^-$ and for $B^+\to\rho^0\pi^+$ for all models as a function of N_c. In Figs. 5 and 6, we show the results for models 1 and 2 in order to make the dependence on form factors explicit.

The numerical results are very sensitive to uncertainties coming from the experimental data. For the branching ratio $B^0\to\rho^+\pi^-$ (Fig. 5), we have a large range of values of N_c and CKM matrix elements over which the theoretical results are consistent with the experimental data from CLEO. However, all models do not give the same result: models 2 and 4 are very close to the experimental data for a large range of N_c, whereas models 1, 3 and 5 are not. The reason is still the magnitude of the form factors. As a result, we have to exclude models 1, 3 and 5 because their form factors are too small.

If we consider numerical results for branching ratio $B^+\to\rho^0\pi^+$ (Fig. 6), it appears that all models are consistent with the experimental data for a large range of N_c. The effect of $\rho-\omega$ mixing (included in our calculations) on the branching ratio $B^+\to\rho^0\pi^+$ is around 30%. Numerical results for models 1, 3, and 5, as well as for models 2 and 4, are very close to each other. The difference between the two branching ratios can be explained by the fact that for the $B^0\to\rho^+\pi^-$ decay, the tree and penguin contributions are both proportional to only one form factor, $F_1(k^2)$. Thus, this branching ratio is very sensitive to the magnitude of this form factor [$F_1(k^2)$ is related to $h_1=0.330$ or 0.625 in models (1,3) and (2,4), respectively]. On the other hand, for the decay $B^+\to\rho^0\pi^+$, both $F_1(k^2)$ and $A_0(k^2)$ are included in the tree and penguin amplitudes, and this branching ratio is less sensitive to the magnitude of the form factors.

If we look at the ratio R between these two branching ratios, $BR(B^+\to\rho^0\pi^+)$ and $BR(B^0\to\rho^+\pi^-)$—shown in Fig. 7—the results indicate that R is very sensitive to the magnitude of the form factors, and that there is a large difference between models 1, 3, and 5 and models 2 and 4. We investigated the ratio R for the limiting CKM matrix elements as a function of N_c, finding that R is consistent with the experimental data over the range $0.98(0.94)<N_c<2.01(1.95)$ [the values outside (inside) brackets correspond to the choice $q^2/m_b^2=0.3(0.5)$]. It should be noted that R, in particular, is not very sensitive to the CKM matrix elements. The small difference which does appear comes from the penguin contributions (which may be neglected). If we just take into account the tree contributions in our calculations, R is clearly independent of the CKM matrix elements [Eq. (42)].

From a comparison of the numerical results and the experimental data, we can extract a range of N_c, within which all results are consistent. In Table III, we have summarized the allowed range of N_c for $B^+\to\rho^0\pi^+$, $B^0\to\rho^+\pi^-$ and R,

TABLE V. Best range of N_c determined from Table IV for $k^2/m_b^2=0.3(0.5)$. One takes the maximum interval of N_c, from Table IV, for each model (2,4). To determine the maximum (minimum) range, one considers all models (2,4) and the largest (smallest) range of N_c. In comparison, we show the range of N_c determined without $\rho-\omega$ mixing.

	$\{N_c\}$ with mixing	$\{N_c\}$ without mixing
model 2	1.00;2.01(0.96;1.94)	0.85;1.74(0.85;1.74)
model 4	0.98;2.01(0.94;1.95)	0.84;1.76(0.84;1.75)
maximum range	0.98;2.01(0.94;1.95)	0.84;1.76(0.84;1.75)
minimum range	1.00;2.01(0.96;1.94)	0.85;1.74(0.85;1.74)

for models 1, 2, 3, 4 and 5, according to various choices of the CKM matrix elements. To determine the best range of N_c, we have to find some intersection of the values of N_c for each model and for each set of CKM matrix elements, for which the theoretical and experimental results are consistent. This is possible and the results are shown in Table IV. In our study, it seems better to use the range intersection $\{N_c\}_{B^+}\cap\{N_c\}_R$ rather than $\{N_c\}_{B^0}\cap\{N_c\}_{B^+}$, for fixing the final interval N_c, since the experimental uncertainties are smaller in the former case, and since we are working to the first order of isospin violation ($\rho-\omega$ mixing). Finally, after excluding models 1, 3 and 5, which are not consistent with all the experimental data, we are able to fix the upper and lower limit of the range of N_c, using the limiting values of the CKM matrix elements (Table V). We find that N_c should be in the range $0.98(0.94)<N_c<2.01(1.95)$, where N_{cmin} and N_{cmax} correspond to (ρ_{min},η_{min}) and (ρ_{max},η_{max}), respectively.

V. SUMMARY AND DISCUSSION

The first aim of the present work was to compare our theoretical results with the latest experimental data from the CLEO Collaboration for the branching ratios $B^+\to\rho^0\pi^+$ and $B^0\to\rho^+\pi^-$. Our next aim was to study direct CP violation for the decay $B^+\to\rho^0(\omega)\pi^+\to\pi^+\pi^-\pi^+$, with the inclusion of $\rho-\omega$ mixing. The advantage of $\rho-\omega$ mixing is that the strong phase difference is large and rapidly varying near the ω resonance. As a result the CP violating asymmetry, a, has a maximum, a_{max}, when the invariant mass of the $\pi^+\pi^-$ pair is in the vicinity of the ω resonance and $\sin\delta=+1$ at this point.

In the calculation of CP violating asymmetry parameters, we need the Wilson coefficients for the tree and penguin operators at the scale m_b. We worked with the renormalization scheme independent Wilson coefficients. One of the major uncertainties is that the hadronic matrix elements for both tree and penguin operators involve nonperturbative QCD. We have worked in the factorization approximation, with N_c treated as an effective parameter. Although one must have some doubts about factorization, it has been pointed out that it may be quite reliable in energetic weak decays [22,23].

We have explicitly shown that the CP violating asymmetry, a, is very sensitive to the CKM matrix elements and the magnitude of the form factors, and we have also determined a range for the maximum asymmetry, a_{max}, as a function of the parameter N_c, the limits of CKM matrix elements and the choice of $k^2/m_b^2=0.3(0.5)$. From all the models investigated, we found that CP violating asymmetry, a_{max}, varies from $-24\%(-19\%)$ to $-59\%(-48\%)$. We stressed that the ratio between the asymmetries associated with the limiting values of CKM matrix elements would be mainly determined by η. Moreover, we also stressed that without $\rho-\omega$ mixing, we cannot have a large CP violating asymmetry, a, since a is proportional to both $\sin\delta$ and r. Even though $\sin\delta$ is large around $N_c=1$, r is very small. As a result, we find a very small value for the CP violation in the decay $B^{\pm}\to\rho^0\pi^{\pm}$ (of the order of a few percent) without mixing. Once mixing is included, the sign of $\sin\delta$ is positive for N_c:$0.98(0.94)<N_c<2.01(1.95)$. Indeed, at the $\pi^+\pi^-$ invariant mass, where the asymmetry, a, is maximum, $\sin\delta=+1$ independent of the parameters used. Thus, by measuring a, we can erase the phase uncertainty $\mathrm{mod}(\pi)$ in the determination of the CKM angle α, which arises from the conventional determination of $\sin 2\alpha$.

The theoretical results for the branching ratios, $B^+\to\rho^0\pi^+$ and $B^0\to\rho^+\pi^-$, were compared with the experimental data from the CLEO Collaboration [6]. These calculations show that it is possible to have theoretical results consistent with the experimental data without needing to invoke contributions from other resonances [24,25]. This data helped us to constrain the magnitude of the various form factors needed in the theoretical calculations of B decays.[1] We determined a range of value of N_c, $0.98(0.94)<N_c<2.01(1.95)$, inside of which the experimental data and the theoretical calculations are consistent for models 2 and 4.

We will need more accurate data in the future to further decrease the uncertainties in the calculation. If we can use both the CP violating asymmetry and the branching ratios, with smaller uncertainties, we expect to be able to determine the CKM matrix elements more precisely. At the very least, it appears that one will be able to unambiguously determine the sign of $\sin\alpha$ and hence, remove the well known discrete uncertainties in α associated with the fact that indirect CP violation determines only $\sin 2\alpha$. We expect that our predictions should provide useful guidance for future investigations and urge our experimental colleagues to seriously plan to measure the rather dramatic direct CP violation predicted here.

ACKNOWLEDGMENTS

This work was supported in part by the Australian Research Council and the University of Adelaide.

[1]We note that BABAR reported preliminary branching ratios for this channel after this paper was prepared [26]. These results are consistent with the CLEO values.

[1] A. B. Carter and A. I. Sanda, Phys. Rev. Lett. **45**, 952 (1980); Phys. Rev. D **23**, 1567 (1981); I. I. Bigi and A. I. Sanda, Nucl. Phys. **B193**, 85 (1981).
[2] *Proceedings of the Workshop on CP Violation*, edited by X.-H. Guo, M. Sevior, and A. W. Thomas (World Scientific, Singapore, 1998).
[3] R. Enomoto and M. Tanabashi, Phys. Lett. B **386**, 413 (1996).
[4] S. Gardner, H. B. O'Connell, and A. W. Thomas, Phys. Rev. Lett. **80**, 1834 (1998).
[5] X.-H. Guo and A. W. Thomas, Phys. Rev. D **58**, 096013 (1998); **61**, 116009 (2000).
[6] CLEO Collaboration, C. P. Jessop *et al.*, Phys. Rev. Lett. **85**, 2881 (2000).
[7] G. Buchalla, A. J. Buras, and M. E. Lautenbacher, Rev. Mod. Phys. **68**, 1125 (1996).
[8] N. G. Deshpande and X.-G. He, Phys. Rev. Lett. **74**, 26 (1995).
[9] R. Fleischer, Int. J. Mod. Phys. A **12**, 2459 (1997); Z. Phys. C **62**, 81 (1994); **58**, 483 (1993).
[10] G. Kramer, W. Palmer, and H. Simma, Nucl. Phys. **B428**, 77 (1994).
[11] Particle Data Group, D. E. Groom *et al.*, Eur. Phys. J. C **15**, 1 (2000).
[12] H. B. O'Connell, A. W. Thomas, and A. G. Williams, Nucl. Phys. **A623**, 559 (1997); K. Maltman, H. B. O'Connell, and A. G. Williams, Phys. Lett. B **376**, 19 (1996).
[13] S. Gardner and H. B. O'Connell, Phys. Rev. D **57**, 2716 (1998).
[14] L. Wolfenstein, Phys. Rev. Lett. **51**, 1945 (1983); **13**, 562 (1984).
[15] M. Bauer, B. Stech, and M. Wirbel, Z. Phys. C **34**, 103 (1987); M. Wirbel, B. Stech, and M. Bauer, *ibid.* **29**, 637 (1985).
[16] S. Mele, Phys. Rev. D **59**, 113011 (1999).
[17] F. Parodi, P. Roudeau, and A. Stocchi, Nuovo Cimento A **112**, 833 (1999); F. Parodi, invited talk presented at the XXIX International Conference on High Energy Physics, Vancouver, 1998; A. Stocchi, hep-ex/9902004.
[18] X.-H. Guo and T. Huang, Phys. Rev. D **43**, 2931 (1991).
[19] Y.-H. Chen, H.-Y. Cheng, B. Tseng, and K.-C. Yang, Phys. Rev. D **60**, 094014 (1999).
[20] P. Ball, J. High Energy Phys. **09**, 005 (1998).
[21] P. Ball and V. M. Braun, Phys. Rev. D **58**, 094016 (1998).
[22] M. J. Dugan and B. Grinstein, Phys. Lett. B **255**, 583 (1991).
[23] H.-Y. Cheng, Phys. Lett. B **335**, 428 (1994); **395**, 345 (1997); H.-Y. Cheng, Phys. Rev. D **58**, 094005 (1998).
[24] A. Deandrea, R. Gatto, M. Ladisa, G. Nardulli, and P. Santorelli, Phys. Rev. D **62**, 036001 (2000).
[25] A. Deandrea, hep-ph/0005014.
[26] BABAR Collaboration, B. Aubert *et al.*, hep-ex/0008058.

ADP-03-124/T561
PCCF-RI-03-0308

QCD Factorization in B Decays into $\rho\pi$[1]

X.-H. Guo[†2], O.M.A. Leitner[†,‡3], A.W. Thomas[†4]

[†] *Department of Physics and*
Special Research Centre for the Subatomic Structure of Matter,
University of Adelaide, Adelaide 5005, Australia
[‡] *Laboratoire de Physique Corpusculaire de Clermont-Ferrand*
IN2P3/CNRS Université Blaise Pascal
F-63177 Aubière Cedex France

Abstract. Based on the QCD factorization approach we analyse the branching ratios for the channel $B \to \rho\pi$. From the comparisons with experimental data provided by CLEO, BELLE and BABAR we constrain the form factor $F^{B\to\pi}(m_\rho^2)$ and propose boundaries for this form factor depending on the CKM matrix element parameters ρ and η.

1. NAIVE FACTORIZATION

The investigation of B decays requires a knowledge of both the soft and hard interactions which control the dynamics of quarks and gluons. Because the energy involved in B decays covers a large range, from m_b down to Λ_{QCD}, it is necessary to describe the phenomenon with accuracy. Recently, the BELLE, BABAR, and CLEO facilities have been providing more and more data which can be compared with theoretical results and hence increase our knowledge in this area.

In any phenomenological treatment of the weak decays of hadrons, the starting point is the weak effective Hamiltonian at low energy [1, 2, 3, 4, 5]. It is obtained by integrating out the heavy fields (e.g. the top quark, W and Z bosons) from the Standard Model Lagrangian. It can be written as,

$$\mathcal{H}_{eff} = \frac{G_F}{\sqrt{2}} \sum_i V_{CKM} C_i(\mu) O_i(\mu) \,, \tag{1}$$

where G_F is the Fermi constant, V_{CKM} is the CKM matrix element, $C_i(\mu)$ are the Wilson coefficients, $O_i(\mu)$ are the operators entering the Operator Product Expansion and μ represents the renormalization scale. In the present case, since we analyse direct CP

---

[1] Presented at Fourth Tropical Workshop, Cairns, Australia, 9-13 June 2003.
[2] xhguo@physics.adelaide.edu.au
[3] oleitner@physics.adelaide.edu.au
[4] athomas@physics.adelaide.edu.au

violation in B decays into $\rho\pi$, we take into account both tree and penguin operators and the effective Hamiltonian is,

$$\mathscr{H}_{eff}^{\Delta B=1} = \frac{G_F}{\sqrt{2}}\left[V_{ub}V_{uq}^*(C_1O_1^q + C_2O_2^q) - V_{tb}V_{tq}^*\sum_{i=3}^{10}C_iO_i\right] + h.c.\,, \tag{2}$$

where $q = d$. Consequently, the decay amplitude can be expressed as follows,

$$A(B \to PV) = \frac{G_F}{\sqrt{2}}\left[V_{ub}V_{uq}^*\left(C_1\langle PV|O_1^q|B\rangle + C_2\langle PV|O_2^q|B\rangle\right) - V_{tb}V_{tq}^*\sum_{i=3}^{10}C_i\langle PV|O_i|B\rangle\right] + h.c.\,, \tag{3}$$

where $\langle PV|O_i|B\rangle$ are the hadronic matrix elements, and $P(V)$ indicates a pseudoscalar (vector) meson. The matrix elements describe the transition between initial and final state at scales lower than μ and include, up to now, the main uncertainties in the calculation because it involves the non-perturbative physics.

The computation of the hadronic matrix elements, $\langle PV|O_i|B\rangle$, is not trivial and requires some assumptions. The general method which has been used is the so-called "factorization" procedure [6, 7, 8], in which one approximates the matrix element as a product of a transition matrix element between a B meson and one final state meson and a matrix element which describes the creation of the second meson from the vacuum. This can be formulated as,

$$\begin{aligned}\langle PV|O_i|B\rangle &= \langle V|J_{2i}|0\rangle\,\langle P|J_{1i}|B\rangle\,,\\ \text{or } \langle PV|O_i|B\rangle &= \langle P|J_{4i}|0\rangle\,\langle V|J_{3i}|B\rangle\,,\end{aligned} \tag{4}$$

where the J_{ji} are the transition currents. This approach is known as *naive* factorization since it factorizes $\langle PV|O_i|B\rangle$ into a simple product of two quark matrix elements, (see Fig. 1). Analytically, Fig. 1 can be written down as,

$$A(B \to PV) \propto \left[\sum_{i=1}^{10}V_{CKM}C_i(\mu)\langle M_1M_2|O_i|B\rangle\right] \propto \left[\sum_{i=1}^{10}V_{CKM}C_i(\mu)\langle M_1|J_{2i}|0\rangle\langle M_2|J_{1i}|B\rangle\right]. \tag{5}$$

A possible justification for this approximation has been given by Bjorken [9]: the heavy quark decays are very energetic, so the quark-antiquark pair in a meson in the final state moves very fast away from the localised weak interaction. The hadronization of the quark-antiquark pair occurs far away from the remaining quarks. Then, the meson can be factorized out and the interaction between the quark pair in the meson and the remaining quark is tiny.

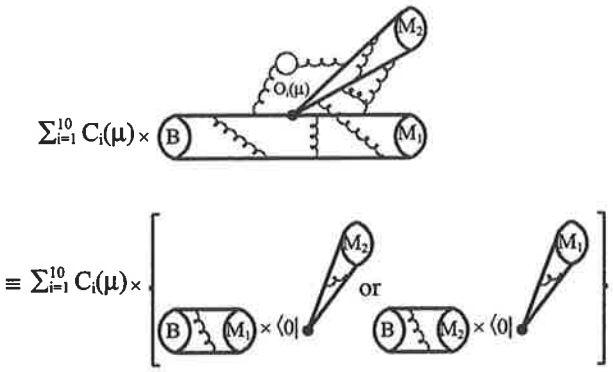

FIGURE 1. Naive factorization, where M_1 and M_2 represent the final meson states.

The main uncertainty in this approach is that the final state interactions (FSI) are neglected. Corrections associated with the factorization hypothesis are parameterized and hence there maybe large uncertainties [10]. In spite of this, there are indications that should give a good estimate of the magnitude of the B decay amplitude in many cases [11, 12]. In order to improve the estimate of the hadronic matrix element, we will briefly present in Section 2 the formalism of QCD factorization, which is an extension of naive factorization. We will see how it is possible to incorporate QCD corrections in order to include the FSI at the first order in α_s into the factorization approach. In Section 3, we will list our numerical results for the branching ratios related to the channels $B \to \rho\pi$ and $B \to \omega\pi$. In Section 4, we will constrain the form factor $F_1^{B\to\pi}$ and propose boundaries for this form factor depending on the CKM matrix element parameters ρ and η. Finally, in the last section we will summarize our analysis and draw some conclusions.

2. QCD FACTORIZATION

Factorization in charmless B decays involves three fundamental scales: the weak interaction scale M_W, the b quark mass scale m_b, and the strong interaction scale Λ_{QCD}. It is well known that the non-leptonic decay amplitude for $B \to PV$ is proportional to:

$$A(B \to PV) \propto \sum_i C_i(\mu)\langle PV|O_i(\mu)|B\rangle \,, \tag{6}$$

where we have omitted the CKM factor and Fermi constant for simplicity. The matrix elements $\langle PV|O_i(\mu)|B\rangle$ contain non-perturbative effects which cannot be accurately evaluated. The coefficients $C_i(\mu)$ include strong interaction effects from the scales M_W down to m_b and is under control. The aim is therefore to obtain a good estimate of the matrix elements without assuming naive factorization. In QCD factorization (QCDF), assuming a heavy quark expansion when $m_b \gg \Lambda_{QCD}$ and soft collinear factorization where

the particle energies are bigger than the scale Λ_{QCD}, the matrix elements $\langle PV|O_i(\mu)|B\rangle$ can be written as [13]:

$$\langle PV|O_i(\mu)|B\rangle = \langle P|j_1|B\rangle\langle V|j_2|0\rangle\left[1+\sum_n r_n\alpha_s^n + \mathcal{O}(\Lambda_{QCD}/m_b)\right], \quad (7)$$

where r_n refers to the radiative corrections in α_s and j_i are the quark currents. It is straightforward to see that if we neglect the corrections at the order α_s, we recover the conventional naive factorization in the heavy quark limit. We can rewrite the matrix elements $\langle PV|O_i(\mu)|B\rangle$, at the leading order in Λ_{QCD}/m_b, in the QCDF approach by using a partonic language and one has [13, 14, 15, 16, 17, 18]:

$$\langle PV|O_i(\mu)|B\rangle = F_j^{B\to P}(m_V^2)\int_0^1 dx T_{ij}^I(x)\phi_V(x) + A_k^{B\to V}(m_P^2)\int_0^1 dy T_{ik}^I(y)\phi_P(y) + \int_0^1 d\xi\int_0^1 dx\int_0^1 dy T_i^{II}(\xi,x,y)\phi_B(\xi)\phi_V(x)\phi_P(y), \quad (8)$$

where ϕ_M (with $M = V,P,B$) are the leading twist light cone distribution amplitudes (LCDA) of valence quark Fock states. The light cone momentum fractions of the constituent quarks of the vector, pseudo-scalar and B mesons are given respectively by x,y, and ξ. The form factors for $B\to P$ and $B\to V$ semi-leptonic decays evaluated at $k^2 = 0$ are denoted by $F_j^{B\to P}(m_V^2)$ and $A_k^{B\to V}(m_P^2)$. Eq. (8) can be understood via Fig. 2 where a graphical representation of the factorization formula is given. The hadronic

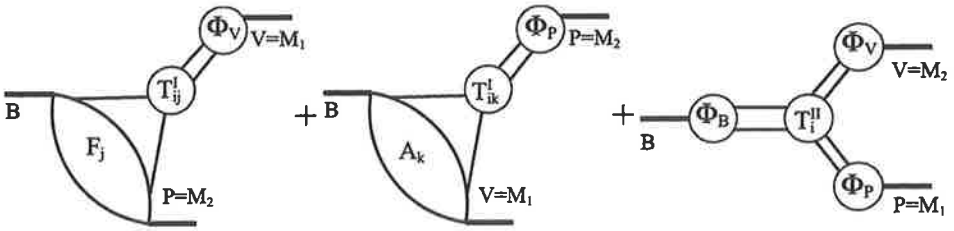

FIGURE 2. Graphical representation of the QCD factorization formula.

decay amplitude involves both soft and hard contributions. At leading order, all the non-perturbative effects are contained in the form factors and the light cone distributions amplitudes. Then, non-factorizable interactions are dominated by hard gluon exchanges (in the case where the $O(\Lambda_{QCD}/m_b)$ terms are neglected) and can be calculated perturbatively, in order to correct the naive factorization approximation. These hard scattering kernels [13, 14, 15, 16, 17, 18, 19], T_{ik}^I and T_i^{II}, are calculable order by order in perturbation theory. The naive factorization terms are recovered by the leading terms of T_{ik}^I coming from the tree level contributions, whereas vertex corrections and penguin corrections are included at higher orders of α_s in T_{ik}^I. The hard interactions (at order $O(\alpha_s)$) between the spectator quark and the emitted meson, at large gluon momentum, are taken into account by T_i^{II}.

2.1. The QCD coefficients a_i

The coefficients a_i [20, 21], have been calculated at next-to-leading order. They contain all the non-factorizable effects at order in α_s. In order to clearly separate every contribution, the coefficients a_i are written as the sum of,

$$a_i = a_{i,I} + a_{i,II} \,, \tag{9}$$

where the first term includes the naive factorization, the vertex and penguin corrections, while the second term contains the hard spectator interactions. According to the final states, the terms a_i have to be expressed for two different cases: case A corresponds to the situation where the recoiling meson M_1 is a vector and the emitted meson M_2 is a pseudoscalar, and vice-versa for case B. For case A, the coefficients a_i take the form [20, 21],

$$\begin{aligned}
a_{1,I} &= C_1 + \frac{C_2}{N_c^{eff}}\left[1 + \frac{C_F\alpha_s}{4\pi}V_M\right], & a_{1,II} &= \frac{\pi C_F\alpha_s}{N_c^{eff2}}C_2 H(BM_1, M_2), \\
a_{2,I} &= C_2 + \frac{C_1}{N_c^{eff}}\left[1 + \frac{C_F\alpha_s}{4\pi}V_M\right], & a_{2,II} &= \frac{\pi C_F\alpha_s}{N_c^{eff2}}C_1 H(BM_1, M_2), \\
a_{3,I} &= C_3 + \frac{C_4}{N_c^{eff}}\left[1 + \frac{C_F\alpha_s}{4\pi}V_M\right], & a_{3,II} &= \frac{\pi C_F\alpha_s}{N_c^{eff2}}C_4 H(BM_1, M_2), \\
a_{4,I}^p &= C_4 + \frac{C_3}{N_c^{eff}}\left[1 + \frac{C_F\alpha_s}{4\pi}V_M\right] + a_{4,I,b}^p, & a_{4,II} &= \frac{\pi C_F\alpha_s}{N_c^{eff2}}C_3 H(BM_1, M_2), \\
a_{5,I} &= C_5 + \frac{C_6}{N_c^{eff}}\left[1 - \frac{C_F\alpha_s}{4\pi}V_M'\right], & -a_{5,II} &= \frac{\pi C_F\alpha_s}{N_c^{eff2}}C_6 H'(BM_1, M_2), \\
a_{6,I}^p &= C_6 + \frac{C_5}{N_c^{eff}}\left[1 - 6\frac{C_F\alpha_s}{4\pi}\right] + a_{6,I,b}^p, & a_{6,II} &= 0, \\
a_{7,I} &= C_7 + \frac{C_8}{N_c^{eff}}\left[1 - \frac{C_F\alpha_s}{4\pi}V_M'\right], & -a_{7,II} &= \frac{\pi C_F\alpha_s}{N_c^{eff2}}C_8 H'(BM_1, M_2), \\
a_{8,I}^p &= C_8 + \frac{C_7}{N_c^{eff}}\left[1 - 6\frac{C_F\alpha_s}{4\pi}\right] + a_{8,I,b}^p, & a_{8,II} &= 0, \\
a_{9,I} &= C_9 + \frac{C_{10}}{N_c^{eff}}\left[1 + \frac{C_F\alpha_s}{4\pi}V_M\right], & a_{9,II} &= \frac{\pi C_F\alpha_s}{N_c^{eff2}}C_{10} H(BM_1, M_2), \\
a_{10,I}^p &= C_{10} + \frac{C_9}{N_c^{eff}}\left[1 + \frac{C_F\alpha_s}{4\pi}V_M\right] + a_{10,I,b}^p, & a_{10,II} &= \frac{\pi C_F\alpha_s}{N_c^{eff2}}C_9 H(BM_1, M_2),
\end{aligned} \tag{10}$$

where the terms $a_{4,I,b}^p, a_{6,I,b}^p, a_{8,I,b}^p$ and $a_{10,I,b}^p$ are,

$$\begin{aligned}
a_{4,I,b}^p &= \frac{C_F\alpha_s}{4\pi}\frac{P_{M,2}^p}{N_c^{eff}}, & a_{6,I,b}^p &= \frac{C_F\alpha_s}{4\pi}\frac{P_{M,3}^p}{N_c^{eff}}, \\
a_{8,I,b}^p &= \frac{\alpha}{9\pi}\frac{P_{M,3}^{p,ew}}{N_c^{eff}}, & a_{10,I,b}^p &= \frac{\alpha}{9\pi}\frac{P_{M,2}^{p,ew}}{N_c^{eff}}.
\end{aligned} \tag{11}$$

In Eqs. (10) and (11) V_M, V'_M represent the vertex corrections, H, H' describe hard gluon exchanges between the spectator quark in the B meson and the emitted meson (pseudoscalar or vector). $P^p_{M,2}, P^p_{M,3}, P^{p,ew}_{M,3}, P^{p,ew}_{M,2}$ are the QCD penguin contributions and electroweak penguin contributions, respectively. These quantities are a result of the convolution of hard scattering kernels G, with meson distribution amplitudes, Φ. We refer the reader to Refs. [13, 14, 15, 16, 17, 18] for more details. Other parameters are $C_i \equiv C_i(\mu)$ (in NDR), $\alpha_s \equiv \alpha_s(\mu)$ (next to leading order), and $C_F = (N_c^2 - 1)/2N_c$ with $N_c = 3$.

3. NUMERICAL RESULTS

Assuming that all of the parameters involved in QCD factorization are constrained by independent studies where the input parameters related to factorization were fitted, we concentrate our efforts on the form factor $F_1^{B\to\pi}$ depending on the CKM matrix parameters ρ and η. In order to reach this aim, we have calculated the branching ratios for B decays such as $B^\pm \to \rho^0\pi^\pm, B^0 \to \rho^\pm\pi^0, B^0 \to \rho^\pm\pi^\mp, B^0 \to \rho^0\pi^0$ and $B^\pm \to \omega\pi^\pm$ where the annihilation and $\rho - \omega$ mixing contributions were taken into account. All the results are shown in Figs. 3, 4 and 5, and the branching ratios are plotted as a function of the form factor $F_1^{B\to\pi}$ and as a function of the values of ρ and η as well.

By taking into account experimental data from CLEO [22, 23, 24, 25, 26, 27], BELLE [28, 29, 30, 31, 32, 33, 34, 35, 36] and BABAR [37, 38, 39, 40, 41, 42, 43, 44], and comparing theoretical predictions with experimental results, we expect to obtain a constraint on the form factor $F_1^{B\to\pi}$ depending on the CKM matrix element parameters ρ and η. Because of the accuracy of the data, we shall mainly use the CLEO and BELLE data for our analysis rather than those from BABAR. We expect that our results should depend more on uncertainties coming from the experimental data than those from the factorization approach (as opposed to naive factorization) applied to calculate hadronic matrix element $\langle\rho\pi|J_\mu|B\rangle$ since in B decays, $1/m_b$ corrections are very small.

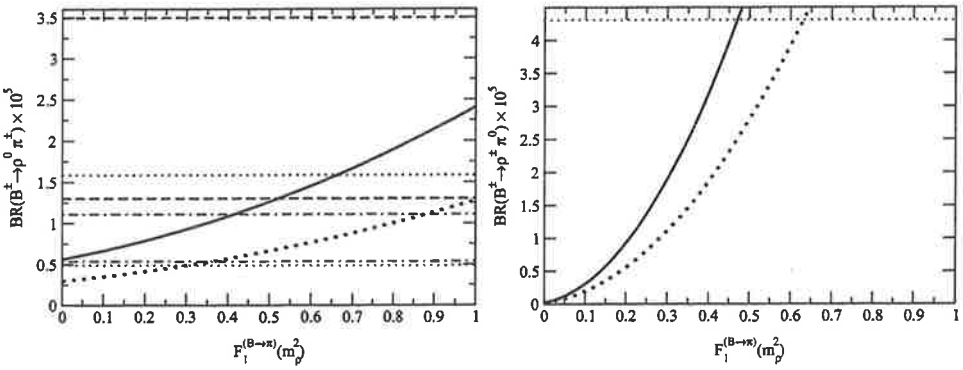

FIGURE 3. Branching ratio for $B^\pm \to \rho^0\pi^\pm$, for limiting values of the CKM matrix elements (Left hand-side). Branching ratio for $B^\pm \to \rho^\pm\pi^0$, for limiting values of the CKM matrix elements (Right hand-side). Solid line (dotted line) for max (min) CKM matrix elements. Notation: horizontal dotted lines: CLEO data; horizontal dashed lines: BABAR data; horizontal dot-dashed lines: BELLE data.

For the branching ratio $B^{\pm} \to \rho^0 \pi^{\pm}$ (Fig. 3), we found total consistency between the theoretical results and experimental data from CLEO and BELLE. However, these results allow us to determine an upper limit (between 0.40 and 0.65) for the value of the form factor $F_1^{B\to\pi}$. The weak dependence of the branching ratio on the form factor, $F_1^{B\to\pi}$, is related to the tree and penguin amplitudes which are mainly governed by the form factor $A_0^{B\to\rho}$ rather than $F_1^{B\to\pi}$. Therefore, this branching ratio cannot be used as an efficient way to constrain the form factor $F_1^{B\to\pi}$. Note also that the comparison with BABAR data shows agreement between theory and experiment when $F_1^{B\to\pi}$ is bigger than 0.5.

For the branching ratio $B^{\pm} \to \rho^{\pm} \pi^0$ (Fig. 3), CLEO gives only an upper limit for the branching ratio whereas BABAR and BELLE do not. Based on this upper limit, the value of the form factor $F_1^{B\to\pi}$ must be lower than 0.62. We emphasize that this branching ratio is strongly dependent on the form factor $F_1^{B\to\pi}$ and hence provides an efficient constraint for the value of $F_1^{B\to\pi}$. For the branching ratio $B^0 \to \rho^{\pm} \pi^{\mp}$ (shown in Fig. 4), BELLE, BABAR and CLEO give consistent experimental data. The decay amplitude related to this branching ratio is proportional to the form factor $F_1^{B\to\pi}$ and thus allows us to constrain the form factor effectively. Requiring agreement between experimental values and theoretical results yields a central value for $F_1^{B\to\pi}$ which is about 0.3. Note that for these three branching ratios their dependence on the CKM matrix elements ρ and η is strong. Hence we expect to be able to determine limits for their values when more B decay channels are taken into account.

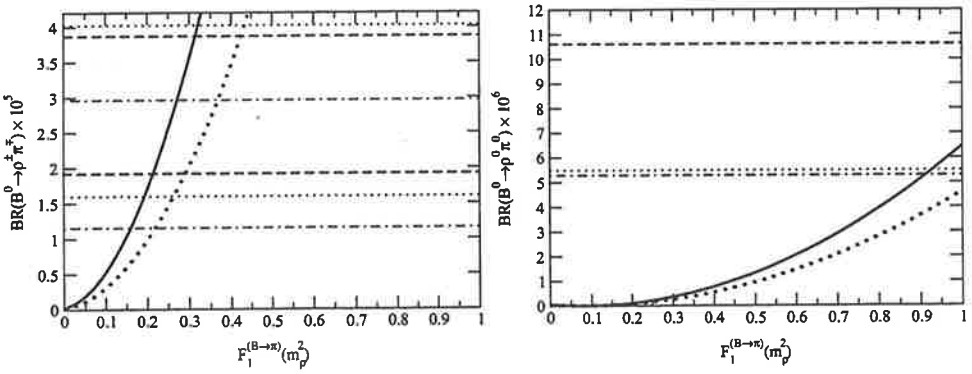

FIGURE 4. Branching ratio for $B^0 \to \rho^{\pm}\pi^{\mp}$, for limiting values of the CKM matrix elements (Left hand-side). Branching ratio for $B^0 \to \rho^0\pi^0$, for limiting values of the CKM matrix elements (Right hand-side). Solid line (dotted line) for max (min) CKM matrix elements. Notation: horizontal dotted lines: CLEO data; horizontal dashed lines: BABAR data; horizontal dot-dashed lines: BELLE data.

For the branching ratio $B^0 \to \rho^0 \pi^0$ (Fig. 4), BABAR, BELLE and CLEO only give an upper limit for the branching ratio. However, the branching ratio does not appear to be very sensitive to the CKM matrix elements ρ and η. That could help us to obtain an upper limit for $F_1^{B\to\pi}$ which is not sensitive to ρ and η. We therefore need new data to go further in this case. Finally, we focus on the branching ratio $B^{\pm} \to \omega \pi^{\pm}$, plotted in Fig. 5. There is no agreement with the CLEO data for values of the form factor $F_1^{B\to\pi}$ lower than 0.25 whereas there is a good agreement with BABAR and BELLE for any

value of $F_1^{B\to\pi}$. Note that in this case the sensitivity of the branching ratio to the CKM matrix elements is bigger than that to the form factor $F_1^{B\to\pi}$ and does not allow us to draw any conclusions regarding the value of $F_1^{B\to\pi}$.

To remove systematic errors in branching ratio data given by the B factories, we can look at the ratio R_π of the two following branching ratios: $\mathscr{B}(B^0 \to \rho^\pm\pi^\mp)$ and $\mathscr{B}(B^\pm \to \rho^0\pi^\pm)$. In Fig. 5 we show the ratio, R_π, as a function of the form factor $F_1^{B\to\pi}$. All the B factory data are in good agreement with theoretical predictions. The results indicate that the ratio is not sensitive to the CKM matrix elements ρ and η whereas it is very sensitive to the value of $F_1^{B\to\pi}$. Comparison with the data shows that $F_1^{B\to\pi}$ is between 0.13 and 0.30 (BELLE), 0.05 and 0.20 (BABAR), and 0.10 and 0.35 (CLEO), respectively. Assuming that the value of $F_1^{B\to\pi}$ at $k^2 = m_\rho^2$ is around 0.30, we have $\mathscr{B}(B^0 \to \rho^\pm\pi^0) \approx 14.2 \times 10^{-6}$ and $\mathscr{B}(B^0 \to \rho^0\pi^0) < 1 \times 10^{-6}$.

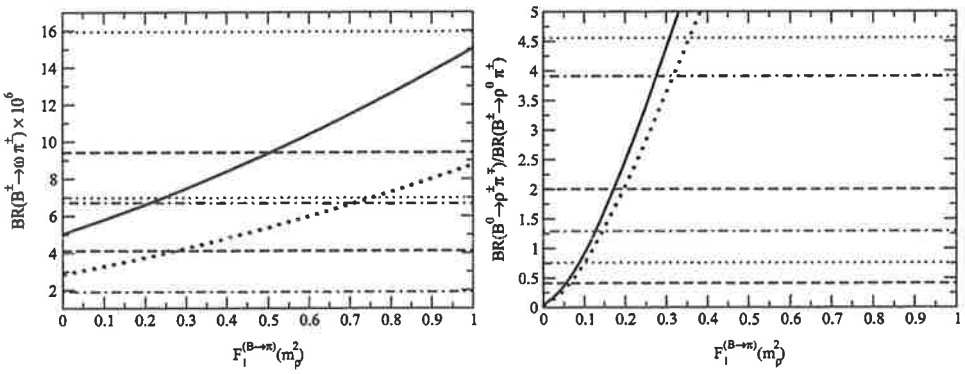

FIGURE 5. Branching ratio for $B^\pm \to \omega\pi^\pm$, for limiting values of the CKM matrix elements (Left hand-side) . The ratio of two $\rho\pi$ branching ratios limiting values of the CKM matrix elements (Right hand-side). Solid line (dotted line) for max (min) CKM matrix elements. Notation: horizontal dotted lines: CLEO data; horizontal dashed lines: BABAR data; horizontal dot-dashed lines: BELLE data.

It has to be pointed out that the annihilation contributions in B decays play an important role since they contribute significantly to the magnitude of the amplitude. The annihilation diagram contribution to the total decay amplitude strongly modifies (in a positive or negative way) the branching ratio $B^- \to \rho^0\pi^-$ according to the value chosen for the phase ϕ_A. This contribution could be bigger than that of $\rho - \omega$ mixing but carries more uncertainties because of its endpoint divergence. We emphasise that these two contributions ($\rho - \omega$ mixing effects and annihilation contributions) are not just simple corrections to the total amplitude, but are important in obtaining a correct description of B decay amplitude.

4. FORM FACTOR $F_1^{B\to\pi}$

Form factors play a major role in the factorization method (naive or QCDF) since they represent the transition between two hadronic states. Their computation is non trivial and may carry large uncertainties, depending on models being used. These models include,

say, QCD sum rules, heavy quark effective theory, lattice QCD and light cone QCD. With the available experimental data for the branching ratios, it is now possible for us to constrain $F_1^{B\to\pi}$ in a model-independent way in QCDF.

It has to be noticed that the branching ratios depend on both $F_1^{B\to\pi}$ and N_c^{eff}. In Fig. 6 we show the results regarding the form factor $F_1^{B\to\pi}(m_\rho^2)$ as a function of N_c^{eff}, where we require that all the branching ratios for B decaying into $\rho\pi$ and $\omega\pi$ be consistent with the experimental data provided by CLEO and BELLE. We have excluded the data from BABAR since they are currently not numerous and accurate enough. We have included uncertainties from the CKM matrix element parameters ρ ($0.190 < \rho < 0.268$) and η ($0.284 < \eta < 0.366$) and we have applied the QCD factorization method where all of the final state interaction corrections arising at order α_s are incorporated. We emphasize that the results are model independent.

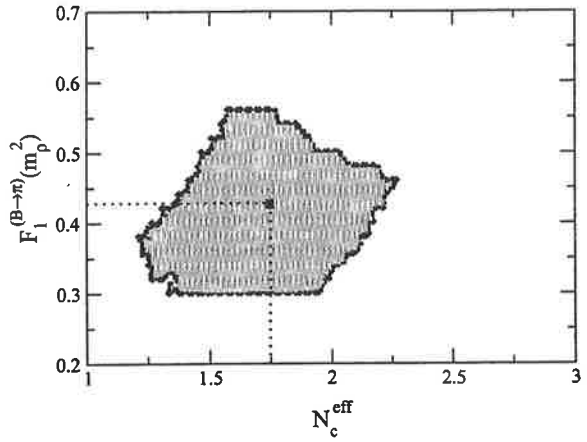

FIGURE 6. $F_1^{B\to\pi}$ as a function of N_c^{eff}. Plot obtained by comparing theoretical results from QCFD with experimental data from BELLE and CLEO for the branching ratios $B \to \rho\pi$ and $B \to \omega\pi$. The plot includes the uncertainties from the CKM matrix element parameters ρ and η.

We found a large common region between BELLE and CLEO for the B decay into $\rho\pi$. From our analysis, $F_1^{B\to\pi}(m_\rho^2)$ varies between 0.3 and 0.57 and N_c^{eff} can take values from 1.25 to 2.25. Their central values are $F_1^{B\to\pi}(m_\rho^2) = 0.43$ and $N_c^{eff} = 1.75$. The result obtained for the form factor $F_1^{B\to\pi}(m_\rho^2)$ reduces one of the main uncertainties in the factorization process. That obtained for the effective number of colours, N_c^{eff}, confirms previous analysis where naive factorization was applied for the same decays.

It is well known that the CKM matrix element parameters ρ and η are the main "key" to *CP* violation within the Standard Model. Recall that the weak phase is mainly governed by the parameter η that provides the imaginary part which is absolutely necessary to obtain an asymmetry between matter and antimatter. Based on our analysis, we are not able to efficiently constrain the CKM matrix parameters ρ and η from the branching ratios for $B \to \rho\pi$. In fact, the common region allowed by CLEO and BELLE data for branching ratios for $B \to \rho\pi$ does not constrain the parameters ρ and η. In the analysis we used the values $0.190 < \rho < 0.268$ and $0.284 < \eta < 0.366$ [45, 46], to which the common region corresponds. However, we can try (as an example) to get

some constraints on ρ and η by only taking into account the central values for the form factor $F_1^{B\to\pi}(m_\rho^2)$ and for the effective number of colours N_c^{eff}. According to our work, we find the following limits: $0.205 < \rho < 0.251$ and $0.300 < \eta < 0.351$.

5. CONCLUSION

The calculation of the hadronic matrix elements that appear in the B decay amplitude is non trivial. The main difficulty is to express the hadronic matrix elements which represent the transition between the meson B and the final state.

We have investigated the branching ratios for $B \to \rho\pi, B \to \omega\pi$ within the QCDF approach. Comparisons were made with experimental results from BABAR, BELLE and CLEO. Based on our analysis of branching ratios in B decays, we have constrained the form factor, $F_1^{B\to\pi}(m_\rho^2)$, and the effective number of colours, N_c^{eff}. More accurate experimental data regarding branching ratios in B decays will provide more accurate results, which will be helpful in gaining further knowledge of direct CP violation in B decays.

This work could be extended to more B decays. It would be very interesting to constrain our parameters by investigating channels other than $\rho\pi$ for branching ratios and asymmetries. By including more channels, we will use more experimental data and hence be able to obtain better results for our parameters. In the QCD factorization framework, annihilation contributions could be subject to discussions. Clarifying this point would be very helpful in obtaining more accurate theoretical predictions. For example, it is important to solve the problem related to the end point integral divergence [13] which is parameterized without any strong physical motivation. Moreover, the annihilation contributions have not been included within the QCDF method. To obtain a consistent framework, it would be better to find a way to include them within QCDF.

Acknowledgements
This work was supported in part by the Australian Research Council and the University of Adelaide.

REFERENCES

1. Buras, Andrzej J., Lect. Notes Phys. **558** (2000) 65.
2. Buras, Andrzej J., hep-ph/9806471.
3. Buchalla, Gerhard and Buras, Andrzej J. and Lautenbacher, Markus E., Rev. Mod. Phys. **68** (1996) 1125.
4. Stech, Berthold, hep-ph/9706384.
5. Buras, Andrzej J., Nucl. Instrum. Meth. **A368** (1995) 1.
6. Fakirov, Dotcho and Stech, Berthold, Nucl. Phys. **B133** (1978) 315.
7. Cabibbo, N. and Maiani, L., Phys. Lett. **B73** (1978) 418.
8. Dugan, Michael J. and Grinstein, Benjamin, Phys. Lett. **B255** (1991) 583.
9. Bjorken, James D., Nucl. Phys. Proc. Suppl. **11** (1989) 325.
10. Quinn, Helen R., hep-ph/9912325.
11. Cheng, Hai-Yang, Phys. Lett. **B335** (1994) 428.

12. Cheng, Hai-Yang, Phys. Lett. **B395** (1997) 345.
13. Beneke, M. and Buchalla, G. and Neubert, M. and Sachrajda, Christopher T., Phys. Rev. Lett. **83** (1999) 1914.
14. Neubert, Matthias, AIP Conf. Proc. **602** (2001) 168.
15. Neubert, Matthias, Nucl. Phys. Proc. Suppl. **99B** (2001) 113.
16. Beneke, M. J., Phys. **G27** (2001) 1069.
17. Beneke, M., hep-ph/0207228.
18. Beneke, M., hep-ph/9910505.
19. Beneke, M. and Buchalla, G. and Neubert, M. and Sachrajda, Christopher T., hep-ph/0007256.
20. Beneke, M. and Buchalla, G. and Neubert, M. and Sachrajda, Christopher T., Nucl. Phys. **B606** (2001) 245.
21. Beneke, M. and Buchalla, G. and Neubert, M. and Sachrajda, Christopher T., Nucl. Phys. **B591** (2000) 313.
22. Gao, Yongsheng and Wurthwein, Frank, CLEO collaboration, hep-ex/9904008.
23. Jessop, C. P. and others, CLEO collaboration, Phys. Rev. Lett. **85** (2000) 2881.
24. Schwarthoff, H., CLEO collaboration, hep-ex/0205015.
25. De Monchenault, Gautier Hamel, hep-ex/0305055.
26. Briere, Roy A., CLEO collaboration, AIP Conf. Proc. **618** (2002) 159.
27. Zhao, Xin, hep-ex/0101013.
28. Abe, K. and others, BELLE collaboration, hep-ex/0107051.
29. Bozek, A., BELLE collaboration, hep-ex/0104041.
30. Lu, R. S. and others, BELLE collaboration, Phys. Rev. Lett. **89** (2002) 191801.
31. Casey, B. C. K. and others, BELLE collaboration, Phys. Rev. **D66** (2002) 092002.
32. Abe, K. and others, BELLE collaboration, Phys. Rev. **D65** (2002) 092005.
33. Garmash, Alexei, BELLE collaboration, hep-ex/0207003.
34. Gordon, A. and others, BELLE collaboration, Phys. Lett. **B542** (2002) 183.
35. Iijima, Toru, BELLE collaboration, hep-ex/0105005.
36. Kinoshita, Kay, BELLE collaboration, Nucl. Instrum. Meth. **A462** (2001) 77.
37. Aubert, B. and others, BABAR collaboration, Phys. Rev. Lett. **87** (2001) 221802.
38. Aubert, B. and others, BABAR collaboration, hep-ex/0206004.
39. Olsen, J., BABAR collaboration, Int. J. Mod. Phys. **A16S1A** (2001) 468.
40. Aubert, B. and others, BABAR collaboration, hep-ex/0008058.
41. Schietinger, Thomas, BABAR collaboration, hep-ex/0105019.
42. Sciolla, G., BABAR collaboration, Nucl. Phys. Proc. Suppl. **99B** (2001) 135.
43. Cavoto, Gianluca, BABAR collaboration, hep-ex/0105018.
44. Aubert, B. and others, BABAR collaboration, Phys. Rev. Lett. **87** (2001) 151802.
45. Abbaneo, D. and others, hep-ex/0112028.
46. Groom, D. E. and others, Eur. Phys. J. **C15** (2000) 1.

PCCF-RI-03-03
ADP-03-111/T549

Direct CP Violation In $B \to \pi^+\pi^- V$ With $\rho^0 - \omega$ Mixing Effects: Phenomenological Approach

Z.J. Ajaltouni[1*], O. Leitner[1,2†], P. Perret[1‡], C. Rimbault[1§], A.W. Thomas[2¶]

[1] *Laboratoire de Physique Corpusculaire de Clermont-Ferrand*
IN2P3/CNRS Université Blaise Pascal
F-63177 Aubière Cedex France
[2] *Department of Physics and Mathematical Physics and*
Special Research Centre for the Subatomic Structure of Matter,
University of Adelaide, Adelaide 5005, Australia

Abstract

We present a detailed study of direct CP violation and branching ratios in the channels $B^{0,\pm} \to \pi^+\pi^- V^{0,\pm}$, where V is a vector meson ($K^{*0,\pm}$ or $\rho^{\pm}$). Emphasis is placed upon the important role played by $\rho^0 - \omega$ mixing effects in the estimation of the CP-violating asymmetry parameter, a_{cp}, associated with the difference of B and $\bar{B}$ decay amplitudes. A thorough study of the helicity amplitudes is presented as a function of the pion-pion invariant mass. All of the calculations and simulations considered correspond to channels which will be analyzed at the LHCb facility.

PACS Numbers: 11.30.Er, 12.39.-x, 13.25.Hw.

*ziad@clermont.in2p3.fr
†oleitner@physics.adelaide.edu.au
‡perret@clermont.in2p3.fr
§rimbault@clermont.in2p3.fr
¶athomas@physics.adelaide.edu.au

1 Introduction

Understanding the physical origin of the violation of CP (Charge Conjugation $\times$Parity) symmetry is one of the main goals of Particle Physics at the present time. Recent experiments at e^+e^- colliders (BaBar, Belle) have produced fundamental results which strengthen the CKM picture of CP violation [1, 2] in the B meson sector [3, 4]. However, the main results of these two collaborations are related to B decays into pairs of pseudo-scalar mesons or into a vector plus a pseudo-scalar meson.

A very broad physics program can also be carried out in the sector with two vector mesons in the final state, following B decay. Apart from measuring the *standard angles*, α, β and γ of the Unitary Triangle (UT), the vector mesons are *polarized* and their decay products (usually long-lived 0^{-+} mesons) are *correlated*. This opens the possibility of making interesting cross-checks of the Standard Model predictions as well testing some specific models of CP violation beyond the SM approach (BSM).

In the special case of two neutral vector mesons, the orbital angular momentum, ℓ, and the total spin, S, of the $V_1^0 V_2^0$ system satisfy the equality $\ell = S = 0, 1, 2$. The CP eigenvalues are defined as $(-1)^\ell$. Because of the allowed values for the angular momentum, ℓ, one has a very clear indication of any *mixing* of different CP eigenstates and hence of CP non-conservation. The separation of the different CP eigenstates requires a detailed analysis of the final angular distributions [5]. However, because this analysis can be carried out in a model-independent way, it provides a significant constraint on any model.

After explaining the helicity formalism (Section II), a special study is devoted to the final state interactions (FSI) and the key role of $\rho^0 - \omega$ mixing (Section III). A complete and realistic determination of the helicity amplitudes, in the framework of the effective Hamiltonian approach, is introduced in Section IV. Then, the main results of the Monte-Carlo simulations, providing estimates of the various density matrix elements h_{ij}, are shown in Section V. In the following section (Section VI) the numerical analysis and discussions about the branching ratios and asymmetries for B decays into two vectors ($B \to \rho^0(\omega) V_2$, with $V_2 = K^{*0}, \bar{K}^{*0}, K^{*-}, K^{*+}, \rho^+, \rho^-$) are given in detail. These two vectors, $\rho^0(\omega)$ and V_2, each decay into two pseudo-scalars. Emphasis is put on the angular distributions of the pseudo-scalar mesons in both the helicity and transversity frames. Finally, in the last section, we summarize our results for the different channels which will be investigated in future experiments at $p\bar{p}$ colliders and make some concluding remarks.

2 General formalism for $B \to V_1 V_2$ decays

2.1 Helicity frame

Because the B meson has spin 0, the final two vector mesons, V_1 and V_2, have the same helicity, $\lambda_1 = \lambda_2 = -1, 0, +1$, and their angular distribution is isotropic in the B rest frame. Let H_w be the weak Hamiltonian which governs the B decays. Any transition amplitude between the initial and final states will have the following form:

$$H_\lambda = \langle V_1(\lambda) V_2(\lambda) | H_w | B \rangle \ , \tag{1}$$

where the common helicity is $\lambda = -1, 0, +1$. Then, each vector meson V_i will decay into two pseudo-scalar mesons, a_i, b_i, where a_i and b_i can be either a pion or a kaon, and the angular distributions of a_i and b_i depend on the polarization of V_i.

The helicity frame of a vector-meson V_i is defined in the B rest frame such that the direction of the Z-axis is given by its momentum, $\vec{p}_i$. Schematically, the whole process gets the form:

$$B \longrightarrow V_1 + V_2 \longrightarrow (a_1 + b_1) + (a_2 + b_2) \ .$$

The corresponding decay amplitude, $M_\lambda\big(B \to \sum_{i=1}^{2}(a_i + b_i)\big)$, is factorized out according to the relation,

$$M_\lambda\big(B \to \sum_{i=1}^{2}(a_i + b_i)\big) = H_\lambda(B \to V_1 + V_2) \times \prod_{i=1}^{2} A_i(V_i \to a_i + b_i) \ , \tag{2}$$

where the amplitudes $A_i(V_i \to a_i + b_i)$ are related to the decay of the resonances V_i. The $A_i(V_i \to a_i + b_i)$ are given by the following expressions:

$$\begin{aligned} A_1(V_1 \to a_1 + b_1) &= \sum_{m_1=-1}^{1} c_1 D^1_{\lambda,m_1}(0, \theta_1, 0) \ , \\ A_2(V_2 \to a_2 + b_2) &= \sum_{m_2=-1}^{1} c_2 D^1_{\lambda,m_2}(\phi, \theta_2, -\phi) \ . \end{aligned} \tag{3}$$

These equalities are an illustration of the Wigner-Eckart theorem. In Eq. (3), the c_1 and c_2 parameters represent, respectively, the *dynamical decays* of the V_1 and V_2 resonances. The term $D^1_{\lambda,m_i}(\phi_i, \theta_i, -\phi_i)$ is the Wigner rotation matrix element for a spin-1 particle and we let $\lambda(a_i)$ and $\lambda(b_i)$ be the respective helicities of the final particles a_i and b_i in the V_i rest frame. θ_1 is the polar angle of a_1 in the V_1 helicity frame. The decay plane of V_1 is identified with the (X-Z) plane and consequently the azimuthal angle ϕ_1 is set to 0. Similarly, θ_2 and ϕ are respectively the polar and azimuthal angles of particle a_2 in the V_2 helicity frame. Finally, the coefficients m_i are defined as:

$$m_i = \lambda(a_i) - \lambda(b_i) \ . \tag{4}$$

Our convention for the $D^1_{\lambda,m_i}(\alpha, \beta, \gamma)$ matrix element is given in Rose's book [6], namely:

$$D^1_{\lambda,m_i}(\alpha, \beta, \gamma) = \exp[-i(\lambda\alpha + m_i\gamma)]\ d^1_{\lambda,m_i}(\beta) \ . \tag{5}$$

The most general form of the decay amplitude $\mathcal{M}\big(B \to \sum_{i=1}^{2}(a_i + b_i)\big)$ is a *linear superposition* of the previous amplitudes $M_\lambda\big(B \to \sum_{i=1}^{2}(a_i + b_i)\big)$ denoted by,

$$\mathcal{M}\big(B \to \sum_{i=1}^{2}(a_i + b_i)\big) = \sum_{\lambda} M_\lambda\big(B \to \sum_{i=1}^{2}(a_i + b_i)\big) \ . \tag{6}$$

The decay width, $\Gamma(B \to V_1V_2)$, can be computed by taking the square of the modulus, $\Big|\mathcal{M}\big(B \to \sum_{i=1}^{2}(a_i + b_i)\big)\Big|$, which involves the three kinematic parameters θ_1, θ_2 and ϕ. This leads to the following general expression:

$$d^3\Gamma(B \to V_1V_2) \propto \Big|\sum_{\lambda} M_\lambda\big(B \to \sum_{i=1}^{2}(a_i + b_i)\big)\Big|^2 = \sum_{\lambda,\lambda'} h_{\lambda,\lambda'} F_{\lambda,\lambda'}(\theta_1) G_{\lambda,\lambda'}(\theta_2, \phi) \ , \tag{7}$$

which involves three density-matrices, $h_{\lambda,\lambda'}, F_{\lambda,\lambda'}(\theta_1)$ and $G_{\lambda,\lambda'}(\theta_2,\phi)$. The factor $h_{\lambda,\lambda'} = H_\lambda H^*_{\lambda'}$ is an element of the density-matrix related to the B decay, while $F_{\lambda,\lambda'}(\theta_1)$ represents the density-matrix of the decay $V_1 \to a_1 + b_1$. In a similar way, $G_{\lambda,\lambda'}(\theta_2,\phi)$ represents the density-matrix of the decay $V_2 \to a_2 + b_2$.

The analytic expression in Eq. (7) exhibits a very general form. It depends on neither the specific nature of the intermediate resonances nor their decay modes (except for the spin of the final particles). This approach also presents three key advantages. The first one comes from the fact that all the dynamics of the B decay is introduced into the coefficients $h_{\lambda,\lambda'}$. This allows us to use various theoretical models involving different dynamical processes and form factors. The second is associated with the fact that the formal expressions for $F_{\lambda,\lambda'}(\theta_1)$ and $G_{\lambda,\lambda'}(\theta_2,\phi)$, which are related to the polarization of the intermediate resonances, remain unchanged whatever the coefficients $h_{\lambda,\lambda'}$ happen to be. Finally, correlations among final particles arise in a straightforward way because of the previous expression which relates the angles θ_1, θ_2 and ϕ. Consequently, a probability density function (pdf) can be inferred from the general expression and one gets:

$$f(\theta_1,\theta_2,\phi) = \frac{d^3\Gamma(B \to V_1V_2)}{\Gamma(B \to V_1V_2)d(\cos\theta_1)d(\cos\theta_2)d\phi} \ , \tag{8}$$

where the angles θ_1, θ_2 and ϕ were defined earlier and $\Gamma(B \to V_1V_2)$ is the partial decay width. This function allows one to compute three other pdfs separately for the variables θ_1, θ_2 and ϕ.

The previous calculations are illustrated by the reaction $B^0 \to K^{*0}\rho^0$ where $K^{*0} \to K^+\pi^-$ and $\rho^0 \to \pi^+\pi^-$. In this channel, since all the final particles have spin zero, the coefficients m_1 and m_2, defined in Eq. (4), are equal to zero. The three-fold differential width has the following form:

$$\begin{aligned}\frac{d^3\Gamma(B \to V_1V_2)}{d(\cos\theta_1)d(\cos\theta_2)d\phi} &\propto (h_{++} + h_{--})\sin^2\theta_1\sin^2\theta_2/4 + h_{00}\cos^2\theta_1\cos^2\theta_2 \\ &+ \Big\{\mathscr{R}e(h_{+0})\cos\phi - \mathscr{I}m(h_{+0})\sin\phi + \mathscr{R}e(h_{0-})\cos\phi - \mathscr{I}m(h_{0-})\sin\phi\Big\}\sin 2\theta_1\sin 2\theta_2/4 \\ &+ \Big\{\mathscr{R}e(h_{+-})\cos 2\phi - \mathscr{I}m(h_{+-})\sin 2\phi\Big\}\sin^2\theta_1\sin^2\theta_2/2 \ , \end{aligned} \tag{9}$$

where all the terms in Eq. (9) have been already specified. It is worth noticing that the expression in Eq. (9) is *completely symmetric* in θ_1 and θ_2 and consequently, the angular distributions of a_1 in the V_1 frame is identical that of a_2 in the V_2 frame. From Eqs. (8) and (9) the normalized pdfs of θ_1, θ_2 and ϕ can be derived and one finds:

$$\begin{aligned} f(\cos\theta_{1,2}) &= (3h_{00} - 1)\cos^2\theta_{1,2} + (1 - h_{00}) \ , \\ g(\phi) &= 1 + 2\ \mathscr{R}e(h_{+-})\cos 2\phi - 2\ \mathscr{I}m(h_{+-})\sin 2\phi \ . \end{aligned} \tag{10}$$

2.2 Transversity frame

Initially, the transversity frame (TF) was introduced by A. Bohr [7] in order to facilitate the determination of the spin and parity of a resonance decaying into stable particles. It can be extended to a system of two vector mesons coming from a heavy meson, B or $\bar{B}$, in order to perform tests of CP symmetry. In displaying new angular distributions, the TF

provides complementary physical information to that seen in the standard helicity frame. The construction of the TF and its use require several steps. For a clear illustration, see Fig. 1, where the channel $B^0 \to \rho^0 K^{*0}$ is chosen.

Departing from the B rest frame, the common helicity axis, (Δ_H), is given by the direction of the momentum $\vec{p_1}$. This and the decay plane, (Π_D), of the vector meson $(K^{*0} \to K^+\pi^-)$ are the main ingredients of the TF. The vector meson ρ^0 is taken at rest (origin of the frame) and the X-axis is given by (Δ_H). In the decay plane, (Π_D), the Y-axis which is orthogonal to the X-axis, is chosen in such a way that the K^+ meson has the Y-component of its momentum greater than or equal to zero. The Z-axis, which is orthogonal to the plane (Π_D), is obtained by the classical relation $\vec{e}_Z = \vec{e}_X \times \vec{e}_Y$.

The angular distributions of the $\pi^\pm$ coming from the ρ^0 decay are referred to the new Z-axis. It is worthy noticing that, in the TF, the flying meson and its decay products are very energetic compared to the B frame. Explicitly, the ρ^0 energy is given by the relation,

$$E_{\rho^0} = ({m_B}^2 - {m_1}^2 - {m_2}^2)/2m_1 \approx 17 \text{ GeV} , \tag{11}$$

where m_1 and m_2 refer to the masses of the K^{*0} and ρ^0 resonances, respectively. As far as the transition amplitudes in the TF are concerned, they are a simple linear combination of the helicity amplitudes, namely:

$$H_P = \frac{H_+ + H_-}{\sqrt{2}} , \text{ and } H_T = \frac{H_+ - H_-}{\sqrt{2}} , \tag{12}$$

while H_0 remains unchanged. We can rewrite the angular distributions given in Eq. (10) by using the relations from Eq. (12) and angles $\theta_{1,2}, \phi$ expressed in the transversity frame. Thus one gets,

$$\begin{aligned} f_T(\cos\theta_{1,2}) &= \left(3|H_T|^2 - 1\right)\cos^2\theta_{1,2} + \left(1 - |H_T|^2\right) , \\ g_T(\phi) &= \left(1 + |H_0|^2 - |H_P|^2\right)\cos 2\phi . \end{aligned} \tag{13}$$

3 Final state interactions and $\rho^0 - \omega$ mixing

3.1 Factorization hypothesis

Final state interactions (FSI) represent unavoidable effects in hadronic physics and they play a crucial role in heavy resonance decays [8]. In the case of a B meson, characterized by a center-of-mass energy $\sqrt{s} \approx 5.3$ GeV, the charmless weak decays of the b-quark lead to *light energetic* quarks which can exchange several gluons amongst themselves as well as with the spectator quark in the B meson. This fundamental process occurs in decays described by tree, penguin and annihilation diagrams and is characterized by two regimes: perturbative and non-perturbative. In order to handle the FSI in both regimes, the usual method is inspired by the effective Lagrangian approach. Perturbative calculations at next-to-leading order (NLO) are performed for a scale higher than m_b (since our analysis is focused on B decays) and the non-perturbative effects are inserted for a scale lower than m_b. This general method is called the *factorization procedure* [9] and further details are given below.

In the factorization approximation, either the vector meson $\rho^0(\omega)$ or the K^* is generated by one current in the effective Hamiltonian which has the appropriate quantum

numbers. For the B decay processes considered here, two kinds of matrix element products are involved after factorization (i.e. omitting Dirac matrices and color labels): $\langle\rho^0(\omega)|(\bar{u}u)|0\rangle\langle K^*|(\bar{q}_iq_j)|B^{\pm,0}\rangle$ and $\langle K^*|(\bar{q}_iq_j)|0\rangle\langle\rho^0(\omega)|(\bar{u}b)|B^{\pm,0}\rangle$, where q_i and q_j could be either u, s or d. We will calculate them in two phenomenological quark models.

The matrix elements for $B \to X^*$ (where X^* denotes a vector meson) can be decomposed as follows [10],

$$\langle X^*|J_\mu|B\rangle = \frac{2}{m_B + m_{X^*}}\epsilon_{\mu\nu\rho\sigma}\epsilon^{*\nu}p_B^\rho p_{X^*}^\sigma V(k^2) + i\Big\{\epsilon_\mu^*(m_B + m_{X^*})A_1(k^2) - \frac{\epsilon^*\cdot k}{m_B + m_{X^*}}(P_B + P_{X^*})_\mu A_2(k^2) - \frac{\epsilon^*\cdot k}{k^2}2m_{X^*}\cdot k_\mu A_3(k^2)\Big\} + i\frac{\epsilon^*\cdot k}{k^2}2m_{X^*}\cdot k_\mu A_0(k^2)\ , \quad (14)$$

where J_μ is the weak current, defined as $J_\mu = \bar{q}\gamma^\mu(1-\gamma_5)b$ with $q = u, d, s$ and $k = p_B - p_{X^*}$ and ϵ_μ is the polarization vector of X^*. The form factors A_0, A_1, A_2, A_3 and V describe the transition $0^- \to 1^-$. Finally, in order to cancel the poles at $q^2 = 0$, the form factors respect the condition:

$$A_3(0) = A_0(0)\ , \quad (15)$$

and they also satisfy the following relations:

$$A_3(k^2) = \frac{m_B + m_{X^*}}{2m_{X^*}}A_1(k^2) - \frac{m_B - m_{X^*}}{2m_{X^*}}A_2(k^2)\ . \quad (16)$$

In the evaluation of matrix elements, the effective number of colors, N_c^{eff}, enters through a Fierz transformation. In general, for an operator O_i, one can write,

$$\frac{1}{(N_c^{eff})_i} = \frac{1}{3} + \xi_i\ , \text{with } i = 1, \cdots, 10\ , \quad (17)$$

here ξ_i describes non-factorizable effects. ξ_i is assumed to be universal for all the operators O_i. Naive factorization assumes that we can replace -in a heavy quark decay- the matrix element of a four fermion operator by the product of the matrix elements of two currents. This reduces to the product of a form factor and a decay constant. This assumption is only rigorously justified at large values of N_c. But it is known that naive factorization may give a good estimate of the magnitude of the B decay amplitude in many cases [11].

3.2 FSI at the quark level: strong phase generated by the penguin diagrams

Let A be the amplitude for the decay $B \to \rho^0(\omega)K^* \to \pi^+\pi^-K^*$ (a similar procedure applies in the case where we have a $\rho^\pm$ [12] instead of the K^*), then one has,

$$A = \langle K^*\pi^-\pi^+|H^T|B\rangle + \langle K^*\pi^-\pi^+|H^P|B\rangle\ , \quad (18)$$

with H^T and H^P being the Hamiltonians for the tree and penguin operators. We can define the relative magnitude and phases between these two contributions as follows,

$$\begin{aligned} A &= \langle K^*\pi^-\pi^+|H^T|B\rangle[1 + re^{i\delta}e^{i\phi}] \ , \\ \bar{A} &= \langle \bar{K}^*\pi^+\pi^-|H^T|\bar{B}\rangle[1 + re^{i\delta}e^{-i\phi}] \ , \end{aligned} \tag{19}$$

where δ and ϕ are strong and weak phases, respectively. The phase ϕ arises from the appropriate combination of CKM matrix elements, $\phi = \arg[(V_{tb}V_{ts}^*)/(V_{ub}V_{us}^*)]$. As a result, $\sin\phi$ is equal to $\sin\gamma$, with γ defined in the standard way [13]. The parameter, r, is the absolute value of the ratio of tree and penguin amplitudes:

$$r \equiv \left| \frac{\langle \rho^0(\omega)K^*|H^P|B\rangle}{\langle \rho^0(\omega)K^*|H^T|B\rangle} \right| . \tag{20}$$

3.3 Strong phase generated by the $\rho^0 - \omega$ mixing

In the vector meson dominance model [14], the photon propagator is dressed by coupling to vector mesons. From this, the $\rho^0 - \omega$ mixing mechanism [15] was developed. In order to obtain a large signal for direct CP violation, we need some mechanism to make both $\sin\delta$ and r large. We stress that $\rho^0 - \omega$ mixing has the dual advantages that the strong phase difference is large (passing through 90° at the ω resonance) and well known [12, 16]. With this mechanism, to first order in isospin violation, we have the following results when the invariant mass of the $\pi^+\pi^-$ pair is near the mass of the ω resonance,

$$\begin{aligned} \langle K^*\pi^-\pi^+|H^T|B\rangle &= \frac{g_\rho}{s_\rho s_\omega}\tilde{\Pi}_{\rho\omega}t_\omega + \frac{g_\rho}{s_\rho}t_\rho \ , \\ \langle K^*\pi^-\pi^+|H^P|B\rangle &= \frac{g_\rho}{s_\rho s_\omega}\tilde{\Pi}_{\rho\omega}p_\omega + \frac{g_\rho}{s_\rho}p_\rho \ . \end{aligned} \tag{21}$$

Here t_V ($V = \rho$ or ω) is the tree amplitude and p_V the penguin amplitude for producing a vector meson, V, g_ρ is the coupling for $\rho^0 \to \pi^+\pi^-$, $\tilde{\Pi}_{\rho\omega}$ is the effective $\rho^0 - \omega$ mixing amplitude, and s_V is the inverse propagator of the vector meson V,

$$s_V = s - m_V^2 + im_V\Gamma_V \ , \tag{22}$$

with $\sqrt{s}$ being the invariant mass of the $\pi^+\pi^-$ pair. We stress that the direct coupling $\omega \to \pi^+\pi^-$ is effectively absorbed into $\tilde{\Pi}_{\rho\omega}$ [17], leading to the explicit s dependence of $\tilde{\Pi}_{\rho\omega}$. Making the expansion $\tilde{\Pi}_{\rho\omega}(s) = \tilde{\Pi}_{\rho\omega}(m_\omega^2) + (s - m_\omega^2)\tilde{\Pi}'_{\rho\omega}(m_\omega^2)$, the $\rho^0 - \omega$ mixing parameters were determined in the fit of Gardner and O'Connell [18]: $\mathscr{R}e\ \tilde{\Pi}_{\rho\omega}(m_\omega^2) = -3500 \pm 300\ \mathrm{MeV}^2$, $\mathscr{I}m\ \tilde{\Pi}_{\rho\omega}(m_\omega^2) = -300 \pm 300\ \mathrm{MeV}^2$, and $\tilde{\Pi}'_{\rho\omega}(m_\omega^2) = 0.03 \pm 0.04$. In practice, the effect of the derivative term is negligible. From Eqs. (18) and (21) one has

$$re^{i\delta}e^{i\phi} = \frac{\tilde{\Pi}_{\rho\omega}p_\omega + s_\omega p_\rho}{\tilde{\Pi}_{\rho\omega}t_\omega + s_\omega t_\rho} \ . \tag{23}$$

Defining

$$\frac{p_\omega}{t_\rho} \equiv r'e^{i(\delta_q+\phi)} \ , \quad \frac{t_\omega}{t_\rho} \equiv \alpha e^{i\delta_\alpha} \ , \quad \frac{p_\rho}{p_\omega} \equiv \beta e^{i\delta_\beta} \ , \tag{24}$$

where $\delta_\alpha, \delta_\beta$ and δ_q are partial strong phases (absorptive part) arising from the tree and penguin diagram contributions. Substituting Eq. (24) into Eq. (23), one finds:

$$re^{i\delta} = r'e^{i\delta_q}\frac{\tilde{\Pi}_{\rho\omega} + \beta e^{i\delta_\beta}s_\omega}{s_\omega + \tilde{\Pi}_{\rho\omega}\alpha e^{i\delta_\alpha}} , \tag{25}$$

where the total strong phase, δ, is mainly proportional to the ratio of the penguin and tree diagram contributions.

3.4 Importance of the strong phase for $B\bar{B}$ asymmetry

Under a CP transformation the strong phase, δ, remains unchanged, while the weak phase, ϕ, which is related to the CKM matrix elements, changes sign. Thus, the asymmetry parameter, a_{CP}^{dir}, which can reveal *direct CP violation*, can be deduced in the following way:

$$a_{CP}^{dir} = \frac{A^2 - \bar{A}^2}{A^2 + \bar{A}^2} = \frac{-2\ r\ \sin\delta\ \sin\phi}{1 + r^2 + 2\ r\ \cos\delta\ \cos\phi} . \tag{26}$$

It is straightforward to see that the parameter a_{CP}^{dir} depends on both the strong phase *and* the weak phase and, consequently, that the maximum value of a_{CP}^{dir} can be reached if $\sin\delta = 1$. This is why the strong final state interaction (FSI) among pions coming from $\rho^0 - \omega$ mixing *enhances* the direct CP violation in the vicinity of the mass of the ω resonance.

In the Wolfenstein parametrization [19], the weak phase comes from $[V_{tb}V_{ts}^*/V_{ub}V_{us}^*]$ and one has for the decay $B \to \rho^0(\omega)K^*$,

$$\begin{aligned} \sin\phi &= \frac{-\eta}{\sqrt{\rho^2 + \eta^2}} , \\ \cos\phi &= \frac{-\rho}{\sqrt{\rho^2 + \eta^2}} , \end{aligned} \tag{27}$$

while the weak phase comes from $[V_{tb}V_{td}^*/V_{ub}V_{ud}^*]$ for the decay $B \to \rho^0(\omega)\rho$,

$$\begin{aligned} \sin\phi &= \frac{\eta}{\sqrt{[\rho(1-\rho) - \eta^2]^2 + \eta^2}} , \\ \cos\phi &= \frac{\rho(1-\rho) - \eta^2}{\sqrt{[\rho(1-\rho) - \eta^2]^2 + \eta^2}} . \end{aligned} \tag{28}$$

The values used for ρ and η will be discussed in Section V.

4 Explicit calculations according to the effective Hamiltonian

4.1 Generalities concerning the OPE for weak hadronic decays

4.1.1 Operator product expansion

The operator product expansion (OPE) [20] is an extremely useful tool in the analysis of weak interaction processes involving quarks. Defining the decay amplitude $A(M \to F)$ as

$$A(M \to F) \propto C_i(\mu)\langle F|O_i(\mu)|M\rangle \ , \tag{29}$$

where $C_i(\mu)$ are the Wilson coefficients (see Section 4.1.2), $O_i(\mu)$ are the operators given by the OPE and μ is an energy scale, one sees that the OPE separates the calculation of the amplitude, $A(M \to F)$, into two distinct physical regimes. One is related to *hard* or short-distance physics, represented by $C_i(\mu)$ and calculated by a perturbative approach. The other is the *soft* or long-distance regime. This part must be treated by non-perturbative approaches such as the $1/N$ expansion [21], QCD sum rules [22], hadronic sum rules or lattice QCD.

The operators, O_i, are local operators which can be written in the general form:

$$O_i = (\bar{q}_i \Gamma_{n1} q_j)(\bar{q}_k \Gamma_{n2} q_l) \ , \tag{30}$$

where Γ_{n1} and Γ_{n2} denote a combination of gamma matrices and q the quark flavor. They should respect the Dirac structure, the color structure and the types of quarks relevant for the decay being studied. They can be divided into two classes according to topology: tree operators (O_1, O_2), and penguin operators (O_3 to O_{10}). For tree contributions (where $W^{\pm}$ is exchanged), the Feynman diagram is shown in Fig. 2 (left). The current-current operators related to the tree diagram are the following:

$$\begin{aligned} O_1^s &= \bar{q}_\alpha \gamma_\mu (1-\gamma_5) u_\beta \bar{s}_\beta \gamma^\mu (1-\gamma_5) b_\alpha \ , \\ O_2^s &= \bar{q} \gamma_\mu (1-\gamma_5) u \bar{s} \gamma^\mu (1-\gamma_5) b \ , \end{aligned} \tag{31}$$

where α and β are the color indices. The penguin terms can be divided into two sets. The first is from the QCD penguin diagrams where gluons are exchanged, while the second is from the electroweak penguin diagrams (where either a γ or a Z^0 is exchanged). The Feynman diagram for the QCD penguin diagram is shown in Fig. 2 (right) and the corresponding operators are written as follows:

$$\begin{aligned} O_3 &= \bar{q} \gamma_\mu (1-\gamma_5) b \sum_{q'} \bar{q}' \gamma^\mu (1-\gamma_5) q' \ , \\ O_4 &= \bar{q}_\alpha \gamma_\mu (1-\gamma_5) b_\beta \sum_{q'} \bar{q}'_\beta \gamma^\mu (1-\gamma_5) q'_\alpha \ , \end{aligned} \tag{32}$$

$$\begin{aligned} O_5 &= \bar{q} \gamma_\mu (1-\gamma_5) b \sum_{q'} \bar{q}' \gamma^\mu (1+\gamma_5) q' \ , \\ O_6 &= \bar{q}_\alpha \gamma_\mu (1-\gamma_5) b_\beta \sum_{q'} \bar{q}'_\beta \gamma^\mu (1+\gamma_5) q'_\alpha \ , \end{aligned} \tag{33}$$

where $q' = u, d, s, c$. Finally, the electroweak penguin operators arise from the two Feynman diagrams represented in Fig. 3 (left) and Fig. 3 (right) where Z, γ is exchanged from a quark line and from the W line, respectively. They have the following expressions:

$$\begin{aligned}
O_7 &= \frac{3}{2}\bar{q}\gamma_\mu(1-\gamma_5)b\sum_{q'} e_{q'}\bar{q}'\gamma^\mu(1+\gamma_5)q' \ , \\
O_8 &= \frac{3}{2}\bar{q}_\alpha\gamma_\mu(1-\gamma_5)b_\beta\sum_{q'} e_{q'}\bar{q}'_\beta\gamma^\mu(1+\gamma_5)q'_\alpha \ , \\
O_9 &= \frac{3}{2}\bar{q}\gamma_\mu(1-\gamma_5)b\sum_{q'} e_{q'}\bar{q}'\gamma^\mu(1-\gamma_5)q' \ , \\
O_{10} &= \frac{3}{2}\bar{q}_\alpha\gamma_\mu(1-\gamma_5)b_\beta\sum_{q'} e_{q'}\bar{q}'_\beta\gamma^\mu(1-\gamma_5)q'_\alpha \ ,
\end{aligned} \tag{34}$$

where $e_{q'}$ denotes the electric charge of q'.

4.1.2 Wilson coefficients

As we mentioned in the preceding subsection, the Wilson coefficients [23], $C_i(\mu)$, represent the physical contributions from scales higher than μ (the OPE describes physics for scales lower than μ). Since QCD has the property of asymptotic freedom, they can be calculated in perturbation theory. The Wilson coefficients include the contributions of all heavy particles, such as the top quark, the W bosons, and the charged Higgs boson. Usually, the scale μ is chosen to be of $\mathcal{O}(m_b)$ for B decays. The Wilson coefficients have been calculated to next-to-leading order (NLO). The evolution of $C(\mu)$ (the matrix that includes $C_i(\mu)$) is given by,

$$C(\mu) = U(\mu, M_W)C(M_W) \ , \tag{35}$$

where $U(\mu, M_W)$ is the QCD evolution matrix:

$$U(\mu, M_W) = \left[1 + \frac{\alpha_s(\mu)}{4\pi}J\right]U^0(\mu, M_W)\left[1 - \frac{\alpha_s(M_W)}{4\pi}J\right] \ , \tag{36}$$

with J the matrix summarizing the next-to-leading order corrections and $U^0(\mu, M_W)$ the evolution matrix in the leading-logarithm approximation. Since the strong interaction is independent of quark flavor, the $C(\mu)$ are the same for all B decays. At the scale $\mu = m_b = 5$ GeV, $C(\mu)$ take the values summarized in Table 1. To be consistent, the matrix elements of the operators, O_i, should also be renormalized to the one-loop order. This results in the effective Wilson coefficients, C_i', which satisfy the constraint,

$$C_i(m_b)\langle O_i(m_b)\rangle = C_i'\langle O_i\rangle^{tree} \ , \tag{37}$$

here $\langle O_i\rangle^{tree}$ are the matrix elements at the tree level. These matrix elements will be evaluated within the factorization approach. From Eq. (37), the relations between C_i' and

C_i are [24, 25]:

$$\begin{aligned} C_1' &= C_1 \ , & C_2' &= C_2 \ , \\ C_3' &= C_3 - P_s/3 \ , & C_4' &= C_4 + P_s \ , \\ C_5' &= C_5 - P_s/3 \ , & C_6' &= C_6 + P_s \ , \\ C_7' &= C_7 + P_e \ , & C_8' &= C_8 \ , \\ C_9' &= C_9 + P_e \ , & C_{10}' &= C_{10} \ , \end{aligned} \tag{38}$$

where,

$$\begin{aligned} P_s &= (\alpha_s/8\pi)C_2(10/9 + G(m_c, \mu, q^2)) \ , \\ P_e &= (\alpha_{em}/9\pi)(3C_1 + C_2)(10/9 + G(m_c, \mu, q^2)) \ , \end{aligned} \tag{39}$$

and

$$G(m_c, \mu, q^2) = 4\int_0^1 dx\ x(x-1)\ln\frac{m_c^2 - x(1-x)q^2}{\mu^2} \ . \tag{40}$$

Here q^2 is the typical momentum transfer of the gluon or photon in the penguin diagrams and $G(m_c, \mu, q^2)$ has the following explicit expression [26],

$$\begin{aligned} \mathscr{R}e\ G &= \frac{2}{3}\left(\ln\frac{m_c^2}{\mu^2} - \frac{5}{3} - 4\frac{m_c^2}{q^2} + \left(1 + 2\frac{m_c^2}{q^2}\right)\sqrt{1 - 4\frac{m_c^2}{q^2}}\ln\frac{1 + \sqrt{1 - 4\frac{m_c^2}{q^2}}}{1 - \sqrt{1 - 4\frac{m_c^2}{q^2}}}\right) , \\ \mathscr{I}m\ G &= -\frac{2}{3}\left(1 + 2\frac{m_c^2}{q^2}\right)\sqrt{1 - 4\frac{m_c^2}{q^2}} \ . \end{aligned} \tag{41}$$

Based on simple arguments at the quark level, the value of q^2 is chosen in the range $0.3 < q^2/m_b^2 < 0.5$ [12, 27]. From Eqs. (38-41) we can obtain numerical values for C_i'. These values are listed in Table 2, where we have taken $\alpha_s(m_Z) = 0.112$, $\alpha_{em}(m_b) = 1/132.2$, $m_b = 5$ GeV, and $m_c = 1.35$ GeV.

4.1.3 Effective Hamiltonian

In any phenomenological treatment of the weak decays of hadrons, the starting point is the weak effective Hamiltonian at low energy [28]. It is obtained by integrating out the heavy fields (e.g. the top quark, W and Z bosons) from the standard model Lagrangian. It can be written as:

$$\mathcal{H}_{eff} = \frac{G_F}{\sqrt{2}}\sum_i V_{CKM}C_i(\mu)O_i(\mu) \ , \tag{42}$$

where G_F is the Fermi constant, V_{CKM} is the CKM matrix element (see Section 4.3), $C_i(\mu)$ are the Wilson coefficients (see Section 4.1.2), $O_i(\mu)$ are the operators from the operator product expansion (see Section 4.1.1), and μ represents the renormalization scale. We emphasize that the amplitude corresponding to the effective Hamiltonian for a given decay is independent of the scale μ. In the present case, since we analyze direct CP violation in B decays, we take into account both tree and penguin diagrams. For the

penguin diagrams, we include all operators O_3 to O_{10}. Therefore, the effective Hamiltonian used will be,

$$\mathcal{H}_{eff}^{\Delta B=1} = \frac{G_F}{\sqrt{2}}\left[V_{ub}V_{us}^*(C_1O_1^s + C_2O_2^s) - V_{tb}V_{ts}^*\sum_{i=3}^{10} C_iO_i\right] + H.c.\,, \tag{43}$$

and consequently, the decay amplitude can be expressed as follows,

$$A(B \to V_1V_2) = \frac{G_F}{\sqrt{2}}\Big[V_{ub}V_{us}^*\big(C_1\langle V_1V_2|O_1^s|B\rangle + C_2\langle V_1V_2|O_2^s|B\rangle\big) - V_{tb}V_{ts}^*\sum_{i=3}^{10} C_i\langle V_1V_2|O_i|B\rangle\Big] + H.c.\,, \tag{44}$$

where $\langle V_1V_2|O_i|B\rangle$ are the hadronic matrix elements. They describe the transition between the initial state and the final state for scales lower than μ and include, up to now, the main uncertainties in the calculation since they involve non-perturbative effects.

4.2 New expression of helicity amplitudes h_{ij} according to Wilson Coefficients

4.2.1 General helicity amplitude

The weak hadronic matrix element is expressed as the sum of three helicity matrix elements, each of which takes the form $H_\lambda\big(B \to \rho^0(\omega)V_2\big) = \langle V_1V_2|H_w{}^{eff}|B\rangle$, and is defined by gathering all the Wilson coefficients of both the tree and penguin operators. Linear combinations of those coefficients arise, such as $c_{t_i}^{V_i}$ (tree diagram contribution) and $c_{p_i}^{V_i}$ (penguin diagram contribution). Then, in the case of $B \to \rho^0(\omega)V_2$, ($V_1 = \rho^0$ or ω), the helicity amplitude $H_\lambda\big(B \to \rho^0(\omega)V_2\big)$ has the general following expression:

$$\begin{aligned}
H_\lambda\big(B \to \rho^0(\omega)V_2\big) &= \Big(V_{ub}V_{us}^*c_{t_1}^\rho - V_{tb}V_{ts}^*c_{p_1}^\rho\Big)\Big\{\beta_1^\rho\varepsilon_{\alpha\beta\gamma\delta}\epsilon_{V_2}^{*\alpha}(\lambda)\epsilon_\rho^{*\beta}(\lambda)P_B^\gamma P_{V_2}^\delta \\
&+ i\Big(\beta_2^\rho\epsilon_{V_2}^*(\lambda)\epsilon_\rho^*(\lambda) - \beta_3^\rho(\epsilon_{V_2}^*(\lambda)\cdot P_B)(\epsilon_\rho^*(\lambda)\cdot P_B)\Big)\Big\} + \Big(V_{ub}V_{us}^*c_{t_2}^\rho - V_{tb}V_{ts}^*c_{p_2}^\rho\Big) \\
&\Big\{\beta_4^\rho\varepsilon_{\alpha\beta\gamma\delta}\epsilon_\rho^{*\alpha}(\lambda)\epsilon_{V_2}^{*\beta}(\lambda)P_B^\gamma P_\rho^\delta + i\Big(\beta_5^\rho\epsilon_\rho^*(\lambda)\epsilon_{V_2}^*(\lambda) - \beta_6^\rho(\epsilon_\rho^*(\lambda)\cdot P_B)(\epsilon_{V_2}^*(\lambda)\cdot P_B)\Big)\Big\} \\
&+ \frac{\tilde{\Pi}_{\rho\omega}}{(s_\rho - m_\omega^2) + im_\omega\Gamma_\omega}\Bigg[\Big(V_{ub}V_{us}^*c_{t_1}^\omega - V_{tb}V_{ts}^*c_{p_1}^\omega\Big)\Big\{\beta_1^\omega\varepsilon_{\alpha\beta\gamma\delta}\epsilon_{V_2}^{*\alpha}(\lambda)\epsilon_\omega^{*\beta}(\lambda)P_B^\gamma P_{V_2}^\delta \\
&+ i\Big(\beta_2^\omega\epsilon_{V_2}^*(\lambda)\epsilon_\omega^*(\lambda) - \beta_3^\omega(\epsilon_{V_2}^*(\lambda)\cdot P_B)(\epsilon_\omega^*(\lambda)\cdot P_B)\Big)\Big\} + \Big(V_{ub}V_{us}^*c_{t_2}^\omega - V_{tb}V_{ts}^*c_{p_2}^\omega\Big) \\
&\Big\{\beta_4^\omega\varepsilon_{\alpha\beta\gamma\delta}\epsilon_\omega^{*\alpha}(\lambda)\epsilon_{V_2}^{*\beta}(\lambda)P_B^\gamma P_\omega^\delta + i\Big(\beta_5^\omega\epsilon_\omega^*(\lambda)\epsilon_{V_2}^*(\lambda) - \beta_6^\omega(\epsilon_\omega^*(\lambda)\cdot P_B)(\epsilon_{V_2}^*(\lambda)\cdot P_B)\Big)\Big\}\Bigg]\,,
\end{aligned} \tag{45}$$

with $\epsilon_{V_2,\rho,\omega}(\lambda)$ being the K^*, ρ^0 and ω polarization vectors expressed in the B rest frame. Finally $\varepsilon_{\alpha\beta\gamma\delta}$ is the antisymmetric tensor in Minkowski space.

In Eq. (45) the parameters β_i are mainly the form factors describing transitions between vector mesons. They take the form:

$$\beta_{1,4}^{V_1} = \frac{G_F}{2} f_{V_1,V_2} m_{V_1,V_2} \frac{2}{m_B + m_{V_2,V_1}} V^{B\to V_2,V_1}(m^2_{V_1,V_2}) \ , \tag{46}$$

$$\beta_{2,5}^{V_1} = \frac{G_F}{2} f_{V_1,V_2} m_{V_1,V_2} (m_B + m_{V_2,V_1}) A_1^{B\to V_2,V_1}(m^2_{V_1,V_2}) \ , \tag{47}$$

$$\beta_{3,6}^{V_1} = \frac{G_F}{2} f_{V_1,V_2} m_{V_1,V_2} \frac{2}{m_B + m_{V_2,V_1}} A_2^{B\to V_2,V_1}(m^2_{V_1,V_2}) \ , \tag{48}$$

here f_{V_1,V_2} is either the ρ^0, ω or K^* decay constant. $V^{B\to V_2,V_1}$ and $A_i^{B\to V_2,V_1}$ are respectively the vector and axial form factors defined in Eqs. (14-16). It is worth noticing that the tensorial terms which enter $H_\lambda\big(B \to \rho^0(\omega)V_2\big)$ become simplified in the B rest frame because the four-momentum of the B is given by $P_B = (m_B, \vec{0})$. Then, using the orthogonality properties of $\epsilon_{V_i}(\lambda)$, the helicity amplitude $H_\lambda\big(B \to \rho^0(\omega)V_2\big)$ acquires a much simpler expression than above:

$$H_\lambda\big(B \to \rho^0(\omega)V_2\big) = iB_\lambda^\rho (V_{ub}V_{us}^* c_{t_1}^\rho - V_{tb}V_{ts}^* c_{p_1}^\rho) + iC_\lambda^\rho (V_{ub}V_{us}^* c_{t_2}^\rho - V_{tb}V_{ts}^* c_{p_2}^\rho) + \frac{\tilde{\Pi}_{\rho\omega}}{(s_\rho - m_\omega^2) + im_\omega\Gamma_\omega}\Big[iB_\lambda^\omega (V_{ub}V_{us}^* c_{t_1}^\omega - V_{tb}V_{ts}^* c_{p_1}^\omega) + iC_\lambda^\omega (V_{ub}V_{us}^* c_{t_2}^\omega - V_{tb}V_{ts}^* c_{p_2}^\omega)\Big] \ , \tag{49}$$

where the terms $B_\lambda^{V_1}$ and $C_\lambda^{V_1}$ take the following forms for the helicity (λ) values, $-1, 0, +1$:

$$B_{\lambda=0}^{V_1} = \beta_2^{V_1} \frac{m_B^2 - (m_{V_2}^2 + m_{V_1}^2)}{2m_{V_2}m_{V_1}} - \beta_3^{V_1} \frac{|\vec{p}|^2 m_B^2}{m_{V_2}m_{V_1}} \ , \tag{50}$$

$$C_{\lambda=0}^{V_1} = \beta_5^{V_1} \frac{m_B^2 - (m_{V_2}^2 + m_{V_1}^2)}{2m_{V_2}m_{V_1}} - \beta_6^{V_1} \frac{|\vec{p}|^2 m_B^2}{m_{V_2}m_{V_1}} \ , \tag{51}$$

$$B_{\lambda=\pm1}^{V_1} = \mp\beta_1^{V_1} m_B |\vec{p}| - \beta_2^{V_1} \ , \tag{52}$$

$$C_{\lambda=\pm1}^{V_1} = \mp\beta_4^{V_1} m_B |\vec{p}| - \beta_5^{V_1} \ . \tag{53}$$

In the above equations, $|\vec{p}|$ is the momentum common to the V_1 and V_2 particles in the B rest frame. It takes the form:

$$|\vec{p}| = \frac{\sqrt{[m_B^2 - (m_{V_1} + m_{V_2})^2][m_B^2 - (m_{V_1} - m_{V_2})^2]}}{2m_B} \ , \tag{54}$$

where m_1 and m_2 are the vector masses. Taking into account the previous relations, we arrive at the final form for the amplitudes $H_\lambda\Big(B \to \rho^0(\omega)V_2\Big)$:

$$\begin{aligned} H_{\lambda=^0_{\pm1}}\Big(B \to \rho^0(\omega)V_2\Big) = \\ A\lambda^2\Bigg\{\Big[R_1^\rho B_{\lambda=^0_{\pm1}}^\rho + R_2^\rho C_{\lambda=^0_{\pm1}}^\rho\Big] + i\Big[I_1^\rho B_{\lambda=^0_{\pm1}}^\rho + I_2^\rho C_{\lambda=^0_{\pm1}}^\rho\Big]\Bigg\} \\ + \frac{\tilde{\Pi}_{\rho\omega}}{(s_\rho - m_\omega^2) + im_\omega\Gamma_\omega}\Bigg[A\lambda^2\Bigg\{\Big[R_1^\omega B_{\lambda=^0_{\pm1}}^\omega + R_2^\omega C_{\lambda=^0_{\pm1}}^\omega\Big] \\ + i\Big[I_1^\omega B_{\lambda=^0_{\pm1}}^\omega + I_2^\omega C_{\lambda=^0_{\pm1}}^\omega\Big]\Bigg\}\Bigg] \ , \end{aligned} \tag{55}$$

where one defines,

$$R_i^{V_1} = \eta\lambda^2 c_{t_i}^{V_1} - \mathscr{I}m(c_{p_i}^{V_1}) \,, \tag{56}$$

$$I_i^{V_1} = \rho\lambda^2 c_{t_i}^{V_1} + \mathscr{R}e(c_{p_i}^{V_1}) \,, \tag{57}$$

with V_1 being either ρ^0 or ω. From Eq. (55), the density-matrix elements $h_{\lambda,\lambda'}$ can be derived automatically and on has:

$$h_{\lambda,\lambda'} = H_\lambda\big(B \to \rho^0(\omega)V_2\big) H^*_{\lambda'}\big(B \to \rho^0(\omega)V_2\big) \,. \tag{58}$$

Because of the hermiticity of the matrix $(h_{\lambda,\lambda'})$, only six elements must be calculated.

4.2.2 Explicit amplitudes for the B decays investigated

By applying the formalism described in Section III, one gets in the case of the ρ^0 production, the following linear combinations of the effective Wilson coefficients:
for the decay $\bar{B}^0 \to \bar{K}^{*0}\rho^0$:

$$\begin{aligned} c_{t_1}^{\rho} &= C_1' + \frac{C_2'}{N_c} \,, & c_{p_1}^{\rho} &= \frac{3}{2}\Big(C_9' + \frac{C_{10}'}{N_c} + C_7' + \frac{C_8'}{N_c}\Big) \,, \\ c_{t_2}^{\rho} &= 0 \,, & c_{p_2}^{\rho} &= -\Big(C_4' + \frac{C_3'}{N_c}\Big) + \frac{1}{2}\Big(C_{10}' + \frac{C_9'}{N_c}\Big) \,, \end{aligned} \tag{59}$$

where C_i' are listed in Table 2. The coefficients, $c_{t_i}^{\rho}$, relate to the tree diagrams and $c_{p_i}^{\rho}$ to the penguin diagrams. To simplify the formulas we used N_c for N_c^{eff} in the expressions (Eqs. (59)-(62)).
for the decay $B^- \to K^{*-}\rho^0$:

$$\begin{aligned} c_{t_1}^{\rho} &= C_1' + \frac{C_2'}{N_c} \,, & c_{p_1}^{\rho} &= \frac{3}{2}\Big(C_9' + \frac{C_{10}'}{N_c} + C_7' + \frac{C_8'}{N_c}\Big) \,, \\ c_{t_2}^{\rho} &= C_2' + \frac{C_1'}{N_c} \,, & c_{p_2}^{\rho} &= C_4' + \frac{C_3'}{N_c} + C_{10}' + \frac{C_9'}{N_c} \,. \end{aligned} \tag{60}$$

In the case of ω production one obtains the following linear combinations of effective Wilson coefficients:
for the decay $\bar{B}^0 \to \bar{K}^{*0}\omega$:

$$\begin{aligned} c_{t_1}^{\omega} &= 0 \,, & c_{p_1}^{\omega} &= -C_4' - \frac{C_3'}{N_c} + \frac{1}{2}\Big(C_{10}' + \frac{C_9'}{N_c}\Big) \,, \\ c_{t_2}^{\omega} &= C_1' + \frac{C_2'}{N_c} \,, & c_{p_2}^{\omega} &= 2\Big(C_3' + \frac{C_4'}{N_c} + C_5' + \frac{C_6'}{N_c}\Big) + \frac{1}{2}\Big(C_9' + \frac{C_{10}'}{N_c} + C_7' + \frac{C_8'}{N_c}\Big) \,. \end{aligned} \tag{61}$$

for the decay $B^- \to K^{*-}\omega$:

$$\begin{aligned} c_{t_1}^{\omega} &= C_2' + \frac{C_1'}{N_c} \,, & c_{p_1}^{\omega} &= C_4' + \frac{C_3'}{N_c} + \Big(C_{10}' + \frac{C_9'}{N_c}\Big) \,, \\ c_{t_2}^{\omega} &= C_1' + \frac{C_2'}{N_c} \,, & c_{p_2}^{\omega} &= 2\Big(C_3' + \frac{C_4'}{N_c} + C_5' + \frac{C_6'}{N_c}\Big) + \frac{1}{2}\Big(C_9' + \frac{C_{10}'}{N_c} + C_7' + \frac{C_8'}{N_c}\Big) \,. \end{aligned} \tag{62}$$

We refer to Appendix A for details of the helicity amplitudes, while for the channel $B^\pm \to \rho^0(\omega)\rho^\pm$ we refer to Appendix B.

4.3 CKM matrix and form factors

In phenomenological applications, the widely used representation of the CKM matrix is the *Wolfenstein parametrization* [19]. In this approach, the four independent parameters are λ_c, A, ρ and η. Then, by expanding each element of the matrix as a power series in the parameter $\lambda_c = \sin\theta_c = 0.2209$ (θ_c is the Gell-Mann-Levy-Cabibbo angle), one finds ($O(\lambda_c^4)$ is neglected)

$$\hat{V}_{CKM} = \begin{pmatrix} 1-\frac{1}{2}\lambda_c^2 & \lambda_c & A\lambda_c^3(\rho - i\eta) \\ -\lambda_c & 1-\frac{1}{2}\lambda_c^2 & A\lambda_c^2 \\ A\lambda_c^3(1-\rho-i\eta) & -A\lambda_c^2 & 1 \end{pmatrix} , \tag{63}$$

where η plays the role of the CP-violating phase. In this parametrization, even though it is an approximation in λ_c, the CKM matrix satisfies unitarity exactly, which means,

$$\hat{V}_{CKM}^{\dagger} \cdot \hat{V}_{CKM} = \hat{I} = \hat{V}_{CKM} \cdot \hat{V}_{CKM}^{\dagger} \cdot \tag{64}$$

The form factors, $V(k^2)$ and $A_j(k^2)$, depend on the inner structure of the hadrons. Here we will adopt two different theoretical approaches. The first was proposed by Bauer, Stech, and Wirbel [10] (BSW), who used the overlap integrals of wave functions in order to evaluate the meson-meson matrix elements of the corresponding current. In that case the momentum dependence of the form factors is based on a single-pole ansatz. The second approach was developed by Guo and Huang (GH) [29], who modified the BSW model by using some wave functions described in the light-cone framework. Nevertheless, both of these models use phenomenological form factors which are parametrized by making the assumption of nearest pole dominance. The explicit k^2 dependence of the form factor is [10, 30]:

$$V(k^2) = \frac{h_V}{\left(1-\frac{k^2}{m_V^2}\right)} , \qquad A_j(k^2) = \frac{h_{A_j}}{\left(1-\frac{k^2}{m_{A_j}^2}\right)} , \tag{65}$$

where m_{A_j} and m_V are the pole masses associated with the transition current and h_V and h_{A_j} are the values of the form factors at $q^2 = 0$.

5 Monte-Carlo simulations: computation of h_{ij} and general results

5.1 Numerical inputs

5.1.1 CKM values

In our numerical calculations we have several parameters: q^2, N_c^{eff} and the CKM matrix elements in the Wolfenstein parametrization. As mentioned in Section IV, the value of q^2 is conventionally chosen to be in the range $0.3 < q^2/{m_b}^2 < 0.5$. The CKM matrix, which should be determined from experimental data, is expressed in terms of the Wolfenstein parameters, A, λ_c, ρ, and η [19]. Here, we shall use the latest values [31], which were extracted from charmless semileptonic B decays, ($|V_{ub}|$), charmed semileptonic B decays,

($|V_{cb}|$), s and d mass oscillations, $\Delta m_s, \Delta m_d$, and CP violation in the kaon system (ϵ_K), (ρ, η). Hence, one has,

$$\lambda_c = 0.2237 \ , \ \ A = 0.8113 \ , \ \ 0.190 < \rho < 0.268 \ , \ \ 0.284 < \eta < 0.366 \ . \tag{66}$$

These values respect the unitarity triangle as well (see also Table 3). In our numerical simulations, we will use the average values of ρ and η.

5.1.2 Quark masses

The running quark masses are used in order to calculate the matrix elements of penguin operators. The quark mass is evaluated at the scale $\mu \simeq m_b$ in B decays. Therefore one has [32],

$$\begin{aligned} m_u(\mu = m_b) &= 2.3 \text{ MeV} \ , & m_d(\mu = m_b) &= 4.6 \text{ MeV} \ , \\ m_s(\mu = m_b) &= 90 \text{ MeV} \ , & m_b(\mu = m_b) &= 4.9 \text{ GeV} \ , \end{aligned} \tag{67}$$

which corresponds to $m_s(\mu = 1 \text{ GeV}) = 140$ MeV. For meson masses, we shall use the following values [13]:

$$\begin{aligned} m_{B^\pm} &= 5.279 \text{ GeV} \ , & m_{K^{*0}} &= 0.896 \text{ GeV} \ , & m_\omega &= 0.782 \text{ GeV} \ , \\ m_{B^0} &= 5.279 \text{ GeV} \ , & m_{\rho^\pm} &= 0.770 \text{ GeV} \ , & m_{\pi^\pm} &= 0.139 \text{ GeV} \ , \\ m_{K^{*\pm}} &= 0.892 \text{ GeV} \ , & m_{\rho^0} &= 0.770 \text{ GeV} \ , & m_{\pi^0} &= 0.135 \text{ GeV} \ . \end{aligned} \tag{68}$$

5.1.3 Form factors and decay constants

In Table 4 we list the relevant form factor values at zero momentum transfer [10, 29, 33] for the $B \to K^*$, $B \to \rho$ and $B \to \omega$ transitions. The different models are defined as follows : model (1) is the BSW model where the q^2 dependence of the form factors is described by a single-ansatz. Model (2) is the GH model with the same momentum dependence as model (1). Finally, we define the decay constant for vector (f_V) meson as usual by,

$$\begin{aligned} \sqrt{2}\langle \rho(q)|\bar{q}_1\gamma_\mu q_2|0\rangle &= f_\rho m_\rho \epsilon_\rho \ \text{ for } \rho \ \text{ and otherwise} \ , \\ \langle V(q)|\bar{q}_1\gamma_\mu q_2|0\rangle &= f_V m_V \epsilon_V \ , \end{aligned} \tag{69}$$

with q being the momentum of the vector meson and m_V and ϵ_V being the mass and polarization vector of the vector meson, respectively. Numerically, in our calculations, we take [13],

$$f_{K^*} = 214 \text{ MeV} \ , \ f_\rho = 221 \text{ MeV} \ , \ f_\omega = 195 \text{ MeV} \ . \tag{70}$$

Finally, the free parameter (effective number of color, N_c^{eff}) is taken to lie between the lower(upper) limits 0.66(2.84) for $b \to s$ transition. Nevertheless, we focus our analysis on values of N_c^{eff} bigger than 1, as suggested in [34]. Regarding the $b \to d$ transition, the lower(upper) limits for N_c^{eff} are 0.98(2.01) [34].

5.2 Simulation of the $\rho^0 - \omega$ mixing

All the channels studied here include at least one ρ^0 meson which mixes with the ω meson. The other vector mesons are either a $K^{*0,\pm}$ or a $\rho^{\pm}$. Thus, the mass of each resonance is generated according to a relativistic Breit-Wigner:

$$\frac{d\sigma}{dM^2} = C_N \frac{\Gamma_R M_R}{\left(M^2 - M_R^2\right)^2 + \left(\Gamma_R M_R\right)^2} \ , \tag{71}$$

where C_N is a normalization constant. In Eq. (71), M_R and Γ_R are respectively the mass and the width of the vector meson which have been determined experimentally. M is the mass of the generated resonance. A simple and phenomenological relation describing the amplitude for $\rho^0 - \omega$ mixing is used for the Monte-Carlo simulations [35]. In the expression for the Breit-Wigner, the ρ^0-propagator is replaced by the following one:

$$\frac{1}{s_{\rho\omega}} = \frac{1}{s_\rho} + \frac{T_\omega}{T_\rho} \frac{\Pi_{\rho\omega}}{s_\rho s_\omega} \ , \tag{72}$$

where T_ω and T_ρ are respectively the ω and ρ production amplitudes. In addition, $\tilde{\Pi}_{\rho\omega}$ is the mixing parameter for which recent values come from $e^+e^- \to \pi^+\pi^-$ annihilations. Explanations have been already been given in Section III. Finally, $1/s_V$ has the same definition as in Eq. (22). Because the same physical processes enter the production of both the ρ^0 and ω resonances (they are both made out from $u\bar{u}$ and $d\bar{d}$ quark pairs with the same weight $1/2$), it seems natural to choose $T_\omega/T_\rho = 1$. So, the invariant mass distribution of the $\pi^+\pi^-$ system becomes simplified, being given by,

$$d\sigma/dm^2 \propto \left|\mathcal{A}(\rho^0(\omega))\right|^2 \ , \tag{73}$$

where $\mathcal{A}(\rho^0(\omega))$ is the amplitude of the two mixed Breit-Wigner distributions and m is the $\pi^+\pi^-$ invariant mass. In Fig. 4, the $\pi^+\pi^-$ invariant mass spectra for $\rho^0 - \omega$ mixing is displayed. Because of the very narrow width of the ω, ($\Gamma_\omega = 8.44$ MeV), we notice a high and narrow peak at the ω pole (≈ 782 MeV).

5.3 Density matrix $h_{\lambda,\lambda'}$

Three main parameters remain free in our simulations: the ratio q^2/m_b^2 (related to the penguin diagrams), the form factor model (GH or BSW) and the effective number of colors, N_c^{eff} (associated with the factorization hypothesis). The histograms plotted in Fig. 5 display spectra of the diagonal and normalized density matrix elements $h_{i,i}$, for the channels $B^0 \to \rho^0(\omega)K^{*0}$ (left hand-side) and $B^+ \to \rho^0(\omega)\rho^+$ (right hand-side). The input numerical parameters are $q^2/m_b^2 = 0.3$, $N_c^{eff} = 2.84$ (left hand-side figure) or $N_c^{eff} = 2.01$ (right hand-side figure), and the GH form factor model is applied for both decays. Note also that the average values of CKM parameters ρ and η are used. The wide spectrum of values of the density matrix element $h_{\lambda,\lambda}$, is caused by the resonance widths (especially that of the ρ) which provides, in turn, a large spectrum for the common momentum p_V in the B rest-frame. Whatever the $\rho^0(\omega)V_2$ channel is, $h_{00} = |H_0|^2$, which corresponds to longitudinal polarization, is the dominant value. Numerically, for the $B^0 \to \rho^0(\omega)K^{*0}$ decay, the mean value of h_{00} is around 0.87 while it is of order 0.90 for $B^+ \to \rho^0(\omega)\rho^+$. The dominance of the longitudinal polarization has already

been confirmed experimentally, since recent experimental data related to the channel $B \to J/\psi K^*$ show clearly that the longitudinal decay amplitude dominates in that case, with $|H_0|^2 = 0.59 \pm 0.06 \pm 0.01$ [36]. Extrapolating these results to the charmless vector meson final states requires some modifications of the form factors without a big change of the relative contributions of the polarization states. Regarding $h_{--} = |H_{-1}|^2$, it represents less than 0.5% of the total amplitude for both decays. This numerical result is confirmed by complete analytical calculations.

In Figs. 6 and 7, the real and imaginary parts of the non-diagonal and normalized density matrix elements $h_{i,j}$ are shown for the channels $B^0 \to \rho^0(\omega)K^{*0}$ and $B^+ \to \rho^0(\omega)\rho^+$, respectively. The input parameters are the same as previously mentioned. The main feature of the non-diagonal matrix elements, $h_{i,j}$, is the smallness of both the imaginary and real parts – the imaginary part being at least one order of magnitude smaller than the real part one. For the $B^+ \to \rho^0(\omega)\rho^+$ decay, we observe that the mean value of all the imaginary parts is zero, whereas it can vary for the other decay. Note also that each of the three real parts are quite similar for both decays. Because of the tiny value of $h_{--} = |H_{-1}|^2$, the moduli of the non-diagonal elements, $h_{+-} = H_+ H_-^*$ and $h_{0-} = H_0 H_-^*$, are very small, while the modulus of $h_{+0} = H_+ H_0^*$ is around 0.3 for both decays. As a first conclusion, the general behavior of the density matrix seems to be similar whatever the decay is. Experimentally, only the mean values of the diagonal elements and h_{+-} will be able to be measured through the angular distributions.

These angular distributions are plotted in Figs. 8 and 9 in the helicity frame and in the transversity frame, respectively for $B^0 \to \rho^0(\omega)K^{*0}$ and for the usual input parameters. Their normalized pdfs have been displayed above in Eq. (10). As a consequence of the small value of $\langle h_{+-} \rangle$, the azimuthal angle distribution in the helicity frame is nearly flat, whereas it is sinusoidal in the transversity frame. From the distribution as a function of polar angle (in the TF) displayed in Eq. (13), one can infer a mean value of the H_T amplitude. This represents an additional piece of information through which one can access the dynamics of $B(\bar{B})$ decays into two charmless hadrons.

6 Branching ratio and asymmetry in B decays into two vector mesons

The analytic expressions for the density matrix elements, h_{ij} allow us to calculate the hadronic branching ratios $\mathscr{B}(B \to \rho^0(\omega)V_2)$ and to estimate the asymmetries related to B and $\bar{B}$ decays. All these physical observables depend primarily on a subset of the parameters mentioned previously, such as the form factors, the ratio $q^2/{m_b}^2$ (where q^2 is the mass of the virtual gluon in the penguin diagram), the effective number of colors, N_c^{eff} (used as a free parameter in the framework of the factorization hypothesis), and the CKM matrix element parameters ρ and η.

6.1 Branching ratio: results and discussions

Departing from the definition of the branching ratio ($\mathscr{B}(B \to f)$),

$$\mathscr{B}(B \to f) = \frac{\Gamma(B \to f)}{\Gamma(B \to All)}\,, \tag{74}$$

the width $\Gamma(B \to V_1 V_2)$ can be inferred from its differential form given by the standard relation [37]:

$$d\Gamma(B \to V_1 V_2) = \frac{1}{8\pi^2 M} |\mathcal{M}(B \to V_1 V_2)|^2 \frac{d^3\vec{p}_1}{2E_1} \frac{d^3\vec{p}_2}{2E_2} \delta^4(P - p_1 - p_2) . \qquad (75)$$

In Eq. (75), $P = (M, \vec{0})$, where $M = m_b$ and $(E_1, \vec{p}_1)$ and $(E_2, \vec{p}_2)$ are the 4-momenta of V_1 and V_2, respectively, in the B rest frame. Because of the large width of the ρ^0 meson ($\Gamma_\rho \approx 150$ MeV) and the K^* meson ($\Gamma_{K^*} \approx 50$ MeV), the energy, E_i, and the momentum, p_i, of each vector meson vary according to the generated event. Computation of $\Gamma(B \to \rho^0(\omega) V_2)$ could not be done analytically but numerically by Monte-Carlo methods. A total number of 50000 events have been generated in order to obtain a precise estimate of this decay width.

In Tables 5 and 6 we list (respectively) the branching ratios for $\bar{B} \to \rho^0(\omega)\bar{V}_2$ and $B \to \rho^0(\omega) V_2$ and their dependence on the form factor models (BSW and GH), q^2/m_b^2, N_c^{eff} and the average values of the CKM parameters ρ and η. For a fixed value of $q^2/{m_b}^2$, there are important variations of the branching ratios, depending on the form-factor model. They can vary by up to a factor two. In the framework of a given form-factor model, some branching ratio modifications appear with $q^2/{m_b}^2$, especially in the channels including a K^*. However, these changes do not exceed 34%. Regarding the ratio between $\mathcal{B}(B^0 \to \rho^0(\omega) K^{*0})$ and $\mathcal{B}(B^+ \to \rho^0(\omega) K^{*+})$, its value is found to be of the order 0.40 for the BSW model and 0.34 for the GH model.

Finally, we observe that the relative difference between two conjugate branching ratios, $\mathcal{B}(B \to f)$ and $\mathcal{B}(\bar{B} \to \bar{f})$, is almost independent of the form-factor models, for a fixed value of $q^2/{m_b}^2$. It can be computed from the two tables just mentioned and, usually, it does not exceed 20%. The exception is for the $K^{*\pm}\rho^0(\omega)$ channels, where it reaches 39%.

6.2 Asymmetry: results and discussions

A search for direct CP violation requires asymmetries between conjugate final states coming from B and $\bar{B}$ decays respectively. In our case, these searches are performed in two complementary ways. We consider first the global CP-violating asymmetry a_{CP}, calculated from branching ratios:

$$a_{CP} = \frac{\mathcal{B}(B \to f) - \overline{\mathcal{B}}(\bar{B} \to \bar{f})}{\mathcal{B}(B \to f) + \overline{\mathcal{B}}(\bar{B} \to \bar{f})} . \qquad (76)$$

Secondly, we use the partial widths of $B(\to f)$ and $\bar{B}(\to \bar{f})$, calculated as described above together with the differential asymmetries investigated as a function of the $\pi^+\pi^-$ invariant mass in the whole range of the ρ^0 Breit-Wigner resonance. Hence, $a_{CP}(m)$ takes the following form:

$$a_{CP}(m) = \frac{\Gamma_m(B \to f) - \bar{\Gamma}_m(\bar{B} \to \bar{f})}{\Gamma_m(B \to f) + \bar{\Gamma}_m(\bar{B} \to \bar{f})} , \qquad (77)$$

where m is the $\pi^+\pi^-$ invariant mass. $\Gamma_m(B \to f)$ and $\bar{\Gamma}_m(\bar{B} \to \bar{f})$ in Eq. (77) are the partial widths written as a function of m.

In Table 7 we list the global CP-violating asymmetry between the B and $\bar{B}$ decays for the channels under investigation. It can be noticed that, for a fixed value of $q^2/{m_b}^2$,

the two form factor models provide quite similar results. For different $q^2/{m_b}^2$ values, the corresponding results could vary, especially in the $K^{*\pm}\rho^0(\omega)$ channels. In Figs. 10 and 11 we show, respectively, the histogram of the direct CP-violating asymmetry parameter $a_{CP}(m)$, for the decays $B^0 \to \rho^0(\omega)K^{*0}$ and $B^+ \to \rho^0(\omega)\rho^+$, as a function of the $\pi^+\pi^-$ invariant mass in the ω mass region and for both form factor models. The asymmetry reaches its maximum when $\sqrt{s}$ is around 780 MeV. However, outside the displayed windows, the asymmetry goes to zero in any case. The peak of the asymmetry is emphasized when the GH form factor model is used in our simulations. For the $K^{*0}\rho^0(\omega)$ channels, the maximum of the CP violating asymmetry is around 13% and 16%, for the BSW model and the GH model, respectively. Finally, we emphasise that the $\rho^{\pm}\rho^0(\omega)$ channels present the most intriguing results because, in any case, their asymmetry is at least 80% (BSW model) and can reach 95% (GH model). This last channel is highly recommended for a direct search for CP violation.

7 Perspectives and conclusions

We have studied direct CP violation in decay process such as $B \to \rho^0(\omega)V_2 \to \pi^+\pi^-V_2$, where V_2 is either $K^{*0,\pm}$ or $\rho^{\pm}$, with the inclusion of $\rho^0 - \omega$ mixing. When the invariant mass of the $\pi^+\pi^-$ pair is in the vicinity of the ω resonance, it is found that the CP-violating asymmetry, $a_{CP}(m)$, reaches its maximum value. In our analysis we have also investigated the branching ratios for the same channels. Thanks to the standard helicity and transversity formalisms, rigorous and detailed calculations of the $B^{0\pm}$ decays into two charmless vector mesons have been carried out completely. Using the effective Hamiltonian based on the operator product expansion with the appropriate Wilson coefficients, we derived in detail the amplitudes corresponding to $B \to \rho^0(\omega)V_2 \to \pi^+\pi^-V_2$ decay and the density matrix, $h_{\lambda\lambda'}$ as well.

In order to apply our formalism, we used a Monte-Carlo method for all the numerical simulations. Moreover, we dealt at length with the uncertainties coming from the input parameters. In particular, these include the Cabibbo-Kobayashi-Maskawa matrix element parameters, ρ and η, the effective number of colors, N_c^{eff}, coming from the naive factorization and two phenomenological models in order to show the possible dependence on form factors, GH or BSW. These form factors vary slightly according to the final states. Recall that this work was achieved by applying a phenomenological treatment, where some assumptions regarding the evaluation of the hadronic matrix elements have been made. In this approach, corrections associated with the limit of validity of the factorization hypothesis were parameterized phenomenologically and may involve large uncertainties.

As a major result, the predominance of the longitudinal polarization, h_{00}, has been pointed out in all the investigated decays. We also found a large direct CP-violating asymmetry in these B decays into two charmless vector mesons. We stress that, without the inclusion of $\rho^0-\omega$ mixing, we would not have a large CP-violating asymmetry. Finally, we predicted branching ratios to be of the order $0.7 - 2.1 \times 10^{-6}$ for $K^{*0}\rho^0(\omega)$ and of the order $2.3-6.6\times10^{-6}$ for $K^{*\pm}\rho^0(\omega)$ (depending on the different phenomenological models). For the channel $\rho^{\pm}\rho^0(\omega)$, we found the branching ratios to be of the order $11 - 24 \times 10^{-6}$.

Two main conclusions can be drawn. The first is the relative importance of the form factor model which is used, since some branching ratios in $B \to \rho^0(\omega)V_2$ could change by

up to a factor two. The second is the important role of $\rho^0 - \omega$ mixing, which can enhance considerably the asymmetry parameter a_{CP}, between the conjugate final states coming, respectively, from B and $\bar{B}$ decays.

Beside the "standard" ways to look for direct CP violation, such as the difference between branching ratios and/or discrepancies in the angular distributions of the decay products, we have presented a detailed discussion of a new method. This involves the variation of a_{CP} as a function of the $\pi^+\pi^-$ invariant mass over the whole range of the ρ^0 resonance [12, 34]. We believe that this method will be very fruitful for future experiments and has already been implemented in the generator of the LHCb experiment. Indeed, we look forward to being able to apply the formalism developed here to the analysis of experimental data for decays such as $B \to \rho^0(\omega)V_2$ (with V_2 being either a K^* or a $\rho^\pm$) in the near future.

Acknowledgements

This work was supported in part by the Australian Research Council and the University of Adelaide. The LHCb Clermont-Ferrand group would like to acknowledge G. Menessier from the LPTM, for many illuminating discussions regarding the exciting question of FSI in hadronic physics.

Appendix

A Practical calculations of the helicity amplitudes

The helicity formalism in the case of vector mesons requires the introduction of three polarization four-vectors for each spin 1 particle [38]:

$$\epsilon(1) = (0, \vec{\epsilon}(1)) \ , \quad \epsilon(2) = (0, \vec{\epsilon}(2)) \ , \text{ and } \ \epsilon(3) = \left(|\vec{k}|/m, E\hat{k}/m\right) . \tag{78}$$

They also satisfy the following relations as well:

$$\epsilon(i)^2 = -1 \ , \text{ and } \ \epsilon(i) \cdot \epsilon(j) = 0 \ , \quad \text{with } i \neq j \ , \tag{79}$$

where m, E and $\vec{k}$ are respectively the mass, the energy and the momentum of the vector meson. $\hat{k}$ is defined as the unit vector along the vector momentum, $\hat{k} = \vec{k}/|\vec{k}|$. The three vectors $\vec{\epsilon}(1), \vec{\epsilon}(2)$ and $\vec{\epsilon}(3) = E\hat{k}/m$ form an orthogonal basis. $\vec{\epsilon}(1)$ and $\vec{\epsilon}(2)$ are the *transverse polarization* vectors while $\vec{\epsilon}(3)$ is the *longitudinal polarization* vector. These three vectors allow one to define the *helicity basis*:

$$\epsilon(+) = \frac{(\epsilon(1) + i\,\epsilon(2))}{\sqrt{2}} \ , \quad \epsilon(-) = \frac{(\epsilon(1) - i\,\epsilon(2))}{\sqrt{2}} \ , \text{ and } \ \epsilon(0) = \epsilon(3) \ . \tag{80}$$

These 4-vectors are *eigenvectors* of the helicity operator $\mathcal{H}$ corresponding, respectively, to the eigenvalues $\lambda = +1, -1$ and 0. In the $B^{0\pm}$ rest-frame, the vector mesons have opposite momentum $\vec{k}_1 = -\vec{k}_2$ and their respective polarization vectors are *correlated*. This implies the following expressions,

$$\vec{k}_K = -\vec{k}_\rho = \vec{k} = \begin{pmatrix} k\sin\theta\cos\phi \\ k\sin\theta\sin\phi \\ k\cos\theta \end{pmatrix} \ ,$$

where θ and ϕ are respectively polar and azimuthal angles of the produced K^*. In our case, one has for the transversal polarization vectors (K^* and ρ) the expressions:

$$\vec{\epsilon}_K(1) = \begin{pmatrix} \cos\theta\cos\phi \\ \cos\theta\sin\phi \\ -\sin\theta \end{pmatrix} = \vec{\epsilon}_\rho(1) \ ,$$

and,

$$\vec{\epsilon}_K(2) = \begin{pmatrix} -\sin\phi \\ \cos\phi \\ 0 \end{pmatrix} = -\vec{\epsilon}_\rho(2) \ .$$

Regarding the longitudinal polarization, $\epsilon_K(3)$ and $\epsilon_\rho(3)$ take the form:

$$\epsilon_K(3) = \left(\frac{|\vec{k}|}{m_K}, \frac{E_K}{m_K}\hat{k}\right) \ , \quad \epsilon_\rho(3) = \left(\frac{|\vec{k}|}{m_\rho}, \frac{E_\rho}{m_\rho}(-\hat{k})\right) \ . \tag{81}$$

By applying the relations from Eq. (80), one can expressed vectors $\vec{\epsilon}(i)$ in the helicity basis and one gets $\vec{\epsilon}(\pm)$:

$$\vec{\epsilon}_K(+) = \begin{pmatrix} \cos\theta\cos\phi - i\sin\phi \\ \cos\theta\sin\phi + i\cos\phi \\ -\sin\theta \end{pmatrix} /\sqrt{2} = \vec{\epsilon}_K^*(-) = \vec{\epsilon}_\rho(-) \ , \tag{82}$$

$$\vec{\epsilon}_K(-) = \begin{pmatrix} \cos\theta\cos\phi + i\sin\phi \\ \cos\theta\sin\phi - i\cos\phi \\ -\sin\theta \end{pmatrix} /\sqrt{2} = \vec{\epsilon}_K^*(+) = \vec{\epsilon}_\rho(+) \ . \tag{83}$$

The weak hadronic amplitude is therefore decomposed, in the helicity basis, according to the general method developed by Bauer, Stech and Wirbel [10]. This will allow one to obtain two interesting results. Firstly, one can isolate the contribution of each helicity state to the total amplitude. Secondly, the contributions of the *tree* and *penguin* operators to the total amplitude can be separated via the helicity states.

The knowledge of the main input parameters $\rho, \eta, A, \sin\theta_c (= \lambda_c)$ and the masses and widths of the intermediate resonances allow a complete determination of the three helicity amplitudes $H_\lambda(B \to \rho^0(\omega)V_2)$, where the helicity λ can take the values -1,0 or +1.

B Channel $B^\pm \to \rho^0(\omega)\rho^\pm$

The formalism applied in case of $B \to \rho^0(\omega)K^*$ can be extend to $B^\pm \to \rho^0(\omega)\rho^\pm$. Nevertheless, in the last case one has $b \to d$ transition instead of $b \to s$. The amplitude

$H_\lambda(B \to \rho^0(\omega)V_2)$ has the form:

$$H_{\lambda=^0_{\pm1}}(B \to \rho^0(\omega)V_2) =$$
$$A\lambda^3\Bigg\{\Big[R_1^\rho B^\rho_{\lambda=^0_{\pm1}} + R_2^\rho C^\rho_{\lambda=^0_{\pm1}}\Big] + i\Big[I_1^\rho B^\rho_{\lambda=^0_{\pm1}} + I_2^\rho C^\rho_{\lambda=^0_{\pm1}}\Big]\Bigg\}$$
$$+\frac{\tilde{\Pi}_{\rho\omega}}{(s_\rho - m_\omega^2) + im_\omega\Gamma_\omega}\Bigg[A\lambda^3\Bigg\{\Big[R_1^\omega B^\omega_{\lambda=^0_{\pm1}} + R_2^\omega C^\omega_{\lambda=^0_{\pm1}}\Big]$$
$$+ i\Big[I_1^\omega B^\omega_{\lambda=^0_{\pm1}} + I_2^\omega C^\omega_{\lambda=^0_{\pm1}}\Big]\Bigg\}\Bigg], \quad (84)$$

where one defines,

$$R_i^{V_1} = (1-\frac{\lambda^2}{2})\eta c_{t_i}^{V_1} + \eta\,\mathscr{R}e(c_{p_i}^{V_1}) - (1-\rho)\,\mathscr{I}m(c_{p_i}^{V_1}), \quad (85)$$
$$I_i^{V_1} = (1-\frac{\lambda^2}{2})\rho c_{t_i}^{V_1} + \eta\,\mathscr{I}m(c_{p_i}^{V_1}) + (1-\rho)\,\mathscr{R}e(c_{p_i}^{V_1}), \quad (86)$$

with V_1 being either ρ^0 or ω.

$$\text{If } V_1 \equiv \rho \text{ and } i = 2 \text{ then } R_i^{V_1} = I_i^{V_1} = 0\,. \quad (87)$$

The expressions for $c_{t_i}^{V_1}$ and $c_{p_i}^{V_1}$, which correspond to the investigated channel, take the following form:
for the decay $B^- \to \rho^0\rho^-$:

$$c_{t_1}^\rho = C_1' + \frac{C_2'}{N_c} + C_2' + \frac{C_1'}{N_c},$$
$$c_{p_1}^\rho = \frac{3}{2}\Big(C_7' + \frac{C_8'}{N_c} + C_9' + \frac{C_{10}'}{N_c} + C_{10}' + \frac{C_9'}{N_c}\Big)\,. \quad (88)$$

In the case of ω production, one obtains the linear combinations of the effective Wilson coefficients:
for the decay $B^- \to \omega\rho^-$:

$$c_{t_1}^\omega = C_2' + \frac{C_1'}{N_c}, \quad c_{p_1}^\omega = C_4' + \frac{C_3'}{N_c} + \Big(C_{10}' + \frac{C_9'}{N_c}\Big),$$
$$c_{t_2}^\omega = C_1' + \frac{C_2'}{N_c}, \quad c_{p_2}^\omega = 2\Big(C_3' + \frac{C_4'}{N_c} + C_5' + \frac{C_6'}{N_c}\Big)$$
$$+\frac{1}{2}\Big(C_9' + \frac{C_{10}'}{N_c} + C_7' + \frac{C_8'}{N_c} - C_{10}' - \frac{C_9'}{N_c}\Big)\,. \quad (89)$$

All the terms used in the appendix have been defined in Section IV.

References

[1] A.B. Carter and A.I. Sanda, Phys. Rev. Lett. **45** (1980) 952, Phys. Rev. **D23** (1981) 1567; I.I. Bigi and A.I. Sanda, Nucl. Phys. **B193** (1981) 85.

[2] Proceedings of the Workshop on CP Violation, Adelaide 1998, edited by X.-H. Guo, M. Sevior and A.W. Thomas (World Scientific, Singapore).

[3] A. Bozek (BELLE Collaboration), in Proceedings of the 4th International Conference on B Physics and CP Violation, Ise-Shima, Japan, February 2001, hep-ex/0104041; K. Abe, *et al.* (BELLE Collaboration), in Proceedings of the XX International Symposium on Lepton and Photon Interactions at High Energies, July 2001, Roma, Italy, BELLE-CONF-0115 (2001); K. Abe, *et al.* (BELLE Collaboration), Phys. Rev. **D65** (2002) 092005; R.S. Lu, *et al.* (BELLE Collaboration), Phys. Rev. Lett. **89** (2002) 191801.

[4] T. Schietinger (BABAR Collaboration), Proceedings of Lake Louise Winter Institute on Fundamental Interactions, Alberta, Canada, February 2001, hep-ex/0105019; B. Aubert, *et al.* (BABAR Collaboration), hep-ex/0008058; B. Aubert, *et al.* (BABAR Collaboration), Phys. Rev. Lett. **87** (2001) 221802.

[5] I. Dunietz et al, Phys. Rev. **D43** (1991) 2193.

[6] M.E. Rose, *"Elementary theory of angular momentum"*, Dover.

[7] A. Bohr, Nuclear Physics **10** (1959) 486.

[8] H. Quinn, *"Hadronic effects in two-body B decays"*. Lectures at SLAC Summer Institute (1999).

[9] J. Schwinger, Phys. Rev. **12** (1964) 630; D. Farikov and B. Stech, Nucl. Phys. **B133** (1978) 315; N. Cabibbo and L. Maiani, Phys. Lett. **B73** (1978) 418; M.J. Dugan and B. Grinstein, Phys. Lett. **B255** (1991) 583.

[10] M. Bauer, B. Stech and M. Wirbel, Z. Phys. **C34** (1987) 103; M. Wirbel, B. Stech and M. Bauer, Z. Phys. **C29** (1985) 637.

[11] M. Beneke, G. Buchalla, M. Neubert and C. T. Sachrajda, Nucl. Phys. **B591** (2000) 313.

[12] S. Gardner, H. B. O'Connell and A. W. Thomas, Phys. Rev. Lett. **80** (1998) 1834 [arXiv:hep-ph/9705453].

[13] The Particle Data Group, D.E. Groom *et al.*, Eur. Phys. J. **C15** (2000) 1.

[14] J.J. Sakurai, *Currents and Mesons*, University of Chicago Press (1969).

[15] H.B. O'Connell, B.C. Pearce, A.W. Thomas and A.G. Williams, Prog. Part. Nucl. Phys. **39** (1997) 201; H.B. O'Connell, A.G. Williams, M. Bracco and G. Krein, Phys. Lett. **B370** (1996) 12; H.B. O'Connell, Aust. J. Phys. **50** (1997) 255.

[16] X.-H. Guo and A.W. Thomas, Phys. Rev. **D58** (1998) 096013, Phys. Rev. **D61** (2000) 116009.

[17] H.B. O'Connell, A.W. Thomas and A.G. Williams, Nucl. Phys. **A623** (1997) 559; K. Maltman, H.B. O'Connell and A.G. Williams, Phys. Lett. **B376** (1996) 19.

[18] S. Gardner and H.B. O'Connell, Phys. Rev. **D57** (1998) 2716.

[19] L. Wolfenstein, Phys. Rev. Lett. **51** (1983) 1945, Phys. Rev. Lett. **13** (1964) 562.

[20] A.J. Buras, Lect. Notes Phys. **558** (2000) 65, also in 'Recent Developments in Quantum Field Theory', Springer Verlag, edited by P. Breitenlohner, D. Maison and J. Wess (Springer-Verleg, Berlin, in press), hep-ph/9901409.

[21] V.A. Novikov, M.A. Shifman, A.I. Vainshtein and V.I. Zakharov, Nucl. Phys. **B249** (1985) 445, Yad. Fiz. **41** (1985) 1063.

[22] M.A. Shifman, A.I. Vainshtein and V.I. Zakharov, Nucl. Phys. **B147** (1979) 385, Nucl. Phys. **B147** (1979) 448.

[23] A.J. Buras, Published in 'Probing the Standard Model of Particle Interactions', eds. 1998, Elsevier Science B.V., hep-ph/9806471.

[24] N.G. Deshpande and X.-G. He, Phys. Rev. Lett. **74** (1995) 26.

[25] R. Fleischer, Int. J. Mod. Phys. **A12** (1997) 2459, Z. Phys. **C62** (1994) 81, Z. Phys. **C58** (1993) 483.

[26] G. Kramer, W. Palmer and H. Simma, Nucl. Phys. **B428** (1994) 77.

[27] R. Enomoto and M. Tanabashi, Phys. Lett. **B386** (1996) 413.

[28] G. Buchalla, A.J. Buras and M.E. Lautenbacher, Rev. Mod. Phys. **68**, (1996) 1125.

[29] X.-H. Guo and T. Huang, Phys. Rev. **D43** (1991) 2931.

[30] Y.-H. Chen, H.-Y. Cheng, B. Tseng and K.-C. Yang, Phys. Rev. **D60** (1999) 094014.

[31] By ALEPH, CDF, DELPHI, L3, OPAL and SLD Collaborations (D. Abbaneo *et al.*), hep-ex/0112028.

[32] H.-Y. Cheng and A. Soni, Phys. Rev. **D64** (2001) 114013.

[33] D. Melikhov and B. Stech, Phys. Rev. **D62** (2000) 014006.

[34] O. Leitner, X.-H. Guo and A.W. Thomas, Phys. Rev. **D66** (2002) 096008; X.-H. Guo, O. Leitner and A.W. Thomas, Phys. Rev. D**63** (2001) 056012.

[35] P. Langacker, Phys. Rev. **D20** (1979) 2983.

[36] T. Affolder et al., Phys. Rev. Let. **85**, 4668 (November 2000) and references therein.

[37] J.D. Jackson, Il Nuovo Cimento, Vol.XXXIV, (1964) 1644.

[38] De Wit and J. Smith, *Field Theory in Particle Physics*, Nort-Holland (1986).

Figure captions

- Fig. 1 Transversity frame for $B \to \rho^0 K^*$.
- Fig. 2 Tree diagram (left), and QCD-penguin diagram (right), for B decays.
- Fig. 3 Electroweak-penguin diagram (left), and electroweak-penguin diagram with coupling between Z, γ and W (right), for B decays.
- Fig. 4 Spectrum of $\rho^0 - \omega$ mixing (in MeV/c^2), simulated by the interference of two Breit-Wigner curves.
- Fig. 5 Spectrum of h_{--}, h_{00}, h_{++}. Histograms on the left correspond to the channel $B^0 \to \rho^0(\omega)K^{*0}$ where the parameters used are: $q^2/m^2{}_b = 0.3$, $N_c^{eff} = 2.84$, $\rho = 0.229, \eta = 0.325$ and form factors from the GH model . Histograms on the right correspond to the channel $B^+ \to \rho^0(\omega)\rho^+$ for the same parameters with $N_c^{eff} = 2.01$.
- Fig. 6 Spectrum of $\mathscr{R}e(h_{ij})$ and $\mathscr{I}m(h_{ij})$ where $i \neq j$. Histograms correspond to the channel $B^0 \to \rho^0(\omega)K^{*0}$ where the parameters used are: $q^2/m^2{}_b = 0.3$, $N_c^{eff} = 2.84$, $\rho = 0.229, \eta = 0.325$ and form factors from the GH model.
- Fig. 7 Spectrum of $\mathscr{R}e(h_{ij})$ and $\mathscr{I}m(h_{ij})$ where $i \neq j$. Histograms correspond to the channel $B^+ \to \rho^0(\omega)\rho^+$ where the used parameters are: $q^2/m^2{}_b = 0.3$, $N_c^{eff} = 2.01$, $\rho = 0.229, \eta = 0.325$ and form factors from the GH model.
- Fig. 8 Spectrum of polar angle (upper figure) and azimuthal angle (lower one) in the helicity frame for the channel $B^0 \to \rho^0(\omega)K^{*0}$. Parameters are: $q^2/m^2{}_b = 0.3$, $N_c^{eff} = 2.84$, $\rho = 0.229, \eta = 0.325$ and form factors from the GH model.
- Fig. 9 Spectrum of polar angle (upper figure) and azimuthal angle (lower one) in the transversity frame for the channel $B^0 \to \rho^0(\omega)K^{*0}$. Parameters are: $q^2/m^2{}_b = 0.3$, $N_c^{eff} = 2.84$, $\rho = 0.229, \eta = 0.325$ and form factors from the GH model.
- Fig. 10 CP-violating asymmetry parameter $a_{CP}(m)$, as a function of the $\pi^+\pi^-$ invariant mass in the vicinity of the ω mass region for the channel $B^0 \to \rho^0(\omega)K^{*0}$. Parameters are: $q^2/m^2{}_b = 0.3$, $N_c^{eff} = 2.84$, $\rho = 0.229, \eta = 0.325$. Solid triangles up and circles correspond to the BSW and GH form factor models respectively.
- Fig. 11 CP-violating asymmetry parameter $a_{CP}(m)$, as a function of the $\pi^+\pi^-$ invariant mass in the vicinity of the ω mass region for the channel $B^+ \to \rho^0(\omega)\rho^+$. Parameters are: $q^2/m^2{}_b = 0.3$, $N_c^{eff} = 2.01$, $\rho = 0.229, \eta = 0.325$. Solid triangles down and circles correspond to the BSW and GH form factor models respectively.

Table captions

- Table 1 Wilson coefficients to the next-leading order.
- Table 2 Effective Wilson coefficients related to the tree operators, electroweak and QCD-penguin operators.
- Table 3 Values of the CKM unitarity triangle for limiting values of the CKM matrix elements.
- Table 4 Form factor values for $B \to \rho$, $B \to \omega$ and $B \to K$ at $q^2 = 0$.
- Table 5 $\bar{B}^0, B^-$ branching ratios (in units of 10^{-6}) using either the BSW or GH form factor models, for $q^2/m_b^2 = 0.3(0.5)$, with $N_{cmax}^{b\to s} = 2.84(2.82)$, $N_{cmax}^{b\to d} = 2.01(1.95)$, $\rho = 0.229$ and $\eta = 0.325$.
- Table 6 B^0, B^+ branching ratios (in units of 10^{-6}) using either the BSW or GH form factor models, for $q^2/m_b^2 = 0.3(0.5)$, with $N_{cmax}^{b\to s} = 2.84(2.82)$, $N_{cmax}^{b\to d} = 2.01(1.95)$, $\rho = 0.229$ and $\eta = 0.325$.
- Table 7 Global CP-violating asymmetries (in percents) using either the BSW or GH form factor models, for $q^2/m_b^2 = 0.3(0.5)$, with $N_{cmax}^{b\to s} = 2.84(2.82)$, $N_{cmax}^{b\to d} = 2.01(1.95)$, $\rho = 0.229$ and $\eta = 0.325$.

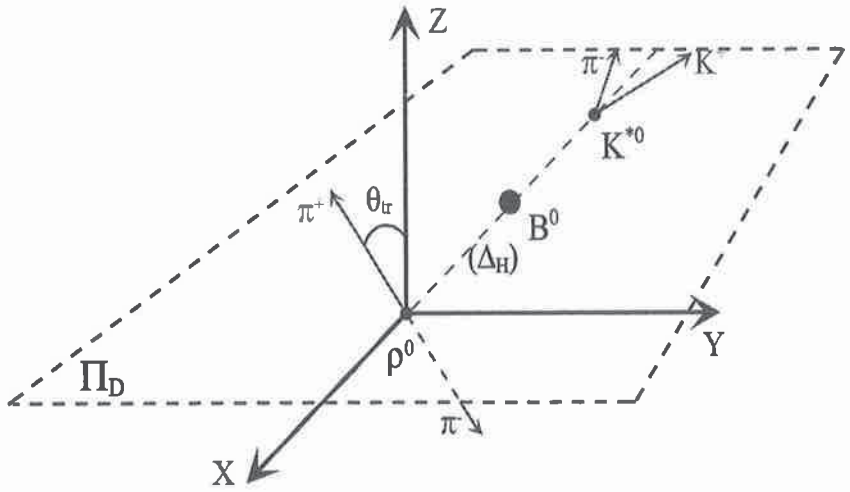

Figure 1: Transversity frame for $B \to \rho^0 K^*$.

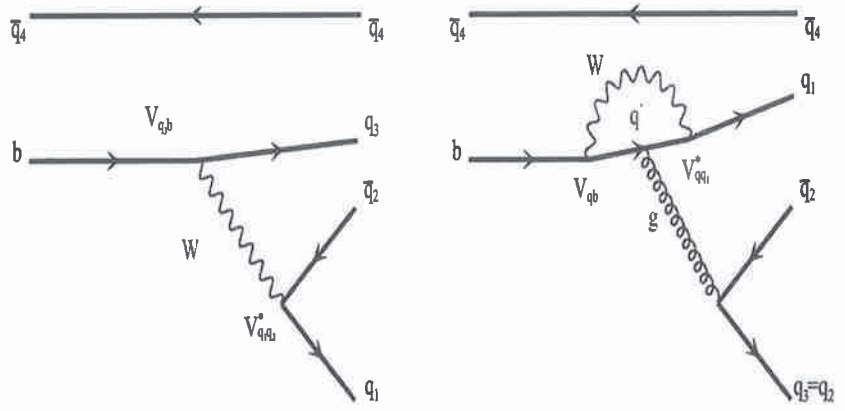

Figure 2: Tree diagram (left), and QCD-penguin diagram (right), for B decays.

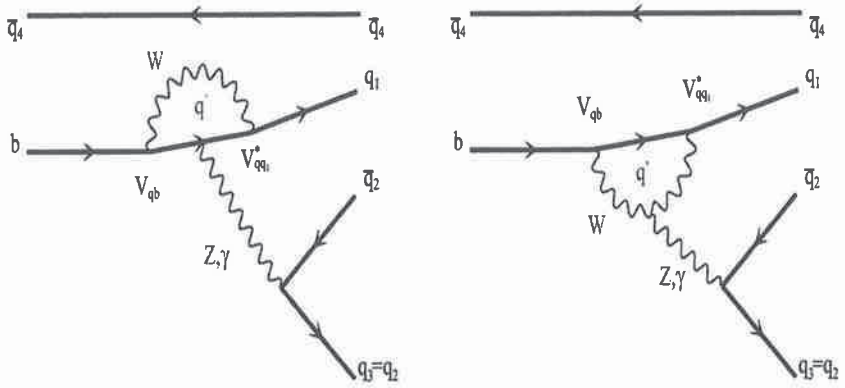

Figure 3: Electroweak-penguin diagram (left), and electroweak-penguin diagram with coupling between Z, γ and W (right), for B decays.

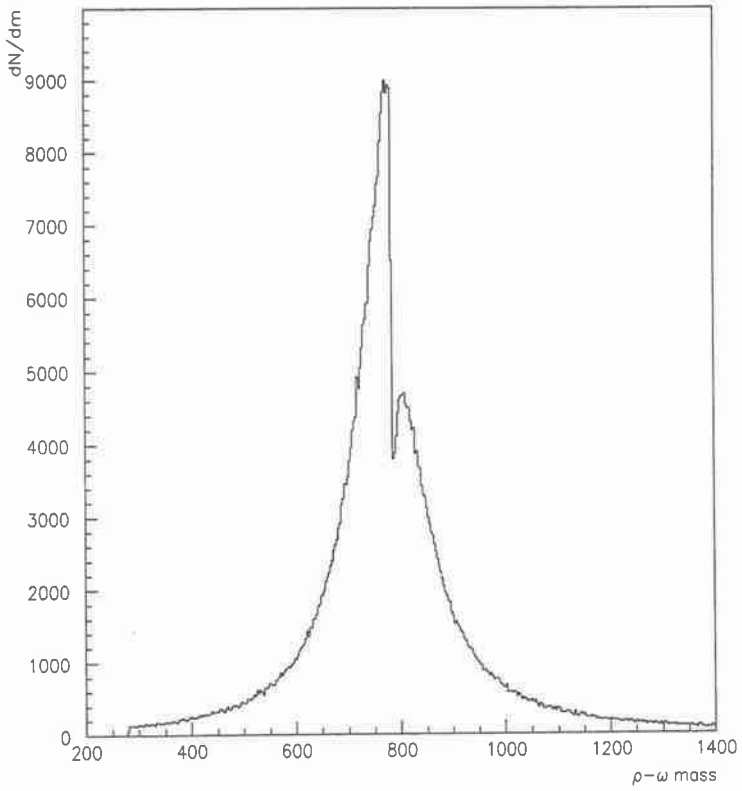

Figure 4: Spectrum of $\rho^0 - \omega$ mixing (in MeV/c^2), simulated by the interference of two Breit-Wigner curves.

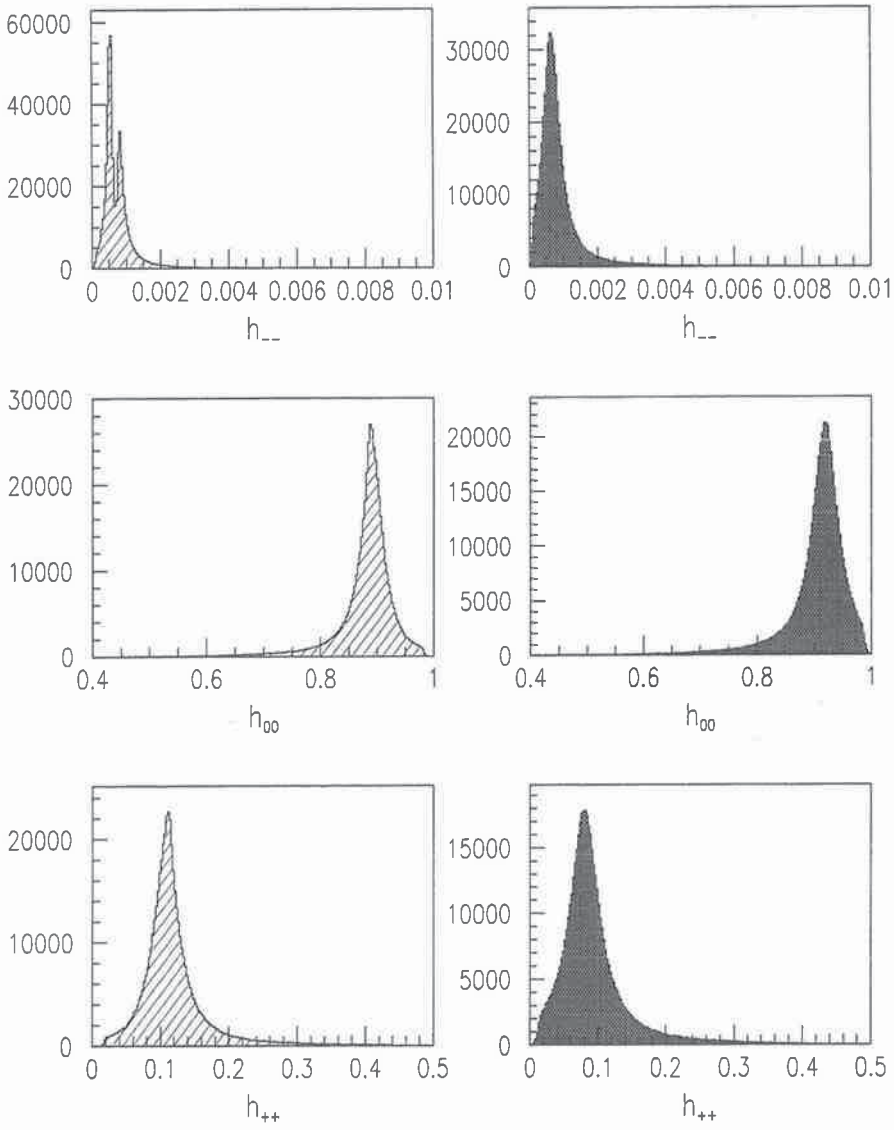

Figure 5: Spectrum of h_{--}, h_{00}, h_{++}. Histograms on the left correspond to the channel $B^0 \to \rho^0(\omega)K^{*0}$ where the parameters used are: $q^2/m^2_b = 0.3$, $N_c^{eff} = 2.84$, $\rho = 0.229, \eta = 0.325$ and form factors from the GH model. Histograms on the right correspond to the channel $B^+ \to \rho^0(\omega)\rho^+$ for the same parameters with $N_c^{eff} = 2.01$.

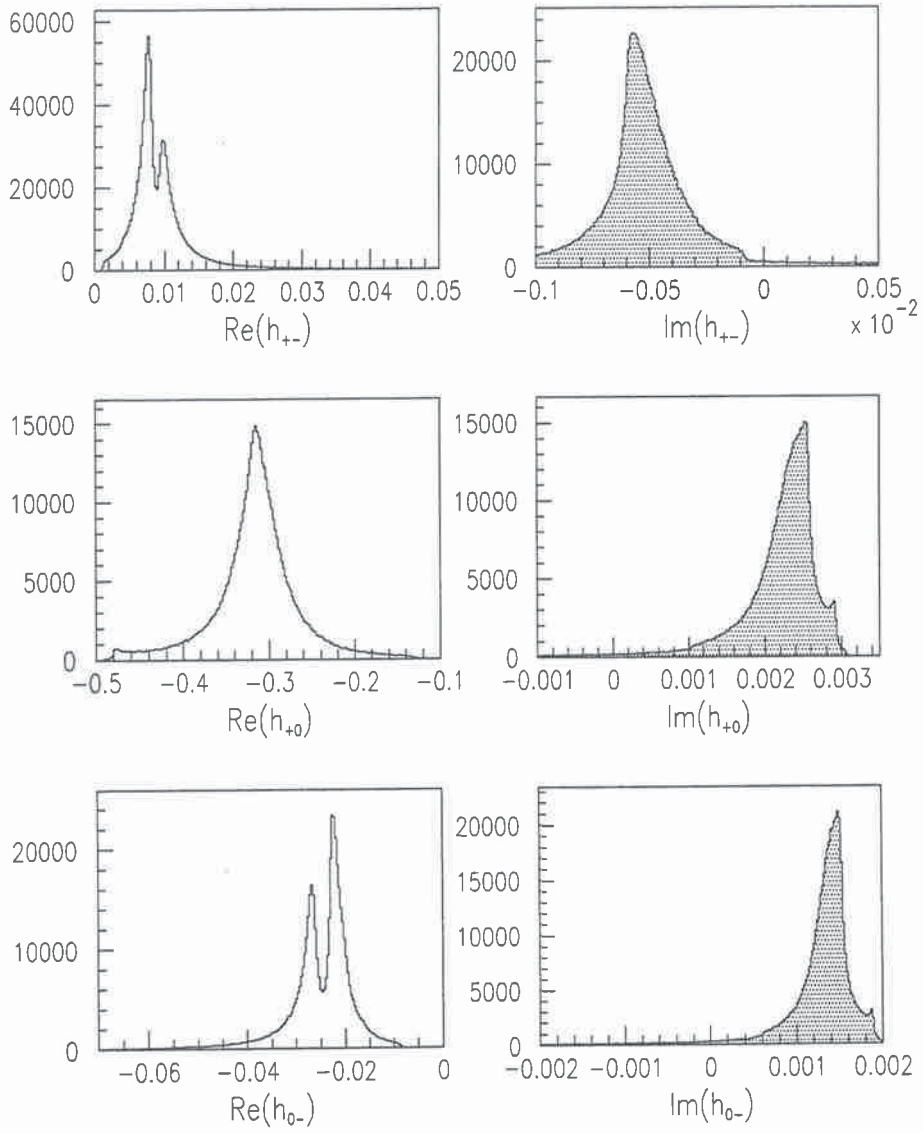

Figure 6: Spectrum of $\mathscr{R}e(h_{ij})$ and $\mathscr{I}m(h_{ij})$ where $i \neq j$. Histograms correspond to channel $B^0 \to \rho^0(\omega)K^{*0}$ where the used parameters are: $q^2/m^2_b = 0.3$, $N_c^{eff} = 2.84$, $\rho = 0.229, \eta = 0.325$ and form factors from the GH model.

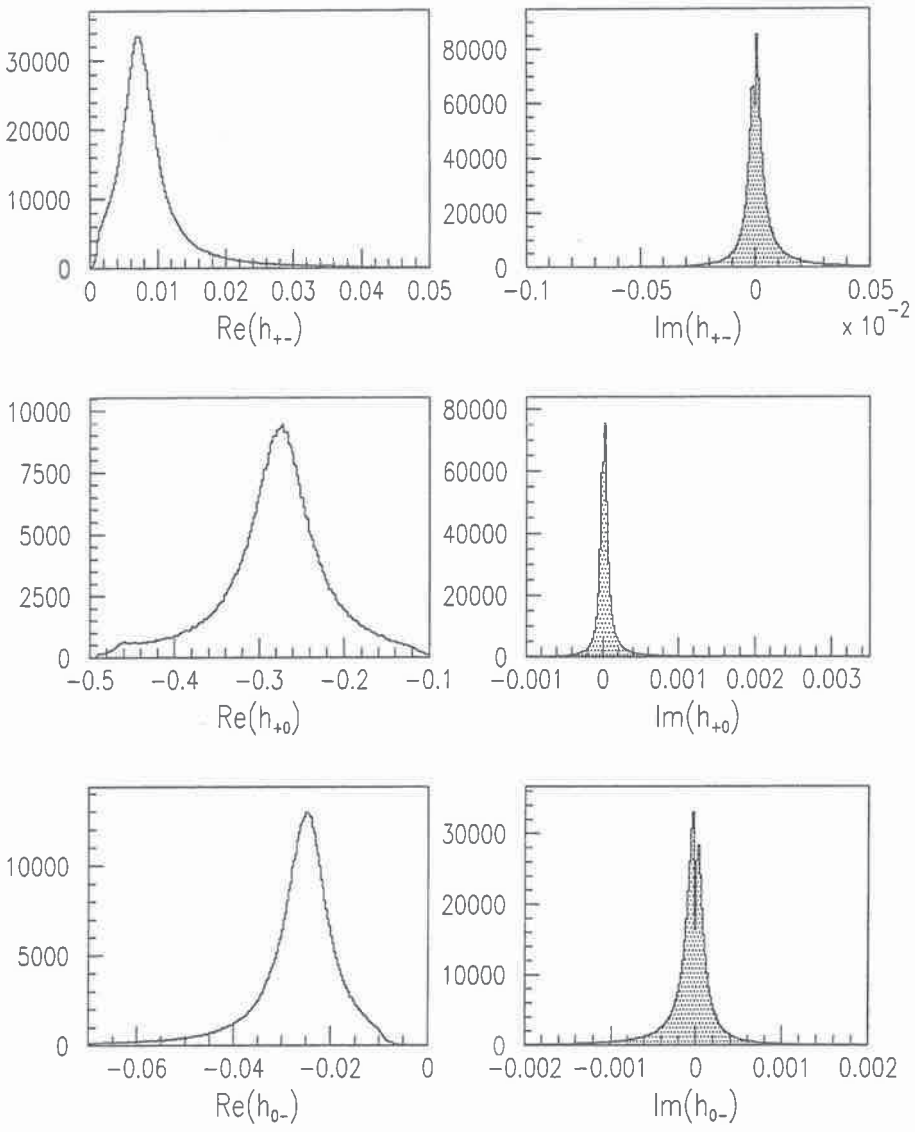

Figure 7: Spectrum of $\mathscr{R}e(h_{ij})$ and $\mathscr{I}m(h_{ij})$ where $i \neq j$. Histograms correspond to the channel $B^+ \to \rho^0(\omega)\rho^+$ where the used parameters are: $q^2/m^2{}_b = 0.3$, $N_c^{eff} = 2.01$, $\rho = 0.229, \eta = 0.325$ and form factors from the GH model.

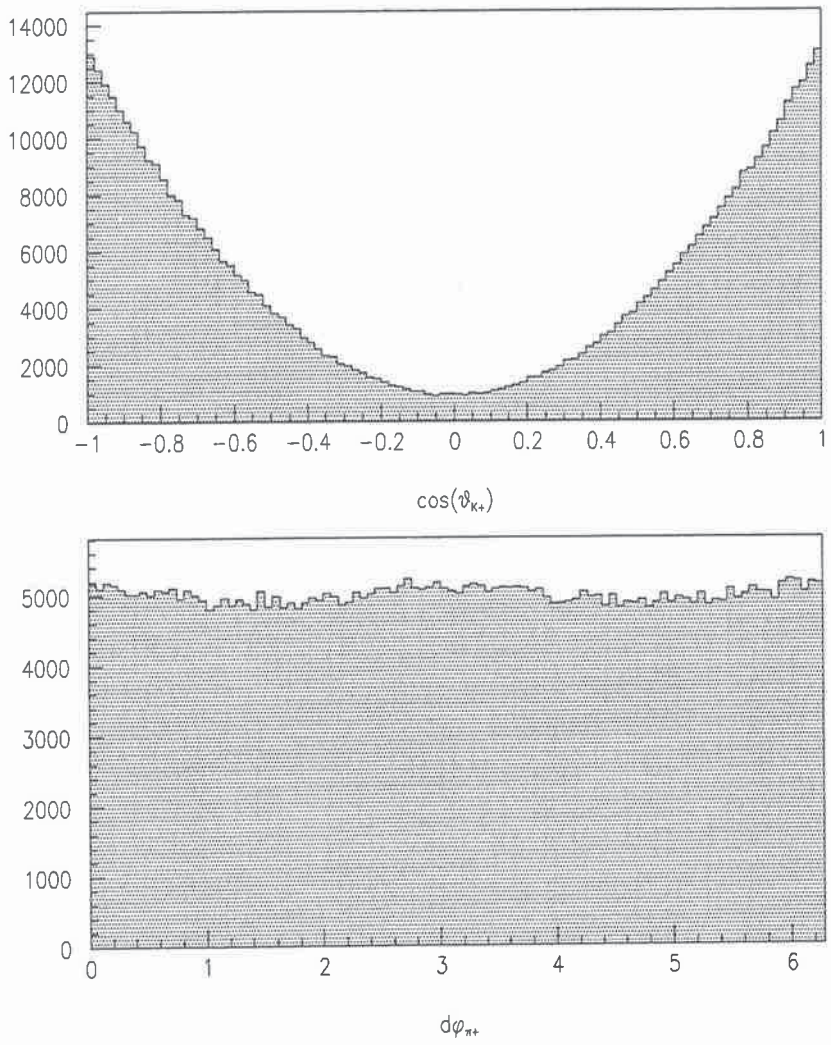

Figure 8: Spectrum of polar angle (upper figure) and azimuthal angle (lower one) in the helicity frame for the channel $B^0 \to \rho^0(\omega)K^{*0}$. Parameters used are: $q^2/m^2_b = 0.3$, $N_c^{eff} = 2.84$, $\rho = 0.229, \eta = 0.325$ and form factors from the GH model.

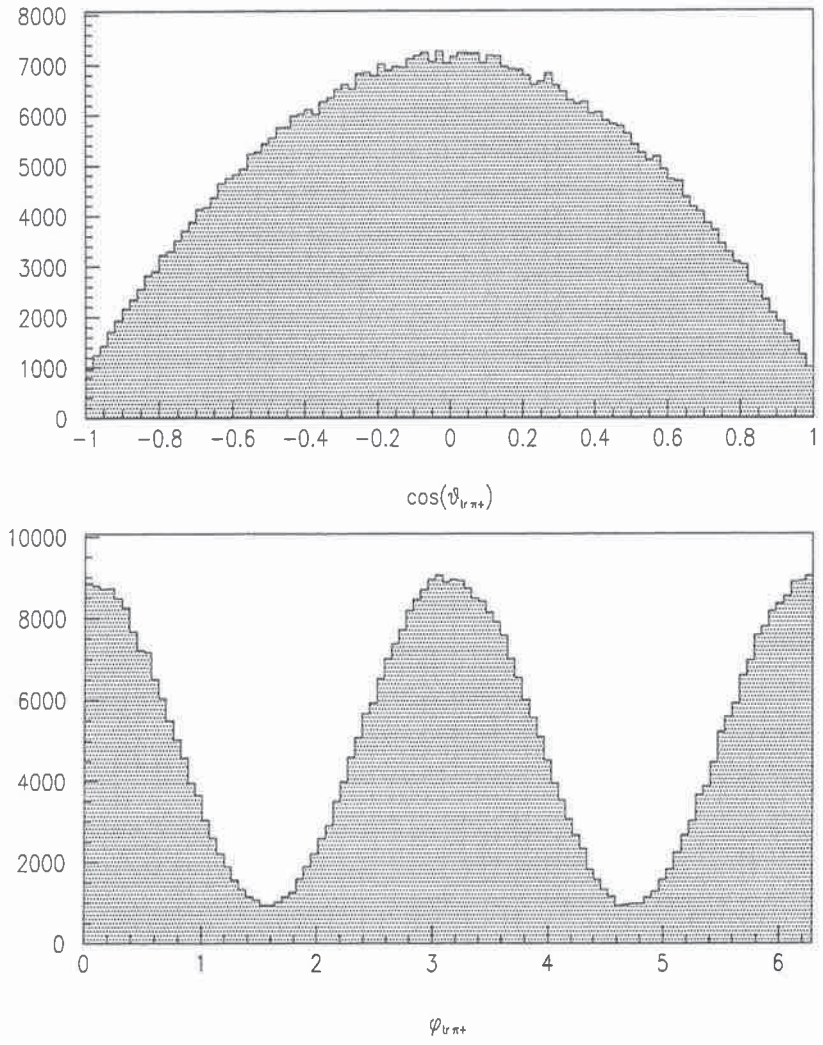

Figure 9: Spectrum of polar angle (upper figure) and azimuthal angle (lower one) in the transversity frame for the channel $B^0 \to \rho^0(\omega)K^{*0}$. Parameters are: $q^2/m^2_b = 0.3$, $N_c^{eff} = 2.84$, $\rho = 0.229, \eta = 0.325$ and form factors from the GH model.

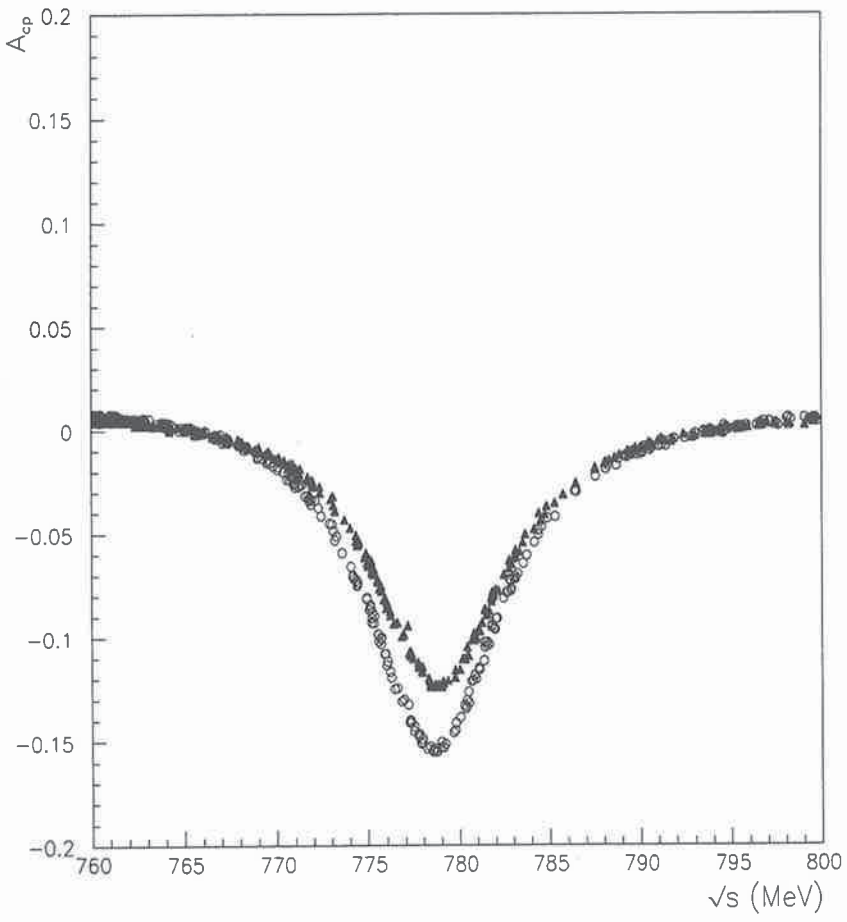

Figure 10: CP-violating asymmetry parameter $a_{CP}(m)$, as a function of the $\pi^+\pi^-$ invariant mass in the vicinity of the ω mass region for the channel $B^0 \to \rho^0(\omega)K^{*0}$. Parameters are: $q^2/m^2{}_b = 0.3$, $N_c^{eff} = 2.84$, $\rho = 0.229, \eta = 0.325$. Solid triangles up and circles correspond to the BSW and GH form factor models respectively.

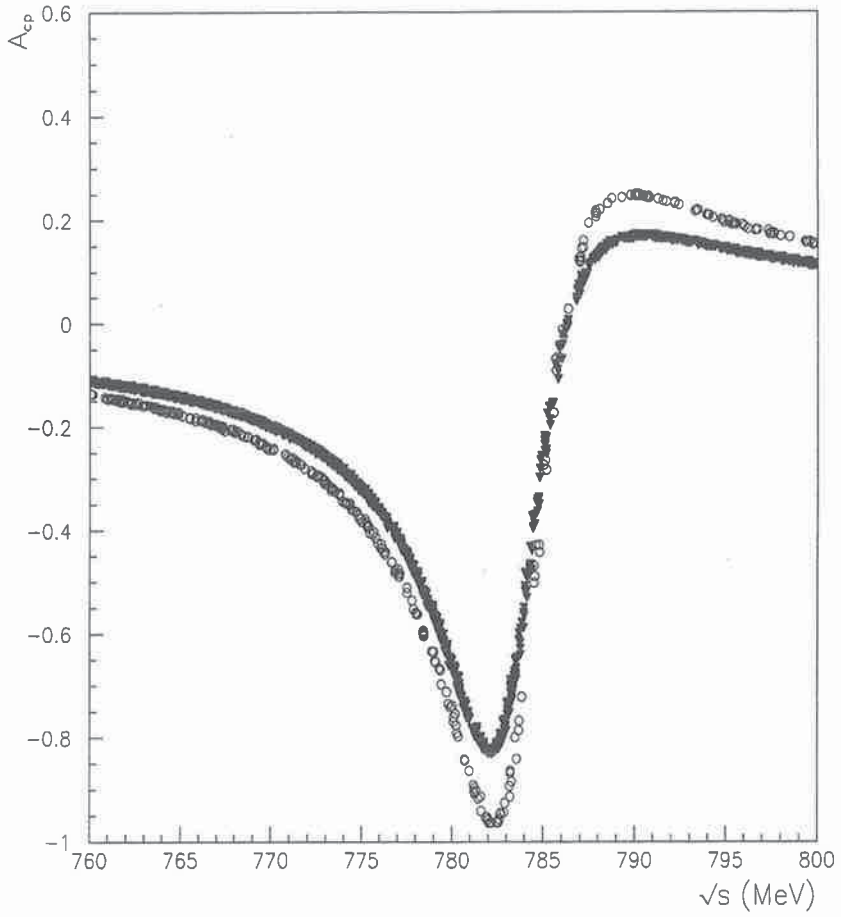

Figure 11: CP-violating asymmetry parameter $a_{CP}(m)$, as a function of the $\pi^+\pi^-$ invariant mass in the vicinity of the ω mass region for the channel $B^+ \to \rho^0(\omega)\rho^+$. Parameters are: $q^2/m^2_b = 0.3$, $N_c^{eff} = 2.01$, $\rho = 0.229, \eta = 0.325$. Solid triangles down and circles correspond to the BSW and GH form factor models respectively.

$C_i(\mu)$ for $\mu = 5$ GeV			
	C_1	-0.3125	
	C_2	$+1.1502$	
C_3	$+0.0174$	C_5	$+0.0104$
C_4	-0.0373	C_6	-0.0459
C_7	-1.050×10^{-5}	C_9	-0.0101
C_8	$+3.839 \times 10^{-4}$	C_{10}	$+1.959 \times 10^{-3}$

Table 1: Wilson coefficients to the next-leading order (see the reference in text).

C_i'	$q^2/m_b^2 = 0.3$	$q^2/m_b^2 = 0.5$
C_1'	-0.3125	-0.3125
C_2'	$+1.1502$	$+1.1502$
C_3'	$+2.433 \times 10^{-2} + 1.543 \times 10^{-3}i$	$+2.120 \times 10^{-2} + 2.174 \times 10^{-3}i$
C_4'	$-5.808 \times 10^{-2} - 4.628 \times 10^{-3}i$	$-4.869 \times 10^{-2} - 1.552 \times 10^{-2}i$
C_5'	$+1.733 \times 10^{-2} + 1.543 \times 10^{-3}i$	$+1.420 \times 10^{-2} + 5.174 \times 10^{-3}i$
C_6'	$-6.668 \times 10^{-2} - 4.628 \times 10^{-3}i$	$-5.729 \times 10^{-2} - 1.552 \times 10^{-2}i$
C_7'	$-1.435 \times 10^{-4} - 2.963 \times 10^{-5}i$	$-8.340 \times 10^{-5} - 9.938 \times 10^{-5}i$
C_8'	$+3.839 \times 10^{-4}$	$+3.839 \times 10^{-4}$
C_9'	$-1.023 \times 10^{-2} - 2.963 \times 10^{-5}i$	$-1.017 \times 10^{-2} - 9.938 \times 10^{-5}i$
C_{10}'	$+1.959 \times 10^{-3}$	$+1.959 \times 10^{-3}$

Table 2: Effective Wilson coefficients related to the tree operators, electroweak and QCD penguin operators (see the reference in text).

	α	β	γ
(ρ_{min}, η_{min})	104°47	19°32	56°21
(ρ_{min}, η_{max})	93°13	24°31	62°56
(ρ_{max}, η_{min})	112°14	21°20	46°66
(ρ_{max}, η_{max})	99°66	26°56	53°78

Table 3: Values of the CKM unitarity triangle for limiting values of the CKM matrix elements.

$B \to \rho$						
	h_V	$h_{A_0} = h_{A_3}$	h_{A_1}	h_{A_2}	m_V (GeV^2)	m_{A_i} (GeV^2)
model (1)	0.329	0.281	0.283	0.283	5.32	5.32
model (2)	0.394	0.345	0.345	0.345	5.32	5.32
$B \to \omega$						
	h_V	$h_{A_0} = h_{A_3}$	h_{A_1}	h_{A_2}	m_V (GeV^2)	m_{A_i} (GeV^2)
model (1)	0.328	0.280	0.281	0.281	5.32	5.32
model (2)	0.394	0.345	0.345	0.345	5.32	5.32
$B \to K^*$						
	h_V	$h_{A_0} = h_{A_3}$	h_{A_1}	h_{A_2}	m_V (GeV^2)	m_{A_i} (GeV^2)
model (1)	0.369	0.321	0.328	0.331	5.43	5.43
model (2)	0.443	0.360	0.402	0.416	5.43	5.43

Table 4: Form factor values for $B \to \rho$, $B \to \omega$ and $B \to K^*$ at $q^2 = 0$ (see the reference in text).

channel	$\frac{q^2}{m_b^2}$	BSW	GH
$\bar{B}^0 \to \bar{K}^{*0}\rho^0(\omega)$	0.3	2.1	1.0
	0.5	1.5	0.73
$B^- \to K^{*-}\rho^0(\omega)$	0.3	6.6	3.9
	0.5	6.2	3.6
$B^- \to \rho^-\rho^0(\omega)$	0.3	24	13
	0.5	24	14

Table 5: $\bar{B}^0, B^-$ branching ratios (in units of 10^{-6}) using either the BSW or GH form factor models, for $q^2/m_b^2 = 0.3(0.5)$, with $N_{cmax}^{b\to s} = 2.84(2.82)$, $N_{cmax}^{b\to d} = 2.01(1.95)$, $\rho = 0.229$ and $\eta = 0.325$.

channel	$\frac{q^2}{m_b^2}$	BSW	GH
$B^0 \to K^{*0}\rho^0(\omega)$	0.3	2.1	1.0
	0.5	1.7	0.88
$B^+ \to K^{*+}\rho^0(\omega)$	0.3	5.8	3.4
	0.5	3.8	2.3
$B^+ \to \rho^+\rho^0(\omega)$	0.3	20	11
	0.5	20	11

Table 6: B^0, B^+ branching ratios (in units of 10^{-6}) using either the BSW or GH form factor models, for $q^2/m_b^2 = 0.3(0.5)$, with $N_{cmax}^{b\to s} = 2.84(2.82)$, $N_{cmax}^{b\to d} = 2.01(1.95)$, $\rho = 0.229$ and $\eta = 0.325$.

channel	$\frac{q^2}{m_b^2}$	BSW	GH
$\bar{K}^{*0}(K^{*0})\rho^0(\omega)$	0.3	+0.36	−0.45
	0.5	+4.70	+5.90
$K^{*-}(K^{*+})\rho^0(\omega)$	0.3	−6.6	−6.37
	0.5	−23.0	−22.0
$\rho^-(\rho^+)\rho^0(\omega)$	0.3	−8.5	−9.6
	0.5	−8.7	−9.9

Table 7: Global CP-violating asymmetries (in percents) using either the BSW or GH form factor models, for $q^2/m_b^2 = 0.3(0.5)$, with $N_{cmax}^{b\to s} = 2.84(2.82)$, $N_{cmax}^{b\to d} = 2.01(1.95)$, $\rho = 0.229$ and $\eta = 0.325$.

LHCb-PHYS-2001-041
PHYSICS
ADP-01-11/T446
PCCF-RI-01-04

$B^{0(\pm)}$ decays into two vector mesons

Physical motivations and a general method for simulations

Z.J.Ajaltouni[1*], O.Leitner[1,2†], C.Rimbault[1‡]

[1] *Laboratoire de Physique Corpusculaire de Clermont-Ferrand*
IN2P3/CNRS Université Blaise Pascal
F-63177 Aubière Cedex France
[2] *Department of Physics and Mathematical Physics and Special Research Centre for the Subatomic Structure of Matter*
Adelaide University
Adelaide 5005, Australia

Abstract

In this paper, a complete description of the channels $B \to V_1 V_2$ is given. Emphasis is put on the determination of the dynamical density matrix which elements are computed according to the Wilson operator product expansions entering into the formulation of the weak effective hamiltonian.

Kinematical consequences related to the particular channel $B \to K^* \rho^0(\omega)$ are described in details.

*ajaltouni@in2p3.fr
†oleitner@physics.adelaide.edu.au
‡rimbault@clermont.in2p3.fr

1 Introduction

In a previous note [1], an exhaustive study of the channel simulations:

$$B \to V_1 V_2, \quad \gamma V, \quad PV, \quad PP,$$

$(V = 1^-, P = 0^-)$ has been performed by stressing the helicity formalism and its consequences. General formulas have been established, notably those giving the final angular distributions in the case of the production of two vector mesons decaying into pseudoscalar mesons.

The squared modulus of the decay amplitude has the following form:

$$|A|^2 \propto h_{\lambda,\lambda'} F_{\lambda,\lambda'}(\theta_1) G_{\lambda,\lambda'}(\theta_2, \phi), \tag{1}$$

where (summation over $\lambda(\lambda')$ is omitted):

- $h_{\lambda,\lambda'}$ is the matrix density element constructed from the weak effective hamiltonian H_w^{eff} taken between the initial state (B_0) and the final state f.
- $F_{\lambda,\lambda'}(\theta_1)$ and $G_{\lambda,\lambda'}(\theta_2, \phi)$ are the matrix elements related to the decays $V_1 \to a_1 + b_1$ and $V_2 \to a_2 + b_2$ respectively.
- θ_j is the polar angle of particle a_j in the rest frame of the resonance V_j while ϕ is the angular difference $\phi_2 - \phi_1$, where ϕ_j is the polar angle of a_j in V_j rest frame.

$\lambda(\lambda')$ being the helicity state of the vector mesons; $\lambda = -1, 0, +1$.

As it can be noticed, the essential parameters for the determination of the decay dynamics are the *unknown matrix elements* $h_{\lambda,\lambda'}$; while the two other ones, $F_{\lambda,\lambda'}(\theta_1)$ and $G_{\lambda,\lambda'}(\theta_2, \phi)$, are kinematic (or geometric) parameters because they are completely determined from the Wigner rotation matrices. The reader is referred to the note $99-051$ for a full kinematic description of the B^0 decay and the physical significance of the angles $\theta_{1,2}$ and ϕ.

Before dealing with the mathematical determinations of the $h_{\lambda,\lambda'}$ elements, a simple justification of the two vector meson channel is given below.

2 Quantum numbers of the ${V_1}^0{V_2}^0$ system

In the case of two vector meson B^0 decay, the most interesting case is the one related to neutral mesons supplemented by the condition $C|{V^0}_i\rangle = -|{V^0}_i\rangle$, where C is the charge conjugation operator and ${V^0}_i$ is a neutral vector meson *eigenstate* of C. Some examples of these channels are:

$$\rho^0\rho^0, \quad J/\Psi\rho^0, \quad J/\Psi\Phi, \quad \Phi\Phi \ldots$$

These vector mesons have, in addition, the *parity* quantum number equal to -1. Noticing that the total angular momentum of the $V_1^0V_2^0$ system: $\vec{J} = \vec{\ell} + \vec{S} = \vec{s_B}$ is equal to zero and because the total spin $\vec{S} = \vec{s_1} + \vec{s_2}$, with $s_1 = s_2 = 1$, the orbital angular momentum can have three different values: $\ell = S = 0, 1, 2$.

Thus, parity, charge conjugation and CP quantum numbers of the $V_1^0V_2^0$ system can be computed:

$$P(V_1^0V_2^0) = (-1)^2(-1)^\ell, \quad C(V_1^0V_2^0) = (-1)^2,$$

$$\Downarrow$$

$$CP(V_1^0V_2^0) = (-1)^\ell.$$

We are led to the important result that the CP value of $V_1^0V_2^0$ is a **mixing** of two different eigenvalues $+1$ and -1 whatever the initial state (B^0 or $\bar{B}^0$) is. A direct consequence of this result is that *CP symmetry is not an exact one.*

The above relation does not hold for reactions involving a neutral K^* like:

$$B_d^0 \to K^{*0}\rho^0, \quad J/\Psi K^{*0} \ldots$$

because K^{*0} and $\bar{K}^{*0}$ are two *distinct particles*; $C|K^{*0}\rangle = |\bar{K}^{*0}\rangle \neq |K^{*0}\rangle$.

However, it is worth noticing two interesting features for channels with an intermediate resonance like $K^{*0}(\bar{K}^{*0})$:

$$K^{*0} \to K^+\pi^-, \quad K^0\pi^0,$$

$$\bar{K}^{*0} \to K^-\pi^+, \quad \bar{K}^0\pi^0.$$

The decay channels are in the ratio $2/3$ and $1/3$ respectively. On one hand, the sign of the charged kaon shows clearly the nature of the neutral K^* from which it comes and consequently the *flavour* of the original $B^0(\bar{B}^0)$. So, a neutral K^* decay is a direct way for B^0 *flavour tagging.*

On the other hand, when a neutral $K^{*0}(\bar{K}^{*0})$ decays into $K^0(\bar{K}^0)\pi^0$, the neutral kaon $K^0(\bar{K}^0)$ is not the true physical particle, because approximately 50% of the $K^0(\bar{K}^0)$ go into K_S^0 and 50% into K_L^0 respectively and the true *detectable* particle is K_S^0 which goes to $\pi^+\pi^-$.

Thus, in the special channel:

$$B^0(\bar{B}^0) \to K^{*0}(\bar{K}^{*0})\rho^0,$$

$$\rightarrow K_S^0\pi^0,$$

tagging the original B^0 is no longer possible but, the $K_S^0\pi^0$ being a *common final state* to both B^0 and $\bar{B}^0$, the above relation $CP = (-1)^\ell$ is still available [2].

In the following, emphasis will be put on the channels $K^{*0(\pm)}\rho^0(\omega)$ and the physical importance of the $\rho^0(\omega)$ mixing for the determination of **CP** violation.

$$B_d^0 \longrightarrow K^{*0}\ \rho^0(\omega)$$

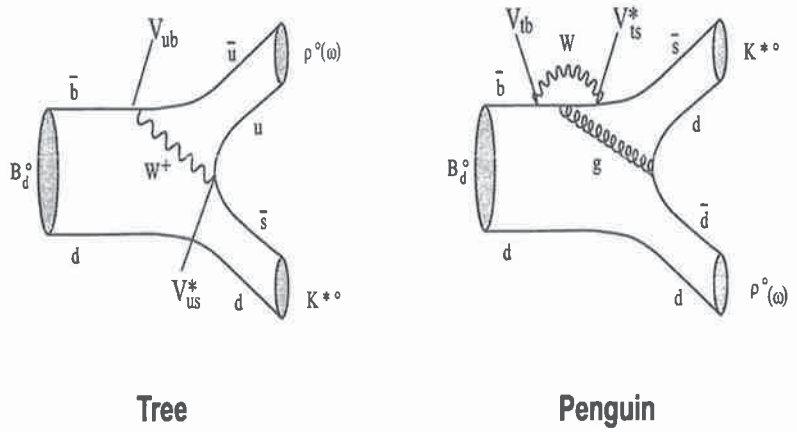

Figure 1: *Tree and Penguin diagrams for the decay* $B^0 \rightarrow K^{*0}\rho^0(\omega)$.

3 $\rho^0(\omega)$ mixing and its consequence

It is well known from hadronic physics that the neutral isovector ρ_8 and the isosinglet ω_8 mix together, leading to the "true" physical resonances ρ^0 and ω. On the phenomenological level, this mixing is made possible because of the existence of a common final state to both ρ^0 and ω decays [5]:

$$\rho^0 \rightarrow \pi^+\pi^-, \qquad (BR \approx 100\%),$$
$$\omega \rightarrow \pi^+\pi^-, \qquad (BR \approx 2.2\%).$$

In the same framework, it has been established that the $\pi\pi$ final state interaction provides a phase shift δ which reaches 90° when the $\pi\pi$ invariant mass is at the ω pole ($M_\omega = 782\ MeV$) [6].

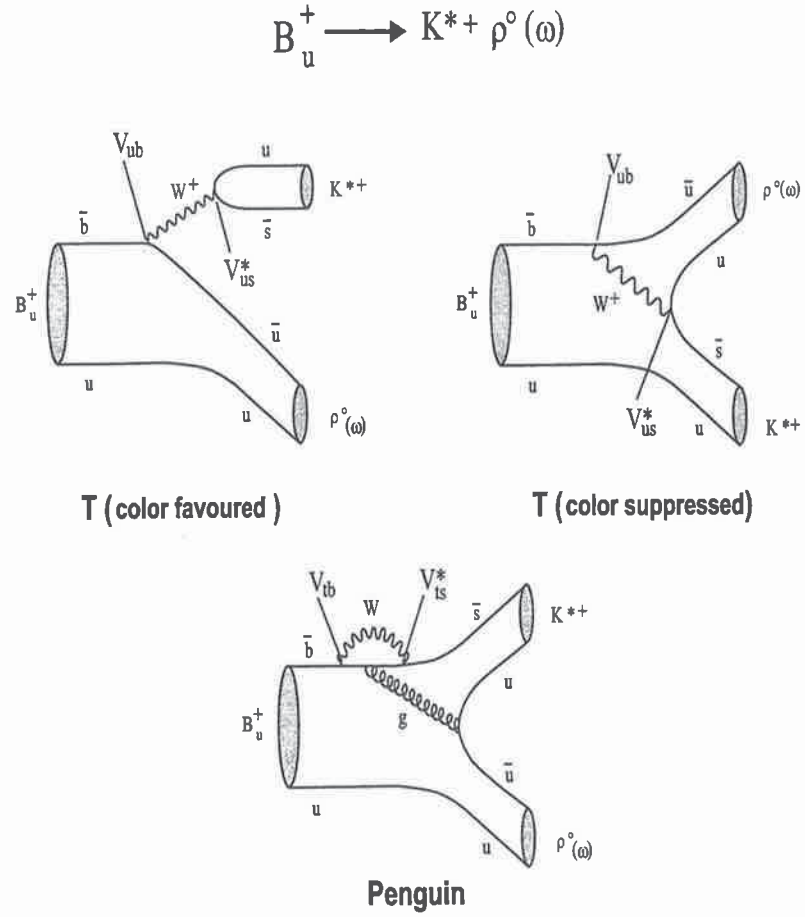

Figure 2: *Tree and Penguin diagrams for the decay* $B^+ \to K^{*+}\rho^0(\omega)$.

This interesting physical property has important consequences in the case where a ρ^0 resonance is produced in some $B^{0\pm}$ decays like:

$$B^0 \to K^{*0}\rho^0, \quad (Fig.1)$$

$$B^+ \to K^{*+}\rho^0, \quad B^- \to K^{*-}\rho^0, \quad (Fig.2)$$

These decays require both tree (T) and penguin (P) diagrams. As it is emphasized in reference [7], the amplitude A and $\bar{A}$ respectively for B^+ and B^- decays can be set in the following form:

$$A = A^T + A^P = A^T(1 + r\exp(i\delta)\exp(i\phi)), \tag{2}$$

$$\bar{A} = \bar{A}^T + \bar{A}^P = A^T(1 + r\exp(i\delta)\exp(-i\phi)), \tag{3}$$

where:

$$r = \left|\frac{A^P}{A^T}\right|, \tag{4}$$

$$\bar{A}^T = A^T, \quad \bar{A}^P = |A^P|\exp(i\delta)\exp(-i\phi). \tag{5}$$

Expressions of A and $\bar{A}$ displayed above suppose that final state interactions (FSI) arise essentially from the penguin diagrams; this hypothesis is supported by the fact that, to order $G_F\alpha_s$ (G_F and α_s are respectively the Fermi constant and the QCD fine-structure constant), the *absorptive* part of the transition amplitude is obtained from the penguin diagrams [8].

In the special case of $\rho^0 - \omega$ mixing, another hypothesis is made using more intuitive arguments: the phase shift due to the mixing is included in the FSI and it is *predominating* at the ω pole, justifying the above expressions of A and $\bar{A}$ that the phase shift δ is principally the one generated by the $\rho^0 - \omega$ mixing.

By CP transformation, the strong phase δ remains unchanged while the weak phase ϕ, which is related to the CKM matrix elements, changes sign. Thus, the asymmetry parameter a_{CP}^{dir} which can reveal *direct CP violation* can be deduced in the following way:

$$a_{CP}^{dir} = \frac{A^2 - \bar{A}^2}{A^2 + \bar{A}^2} = \frac{-2\sin\delta\sin\phi}{1 + r^2 + 2r\cos\delta\cos\phi}. \tag{6}$$

It is straightforward to notice that the parameter a_{CP}^{dir} depends both on the strong phase *and* the weak phase and, consequently, the maximum value of a_{CP}^{dir} can be reached if $\sin\delta = 1$, which allows us to state that the strong final state interaction (FSI) among pions coming from the $\rho^0 - \omega$ decays *enhances* the direct CP violation in the vicinity of the resonance ω mass.

Simulation of the $\rho^0 - \omega$ mixing

A simple and phenomenological relation describing the amplitude of the $\rho^0 - \omega$ mixing is used for the Monte-carlo simulations [9]. In the ρ^0 Breit-Wigner, the (ρ^0) propagator is replaced by the following one:

$$\mathcal{A} = \frac{1}{s_\rho} + \frac{T_\omega}{T_\rho}\frac{\Pi_{\rho\omega}}{s_\rho s_\omega}, \tag{7}$$

where

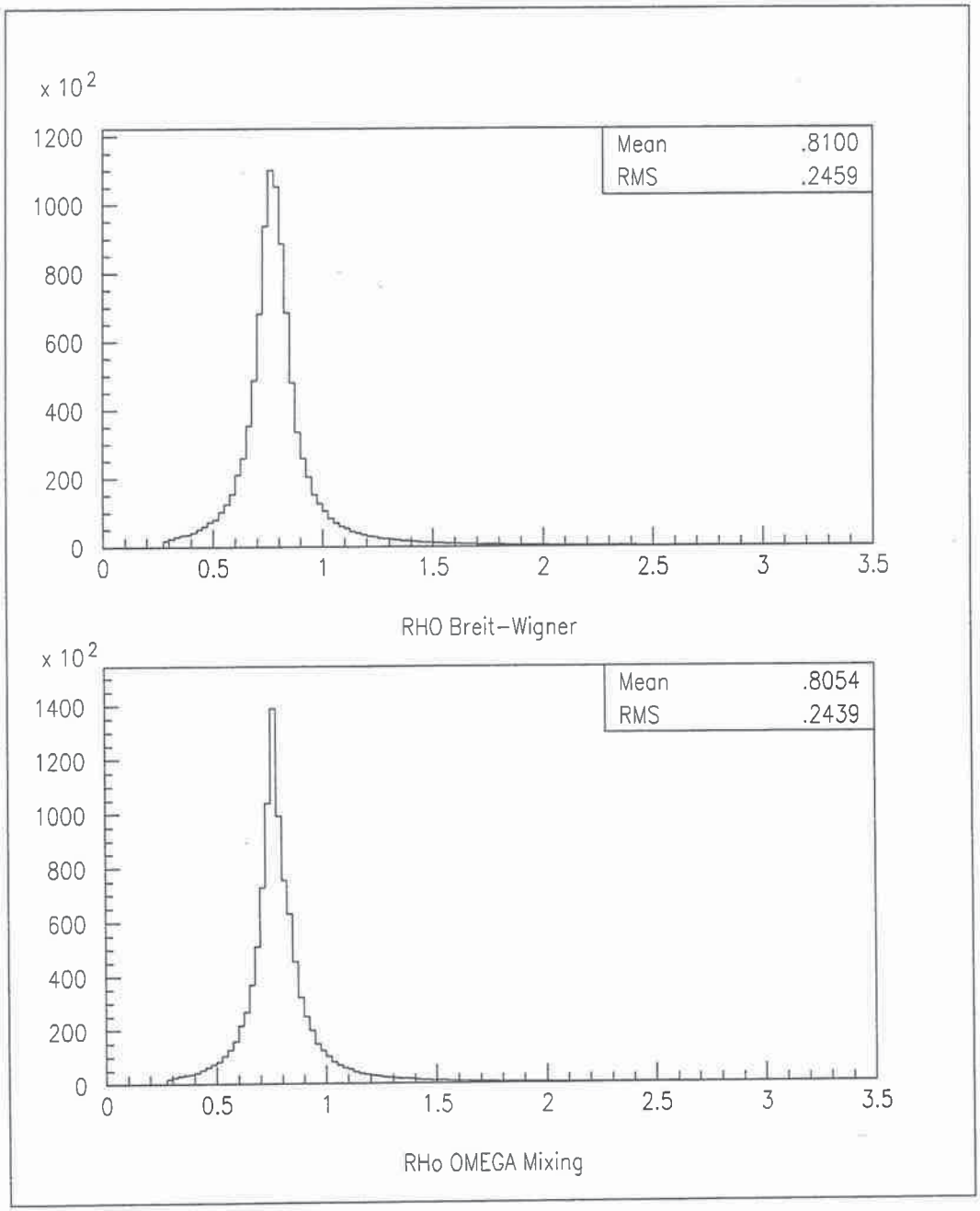

Figure 3: *Spectrum (in GeV/c^2) of ρ^0 Breit-Wigner (upper histogram) and $\rho^0 - \omega$ mixing (lower histogram).*

- $1/s_V = 1/(s - {M_V}^2 + i\Gamma_V M_V)$ is the V resonance propagator, M_V and Γ_V being respectively the mass and the width of the resonance V.
- T_ω and T_ρ are respectively the ω and ρ production amplitudes.
- $\Pi_{\rho\omega}$ is the mixing parameter for which recent values come from e^+e^- annihilations:

$\Re e(\Pi_{\rho\omega}) = -3500 \pm 300 \ \ MeV^2$ and $\Im m(\Pi_{\rho\omega}) = -300 \pm 300 \ \ MeV^2$.

Due to the same physical processes which enter into the production of the ρ^0 and ω resonances (they are both made out from $u\bar{u}$ and $d\bar{d}$ quark pairs with the same weight 1/2), it seems natural to choose $T_\omega/T_\rho = 1$. So, the squared mass distribution of the $\pi\pi$ system becomes simplified and it is given by:

$$d\sigma/dm^2 \propto \left|\mathcal{A}(\rho^0(\omega))\right|^2, \tag{8}$$

where $\mathcal{A}$ is the amplitude of the two Breit-Wigner given above and m is the $\pi\pi$ invariant mass.

In Figure 3, are displayed the $\pi\pi$ invariant mass spectra for the ρ^0 Breit-Wigner and the $\rho^0 - \omega$ mixing respectively. Because of the very narrow ω width ($\Gamma_\omega = 8.44 \ MeV$), we notice a high and narrow peak at the ω pole ($\approx 782 \ MeV$).

4 Dynamics of the $B \to V_1 V_2$ decay

The formalism describing the $B^{0(\pm)}$ decay into two vector mesons is derived from the general formalism related to the hadronic weak decay of a heavy meson (or heavy quark). It is based on the new concepts introduced by the Heavy Quark Effective Theory (**HQET**) which involves additionnal symmetry due to the high mass of the heavy quark (b or c quark) [10]. Technical calculations require a weak effective hamiltonian, H_w^{eff}, by using the "Operator Product Expansions" (**OPE**) pioneered by Wilson and which involve field operators describing both *tree* and *penguin* diagrams, the last ones include both QCD and electroweak penguins (Figures 1 and 2).

The general form of H_w^{eff} is given by:

$${H_w}^{eff} = \frac{G_F}{\sqrt{2}} \sum\nolimits_{q=d,s} \Big(V_{ub}V_{uq}^*(c_1O_1 + c_2O_2) - V_{tb}V_{tq}^* \sum\nolimits_{i=3}^{10} c_iO_i \Big), \tag{9}$$

where c_i are the Wilson coefficients and O_i are field operators with dimension $d \geq 4$; they are computed at an energy scale μ which is identified, here, with the b quark mass m_b.

In the case of charmless B decays, Wilson coefficients have been calculated by Buchalla et al [11]. These coefficients represent the *perturbative part* of the weak hamiltonian, they are estimated by the Renormalization Group techniques and their values depend on the renormalization scheme which is used. Their physical significance is the *weight* of each

field operator $O_i(\mu)$ entering in the weak hamiltonian H_w^{eff}. From reference [12], the values of c_i which have been computed at the energy scale $\mu = m_b$ are:

$$\begin{aligned} c_1 &= -0.3125, \quad c_2 = 1.1502, \\ c_3 &= 0.0174, \quad c_4 = -0.0373, \\ c_5 &= 0.0104, \quad c_6 = -0.0459, \\ c_7 &= -1.050 \times 10^{-5}, \quad c_8 = 3.839 \times 10^{-4}, \\ c_9 &= -0.0101, \quad c_{10} = 1.959 \times 10^{-3}. \end{aligned} \tag{10}$$

The first two coefficients, c_1 and c_2, are related to the *tree* diagrams and they show clearly their dominance with respect to the *penguin* ones. Coefficients $c_3 - c_6$ correspond to QCD penguin operators while $c_7 - c_{10}$ are related to the EW ones.

However, those values of c_i must be modified when renormalization of operator O_i at one-loop order is taken into account.

Detailed expressions of operators $O_i(\mu)$ and their physical interpretation are given in reference [13].

Thus, a general form for the weak decay amplitude into a final state f can be expressed like:

$$A(B^0 \to f) = \langle f|H_w^{eff}|B^0\rangle = \frac{G_F}{\sqrt{2}} \sum_{i=1}^{10} \sum_{q=d,s} {\lambda_q}^i c_i(\mu) \langle f|O_i(\mu)|B^0\rangle, \tag{11}$$

where ${\lambda_q}^i$ is the product of two CKM matrix elements: $V_{ub}V_{uq}^*$ (for $i = 1, 2$) or $(V_{tb}V_{tq}^*)$ (for $i = 3, \ldots, 10$).

The hadronic matrix elements $\langle f|O_i(\mu)|B^0\rangle$ represent the *non-perturbative contribution* to the amplitude $A(B^0 \to f)$. Usually, they are estimated according to some specific models: Non Relativistic Quark Model (NRQM), Form Factor models (BSW) and especially the Lattice QCD calculations.

In the following, calculation of the hadronic matrix elements is performed in the framework of the BSW model [14] from which form factors are derived by the knowledge of the hadronic wave functions for both initial and final states.

5 Determination of the density-matrix elements

The B^0 decay into two vector mesons requires the helicity formalism which has been intensively used in the previous paper [1]. To each vector meson (spin 1) is assigned a set of three polarization 4-vectors defined in this way:

$$\epsilon_1 = (0, \vec{\epsilon_1}), \quad \epsilon_2 = (0, \vec{\epsilon_2}), \quad \epsilon_3 = \left(|\vec{k}|/m, E\hat{k}/m\right), \tag{12}$$

and verifying the following relations:

$$\epsilon_i{}^2 = -1, \quad \epsilon_i \cdot \epsilon_j = 0, \quad \text{with } i \neq j, \tag{13}$$

where $m, E, \vec{k}$ are respectively the mass, the energy and the momentum of the vector meson; $\hat{k}$ is defined as the unit vector along the vector momentum, $\hat{k} = \vec{k}/|\vec{k}|$.

The three vectors $\vec{\epsilon_1}, \vec{\epsilon_2}$ and $\vec{\epsilon_3} = E\hat{k}/m$ form an orthogonal basis; ϵ_1 and ϵ_2 are called the *transverse polarization* vectors while $\vec{\epsilon_3}$ is the *longitudinal polarization* one.

From that basis, an *helicity basis* is defined according to:

$$\epsilon(+) = \frac{(\epsilon_1 + i\epsilon_2)}{\sqrt{2}}, \quad \epsilon(-) = \frac{(\epsilon_1 - i\epsilon_2)}{\sqrt{2}}, \quad \epsilon(0) = \epsilon_3. \tag{14}$$

These 4-vectors are *eigenvectors* of the helicity operator $\mathcal{H}$ with the eigenvalues $\lambda = +1, -1$ and 0 respectively. For a clear account of the helicity basis for a spin 1 particle, the reader can consult the book of Dewitt-Smith [15].

In the case of two vector mesons coming from the B decay, their 4-momenta are defined in the B rest frame and their corresponding polarization vectors are *correlated* because $\hat{k_1} = -\hat{k_2}$. For an explicit calculation of their spatial components, see the appendix A.

The weak hadronic amplitude is then decomposed on the helicity basis according to the general formalism developed by the authors BSW [14]. This method allows one to obtain two interesting results:

- the contribution of the *tree* and *penguin* operators to the global amplitude via the helicity states.
- the total contribution of each helicity state.

A way of illustrating this method is to study the channel: $B^0(\bar{B}^0) \to K^{*0}(\bar{K}^{*0})\rho^0$.

(i) First of all, the mass of each resonance (K^{*0} and ρ^0) is generated according to a relativistic Breit-Wigner:

$$\frac{d\sigma}{dM^2} = C\frac{\Gamma_R M_R}{(M^2 - M_R^2)^2 + (\Gamma_R M_R)^2}, \tag{15}$$

C being a normalization constant.

(ii) The weak hadronic matrix element is expressed as the **sum** of three helicity matrix elements; each one of the form, $H_\lambda = \langle V_1 V_2 | H_w{}^{eff} | B \rangle$, is defined by gathering all the Wilson coefficients of both tree and penguin operators. Linear combinations of those coefficients arise like: c'_{t1}, c'_{p1}, and c'_{p2} (see Appendix B) and the *helicity amplitude* H_λ gets the following expression:

$$
\begin{aligned}
H_\lambda = &\Big(V_{ub}V_{us}^* c_{t_1}^\rho - V_{tb}V_{ts}^* c_{p_2}^\rho\Big)\Big\{\beta_1 \varepsilon_{\alpha\beta\gamma\delta}\epsilon_K^{*\alpha}(\lambda)\epsilon_\rho^{*\beta}(\lambda)P_B^\gamma P_K^\delta \\
&+i\Big(\beta_2 \epsilon_K^*(\lambda)\epsilon_\rho^*(\lambda) - \beta_3(\epsilon_K^*(\lambda).P_B)(\epsilon_\rho^*(\lambda).P_B)\Big)\Big\} \\
&+\Big(-V_{tb}V_{ts}^* c_{p_1}^\rho\Big)\Big\{\beta_4 \varepsilon_{\alpha\beta\gamma\delta}\epsilon_\rho^{*\alpha}(\lambda)\epsilon_K^{*\beta}(\lambda)P_B^\gamma P_\rho^\delta, \\
&+i\Big(\beta_5 \epsilon_\rho^*(\lambda)\epsilon_K^*(\lambda) - \beta_6(\epsilon_\rho^*(\lambda).P_B)(\epsilon_K^*(\lambda).P_B)\Big)\Big\}
\end{aligned} \tag{16}
$$

with:

- $\varepsilon_{\alpha\beta\gamma\delta}$: antisymmetric tensor in the Minkowski space.
- $\beta_{1,4} = \frac{G_F}{2} f_{\rho,K} m_{\rho,K^*} \frac{2}{m_B + m_{K^*,\rho}} V^{B\to K^*,\rho}(m^2_{\rho,K^*})$.
- $\beta_{2,5} = \frac{G_F}{2} f_{\rho,K} m_{\rho,K^*}(m_B + m_{K^*,\rho}) A_1^{B\to K^*,\rho}(m^2_{\rho,K^*})$.
- $\beta_{3,6} = \frac{G_F}{2} f_{\rho,K} m_{\rho,K^*} \frac{2}{m_B + m_{K^*,\rho}} A_2^{B\to K^*,\rho}(m^2_{\rho,K^*})$.
- f_K, f_ρ: respectively K^{*0} and ρ^0 decay constants.
- $V^{B\to K^*,\rho}$, $A_i^{B\to K^*,\rho}$: respectively Vector and Axial form factors (see Appendix C).
- $\epsilon_{K,\rho}(\lambda)$: K^{*0}, ρ^0 polarization vectors expressed in the B rest frame.

It is worth noticing that the tensorial terms which enter H_λ become simplified in the B rest frame because the B 4-momentum is given by $P_B = (m_b, \vec{0})$. Then, using the orthogonality properties of $\epsilon_j(\lambda)$, the helicity amplitude H_λ acquires a much simpler expression than above:

$$
H(\lambda) = iB(\lambda)(V_{ub}V_{us}^* c_{t_1}^\rho - V_{tb}V_{ts}^* c_{p_2}^\rho) + iC(\lambda)(-V_{tb}V_{ts}^* c_{p_1}^\rho), \tag{17}
$$

with:

$$
\begin{aligned}
B(0) &= \beta_2 \frac{m_B^2 - (m_K^2 + m_\rho^2)}{2m_K m_\rho} - \beta_3 \frac{|\vec{p}|^2 m_B^2}{m_K m_\rho}, \\
C(0) &= \beta_5 \frac{m_B^2 - (m_K^2 + m_\rho^2)}{2m_K m_\rho} - \beta_6 \frac{|\vec{p}|^2 m_B^2}{m_K m_\rho}, \\
B(\pm 1) &= \mp\beta_1 m_B |\vec{p}| - \beta_2, \\
C(\pm 1) &= \mp\beta_4 m_B |\vec{p}| - \beta_5,
\end{aligned} \tag{18}
$$

$|\vec{p}|$ being the common momentum to V_1 and V_2 particles in the B rest frame.

(*iii*) Expressing the CKM matrix elements according to Wolfenstein parametrization [16]:

$$V_{CKM} = \begin{bmatrix} 1-\frac{\lambda^2}{2} & \lambda & A\lambda^3(\rho - i\eta) \\ -\lambda & 1-\frac{\lambda^2}{2} & A\lambda^2 \\ A\lambda^3(1-\rho-i\eta) & -A\lambda^2 & 1 \end{bmatrix} + O(\lambda^4), \qquad (19)$$

where we use[17]:

$$A = 0.815, \quad \lambda = 0.2205: \text{ well known}$$
$$0.09 < \rho < 0.254, \quad 0.323 < \eta < 0.442.$$

Taking into account the preceding relations, we arrive at the final form for the amplitudes H_λ:

$$H\begin{pmatrix} 0 \\ \pm 1 \end{pmatrix} = A\lambda^2 \Big\{ \Big[\Big(\eta\lambda^2 c^{\rho}_{t_1} - \Im m(c^{\rho}_{p_2}) \Big) B\begin{pmatrix} 0 \\ \pm 1 \end{pmatrix} - \Im m(c^{\rho}_{p_1}) C\begin{pmatrix} 0 \\ \pm 1 \end{pmatrix} \Big]$$
$$+ i \Big[\Big(\rho\lambda^2 c^{\rho}_{t_1} + \Re e(c^{\rho}_{p_2}) \Big) B\begin{pmatrix} 0 \\ \pm 1 \end{pmatrix} + \Re e(c^{\rho}_{p_1}) C\begin{pmatrix} 0 \\ \pm 1 \end{pmatrix} \Big] \Big\}, \qquad (20)$$

from which the density-matrix elements $h_{\lambda,\lambda'}$ can be derived automatically;
$\Rightarrow h_{\lambda,\lambda'} = H_\lambda {H_{\lambda'}}^*$.

Due to the *hermiticity* of the matrix $(h_{\lambda,\lambda'})$, only six elements must be calculated and, furthermore, a normalization condition is applied:

$$N\ (h_{++} + h_{00} + h_{--}) \ = \ 1, \qquad (21)$$

(N being the normalization constant) which makes easier the comparison of the modulus of the different matrix elements.

In the next histograms (Fig.4 - Fig.9) are displayed the spectra of $h_{\lambda,\lambda'}$ for different values of the Wolfenstein parameters ρ and η. In our study, these spectra are obtained for the four couples of values: $(0.09, 0.323)$; $(0.09, 0.442)$; $(0.254, 0.323)$ and $(0.254, 0.442)$. But, due to the fact that some density matrix elements do not vary too much with ρ and η, in most cases only the spectra corresponding to the first couple of values are shown. All the histograms correspond to a sample of 20000 generated events.

It is important to notice that large spectrum of values for $h_{\lambda,\lambda'}$ are obtained and *not single ones* because of the broad range of both the ρ^0 resonance mass and the common momentum $|\vec{p}|$ (see the analytical expressions of $B(\lambda)$ and $C(\lambda)$ given above).

- Whatever the values of ρ and η are, the dominant value of $h_{++} = |H_{+1}|^2$ is $\leq 10^{-2}$, numerical result which is proved too by complete analytical calculations. Thus the dominant polarization state is the **longitudinal** one because $h_{00} = |H_0|^2 \geq 60\%$, its mean value being around 85% (Fig.4).

- Due to the tiny value of $|H_{+1}|$, the modulus of the non-diagonal elements $h_{+-} = H_+ H_-{}^*$ and $h_{+0} = H_+ H_0{}^*$ are usually smaller than 0.2; while the modulus of $h_{-0} = H_- H_0{}^*$ can reach 0.5 (Fig.5).

Fig.6 and Fig.7 display the variations of the diagonal matrix elements h_{--}, h_{00} and h_{++} with respect to the four sets of ρ and η values: it can be seen that h_{++} has always a tiny value and h_{00} is always dominant. Other physical features appear: h_{00} is very *sensitive* to the parameter η; its spectrum is rather wide for $\eta = 0.323$, while it is bounded between 0.8 and 1.0 for $\eta = 0.442$. For a fixed value of η, no noticeable variation with the parameter ρ is seen.

Fig.8 shows the real and imaginary parts of the non-diagonal elements h_{-0}, h_{+-}, h_{+0} respectively for $\rho = 0.09$ and $\eta = 0.323$. It is worth noticing that both real and imaginary parts of h_{+-} and h_{+0} are too small and close to zero.

Due to the importance of h_{+-} matrix element in the ϕ angle distribution (see Section 6), a full study of both real and imaginary parts of h_{+-} has been done. Fig.9 shows the corresponding spectra according to the values of ρ and η. It can be deduced that the real and imaginary parts have very similar distributions and both are dominated by small values (≤ 0.05).

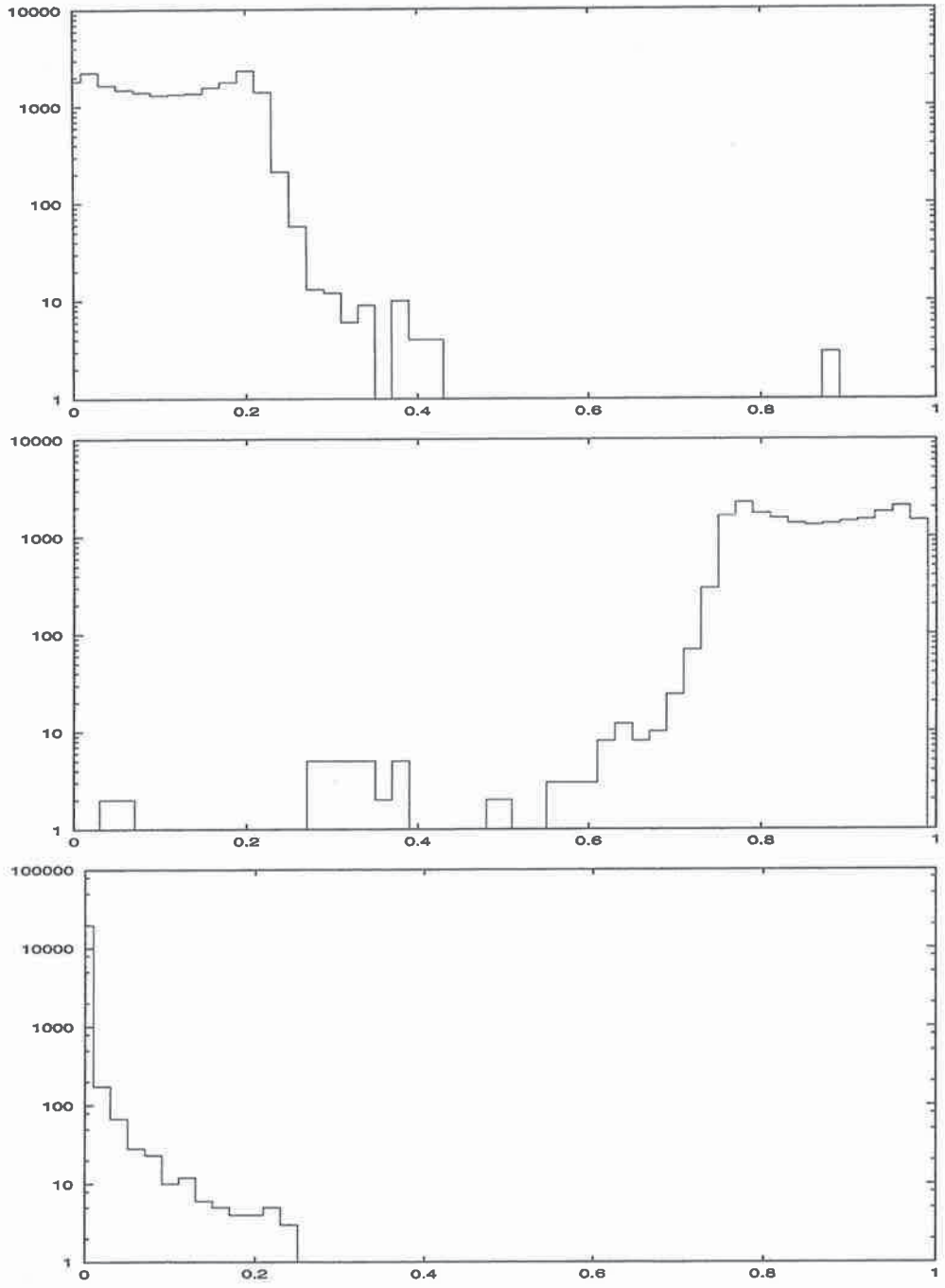

Figure 4: *Diagonal matrix elements:* h_{--}, h_{00}, h_{++} *respectively for* $\rho = 0.09$, $\eta = 0.323$.

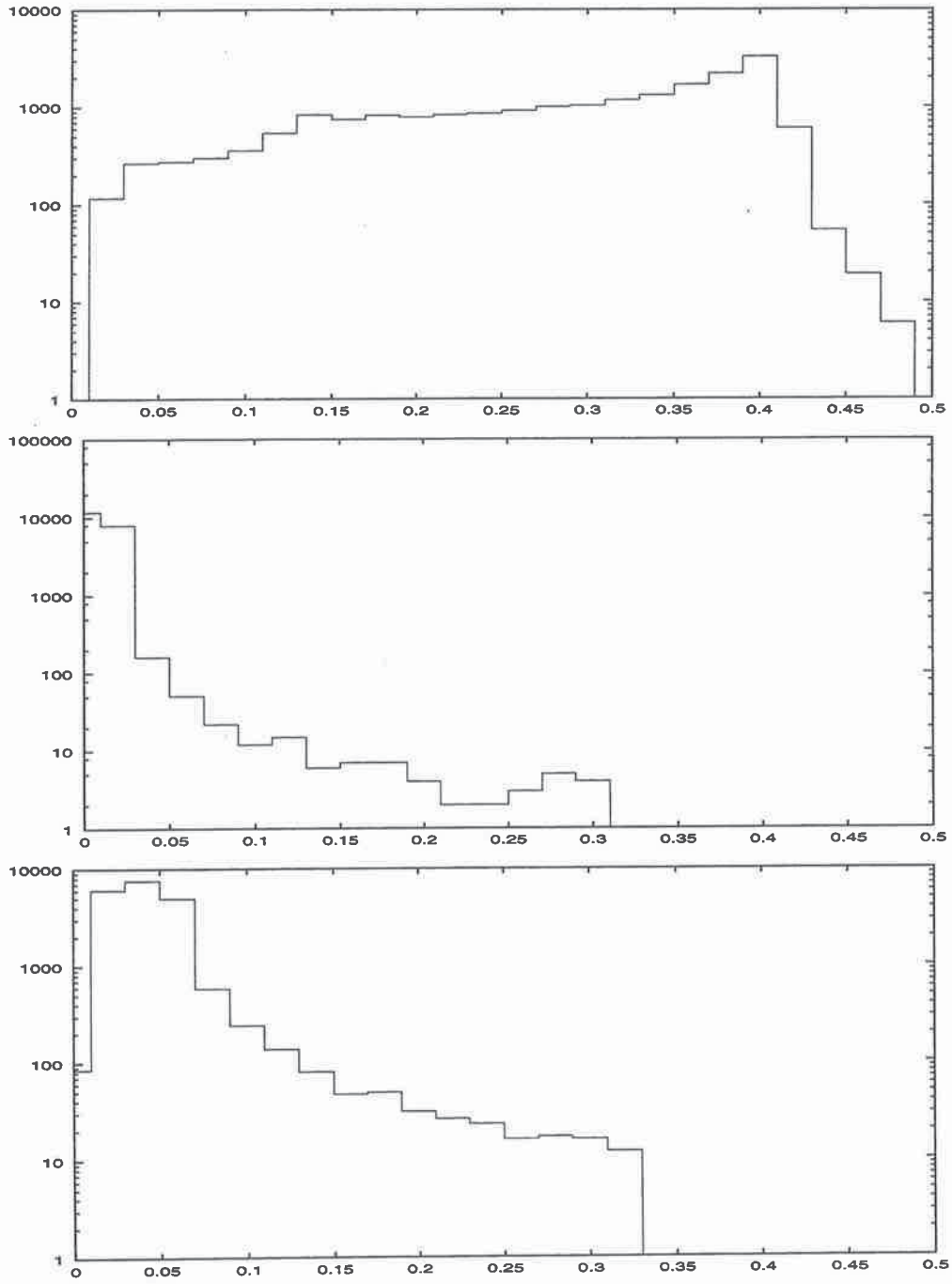

Figure 5: *Modulus of non diagonal matrix elements:* h_{0-}, h_{+-}, h_{+0} *respectively for* $\rho = 0.09, \eta = 0.323$.

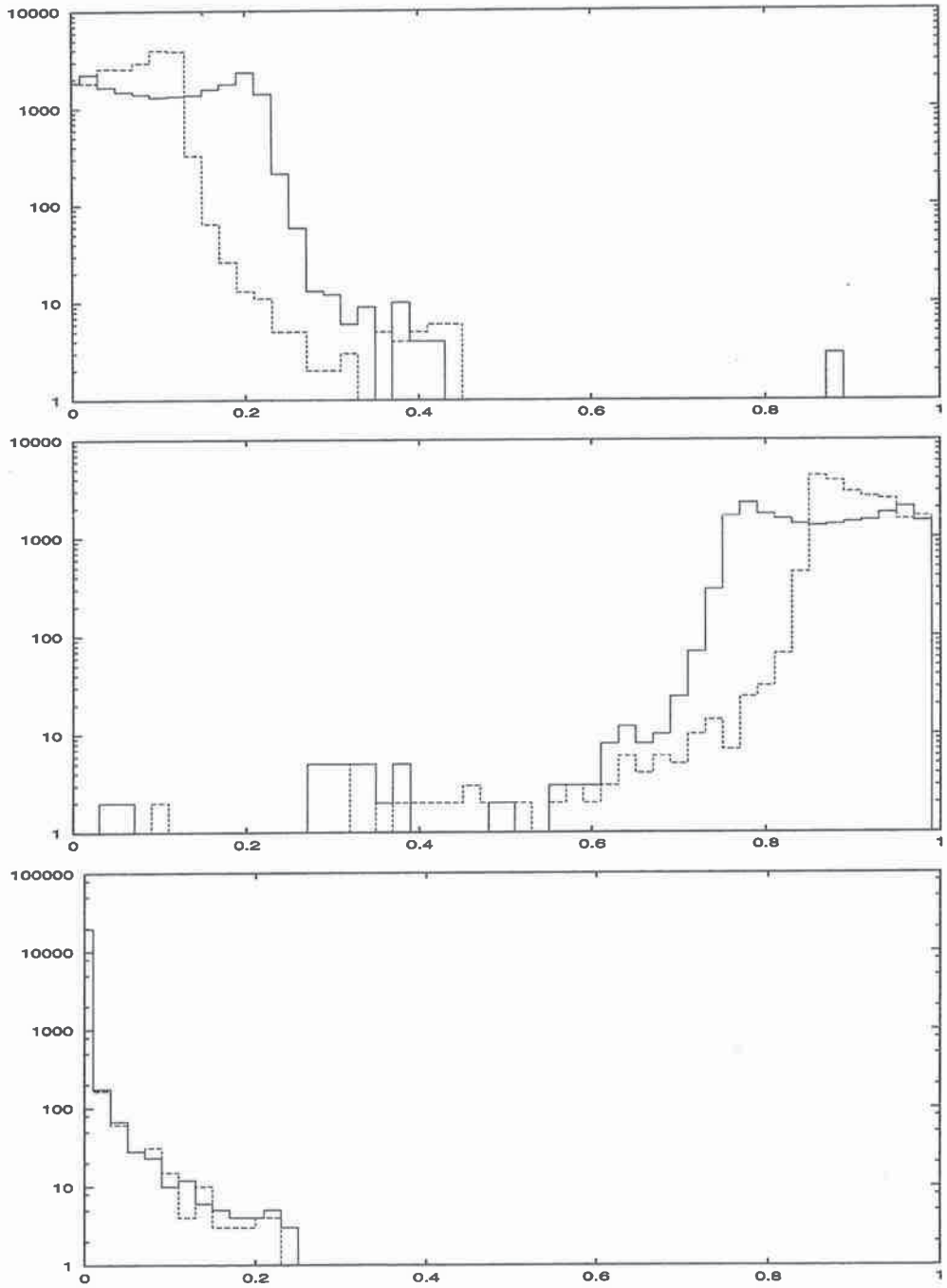

Figure 6: *Variations of* h_{--}, h_{00}, h_{++} *according to Wolfenstein parameters:* $\rho = 0.09, \eta = 0.323$ *(full line) and* $\eta = 0.442$ *(dashed line).*

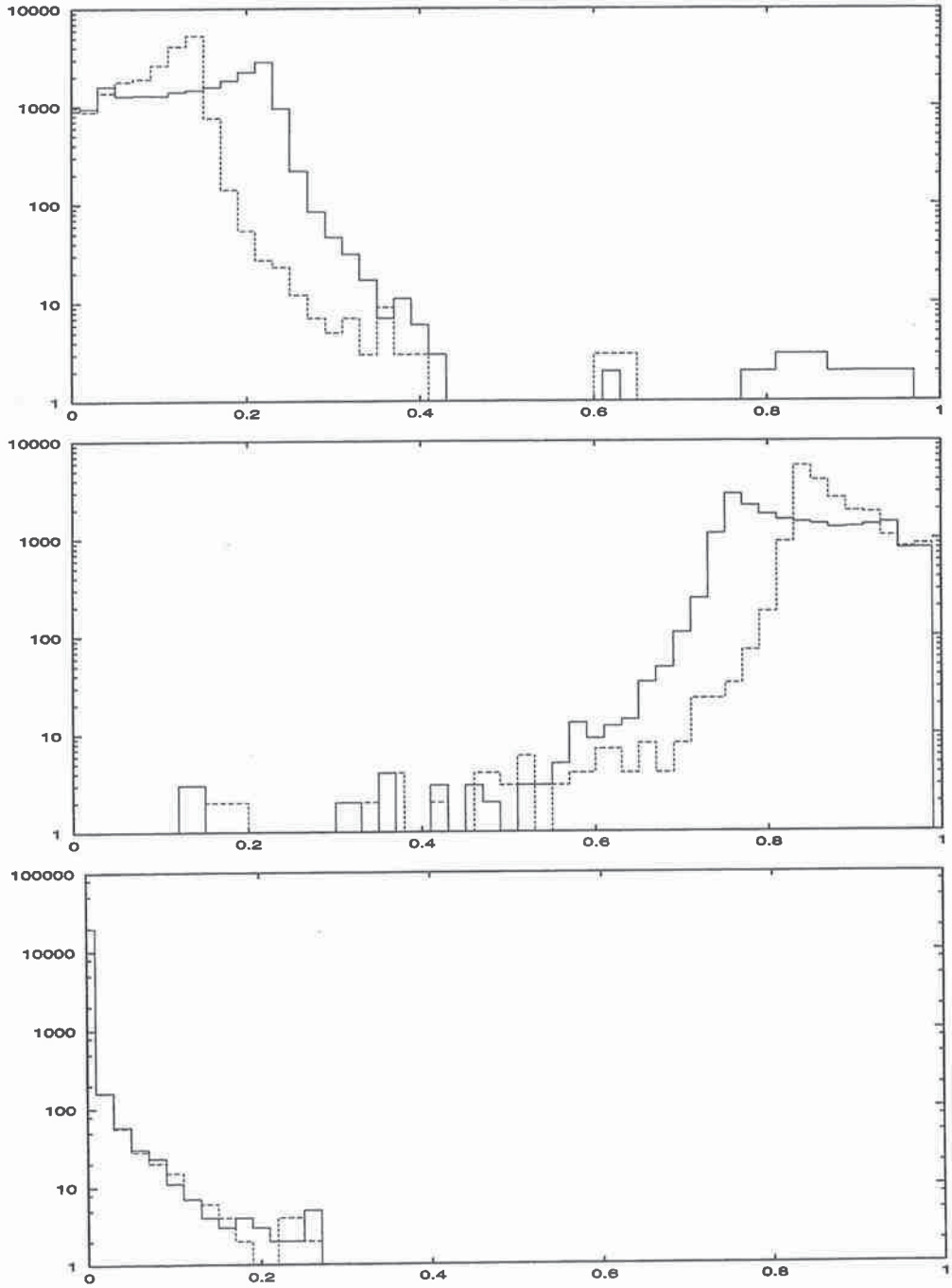

Figure 7: *Variations of* h_{--}, h_{00}, h_{++} *according to Wolfenstein parameters:* $\rho = 0.254, \eta = 0.323$ *(full line) and* $\eta = 0.442$ *(dashed line).*

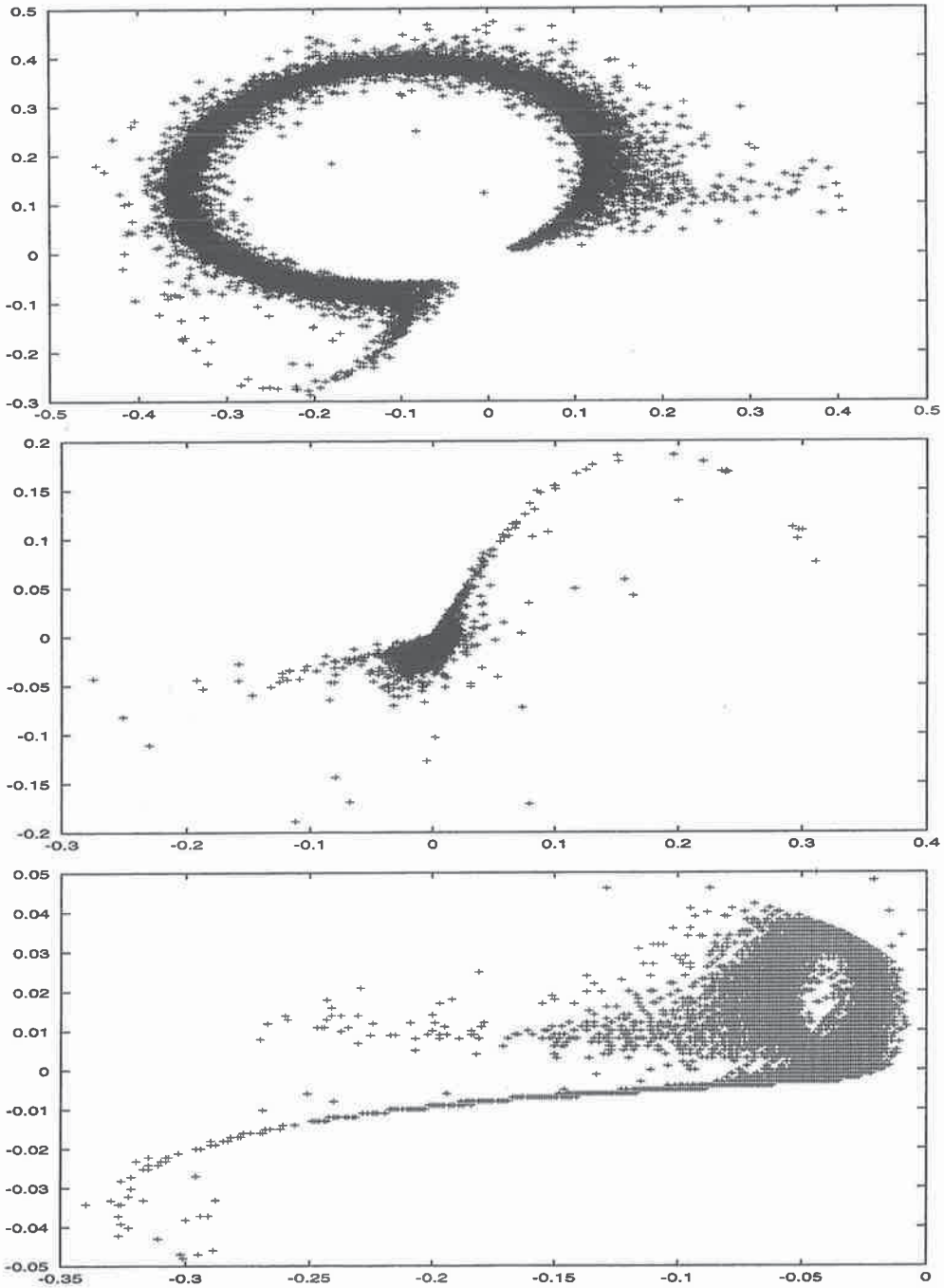

Figure 8: *Imaginary part vs Real part of matrix elements* h_{0-}, h_{+-}, h_{+0} *respectively for* $\rho = 0.09, \eta = 0.323$.

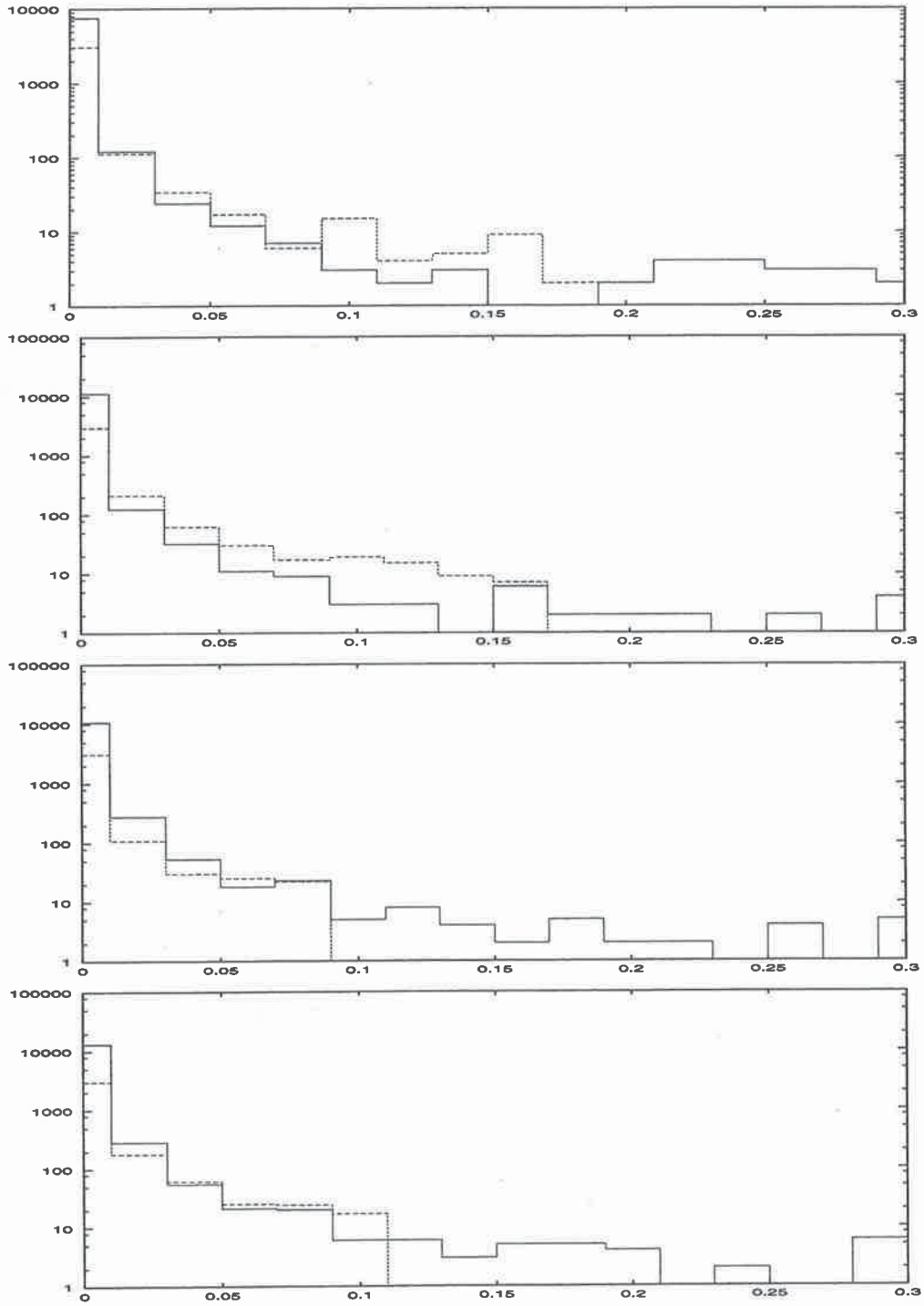

Figure 9: *Real part (full line) and Imaginary part (dashed line) of h_{+-} matrix element for (ρ, η) = (0.09, 0.323); (0.09, 0.442); (0.254, 0.323) and (0.254, 0.442) respectively.*

6 Decays of vector mesons V_1 V_2 into two pseudoscalar mesons

The matrix elements derived above allow us to compute the *degrees of polarization* of each resonance like K^* or ρ^0. The angular distributions of the pseudoscalar mesons in each V_i rest frame depend on:
(i) the spin 1 of the vector meson V_i.
(ii) the weight of each helicity state.
(iii) the correlations among the helicity states of the two vector mesons.

Complete analytical expression of the final angular distributions is the following one:

$$\begin{aligned}\frac{d^3\Gamma}{d\cos\theta_1 d\cos\theta_2 d\phi} \propto\ & (h_{++}+h_{--})\sin^2\theta_1\sin^2\theta_2/4 + h_{00}\cos^2\theta_1\cos^2\theta_2 \\ & + (\Re e(h_{+0})\cos\phi - \Im m(h_{+0})\sin\phi + \Re e(h_{0-})\cos\phi - \Im m(h_{0-})\sin\phi)\sin 2\theta_1\sin 2\theta_2/4 \\ & + (\Re e(h_{+-})\cos 2\phi - \Im m(h_{+-})\sin 2\phi)\sin^2\theta_1\sin^2\theta_2/2. \qquad (22)\end{aligned}$$

Angles θ_1 , θ_2 and ϕ have been defined in Section 1.

Explicit angular distributions for polar and azimuthal angles can be derived from the relation above. It is interesting to notice that, due to the pseudoscalar nature of the final particles, angles θ_1 and θ_2 have the *same* distributions:

- $d\sigma/d\cos\theta_{1,2} \propto (3h_{00}-1)\cos^2\theta_{1,2} + (1-h_{00})$.
- $d\sigma/d\phi \propto (1 + 2(\Re e(h_{+-})\cos 2\phi - \Im m(h_{+-})\sin 2\phi))$.

In Fig.10 are displayed respectively the $\cos\theta$ distribution and the azimuthal angle ϕ one. Some comments on these curves are necessary:

- The $\cos\theta$ distribution is practically the same whatever the values of ρ and η are; no sensitivity to particular values of ρ and η is seen.
- As far as angle ϕ is concerned, its distribution depends on the matrix element h_{+-}. Despite the fact that $\Re e(h_{+-})$ and $\Im m(h_{+-})$ do not exhibit sensitive differences (see Fig.9), those parameters present some dependence upon ρ and η: full curve corresponds to $\rho = 0.09, \eta = 0.323$; while dashed one is related to $\rho = 0.254, \eta = 0.442$. A visible discrepancy among these two curves is seen.

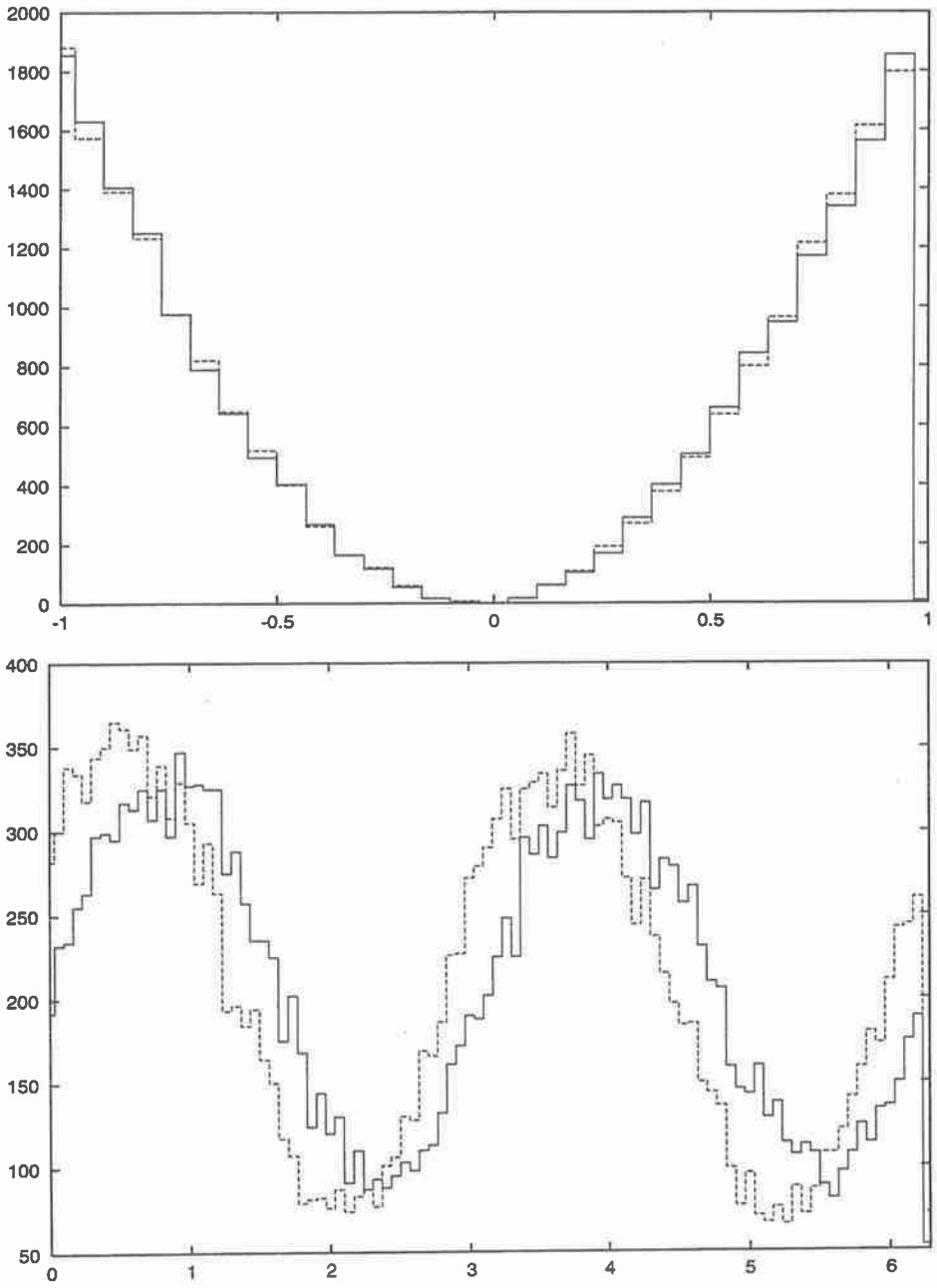

Figure 10: *Cosθ distribution (upper figure) and azimuthal angle ϕ distribution (lower figure) for $\rho = 0.09, \eta = 0.323$ (full line) and $\rho = 0.254, \eta = 0.442$ (dashed line) respectively.*

7 Perspectives and conclusion

• Thanks to the HQET approach and the OPE formalism which is used, we have at our disposal rigorous and *complete calculations* of the dynamics of the $B^{0\pm}$ decays into two vector mesons. This formalism is available for all charmless B decays provided the spin of the intermediate resonance(s) is less or equal 1; the only changes which must be taken into account are the V_{CKM} matrix elements, the masses and the widths of the resonances involved in each decay.

• In the case of leptonic decay of one resonance, like $J/\Psi \rightarrow e^+e^-, \mu^+\mu^-$, the angular distributions are modified because of the spin 1/2 final leptons; which require the use of other Wigner rotation matrices. Those calculations have been already done in our first paper [1].

• In the case where a $(c\bar{c})$ bound state or a charmed meson is produced like:

$$B^0 \rightarrow J/\Psi\rho^0, D^*X(X = \rho^0, \omega, K^{*0}),$$

the Wilson coefficients involved in the effective hamiltonian have to be modified, but we do not expect big change with respect to the $c_i(c_i')$ coefficients used in the present paper.

• Other interesting consequences arise from this formalism: it can be easily extended to the numerous channels like: $B \rightarrow VP,\ PP$ where one or two pseudoscalar mesons $(P = 0^{-+})$ are produced directly from the B decay. Because of the simple equality $\lambda(P) = \lambda(V) = 0$, the number of helicity states is reduced from 3 to 1.

• An important point which has been mentionned in the present note is the role of the $\rho^0 - \omega$ *mixing* and its consequence for the determination of the direct CPV parameter (Section 3 and reference [7]). Tagging of B^+ and B^- is made easy thanks to the K^+ and K^- mesons coming from the cascade decays. In our opinion, we can also exploit all the angular distributions of the final particles (and their correlations) in order to detect an eventual discrepancy which can arise between the B^+ and B^- decays respectively. However, a complete study of those channels and their simulations require the knowledge of the strong phase shift δ (mentionned in Section 3) according to the $\pi\pi$ invariant mass. Work is in progress.

• Those calculations and simulations can be implemented into **SICBMC**, the Monte-Carlo generator of the LHCb experiment, in order to perform afterwards a full analysis of the simulated channels.

Acknowledgements

The authors are very grateful to Dr P.Perret, leader of the LHCb Clermont-Ferrand team, for his advices and his suggestions.

One of us (Z.J.A.) is very indebted to Professor A.W.Thomas, Director of the Special Research Centre for the Subatomic Structure of Matter, for the very exciting and illuminating discussions he got with him about the QCD penguin diagrams and their importance in the evaluation of the B^0 decay width.

This work was supported in part by the Australian Research Council and the University of Adelaide.

Appendix

A Polarizations in B_d^0 rest frame

Momentum:

$$\vec{k}_K = -\vec{k}_\rho = \vec{k} = \begin{pmatrix} k\sin\theta\cos\phi \\ k\sin\theta\sin\phi \\ k\cos\theta \end{pmatrix},$$

where θ and ϕ are respectively polar and azimuthal angles of the produced K^{*0}.

Longitudinal polarization:

$$\epsilon_K(0) = \left(\frac{|\vec{k}|}{m_K}, \frac{E_K}{m_K}\hat{k}\right), \quad \epsilon_\rho(0) = \left(\frac{|\vec{k}|}{m_\rho}, \frac{E_\rho}{m_\rho}(-\hat{k})\right).$$

Tranversal polarizations :

$$\vec{\epsilon}_K(1) = \begin{pmatrix} \cos\theta\cos\phi \\ \cos\theta\sin\phi \\ -\sin\theta \end{pmatrix} = \vec{\epsilon}_\rho(1),$$

$$\vec{\epsilon}_K(2) = \begin{pmatrix} -\sin\phi \\ \cos\phi \\ 0 \end{pmatrix} = -\vec{\epsilon}_\rho(2).$$

Helicity frame :

$$\epsilon_K(+) = (\epsilon(1) + i\epsilon(2))/\sqrt{2}, \quad \epsilon_K(-) = (\epsilon(1) - i\epsilon(2))/\sqrt{2},$$

$$\vec{\epsilon}_K(+) = \begin{pmatrix} \cos\theta\cos\phi - i\sin\phi \\ \cos\theta\sin\phi + i\cos\phi \\ -\sin\theta \end{pmatrix}/\sqrt{2} = \vec{\epsilon}_K^*(-) = \vec{\epsilon}_\rho(-),$$

$$\vec{\epsilon}_K(-) = \begin{pmatrix} \cos\theta\cos\phi + i\sin\phi \\ \cos\theta\sin\phi - i\cos\phi \\ -\sin\theta \end{pmatrix}/\sqrt{2} = \vec{\epsilon}_K^*(+) = \vec{\epsilon}_\rho(+).$$

B Wilson's coefficients

We use, in the case of the ρ^0 production, the following linear combinations of the effective Wilson coefficients:

$$c_{t1}^{\rho} = c_1' + \frac{c_2'}{N_c},$$
$$c_{p1}^{\rho} = -(c_4' + \frac{c_3'}{N_c}) + \frac{1}{2}(c_{10}' + \frac{c_9'}{N_c}),$$
$$c_{p2}^{\rho} = \frac{3}{2}(c_7' + \frac{c_8'}{N_c} + c_9' + \frac{c_{10}'}{N_c}),$$

where c_{t1}^{ρ} relative to tree diagram, c_{pi}^{ρ} relative to penguin diagram and $0.98 < N_c < 2.01$.

When $q^2/m_b^2 = 0.3$:

$c_1' = -0.3125, \quad c_2' = 1.1502,$

$c_3' = 2.443 \times 10^{-2} + 1.543 \times 10^{-3}i, \quad c_4' = -5.808 \times 10^{-2} - 4.628 \times 10^{-3}i,$

$c_5' = 1.733 \times 10^{-2} + 1.543 \times 10^{-3}i, \quad c_6' = -6.668 \times 10^{-2} - 4.628 \times 10^{-3}i,$

$c_7' = -1.435 \times 10^{-4} - 2.963 \times 10^{-5}i, \quad c_8' = 3.839 \times 10^{-4},$

$c_9' = -1.023 \times 10^{-2} - 2.963 \times 10^{-5}i, \quad c_{10}' = 1.959 \times 10^{-3}.$

When $q^2/m_b^2 = 0.5$:

$c_1' = -0.3125, \quad c_2' = 1.1502,$

$c_3' = 2.120 \times 10^{-2} + 2.174 \times 10^{-3}i, \quad c_4' = -4.869 \times 10^{-2} - 1.552 \times 10^{-2}i,$

$c_5' = 1.420 \times 10^{-2} + 5.174 \times 10^{-3}i, \quad c_6' = -5.729 \times 10^{-2} - 1.552 \times 10^{-2}i,$

$c_7' = -8.340 \times 10^{-5} - 9.938 \times 10^{-5}i, \quad c_8' = 3.839 \times 10^{-4},$

$c_9' = -1.017 \times 10^{-2} - 9.938 \times 10^{-5}i, \quad c_{10}' = 1.959 \times 10^{-3}.$

C Form factors (BSW model)

	V	A_1	A_2
$B \to K^*$	$\frac{0.369}{1-m_\rho^2(GeV^2)/5.43^2(GeV^2)}$	$\frac{0.328}{1-m_\rho^2(GeV^2)/5.43^2(GeV^2)}$	$\frac{0.331}{1-m_\rho^2(GeV^2)/5.43^2(GeV^2)}$
$B \to \rho$	$\frac{0.329}{1-m_{K^*}^2(GeV^2)/5.32^2(GeV^2)}$	$\frac{0.283}{1-m_{K^*}^2(GeV^2)/5.32^2(GeV^2)}$	$\frac{0.283}{1-m_{K^*}^2(GeV^2)/5.32^2(GeV^2)}$

For further details, see reference [7] and literature quoted therein.

References

[1] **Towards a unified Monte-Carlo for B meson decay simulations**
Z.J.Ajaltouni et al, LHCb 99-051, PHYSICS, December 1999.

[2] **R.Fleischer**, private communication.

[3] **Dynamics of the Standard Model**
Donoghue et al, Cambridge monographs on Particle Physics (1994).

[4] **Weak Hamiltonian, CP Violation and Rare Decays**
A.J.Buras, hep-ph/9806471
("Probing the Standard Model of Particle Interactions" , F.David and R.Gupta eds, Elsevier Science).

[5] Review of Particle Physics, **EPJC C15**, 2000.

[6] $\rho\omega$ **mixing and direct CP violation in hadronic B decays**
S.Gardner et al, Phys.Rev.Lett. **80**, 1834 (1998) and references therein.

[7] **Enhanced direct CP violation in** $B^{\pm} \to \rho^0\pi^{\pm}$
X.-H.Guo, O.Leitner and A.W.Thomas, Phys.Rev.D**63** (2001) 056012.

[8] Myron Bander et al, Phs.Rev.Lett. **43** (1979) 242.
Harry Lipkin, Phy.Lett. **B 415** (1997) 186.

[9] P.Langacker, Phys.Rev.D20, (1979) 2983.

[10] **Heavy Quark Symmetry**
M.Neubert, Physics Reports **245** (1994) 259-395.

[11] **Weak decays beyond leading logarithms**
G.Buchalla et al, Reviews of Modern Physics, Vol.68, 1125 (October 1996).

[12] N.G.Deshpande et al, Phys.Rev.Lett. **74**, 26 (1995).

[13] **CP Violation and the role of electroweak penguins in nonleptonic B decays**
R.Fleischer, International Journal of Modern Physics **A12**, 2459 (1997).

[14] M.Bauer, B.Stech and M.Wirbel, Z.Phys. **C34**, 103 (1987) ;
M.Bauer et al, Z.Phys. **C29**, 637 (1985).

[15] **Field Theory in Particle Physics**
De Wit and J.Smith, Nort-Holland (1986).

[16] Review of Particle Physics, **EPJC C15** (2000), 110.

[17] F.Parodi, P.Roudeau and A.Stocchi, Nuo.Cim. **A112** (1999) 833.

Leitner, O., Guo, X-H., and Thomas, A.W., (2003) Direct CP violation in $B \to \pi^+\pi^-\pi$: determination of α without discrete ambiguity. *European Physical Journal C, v. 31 (2), pp. 215-226.*